Disrupt and Deliver:
Towards an Ultrasound-sensitive Lipid-based Drug Delivery System Against Biofilm Infections



Victoria K. Chris

Keble College, University of Oxford

25th April 2026

Supervisors:

Dr. Dario Carugo, Professor Alethea B. Tabor,

Dr. Sara Keller, Dr. Ramon Garcia-Maset, Dr. Gareth LuTheryn

This thesis is submitted to the Nuffield Department of Orthopaedics, Rheumatology and Musculoskeletal Sciences, University of Oxford, in fulfilment of the requirements for the degree of Doctor of Philosophy

Abstract

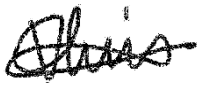
Urinary tract infections (UTIs) are the second most common type of infection, caused by uropathogenic bacteria that are able to grow and survive as biofilms (structured communities of bacteria). Biofilm formation is responsible for increased pathogenic virulence and retention, which play a significant role in the progression and persistence of infection. Therefore, biofilms are an important target to disrupt when treating UTIs. Liposomes have shown promise in antibacterial applications by increasing antibiotic efficacy against resistant bacteria. However, not all formulations have been shown to have biofilm-disrupting activity and there are presently no formulations in clinical use against UTIs. This DPhil aimed to explore the conjugation of drug-loaded liposomes to an effective biofilm dispersal agent, ultrasound (US)-sensitive lipid-coated microbubbles (MBs), as a strategy to simultaneously disrupt biofilms and deliver antibiotics. Nitrofurantoin (NIF), the first-line antibiotic treatment for UTIs, and vancomycin (VAN), a potent antibiotic used against severe Gram-positive bacterial infections, were loaded into cationic (positively-charged) or fusogenic (membrane fusing) liposomes and evaluated against planktonic (free-swimming) and biofilm models of *E. coli* and *E. faecalis*. For the VAN-loaded liposomes, the cationic formulation was of comparable efficacy to free VAN against both *E. coli* and *E. faecalis*, whilst the fusogenic formulation was only able to facilitate the killing of planktonic *E. faecalis*. Both NIF-loaded liposome formulations showed reduced efficacy (up to 16-fold) against planktonic *E. coli* or *E. faecalis* compared to free NIF. The fusogenic formulation largely matched free NIF activity against *E. faecalis* biofilm, but these liposomes decreased the viability of biofilm-associated *E. faecalis* cells up to 50% more effectively than free NIF at lower drug concentrations (<62.5 μg/mL). NIF-loaded fusogenic liposomes were conjugated to MBs via maleimide-thiol click chemistry and the resulting liposome-loaded MBs (LMBs) showed a reduced sensitivity to US (at 1.1 MHz, 1 MPa peak negative pressure) compared to unconjugated MBs. When evaluated against *E. faecalis* biofilm, LMBs did not significantly increase biofilm clearance but did significantly increase cell

death of the remaining biofilm (around 2-fold; $p<0.05$) when compared to an untreated control. Interestingly, MBs co-administered with free NIF showed an increased acoustic response and significant biofilm clearance (up to 71% more; $p<0.0001$) when compared to MBs alone and LMBs. This suggests that MB co-administration with NIF may be a more promising anti-biofilm treatment modality than LMBs, using the examined US parameters and particle formulations. This thesis demonstrates the potential for the US-mediated disruption of bacterial biofilms alongside liposomal and lipophilic drug delivery as a therapeutic approach to UTIs.

Statement of Originality

I hereby declare that this submission is my own work, and to the best of my knowledge, it contains no materials previously published or written by another person or substantial proportions of material that have been accepted for the award of any other degree or diploma at the University of Oxford, or any other educational institution, except where due acknowledgement is made in the thesis.

Any contribution made to the research by others with whom I have worked at the University of Oxford, or elsewhere, is explicitly acknowledged in the thesis. I also declare that the intellectual content of this thesis is the product of my own work, except to the extent that assistance from others in the project's design and conception or style, presentation and linguistic expression is acknowledged.



Victoria K. Chris

25th April 2026

Acknowledgements

Completing this DPhil has been a journey shaped by the guidance, support, and encouragement of many individuals, to whom I am deeply grateful.

Many thanks to the UCL School of Pharmacy for giving me the privilege of embarking on this research journey by accepting me onto the EPSRC-SFI CDT in Transformative Pharmaceutical Technologies back in 2021, when the uncertainty caused by the pandemic was still being felt. I'm glad to have been part of the 2021 cohort, especially the UCL girls, whose friendship brought so many enjoyable moments and made the challenges of research feel far less daunting. I would also like to thank the NDORMS Graduate Studies team for a smooth and easy transfer to the University of Oxford, and both the EPSRC and NIHR for funding my DPhil (EP/S023054/1).

I would like to sincerely thank Dr. Dario Carugo, Prof. Alethea Tabor, Dr. Sara Keller, Dr. Ramon Garcia-Maset, and Dr. Gareth LuTheryn for being an incredible supervisory team; the exceptional guidance and friendly support throughout these 4 years of research helped me to grow not only as a research student, but also as an individual. I am also thankful for my wonderful colleagues across the μDRIP group, Hailes-Tabor Lab, and the BUBBL group, who have shared their invaluable experimental expertise time and time again, been an observant eye and listening ear when I was silently struggling, as well as provided continuous inspiration and encouragement.

I am so grateful to my family for encouraging my pursuit of science and knowledge, giving me the freedom to fully immerse myself in my research whilst keeping me grounded. I'd also like to thank my amazing fiancé, Odu, for all your love, support, and curiosity that fuelled my enthusiasm for this research, and, of course, for being the soundboard for my early-morning or late-night liposome- and bioengineering-related thoughts. Finally, I'd like to thank God for bringing me this opportunity at exactly the right time and place, and giving me the strength to see it through to the end.

Attributions

Chapters 1, 3, 4, 5

V. K. Chris conceived the studies, designed the research, conducted the experiments, analysed and visualised the data, and wrote the chapters.

Chapter 2

V. K. Chris conceived the studies, analysed and visualised the data, and wrote the chapter. V. K. Chris also designed the research and conducted the experiments of all but the long-term storage stability studies mentioned in section **2.3.3** and drug release studies mentioned in section **2.3.4**, where M. N. Barrios designed the research and conducted the experiments as part of an MSc Pharmacology project that V. K. Chris co-supervised.

Table of contents

List of figures 12

List of tables 17

Abbreviations 18

1 Introduction and Literature Review 21

1.1 Antimicrobial Resistance 21

1.1.1 Antibiotics: a brief history and the current state 21

1.1.2 Human contributions to resistance 24

1.1.3 Bacterial mechanisms of resistance 26

1.2 Biofilm and Resistance 35

1.2.1 Biofilm formation 35

1.2.2 Biofilm structure and function 37

1.2.3 Implications in modern medicine 42

1.3 Bacteria in Urinary Tract Infections (UTIs) 50

1.3.1 Types and causes 50

1.3.2 Current landscape of UTI treatment 54

1.3.3 Future of UTI treatment and management 58

1.4 Liposomes: lipid-based nanoparticles for drug delivery 61

1.4.1 Nanoparticles for drug delivery: a brief overview 61

1.4.2 Liposomes: types and mechanisms 65

1.4.3 Liposome manufacturing methods 71

1.4.3.1 Production methods 71

1.4.3.2 Drug-loading methods 74

1.4.3.3 Characterisation methods 75

1.4.4 Clinical applications of liposomes: uses in bacterial infection 77

1.5 Ultrasound-mediated methods of treatment 83

1.5.1 A background on ultrasound, cavitation and microbubbles 83
1.5.2 Microbubble manufacturing methods 90
1.5.2.1 Production methods 91
1.5.2.2 Characterisation methods 92
1.5.3 Therapeutic ultrasound and microbubbles: uses in bacterial infections 94
1.5.4 Integrating ultrasound with drug delivery systems 97
1.6 Aims and Objectives 102
2 Formulation and characterisation of drug-loaded liposomes 104
2.1 Introduction 104
2.2 Materials and Methods 109
2.2.1 Materials 109
2.2.2 Liposome production 110
2.2.3 Liposome characterisation 113
2.2.4 Encapsulation efficiency (EE) 113
2.2.5 Drug release assays on vancomycin-loaded liposomes 114
2.2.6 Statistical analyses 115
2.3 Results and Discussion 116
2.3.1 Formulation of cationic and fusogenic liposomes 116
2.3.2 Loading and labelling of liposome formulations 120
2.3.3 Long-term stability of VAN-loaded cationic liposomes 122
2.3.4 Passive drug release from VAN-loaded cationic liposomes 124
2.4 Conclusions 126
3 Assessment of antibacterial activity of liposomal antibiotics 129
3.1 Introduction 129
3.2 Materials and Methods 133
3.2.1 Materials 133
Microbial strains 133
3.2.2 Microbiological assays 134

3.2.2.1 Minimum inhibitory concentration 134
3.2.2.2 Minimum bactericidal concentration 135
3.2.2.3 Minimum biofilm eradication concentration 136
3.2.2.4 Minimum biofilm-associated bactericidal concentration 138
3.2.3 Confocal imaging with VAN-loaded liposomes 139
3.2.4 Super-resolution imaging 140
3.2.5 Data processing 141
3.3 Results and Discussion 142
3.3.1 Investigating liposomal vancomycin activity against planktonic bacteria 142
Liposomal VAN activity against planktonic *E. coli* 143
Liposomal VAN activity against planktonic *E. faecalis* 146
The effect of unloaded liposomes on bacterial viability 149
3.3.2 Preliminary findings from confocal imaging of *E. coli* and *E. faecalis* after liposome treatment 153
3.3.3 Preliminary observations of liposome interactions using super-resolution microscopy 160
3.3.4 Investigating the effect of liposomal PEG content on bacterial interaction 163
3.3.5 Investigating liposomal nitrofurantoin activity against planktonic bacteria 171
Liposomal NIF activity against planktonic *E. coli* 173
Liposomal NIF activity against planktonic *E. faecalis* 175
3.3.6 Testing liposomal antibiotics against monospecies biofilms 177
3.4 Conclusions 184
4 Formulation of microbubbles, conjugation to drug-loaded liposomes, and assessment of the activity of the liposome-microbubble system 187
4.1 Introduction 187
4.2 Materials and Methods 189
4.2.1 Materials 189
4.2.2 Ultrasound instrumentation and parameters 190

4.2.3 Microbubble production ... 192
4.2.4 Microbubble characterisation ... 193
4.2.5 Liposome-microbubble conjugation optimisation and particle characterisation ... 194
4.2.6 Assessment of anti-biofilm activity of liposome-microbubble particles ... 195
4.2.7 Statistical analysis ... 197
4.3 Results and Discussion ... 198
4.3.1 Microbubble formulation and characterisation ... 198
4.3.2 Characterisation of optimised liposome-loaded microbubbles ... 202
4.3.3 Evaluation of anti-biofilm and cavitation activity of liposome-microbubble construct ... 208
4.3.3.1 Pre-application acoustic response of treatments ... 208
4.3.3.2 Post-application acoustic response and anti-biofilm activity of treatments ... 212
4.4 Conclusions ... 222
5 Conclusions ... 224
5.1 Summary of research ... 224
5.2 Perspectives and future work ... 227
5.2.1 Limitations of the study ... 227
5.2.2 Suggestions for future work ... 229
5.3 Closing remarks ... 232
6 Supplementary ... 233
6.1 Liposome manufacturing ... 233
6.1.1 Calibration curves ... 233
6.1.2 Rehydration difficulties ... 233
6.1.3 Freeze-thaw method attempts ... 234
6.1.4 Liposome contribution to absorbance ... 235
6.2 Cationic liposome aggregation observations ... 237
6.3 Super-resolution microscopy ... 238
6.3.1 Liposome-only sample images ... 238

6.3.2 Proposed in-solution staining protocol 238
6.4 Fusogenic liposome PEG titration 240
6.5 NIF precipitation in microbiological assays 241
6.6 MBEC assays 242
6.6.1 MBEC assay optimisation 242
6.6.2 Biofilm biomass as absorbance values (complementary to Figures 42A and 43A) 247
6.7 Optimisation of liposome-microbubble conjugation 248
6.8 Confocal images of biofilm clearance 256
6.9 Passive cavitation detection analysis MATLAB script 257
References 261

List of figures

Figure 1 | Timeline of antibiotic discovery. 22

Figure 2 | Timeline of discovery of major antibiotics and corresponding emergence of resistance. 23

Figure 3 | General structure of a bacterial cell. 27

Figure 4 | Structural differences in the cell envelopes of Gram-positive and Gram-negative bacteria. 28

Figure 5 | Mechanisms of bacterial resistance to antibiotics. 30

Figure 6 | Canonical routes of horizontal gene transfer. 34

Figure 7 | Biofilm life cycle and constituents. 37

Figure 8 | Resistance mechanisms facilitated by biofilm formation. 40

Figure 9 | Co-trimoxazole (trimethoprim/sulfamethoxazole) mechanism of action. 47

Figure 10 | Diagram of the urinary tract and corresponding infections. 51

Figure 11 | Chemical structure of nitrofurantoin (NIF). 55

Figure 12 | Examples of nanoparticles used in drug delivery. 62

Figure 13 | General liposome structure and classes. 66

Figure 14 | Potential mechanisms of cellular uptake of cationic and fusogenic liposomes. 68

Figure 15 | Schematic representation of lipid organisation during three conventional liposome production methods. 74

Figure 16 | Overview of relevant characteristics that define US fields in medical use.. 85

Figure 17 | Types of microbubble cavitation and its biophysical effects. 88

Figure 18 | Examples of cavitation nuclei. 90

Figure 19 | Types of cavitation detection and a simplified representation of an acoustic pressure spectrum. 94

Figure 20 | Maleimide-thiol conjugation reaction. 100

Figure 21 | Molecular packing and phases of lipid membranes. 106

Figure 22 | Schematic of liposome production process. 111

Figure 23 | Schematic of the ultrafiltration process. 114

Figure 24 | Storage stability of liposome formulations over seven days. 117

Figure 25 | Representative absorbance spectrum showing the presence of VAN and DiO in (fusogenic) liposome formulation. 122

Figure 26 | Storage stability of Cat-8-VAN over 120 days 123

Figure 27 | Drug release (%) of vancomycin from cationic liposomes over time at 4°C and 37°C. 125

Figure 28 | Arrangement of samples in 96-well plate for MIC/MBC assays. 136

Figure 29 | Arrangement of samples in 24-well plate for MBEC assays 138

Figure 30 | Schematic of on-chip staining protocol for super-resolution imaging with ONI. 141

Figure 31 | Bacterial viability of four *E. coli* strains after treatment with VAN formulations in MBC assays. 146

Figure 32 | Bacterial viability of three *E. faecalis* strains after treatment with VAN formulations in MBC assays. 148

Figure 33 | Bacterial viability after treatment of planktonic monospecies models with unloaded liposomes 151

Figure 34 | Confocal images (100×) of UTI89 and EF36 after treatment with liposomal VAN. 157

Figure 35 | Comparison of LDRs and PCCs from confocal images of UTI89 and EF36 after treatment with liposomes 158

Figure 36 | Super-resolution images of UTI89 and EF36 after treatment with Fuso-1-PEG-VAN. 162

Figure 37 | Representative confocal images of UTI89 and EF36 after treatment with fusogenic formulations containing either 2.5% or 1% PEG..... 167

Figure 38 | Comparison of LDRs and PCCs from confocal images of UTI89 and EF36 after treatment with fusogenic liposomes containing either 5% (original), 2.5% or 1% PEG content. 168

Figure 39 | Bacterial viability of UTI89 and EF36 after treatment with fusogenic liposomes containing either 5% (original), 2.5% or 1% PEG content in MBC assay..... 170

Figure 40 | Bacterial viability of four *E. coli* strains after treatment with NIF formulations in MBC assays. 174

Figure 41 | Bacterial viability of three *E. faecalis* strains after treatment with NIF formulations in MBC assays. 177

Figure 42 | Biofilm biomass and bacterial viability of *E. coli* in MBEC and MBaBC assays..... 181

Figure 43 | Biofilm biomass and bacterial viability of *E. faecalis* in MBEC and MBaBC assays.. 183

Figure 44 | Diagram of ultrasound setup..... 191

Figure 45 | Example spectra of analysed cavitation data..... 192

Figure 46 | Representative bright-field images of prepared microbubbles before and after washing. 199

Figure 47 | Representative cavitation profile of microbubbles immediately after production. ... 201

Figure 48 | Representative brightfield and widefield images of FMBs. 203

Figure 49 | Acoustic energy emitted by conjugated and non-conjugated microbubbles after exposure to US. 206

Figure 50 | Representative cavitation profile of conjugated and non-conjugated microbubbles.207

Figure 51 | Acoustic energy emitted by treatment samples after exposure to US in the absence of biofilm..... 210

Figure 52 | Representative cavitation profiles of treatment samples in the absence of biofilm.. 212

Figure 53 | Acoustic energy emitted by microbubble preparations after exposure to US in the presence of biofilm. 214

Figure 54 | Representative cavitation profiles of microbubble preparations exposed to US in the presence of biofilm. 215

Figure 55 | Confocal images (10×) of *E. faecalis* biofilm after incubation with different US-exposed treatments. 220

Figure 56 | Biofilm coverage area vs. inertial collapse duration comparisons. 221

Figure 57 | Mean pixel intensities and ratios of treated biofilm staining with SYTO 9 and PI... 221

List of Supplementary Figures

Supplementary Figure 1 | Calibration curves used for encapsulation efficiency calculations..... 233

Supplementary Figure 2 | Photographs of thin film during hydration step. 233

Supplementary Figure 3 | Photographs of Amicon® filter after ultrafiltration of liposome suspension. 236

Supplementary Figure 4 | Photographs comparing Cat-8-VAN aggregation in MHB and caMHB. 237

Supplementary Figure 5 | Confocal images comparing Cat-8-VAN aggregation in caMHB or PBS. 237

Supplementary Figure 6 | Super-resolution dSTORM image of sample containing only Fuso-1-PEG-VAN labelled with proprietary pan-LNP detection (640 nm, Oxford Nanoimaging, UK). 238

Supplementary Figure 7 | Photographs comparing Fuso1-PEG-VAN containing varying amounts of PEG during the rehydration step. 240

Supplementary Figure 8 | Photograph of NIF precipitation at high concentrations in caMHB. 241

Supplementary Figure 9 | Biofilm biomass of *E. coli* after treatment with VAN formulations in MBEC assays. 244

Supplementary Figure 10 | Biofilm biomass of *E. faecalis* after treatment with VAN formulations in MBEC assays. 245

Supplementary Figure 11 | Comparison of bacterial biofilm biomass when grown in caMHB or TSB for 24 hours. 246

Supplementary Figure 12 | Biofilm biomass (as absorbance values) in MBEC assays. 247

Supplementary Figure 13 | Cavitation profiles of MBs and FMBs conjugated at 4°C or at room temperature. 250

Supplementary Figure 14 | Brightfield and widefield images of FMBs and MBs conjugated by mixing at 4°C or at room temperature. 252

Supplementary Figure 15 | Cavitation profiles of MBs and FMBs conjugated in the presence of room air or PFB gas. 253

Supplementary Figure 16 | Cavitation profiles of MBs and FMBs after gentle mixing or standing at 4°C in the presence of room air. 254

Supplementary Figure 17 | Cavitation profiles of MBs and FMBs after gentle mixing or standing at 4°C in the presence of PFB. 255

Supplementary Figure 18 | Confocal images (40×) of pores and streaks in *E. faecalis* (EF36) biofilm after US exposure with bubble-containing treatments. 256

List of tables

Table 1 | Liposome formulations tested. 112

Table 2 | Average size, PDI and zeta potential of tested unloaded formulations. 120

Table 3 | Average encapsulation efficiency of the formulations for each drug evaluated. 121

Table 4 | Bacterial strains used in the present study. 134

Table 5 | Maximum drug concentrations used in each microbiological assay. 139

Table 6 | Summary of MIC and MBC values of VAN treatments. 143

Table 7 | Summary of properties of fusogenic liposomes containing varying PEG content. 164

Table 8 | Summary of MIC and MBC values of NIF treatments. 172

Table 9 | List of treatments used to evaluate anti-biofilm activity of liposome-loaded microbubbles. 196

List of Supplementary Tables

Supplementary Table 1 | Average size and concentration of MBs and FMBs after being subject to various conjugation conditions. 251

Abbreviations

AMP	Antimicrobial Peptide
AMR	Antimicrobial Resistance
ANOVA	Analysis Of Variance
AST	Antibiotic Susceptibility Test
BLDB	Beta-Lactamase Database
caMHB	Cation-Adjusted Mueller-Hinton II Broth
CAUTI	Catheter-Associated Urinary Tract Infection
CF	Cystic Fibrosis
CFU	Colony Forming Unit
CLSI	Clinical and Laboratory Standards Institute
cUTI	Complicated Urinary Tract Infection
DBCO	Dibenzocyclooctyne
DLS	Dynamic Light Scattering
dSTORM	Direct Stochastic Optical Reconstruction Microscopy
ECM	Extracellular Matrix
eDNA	Exogenous/Extracellular Deoxyribonucleic Acid
EDTA	Ethylenediaminetetraacetic Acid
EE	Encapsulation Efficiency
EPS	Extracellular Polymeric Substance
ESBL	Extended-Spectrum β-Lactamase
EUCAST	European Committee on Antimicrobial Susceptibility Testing
ExPEC	Extraintestinal *Escherichia Coli*
FDA	US Food and Drug Administration

FMB	[Fuso-1-PEG-NIF]-Loaded Microbubble
GLASS	Global Antimicrobial Resistance and Use Surveillance System
HGT	Horizontal Gene Transfer/Transmission
IBC	Intracellular Bacterial Community
LDR	Live/Dead Ratio
LMB	Liposome-Loaded Microbubble
LNP	Lipid Nanoparticle
LPS	Lipopolysaccharide
MBaBC	Minimum Biofilm-associated Bactericidal Concentration
MBC	Minimum Bactericidal Concentration
MBEC	Minimum Biofilm Eradication Concentration
MDR	Multi-Drug Resistant
MGE	Mobile Genetic Elements
MIC	Minimum Inhibitory Concentration
MPS	Mononuclear Phagocytic System
NIF	Nitrofurantoin
NP	Nanoparticle
PBP	Penicillin-Binding Protein
PCC	Pearson's Correlation Coefficient
PCD	Passive Cavitation Detector/Detection
PDI	Polydispersity Index
PDR	Pan-Drug Resistant
PDT	Photodynamic Therapy
PEG	Polyethylene Glycol
PFB	Perfluorobutane

PHE	Public Health England
PLGA	Poly(Lactic-co-Glycolic Acid)
PNP	Peak Negative Pressure
PRF	Pulse Repetition Frequency
PSD	Power Spectral Density
QIR	Quiescent Intracellular Reservoir
QS	Quorum Sensing
ROS	Reactive Oxygen Species
rRNA	Ribosomal Ribonucleic Acid
TSB	Tryptic Soy Broth
UPEC	Uropathogenic *Escherichia Coli*
US	Ultrasound
UTI	Urinary Tract Infection
uUTI	Uncomplicated Urinary Tract Infection
VAN	Vancomycin
VGT	Vertical Gene Transfer/Transmission
VRE	Vancomycin-Resistant Enterococci
WGA	Wheat Germ Agglutinin
WHO	World Health Organisation
XDR	Extensively Drug Resistant

1 Introduction and Literature Review

1.1 Antimicrobial Resistance

1.1.1 Antibiotics: a brief history and the current state

Since the accidental discovery of penicillin by Alexander Fleming in 1928 and its subsequent mass production, antibiotics have been considered 'wonder drugs', redefining humanity's relationship with infectious disease[1,2]. In the pre-antibiotic era, pneumonia was a major cause of mortality, with a mortality rate up to 40% if caused by *Streptococcus pneumonia*[3]. Penicillin treatment reduced this mortality rate to 12%, diminishing the fear of the once-deadly condition[4]. Overall, the discovery and distribution of antibiotics in the 20th century accelerated the decline in infectious disease mortality[5,6]. The 'golden era' of antibiotic discovery, from the 1940s to the 1960s, saw the development and large-scale production of most of the antibiotic classes that we know today (**Figure 1**)[7]. Unfortunately, it was not long after the large-scale (and excessive) use of rapidly discovered antibiotics during this time that resistant bacterial isolates were identified (**Figure 2**)[7,8]. The discovery boom was then followed by a slump in new antibiotic development, leading to the 'discovery void' starting in the late 1980s, where no new classes of antibiotics were brought to market, yet resistance was still being reported[8–11]. The increase in strains resistant to antibiotics along with the decrease in new antibiotic classes discovered paved the way for the current global health crisis known as antimicrobial resistance (AMR).

AMR specifically refers to the ability of microorganisms, especially bacteria, to evolve and become resistant to antimicrobials that they may have been previously susceptible to. The unprecedented rise in AMR has been associated with around 5 million deaths globally in 2019, and was directly attributed to 1.2 million deaths that year[12]. This figure is predicted to increase to 10 million deaths globally per year by 2050, becoming the leading cause of death ahead of cancer and cardiovascular disease[13,14]. Recent surveillance reports show that, between 2018 and 2023, AMR monitored in a range of pathogen-antibiotic combinations increased by 40%, demonstrating that the crisis is still

very much ongoing[15]. Within the UK, over 35,000 deaths are related to AMR each year and NHS England already spends approximately £180 million per year treating AMR infections, with estimates of $900 million being spent across the whole of the UK in inpatient admissions[16,17]. This treatment cost is predicted to increase to a staggering $3.7 billion per year in the UK by 2050[17]. Not only would the cost of treating AMR infections scale with the number of individuals affected, but there would also possibly be a need for more expensive and intensive care, created by further health complications associated with AMR infection.

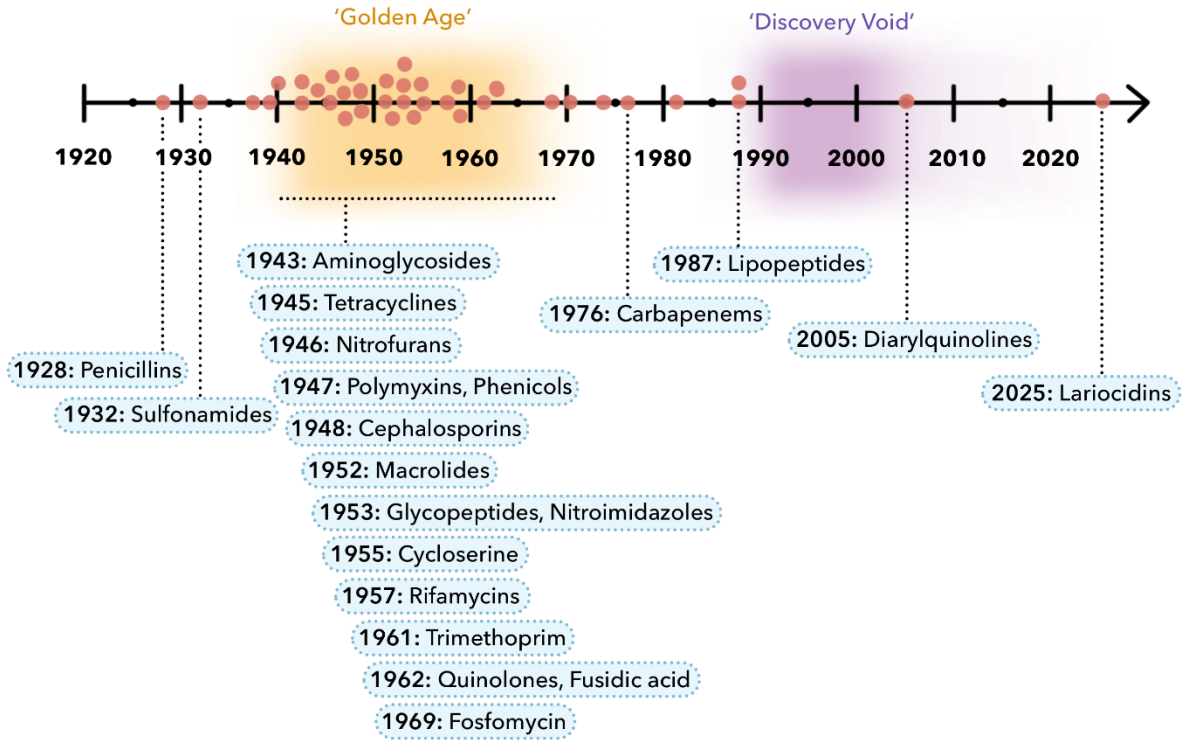


Figure 1 | Timeline of antibiotic discovery. Timeline spanning from 1920s to the present day shows years of discovery of 38 classes of antibiotics as red dots on the timeline. Some major classes of antibiotics and their years of discovery are highlighted in blue. The 'golden age' of antibiotic discovery is indicated by the yellow zone and the 'discovery void' is indicated by the purple zone.

The cost of AMR is not limited to human health and healthcare services; worldwide economic output could also be heavily impacted. The World Bank estimated that 3.8% of global gross domestic product (GDP) could be lost each year, with an annual shortfall of $3.4 trillion by 2030[18,19]. A study by the Global Leaders Group on AMR predicted an average reduction of life expectancy by 1.8 years by 2035[20]. Trade and tourism is also expected to be impacted; fear of

catching a resistant infection at work or on holiday would translate to a reduction in GDP, and work days and productivity lost due to bereavement would rise[21]. Food production and security would also be compromised as antimicrobials used in farming contaminate the food chain and waterways, increasing the likelihood of resistant foodborne diseases and biodiversity loss[22–24]. The social impact could also be devastating with anticipated stigmatisation of infected individuals or those at higher risk of infection, particularly migrants and the elderly, which could then lead to further antibiotic misuse by these individuals[25–27].

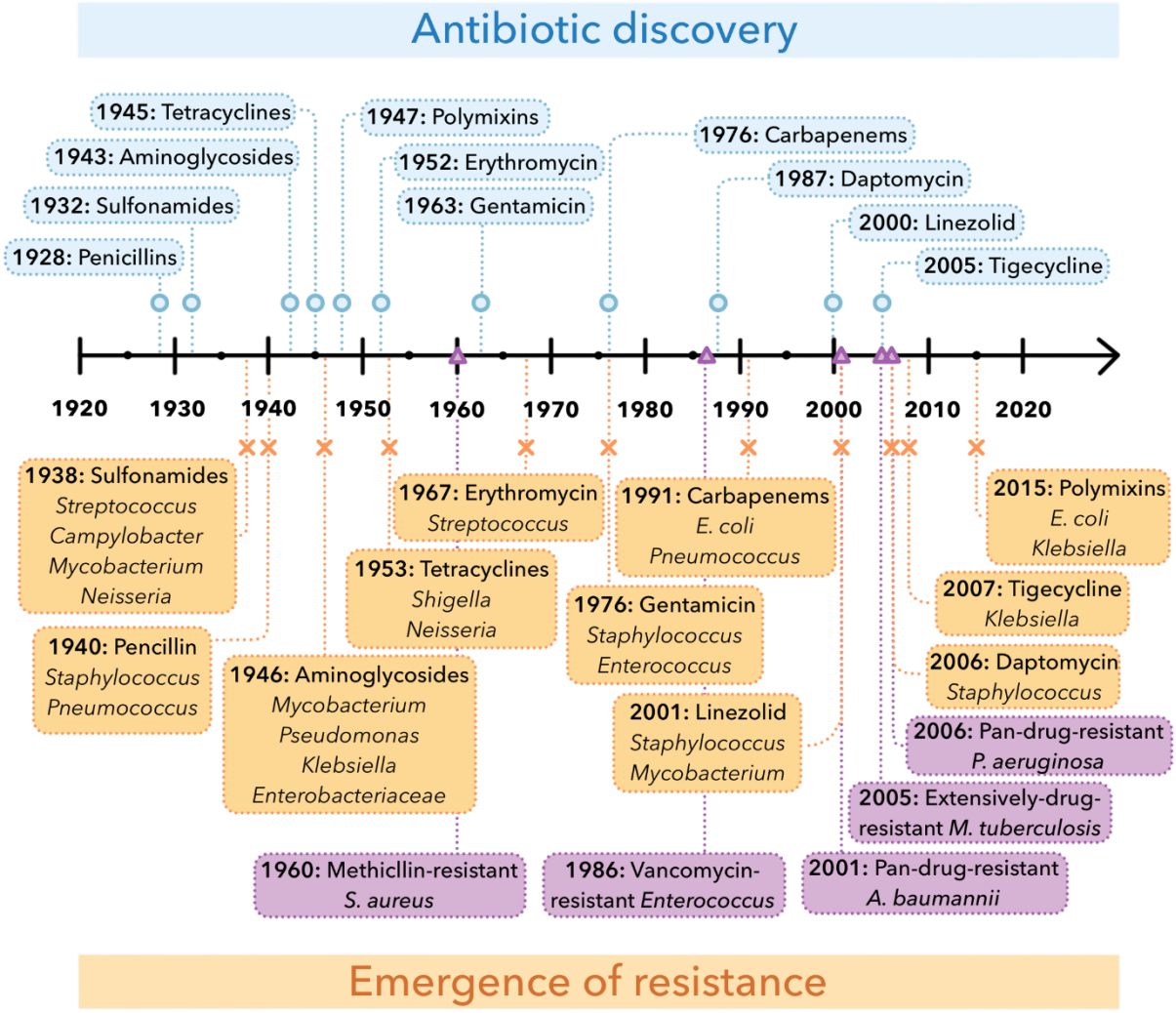


Figure 2 | Timeline of discovery of major antibiotics and corresponding emergence of resistance. Blue circles above the timeline show discovery of 11 different antibiotics/classes. Orange crosses below the timeline indicate the years when resistance was first identified for these antibiotics/classes; various resistant strains are listed for each. Purple triangles highlight the discovery of significant resistant bacterial strains.

Unsurprisingly, the World Health Organisation (WHO), as well as other organisations and groups, have acknowledged that AMR is a major public health threat that requires urgent and coordinated global action[15,28,29]. In response to the call to action, government bodies and organisations across the world have developed national action plans, launched initiatives to improve surveillance and stewardship, as well as encouraged public and private funding of AMR research[15,28–30]. For example, WHO has established a surveillance unit (Global Antimicrobial Resistance and Use Surveillance System; GLASS), published a global AMR research agenda, and runs annual campaigns for World AMR Awareness Week[15,28,29]. Although recent reports and statistics solidify concerns, efforts made by individuals and groups must be intentional and coordinated in order to meaningfully take on a public health threat of this magnitude and reach; setting up and engaging with global initiatives are a crucial step in working towards effectively combatting AMR.

1.1.2 Human contributions to resistance

While AMR is a natural phenomenon that allows microorganisms to evolve, resulting in antibiotics eventually becoming ineffective, human activity has played a significant role in the rapid progression of AMR into a public health crisis. Antibiotic misuse and overuse in humans, animals and farming is the main catalyst of rising AMR, leading to the ultimate selection and spreading of a resistant population of bacteria after susceptible strains have been cleared[28,31]. Antibiotic misuse and overuse in humans include, but is not limited to, not completing a prescribed antibiotic course, self-medicating on antibiotics without a prescription, as well as over-prescription by healthcare professionals[31,32]. Studies by Public Health England (PHE) found that 31% of registered antibiotic prescriptions in England were not linked to any clinical condition, and that 8.8-23% of all antibiotic prescriptions were inappropriate, based on what assumptions were made[33,34]. Not only do these actions directly influence the evolution of pathogenic bacteria, but they also clear commensal strains making up the microbiome that would have otherwise been involved in host protection[35]. Additionally, the overuse of untargeted antibiotics, i.e. broad-spectrum antibiotics, that occurs

when the causative agent has not been correctly identified or confirmed, further leads to the development of resistance[15,36].

Unprescribed antibiotics are also extensively used in agriculture, for prophylactic, metaphylactic and therapeutic use; around 70% of worldwide antibiotics were used in livestock in 2017[23,37,38]. The intensive conditions used in animal farming are optimised for high yield, fostering a stressful environment in which animals become more susceptible to disease, which would in turn reduce their productivity and allow zoonosis to emerge[39–41]. This presents mass-medication of livestock as the cheap and effective option to protect food safety and security. There is also a financial incentive in stimulating animal productivity and growth via antibiotic use, which altogether contributes to the significant overuse of antibiotics in animal farming[42]. Not only is there a risk of transmission of resistant bacteria to farmers through direct contact, but the downstream consumption of animal products containing resistant bacteria also leads to the spread of resistance in other organisms[43]. Environmental exposure to these contaminants via animal (and human) waste means soil and water bodies are either exposed to resistant microorganisms or to sufficiently low concentrations of antibiotics that can induce AMR[23,44,45].

In addition to antibiotic abuse, environmental contamination, poor hygiene and sanitation, human conflict, and global movement are some of the many other ways in which human activity has contributed to the growing issue[31]. Improper disposal of expired or unused antibiotics also contributes to environmental contamination, especially when additives in everyday hygiene products, cosmetics and detergents containing antibiotics and biocides are factored in[46,47]. Poor hygiene and sanitation, particularly in overcrowded public settings, means that there is a varied pool of microorganisms that are able to transfer resistance, and hosts to facilitate this transmission. Lack of access to safe water means water bodies previously exposed to resistant microbes or excreted antibiotics would further drive this AMR spread[48,49]. Disrupted healthcare systems caused by human conflict and war means that antibiotic abuse and lack of sanitation and safe water

previously mentioned become commonplace. This leads to shocking levels of resistance: for example, up to a 300% increase in aztreonam resistance was seen in patients after the 'Great March of Return' Gaza Strip border protests in 2018[50]. Population displacement and global movement allows rapid spreading of resistant strains in distant regions worldwide, ultimately leading to a rise in AMR[51–54]. For example, multidrug-resistant *Mycobacterium tuberculosis* was transmitted from an infectious passenger to other closely-seated individuals during a long-haul flight[55]. Altogether, anthropogenic activities have a significant impact on the evolution of bacterial resistance and its transmission, and has exacerbated the AMR crisis in numerous ways.

1.1.3 Bacterial mechanisms of resistance

Despite human input accelerating AMR, microorganisms themselves possess features that allow them to naturally develop and/or acquire resistance. As previously mentioned, AMR refers to the evolution of microorganisms to become drug-resistant, which often involves the acquisition of new genetic material from external sources, known as extrinsic or acquired resistance. However, this is not always the case: resistance can also be intrinsic, where the microorganism's wild-type genes and natural characteristics confer resistance, or even adaptive, where temporary resistance is expressed in response to specific environmental stimuli[56,57]. Understanding the mechanisms by which resistance is mediated is vital for research addressing rising AMR. In this thesis, I will be focussing on bacteria and bacterial AMR.

Bacteria are single-celled prokaryotic microorganisms that are ubiquitous in the environment – they make up the majority of microorganisms with estimates of 5×10^{30} living bacteria on the planet at any one time[58]. Even though they are typically only a few microns in size, they have very complex and organised structures (as shown in **Figure 3**): the cell cytoplasm is surrounded by a phospholipid plasma membrane with integral membrane proteins, and a peptidoglycan cell wall, made of glycan strands cross-linked via short peptide chains[59,60]. The cytoplasm contains genetic material (chromosomal and plasmid DNA, not within a nucleus), as well as organelles, such as

ribosomes and vesicles. They come in various shapes, for example rod-shaped bacilli and spherical cocci, and often exist in aggregates, such as pairs or chains. Some bacteria also have several surface structures, including flagella, pili, and capsules[60].

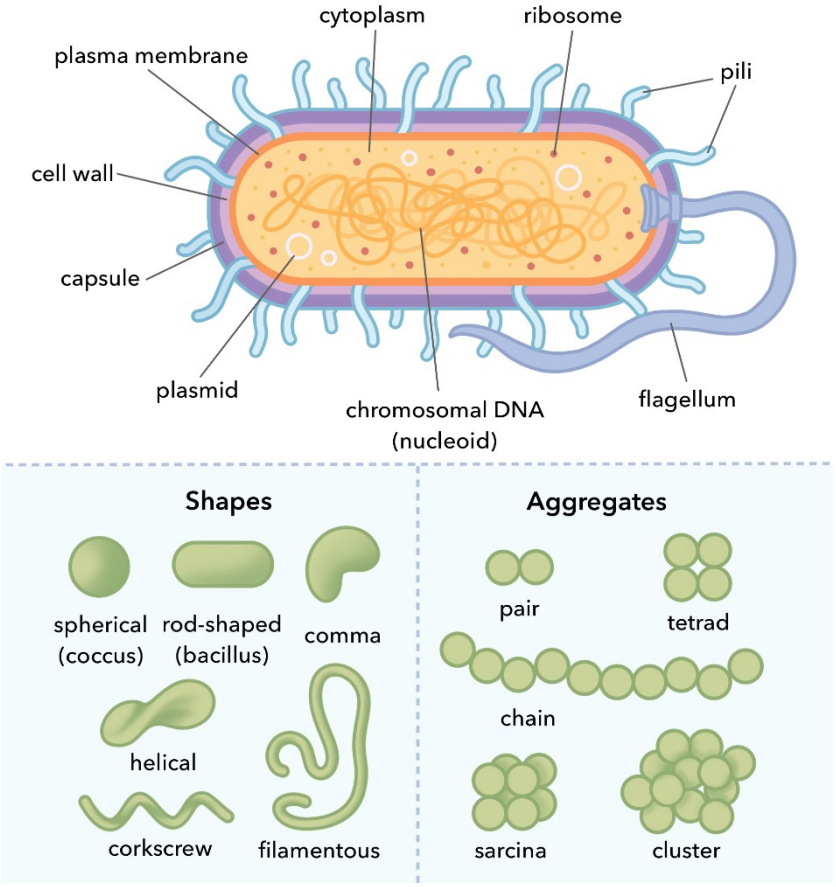


Figure 3 | General structure of a bacterial cell. Common cell shapes and aggregate structures are also shown.

There are two main groups of bacteria, Gram-positive and Gram-negative, defined by the bacterium's ability to retain Gram stain, corresponding to the structural differences present in the cell envelopes of the two classes (**Figure 4**)[61]. Gram-positive bacteria cell envelopes consist of a plasma membrane below a thick peptidoglycan layer (30-100 nm) that is exposed to the external environment[61]. This layer has added teichoic and lipoteichoic acid polymers threaded through to aid with cation-sequestering as well as anchoring the cell wall to the plasma membrane[60,61]. Gram-negative bacteria, on the other hand, have a thin peptidoglycan layer (a few nanometres) between the inner plasma membrane and a second outer membrane (OM), with the area between the two

membranes forming the periplasmic space. This space houses proteins involved in envelope biogenesis, chemotaxis, and degrading toxins, among others[62]. Due to the lack of an outer membrane in Gram-positive bacteria, it is debated whether a small periplasmic space is present between the plasma membrane and cell wall. It is suggested that because of the functional importance the periplasm has in Gram-negative bacteria, it is likely that there is a similar structure present in Gram-positive bacteria to compartmentalise proteins involved in cell wall synthesis, as well as balance osmotic and turgor pressure conditions for the cell[63].

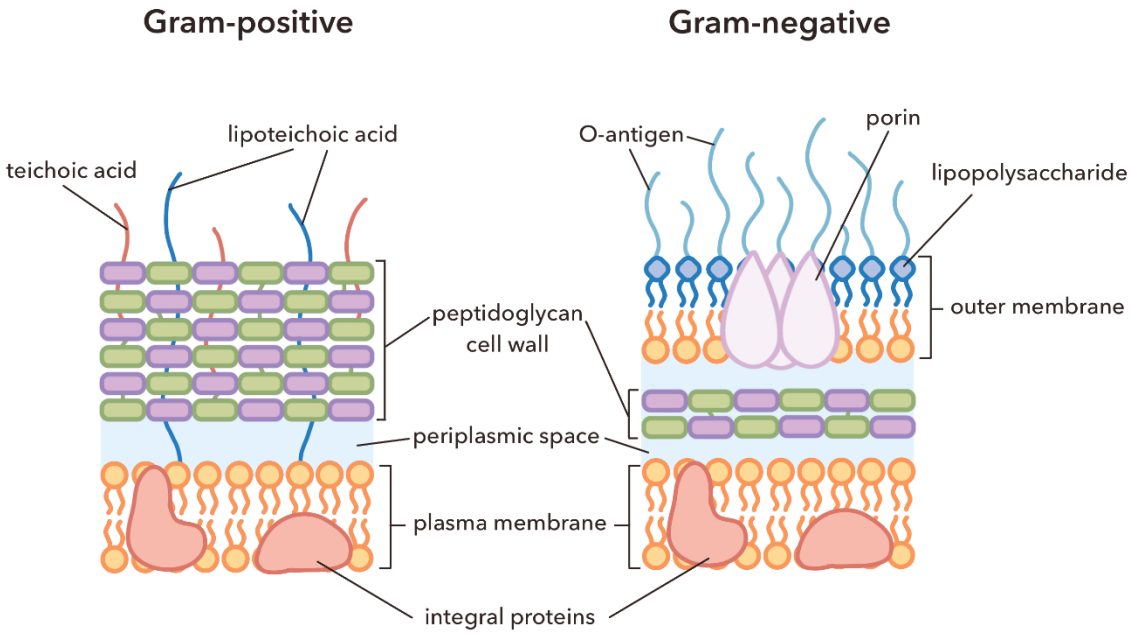


Figure 4 | Structural differences in the cell envelopes of Gram-positive and Gram-negative bacteria. Gram-positive bacteria have a thicker cell wall above their inner membrane, whereas Gram-negative bacteria tend to have thinner cell walls and an additional outer membrane. This outer membrane contains lipopolysaccharides and porins that contribute to modulation of membrane permeability. Adapted from Atanasova (2010)[64].

The OM of Gram-negative bacteria is one of its distinguishing features, composed mainly of the glycolipid lipopolysaccharide (LPS). The densely-packed LPS is crucial for barrier function and controls membrane permeability: the hydrophobic acyl chains decrease hydrophilic molecule entry and the hydrophilic O-antigen side chains reduce permeability to hydrophobic molecules[61,65]. This is one example of bacterial intrinsic resistance with passage of many antibiotic classes being inhibited by the presence of full-length LPS on the OM in the first instance, such as glycopeptides,

macrolides and rifamycins[66]. The OM also contains water-filled channels called porins that allow uptake of hydrophilic molecules up to around 600 daltons in molecular weight[67]. As antibiotics tend to be above this range, they are typically excluded from entering bacterial cells in this way, highlighting porins as another intrinsic resistance mechanism[68]. Porins were commonly considered permanently open channels, however, studies have shown that their conductivity can be quickly modulated in response to changes in transmembrane voltage, pH and polyamine abundance[69–71]. This demonstrates adaptive resistance, where specific conditions can temporarily promote a physiological state that favours drug-resistance.

Efflux pumps are another intrinsic resistance mechanism that are present in both Gram-positive and Gram-negative bacteria[72]. They typically span the (inner) plasma membrane and are able to actively pump unchanged antibiotics out of the cytoplasm, reducing their intracellular concentration, but there are some with OM portions that allow for pumping of toxins out of the cell, across the two membranes of Gram-negative bacteria[73,74]. Many of these efflux pumps can transport a wide range of substrates, and, as such, confer multi-drug resistance to bacteria. This is of particular concern as all of the WHO priority pathogens express efflux pumps that facilitate AMR[72,75]. Additionally, efflux pump expression can be upregulated in response to antibiotic exposure—another example of how bacteria can adapt their resistance based on external stimuli[57,74].

Genetic mutations in bacteria have a frequency between 10^{-5} and 10^{-9}, and specifically for AMR-related mutations have a frequency of 10^{-8}-10^{-9}, which contributes to the spontaneous evolution of intrinsic resistance mechanisms[76]. These mutations can then be transmitted via vertical gene transmission (VGT) to eventually produce resistant populations. Aside from structural features and membrane permeability modulation, there are several other primary mechanisms that confer resistance and are naturally found in some bacteria, some of which may have come about as a result of spontaneous mutation[77,78]. These primary cellular mechanisms include enzymatic

inactivation of antibiotics; alteration, modification or protection of target binding sites; and utilising bypasses in metabolic pathways (**Figure 5**)[56,79].

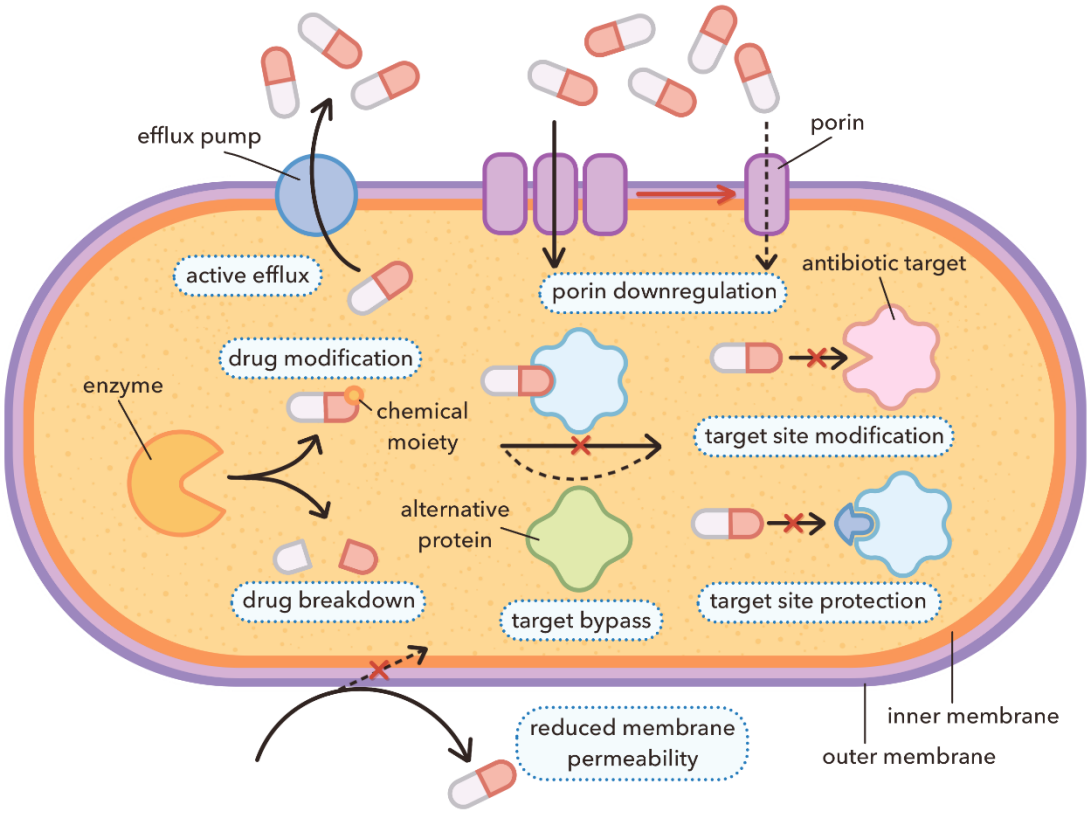


Figure 5 | Mechanisms of bacterial resistance to antibiotics. Bacteria are able to control membrane permeability by modulating efflux pump activity and regulating porin expression. Some bacteria also possess an outer membrane that confers intrinsic resistance to some antibiotics that are excluded from the intracellular environment by this barrier. Antibiotics can be directly targeted via bacterial enzymes that can break down or chemically modify antibiotics. Target proteins can have modified or protected target sites preventing antibiotic binding. Target proteins can also be bypassed completely through use of other proteins as part of alternative metabolic pathways that have the same capacity as the target protein. Adapted from Darby *et al.* (2023)[79].

Enzymatic inactivation

There are a series of enzymes that have evolved to inactivate antibiotics, either through direct breakdown or chemical modification. With over 12,000 entries currently in the Beta-Lactamase Database (BLDB), β-lactamases are the most common inactivating enzymes that evolved alongside β-lactams' clinical introduction[80]. They work by hydrolysing amide and ester bonds in the β-lactam ring found in all β-lactam antibiotics, such as penicillins and monobactams. This makes them unable to covalently bond to and inhibit the activity of penicillin-binding proteins (PBPs) involved

in peptidoglycan cross-linking and cell wall formation[81]. The emergence of extended-spectrum β-lactamases (ESBLs) heightened concerns as resistance to whole classes of antibiotics—penicillins, third-generation cephalosporins, and even non-β-lactams like fluoroquinolones and aminoglycosides—became more commonplace[56]. This led to increased use of carbapenems, widely used as potent last-line broad-spectrum antibiotics, which has ultimately resulted in the evolution of carbapenem-hydrolysing carbapenemases[82,83].

In addition to hydrolysis, antibiotics can be inactivated via transferral of chemical groups. For example, exposed hydroxyl or amino groups found in aminoglycosides can be modified by transfer of an acetyl, phosphoryl or nucleotidyl group by bacterial enzymes[84]. This prevents aminoglycoside hydrogen-bonding with the 16S ribosomal RNA (rRNA) of the 30S ribosomal subunit, an interaction that would otherwise inhibit bacterial protein synthesis[85]. Aminoglycoside-modifying enzymes have been identified in many priority Gram-positive and Gram-negative strains, including *Staphylococcus aureus* and *Pseudomonas aeruginosa*[86,87]. With acetylation being heavily involved in regulating bacterial motility and metabolism, the evolution of antibiotic-inactivating acetyltransferases is not surprising; it is a common resistance mechanism observed against fluoroquinolones and chloramphenicol[88–90].

Target modification

To inhibit the activity of antibiotics, it is not necessary for the antibiotic itself to be altered; the target protein could be the one modified instead. Random point mutations in or chemical modifications to the target binding sites can reduce the affinity of the antibiotic for its target, reducing the drug's efficacy[56]. For example, four amino acid insertions in PBP3 targeted by the β-lactam aztreonam has been found to confer resistance to aztreonam and avibactam[91]. Methylation of bacterial 23S rRNA by the methyltransferase encoded by the *cfr* gene found in *S. aureus* and *Escherichia coli* were observed to confer resistance to phenicols, lincosamides and oxazolidinones[92]. Bacteria are also able to protect the target site by expressing target mimics to bind the antibiotic,

reducing the effective concentration of the antibiotic, or expressing drug mimics that prevent antibiotic binding and subsequent target inactivation. These methods have been identified as the basis for fluoroquinolone and tetracycline resistance in *M. tuberculosis* and *E. coli*, respectively[93,94].

Target bypass

In addition to modifying the target itself, there is also the option for bacteria to bypass the target altogether in the metabolic pathway to evade interaction with antibiotics. Replacement of PBPs is one common example of this: for example, *Staphylococcus spp.* can express an alternative PBP from its *mecA* gene, PBP2a, that has reduced β-lactam affinity, conferring a high level of resistance to methicillin[95]. In another example, vancomycin-resistant enterococci (VRE) are able to substitute the terminal amino acids of the peptidoglycan chain via the *van* genes, reducing the hydrogen-bonding interaction of vancomycin, making the cell wall synthesis process resistant to inhibition[96].

Bacteria have countless mechanisms through which they manifest resistance to antibiotics—the methods described above are representative but are by no means comprehensive. Altogether, structural features, modulating membrane permeability, enzymatic inactivation of drugs, target site alteration, and target bypass already make a robust toolkit to diminish the effectiveness of administered antibiotics.

Gene transfer

All bacteria possess a selection of intrinsic resistance mechanisms, with many of these encoded on extrachromosomal mobile genetic elements (MGEs), such as plasmids, transposons and integrons[97,98]. Plasmids are circular pieces of DNA that can be up to hundreds of kilobase pairs in size, distinct from the larger chromosomal bacterial DNA that goes up to several thousand of kilobase pairs[99,100]. Although chromosomal DNA holds most of the resistance genes found in bacteria, plasmids contain a much higher proportion of AMR genes and the ability of plasmids to self-replicate and transfer readily makes them perfect vehicles for AMR[101,102]. Transposons are small pieces of DNA, present on both plasmids and chromosomal DNA, that encode enzymes

that facilitate the 'jumping' of inserted sequences from one DNA molecule to another to increase gene variation. An integron is a type of transposon that uses site-specific recombination to capture whole genes in 'gene cassettes', allowing for the rearrangement of bacterial genomes[103,104]. The mobile nature of these elements allows resistance genes to be rapidly transferred intracellularly between different pieces of DNA, but also intercellularly with other bacteria. Intercellular genetic mobility is the basis of extrinsic or acquired resistance, where bacteria acquire resistance genes from external sources via horizontal gene transfer (HGT) and is, arguably, the most important driver for the swift and widespread transmission of AMR[105].

HGT occurs through three main routes: conjugation, transformation, and transduction (**Figure 6**)[106]. Conjugation, sometimes referred to as 'bacterial "sex"', is one of the most crucial routes of HGT contributing to the rise of AMR in healthcare settings[107]. It requires direct physical contact between bacterial cells via conjugative pili, essentially establishing a small cargo tunnel for efficient transferral of MGEs between a broad range of bacterial hosts[108,109]. For example, $bla_{CTM\text{-}X}$ ESBL genes found in *Enterobacteriaceae* are known to have been widely spread across different bacterial species via conjugative plasmids[110]. Transformation involves uptake of exogenous DNA (passively released from dying bacteria or actively released during the growth cycle) from the environment and subsequent incorporation into the host bacterial genome, forming mosaic genes. This method not only requires a source of naked genetic material, but also competent bacteria that are able to successfully take up and integrate exogenous DNA into their own without it being degraded by nucleases. For clinically relevant species, this ability is not as prolific as conjugation[56,107]. *Streptococcus pneumoniae* was the first naturally transformable species discovered, known to have mosaic genes encoding penicillin resistance[111,112]. Lastly, transduction occurs when bacteriophages (viruses that infect bacteria) facilitate the transferal of DNA packaged from a donor bacterium to a recipient cell during infection. The transferred DNA could be a combination of both viral and bacterial DNA, which is then integrated into the recipient genome and used to package more DNA into new phage particles, ready for transfer to another recipient[56]. In this way, bacteriophages can

mediate the transfer of resistance genes between bacterial cells. For example, the *bla*$_{SHV-2}$ ESBL gene has been reported to be carried by bacteriophages that infect *E. coli*[113]. As bacteriophages tend to have high host-specificity, transduction normally happens in an intraspecies manner; however, bacteriophages that are capable of interspecies transduction have been documented[114]. There are other 'non-canonical' HGT mechanisms suggested in the literature: sharing of genetic material via membrane vesicles, using intercellular 'nanotubes' (distinct from pili), and some bacteria producing phage-like particles called gene transfer agents[115–117].

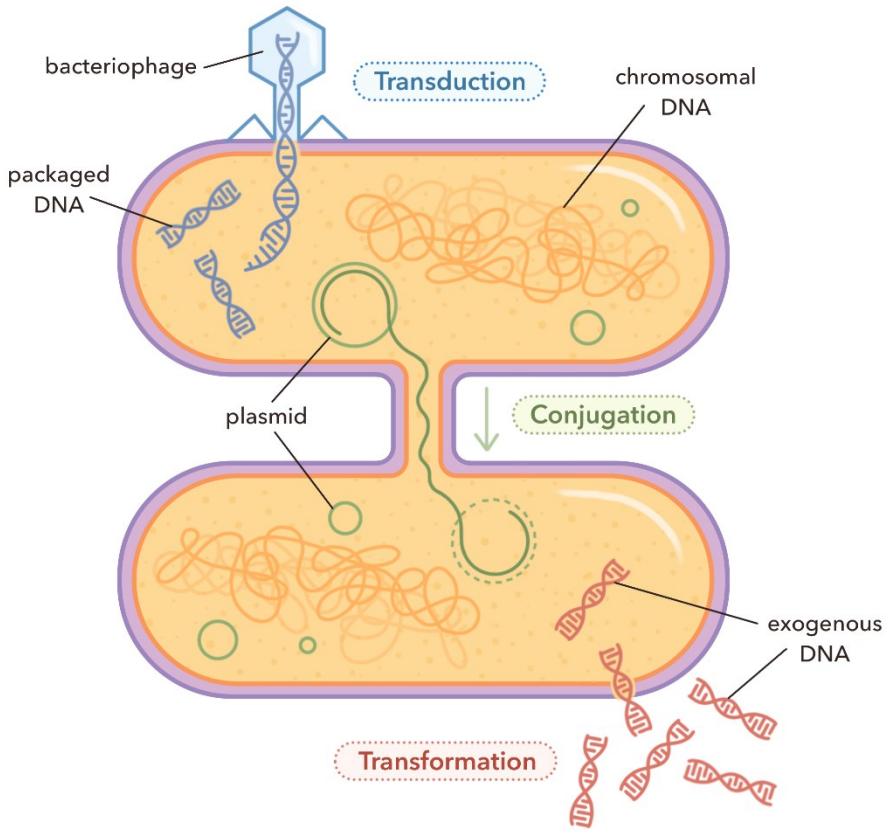


Figure 6 | Canonical routes of horizontal gene transfer. Bacteriophages can inject genetic material—packaged DNA can be both viral and bacterial—into an infected bacterial cell (transduction). Cell-to-cell contact via conjugative pili can be used to directly transfer mobile genetic elements, such as plasmids, between cells (conjugation). Some bacteria can acquire genetic material by picking up exogenous DNA released from other bacterial cells (transformation).

1.2 Biofilm and Resistance

1.2.1 Biofilm formation

On a cellular level, bacteria are able to adopt many mechanisms that contribute to the development of AMR and, unfortunately, many of these traits have been selected for by the increased use of antibiotics worldwide[109]. The accumulation of these mutations and resistance genes over time have allowed many species of bacteria to become multi-drug resistant (MDR), extensively drug resistant (XDR), or even pan-drug resistant (PDR), categories used to describe the varying degrees of AMR[118,119]. However, these cellular mechanisms are not the full story; bacteria are not only able to acquire resistance on an individual level, but they are also able to respond to their surroundings and facilitate AMR as a highly organised population, known as biofilm.

Bacterial biofilm is a heterogeneous 3D aggregation of bacterial cells attached to a surface and embedded in an extracellular matrix (ECM) of self-secreted extracellular polymeric substances (EPS)[120]. These structures are able to persist on both biotic and abiotic surfaces, such as human tissues and medical devices, but also as intercellularly-attached 'free-floating' aggregates, with between 40 and 80% of all bacterial cells having the capacity to form biofilm[121,122]. Biofilm formation is facilitated by intercellular communication via quorum sensing (QS), a cell-density based cell-to-cell communication system that involves secretion of a signalling compound (autoinducer). QS was first discovered in the marine photobacterium, *Vibrio fischeri*, that colonises the light organs of the bob-tail squid in a symbiotic relationship. It was observed that when there was a high cell density of *V. fischeri*, there were also increased autoinducer concentrations and once a critical threshold was reached, bioluminescence occurred. At lower cell densities, with reduced autoinducer concentrations, bioluminescence was inactive[123,124]. In general, QS functions when autoinducer concentrations reach a threshold and trigger the upregulation of specific genes via intracellular receptor binding[125]. Using *V. fischeri* as an example, its luminescence QS system involves the *lux* operon that encodes several proteins and luminescence enzymes—LuxI, LuxR and LuxCDABE. LuxI synthesises an autoinducer that binds to and activates transcriptional

activator LuxR. LuxR can then activate the transcription of the *lux* operon itself. This increases the amount of LuxI present and, in turn, autoinducer and activated LuxR, thereby creating a positive feedback loop resulting in population density-regulated bioluminescence[126]. Biofilm formation can be facilitated by systems similar to the *lux* system in many pathogenic bacteria, such as *P. aeruginosa*, *S. aureus* and *E. coli*, where the activated genes tend to be ones involved in EPS production and secretion, adhesion, cell motility and virulence[127]. As biofilm formation is metabolically expensive, particularly matrix production, it would make sense for bacteria to move towards biofilm form only when there are enough bacterial cells in the vicinity to establish an effective biofilm[128]. In this way, QS was shown to be a system that allows cell-density-based population changes within bacterial biofilms in a coordinated manner.

There are several steps in the biofilm life cycle (**Figure 7**). Firstly, planktonic (free-swimming) bacterial cells need to adhere irreversibly to a surface (or intercellularly to other bacterial cells) and accumulate. Attachment can be facilitated via bacterial extensions, i.e. pili, and/or a combination of physical forces, including hydrophobic, electrostatic and steric forces. Initially, this attachment is reversible but as the forces increase in magnitude, attachment becomes irreversible[129]. As the cells aggregate and form microcolonies, they use QS to stimulate the production of nutrient-rich EPS, containing proteins, nucleic acids, and carbohydrates. These substances are secreted to form the ECM that enhances attachment and further cell aggregation to promote biofilm development. Biofilm-related genes, including stress pathways and virulence factors, are upregulated and eventually progress into a mature biofilm, complete with an increased cell density and thickness, nutrient gradients, and metabolic heterogeneity. After a stable biofilm is formed, programmed dispersal of cells occurs as a result of biofilm overgrowth or to prevent overgrowth, or perhaps both. In a mature or overgrown biofilm, there is a buildup of toxic byproducts and scarcity of nutrients and oxygen, prompting an increase in cell dispersal. During this stage, EPS degradation pathways and planktonic lifestyle genes are upregulated, while EPS synthesis and adhesion genes

are downregulated[130]. The resulting matrix breakdown releases planktonic and highly virulent bacterial cells into the surrounding environment, where they can colonise new areas[120,129].

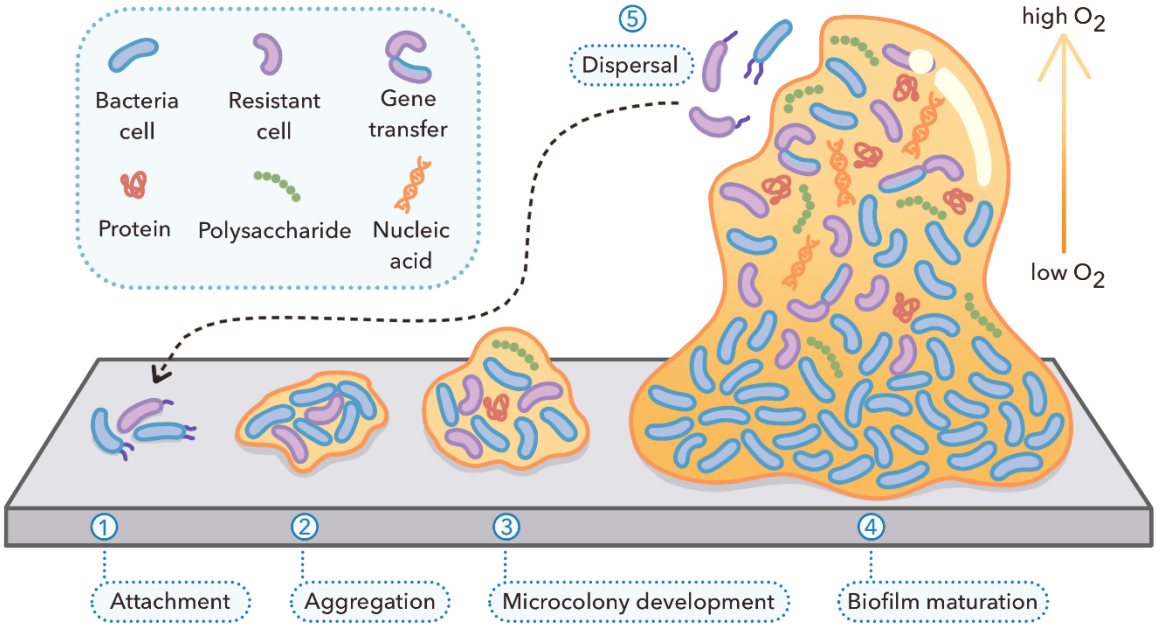


Figure 7 | Biofilm life cycle and constituents. Initial attachment, aggregation of cells, and microcolony development followed by maturation of the biofilm structure as EPS is produced. Biofilm contains bacterial cells along with nutrients such as proteins, nucleic acids and oxygen embedded in a polysaccharide matrix. Resources are not evenly distributed throughout this matrix, with more nutrients being more abundant towards the surface, leaving dormant and more susceptible cells buried towards the bottom of the structure. After a stable biofilm is formed, programmed dispersal of cells occurs–the released cells can form biofilm elsewhere.

1.2.2 Biofilm structure and function

The EPS matrix makes up most of the biofilm mass, accounting for up to 80% of the total volume[125]. It consists of polysaccharides, proteins, extracellular DNA (eDNA), lipids and metal ions that are secreted as a result of QS pathway activation. Biofilm is an aqueous environment, with around 97% of the matrix being water, and the solubility of many of these polymeric substances contribute to their function[120]. For example, dissolved polysaccharides increase biofilm viscosity due to their large molecular mass and give the characteristic stickiness of the matrix. This allows for efficient embedding of bacteria and scaffolding of other polymeric substances in the biofilm[131]. Proteins found in the biofilm can be secretory or membrane-associated, contributing to matrix stability or adherence and aggregation. In *P. aeruginosa*, LecA and LecB lectins are proteins

necessary for biofilm formation on stainless steel and glass surfaces[132]. The presence of eDNA is also vital for biofilm formation: in a structural capacity, it associates with bacterial membranes to promote adherence to surfaces, and as genetic material, it contributes to AMR via HGT between cells[133]. It has also been reported that eDNA impedes the movement of cationic antibiotics through the biofilm with its anionic properties, and also chelates Mg^{2+} ions that leads to a downstream increase in resistance[134].

Historically, and as the name would suggest, it was thought that biofilms were homogeneous flat structures. However, experimental probing into biofilm architecture is a developing field, with more and more evidence demonstrating the heterogeneity and structural complexity of biofilm across different species[135]. For example, confocal laser scanning microscopy (CLSM) has shown that biofilms can vary in thickness, volume, coverage area and roughness: *E. coli* forms small aggregates that cluster together to give a rough biofilm, *Enterococcus faecalis* forms dense, compact and level biofilm, and *P. aeruginosa* biofilms contain mushroom-shaped structures that give widely varying thickness[136]. Of these, the mushroom-like structures of *P. aeruginosa* serve as the primary biofilm model, due to the microorganism's clinical relevance and the distinctive architecture observable in experimental conditions[137]. The mushroom-shaped structures are characterised by narrow stalks and wide upper surfaces, that allow for the existence of pores and channels within the broader biofilm structure. This means that nutrients and water are still able to flow freely throughout this network of channels, despite the high viscosity of the EPS matrix[120,135]. These channels also help to compartmentalise microcolonies and help to establish physiological gradients important for mature biofilm, contributing to the heterogeneity observed[138].

Within biofilms, heterogeneity not only refers to the co-existence of multiple species that may be present within the same biofilm, but can also refer to the various physical and metabolic states that these cells are in, even within a monospecies biofilm. Within the hypoxic base layer, most of the cells are immobile, being dead or metabolically inactive with low transcriptional activity and

nutrient consumption[139]. Towards the surface, where more oxygen is available, the cells are metabolically active and more likely to be in a planktonic state, ready for dispersion[140]. In between these two layers, is an environment where cells attuned for metabolism in oxygen-poor environments are found, upregulating pathways that utilise carbon sources instead, such as lactate, for energy generation[139,141]. These differences in physiological state can also form a sort of feedback loop between metabolism and structure. For example, in low-O_2 environments, matrix production is upregulated, resulting in a higher surface area-to-volume ratio and, ultimately, increased O_2 availability[139]. Altogether, the physical structure and chemical gradients found in biofilms complement each other; population compartmentalisation via structural features allows for differential metabolic and genetic states within the same environment, which in turn contributes to the structure and function of the biofilm.

There are several reasons why biofilm is the predominant state that biofilm-producing bacteria adopt in natural growth conditions[142–144]. Firstly, biofilm allows bacteria to physically stay within favourable conditions, such as within the human body, namely via surface proteins and secreted EPS. This prevents the bacteria from being easily uprooted by shear forces and taken away from a nutrient-rich environment[143]. Secondly, multicellular coordination and the 'division of labour' within biofilms means bacteria with different requirements and metabolic states are able to grow effectively together[139,145]. The physicochemical environment within the biofilm itself is one that promotes bacterial survival: the structural features, nutrient gradients and QS support a self-regulating and dynamic system able to adapt to the needs of a heterogeneous bacterial population. Thirdly, the defensive properties of biofilms protect bacteria from adverse external biochemical changes, such as changes in oxygen levels, pH and osmotic pressure, as well as the host immune system and antibiotics, providing additional antibiotic resistance mechanisms (**Figure 8**)[146].

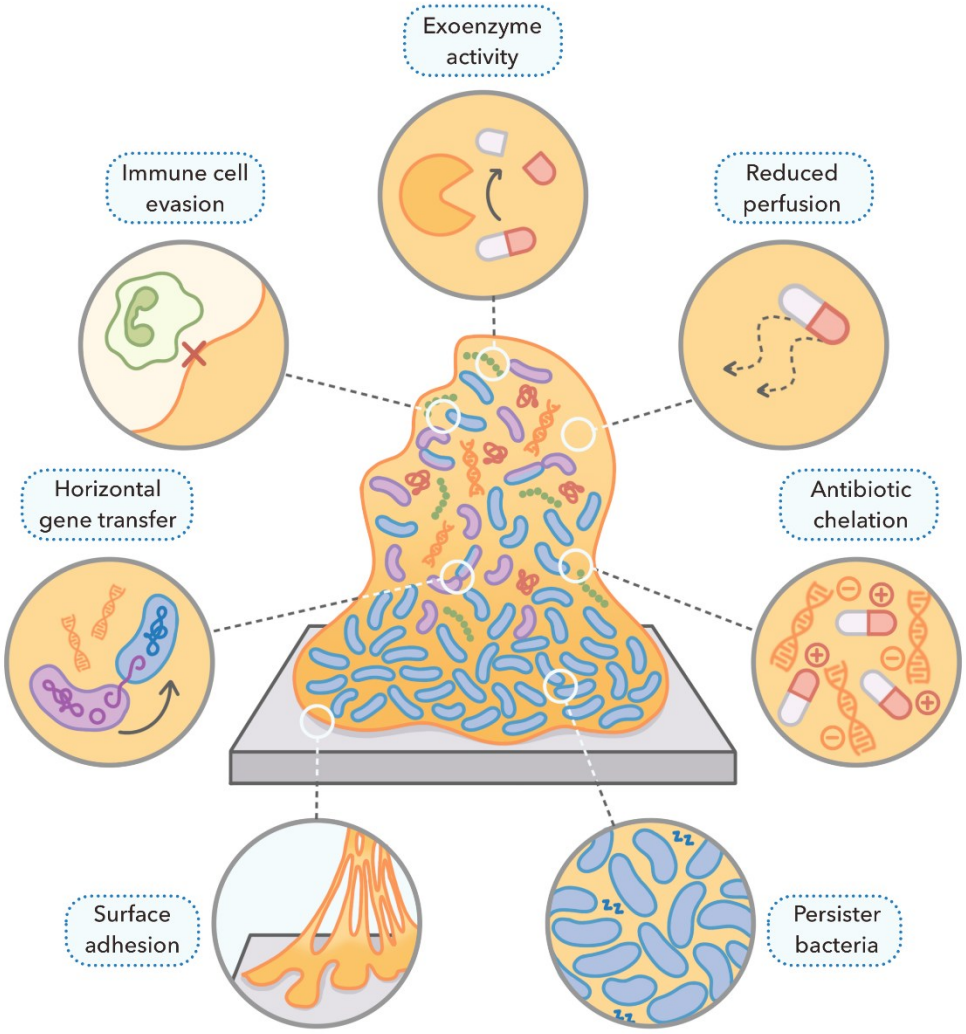


Figure 8 | Resistance mechanisms facilitated by biofilm formation. Within a biofilm, bacteria are embedded in an EPS matrix which attenuates antibiotic permeation and inhibits immune cell entry. This slows down penetration allowing for bacterial exoenzymes to modify and inactivate antibiotics, and for negatively-charged extracellular DNA to chelate cationic antibiotics. Biofilms also provide a suitable environment for increased horizontal gene transfer where resistance genes can be shared. Adhesion proteins upregulated via quorum sensing systems mean that these bacterial communities can effectively attach to a variety of surfaces, resisting being washed away from a colonised surface. Biochemical gradients give rise to metabolic heterogeneity that encourages the existence of persister subpopulations that are typically metabolically dormant and more tolerant to antibiotics.

As one might expect, HGT is enhanced within biofilm structures with metabolically active bacterial cells and eDNA being within close proximity and at high densities; there is an increased frequency of HGT in biofilms compared to planktonic bacteria, and, as such, more spreading of resistance genes[147,148]. It has also been proposed that HGT is, in fact, essential for cohesion and equilibrium within mono- and multi-species biofilms to create a stable system that supports the heterogeneous

population[149]. High cell densities mean that conjugation can happen more readily in biofilms and increased eDNA availability increases the likelihood of successful bacterial transformation. As previously mentioned, eDNA within the biofilm matrix is incredibly versatile: in addition to carrying resistance genes to be shared via HGT, it contributes to the structural integrity and adherent properties of the biofilm, and the negative charge allows for cation chelation facilitating antibiotic resistance[150,151].

The EPS matrix not only provides a good platform for eDNA retention, but is also an effective diffusion barrier, slowing and reducing the penetration of the immune system and antibiotics. The high viscosity of the matrix makes it difficult for macromolecules and immune system components to diffuse through to resident bacteria and its negatively-charged constituents contribute to the sequestering of positively-charged antibiotics, likely through electrostatic interactions[152]. Small molecule antibiotics that are able to penetrate the matrix often do so at a reduced speed, which is particularly problematic if the antibiotic is modified by exoenzymes associated with the matrix before it reaches the target bacteria. An example of this is the slow penetration and subsequent degradation of the β-lactam, imipenem, by β-lactamases expressed in *P. aeruginosa* biofilms[153].

The metabolic heterogeneity of bacteria within the biofilm also has a role to play: reduced metabolic activity and growth rate in the deeper layers of the biofilm means that antibiotics that are mostly effective on rapidly growing cells have minimal effect. For example, tobramycin inhibits protein synthesis and ciprofloxacin inhibits DNA replication, with both being able to penetrate *P. aeruginosa* biofilms. However, it was reported that cells deep in the biofilm were able to tolerate tobramycin and ciprofloxacin treatment, likely because of reduced oxygen levels triggering a state of reduced metabolic activity and, hence, reduced DNA replication and protein synthesis[154]. These dormant cells are typically more tolerant of antibiotics in this way and form the basis of 'persister cells' that are able to survive treatment and subsequently proliferate to re-establish the biofilm once antibiotic availability is low. This persister subpopulation often upregulates stress responses

as a result of nutrient scarcity and antibiotic exposure, ultimately making them slow-growing, metabolically-dormant, and tolerant to a wide range of antibiotics[138,155]. Because of this, persister cells are a major cause of chronic, recurring infections and can lead to consequential treatment failure[156].

Biofilm is evidently advantageous to bacterial communities but it is a double-edged sword in the context of human health; biofilm formation plays a beneficial defensive role for humans (i.e. microbiomes in the gastrointestinal tract), but it also significantly contributes to pathogenic AMR fuelling the global health crisis. Increased HGT, reduced antibiotic penetration, increased antibiotic tolerance and infection persistence are some of the ways in which biofilm formation contributes to AMR and the growing clinical concern.

1.2.3 Implications in modern medicine

With up to 80% of all bacterial species being able to form biofilm, it is unsurprising that biofilms are implicated in an estimated 80% of human infections and 65% of nosocomial (hospital-acquired) infections[121,157,158]. This is of particular concern considering that biofilms can be 10-1000 times more resistant to antibiotics than their planktonic counterparts, majorly contributing to public health concerns[158]. The combination of resistance mechanisms previously described in sections **1.1.3** and **1.2.2** explains how this can be the case and this increased resistance highlights why a focus on targeting biofilm structures, in addition to individual bacterial cells, is crucial in modern medicine. As biofilms can form on both biotic and abiotic surfaces, they can be found directly on human tissue, such as teeth and lungs, as well as associated with medical devices, such as catheters and implants[144,159]. There are several examples of how biofilm formation in human infection, often by opportunistic bacteria, progresses disease and worsens patient prognosis, some of which will be discussed below.

Cystic fibrosis (CF) is a genetic condition that causes the buildup of thick, sticky mucus primarily in the lungs and digestive system, that would ordinarily be cleared. The progressive damage to

these organs makes this condition life-limiting. The mucus of the CF airway is prime for bacterial aggregation and biofilm formation, resulting in chronic cycles of inflammation and infection characteristic of CF. Biofilm-forming *P. aeruginosa* is the leading cause of morbidity and mortality in CF patients; more than 80% of patients with CF have chronic pulmonary infection with *P. aeruginosa* that later results in respiratory failure[160]. Although these patients frequently use antibiotics, because of the nature of the biofilm and CF environment, the local concentrations of these antibiotics vary, leading to subinhibitory concentrations that increase bacterial virulence and persistence[161].

The CF airway is not the only space that holds favourable conditions for biofilm formation; the moist, necrotic and hypoxic environment of chronic wounds promotes bacterial attachment and aggregation, with up to 60% of chronic wounds having some form of biofilm growth[162]. Chronic wounds are formed when a wound does not heal as normal, taking longer than 4 weeks even with treatment—a trend seen in increasingly elderly patients with underlying complications[163]. These chronic wounds typically fall into the category of diabetic ulcers, venous ulcers and pressure sores, and can progress to a stage requiring amputation to prevent loss of life or limb. Biofilm formation was found to be a major driver of chronicity, with *S. aureus* and *P. aeruginosa* being the most prevalent species[164]. Due to the physiology of chronic wounds, bacterial populations are able to aggregate in deeper layers of skin and persist even after the use of harsh debridement methods[165]. Biofilm presence may also stimulate a continued immune response, contributing to chronic inflammation, which in turn exacerbates wound pathophysiology[164].

Infective endocarditis (IE) is a rare, life-threatening condition where pathogenic bacteria, largely *Streptococcus*, *Staphylococcus* and *Enterococcus*, colonise the inner lining of the heart[166]. Bacteria that have entered the bloodstream are able to attach and grow biofilms on damaged heart valves or even prosthetic implants, incorporating fibrin and platelets from the extracellular environment[167]. These biofilms, as expected, have decreased antibiotic penetration but also cause leaky valves and

continuous bloodstream infection, which manifests as recurrent fever and fatigue, among other symptoms[168,169]. Again, persister cells are able to evade antibiotic activity to re-establish biofilm and induce dispersal, potentially leading to embolization, with detached biofilm blocking blood vessels elsewhere[169]. In the case of implanted valves, the foreign biomaterial used additionally induces an immune response that dampens the overall antibacterial activity of the immune system, augmenting bacterial immune evasion[170].

Aside from cardiac implants, there are other medical devices that are significantly impacted by biofilm growth. One such example is catheters frequently used in the urinary tract. Urinary tract infections (UTIs) are the most common type of bacterial infection with uropathogenic *E. coli* (UPEC) being the most common causative agent. Although there are many non-catheter-associated cases, attachment of bacteria to the catheter surface and subsequent biofilm development in UTIs make up 40% of hospital-acquired infections and 80% of hospital-acquired UTIs[171,172]. Like cardiovascular implants, catheters are foreign bodies that trigger the immune system. Part of this response is to produce fibrinogen, which aids with tissue injury but also provides beneficial properties for bacterial adhesion and aggregation that later develops into a catheter-associated biofilm[172,173]. Because the insertion of urinary catheters, usually during hospital visits, breaches natural barriers, urinary pathogens can migrate and colonise the bladder[171]. Here, biofilm formation is responsible for increased pathogenic retention amidst urine flow, providing a reservoir for bacterial release to other areas and urinary obstruction. For patients, this leads to urinary urgency and frequency, and lower back and abdominal pain. It also plays a role in the recurrence of infection becoming chronic UTIs[172].

The global market for implantable biomaterials is rapidly expanding with better access to advanced healthcare and innovation of suitable materials[174]. With increasing use of medical devices and clinical equipment in modern medicine, device-associated infections are also on the rise[175,176]. Elevated medical device usage can be attributed to the worldwide ageing population, who are more

prone to injury and other age-related conditions, such as osteoporosis and diabetes[177]. This means more surgeries and implants, such as prosthetic joints in replacement surgery. *Staphylococcus* and *Enterococcus* species are commonly found to infect prosthetic joints, where biofilms attach to the bone, prosthetic and surrounding tissue leading to pain, swelling and implant loosening[178]. The viscous synovial joint fluid, containing fibrinogen, albumin and other proteins, facilitates biofilm aggregation on and around the implant[179,180]. Increased antibiotic resistance in periprosthetic joint infections increases the frequency of recurrence and leaves implant replacement as the main viable treatment option, despite the risk of reintroducing an infection. Many elderly patients also have poly-morbidities that can become more complicated to treat with the involvement of biofilm infections, particular those that are multi-drug resistant. Furthermore, poor quality of life in younger demographics, in the form of poor diets and increased accidents, also contributes to the growing demand for implanted biomaterials and risky surgeries[174].

With biofilm-associated infections posing such a widespread threat to public health, it is clearly important to target biofilm structures, as well as individual bacterial cells, for effective clearance of infection long-term. Not only would biofilm dispersal enable access to deeper biofilm layers and the bacteria therein, but could also (re)sensitise the released bacterial cells to antibiotic[181]. Thus, specifically targeting biofilm in infection has major advantages. Depending on the infected tissue, patient health and the stage of the biofilm formation, treatment options vary[144,182]. Antibiotics are naturally the first port of call for many bacterial infection treatment plans, but to avoid promoting AMR they are now often used in combination therapies which typically include two or three different antibiotics[183]. Combinatorial antibiotic treatments tend to target more than one bacterial cell type, making them harder to circumvent with resistance mechanisms, leading to synergistic effects. For example, co-trimoxazole is a combination of trimethoprim and sulfamethoxazole clinically used for UTIs. These two antibiotics both work to inhibit bacterial DNA synthesis by disrupting folic acid synthesis but have different target proteins at two different stages of the pathway; trimethoprim binds to dihydrofolate reductase and sulfamethoxazole binds to

dihydropteroate synthetase (**Figure 9**)[184]. There are more and more studies underway trying new combinations that restore or enhance efficacy of existing antibiotics, particularly with increased anti-biofilm effects[183]. Colistin is a cationic antibiotic that interacts with LPS in the place of magnesium and calcium ions, disrupting the bacterial outer membrane[185]. As a last-resort antibiotic, this drug is of particular use in hospital intensive care units against multi-drug-resistant Gram-negative infections, including *P. aeruginosa* and carbapenem-resistant *Klebsiella pneumoniae*. However, reports of rising catheter-associated colistin-resistant *K. pneumoniae* strains brings the current efficacy of colistin into question[186,187]. Recent studies combining colistin with EDTA (a metal chelator that destabilises the EPS matrix) have demonstrated that synergy between the two can restore antibacterial effects as well as enhance anti-biofilm activity[188,189].

While antibiotic combinations show promise, it is important to practice therapies that are not heavily reliant on antibiotic use in order to take tolerant biofilms, spreading AMR and drug combination restrictions into account[190]. For oral biofilms and chronic wounds, irrigation and mechanical debridement using water jets are commonly used to physically clear biofilm. This is normally followed by a course of prophylactic antibiotics and antiseptics to prevent biofilm regrowth, but often fails, likely due to recalcitrant persister cells[191]. For chronic wounds, surgical debridement to cut out unhealthy tissue is considered the gold standard but for patients unable or unwilling to undergo surgery, other options like biological debridement can also be used, where larva is used to eat away at the wound debris[192]. For some implants and periprosthetic infections, complete implant removal and/or replacement is the only viable option to reduce the bacterial load, but even then the risk of recurrence remains[193]. Implants are often manufactured with anti-adhesive and/or bactericidal coatings, such as hyaluronic acid, polyethylene glycol (PEG) chains, and chitosan, to prevent bacterial attachment and aggregation in an effort to prolong the longevity of the implant[194]. Prophylactic vaccines are a relatively new clinical treatment used for some types of bacterial infections. For example, Uromune® is a vaccine for recurrent UTI patients that uses

inactivated bacterial cells to stimulate the host immune system, with a UTI-free rate of up to 58%[195]. However, it has been documented that the protective effect of the vaccine reduces over time, suggesting that repeated administration and/or complementary therapies may be necessary[196,197].

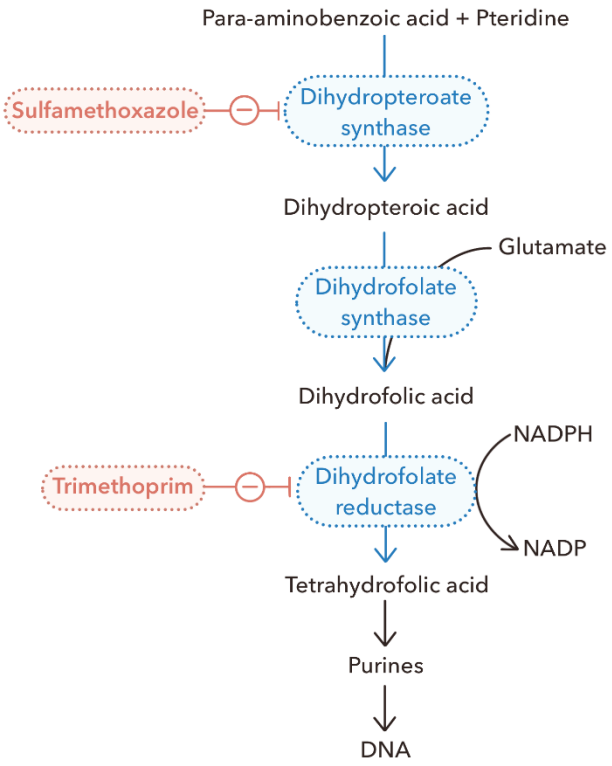


Figure 9 | Co-trimoxazole (trimethoprim/sulfamethoxazole) mechanism of action. Sulfamethoxazole inhibits dihydropteroate synthase, preventing dihydropteroic acid production. Trimethoprim inhibits dihydrofolate reductase, preventing tertrahydrofolic acid production. Together, this combination prevents downstream synthesis of DNA by targeting two different enzymes in this pathway.

Fortunately, in recent years, there has been more research into novel anti-biofilm techniques, including nanoparticles (NPs), antimicrobial peptides (AMPs), photodynamic therapy (PDT) and phage therapy. NPs are nano-sized drug carriers that are typically 100 nm or smaller and can be made from a variety of materials, such as metals, lipids, or polymers, conferring different properties[198]. They are of particular interest in anti-biofilm research due to their ability to increase antibiotic stability and biofilm permeability, reduce off-target effects, as well as be targeted to and degrade bacterial structures[199,200]. The small size of NPs also lends itself well to biofilm penetration, which can be further enhanced through surface modifications. The components of the NP itself,

as well as its cargo, can also play a role in biofilm penetration, matrix degradation and QS inhibition[201]. For example, silver NPs can show antibacterial and anti-biofilm activity through the production of reactive oxygen species (ROS) and downregulation of QS-regulated genes[202,203]. AMPs are largely cationic oligopeptides made of up to 50 amino acids and can be naturally derived or synthetically developed, with some showing anti-biofilm activity via a variety of mechanisms[204,205]. For example, AMPs can neutralise LPS as their amphipathic nature allows for electrostatic interaction with LPS and insertion into the lipid bilayer, ultimately destabilising bacterial membranes[206]. The Cec4 peptide has been demonstrated to reduce *Acinetobacter baumannii* biofilm adherence through membrane disruption[207]. QS systems can also be disrupted by AMPs to have an effect on biofilm development: the human-derived AMP, LL-37, was able to interfere with two QS systems and promote a planktonic lifestyle in *P. aeruginosa*, reducing biofilm development[208]. The 1018 peptide was also found to prevent intracellular accumulation of a stress response signal, (p)ppGpp, and inhibit *P. aeruginosa* biofilm growth[209]. The biofilm matrix is another important target for AMPs as its degradation compromises biofilm integrity and promotes dispersal. FLIP7 from medicinal maggots is an AMP that degrades the matrix of and kills *A. baumannii*, *S. aureus* and *E. coli* strains[210]. Furthermore, AMPs can modulate host immune cell activity; IP-1 was shown to induce autophagy in macrophages infected with *M. tuberculosis*, restricting infection progression[211]. AMPs can also be incorporated into NPs to protect, target and enhance delivery to biofilm[212]. PDT is a low patient-risk therapy that involves the production of ROS by a photosensitizer exposed to light in the presence of oxygen. These generated ROS can lead to the accumulation of oxidative damage in bacteria, ultimately killing those cells[213]. They have been shown to have anti-adhesive and anti-biofilm effects, and can also be combined with NPs to increase stability and efficacy[214]. Bacteriophages are valuable biological platforms to be engineered as an anti-biofilm treatment due to their natural targeting to bacterial strains as well as their ability to penetrate and disperse biofilms[215]. Multiple phages can be combined into a 'cocktail' to increase the range of targeted bacterial receptors as they tend to be very species-specific[216]. Phages are also

often combined with antibiotics to give a synergistic effect as well as avoid the emergence of phage resistance; interestingly, upregulated phage resistance can sensitise bacteria to antibiotics, potentially by forcing bacteria to choose between resistance pathways[217–219]. With the aim of specifically targeting the EPS matrix, microbial enzymes are also proving to be an effective tool to breakdown EPS components and degrade the biofilm matrix[220]. Degrading enzymes, such as proteases and deoxyribonucleases, can cleave substrates integral to biofilm matrix structure and function, including eDNA, proteins and polysaccharides. These enzymes are naturally secreted by microorganisms and can be isolated for use as an anti-biofilm agent[221]. For example, α-amylase (isolated from seawater samples or animal sources) is a glycoside hydrolase that breaks down polysaccharides within the EPS matrix and has been shown to have effective biofilm dispersal activity[222,223].

The ubiquity of bacteria and biofilms in the environment make it unsurprising that biofilms are having a significant impact on modern human medicine. In the era of an increasing ageing population and widespread access to advanced healthcare, it is imperative to stay diligent and keep up with bacterial evolution and AMR. Currently, most of the approved clinical treatments of biofilm-associated infections involve direct antibiotic use and/or physical removal. In order to stay ahead of the AMR curve, combining and developing more types of therapies with a focus on biofilm elements is beneficial; as discussed, researchers have already started exploring options specific to biofilm permeation, matrix degradation, and QS inhibition. Although there are many promising anti-biofilm methods currently being researched pre-clinically, extensive tests are necessary to dispel any safety, *in vivo* efficacy and cost concerns for clinical use.

1.3 Bacteria in Urinary Tract Infections (UTIs)

1.3.1 Types and causes

Urinary tract infections (UTIs) are the second most common type of infection, widespread in both healthcare and community settings[224]. UTIs affected more than 400 million individuals worldwide, and caused around 230,000 deaths in 2019[225]. Within two years, the number of affected individuals increased to almost 450 million, with over 300,000 deaths globally[226]. In the UK, around 1.8 million admissions to hospital involved UTIs between 2018 and 2023 and treatment of UTIs on the whole cost the NHS over £600 million in 2023, demonstrating the immense healthcare and economic burden UTIs currently pose[227,228].

UTI is a broad term that refers to several types of infections that can occur at different points within the urinary tract. The urinary tract is made up of the kidneys, ureters, bladder, and urethra, and is overall important for the filtering of waste products out of the blood to produce urine that is then excreted—essentially, the body's drainage system. The kidney regulates water and electrolytes in the blood through filtration and reabsorption; the ureters transport this urine through to the bladder where it is stored temporarily until it passes out of the system via the urethra[229]. A healthy urinary tract has natural defences against bacterial colonisation: urethral sphincters to keep the urinary tract closed, urothelium that lines the urinary tract forming a protective mucosal barrier, immune system recruitment via the urothelium, as well as the unidirectional flow of urine preventing bacteria from moving up the tract[230,231]. If these barriers are breached, e.g. by catheter insertion, uropathogens typically found in the gastrointestinal tract can migrate and colonise the urethra (urethritis) and bladder (cystitis) of the lower urinary tract and the ureters (ureteritis) and kidneys (pyelonephritis) of the upper urinary tract (**Figure 10**)[232].

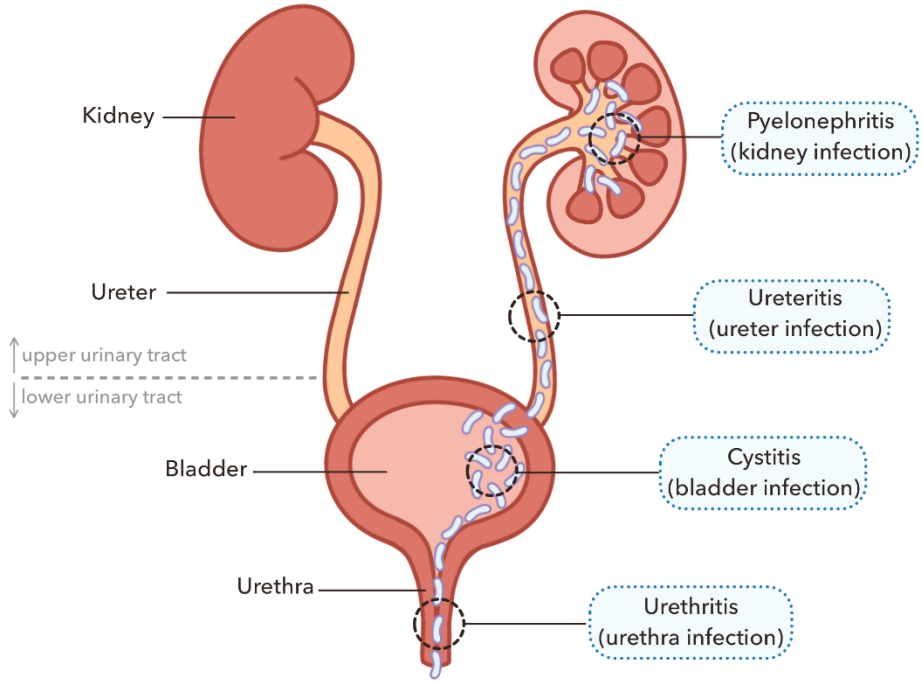


Figure 10 | Diagram of the urinary tract and corresponding infections. The urinary tract contains the kidneys and ureters in the upper urinary tract, and the bladder and urethra in the lower urinary tract. The term 'urinary tract infection' refers to the collection of infections that can affect different parts of this system.

In the current clinical landscape, UTIs are split into uncomplicated and complicated UTIs (uUTIs and cUTIs, respectively), although there have been recent calls for a more standardised classification[233]. uUTIs refer to infections of healthy individuals with no urinary tract abnormalities, whereas cUTIs occur when there are underlying conditions or structural abnormalities that complicate the infection, such as renal failure, catheterisation, and pregnancy[234]. Due to anatomical differences between men and women, UTIs affect women significantly more; over a woman's lifetime, there is a 60% chance of being affected by at least one UTI, with around 11% of women affected by at least one UTI every year, whereas men account for 20% of all UTIs[235,236]. UTIs can also be described by their occurrence, either primary or recurrent, where primary refers to a first-time isolated infection and recurrent describes two or more infections within six months or three or more infections within a year[232]. Unfortunately, recurrent UTIs are particularly common for women, with 26% reporting a recurrence six months after initial treatment and 36-53% of women reporting a recurrence within a year[237,238]. They can be caused by a relapse with the same bacterial

strain or reinfection with a new bacterial strain, but it is often due to persister bacteria re-establishing infection soon after treatment[239,240]. A shorter urethra, changing hormone levels particularly during pregnancy, sexual activity, and disturbances to vaginal microflora all contribute to the increased UTI risk in women[241]. Age-related conditions, such as increased catheterisation, menopause and prostate enlargement, are also contributing factors to UTIs in both men and women: 15% of hospitalisations for over-65s are due to UTIs, making up 56% of UTI admissions[224,227,242]. Typical lower UTI symptoms include increased urinary frequency and urgency, abdominal pain, and a burning sensation or bleeding during urination. For upper UTIs, there may be symptoms of fever, nausea and lower back pain, sometimes in addition to lower UTI symptoms. However, UTIs can also be asymptomatic with elevated bacterial presence in urine ($>10^5$ colony forming units/mL) but no symptoms shown[243].

Uropathogenic *E. coli* (UPEC) is the predominant bacterial species that causes UTIs, implicated in 65-75% of all UTIs[235]. Although most *E. coli* strains are present in the human gastrointestinal tract as part of the commensal flora, UPEC makes up part of the extraintestinal pathogenic *E. coli* (ExPEC) group that started as commensal organisms but evolved to become virulent[244]. UTI pathogenesis starts with bacterial contamination of the vaginal and periurethral areas, with these uropathogens normally found in the gastrointestinal tract. Despite the numerous natural barriers of the urinary tract, UPEC strains possess various virulence factors and tactics that facilitate migration into and colonisation of the urinary tract via the urethra and bladder. For example, expression of flagella, type 1 fimbriae and secreted adhesins are vital for the invasion and attachment to urothelial cells[234]. The type 1 fimbriae, containing FimH adhesins at the tip, are bacterial appendages responsible for inducing cytoskeletal rearrangement in the attached host cell, leading to subsequent internalisation of the bacterial cell. If these bacterial cells are unable to be ejected through exocytosis triggered by bacterial LPS recognition, UPEC is able to persist and rapidly multiply to form intracellular bacterial communities (IBCs). IBCs are biofilm-like in nature and act as reservoirs of UPEC that can go on to invade other cells. UPEC can also form

metabolically-dormant counterparts, known as quiescent intracellular reservoirs (QIRs), that persist in a membrane-associated compartment within the host cell as a source of recurrent infection. Whilst within a host cell, UPEC can evade the active host immune system and is sheltered from antibiotic treatment. Other types of fimbriae expressed by UPEC are essential for ascension up the urinary tract, such as type 2 fimbriae, while others are involved in interactions with receptors specific to the different urinary organs, such as S fimbriae[232]. Many secreted virulence factors have toxic effects, such as apoptosis-inducing cytotoxic necrotising factor 1 (CNF1), pore-forming α-haemolysin (HlyA), and iron-scavenging siderophores[245]. In addition to this, UPEC strains are able to form biofilm within the urinary tract, with a rate of around 84% across all UTIs[246–248]. Once established, bacteria within the biofilm have the advantage of upregulated expression of virulence factors among other resistance mechanisms, some of which are discussed in section **1.2.2**[249–252].

K. pneumonia (6-8%), *Proteus mirabilis* (2%), and *Enterococcus* (5-11%) species are also often cited as common causes of UTIs[224,234,235,243]. *K. pneumonia* and *P. mirabilis* possess specialised fimbriae that enhance attachment and aggregation on catheters and other medical devices, with both species contributing to around 10% of catheter-associated UTIs (CAUTIs)[253]. *P. mirabilis* additionally produces urease that hydrolyses urea, increasing urine pH and leading to the formation of crystalline biofilm in association with calcium crystals and ammonium phosphate precipitates[254]. For *Enterococcus faecalis*-associated CAUTIs, fibrinogen deposition onto the catheter (as a result of inflammation response after catheter insertion into the bladder) is crucial for *E. faecalis* adhesins and pili to attach and facilitate biofilm formation[255]. All of these species are able to form biofilm as polymicrobial communities within the urinary tract that are significant in the progression and persistence of infection[249,256]. As such, it is important to consider these biofilms for effective treatment and management of UTIs.

1.3.2 Current landscape of UTI treatment

Widespread use of amoxicillin as a first-line medication for UTIs in the 1970s induced the development of resistance, prompting a decline in amoxicillin use[257]. Currently, nitrofurantoin (NIF) is the first-line treatment for UTIs internationally as it is one of the few antibiotics that are still effective against most Gram-positive and Gram-negative uropathogens[258,259]. In the UK, a three-day course of twice daily doses of NIF is the recommended treatment option for uUTIs; in other countries, like Switzerland, India and Brazil, a five to seven day course is prescribed[259].

NIF is a member of the nitrofuran class of broad-spectrum antibiotics, containing a furan ring linked to a nitro group (**Figure 11**). Due to its chemical structure and composition, NIF is only slightly water soluble and gives low plasma concentrations, which may explain low tissue penetration and systemic activity[260]. However, with an oral bioavailability of 80%, it is well absorbed in the gastrointestinal tract and rapidly accumulates in urine (200 μg/mL per 100 mg oral dose), where up to 25% is excreted unchanged[258]. This is particularly advantageous in the context of UTIs, where high urinary concentrations means NIF can effectively reach bacteria within the bladder and urinary tract, but also have its activity enhanced by urine acidity[261]. After NIF activation via reduction of the nitro group, the reactive intermediates bind to and disrupt bacterial ribosomes and enzymes, interfering with DNA and cell wall synthesis, as well as other metabolic pathways[258,262]. Likely due to its wide-ranging activity, resistance rates remain low in *E. coli* and *Enterococcus spp.*, species normally found in UTIs[263]. NIF is typically used to treat uncomplicated lower UTIs and frequently used as a prophylactic, with long-term low-doses administered to individuals with chronic and recurrent UTIs[237,264]. Unfortunately, long-term use has been linked to eventual pulmonary toxicity and hepatic injury[264–266]. It has also been reported that sub-lethal concentrations of NIF in some cases does not affect growth rate and can in fact induce stronger biofilm formation, which could partially be contributing to recurrence of infection[267–269]. Therefore, combining other antibiotics or treatment strategies may prove to be beneficial for a more sustained eradication of infection.

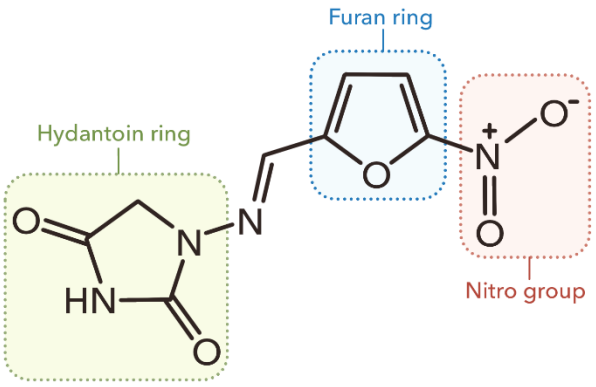


Figure 11 | Chemical structure of nitrofurantoin (NIF). NIF is a synthetic antibiotic consisting of a furan ring linked to a nitro group and a hydantoin side chain.

Combination antibiotics are increasingly used in UTI treatment to target multiple bacterial systems at once, in an effort to avoid promoting AMR. Co-trimoxazole is a relatively old combination of trimethoprim and sulfamethoxazole often used in the treatment and prophylactic management of recurrent UTIs[270,271]. As described in section **1.2.3**, these two antibiotics both work synergistically to inhibit bacterial DNA synthesis by disrupting folic acid synthesis. They do this by targeting proteins at two different stages of the pathway; trimethoprim inhibits dihydrofolate reductase and sulfamethoxazole inhibits dihydropteroate synthetase (**Figure 9**)[184]. Unfortunately, co-trimoxazole use has seen a decline since the rising rate of resistance was observed, particularly in treatments of cUTIs and pyelonephritis[272,273]. Despite the reduced usage frequency, it appears as though resistance levels have not dropped significantly in the past several decades, highlighting the need to diversify the antibiotic arsenal and be vigilant about antimicrobial stewardship[274].

As alternatives to antibiotics, there are several non-antibiotic strategies that are recommended for UTI treatment and management in the face of AMR[275]. Many mild uUTIs actually clear up on their own over time, and some lifestyle adjustments can serve as preventative measures for future infections[276]. For example, drinking plenty of water to encourage more frequent passing of clear urine and flush out bacteria, practicing good genital and sexual hygiene, and avoiding fluids that irritate the bladder, such as alcohol and caffeine[243,277]. Interestingly, cranberry juice is often used by

women as a substance to reduce UTI occurrence. While there is still scepticism about its effectiveness, multiple reviews have found that there is reason to believe that cranberries can truly serve as a natural remedy to UTIs[278,279]. It is thought that a phytonutrient, proanthocyanidins, found in cranberries interferes with bacterial adhesion to urothelial cells, and because adherence is essential for pathogenesis, this reduces the instances and recurrence of UTIs[275]. It is also proposed that the acidic nature of cranberry juice influences urine pH, creating a harsh acidic environment for pathogenic bacteria[243]. This is similar to one of the mechanisms commensal *Lactobacillus spp.* use to prevent uropathogenic colonisation; their secretion of lactic acid and other organic acids has been linked to the inhibition of growth of other bacterial species[280]. In addition to this, lactobacilli are able to co-aggregate with uropathogens and compete for adhesion receptors, produce toxins, such as hydrogen peroxide, that facilitates a killing effect, and modulate the host immune response[275]. These reasons would explain why probiotic consumption is also increasingly explored as a non-antibiotic UTI therapy; boosting *Lactobacillus* levels in women has been shown to be a largely safe and effective preventative measure, although larger trials are needed before these clinical recommendations can be made[281,282].

Immunostimulation via vaccines is also proving to be a capable prophylactic measure for UTIs. Uromune® (MV140) is a vaccine for recurrent UTI patients that uses inactivated uropathogenic bacterial cells to induce a potent host immune response, with a UTI-free rate of up to 58%[195]. Protection is likely enabled through induction of dendritic cells that produce T-helper cells and stimulates antibody secretion, but more studies are required to better understand the mechanism behind MV140's activity[283]. A 2015 study showed that only 9.7% of patients given a three-month course of MV140 saw a return of infection after 12 months, whereas all of those that took a six-month prophylactic course of nitrofurantoin or co-trimoxazole experienced a new UTI episode[284]. UTI vaccines are a relatively new clinical option with increasing exploration into different vaccine components and targets, which are touched on in the next section (**1.3.3**).

In hospital settings, CAUTIs are the most common hospital-acquired infection, making up around 75% of nosocomial infections[285]. Indwelling urinary catheters are extremely common in hospitals—used by up to 25% of adult inpatients—and with an increasing ageing population, this is not likely to decline[286]. CAUTIs may be the most preventable hospital-acquired infection with up to 40% of indwelling catheter use being deemed as unjustified or inappropriate[287,288]. Because CAUTI pathogenesis is enabled by the catheter itself, one of the biggest risk factors associated with infection is the duration of catheterisation. The link between catheterisation duration and UTI risk is well documented: the daily UTI risk with an indwelling catheter is between 3 and 7%, and can be higher for female, geriatric, and other vulnerable patients[289–291]. As such, evidence-based clinical guidelines stipulate limited instances in which catheters should be used, to avoid the inappropriate use of indwelling catheters [292,293]. If they are used, it is recommended that catheters are replaced every four weeks or removed as soon as they are not needed, and when inserted, they are done so using aseptic technique and with a monitoring and maintenance plan in place.

Surface coatings are also implemented during the designing and production of catheters as a measure to reduce potential bacterial colonisation[294,295]. Latex and silicone are the most commonly used materials for urinary catheters, but their large hydrophobic properties make them more suitable for bacterial adhesion and subsequent biofilm formation. Therefore, catheter surfaces are commonly functionalised using antibacterial and antifouling coatings. Antibiotic formulations can be added to inhibit bacterial growth on urinary catheters; for example, coating catheters with a nitrofurazone-silicone matrix was found to effectively inhibit growth of uropathogenic isolates by 75%[296]. Unfortunately, nitrofurazone catheters are associated with more patient pain and discomfort, which highlights the importance of considering patient experience in addition to biological function for coating options[297]. Coated catheters can also act as an antibiotic reservoir: azithromycin and ciprofloxacin-infused silicone catheters had a constant antimicrobial activity over a period of a year, preventing bacterial adherence long-term[298]. It is also common to use metals, such as silver, as a bactericidal coating and many clinical trials have demonstrated the effectiveness

of silver complexes as an antibacterial catheter coating[299–301]. However, there are some studies that show no difference in UTI incidence between silver-coated and non-coated catheters, which calls its efficacy into question[302,303].

Currently, many of the clinically approved treatments for UTIs still depend heavily on antibiotic use, despite the risk of inducing AMR. There has been a move towards exploring immune-modulatory and biomaterial-focused strategies, as well as non-antibiotic recommendations. However, more clinical trials and updated guidelines for these are needed in order to encourage widespread implementation. There is also a need for more approved advanced therapeutics, particularly those expressly targeting biofilm-related structures and pathways.

1.3.3 Future of UTI treatment and management

Fortunately, the UTI research landscape has evolved to additionally explore more options beyond antibiotics. The repertoire of clinical strategies in development for UTIs is rapidly expanding, with increasing research into more biofilm-targeted techniques[304].

One such treatment being increasingly researched for antibacterial and anti-biofilm activity—and is of significance to this project—is nanoparticle-based drug delivery. Nanoparticles are nano-sized drug carriers that are typically 100 nm or smaller and can be made from a variety of materials, such as metals, lipids, or polymers, conferring different properties[198]. In UTI research, nanoparticles are an increasingly popular therapeutic tool for drug delivery because of their versatility; antibiotic encapsulation in or immobilisation on nanoparticles can improve the efficacy of existing antibiotics, or nanoparticles themselves can hold antibacterial properties[201,305]. The size, composition, surface functionalisation capacity and drug carrying ability all contribute to the high potential of nanoparticles as an effective UTI therapy. For example, silver boron nanoparticles were used to inhibit *E. coli* and *S. aureus* biofilms, β-lactam antibiotics were used in combination with zinc oxide nanoparticles to enhance bacterial killing of *E. coli* and *K. pneumoniae*, and ciprofloxacin-loaded albumin nanoparticles had increased antibiotic efficacy when used against *E.*

coli, *E. faecalis*, *S. aureus*, and *P. aeruginosa*[306–308]. Other antibacterial agents, such as AMPs and bacteriophages, can also be combined with nanoparticle technologies to protect, target and enhance delivery to biofilm[212].

As previously described, AMPs are amphipathic oligopeptides made of up to 50 amino acids, with some showing antibacterial and anti-biofilm activity via a variety of mechanisms: membrane destabilisation, bacterial cell signalling interference, matrix degradation, QS disruption and promotion of biofilm dispersion[204,205]. As AMPs are largely secreted from (epithelial) cells that regularly encounter microorganisms, the urinary tract naturally produces many different peptides that can be isolated and built upon for UTI treatment. Human LL-37 is one such AMP—generated from the cleaving of the human cationic antimicrobial protein hCAP18, which is constitutively expressed by the urothelium—that is actively researched for its anti-biofilm and immunomodulatory properties[309]. Not only has LL-37 been shown to inhibit biofilm adherence and growth by preventing curli fimbriae formation in UPEC, but also facilitate the formation of neutrophil extracellular traps involved in bacterial clearance by the innate immune system[310,311].

Bacteriophage therapy involves infecting bacteria with engineered versions of viruses that naturally target specific bacterial strains and receptors. Phages can penetrate and damage the biofilm matrix and use the resident bacteria as phage-replication machines, eventually resulting in bacterial cell lysis[215]. Several clinical studies are underway probing the efficacy and safety of phage therapy as a UTI management strategy[312]. As they are so specific, they are often being tested as 'phage cocktails' where multiple phages with different targets are combined into a single treatment, simplifying preparation and administration[216]. This would be particularly important in the treatment of multispecies biofilms, as demonstrated by the successful use of a phage cocktail on a *P. aeruginosa* and *P. mirabilis* biofilm in an *in vitro* CAUTI model[313]. Phages are also often combined with antibiotics to give a synergistic effect as well as avoid the emergence of phage resistance; for

example, they have been combined with amoxicillin to significantly reduce the bacterial load of *K. pneumoniae* biofilms[314].

Immunotherapy is another rising field that holds promise for enhancing host immune responses to UTIs, e.g. through the development of new vaccines and monoclonal antibody treatments. Most of the clinically tested and approved UTI vaccines contain whole inactivated or heat-killed bacterial cells to stimulate the immune system[275]. New vaccines are now exploring the possibilities beyond inactivated or dead bacterial cells; they can contain bacterial toxins, proteases, and siderophores. ExPEC4V, a vaccine made of four conjugated O-antigens from ExPEC strains, is such an example that has successfully and safely induced antibody production in clinical trials[315,316]. Vaccines can also contain adhesin complexes that stimulate the immune system to target bacterial adhesion components, increasing the likelihood of interfering with bacterial attachment and colonisation[234]. For example, a vaccine (SEQ-400) containing FimH adhesin protein as the antigen is in development, and a clinical study of this vaccine showed host immunity facilitated by the production of FimH-specific antibodies[317]. It is likely that this vaccine enhances host immune activity to prevent bacterial adherence as well as reduce the infection recurrence rate. Monoclonal antibodies against FimH are also being investigated as a prophylactic strategy to protect against UTIs[318]. There are also recent experiments modulating the immune system as a way to reduce the collateral damage done as a result of increased inflammation during UTI pathogenesis[319]. For example, matrix metalloproteases (MMPs) are enzymes used in tissue remodelling and wound healing but are often upregulated during hyper-inflammation and implicated in acute cystitis pathogenesis. Using an MMP inhibitor, such as Batimastat (BB-94), in an acute cystitis model led to reduced bacterial counts and showed therapeutic effects, highlighting selective immune dampening as a viable therapeutic approach[320].

Another interesting approach for UTI treatment that is emerging—and is of interest to this project, along with nanoparticles—is therapeutic ultrasound. This technique is discussed in depth in

section **1.5** but, briefly, it involves the use of ultrasonic energy to induce the volumetric oscillation (cavitation) of gas-filled microparticles, known as microbubbles. The cavitation activity can have a series of physical and biochemical effects on the surrounding medium and in the case of UTIs and biofilm-associated infections, this action can disrupt biofilm structures and increase cell permeability[321,322]. Ultrasound technology can be used in conjunction with other therapies to enhance drug delivery: using ultrasound-activated microbubbles in combination with gentamycin-loaded lipid nanoparticles significantly increased intracellular drug delivery to *E. faecalis* in a human bladder model[323].

Despite antibiotics still being largely used in UTI treatment and management, there are plenty of novel approaches moving away from heavy antibiotic use in the research pipeline. With biofilms being strongly associated with UTIs, it is important that new techniques addressing biofilm formation and growth are developed to make a better effort at reducing recurrence rates. The following sections will further explore nanoparticles, specifically liposomes, and therapeutic ultrasound as anti-biofilm technologies within UTI treatment.

1.4 Liposomes: lipid-based nanoparticles for drug delivery

1.4.1 Nanoparticles for drug delivery: a brief overview

When designing antibacterial formulations, overcoming limitations, such as low bioavailability due to host interaction with the drug, poor targeting or penetration due to AMR, and side effects of toxicity particularly associated with long courses of antibiotics, are of top priority[324]. This has led to expanding research into drug delivery systems that show promise in enhancing therapeutic efficacy and safety. An ideal drug delivery system should be biocompatible, efficiently transport cargo across biological barriers, improve the solubility, stability and circulation time of the cargo, enhance efficacy and reduce toxicity, as well as be a canvas for surface functionalisation[325,326]. Nanoparticles (NPs) have emerged as one such versatile platform for drug delivery, with intrinsic properties that often offer improved pharmacokinetics and therapeutic results over conventional

medicines[198]. NPs are particles between 1 and 100 nm in size in at least one dimension, where their small size and high surface-area-to-volume ratio can facilitate distinct molecular interactions and surface modification options. They can also be made of various materials that influence their physicochemical characteristics and allows for their classification into three main types: carbon-based, inorganic, and organic NPs (**Figure 12**).

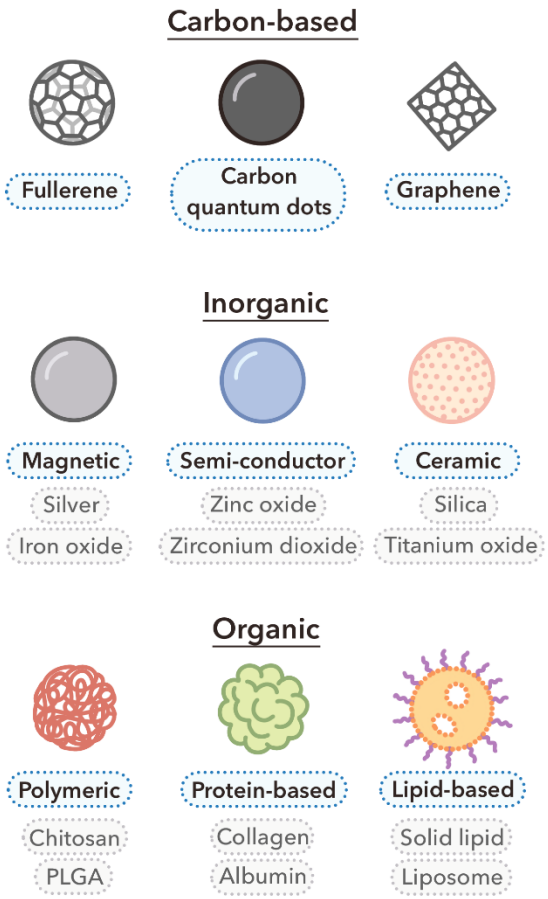


Figure 12 | Examples of nanoparticles used in drug delivery. The three main classes of nanoparticles (carbon-based, inorganic and organic) can be split into multiple subclasses, some of which are highlighted in blue, along with some examples within each subclass (highlighted in grey). PLGA = poly(lactic-co-glycolic acid).

Carbon-based NPs, including fullerenes and carbon quantum dots, are nanostructures made of carbon that come in all shapes and sizes, from single sheets to nanotubes[327]. They are often very small (up to 10 nm) and their chemical stability and structural versatility make them effective for drug delivery. For example, football-shaped fullerenes have a unique morphology that allows for efficient loading with therapeutic agents and also possess physical properties of biocompatibility

and photosensitivity. C_{60} fullerenes have been conjugated with doxorubicin (C_{60}-DOX) in a novel anticancer therapy where ROS generation induced by light exposure contributed to cell death directly, but was also responsible for drug release from the conjugate[328]. Their conductivity and optical properties also make them well-suited for imaging and diagnostic purposes, together presenting carbon-based NPs as a promising theranostic tool.

Inorganic NPs constitute of crystallised salts of inorganic materials, like silver, silica and zinc oxide, forming 3D covalently- or metallically-bonded arrangements that can be engineered into various shapes and sizes[329]. Due to their metallic, ceramic or semi-conducting properties, these NPs are commonly produced for anticancer and antibacterial therapies. For example, metallic silver NPs (AgNPs) have been shown to inhibit cancer cell angiogenesis, as well as bacterial cell replication through the electrostatic interaction of Ag^+ ions with the bacterial cell wall and nucleic acids[330,331]. It is also thought that AgNPs actuate their effect through the steady release of Ag^+ ions that promote the production of ROS, leading to downstream anticancer and antibacterial activity by inducing oxidative stress[332,333]. A similar mechanism has been suggested for semi-conducting zinc oxide NPs (ZnONPs); they have been shown to selectively induce apoptosis in cancerous human myeloblastic leukaemia cells and degrade the wall and membrane of *E. coli* cells[334,335].

Being made of organic molecules, like proteins, lipids, and carbohydrates, organic NPs possess biocompatible and biodegradable qualities, which makes them excellent for use in biomedicine[198,336]. There are several different subtypes, including protein-based, polymeric and lipid-based organic NPs. Protein-based NPs are considered very promising drug delivery vehicles as the constituent proteins are biodegradable and non-antigenic, with extensive capacity for surface modification[337]. Their amphiphilicity also facilitates interactions with hydrophobic molecules and transportation in hydrophilic cellular environments, greatly increasing bioavailability. For example, albumin NPs reversibly bound to hydrophobic paclitaxel have been utilised in anti-cancer therapy for targeting in the aqueous tumour microenvironment, where albumin naturally readily

accumulates[338]. It was also found to reduce hypersensitivity reactions and improve overall patient prognosis—this has been clinically approved for use as Abraxane® since 2005, showcasing the potential of protein-based NPs[339]. Polymeric NPs, derived from either natural or synthetic polymers arranged into a solid matrix, show similar benefits in biocompatibility, biodegradability, and enhanced drug stability and efficacy[340]. For instance, PLGA NPs have also been combined with paclitaxel to enhance cellular internalisation of drug in triple-negative breast cancer cells[341]. Additionally, in antibacterial research, chitosan NPs have been used to enhance the activity of metal ions and biomolecules; loading chitosan NPs with lysozyme has been shown to enhance antibacterial activity against *E. coli*, and hybrid chitosan-alginate NPs increased loaded plant extract stability to result in effective bactericidal activity against methicillin-resistant *S. aureus* (MRSA)[342,343]. The diversity of polymers allows for a variety of structures and functions, as well as favourable interactions with a wide range of medicinal agents, making them a safe and advantageous option for drug delivery.

Lipid-based NPs are one of the most widely used NPs in the current biomedical landscape, particularly due to their stability, versatility, safety and relatively easy and low-cost large-scale production. There are four main lipid components that make up these NPs in different combinations: phospholipids, cholesterol, ionizable lipids, and PEGylated lipids. Each of these have a role to play towards particle stability, drug-loading capacity and cellular internalisation abilities[344]. The high therapeutic potential of lipid-based NPs, paired with commercial scalability, likely explains why they were utilised in groundbreaking COVID-19 mRNA vaccines, BNT162b2 (Comirnaty®) and mRNA-1273 (Spikevax). Encapsulating mRNA within a lipid-based NP protects it from degradation and allows internalisation by host cells, leading to a downstream immune response and subsequent immunisation[345,346]. There are many types of lipid-based NPs that are used for drug and gene delivery, including solid lipid NPs (SLNPs), nanostructured lipid carriers (NLCs) and liposomes. SLNPs consist of a solid lipid core that forms a crystalline structure where drug can be captured, providing good drug stability and robustness during manufacturing

processes[347]. However, this crystalline structure is also responsible for a relatively low drug loading capacity—an issue sought to be addressed through incorporation of liquid lipids along with solid lipids in their core, giving rise to NLCs with better stability and drug loading capacity[348]. Liposomes are also incredibly versatile with a longer history of clinical use compared to SLNPs and NLCs, as the earliest generation of lipid-based NPs[349]. Their established presence in the clinical landscape, pharmaceutical manufacturing and biomedical regulation makes them a sensible foundation for developing novel therapies in drug delivery with the aim of clinical translation. As such, liposomes were chosen as the primary drug delivery system for this project and will be explored in more depth in the rest of this chapter.

1.4.2 Liposomes: types and mechanisms

Liposomes are a small vesicular drug delivery system, typically between 20 and 1000 nm in size, composed of a lipid bilayer surrounding an aqueous core (**Figure 13A**)[349]. Because of this structure, they make excellent carriers of both hydrophilic and hydrophobic drugs, either within the aqueous compartment or the lipid bilayer. Constituent lipids naturally self-assemble in aqueous medium to form spherical lipid nanostructures that can have different sizes and lamellarities (**Figure 13B**). This diversity in liposome structure is largely influenced by the preparation methods, some of which are discussed in section **1.4.3**. Phospholipids, such as phosphatidylethanolamines and phosphatidylcholines, along with cholesterols are common liposome components that also impact the particle's properties, including size, stability, surface charge, membrane fluidity and rigidity, drug loading capacity, and surface modification options[350]. Together, the range of liposome structures and formulations allow for diverse applications within the biomedical, cosmetic and food industries[351–353].

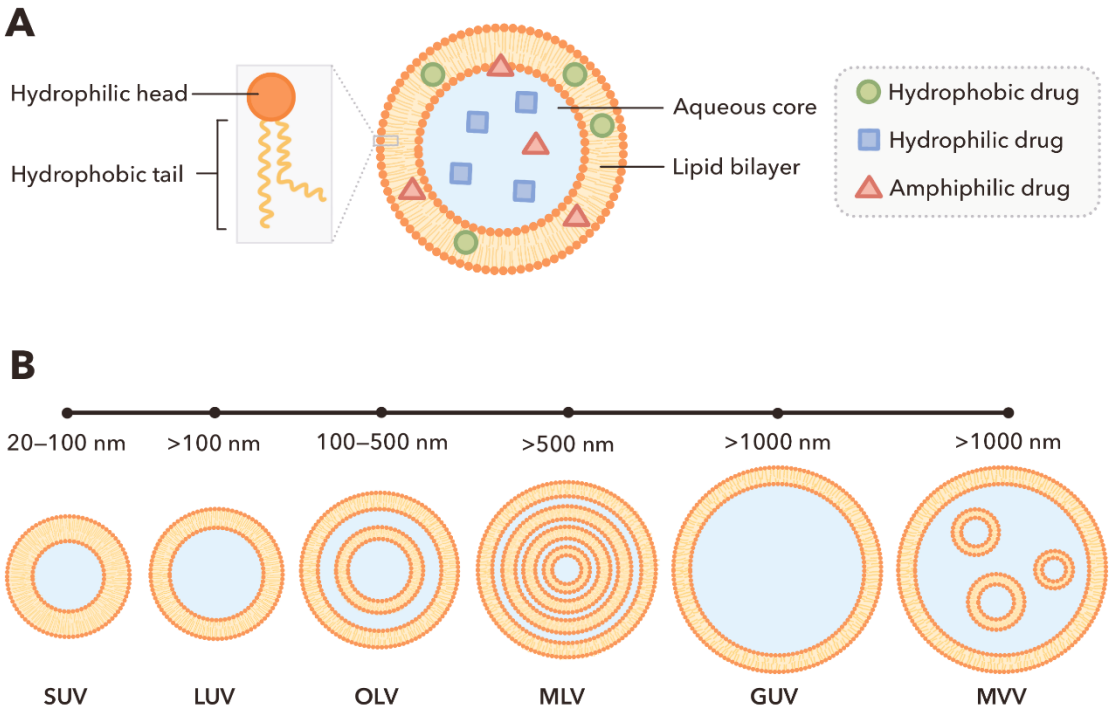


Figure 13 | General liposome structure and classes. (A) Structure of a unilamellar liposome, constituent phospholipid, and drug loading compartments. (B) The 6 different classes of liposomes based on size and lamellarity. SUV = small unilamellar vesicle; LUV = large unilamellar vesicle; OLV = oligolamellar vesicle; MLV = multilamellar vesicle; GUV = giant unilamellar vesicle; MVV = multivesicular vesicle. Most pharmaceutically approved liposomes are between 50 and 300 nm in size[354]. Panel B adapted from Luiz *et al.* (2023)[355].

Since the first approval of liposomal doxorubicin (Doxil®) by the FDA in 1995, liposomes have become widely recognised as excellent drug delivery vehicles in medical practice[351]. There are numerous benefits of liposomal drug encapsulation, including improved stability, targeting and efficacy. The lipid membrane of liposomes provides an effective barrier to exclude loaded drugs from the external environment. It can help to create intravesicular conditions tailored to the loaded drugs, e.g. allowing for an acidic environment to improve stability of pH-sensitive drugs during transport, but also protect the loaded cargo from unsuitable external conditions, e.g. shielding drugs from degradation during processing, storage and by cellular enzymes[356,357]. In this way, bioavailability can be enhanced as larger amounts of active drug are able to circulate. The versatility of the lipid membrane also means that liposomes can be functionalised with disease-specific ligands for selective targeting[358]. This also works to reduce toxicity and off-target effects, as drugs

can accumulate at the relevant target site. Simply encapsulating drugs within a lipid vesicle can greatly improve therapeutic potency and efficacy in these ways.

As previously mentioned, the substituent lipids have a great impact on the properties of liposomal formulations, giving rise to different types of liposomes that offer specific additional benefits. The first-generation of liposomes were made using mostly phospholipids, with or without cholesterol to adjust bilayer fluidity and rigidity. However, their simplicity meant they showed physical instability over time, seen as aggregation, fusion or drug-leakage[359]. Rapid uptake and clearance by the mononuclear phagocytic system (MPS) also led to short blood circulation times[360,361]. In some cases, uptake by macrophages is an intentional result; liposomes have been demonstrated to enhance penetration into macrophages infected by intracellular communities of *M. tuberculosis*[362]. However, in general, rapid MPS clearance is associated with reduced blood circulation times, impairing the function of conventional liposome formulations. Therefore, new lipid compositions and modifications were developed to overcome these limitations. For example, charged liposomes show better physicochemical stability due to the charge providing repulsive forces to reduce particle aggregation and fusion[363,364]. Furthermore, charged liposomes can improve encapsulation of charged cargo; cationic liposomes are commonly used in gene delivery due to electrostatic interactions between the positively-charged liposome and negatively-charged nucleic acid facilitating efficient encapsulation[365]. Their positive charge also likely contributes to increased intracellular uptake via endocytosis. Here, it is thought that cationic liposomes can favourably interact with negatively-charged cell membranes (as well as form a protein corona in physiological conditions) to increase cellular uptake via the endocytic pathway leading to downstream drug release from the endosome (**Figure 14A**)[366–368]. Cationic liposomes have also demonstrated potential for drug delivery beyond the blood-brain-barrier via transcytosis, a mode of transport across a polarised cell involving endocytic components[369]. However, one drawback is that these liposomes can sometimes become entrapped and degraded within the endocytic pathway, rendering encapsulated cargo inactive[370]. Fusogenic liposomes are an (often charged) alternative

that potentially bypass the endocytic pathway by fusing with the target membrane to directly release their cargo, and reducing the risk of subsequent entrapment and degradation (**Figure 14B**)[371–373].

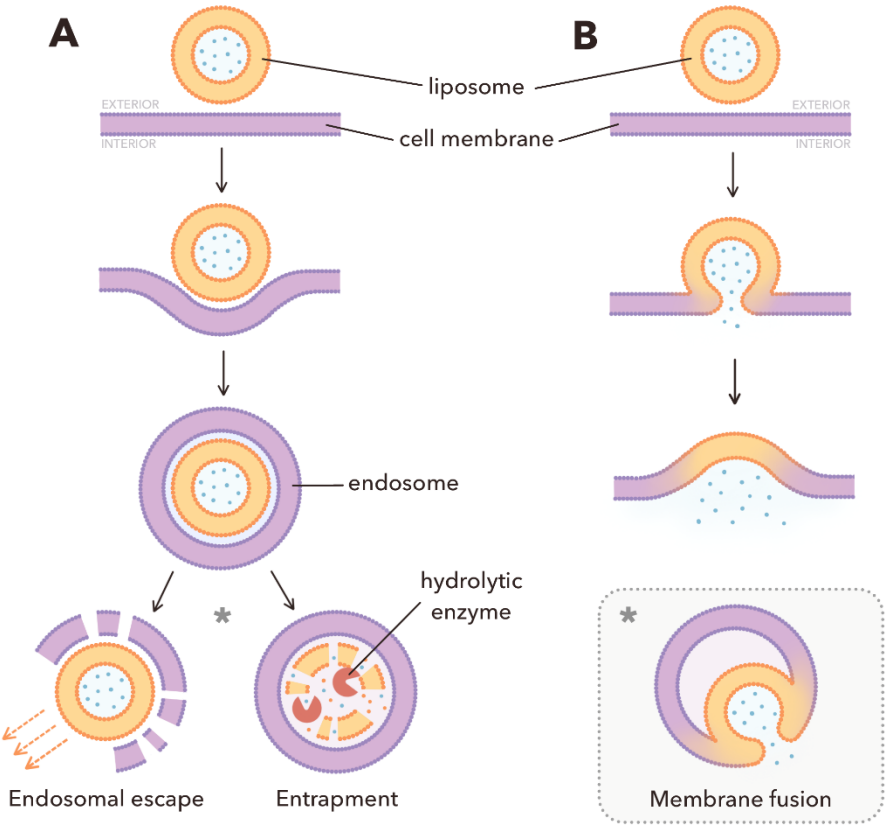


Figure 14 | Potential mechanisms of cellular uptake of cationic and fusogenic liposomes. (A) Possible outcomes of (cationic) liposome uptake via the endocytic pathway–entrapment and subsequent degradation within the endosome or endosomal escape releasing the liposome into the cell. (B) Proposed mechanism of fusogenic liposomes fusing to target membranes and directly releasing cargo without involving the endocytic pathway. (*) Fusogenic liposomes can also potentially be taken up via endocytosis, but their properties may increase the likelihood of cargo release through membrane fusion.

Another option to improve conventional liposome stability and reduce clearance by immune cells is to modify the surface of the liposomes with polymers, most commonly PEG, forming a class of 'stealth stabilised' liposomes. PEG is a neutral, hydrophilic polymer that can provide a steric barrier through surface hydration and acquisition of a protein corona as it interacts with serum proteins, contributing to the 'stealth' effect[374]. The degree of liposome 'stealth stabilisation' through PEGylation is influenced by both the PEG density and PEG chain length; low molecular weights

and densities result in a collapsed 'mushroom' conformation, whereas higher molecular weights and densities result in an extended 'brush' conformation on the liposome surface[375,376]. By incorporating PEGylated lipids—particularly at weights and densities that adopt a 'brush' conformation—into a liposome formulation, a hydrophilic steric barrier is introduced that decreases surface opsonisation, which is a necessary prerequisite for MPS recognition and subsequent clearance, thus improving circulation times[377]. Addition of PEG chains also helps to increase liposome stability by reducing aggregation but this effect diminishes as larger amounts of PEG are incorporated into a liposome membrane[378,379]. Large amounts and/or high molecular weights of PEG can actually also work to obstruct target membrane interactions and block cellular uptake and endosomal escape in what is branded as the 'PEG dilemma'[376,379,380]. Therefore, there's a balance to be struck when modifying liposome surfaces with PEG chains in order to not compromise drug delivery ability for the sake of immune system evasion.

PEG chains are not the only modification that can be made to improve liposome function; disease-specific ligands can be conjugated to liposome surfaces to allow for active targeting. Ordinarily, liposomes can passively target disease sites, such as tumours, through the enhanced permeation and retention (EPR) effect[358]. This is where highly permeable blood vessels within a tumour microenvironment enable small NPs to leak out of the blood and accumulate in tumour tissue. However, this passive targeting does not allow for precise discrimination between healthy and diseased cells, which is why ligand-conjugated liposomes were developed[381]. These ligands, e.g. receptors, antibodies, and hormones, would enable increased receptor-mediated internalisation of liposomes in areas where target biomarkers are present, delivering more drug to the relevant site[382–384]. Therefore, liposomal encapsulation can reduce drug doses and off-target effects through increased internalisation at target sites, rather than depending on enhanced passive accumulation[385].

Liposomes can also be engineered to be responsive to a range of stimuli, releasing drug when specific conditions are met. The stimuli could be specific features of a disease environment, such as the acidic conditions found in biofilms, but could also be external stimuli, such as light, ultrasound or magnetic field exposure as part of treatment[386]. Stimuli-responsive liposomes typically become unstable when exposed to the intended stimuli, triggering drug release. For example, pH-responsive liposomes contain specific lipids, such as 1,2-dioleoyl-sn-glycero-3-phosphoethanolamine (DOPE) and cholesteryl hemisuccinate (CHEMS), whose functional groups become protonated in acidic conditions[358,386]. This biochemical change is linked to conformational changes in the lipid structure, leading to destabilisation of the lipid bilayer and cargo release[387,388]. Zwitterionic liposomes take this one step further: they can reverse their charge depending on whether the external pH is above or below its iso-electric point (the pH at which the liposome has no net charge)[389]. This allows for liposomes that carry a neutral charge at physiological pH and avoid interactions with blood components to become positively-charged at acidic pH and facilitate better interaction with and internalisation at negatively-charged target membranes[390]. Heat and light are also increasingly used stimuli, where drug release can be linked to local temperature increases, e.g. during a fever, or directed by light exposure, e.g. as part of PDT[358,386]. When a liposome is heated above its phase transition temperature, it shifts from a gel-like solid phase to a more permeable liquid phase, triggering drug release[391]. During PDT, UV irradiation of photo-polymerizable lipids, such as $DC_{8,9}PC$ (1,2-bis(tricosa-10,12-diynoyl)-*sn*-glycero-3-phosphocholine), initiates polymerisation within the lipid bilayer and destabilises the membrane structure, leading to drug release at the site of light exposure[392]. In this way, stimuli-responsive liposomes can be used for spatially- and temporally-controlled and sustained release of cargo.

Overall, the versatility of liposomes for drug delivery is demonstrated in the wide range of liposome types that have been documented to date. By modulating lipid composition, surface

additions, and even preparation methods, liposome function can be fine-tuned for different disease contexts.

1.4.3 Liposome manufacturing methods

There are numerous ways in which liposomes can be manufactured that vary in multiple factors, including complexity, time and financial cost, and scalability, making liposome production feasible in many different settings[393]. The method used also influences the physicochemical properties of the resulting liposomes, so this choice needs to be carefully considered during the formulation stage in addition to the lipid composition and drug options. This section will give an overview of some of the key methods used in the manufacturing process, from production to characterisation, to highlight the breadth of techniques available.

1.4.3.1 Production methods

Liposome production typically involves dissolving constituent lipids in an organic solvent that is later removed. When subject to an aqueous environment, these lipids self-assemble into liposomes that can then undergo further downstream processing[394]. Three of the most commonly used methods for the preparation of liposomes are the thin-film hydration method (Bangham method), the ethanol injection method and the reverse-phase evaporation method, which are described below. There are also more recent techniques, such as the microfluidic method and the freeze-drying method, that are extensively reviewed elsewhere[393–396].

Thin-film hydration method (Bangham method)

The thin-film hydration method, also known as the Bangham method, is considered the earliest established method of liposome production since its description by Alec Bangham in 1965[397]. It is a simple protocol that involves dispersing lipids in an organic solvent (e.g. chloroform) and evaporating this solvent to form a thin lipid film[397,398]. This thin film is then hydrated in an aqueous buffer which results in the production of a suspension of MLVs (**Figure 15A**)[395]. Disadvantages of this technique are that the resulting suspension contains liposomes that are heterogeneous in

size and lamellarity and the encapsulation efficiency can be quite low, particularly for hydrophilic drugs, as it relies on passive loading[394]. Fortunately, additional extrusion through polycarbonate membrane filters of a specific size or sonication steps can be used to reduce liposome size and size dispersity, producing more uniform unilamellar liposomes. These steps can also increase encapsulation efficiency, along with other processes, such as freeze-thaw cycles and dialysis[399,400]. With thin-film hydration being relatively simple and straightforward, it is efficient for manufacturing in small batches, as would be the case in most laboratory settings, and can be used on different lipid combinations and concentrations[401]. However, this technique has poor scalability due to the large amounts of organic solvent needed as well as inefficient hydration and mixing at large scales, contributing to batch variability. Additionally, thorough extraction of the organic solvent and liposome size adjustments via extrusion can be time-consuming and difficult. Despite this, this technique is well-documented in the literature and is a popular choice for liposome manufacturing in early formulation stages[394].

Ethanol injection method

Since its first description in the 1970s, ethanol injection has been used as a rapid and reproducible method of liposome production[402]. It involves dissolving lipids in ethanol and rapidly injecting the lipidic solution into a large amount of heated aqueous buffer. As the ethanol is dispersed, small unilamellar liposomes spontaneously form through the fusion of lipid fragments (**Figure 15B**)[403]. Whilst this method does not require downstream extrusion or sonication to produce SUVs, it demands additional solvent removal steps, such as evaporation or dialysis, to get rid of residual ethanol and often gives low liposome concentrations[351]. Due to ethanol's ability to form an azeotrope with water, the solvent extraction process can be quite difficult as they cannot be separated by simple distillation[393]. Diethyl ether is sometimes used as an alternative organic solvent as it is insoluble in an aqueous environment, so allows for direct removal through evaporation (without further removal steps) and forms a more concentrated liposome suspension with

improved encapsulation efficiencies[395]. However, ether is a harmful solvent and residual amounts are not accepted by regulatory bodies[404]. Additionally, cooling effects during ether injection can cause blockages in the injection equipment that contribute to MLV formation[395]. Efficient mixing is required to make sure homogeneous liposomes are produced which may be difficult to attain manually. In combination with microfluidic systems and in-line mixers, this method has been used for very controlled and continuous liposome production at industrial scales[401].

Reverse-phase evaporation method

Reverse-phase evaporation, as a method to produce liposomes, was also introduced in the 1970s as a relatively simple protocol that achieves efficient encapsulation of hydrophilic drugs[405]. In this method, lipids dissolved in organic solvent are mixed with drug dissolved in an aqueous medium to form a water-in-oil emulsion containing inverted micelles (**Figure 15C**)[395]. The solvent is then slowly removed by evaporation to produce a gel-like phase, which eventually collapses, dispersing some of the inverted micelles. Hydration of this gel-like phase allows the excess phospholipids to form a bilayer around the remaining micelles, leading to the formation of LUVs. Although high encapsulation efficiencies can be achieved, this method can be time-consuming and uses large quantities of organic solvent that eventually needs to be removed, making it difficult to scale up[401]. The presence of residual organic solvent is also a concern that adds complexity to the production process. Additionally, the resulting size and distribution cannot be well controlled, which might contribute to reproducibility issues at an industrial scale[394]. Furthermore, not all drug cargo is suitable for this method; while large macromolecular drugs can be loaded, fragile molecules such as DNA and peptides can be disrupted by exposure to organic solvent and periods of sonication needed for emulsification[406]. This highlights how the nature of the loaded drug can place restrictions on the choice of liposome manufacturing method.

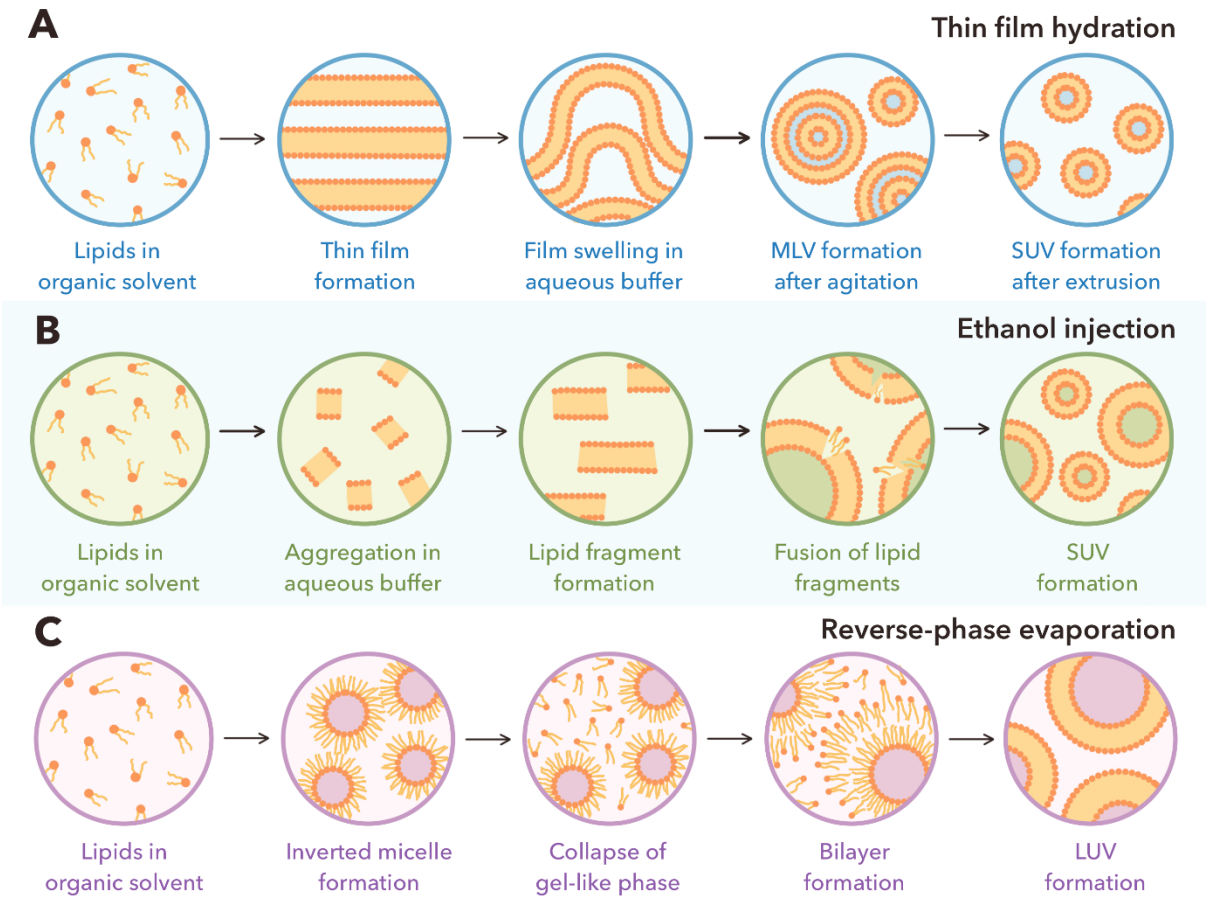


Figure 15 | Schematic representation of lipid organisation during three conventional liposome production methods. (**A**) Thin film hydration (Bangham method). (**B**) Ethanol injection method. (**C**) Reverse-phase evaporation method. MLV = multilamellar vesicle; SUV = small unilamellar vesicle; LUV = large unilamellar vesicle.

1.4.3.2 Drug-loading methods

Even if a manufacturing method gives a relatively low encapsulation efficiency, there are numerous ways in which drugs can be loaded. As hydrophilic drugs partition into the aqueous core, they can either be encapsulated during liposome formation (i.e. passively) or after liposome formation (i.e. actively). Typically, passive drug loading results in lower encapsulation efficiencies but there are some techniques that aim to improve passive drug entrapment. For example, freeze-thaw cycles that involve rounds of rapid freezing (e.g. using liquid nitrogen) followed by a period of thawing were found to increase the amount of entrapped drug to almost 90% compared to 5.8% without[407,408]. This technique is thought to increase drug encapsulation through cryo-concentration, where drug molecules are concentrated into zones upon freezing which increases diffusion into

liposomes as thawing occurs[399]. Since holding liposomes at a sub-zero temperature during the thawing process is thought to be the point at which drug diffusion into liposomes takes place, a variation of freeze-thawing that involved a period of 'annealing' was demonstrated to further increase encapsulation efficiency[399]. For active drug loading of a hydrophilic drug that is an amphipathic weak base, a transmembrane pH gradient, often of ammonium sulphate buffer, can be used to drive drug loading. Where ammonium sulphate concentration is greater than in the surrounding medium, base exchange with ammonium ions facilitates active loading of the drug[409]. This technique has been used to efficiently load doxorubicin into liposomes to a level of up to 98% and is actively used to produce clinical Doxil® formulations[410–412]. Hydrophobic drugs can be directly incorporated into the liposome bilayer during liposome production, e.g. being dissolved with constituent lipids in organic solvent. Alternatively, drug-lipid conjugates can be used as liposome constituents as a loading method for both hydrophilic and hydrophobic drugs.

1.4.3.3 Characterisation methods

After production, particle characterisation is imperative to assess physicochemical properties that contribute to *in vitro* and *in vivo* performance and pharmacokinetics, as well as to meet regulatory standards, such as guidelines stipulated by the FDA[413,414]. Properties including but not limited to size and size distribution, zeta potential, structure and composition, encapsulation efficiency, storage stability and drug release are frequently characterised[414,415].

Size, size distribution and zeta potential

Dynamic light scattering (DLS) is a commonly used technique to measure liposome size, size distribution (polydispersity index) and zeta potential. It is a simple, quick and consistent method, contributing to its popularity in particle characterisation. DLS is most accurate on suspensions with a very narrow size distribution and requires low particle concentrations[416]. The size is normally given as the average diameter with high sensitivity to the presence of aggregates. Size distribution is quantified through a polydispersity index (PDI), where a PDI < 0.1 indicates a very narrow size

distribution and a PDI < 0.3 is generally considered acceptable for nanoparticles involved in drug delivery[417]. Zeta potential describes the surface charge of a nanoparticle that develops between the solid surface of the particle and the surrounding polar medium. Measurements between -30 mV and +30 mV correspond to particles that tend to aggregate and have reduced stability, but this range varies depending on the type of particle[418]. As such zeta potential is used to predict colloidal stability of liposome suspensions. DLS uses scattering of light to measure particle size and zeta potential based on their Brownian motion and electrophoretic mobility, respectively[419]. Nanoparticle tracking analysis (NTA) is another popular technique for measuring particle size and dispersity, which utilises light scattering to track particles under Brownian motion, relating movement speed to particle size[420].

Structure and composition

Microscopy is a versatile tool when it comes to liposome characterisation; shape, morphology and lamellarity can all be visualised using electron microscopy. Transmission electron microscopy (TEM) and cryo-TEM are particularly useful for confirming particle shape and vesicular structure (i.e. lamellarity)[421]. Scanning electron microscopy (SEM) aids with visualising surface morphology and can also provide information on size and dispersity[422]. Small-angle X-ray scattering (SAXS) is another technique often used for information on lamellarity, bilayer thickness and spacing, and NMR can be used to directly assess liposome surface modifications[396,423,424]. Lipid composition is also an important property to measure to meet regulatory requirements and this can be done using liquid chromatography followed by e.g. mass spectrometry detection after disruption of the liposome membrane[394,425].

Encapsulation efficiency

The encapsulation/entrapment efficiency describes the extent of successful drug loading into a liposome and typically requires the separation of loaded liposomes from excess unloaded drug, followed by destruction of the liposomes to liberate encapsulated drug. Techniques used to

measure encapsulation efficiency differ depending on the properties of the drug and how the drug is partitioned into the liposome[426]. For example, centrifugal ultrafiltration involving the centrifugation of a liposome suspension through a polymer filter of a particular size is a popular and straightforward protocol for separation[427,428]. Dialysis and size-exclusion chromatography are also effective methods for separation and the fractions are then subject to quantification using detection methods like spectroscopy and liquid chromatography[427,428]. These techniques can also serve as drug removal steps suitable for liposome purification, and can also be adjusted for the assessment of *in vitro* drug release[415].

Storage stability

The shelf-life of these suspensions is of great importance when thinking about liposome stability, especially as liposome integrity may not be maintained over time[429]. Storage stability studies may involve the continued probing of aforementioned properties over a period of time and in specific conditions. For example, liposome aggregation and drug retention changes are considered to be 'liposome stability problems' that can be monitored through stability studies[430].

Characterising this wide breadth of properties is necessary for clinical approval and quality control purposes, as well as giving insights into links between structure, function and performance.

1.4.4 Clinical applications of liposomes: uses in bacterial infection

Most of the clinically approved liposomal formulations are currently used in anti-cancer therapies, with several others in the fungal disease, viral vaccine and pain management markets[354]. These include Doxil®, the first FDA-approved nano-drug utilising PEGylated liposome technology for cancer management, AmBisome® that incorporates Amphotericin B into the lipid membrane for severe fungal infections, and Visudyne®, a light-sensitive formulation used for age-related macular degeneration[412,431,432]. Interestingly, there are very few antibacterial liposomal formulations in clinical use; as of 2026, Arikayce® was the only expressly antibacterial liposomal treatment available on the market[433].

Arikayce®, also known as amikacin liposome inhalation suspension (ALIS), is a liposomal formulation of amikacin that is nebulised and administered directly to the lungs through inhalation[434,435]. Amikacin (AMK) is an aminoglycoside antibiotic that irreversibly binds to the 30S bacterial ribosomal subunit, disrupting translation and subsequent protein synthesis[436]. In the face of expanding aminoglycoside-modifying enzymes (AMEs) that inactivate aminoglycosides through acetylation, phosphorylation or adenylylation, AMK was still widely used to successfully treat multi-drug resistant infections[437]. Unfortunately, AMK resistance has seen a rise in some regions even though it is the most resistant to inactivation by AMEs, which may explain why a liposomal formulation was explored as a way to maintain or improve its antibacterial activity[438]. In Arikayce®, cationic AMK is encapsulated within a neutral lipid membrane. This pairing works to impair drug diffusion across the membrane, resulting in a slow and sustained release of AMK, but also shields the drug from external anionic sputum components, improving its stability[435,439]. Additionally, encapsulation aids with biofilm penetration and macrophage uptake, which is of particular significance within the infected lung environment[439,440]. The administration and manufacturing process also contribute to Arikayce® activity; using the product-specific nebulizer system, Lamira™, ensures efficient distribution and deposition of drug throughout the lung[434,441]. Furthermore, the high encapsulation efficiency afforded by the in-line infusion manufacturing process ensures that a high concentration of AMK is available for nebulisation[435,442]. This goes to show how formulation, manufacturing and administration all have to be carefully considered, as exemplified by the clinical success that Arikayce® has achieved.

In the context of antibacterial treatments, antibiotic encapsulation in or immobilisation on nanoparticles aims to improve the efficacy of existing antibiotics through controlled and sustained release, prolonged circulation and infection targeting[443,444]. As described in section **1.4.2**, liposomes possess immense versatility and flexibility that makes them a desirable antibiotic carrier. For example, conventional liposomes loaded with vancomycin demonstrated an increased potency over free vancomycin when used against MRSA[445]. In another example, PEGylated liposomes were

found to decrease vancomycin accumulation in the kidneys, reducing nephrotoxicity, whilst increasing distribution into the lungs in an MRSA infection model[446]. A combination of immobilised polymyxin B and encapsulated fosfomycin has been used within a single liposome formulation to synergistically increase killing of *A. baumannii*[447]. Reduced nephrotoxicity and improved bacterial adherence were also observed with this formulation likely due to the adsorption of polymyxin B on the liposome surface. There are numerous instances in the literature where liposomal encapsulation has worked to enhance efficacy and potency of existing antibiotics through many different mechanisms[389,443].

Liposomes also show potential in overcoming bacterial resistance, with hopes to restore antibiotic efficacy of those that have become ineffective due to AMR. For example, liposomal polymyxin B showed increased penetration and enhanced killing of resistant *P. aeruginosa* and other Gram-negative isolates[448]. Vancomycin, which is normally ineffective against Gram-negative bacteria as it can't cross the outer membrane to inhibit cell wall synthesis, has had its spectrum widened through encapsulation in fusogenic liposomes[449]. Liposomes adhering to and fusing with the outer membrane would remove this barrier, introducing vancomycin into the bacterial periplasmic environment that it would usually be excluded from. A similar behaviour has been documented about fusidic acid, an antibiotic that inhibits proteins synthesis and has largely limited activity against Gram-negative bacteria[450,451]. Through loading of fusidic acid into fusogenic liposomes, inhibition of growth was observed on clinical strains of Gram-negative *Staphylococcus epidermidis* and *A. baumannii*[452]. These observations could be due to the liposomes facilitating drug diffusion into the periplasm and beyond, and is one way in which liposomes can be used to overcome bacterial resistance mechanisms. The protection afforded by encapsulation can also prevent antibiotics from being inactivated by bacterial enzymes, avoiding enzymatic resistance—adsorbing the β-lactam, piperacillin, onto the liposome surface was shown to confer protection from hydrolysis by *S. aureus* β-lactamases[453].

With many bacterial infections being associated with biofilm, reducing drug penetration and thus requiring much higher drug doses, liposomal antibiotics have been explored as a route for localised drug delivery to circumvent resistance afforded by biofilm presence[454–456]. One of the main features of a bacterial biofilm is the EPS matrix in which bacterial cells are embedded and shielded from the external environment. By targeting this negatively-charged EPS with cationic liposomes, encapsulated antibiotics can potentially more efficiently penetrate into the matrix and reach bacteria embedded deep within. One comparison of conventional and cationic liposomes found better penetration into *Streptococcus mutans* biofilms, and another study assessing anionic and cationic liposomes saw the positively-charged formulation gave enhanced penetration and inhibition of *S. aureus* and *P. aeruginosa* biofilms[457,458]. Fusogenic liposomes have also been explored as an anti-biofilm strategy; liposomes that contain lipids that destabilise lipid bilayers can fuse directly with bacterial cells and promote interactions with biofilm components. Fusogenic liposome formulations have been shown to increase anti-biofilm capacity on multiple occasions—they gave increased penetration and retention against *S. aureus* biofilms, particularly cationic ones[459]. Formulations containing vancomycin have also been documented to have increased antibiotic efficacy against mature MRSA biofilms, where it is proposed that the destabilising and fusing property is responsible for anti-biofilm function[460].

Not only do liposomes themselves show biofilm penetration potential, but they can also be used in combination with biofilm-dispersing enzymes, focussing on matrix degradation as the first step to improving bacterial uptake of antibiotics. Lysozyme is one such enzyme that has been conjugated to the surface of liposomes loaded with gentamicin, showing increased matrix damage, reducing *P. aeruginosa* and *S. aureus* biofilm mass and inhibiting bacterial growth, when compared to free gentamicin or lysozyme alone[461]. In another study, DNase I and proteinase K enzymes were loaded into cationic liposomes and tested on *Cutibacterium acnes* biofilms in skin and catheter infection models[462]. Reduced biofilm biomass, increased biofilm penetration depth and antibacterial activity both within and outside of the biofilm was observed, likely due to the cationic

targeting combined with degradation of eDNA and extracellular proteins facilitated by the encapsulated enzymes.

Despite liposomal antibiotics in the literature showing encouraging results in the context of AMR and Arikayce® being a stand-out example of the potential of liposomal formulations in antibacterial therapy, there are still very few antibacterial liposomes currently undergoing clinical trials[354,463,464]. This indicates that there may be other factors at play hampering clinical translation. Aside from regulatory and intellectual property matters, there are many complexities to be taken into account, including clinical trial intricacies, manufacturing options, formulation choices and the current scope of research done (pertaining specifically to anti-biofilm effects)[465]. For liposomal formulations, clinical trials require extensive controls to account for different components of the system and regulatory assessments can be multifaceted, making them relatively complicated and costly to evaluate[466,467].

Even though liposomes exhibit numerous benefits on the basis of their physical properties, their physical stability is one factor that can present some disadvantages: size changes and aggregation during storage and premature drug leakage in physiological conditions would affect a formulation's *in vivo* reliability and reproducibility[468,469]. There is also the question of whether the preparation process degrades the encapsulated cargo, especially if drug-loading involves several freeze-thaw cycles or sonication; antibiotics, such as vancomycin and teicoplanin, can lose efficacy as a result of these extreme conditions[470]. Not only can degradation lead to loss of antibacterial activity, but it can also result in hepatoxicity or nephrotoxicity upon administration[471]. Therefore, it is imperative that manufacturing and processing methods are taken into consideration during the initial formulation. Related to this, large-scale production methods often put restrictions on the types of liposomes that can be made to be sterile and stable, so would often demand a level of simplicity when it comes to surface modifications[472]. Additionally, certain production methods are not necessarily suitable for clinical formulations; reverse-phase evaporation is a popular technique

that gives high encapsulation efficiencies of hydrophilic drugs, but may leave traces of organic solvents within the final liposome formulation, posing a toxicity risk[404,473].

Although liposome formulations are typically chosen due to their versatility, biocompatibility and biodegradability, there are some instances where this can be a double-edged sword. The efficacy of cationic liposomes, for example, lies in their ability to passively target negatively-charged bacterial cells and interact with biofilm components. However, this property also allows potential interactions with negatively-charged host cell membranes and proteins, promoting oxidative stress and cytotoxicity[474]. In addition to this, there is a fine balance to be struck between a stable drug-carrying formulation and one that releases the drug when required for pharmaceutical applications. There are some cases where this is not achieved: in a study on aminoglycoside activity against *P. aeruginosa*, liposomal aminoglycosides did not perform better than free drug[475]. It was suggested that this could be due to some drug being retained within the liposomes rather than being released. This may also be the explanation for a PEGylated liposome formulation containing clarithromycin that didn't seem to improve biofilm clearance over free drug[476]. Formulation tweaks can clearly help with improving function—in the last example, modifying the liposome with WGA increased *in vitro* and *in vivo* anti-biofilm efficacy—but these changes may take a lot of time and resources, slowing down its progress into the clinical testing pipeline. Furthermore, not all formulations that show antibacterial effects have been shown to have anti-biofilm activity, which is important to consider with what we now know about bacterial infections in healthcare. Sometimes, the formulation does not possess the right properties to confer anti-biofilm activity; neutral and anionic liposomes have been documented to have minimal effect on bacterial biofilms possibly due to the lack of favourable interactions[477]. There is also the possibility that, when considering the complex and heterogeneous structure of biofilm, some liposomes may not be very efficient at penetrating the entire thickness of the biofilm, so complete clearance cannot be achieved even if growth is inhibited.

With this in mind, using additional agents (that are already in clinical use) to encourage biofilm dispersal and enhance liposomal activity could be an appropriate route to take. As previously discussed, biofilm dispersal would not only enable access to deeper biofilm layers, but can also (re)sensitise the released bacterial cells to antibiotics[181]. Combining liposome use with a clinically-approved biofilm-dispersal agent could clear the path to clinical translation for effective liposomal therapies aimed at biofilm-related infections. One such effector of biofilm dispersal that is already in clinical use, albeit for different purposes, is ultrasound paired with microbubbles, which will be explored in the next section.

1.5 Ultrasound-mediated methods of treatment

1.5.1 A background on ultrasound, cavitation and microbubbles

Sound is mechanical energy that propagates as pressure waves through a medium, consisting of an alternation of high-pressure (compression) and low-pressure (rarefaction) phases[478]. A vibrating source transfers mechanical energy to particles in a medium, causing them to collide and pass the energy along, which propagates sound as a wave[479]. The propagation of this sound wave through a medium produces a deviation in pressure from ambient atmospheric pressure, referred to as the acoustic pressure[480]. Ultrasound (US) is a sound wave with a frequency above the human hearing range (i.e. >20 kHz) and due to its low absorption by water and biological tissues, it is used as a non-invasive, safe and cost-effective medical tool[481].

US is typically produced by probes that contain piezoelectric crystals that convert electrical energy into mechanical energy, which is then converted back to electrical energy after the waves are reflected back by the target (necessary for imaging purposes)[479]. These US waves have particular characteristics fine-tuned for their purpose, and some of the most relevant characteristics defining US fields in medical use are illustrated in **Figure 16**[482]. The frequency, expressed in hertz (Hz), refers to the number of wave cycles per second. A period refers to the amount of time for a single complete wave cycle to occur, while the wavelength is the distance between two successive wave

peaks. The amplitude describes the maximum deviation from the average pressure, with the peak negative pressure (PNP) being a specific measure of amplitude that defines the maximum drop in acoustic pressure, expressed in pascals (Pa). US exposure can have alternating 'on' and 'off' periods in a defined temporal pattern, making up an US burst. The pulse duration is the time for which the US pulse is 'on' and the pulse repetition period is the time from the beginning of one pulse to the beginning of the next. The duty cycle is defined as the pulse duration over the pulse repetition period as a percentage, i.e. describing the amount of time US is actively transmitting ('on') compared to resting ('off'). The power is the rate at which the sound wave delivers energy, typically measured in watts (W), and the intensity describes the power delivered over an area, expressed in W/cm^2. These parameters are all important to understand and consider based on the intended outcome (i.e. diagnostics or therapeutics), the target tissue, and instrumentation used, among other factors, in order to optimise clinical outputs[478]. For medical diagnostics, low intensity (<0.1 W/cm^2) and short US pulses of frequencies between 2 and 12 MHz are typically used, with lower frequencies used for imaging of deeper tissue (due to better penetration depth)[483,484]. For therapeutics, long pulses or continuous waves of up to 3 MHz in frequency and intensities up to 10,000 W/cm^2 are generally used, with lower power settings used for physiotherapy and drug delivery, and higher power applications in surgery and dentistry[485,486].

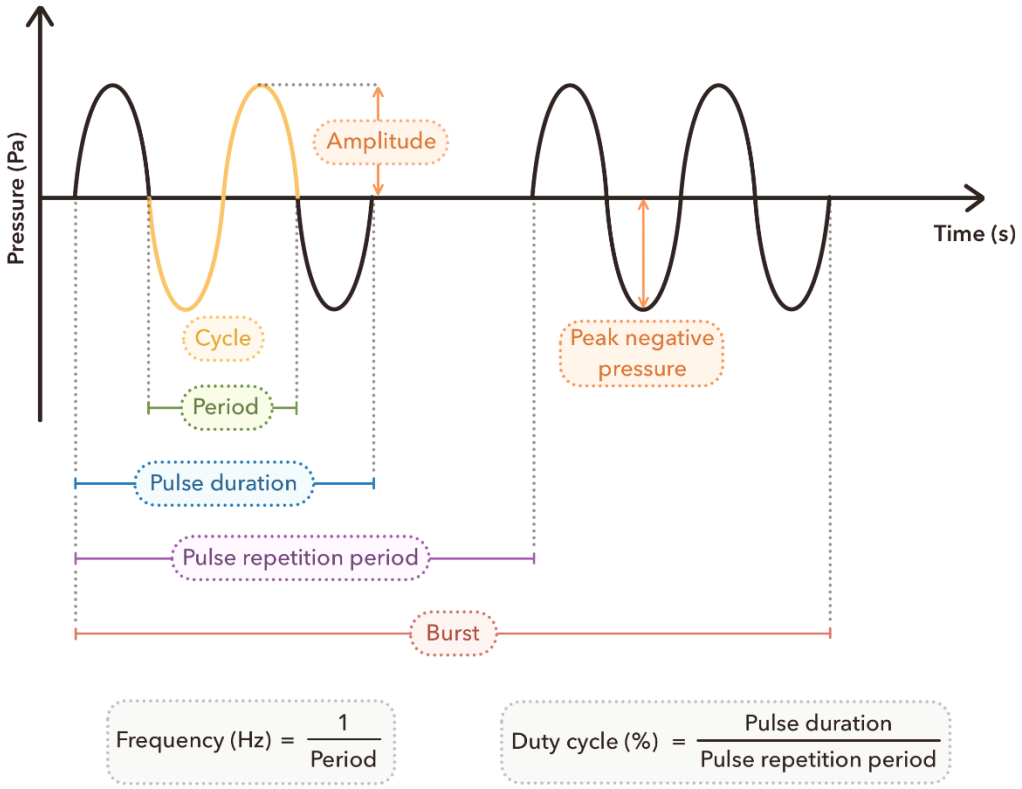


Figure 16 | Overview of relevant characteristics that define US fields in medical use. Adapted from Deprez *et al.* (2021)[482].

As sound passes through tissue, sound waves experience 'resistance' that opposes their propagation, which is described as acoustic impedance. Every tissue possesses different impedance values, and interactions of transmitted sounds waves with tissue and tissue boundaries result in the progressive loss of acoustic energy, known as attenuation[479]. Many factors contribute to acoustic attenuation including reflection, where US bounces directly back to its source; refraction, where US is deflected, particularly at tissue boundaries; scattering, where US is bounced in all directions; and absorption, where US is converted to thermal energy upon collision with particles within a tissue. These effects result in the progressive reduction of US intensity and amplitude over the distance travelled.

These factors also contribute to echogenicity which forms the basis of imaging and diagnostics using US; differences in how adjacent tissues reflect US waves enable image generation from US probes detecting the returning echoes[487]. Tissues that show strong echogenicity (i.e. hyperechoic),

such as nerves and bone, show up white in brightness-mode (B-mode) images, whereas those with low (hypoechoic) or no (anechoic) echogenicity, such as fat and blood vessels, show up as grey or black, respectively. As such, US has long been used in medical diagnostics to generate images of biological matter through measuring US transmission and reflection that differ between tissues[479,488]. For example, the best-known use of US in modern medicine is during pregnancy scans, where differences in tissues' physical properties yield different echo patterns that allow for the visualisation of a foetus in the womb[489]. However, not all tissues provide enough contrast for imaging; for example, tumours with poor or complex vascularisation are not as compatible with standard US techniques and require contrast enhancement for improved diagnosis[490].

US contrast agents in the form of tiny gas bubbles have long been used to enhance medical US images, especially in cardiology for the visualisation of anechoic blood vessels[491]. Gas bubbles enhance contrast by increasing the difference in acoustic impedance between the gas bubbles and the surrounding media, which boosts the echo signal that can be detected[492]. Although free gas bubbles are naturally generated upon exposure to an US field due to changes in temperature and pressure of the exposed media, encapsulated gas bubbles provide the benefits of increased stability during imaging and reduced coalescence[491,493]. Thus, microbubbles (MBs)—small pockets of encapsulated gas between 0.1 and 10 μm in diameter—have been the most commonly used US contrast agent since the 1990s[491,494].

MBs are typically composed of a protein, polymer, or phospholipid shell surrounding a gaseous core[495]. The encapsulated gas of choice was originally air, which was relatively unstable with a short circulation half-life due to its high solubility in water, prompting the shift towards using poorly water soluble perfluorinated gases that improved MB circulation stability[496]. Hence, all of the currently clinically approved and actively used MB formulations contain an inert gas[491,496]. In addition to inert gas, the MB shell also contributes to bubble stability and durability by reducing gas dissolution and surface tension[493]. The gas compressibility is fundamental to the mechanism

of MB activity under US exposure: as US is applied, MBs expand and contract during periodic cycles of low and high pressure, undergoing a volumetric oscillatory motion known as cavitation[482,497]. At low US intensities (<3 W/cm^2), these oscillations are steady and repetitive in a mostly linear fashion, referred to as stable or non-inertial cavitation (**Figure 17A**)[482,498,499]. Asymmetry in this oscillation leads to a movement of local media surrounding the bubble, known as microstreaming (**Figure 17C**), which imparts shear stress onto nearby surfaces causing membrane disruption and pore formation[482,500,501]. If MBs are in close proximity to or interacting with a cell membrane, non-inertial cavitation can also result in a 'massaging' effect that can stimulate endocytosis of therapeutic agents, for example[502,503]. At higher US intensities (≥3 W/cm^2), these bubbles oscillate violently, known as transient or inertial cavitation, and can eventually collapse under the increased pressure (**Figure 17B**), causing microjets or shockwaves (**Figure 17C**)[482,498]. Microjets are a result of asymmetric bubble collapse that causes bubble deformation in a way that releases a high velocity liquid jet. This can have a membrane permeabilization effect through perforation or formation of pits and invaginations[501,504]. Shockwaves emitted after bubble collapse can exert similar shear stresses on nearby cell surfaces. Exposure of tissue to these extreme pressure changes can also cause thermal effects as a result of energy absorption, and can even induce chemical effects in the form of ROS production[505,506]. A rise in temperature can be exploited by heat-sensitive drug carriers to achieve localised drug delivery, while ROS production contributes to tumour killing as part of sonodynamic therapy[507,508]. Therefore, not only is cavitation useful for enhancing imaging and diagnostics through echogenicity, but MBs can also be used as cavitation nuclei in therapeutic contexts through mechanical, thermal and chemical effects[483,500,509].

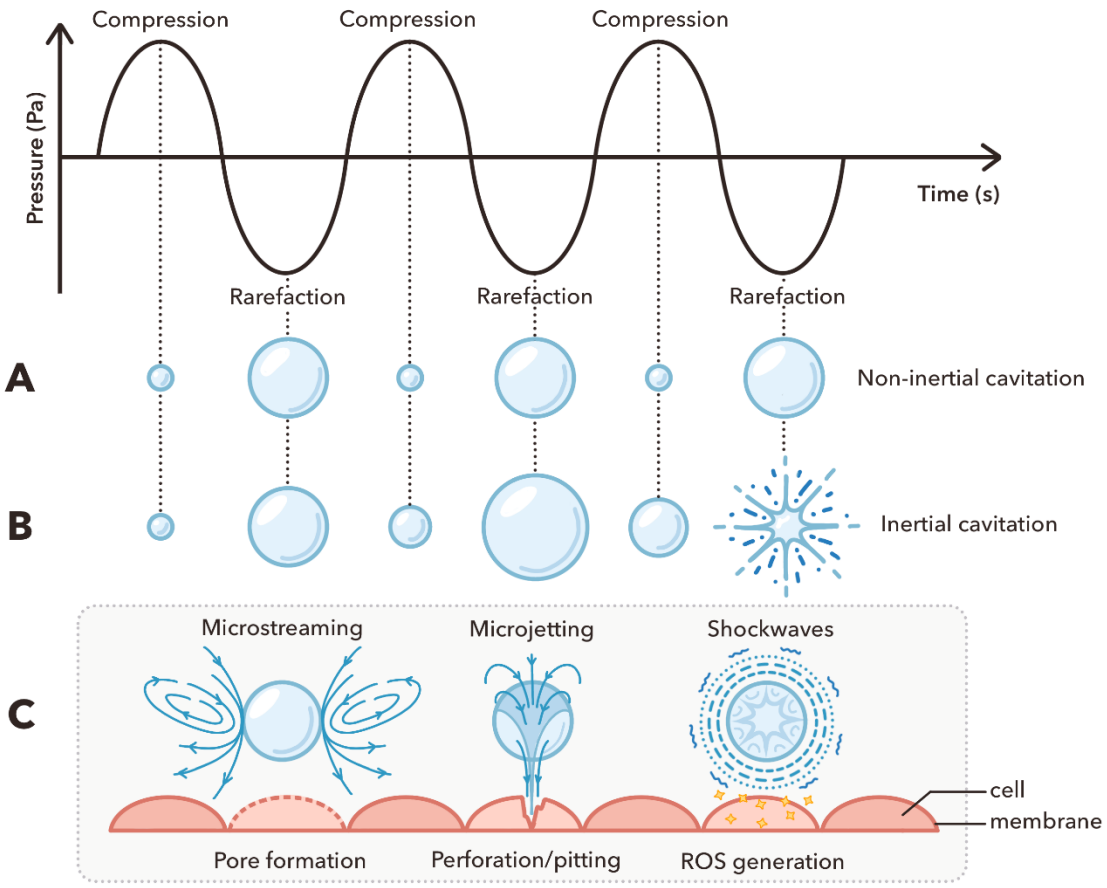


Figure 17 | Types of microbubble cavitation and its biophysical effects. When microbubbles are exposed to a low intensity US field, they undergo (**A**) stable/non-inertial cavitation; at high US intensities, microbubbles undergo (**B**) transient/inertial cavitation. (**C**) This cavitation can have several biophysical effects on the surrounding media and cell surfaces, including the generation of microstreaming flows, microjets and shockwaves that can lead to membrane pore formation, membrane perforation/pitting/invagination and ROS generation.

Aside from MBs, there are several other contrast agents/cavitation nuclei that are in development, including nanocups, nanodroplets, and echogenic liposomes (**Figure 18A**)[510]. These technologies revolve around introducing exogenous US-sensitive material, largely involving gas bubbles in some form, for enhanced cavitation effects: nanocups are polymeric cup-shaped nanoparticles classed as solid cavitation nuclei that stabilise gas bubbles captured in the cup, becoming a site of cavitation activity[511]. Nanodroplets typically consist of a protein, polymer, or phospholipid stabilising shell surrounding a volatile liquid perfluorocarbon core which vaporises to form MBs when exposed to US, and as such they're classified as phase-change liquid droplets[512]. Echogenic liposomes are thought to be similar to liposomes discussed in section **1.4.2** with the difference being the existence

of entrapped gas within either the lipid bilayer, or instead of an aqueous core[513]. The entrapped gas confers US-sensitivity to the liposome as it constitutes a site for cavitation nucleation. All of these (and more) are increasingly explored options for diagnostic and therapeutic purposes but MBs, in particular lipid-coated MBs, still stand out as the most commonly used cavitation nuclei, both pre-clinically and commercially[510]. (Going forward, all mentions of MBs will be specifically referencing lipid-coated MBs, unless stated otherwise.)

Lipid-coated MBs are made of a lipid monolayer encapsulating an inert gas (shown in **Figure 18A**). The thin (~3 nm thick) lipid shell, in a similar fashion to liposome membranes, self-assemble at the gas-liquid interface which works to reduce bubble surface tension to prevent gas dissolution and improve stability[495]. Additionally, the 'weak' hydrophobic and van der Waals interactions between lipid constituents makes this shell compatible with cavitation motions during US exposure[495,514]. Furthermore, like liposome membranes, the MB lipid shell can also serve as a platform for therapeutic modifications (**Figure 18B**). For example, MBs formulated with interleukin-8 antibodies attached to the surface were able to target interleukin-8 on atherosclerotic plaques to reduce associated inflammation upon US exposure[515]. Therapeutic agents can also be loaded directly into the lipid monolayer: hydrophobic paclitaxel has been effectively loaded into MB lipid shells to improve US-responsive tumoricidal activity in human breast cancer models[516]. However, this strategy presents limited drug-loading capacity due to the thin lipid monolayer of the MB, so a thick oil layer can be introduced within the MB shell to improve drug-loading but this does have an effect on acoustic behaviour[517,518]. Although drugs can also be loaded into the MB gas core, as shown with loading of gaseous nitric oxide into MBs to facilitate US-mediated thrombolysis in rats, there are reports of challenges with MB stability and therapeutic gas loading, as well as variation in acoustic response as a result[519–521]. Thus, MB shell coupling or conjugation is often chosen as the more versatile alternative and combinations of these drug-loading modes are used in targeted MB research[522,523].

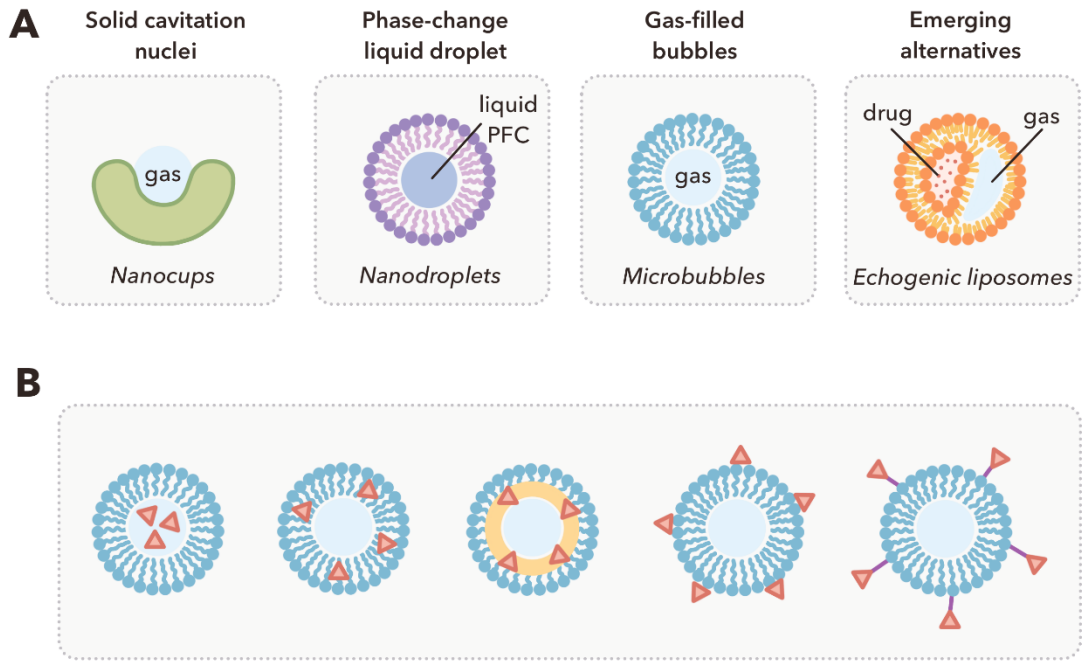


Figure 18 | Examples of cavitation nuclei. (A) There are several types of cavitation nuclei that are currently used or researched for diagnostics and therapeutics. They can be classified as solid cavitation nuclei, phase-change liquid droplets, gas-filled bubbles, along with emerging alternatives like echogenic liposomes. An example of each is shown. (B) Gas-filled bubbles, e.g. lipid-coated microbubbles, can be used to transport drugs in several ways: loading into the gaseous core, incorporation into the lipid shell, incorporation into an oil layer below the lipid shell, non-covalent coupling to the microbubble surface, and conjugation to ligands or carriers. PFC = perfluorocarbon.

1.5.2 Microbubble manufacturing methods

There are several methods by which MBs can be prepared that can be chosen based on target MB properties (like size and coating), time and financial cost, and scalability, for MB production that satisfies a range of conditions[524,525]. Particularly when considering drug-loading and surface modification, the method of preparation may be restricted with some techniques being more suitable than others[525]. Therefore, similar to liposomes, this choice needs to be taken into consideration during the formulation stage. This section will cover a selection of the most commonly used methods in the manufacturing process, from production to characterisation.

1.5.2.1 Production methods

Sonication and agitation

Sonication at low frequency (e.g. 20 kHz) and high power (>50 W) is the most commonly used method for MB production, where the changes in pressure and temperature of the sonicated medium results in the formation of gas-filled cavities[517,524,525]. This method starts off with a process similar to liposome thin-film hydration, where lipids are dispersed in an organic solvent (e.g. chloroform) before evaporation to form a thin lipid film that is then hydrated in an aqueous buffer[524]. Within a sealed vial, the air is replaced with the desired gas that is to constitute the MB core. A sonicator tip/horn is typically placed at the air-liquid interface which allows for the loading of the bulk gas phase into the bulk aqueous phase, forming MBs with a high size dispersity[517,524,526]. Even though the size distribution can be somewhat optimised by adjusting the sonication parameters, fractioning is often required for more monodisperse suspensions[525]. MB size matters, not only for acoustic responsiveness—successful biomedical applications utilise MBs below 10 μm in size—but also to avoid adverse biological outcomes, such as embolism[517,527,528]. Therefore, techniques like differential centrifugation and flotation are used to fractionate MBs based on their size (extensively reviewed by Upadhyay and Dalvi, 2019)[517]. One advantage of the sonication method is that it can be performed as batch or continuous production, allowing for adaptability in small- and large-scale production operations[517].

Mechanical agitation is another commonly used method of MB preparation that involves the vigorous shaking, e.g. using vial mixers, of the hydrated lipid film suspension to form MBs[527]. Although agitation also produces MBs with wide size distributions that require further fractionation, this method has been shown to produce smaller MBs than sonication which may be advantageous for some applications[529].

Flow-focussed techniques

In order to address the issue of high MB size dispersity associated with the aforementioned conventional methods, alternative techniques that utilise continuous flow, such as co-axial electrohydrodynamic atomization (CEHDA) and microfluidic devices, have been established[517,525]. These techniques eliminate the need for post-processing fractionation steps that would ultimately affect MB yield and stability. CEHDA uses electrical force to form droplets from a stream of conducting liquid and gas ejected from a coaxial nozzle, resulting in gas-encapsulated bubbles[525,530]. By varying the applied voltage and flow rate, among other parameters, the size and size distribution of MBs can be tightly controlled[531]. There is also the added benefit that extreme mechanical action, like agitation or sonication, is not required. Microfluidic devices are also able to produce a high yield of MBs in a single step, with different device designs and flow parameters lending themselves to different target sizes: cross flow (T-junction) devices typically give larger MBs than flow-focusing devices that use narrower geometries for smaller MBs[524].

1.5.2.2 Characterisation methods

Physicochemical characterisation

Similarly to liposomes, the physical characteristics of MBs can be evaluated using DLS and NTA for size and size distribution and electron microscopy for size and morphology (see section **1.4.3.3**)[524]. Unfortunately, DLS is known to be unsuitable for suspensions with a high size dispersity, which may be common for MB preparations depending on the production method used. Therefore, optical microscopy (in conjunction with automated sizing software) and electrical impedance particle counting are also commonly used to assess MB size, concentration and size distribution[524,532]. The Coulter Counter is a popular piece of equipment that measures MB size: after dilution in an electrolyte, an electric field is established that forces MBs though an aperture[524,533]. The detected change in electrical impedance allows for particle size and count to be determined. As this technique is quick and easy, it is widely used for MB characterisation, but it

should be noted that there is currently disagreement on which sizing method is the most accurate[532].

Acoustic characterisation

As cavitation is fundamental to MB activity and its downstream biophysical effects, it is important to be able to characterise the acoustic response. The pressure changes in the media as a result of MB cavitation can be detected by a transducer that converts energy between electric and acoustic, in either an active or passive manner (**Figure 19A**)[534]. In the case of active cavitation detection (ACD), a focussed transducer transmits a wave and detects the echoing of that same wave by MBs, essentially actively probing for cavitation using a pulse-echo technique[535–537]. For passive cavitation detection (PCD), an unfocussed transducer is used to capture the acoustic emission noise after US transmission from another transducer[535,538]. PCD is widely used with the resulting cavitation profiles containing spectra of frequency components (**Figure 19B**): the fundamental frequency initially emitted by the transducer; harmonic, sub- and ultra-harmonics associated with non-inertial cavitation; and broadband noise associated with inertial collapse[539–541]. Taken together, this information helps to understand the features of the induced cavitation, including occurrence and intensity, which helps in mapping MB physical characteristics and biological effects to their acoustic response[538].

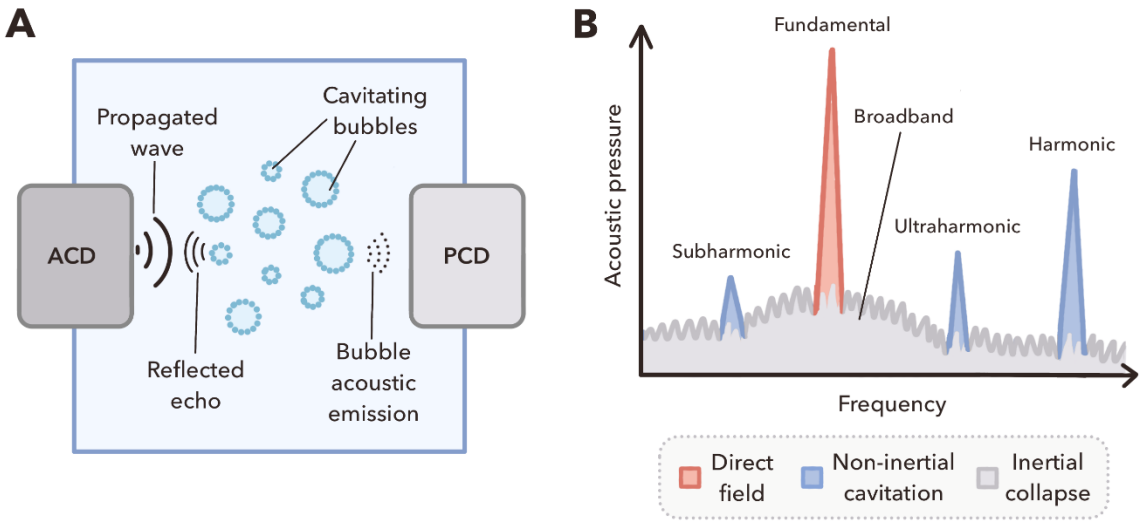


Figure 19 | Types of cavitation detection and a simplified representation of an acoustic pressure spectrum. (A) Active cavitation detection (ACD) and passive cavitation detection (PCD). (B) A simplified acoustic pressure spectrum showing the fundamental (input) frequency, the harmonic, ultraharmonic and subharmonic components, as well as broadband noise. The fundamental frequency is associated with the direct field emitted directly from the transducer (red), the harmonics, ultra-harmonics and sub-harmonics are often associated with non-inertial cavitation (blue), and broadband noise is typically associated with inertial collapse (grey). Adapted from Wu *et al.* (2022)[537].

1.5.3 Therapeutic ultrasound and microbubbles: uses in bacterial infections

In the context of bacterial infections, US has been used alone (i.e. without MBs or antibiotics) to directly kill planktonic cells: Li *et al.* found that a low frequency US programme (20 kHz, 60 W/cm^2) reduced bacterial viability of *E. coli* and *S. aureus* involving ruptures in the cell walls and membranes, likely caused by cavitation effects[509,542]. The role of US in specifically enhancing antibiotic delivery has also long been demonstrated: after applying US at 67 kHz and 0.3 W/cm^2 in combination with gentamicin, Pitt *et al.* showed how planktonic *P. aeruginosa* and *E. coli* viabilities were significantly reduced and even seemed to show decreased antibiotic resistance[543].

Further improving drug delivery with US-responsive MBs is of interest, not only through incorporation of drugs into MB formulations as previously described, but also through the biophysical effects of cavitation directly impacting drug delivery[481]. For instance, the oscillatory motion associated with microstreaming can increase transport and diffusion rates of drugs present in the surrounding medium by virtue of this movement. The shear stresses on nearby membranes

that lead to cell permeabilization can be used to promote drug uptake through membrane pores or endocytosis. Additionally, if MBs are coupled to ligands or drug carriers, US exposure and subsequent cavitation events can be used to disrupt or rupture them in ways that promote drug release and delivery into nearby cells[544,545].

When used in combination with MBs and antibiotics, US can be used as an adjuvant to encourage drug uptake and increase antibiotic efficacy; for example, gentamicin efficacy was significantly increased against planktonic *E. coli* when MBs and US (46.5 kHz, 0.1 W/cm^2, 33% duty cycle) were used together, compared to gentamicin only, as a result of increased bacterial membrane permeabilization, complementing Pitt *et al.*'s findings from 1994[543,546]. In this study, they found that without gentamicin their chosen US parameters had no effect on bacterial viability despite other studies showing planktonic bacteria killing with US alone, which highlights how variations in US fields used across different studies can yield different antibacterial outcomes. Additionally, inconsistencies in the reporting of experimental US field parameters makes it hard to directly compare across studies[547].

Most of the studies involving US, MBs and antibiotics have in fact been on biofilm models[547]. In addition to bacterial cell permeabilization and enhanced drug delivery, US-mediated treatment allows for several anti-biofilm mechanisms: the generation of micropores where sections of biofilm become detached, formation of craters spanning the depth of the biofilm from shockwaves and microjets, and sloughing of biofilm caused by microstreaming-associated stresses[509,548,549]. Pores and channels naturally present in biofilm structures are also thought to enable MBs to penetrate more effectively, aided by US-induced micro-convection throughout the biofilm, followed by internal disruption of the EPS matrix[550]. In these ways, US can be used for biofilm disruption through complete mechanical clearing of biofilm (e.g. ultrasonic scaling of dental biofilm) or removing upper layers to expose deeper layers that become re-sensitised by the new flux of nutrients, ready for subsequent antibiotic treatment[509,551,552]. Additionally, treatment based on

physical phenomena like cavitation do not have to rely on chemical reagents for antibacterial/anti-biofilm effects and thus does not induce further AMR, presenting US as a particularly attractive option[553].

It is important to note that US alone is not enough for anti-biofilm applications; Rediske *et al.* showed that US alone (28.48 kHz, 0.1 or 0.3 W/cm^2) did not have any effect on viable bacteria count within *E. coli* biofilm and this observation has been supported by other studies involving different US fields and biofilm species[554–556]. This justifies why US is frequently combined with MBs for anti-biofilm effects: hole and pore formation, as a result of shear stress on biofilm structures, and increased membrane permeabilization and antibiotic-susceptibility of resident cells have been demonstrated on *S. epidermidis* biofilms using different US parameters[322,552,557]. From these experiments, it is apparent that US and MBs are effective at mechanically removing and sensitising bacteria within a biofilm, but often needs to be followed up with antibiotic treatment for synergistic anti-biofilm effects that result in substantial bacterial death; it was only after the biofilms were treated with vancomycin that significant cell death was observed[557]. This dynamic between biofilm disruption and drug delivery is important to consider—if partial biofilm disruption leaves behind viable/persister cells after treatment, there is a risk of biofilm re-establishment[558]. Additionally, bacteria mechanically released from the biofilm without being killed can potentially facilitate the formation of biofilms elsewhere. Therefore, biofilm disruption being coupled with drug delivery is of importance.

Whilst the prospects of US-mediated anti-biofilm therapies are exciting, there is a concern that US frequencies and intensities used to kill bacteria in *in vitro* studies would not translate effectively and safely *in vivo*, leading to tissue damage. For example, Rediske *et al.* found that low frequency US (28.48 kHz, 0.3 W/cm^2) used in their *in vivo* experiments on rabbits led to skin damage, likely from temperature increases[554]. It is important to note that in this study, US was applied for 24 hours which may not be clinically practical anyway. High intensity US (>10 W/cm^2), which is commonly

used for removal of bacteria from polymer surfaces and in some *in vitro* studies, also lyses and kills eukaryotic cells[509,559]. Fortunately, adding MBs allows for the use of lower intensities while still achieving intense cavitation, and their versatility makes them the anchor of US-responsive drug delivery. Another concern is that certain US environments can actually promote bacterial growth, especially if not followed by antibacterial treatment: low frequency, low intensity sonication (70 kHz, <2 W/cm^2) is proposed to be able to increase oxygen availability and waste elimination within a biofilm, stimulating bacterial metabolism[559]. Therefore, it is necessary to consider the frequencies and intensities used, not only with damage to host tissue in mind but also taking bacterial growth induction into account.

US treatment of bacterial biofilm can be considered a double-edged sword: it can both compromise biofilm structural integrity and stimulate dormant bacterial metabolism to re-sensitise them to antibiotics, but this metabolism boost can also eventually support biofilm formation and growth[560,561]. Literature contains evidence supporting both the destructive and stimulatory properties of US treatment, with differences in reported US parameters and target species adding to the complexity. But one thing is clear—when used in combination with MBs and antibiotics, US has been found to always enhance antibacterial activity compared to antibiotics alone, i.e. US-mediated drug delivery has synergistic anti-biofilm effects[547]. Therefore, it is no wonder that integration of US-mediated biofilm disruption with enhanced drug delivery is of increasing interest.

1.5.4 Integrating ultrasound with drug delivery systems

Co-administration of MBs with drugs is the most straightforward option when it comes to integrating US with drug delivery, where MBs are administered alongside free drug (distinct from conjugation, which requires attachment of the drug to MBs). This utilises the mechanical, thermal and chemical effects of acoustically-activated MBs to increase drug penetration efficiency[562]. For example, MBs have been used to increase intrauterine transfection of naked DNA in foetal mice as a demonstration of US-enhanced gene transfer and have even been used to facilitate killing of

P. aeruginosa biofilms using sub-inhibitory concentrations of gentamicin[563,564]. Drug carriers like liposomes can also be co-administered alongside MBs for improved drug delivery: polymyxin B-loaded liposomes were found to significantly reduce *A. baumannii* biofilm viability when added together with US and MBs more than the liposomes, free drug, or US and MBs alone[565]. Although co-administration has generally been demonstrated to be effective, if the drug and MBs are not in the same vicinity when US is active, the drug might not be subject to cavitation effects that enhance drug uptake, impacting the overall efficiency[562]. Additionally, the therapeutic window may be relatively short given that membrane permeabilization effects can be temporary and revert in as little as a minute[484]. Therefore, ensuring the drug is local to both the MBs and the target site is beneficial. As such, MBs conjugated to drugs or drug carriers are being explored as the more efficient alternative[562].

As previously mentioned, although MBs can be used for drug transport in several ways (**Figure 18B**), MBs themselves do not have the best drug-loading capacity, primarily due to their thin lipid monolayer shell and limited surface area[517,566]. Covalent or non-covalent attachment of separate drug carriers to a MB surface not only increases the effective drug-loading capacity, but also provides targeting benefits—loaded MBs can spatially localise drug release to the US treated area, potentially reducing side effects and unwanted interactions[567]. Additionally, having the drugs in close proximity to the MB itself means the drugs are more likely to be subject to cavitation activity that will increase their uptake[568]. Furthermore, drug-loaded MBs can be used for theranostics, where drug delivery can also be visualised using ultrasonic imaging techniques[569].

Liposomes are a long established and successful drug carrier in the clinical landscape (see section **1.4.2**), but they are known to be weakly echogenic as they lack a gas core[570]. Therefore, conjugation of drug-loaded liposomes to acoustically active MBs makes for an US-responsive drug delivery vehicle, combining the strengths of the two lipid-based systems. Through conjugation, thousands of liposomes can be attached to a single MB without dampening its acoustic response and both

contribute to the synergistic enhancement of drug delivery[570,571]. It has been demonstrated that MB collapse during cavitation can lead to the destruction of conjugated or nearby (non-conjugated) liposomes, liberating their content[544,545]. It has also been shown that some conjugated liposomes stay intact—one study showed that insonated liposome-MB complexes did not completely release their content[544]. These unruptured liposomes could possibly experience the mechanical effects of cavitation that drive delivery into nearby tissue instead, but more studies involving different liposome-MB formulations and US parameters would be beneficial to substantiate this hypothesis.

In the literature, there are a few types of conjugation that can be used for this liposome-MB complex: most commonly through avidin-biotin linkage or click chemistry reactions. This is typically facilitated by the presence of functionalised lipids within both the liposome bilayer and MB shell[572]. If both the liposomes and MBs are biotinylated, they can be non-covalently conjugated through the addition of avidin as a linker[570,572,573]. It is a simple and straightforward process, favoured in pre-clinical research, that yields a very strong and stable bond between the two lipid particles. However, avidin's high non-specificity and immunogenicity (as avidin is derived from chicken eggs) limits its downstream clinical applications[574]. Researchers are turning to click chemistry for conjugation instead to overcome this immunogenicity challenge; click chemistry offers a biorthogonal alternative (i.e. does not interfere with natural biological reactions) for producing stable covalently conjugated liposome-MB complexes[575]. For example, maleimide and thiol functional groups on the liposomes and MBs, respectively (**Figure 20**), have been used for conjugation resulting in increased doxorubicin efficacy under US exposure[576,577]. Again, this conjugation process is very simple and straightforward as it can be done at room temperature and in aqueous buffer, without any additional reagents or catalysts[575]. One issue with the maleimide-thiol conjugation approach, however, is that this bond can react with other thiol compounds at physiological pH and temperature[578]. This can lead to liposome shedding but can also potentially be deployed as a controlled release strategy. Azide-DBCO click chemistry has also been demonstrated to be efficient for liposome-MB conjugation that facilitated the release of the

anticancer drug, iproplatin, following US exposure[579]. A novel conjugation technique involving DNA-lipid tethers has been used to attach liposomes to MBs, using single-strand DNA anchored into the lipid shells via cholesterol to achieve very strong and specific complementary binding[580]. The clinical applications and implications of this technique are yet to be tested given that the use of DNA could induce an immune response, but this goes to show the current innovation of bioconjugation strategies as it pertains to liposome-MB complexes.

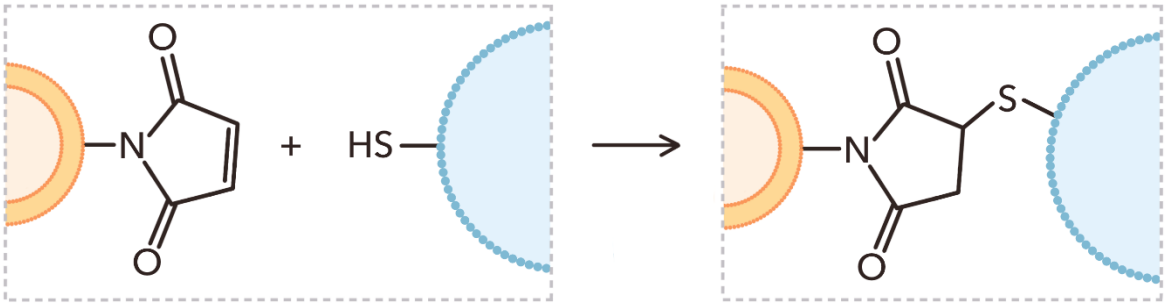


Figure 20 | Maleimide-thiol conjugation reaction. In the literature, maleimide functional groups associated with the liposome lipid bilayer (yellow, left) and thiol functional groups associated with the microbubble lipid shell (blue, right) have been used to conjugate these lipid particles together. This reaction is rapid and can be done at room temperature, in aqueous buffer, and without additional reagents.

Although there are several clinically approved liposomal formulations and commercially available MB contrast agents, clinical applications of liposome-loaded MBs (LMBs) are largely still being investigated, with all published findings so far being from pre-clinical experiments[354,491,581]. Early proof-of-concept experiments by Kheirolomoom *et al.* in 2007 showed that MBs and liposomes can be successfully conjugated via biotin-avidin-biotin bridges to deliver the liposomal payload into a cell monolayer after US exposure[570]. These experiments were complemented by later findings from Malik *et al.* who utilised the same approach to evaluate conjugation efficiency[572]. Since 2007, LMBs have been evaluated in a gradually growing number of studies on mostly anti-cancer and gene delivery approaches[523]: doxorubicin, paclitaxel, irinotecan-oxaliplatin, and irinotecan have been loaded into liposomes and conjugated to MBs (via biotin-avidin or click chemistry reactions) in a handful of studies that all documented increased drug uptake by tumour

cells, increased tumour cell killing and/or more significant tumour reduction when compared to the drug alone[576,577,579,582–584]. The potential for enhanced gene transfer was illustrated in 2007 by Lentacker *et al.* who visualised plasmid DNA uptake from LMBs[573]. After this, a similar approach was taken to deliver small interfering RNA (siRNA) and short hairpin RNA (shRNA) using the LMB system to liver and brain cancer models, respectively[583,585]. Outside of these, there a very few applications of LMBs being explored: one recent study has loaded neurotransmitters highlighting the potential for treating cardiovascular diseases[586]; a couple of studies have focused on gene therapy for hepatic fibrosis, using LMBs for safe and targeted delivery of relevant genetic material[587,588]; and one other study has shown gentamicin-loaded LMBs can be used to kill intracellular UPEC in an organoid UTI model[323]. This single study utilising LMBs in UTI research highlights a current gap in the literature in this field despite the potential it has.

1.6 Aims and Objectives

Liposomes are well known for their drug delivery capacity in protecting and targeting drug cargo, and are successfully used against bacterial infections, as exemplified by the clinically approved Arikayce® for lung infection[435]. Some formulations have also been shown to possess biofilm-penetrating abilities but in some cases, the lack of favourable interactions with the biofilm matrix hampers its antibacterial and anti-biofilm potential[454,477]. Although MBs are not considered drug delivery vehicles as they have a low drug-loading capacity, their compressibility in an US field allows for acoustic responsiveness (i.e. cavitation) that results in mechanical, thermal and chemical effects on its surrounding environment[483,517]. MBs can therefore be used to destroy biofilm structures and disrupt bacterial systems, utilising cavitation effects, but sometimes show limited bactericidal activity on their own and thus ought to be used in conjunction with antibiotics[589]. MBs have been shown to synergistically enhance antibacterial properties when used in combination with antibiotics as well as drug carriers, namely via biofilm destruction and membrane permeabilization effects[509]. Because MB-associated cavitation effects are localised to the area of US exposure and drug delivery would be most improved when drugs are in the vicinity of MBs, it is sensible to ensure colocalization of MBs and drug-loaded liposomes through conjugation to make LMBs[568,570]. This not only increases drug loading capacity of MBs, but also improves their therapeutic potential[523].

LMBs for US-mediated drug delivery is a promising emerging field that has shown pre-clinical success in various applications, including gene therapy, anti-cancer applications, and UTI treatment. However, there is currently only one study by Horsley *et al.* demonstrating the potential that liposome-MB complexes have in treating UTI infections in a bladder model[323]. In that study, gentamicin-loaded liposomes were conjugated to MBs via avidin-biotin linkages to effectively treat intracellular *E. faecalis* in a human-derived bladder organoid model.

This project aims to expand on the work by Horsley *et al.* and address the research gap in using LMB technology specifically against bacterial biofilms. By developing a novel LMB formulation (with an antibiotic other than gentamicin, and using click-chemistry for conjugation) that combines US-mediated disruption of biofilm with bacterial killing by drug-loaded liposomes, this project would be an early step in probing the versatility of LMBs in terms of antibiotic applications against biofilm.

The objectives of this project were to:

I. Formulate antibiotic-loaded liposomes and characterise their physical properties to enable the optimisation of liposome production protocols and selection of suitable formulations for subsequent experiments;

II. Assess the bactericidal properties of these liposomes without US or MBs against monospecies planktonic and biofilm models relevant to UTIs. This will allow for further selection of the most suitable formulation and provide context for when US and MBs are included in the treatment;

III. Formulate MBs and characterise their physical properties before conjugating them to the selected antibiotic-loaded liposomes and evaluating the success of conjugation and its impact on MB activity; and

IV. Determine the antibacterial and anti-biofilm efficacy of the final LMB formulation against a UTI-relevant monospecies biofilm model.

2 Formulation and characterisation of drug-loaded liposomes

2.1 Introduction

Liposomes are commonly used drug delivery vehicles that have been employed to improve antimicrobial efficacy and targeting[444]. These lipid-based drug delivery systems present a versatile option to counter antimicrobial resistance and infection recurrence. Encapsulating antibiotics within a lipid-based nanoparticle means the drug can be protected from premature degradation by the host immune and/or clearance system during transport, and desired biological effects can often be achieved with lower systemic doses, reducing negative side effects[443,590–593]. These lipid particles can also be functionalised for specific targeting to bacteria and biofilms to increase the local antibiotic concentration and enhance its potency[593–596], as well as surface-modified to respond to certain biochemical conditions, such as changes in pH or temperature[597–600].

Cationic liposomes are commonly used in drug delivery, such as gene delivery, because of the electrostatic interaction between the lipid shell and the liposome cargo enhancing encapsulation efficiency[601,602]. These liposomes are also a suitable choice for antibacterial purposes, as the positive charge of cationic liposomes can interact with negatively charged membranes of bacterial cells and with biofilm components, interfering with biofilm formation and bacterial communication[454]. For example, cationic liposomes have been used to effectively target curcumin to *S. aureus* infections in the bone and have been reported to promote nanoparticle retention in *P. aeruginosa* biofilms[603,604]. In both of these cases, the cationic lipid DOTAP was included in the formulation at a 40% molar ratio to give the characteristic positive charge that aids with cell membrane targeting. DOTAP is the most widely used cationic lipid in liposome formulations and is known to enhance nanoparticle dispersibility and membrane fluidity[605]. DOTAP is typically accompanied by helper lipids, such as cholesterol, DPPC and DOPC, which were also included in the aforementioned formulations and are known to improve liposome stability and delivery efficacy[606,607].

Fusogenic liposomes are another type of lipid-based nanoparticle that show promise against bacterial and biofilm-associated infections. Instead of primarily relying on surface charge to promote interaction with bacterial membranes, increasing the likelihood of endocytosis of the nanoparticle, fusogenic liposomes mainly depend on a fluid lipid membrane that can destabilise and fuse directly with nearby biological membranes[472,600]. This typically involves liposome membranes containing an asymmetric or short-chained lipid, such as phosphoethanolamine (PE) or cholesteryl hemisuccinate (CHEMS), and/or lacking cholesterol, producing a less rigid and more fluid membrane[456,459,472]. For anti-biofilm applications, it has been observed that fusogenic liposomes specifically destabilise the bacterial outer membrane and promote bacterial aggregation, therefore compromising biofilm structure and cell integrity[373,459]. This has worked to increase antibiotic efficacy: vancomycin (VAN)-encapsulated fusogenic liposomes were better able to penetrate *S. aureus* biofilms[460] and even seemingly restore antibacterial activity of VAN against Gram-negative *P. aeruginosa* and *A. baumannii*[591]. In both studies, a formulation containing DOPE, DPPC and CHEMS lipids in a 4:2:4 molar ratio was used, where DOPE contributes to the fusogenic property due to its inverted conical shape (**Figure 21A**). This structure makes it prone to forming lipid layers of negative curvature, which destabilises lamellar (L_α) membrane structures to transition into the inverted hexagonal (H_{II}) phase, promoting membrane fusion (**Figure 21B**)[608–610]. This phase transition is often triggered by an acidic environment, as found in a bacterial biofilm, leading to destabilisation of the liposomal and bacterial lipid bilayers, and cargo release. The anionic helper lipid CHEMS is also pH-sensitive and can induce the phase transition as a result of protonation in an acidic environment, enhancing fusogenicity[611].

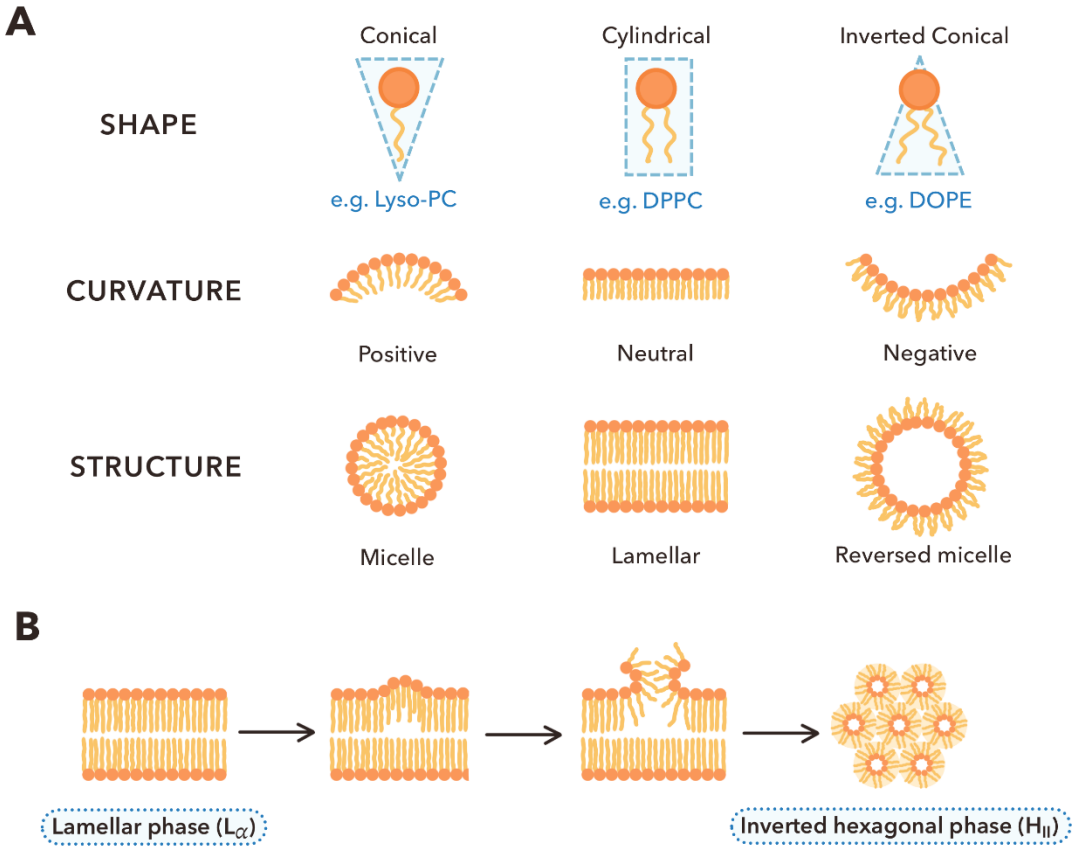


Figure 21 | Molecular packing and phases of lipid membranes. (**A**) Three types of lipid molecular shapes and the corresponding membrane curvature and structures, with examples. (**B**) Schematic of the proposed lamellar-to-inverted hexagonal ($L_\alpha \rightarrow H_{II}$) phase transition mechanism. Triggers, such as water penetration or an acidic environment, can induce packing stress and membrane instability that initiates the phase transition[612-614].

One of the most widely used and well-documented methods of liposome production is the thin-film hydration method, which involves dispersing lipids in a solvent and evaporating this solvent to form a thin lipid film[397,398]. This thin film is then hydrated in an aqueous buffer which results in the production of a suspension containing different sizes and lamellarities of liposomes. Thin-film hydration is a very simple and efficient manufacturing method to carry out in small batches, as would be the case in most laboratory settings, and can be used with different lipid combinations and concentrations[401]. As such, it is a popular manufacturing method in early formulation stages and a good choice for this project. However, this technique has poor scalability due to the large amounts of organic solvent needed as well as inefficient hydration and mixing at such large scales, contributing to batch variability. It also relies on passive drug loading which can result in low drug

encapsulation efficiencies, particularly for hydrophilic drugs[615]. Optional extrusion or sonication techniques can be used to reduce liposome size and produce unilamellar vesicles as well as improve drug encapsulation. Other liposome production methods, such as reverse phase evaporation, provide a high encapsulation efficiency but have their own limitations, namely difficulties with complete elimination of organic solvent and drug exposure to organic solvent and sonication protocols (see section **1.4.3.1**). This highlights how the manufacturing method needs to be carefully considered as part of the formulation process.

The choice of drug also matters in liposomal formulations; not only should it be appropriate for the intended clinical outcome, but it should also have properties that are compatible with the liposome production process. Nitrofurantoin (NIF) is currently the first-line treatment for UTIs as it is one of the few antibiotics that are still effective against most Gram-positive and Gram-negative uropathogens[258]. NIF is a nitrofuran antibiotic, containing a furan ring linked to a nitro group (see **Figure 11**). After NIF activation via reduction of the nitro group, the reactive intermediates bind to and disrupt bacterial ribosomes and enzymes, interfering with DNA and cell wall synthesis, as well as other metabolic pathways[258,262]. In addition to its broad-spectrum activity, NIF also readily accumulates in urine allowing for significant concentrations in the bladder, hence its use against infections of the lower urinary tract[262]. NIF is also frequently used as a prophylactic, with long-term low-doses administered to individuals with chronic and recurrent UTIs[237,264]. Unfortunately, long-term use has been linked to eventual pulmonary toxicity and hepatic injury[264–266]. It has also been reported that sub-lethal concentrations of NIF in some cases do not affect bacterial growth rate and can in fact induce denser biofilm formation, which could partially be contributing to recurrence of infection[267–269]. Therefore, there is a balance to be struck between concentrations of NIF that are high enough to clear infection but low enough to be safe for longer-term use. If high enough doses of NIF could be delivered directly to bacterial cells within biofilms in a system that shields the drug from host cells, there is potential for infections to be more completely cleared over a shorter treatment course, reducing the rate of recurrence. This would

also reduce the risk of side effects, as there is less interaction between NIF and host cells, and possibly also reduce the risk of drug-resistance development. As such, liposomal encapsulation of NIF is a promising option to capitalise on the benefits while reducing the risks.

There are currently no reports of NIF-loaded liposomes in the literature, despite intravesical liposomes being studied for therapeutic effects in the bladder and liposomal antibiotics showing encouraging results in the context of AMR[434,435,616,617]. Many clinically-approved liposomal formulations encapsulate a hydrophilic drug, e.g. doxorubicin in DOXIL® and amikacin in Arikayce®, but due to its chemical structure and composition, NIF is only slightly water soluble and has greatest solubility in dimethylformamide (DMF) or dimethyl sulfoxide (DMSO). This would make it difficult to load NIF into the aqueous compartment of a liposome[618]. Theoretically, hydrophobic NIF should be able to incorporate into the lipid membrane of a liposome[619]. However, it is also almost insoluble in chloroform—a common solvent used in thin-film hydration—which reduces its compatibility with this process. Fortunately, the sodium salt form of the drug (i.e. nitrofurantoin sodium), normally used intravenously, has an increased water solubility that would allow for drug loading into the aqueous liposome core to produce liposomes that resemble clinically successful formulations.

In this chapter, I used the thin-film hydration method to manufacture cationic and fusogenic liposomes and monitored their size and surface charge over time, as an indication of formulation stability and suitability for downstream experiments and applications. I then optimised a protocol for passive loading of these formulations with NIF and VAN. Although VAN is not typically recommended for use against UTIs, particularly ones caused by Gram-negative bacteria, it has previously been shown that VAN-loaded liposomal formulations are able to penetrate bacterial biofilms and even restore activity against some Gram-negative species[449,460]. Additionally, a recent case has been documented showing that intravesicular administration of vancomycin was successfully used to treat cystitis and bladder stones[620]. NIF encapsulation within liposomes has

not previously been reported, but I hypothesised that loading of NIF into liposomes for drug delivery has the potential to provide greater UTI clearance and reduce side effects. Therefore, I loaded liposomes with VAN based on existing findings and used the knowledge acquired throughout this process for encapsulation of NIF within liposomes. I also created formulations containing lipid dyes for future microscopy-based visualisation studies of these liposomes. Lastly, a drug release assay for the VAN-loaded cationic formulation was performed to confirm drug-loaded liposome integrity over time at temperatures reflective of storage or physiological conditions.

2.2 Materials and Methods

2.2.1 Materials

Cholesteryl hemisuccinate (CHEMS), 1,2-dioleoyl-sn-glycero-3-phosphoethanolamine (DOPE), 1,2-dioleoyl-3-trimethylammonium-propane (DOTAP), and 1,2-dipalmitoyl-sn-glycero-3-phosphocholine (DPPC) were purchased from Avanti Polar Lipids USA. L-α-phosphatidylcholine (PC, soybean), cholesterol and 10X phosphate-buffered saline (PBS) stock solution were purchased from Merck Life Sciences, UK. 1,2-dioleoyl-sn-glycero-3-phosphoethanolamine-N-[maleimide(polyethylene glycol)-5000] (DOPE-PEG5000-Maleimide) was purchased from BroadPharm, USA.

Vancomycin hydrochloride (VAN), nitrofurantoin sodium (NIF) and 3,3´-dioctadecyloxacarbocyanine (DiO) were purchased from Cambridge Bioscience, UK. 1,1'-Dioctadecyl-3,3,3',3'-Tetramethylindodicarbocyanine, 4-Chlorobenzenesulfonate Salt (DiD) was purchased from Thermo Fisher Scientific, UK. Chloroform, methanol, UltraPure™ DNase/RNase-free distilled water and other solvents were of analytical grade (Thermo Fisher Scientific, UK).

Millipore Amicon® Ultra-0.5 100 kDa centrifugal filter units were purchased from Merck Life Sciences, UK. Folded capillary zeta cells (DTS1070) were obtained from Malvern Panalytical, UK. Polycarbonate extruder membranes with pore size of 100 nm and 200 nm (diameter of 19 mm) were purchased from Avanti Polar Lipids, USA. Polycarbonate extruder membranes with pore size of 100 nm and diameter of 25 mm were purchased from Genizer, USA.

2.2.2 Liposome production

Liposomes were produced using the thin-film hydration method, similar to the process described by Zhang (2017)[398] and illustrated in **Figure 22**. Lipids were dissolved in a 1:1 mixture of methanol and chloroform in a round-bottom flask. Rotary evaporation was used to remove the bulk of organic solvent, which resulted in the formation of a thin lipid film. The lipid film was then kept under vacuum overnight to remove any residual solvent. 0.1X PBS was used to rehydrate the lipid film. For drug-loaded liposomes, drug was first dissolved in the 0.1X PBS before being used for rehydration. A suspension of multilamellar vesicles (MLVs) was produced after brief vortexing for 30 s and subsequent spinning for one hour at a temperature above the lipid phase transition temperature (information for each formulation is provided in **Table 1**). After being filtered through a 0.45 μm PFTE syringe filter (Thermo Fisher Scientific, UK), the MLVs were immediately extruded, either manually using an Avanti Research™ Mini-Extruder or semi-automatically using a Microfluidics™ LV1 Microfluidizer Homogeniser, to make near-unilamellar vesicles with a final average size of approximately 100 nm.

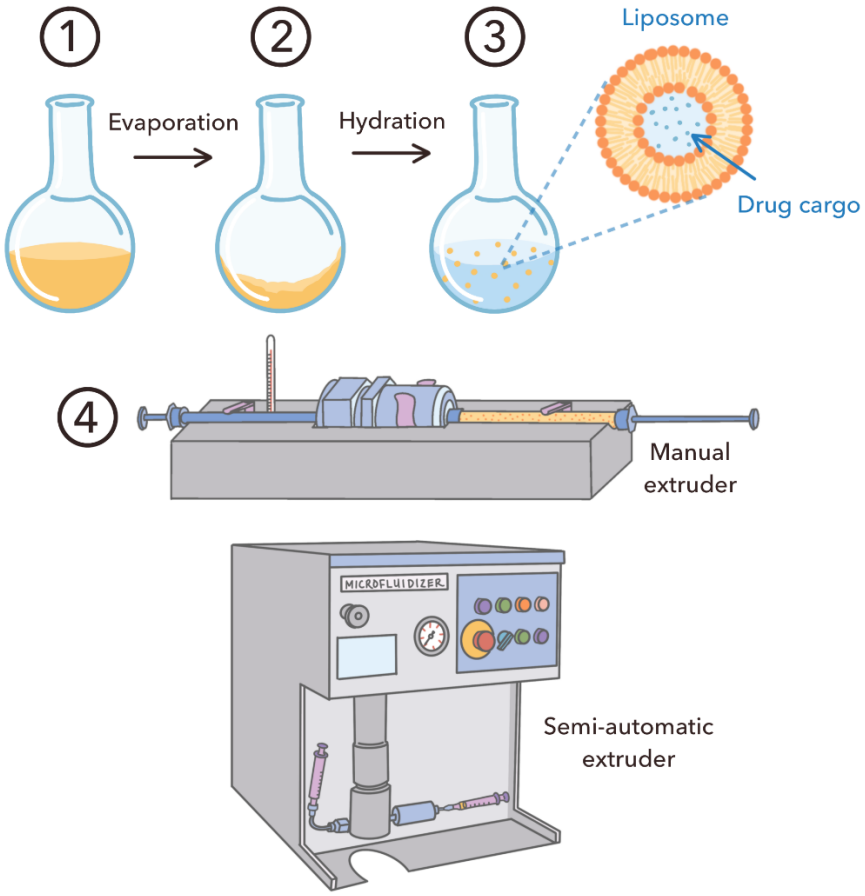


Figure 22 | Schematic of liposome production process. (1) Lipids are dispersed in organic solvent. (2) The solvent is evaporated to form a dry, thin lipid film. (3) The lipid film is rehydrated in aqueous buffer. (4) The liposomes are extruded, either manually or semi-automatically.

Table 1 | Liposome formulations tested. The molar ratios of the constituent lipids are detailed, and the total lipid concentration for each formulation. The transition temperature refers to the transition temperature of the constituent lipid with the highest transition temperature for each formulation.

Formulation	Lipids (Molar Ratio)	Total Lipid Concentration (mg/mL)	Transition Temperature (°C)
Fuso-1	DOPE/DPPC/CHEMS (4:2:4)	15	41
Fuso-1 (DiO or DiD)	DOPE/DPPC/CHEMS/DiO or DiD (4:2:4:0.1)	15	41
Fuso-1-PEG	DOPE/DPPC/CHEMS/ DOPE-PEG5000-Maleimide (7:4:8:1)	15	41
Fuso-1-PEG (DiO or DiD)	DOPE/DPPC/CHEMS/ DOPE-PEG5000-Maleimide/DiO or DiD (7:4:8:1:0.1)	15	41
Fuso-2	DOPE/DOTAP (1:1)	3	< 5
Cat-3	DOTAP/Cholesterol (1:1)	3	-16
Fuso-6	DOPE/DPPC/DOTAP (2:1:2)	3	41
Cat-7	DOTAP/DPPC/Cholesterol (2:1:2)	3	41
Cat-7.1	DOTAP/DPPC/Cholesterol (2.5:1:1.5)	3	41
Cat-7.2	DOTAP/DPPC/Cholesterol (3:1:2)	3	41
Cat-8	PC/Cholesterol/DOTAP (3:4:3)	15	< 5
Cat-8 (DiO or DiD)	PC/Cholesterol/DOTAP/DiO or DiD (3:4:3:0.1)	15	< 5

2.2.3 Liposome characterisation

Average liposome diameter, size distribution (quantified as polydispersity index, PDI) and zeta potential were determined using a Zetasizer (Malvern Instruments, UK). A sample of the final liposome suspension was diluted 1:10 (v/v) in 0.1X PBS and injected into a DTS1070 folded capillary cell (Malvern Instruments, UK) for dynamic light scattering (DLS) measurements. Three measurements were taken for each sample (three samples total), with a 60 s delay between each zeta potential measurement. The minimum number of runs per measurement was 10 and the maximum was 100.

Average liposome concentration was determined using the Corning® Videodrop. The liposomes were diluted up to 2000 times in 0.1X PBS to track between 20 and 50 particles per frame, with a total of at least 300 particles tracked across a maximum of 10 videos per sample. Three measurements were taken for each sample (three samples total).

2.2.4 Encapsulation efficiency (EE)

EE was determined by separating the suspension into liposomal and free drug fractions using ultrafiltration (**Figure 23** and **Supplementary Figure 3**): 100 kDa 500 μL Amicon® filters were filled with liposome suspension and spun for 30 min at 10,000 ×g (Eppendorf Centrifuge 5418 R; Thermo Scientific™ Sorvall™ Legend™ Micro 21 Microcentrifuge). The filters containing the retained liposomes were washed out with 0.1X PBS to make it back up to the original volume and stored at 2-5°C as the final purified liposome suspension. The flowthrough was collected as the free drug fraction. VAN (absorbance at 282 nm) and NIF (absorbance at 381 nm) were detected by UV-Visible spectroscopy (Shimadzu UV-Vis-NIR Spectrophotomer; Implen NanoPhotometer® NP80). The concentration of the free drug fraction and the concentration of the original rehydration stock (which represented total drug concentration) were determined using a calibration curve (**Supplementary Figure 1**). EE was then calculated as follows:

$$\mathbf{EE\ (\%) = \frac{mass_{total} - mass_{free}}{mass_{total}} \times 100} \qquad \textbf{(Eq. 1)}$$

where $\mathbf{mass_{free}}$ refers to the free drug in solution outside the liposomes and $\mathbf{mass_{total}}$ is the sum of the drug present inside and outside of the liposomes.

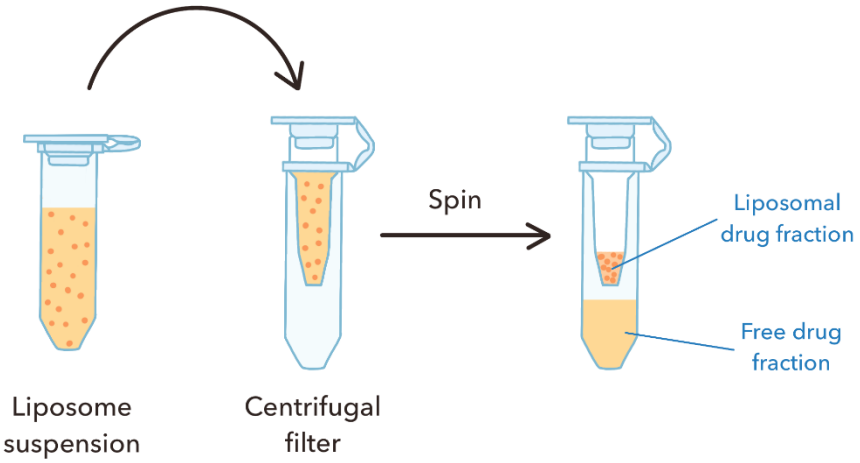


Figure 23 | Schematic of the ultrafiltration process. Liposome suspension is inserted into an Amicon® filter and spun to separate the suspension into a solution of free drug and a fraction containing liposomes with encapsulated drug.

2.2.5 Drug release assays on vancomycin-loaded liposomes

These experiments were performed by Maria Nunez Barrios (under my supervision) as part of the MS Taught Course of Pharmacology at the University of Oxford, contributing to this project. A dialysis system was set up using Slide-A-Lyzer G3 Dialysis Cassettes (Thermo Fisher Scientific, USA), with a molecular weight cut-off of 20 kDa, and used as per the manufacturer's instructions. Briefly, each dialysis cassette was hydrated for 2 min in the dialysis buffer (0.1X PBS) before use. After hydration, 3 mL of sample were loaded into the chamber and gently pressed before closing to remove excess air. Drug release was evaluated at pH 7.4 for 4 h at two different temperatures: either 4°C to simulate liposome storage conditions, or 37 °C to mimic physiological conditions that are more relevant to liposome administration. The setup was protected from light while the assay was running. Samples were taken from the dialysis buffer every hour for analysis, using the sample at 0 h as a blank for drug quantification. VAN (absorbance at 282 nm) was detected by

UV-Visible spectroscopy (Implen NanoPhotometer® NP80) and a calibration curve used to determine the corresponding concentration. Drug release (%) was calculated as follows

$$\textbf{drug release (\%)} = \frac{\textbf{concentration}_{t=x} - \textbf{concentration}_{t=0}}{\textbf{concentration}_{total}} \times 100 \qquad \textbf{(Eq. 2)}$$

where $\textbf{concentration}_{t=x}$ is the mean concentration of drug at a given timepoint, $\textbf{concentration}_{t=0}$ is the mean concentration of drug at the beginning of the experiment (0 h), and $\textbf{concentration}_{total}$ is the total concentration of the encapsulated drug as calculated from prior encapsulation efficiency experiments.

2.2.6 Statistical analyses

Data were visualised using GraphPad Prism 9 (version 9.4.1). This software was also used to perform mixed model analysis of variance (ANOVA) and repeated measures one-way ANOVA tests. The standard p-value cut-off (≤ 0.05) was used to determine statistical significance.

2.3 Results and Discussion

2.3.1 Formulation of cationic and fusogenic liposomes

Cationic (Cat-#) and fusogenic (Fuso-#) liposomes listed in **Table 1** were formed by thin-film hydration followed by extrusion, as described in section **2.2.2**. DOTAP was included in the cationic formulations due to its widely documented use as a cationic lipid in liposome formulations[603–605]. It is also typically accompanied by helper lipids, such as cholesterol, DPPC and DOPC, hence why cholesterol and DPPC were also used in all of the tested formulations[606,607]. For the fusogenic liposomes, DOPE was included in the formulation due to its reported membrane-fusing property, along with helper lipids like DPPC and CHEMS[373,621].

The tested formulations were based on ones found in the literature and adapted with an informed trial-and-error approach: Fuso-1 was based on a formulation reported by Nicolosi *et al.* (2010)[449], with Fuso-1-PEG being a novel variation of this formulation; Fuso-6 was also a variation of Fuso-1, with CHEMS replaced with DOTAP, as DOTAP has also been frequently used in fusogenic formulations[622]; Fuso-2 was based on a fusogenic formulation characterised by Cavalcanti *et al.* (2022)[623]; Cat-3 was based on a commercial cationic liposome formulation (GEN-7001 by Merck Life Science, UK); Cat-7, Cat-7.1, Cat-7.2 and Cat-8 were novel variations of Cat-3, where an additional helper lipid, DPPC or PC, was added to assess the impact on the formulation stability.

The ideal liposome diameter for these experiments was considered to be ~100 nm, as liposomes in the range of 20 to 400 nm in diameter can mimic bacterial extracellular vesicles, potentially encouraging effective uptake into cells, as well as being an appropriate size to evade the immune system and favour cellular uptake[396,624]. Additionally, liposomes within this size range have been reported in the literature to be used for antibacterial purposes[449,625–627]. The average size (diameter), zeta potential and polydispersity index (PDI) of the resulting liposomes were determined using DLS and these measurements were used to choose suitable formulations for subsequent steps of the project.

In order to deem a formulation suitable, it was evaluated whether the liposomes were able to maintain their average diameter and surface charge over time, as an indication of their storage stability. Thus, DLS measurements of formulations kept at 4°C were monitored over a period of seven days (**Figure 24** and **Table 2**). This time-frame was chosen as subsequent experiments involving these liposomes (e.g. microbiological assays) could last up to seven days and it was necessary to be confident that liposome integrity could be maintained for that period.

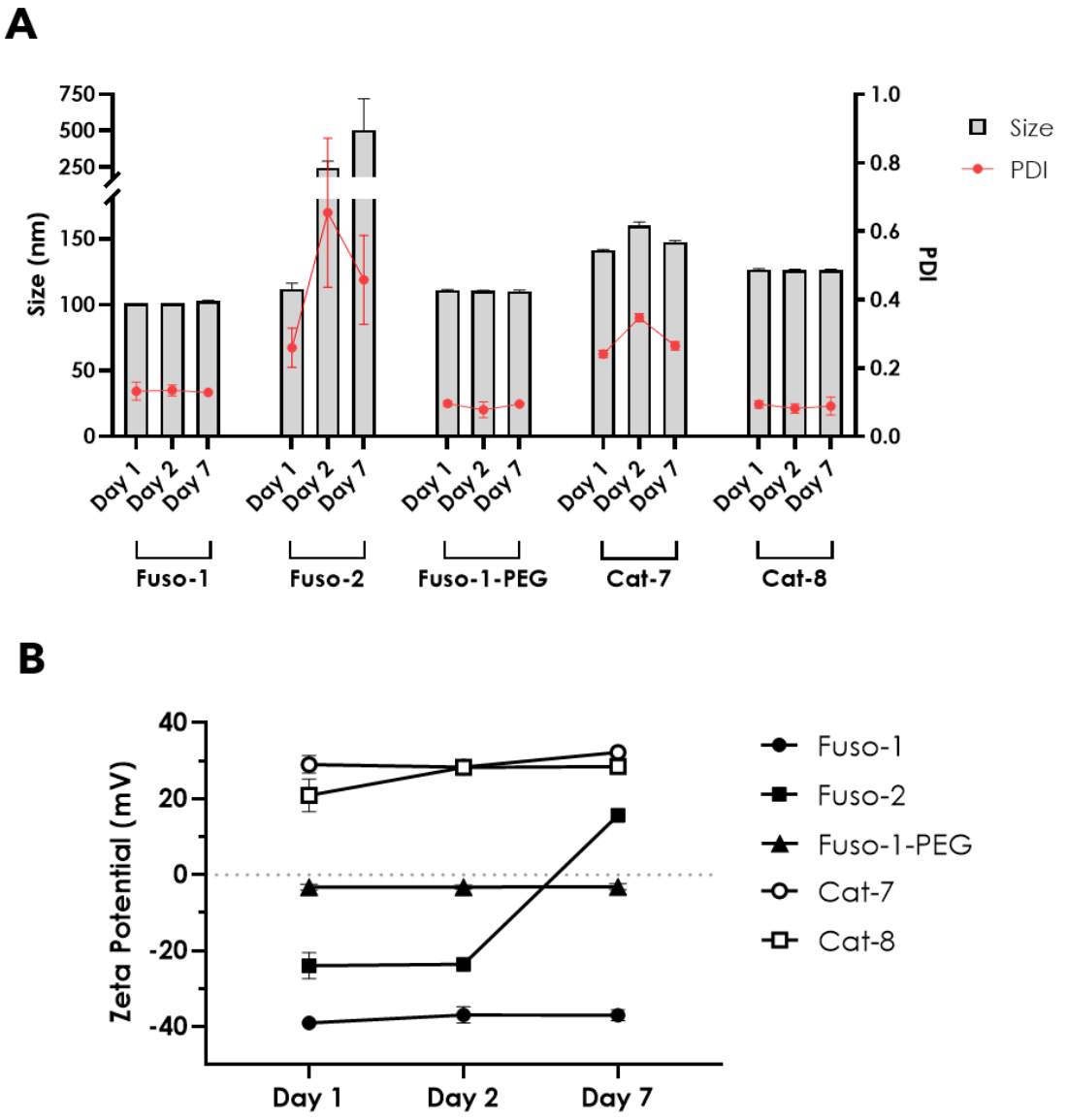


Figure 24 | Storage stability of liposome formulations over seven days. Fuso-1, Fuso-2, Fuso-1-PEG, Cat-7 and Cat-8 liposome properties over a period of seven days. (A) Average liposome size is shown as grey bars and corresponding PDI values as red circles. (B) Average zeta potential values measured at pH 7.4. The five formulations shown here were the ones that were able to be measured by DLS at days 1, 2 and 7; the others gave suspensions unsuitable for DLS measurements so are not shown. Data represents the average of three repeats.

Fuso-1 had an average diameter of 102 ± 1.36 nm and an average zeta potential of -37.8 ± 2.13 mV. This negative charge is as expected due to the presence of CHEMS within the formulation, that also acts to stabilise the fusogenic DOPE lipid as a helper lipid[611,628]. Unfortunately, a year into this project and after a transfer of institution, Fuso-1 liposomes could no longer be produced; the rehydration step was repeatedly unsuccessful (**Supplementary Figure 2**). This could possibly be due to changes in manufacturers and suppliers as a result of transferring experiments between institutions. Therefore, a PEGylated DOPE lipid was introduced into the formulation to stabilise the liposomes in suspension (as well as provide the means for future conjugation experiments), hence, the introduction of the 'Fuso-1-PEG' formulation. Fuso-1-PEG had an average size of 111 ± 0.46 nm and zeta potential of -3.05 ± 0.57 mV. The slight increase in diameter could be due to the introduction of PEG(5000) chains into the formulation. This high molecular weight of PEG was used to encourage an extended 'brush' conformation, making it theoretically more likely for the attached end group (i.e. the maleimide functional group) to be available for subsequent conjugation[375,376]. Despite the relatively neutral zeta potential meaning less repulsive force between the nanoparticles, the liposomes remained dispersed in a suspension that maintained a similar average size and zeta potential over seven days. This is likely due to the presence of PEGylated lipids that are known to have a stabilising effect that reduces nanoparticle aggregation through creating a hydrophilic steric barrier[377,629,630]. Unfortunately, inclusion of PEG in formulations can also work to obstruct target membrane interactions and hinder cellular uptake and endosomal escape[376,379,380]. However, adding PEG allowed for a formulation stable in size and zeta potential where a non-PEGylated version could not be formed. Fuso-1-PEG was thus chosen for subsequent experiments due to the observed time profiles of size and zeta potential of this formulation.

Fuso-2 started with an average diameter of 112 ± 4.33 nm post-production and had a zeta potential of -24 ± 3.42 mV. However, after one day, it more than doubled in mean size, suggesting that the nanoparticles were not stable in the suspension. The lack of a stabilising lipid, such as cholesterol,

may explain why the particles seemed to have aggregated rapidly on day two to form a suspension with a high size dispersity (PDI = 0.65), despite the negative surface charge (-23.60 mV) providing a repulsive force. Additionally, Fuso-2 did not maintain a negative surface charge over the seven-day period; it increased significantly to +15.6 ± 1.04 mV at the same pH. Therefore, Fuso-2 was not chosen as a suitable fusogenic liposome formulation. Although Cat-7 had a stable zeta potential of ~30 mV and a satisfactory size (151 ± 10.70 nm), the PDI increased from 0.24 to 0.35 in a single day, above the generally acceptable threshold of 0.3. Therefore, Cat-7 was also not taken forward as a successful formulation.

Cat-8 had an average size of 126 ± 0.73 nm and zeta potential of +24.6 ± 4.89 mV at neutral pH across the seven days. This positive surface charge is as expected for a formulation that includes the cationic lipid DOTAP[606]. Overall, this formulation showed acceptable stability over the seven-day period and was chosen for subsequent experiments.

It is also of note that most of the formulations showed remarkable reproducibility between batches as evidenced by the relatively small standard deviations in average size, PDI and zeta potential. This could be due to the same optimised protocol, reagent batches and measurement equipment being used for the duration of this experiment. These variables may be important to consider for potential scale-up of production of these formulations, where batch reproducibility will have an influence on drug release kinetics, downstream cellular interactions and approval by regulatory bodies.

Out of nine tested formulations (three fusogenic and five cationic), one of each type was consistently stable for at least one week; therefore, Cat-8 and Fuso-1-PEG were taken forward for comparison in subsequent experiments.

Table 2 | Average size, PDI and zeta potential of tested unloaded formulations. Data shown are averages over a seven-day period. The size refers to nanoparticle hydrodynamic diameter. Zeta potentials were measured at pH 7.4.

Formulation	Average size (nm)	Average PDI	Average zeta potential (mV)
Fuso-1	102 ± 1.36	0.13 ± 0.01	-37.80 ± 2.13
Fuso-1-PEG	110 ± 1.10	0.09 ± 0.01	-3.05 ± 0.57
Fuso-2	288 ± 205.00	0.46 ± 0.22	-7.93 ± 18.30
Cat-3	632 ± 308.00	0.61 ± 0.23	+0.50 ± 5.24
Fuso-6	> 1000	0.83 ± 0.07	+21.00 ± 3.38
Cat-7	151 ± 10.70	0.29 ± 0.06	+28.70 ± 1.49
Cat-7.1	162 ± 3.87	0.49 ± 0.08	+26.60 ± 0.70
Cat-7.2	339 ± 17.50	1.55 ± 0.06	+26.10 ± 0.38
Cat-8	126 ± 0.73	0.09 ± 0.01	+24.60 ± 4.89

2.3.2 Loading and labelling of liposome formulations

The selected liposome formulations were then passively loaded with VAN or NIF. VAN was selected as a model drug because it can be loaded into the aqueous core of the liposome and has been successfully loaded into fusogenic liposomes to increase antibacterial effects against Gram-negative strains[449,460]. NIF was also chosen as it is the first-line medication given to UTI patients, as previously mentioned. The high solubility of the sodium salt form in aqueous solvent allowed the NIF-loaded liposomes to be produced in the same way as the VAN-loaded liposomes. The encapsulation efficiencies (EEs) of both formulations with both drugs are shown in **Table 3**.

NIF appears to be more readily encapsulated within the two liposome formulations than VAN; NIF-loaded formulations together had an average of 63% EE compared to 39% EE for VAN-

loaded liposomes. This could be due to the increased lipophilicity that NIF has compared to VAN, which allows NIF to favourably interact with the lipid bilayer in addition to the aqueous compartment. It has been reported that NIF can incorporate into lipid monolayers, affecting the packing of the phospholipids[619,631], which may explain this observation.

The liposomes were rehydrated with 8 mg/mL VAN or 4 mg/mL NIF, resulting in an average of 3 mg/mL VAN or 2.5 mg/ml NIF successfully loaded within the liposome fraction.

Prior to this, freeze-thaw methods of loading were used which gave very low EE of ~3% (methods described in section **6.1.3**).

Table 3 | Average encapsulation efficiency of the formulations for each drug evaluated.

Formulation	Drug loaded	Encapsulation Efficiency (%)
Cat-8	VAN	45 ± 3
	NIF	64 ± 19
Fuso-1-PEG	VAN	33 ± 4
	NIF	61 ± 14

DiO and DiD were chosen as the fluorescent labels as they both can be incorporated into the lipid shell of liposomes and have minimal overlap between their excitation/emission spectra: 484/501 nm for DiO and 646/668 nm for DiD. The successful incorporation of the dye was assessed using UV-Vis after the liposome fraction had been separated from the free drug fraction. For example, **Figure 25** shows the presence of both VAN and DiO within the retained liposome fraction. In the free drug (flowthrough) fraction, unencapsulated VAN was detected but no DiO was detected. This is likely due to the fact that DiO is lipophilic and so was kept within the lipid membranes of the liposomes that were retained, whereas VAN is hydrophilic and any unencapsulated drug was filtered out into the flowthrough fraction.

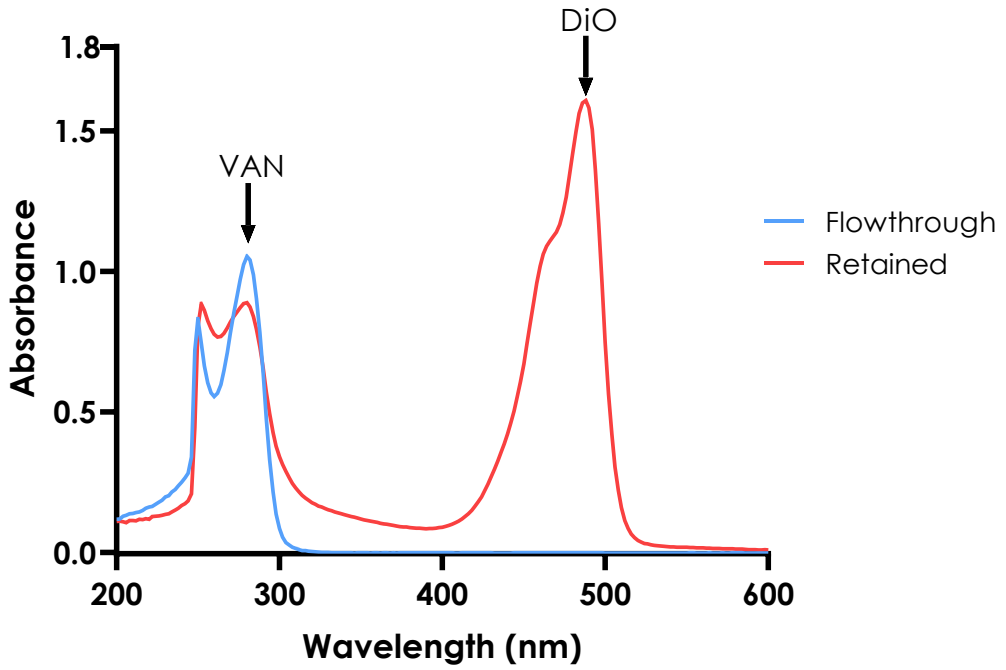


Figure 25 | Representative absorbance spectrum showing the presence of VAN and DiO in (fusogenic) liposome formulation. After separation of the liposome suspension using ultrafiltration, the flowthrough (blue) and retained (red) fractions were analysed using UV-Vis to determine their contents. VAN has max absorbance at 282 nm, DiO at 484 nm. A similar spectrum of DiD-labelled liposomes was obtained but is not shown here.

2.3.3 Long-term stability of VAN-loaded cationic liposomes

As liposomes tend to degrade over time, it is important to assess their long-term shelf life for potential storage and transportation purposes in the future. Refrigeration and protection from light are recommended to prevent lipid hydrolysis and degradation[632]. Aliquots of a Cat-8-VAN batch were stored at 4°C and protected from light for a period of 120 days, with samples taken on days 1, 30, 60 and 120. The size, PDI and surface charge were measured using DLS (**Figure 26**). The size and zeta potential remained consistent across the 120 days, with an average diameter of 116.3 ± 1.9 nm and positive surface charge of +63.4 ± 6.2 mV. The size of Cat-8-VAN did not differ much from its unloaded counterpart (average diameter of 126 nm); however, it seemed as though loading of VAN greatly increased the zeta potential of the suspension (from +24.6 mV to +63.4 mV). This could be because VAN has a net positive charge at physiological pH (7.4) and VAN present outside of the liposome contributes to the positive zeta potential value[633]. The PDI was also consistently below the generally acceptable threshold of 0.3, with an average of 0.167 ± 0.013.

Although there was no statistically significant difference in size (p=0.055), PDI (p=0.1275) or zeta potential (p=0.1433) over the 120 days, this assay was performed on aliquots from a single liposome preparation. Therefore, this could explain the minimal variation (standard deviation) of the different properties measured and this experiment should be repeated with more Cat-8-VAN batches to allow a confident conclusion to be made. From the high reproducibility observed in previous experiments, it is possible that repeats would confirm no significant difference between liposome batches. In addition to repeating this assay with more batches, repeat experiments with NIF-loaded, fusogenic and unloaded liposomes should also be carried out to determine whether this trend is consistent across formulations and provide a more robust comparison between drug-loaded and unloaded liposomes. Subsequent experiments with all drug-loaded liposomes were carried out on the assumption that the formulations were physically stable in the short-term (<7 days), based on observations from sections **2.3.1** and **2.3.3**.

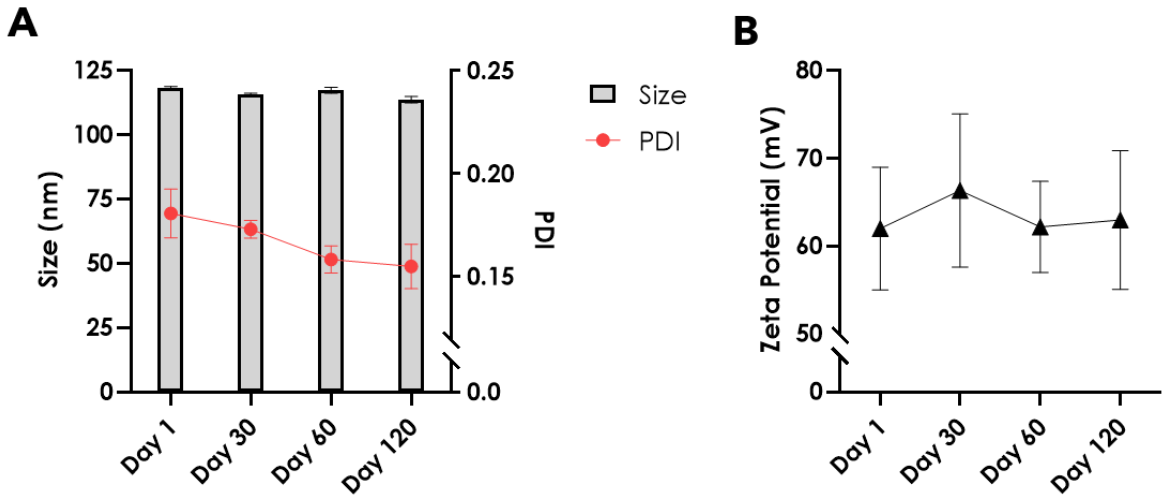


Figure 26 | Storage stability of Cat-8-VAN over 120 days. (A) Size and PDI, and (B) zeta potential of Cat-8-VAN over 120 days. Average liposome size (diameter) is shown as grey bars and corresponding PDI values as red circles. Average zeta potential values measured at pH 7.4. Repeated measures one-way ANOVA tests were performed and showed no significant difference in size (p=0.055), PDI (p=0.1275) or zeta potential (p=0.1433) over the 120 days.

2.3.4 Passive drug release from VAN-loaded cationic liposomes

A drug release assay was performed to determine the extent of drug leakage from the liposome formulation over time. To evaluate this, a dialysis system was set up as described in section **2.2.5** where the extent of drug release from VAN-loaded Cat-8 liposomes (Cat-8-VAN) was assessed over four hours, at either 4°C or 37°C to reflect storage or physiological conditions, respectively. A four-hour window was chosen for these experiments as the intended clinical application of these liposomes involves their administration with conjugated microbubbles (MBs), which have a relatively short circulation half-life (<5 min)[634,635]. Additionally, with the focus being on UTI treatment, intravesicular (bladder) instillations of antibiotics that are currently practiced are typically retained in the bladder for 1-2 hours[636,637]. Therefore, it is likely that patient exposure to the formulation would not exceed the chosen four-hour experimental window.

There was an increase in % drug release over time at both temperatures tested (**Figure 27**); a mixed model ANOVA showed that there was a statistically significant difference between the mean drug release over the different time points ($p=0.0023$). In order to calculate Cat-8-VAN EE, the liposomal suspension was purified using ultrafiltration, removing excess VAN that was not encapsulated. This reduces the likelihood of % drug release increases being due to unencapsulated drug diffusing across the dialysis membrane. The results indicate that there is notable passive leakage of VAN from Cat-8-VAN over the tested time period at both temperatures. However, this finding is not necessarily unexpected; Scriboni *et al.* observed ~45% VAN release from cationic liposomes at 4 hours and González Gómez *et al.* observed 55% VAN release from neutral liposomes within 12 hours[428,460]. This experiment is not directly comparable as different liposome formulations and dialysis conditions were used, but highlights how passive leakage of Cat-8-VAN could potentially follow the same release model as what is reported in the literature. As mentioned previously, the likely treatment exposure time would be relatively short (<2 hours), which would mean that the liposomes would not have ample time to release the majority of their content during treatment; only 14% of VAN was released after two hours at 37°C. Due to the nature of

encapsulation, this is to be expected; not only can VAN be protected from the external environment, it also has a reduced ability to interact directly with bacteria as it would first need to cross the liposome membrane. Administering these liposomes together with MBs could facilitate further drug release in a shorter period of time via ultrasound-induced MB cavitation, an effect that has been previously documented[638]. As such, conjugation of liposomes to MBs can address the concern of relatively slow passive drug release from the liposomes within the intended therapeutic application, whilst utilising the protective and targeting benefits of liposomal encapsulation.

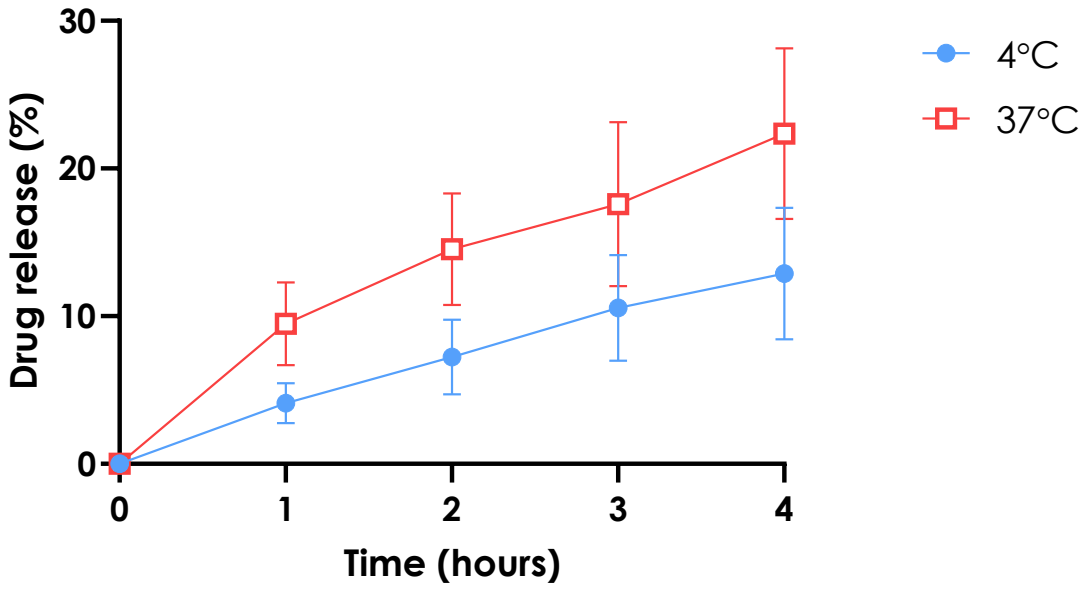


Figure 27 | Drug release (%) of vancomycin from cationic liposomes over time at 4°C and 37°C. The mean values of three independent repeats for each temperature ± the corresponding standard deviation are shown. A mixed model ANOVA was performed to compare % drug release at 4 °C and 37 °C. Temperature was found to have no statistically significant effect on drug release (p=0.1365).

At 4°C, 12% drug release was observed after four hours, and at 37°C, 22% of encapsulated drug had been released. Despite average % drug release at 37°C being around twice as high as at 4°C, there was overall no statistically significant difference between the two temperatures (p=0.1365). It appears as though the rate of drug release is increased at 37°C (particularly within the first two hours), which is to be expected as a higher temperature correlates with a higher molecular diffusion

rate. However, this doesn't necessarily indicate that the liposome membranes became destabilised at higher temperatures; the passive leakage may be the same at both 4°C and 37°C but the increased diffusion rate at 37°C means that a larger quantity of VAN is detected sooner. Therefore, a longer assay (24 hours or longer) would be useful in determining whether temperature has a true effect on liposome stability. If the liposomes were to reach the same plateau in % drug release, but the liposomes at 37°C reached it sooner, it would be likely that liposome membrane integrity is not affected and the higher temperature is what is affecting diffusion kinetics. A free drug sample and an unloaded liposome sample should also be added to this assay as positive and negative controls, respectively. A concentration-matched free VAN sample can be used to evaluate how much temperature contributes to the rate of drug release, and may allow for better assessment of liposome membrane behaviour in the context of drug release. Additionally, it would be useful to know how drug release differs between Fuso-1-PEG and Cat-8 but also between VAN and NIF. Therefore, these experiments should be repeated with the two different formulations and two antibiotics in the future to give insights into how antibiotics can influence liposome formulation choices.

2.4 Conclusions

UTIs are a significant global healthcare concern and economic burden, made worse by the relatively high recurrence of these infections. Most of the first-line therapies involve orally or intravenously administered antibiotics or combinations of antibiotics, some of which may cause serious side effects as a result of prolonged use. Drug delivery systems, such as liposomes, show potential in targeted doses that reduce side effects and protect from premature degradation, increasing antibiotic efficacy. Some formulations, such as fusogenic liposomes, also hold promise for enhanced bacterial targeting though direct membrane fusion with particular benefits in biofilm contexts.

This chapter focussed on establishing liposome formulations and characterising them, specifically assessing their size, surface charge, encapsulation efficiency and drug release profiles. The overall aim was to select candidate liposomes that were able to maintain their physical properties over time, can be passively loaded with VAN and NIF, and have a drug release profile comparable to that in the literature.

Cationic and fusogenic liposomes were formulated and selected for subsequent experiments based on their physical stability—Cat-8 and Fuso-1-PEG were the two formulations taken forward as they showed stable average size (126 nm and 111 nm, respectively) and zeta potential (+24.6 mV and -3.05 mV, respectively) over a period of seven days. Two different types of liposomes were formulated due to the proposed difference in the mechanism of delivery; cationic liposomes are thought to primarily enter a bacterial cell via the endocytic pathway, whereas fusogenic liposomes are thought to fuse directly with nearby membranes due to the presence of DOPE lipid. Both of these formulations were successfully loaded with VAN and NIF, giving average EEs of 39% and 63%, respectively. NIF was chosen based on its status as the first-line medication for UTIs and VAN was chosen for its demonstrated enhanced efficacy within liposome formulations and its potential in intravesicular UTI therapy. Drug-loading was observed not to have a significant effect on the physical stability of liposomes; VAN-loaded liposomes maintained their physical size and zeta potential for up to four months, though they had a slightly more positive zeta potential probably due to the presence of VAN. Further experiments probing NIF-loaded liposomes and fusogenic liposomes would be useful to confirm that this trend holds true for other formulations. Incorporation of lipophilic dyes, DiO and DiD, into the liposome membranes was also successfully shown, which will be of importance in future microscopy experiments. Lastly, drug release experiments modelling how either storage conditions (4°C) or a physiological environment (37°C) would influence passive drug release found that temperature had no significant effect on the drug release profile of Cat-8-VAN ($p=0.1365$). Again, further experiments on NIF-loaded and

fusogenic liposomes are advisable to investigate if formulation differences influence passive drug release.

Here, NIF-loaded liposomes were successfully formulated and characterised to address the gap in liposomal formulations of NIF for UTI treatment. Short-term stability studies were performed on VAN-loaded Fuso-1-PEG, a formulation similar to that produced by Nicolosi *et al.* (2010) for antibacterial purposes. Stability assays were not performed in that study, so the stability experiments carried out here add to the characterisation profile of a similar formulation and may provide useful insight into downstream antibacterial observations.

The research presented in this chapter is the first step towards the aim of this thesis to create a novel ultrasound-mediated lipid-based drug delivery system that is efficient at both disrupting biofilms and delivering antibiotics to bacteria in clinical contexts. In order to assess the antibacterial activity of the formulated liposomes—and suitability for the final acoustically-active drug delivery system—they will be tested on monospecies bacterial models, which is explored in the next chapter.

3 Assessment of antibacterial activity of liposomal antibiotics

3.1 Introduction

Since the first approval of liposomal doxorubicin (Doxil®) by the FDA in 1995, liposomes have become widely recognised as excellent drug delivery vehicles in medical practice[351]. In the context of antibacterial treatments, antibiotic encapsulation in or immobilisation on liposomes aims to improve the efficacy of existing antibiotics through controlled and sustained release, prolonged circulation, and infection targeting[443,444]. Although liposomal antibiotics show potential in the context of combatting AMR (see section **1.4.4**), most of the clinically approved liposomal formulations are currently used in anti-cancer therapies, with several others in the fungal disease, viral vaccine and pain management markets[354]. As of 2022, Arikayce® was the only expressly antibacterial liposomal treatment available on the market and is used to treat lung infection caused by *Mycobacterium avium* complex (MAC); there are no approved liposomal antibiotics used in UTI treatment and management, as discussed in section **1.4.4**[433].

There has not been much research into using liposomes as delivery vehicles for antibiotics into the urinary tract; however, there are a few studies exploring intravesical administration of empty or loaded liposomes to promote bladder wound healing and/or deliver botulinum toxin to overactive bladders[616,617,639]. This at least indicates that liposome use in the urinary tract is potentially viable and beneficial within a disease treatment or management system. Much liposome-antibiotic research is in the pre-clinical stages with many studies focussing on pulmonary infections by *P. aeruginosa*, MAC, and *S. aureus*, but there is a precedent for effective antibiotic drug delivery to bacteria and biofilm using liposomes[444,454]. Of the studies that involve urinary species such as *E. coli*, there was either a gastro-intestinal focus, a desire to test on a model MDR pathogen or no condition specified[640–642]. This demonstrates that there is a research gap into liposomal antibiotic use specifically against UTIs.

UPEC is a Gram-negative bacterium that is also the predominant bacterial species found in UTIs, implicated in 65-75% of UTIs, which makes UPEC strains a relevant model to test novel UTI treatments on[235]. *K. pneumoniae*, *P. mirabilis*, and *Enterococcus* species are also often cited as common causes of UTIs[224,234,235,243]. Of these, *E. faecalis* is of particular interest due to its prevalence in both uUTIs and cUTIs, as well as the fact that it is Gram-positive; when tested on alongside *E. coli*, both species should provide a good initial spread of information about the spectrum activity of a treatment[234].

When testing an antimicrobial treatment, a plethora of microbiological assays under the antibiotic susceptible test (AST) umbrella can be used depending on what information is required. These include minimum inhibitory/bactericidal concentration (MIC/MBC) assays on planktonic bacteria, but also minimum biofilm inhibition/eradication/bactericidal concentration (MBIC/MBEC/MBBC) assays on biofilm growth. The objective of these assays is to be able to identify the lowest concentration of an antibacterial compound needed to inhibit bacterial/biofilm growth without necessarily killing the cells (i.e. inhibitory) or kill 99.9% of the bacteria cells (i.e. bactericidal); however in some cases—particularly for biofilm susceptibility—the definitions are not as clear-cut[643,644].

There are several methods that fall under ASTs[643,645], but here I will focus on broth microdilution assays as they are one of the standardized assays with established guidelines by EUCAST and the Clinical and Laboratory Standards Institute (CLSI)[646,647]. The broth microdilution MIC assay involves serial dilutions of antibiotic prepared in a multi-well plate. A standardized suspension of bacteria is then added and incubated in controlled conditions. The MIC is often identified by eye where there is no visible bacterial growth, but quantitative readings can also be made using a microplate reader. To assess the MBC, dilutions of the suspensions above (and below) the MIC are plated on agar and incubated. The lowest concentration needed to prevent colony growth (i.e. kill 99.9% bacteria) is recorded as the MBC. Alternatively, quantitative data can be obtained

through the resazurin assay, a colorimetric test to identify the MBC: blue resazurin is metabolised to form pink resorufin by living cells that can be quantified through fluorescence intensity or absorbance measurements on a microplate reader[648].

Unfortunately, for biofilm susceptibility testing (BST), there are no clinically standardized methods as there are for MIC assays published by EUCAST or CLSI, which is something that researchers and clinicians are urgently calling out for as it makes comparisons between studies incredibly difficult[644,649]. Due to the vast number of variables that influence biofilm formation, such as media, growth time, temperature, and the physical structure and material of the container used, many factors would need to be taken into consideration which could make it harder to establish a one-size-fits-all gold standard for susceptibility testing. Currently, there are several biofilm susceptibility parameters beyond the MBIC, MBEC and MBBC that have been used in the literature, including the biofilm prevention concentration (BPC) and biofilm tolerance factor (BTF)[649–651]. For the sake of clarity and to avoid confusion, I will provide the definition of MBEC proposed by Coenye[649] and the protocol of this assay that will be used in this chapter.

The MBEC is the lowest antibiotic concentration needed to completely clear an established biofilm[649]. This assay involves allowing a specified amount of time in controlled conditions for the bacteria to establish a biofilm adhered to the wells of a microtiter plate. The Calgary device is a popular alternative to a standard microtiter plate used for BST where plastic pegs attached to the lid of a microtiter plate provide the platform for biofilm adherence and formation[652]. The established biofilm would then be exposed to serial dilutions of antibiotic and incubated. Crystal violet is used to stain the biofilm (both living and dead matter) and absorbance is quantified using a microplate reader to give the biofilm biomass. As crystal violet staining is not specific for live or dead cells, additional data on the bacterial populations is often obtained by colony forming unit (CFU) counting or microscopy[649]. However, the manual rinsing, media renewal and handling of biomass can introduce significant variation and inaccuracies with all of these techniques—a

demonstration of why it may be more difficult than expected to standardize a BST[653]. There is debate around whether this assay does effectively measure biofilm reduction/eradication, rather than the inhibition of further biofilm growth, especially given that pre-treatment biofilm measurements are not always taken or practical to take for comparison[644]. Nevertheless, the MBEC and corresponding devices are still widely used for BST in the absence of standardized methods and definitions[654].

For the drug-loaded liposomes formulated in chapter **2**, it was important to understand how they interact with bacteria before conjugation to microbubbles. This information would confirm whether these liposomes possess antibacterial properties but should also prove useful in comparisons of antibacterial activity before and after ultrasound involvement. As most UTIs are caused by infections with *E. coli* (i.e. UPEC), using clinical isolates from UTI patients was important to test the previously formulated liposomes in a UTI context[235]. Complementary experiments on (Gram-positive) *E. faecalis* using clinical isolates from UTI patients were important to test whether there is any difference in response from Gram-negative and Gram-positive bacteria while still keeping the findings relevant to UTIs. In this chapter, I investigated the activity of cationic and fusogenic liposomal VAN and NIF against planktonic *E. coli* and *E. faecalis* strains via MIC and MBC assays. These experiments were based on findings by Nicolosi *et al.* (2010), where liposomal encapsulation of VAN led to broader spectrum activity against even Gram-negative bacterial species[449]. Preliminary microscopy studies were also carried out to follow-up these assays and probe liposome-bacteria interactions and the differences between the two formulations. Lastly, monospecies biofilm models of *E. coli* and *E. faecalis* were treated with liposomal NIF to investigate its anti-biofilm properties in MBEC assays prior to microbubble conjugation.

3.2 Materials and Methods

3.2.1 Materials

Cholesteryl hemisuccinate (CHEMS), 1,2-dioleoyl-sn-glycero-3-phosphoethanolamine (DOPE), 1,2-dioleoyl-3-trimethylammonium-propane (DOTAP), and 1,2-dipalmitoyl-sn-glycero-3-phosphocholine (DPPC) were purchased from Avanti Polar Lipids. L-α-phosphatidylcholine (PC, soybean), cholesterol and 10X phosphate-buffered saline (PBS) stock solution were purchased from Merck Life Sciences, UK. 1,2-dioleoyl-sn-glycero-3-phosphoethanolamine-N-[maleimide(polyethylene glycol)-5000] (DOPE-PEG5000-Maleimide) was purchased from BroadPharm. Chloroform, methanol, UltraPure™ DNase/RNase-free distilled water and other solvents were of analytical grade (Thermo Fisher Scientific, UK). 3,3´-dioctadecyloxacarbocyanine (DiO) was purchased from Cambridge Bioscience and 1,1'-Dioctadecyl-3,3,3',3'-Tetramethylindodicarbocyanine, 4-Chlorobenzenesulfonate Salt (DiD) and the LIVE/DEAD™ *Bac*Light™ Bacterial Viability Kit, containing SYTO 9 and propidium iodide (PI) dyes, were purchased from Thermo Fisher Scientific, UK. Vancomycin hydrochloride (VAN) and Nitrofurantoin sodium (NIF) were purchased from Cambridge Bioscience, UK.

Cation-adjusted Mueller-Hinton II broth (caMHB), tryptic soy broth (TSB) and lysogeny broth (LB) were made by dissolving broth powder (Merck Life Sciences, UK) in distilled water according to the manufacturer's instructions and autoclaving at 121°C for 15 min to sterilise. Agar and crystal violet (CV, 1% aqueous solution) were also purchased from Merck Life Sciences, UK.

A tailored version of the LNP (lipid nanoparticle) Profiler Kit for super-resolution microscopy was obtained from ONI (Oxford Nanoimaging Ltd., Oxford, UK).

Microbial strains

Details of the strains used are listed in **Table 4**. Frozen stocks of *Escherichia coli* strains (UTI89, CFT073, and K12) were obtained from ATCC. *Escherichia coli* strain 83972 (HM50) was obtained through BEI Resources, NIAID, NIH as part of the Human Microbiome Project. Frozen stocks

of clinical isolates of *Enterococcus faecalis* (EF12-PT12/UEF12, EF36, and EF48-PT38/UEF33) were obtained from University College London (UCL), collected from UTI patients at the Royal Free Hospital, London, UK. The bacteria strains were stored at −80°C in cryovials containing 20% glycerol (v/v) in LB.

Table 4 | Bacterial strains used in the present study.

Strain	Species	Source	Origin
UTI89	*Escherichia coli*	ATCC	Isolated from a patient with acute cystitis infection
CFT073	*Escherichia coli*	ATCC	Isolated from a patient with acute pyelonephritis infection
K12	*Escherichia coli*	ATCC	Faeces of convalescent diphtheria patient. Considered non-pathogenic
HM50/ABU 83972	*Escherichia coli*	BEI	Urine of asymptomatic bacteriuria patient
EF12-PT12/UEF12	*Enterococcus faecalis*	UCL	Isolated from a patient with acute cystitis infection
EF36	*Enterococcus faecalis*	UCL	Isolated from a patient with acute cystitis infection
EF48-PT38/UEF33	*Enterococcus faecalis*	UCL	Isolated from a patient with acute cystitis infection

3.2.2 Microbiological assays

3.2.2.1 Minimum inhibitory concentration

Bacterial strains were inoculated on LB agar plates (Thermo Fisher Scientific, UK) from the frozen stock. After incubation at 37°C for 24 h, three separate colonies were transferred to caMHB and incubated at 37°C, shaking at 180 rpm, for at least 18 h. Then, the optical density at 600 nm (OD_{600}) value was adjusted to roughly the equivalent of 10^8 CFU/mL. This stock was further diluted to 10^6 CFU/ml in caMHB to make a working bacterial suspension. The standard broth microdilution method as set out by the CLSI M100[647] (with a modification of using shaking instead of static

incubation) was used to determine minimum inhibitory concentrations (MICs) of free drug and drug-loaded liposomes for VAN and NIF (**Figure 28**). 100 μL of sterile caMHB was added to all the wells of a 96 well-plate, apart from the ones corresponding to the maximum concentration of drug and the outer wells. Free drug was first dissolved in filtered 0.1X PBS to make stock solutions of up to 10 mg/mL before being diluted to the target concentration in caMHB. Drug-loaded liposomes were prepared as described in section **2.2.2**, and concentrated liposome samples produced through ultrafiltration were diluted to the target concentration in caMHB. These target concentrations differed according to the drug, bacterial species and assay type performed (**Table 5**). 200 μL of free-drug or drug-loaded liposomes were then added to the maximum concentration column (column 4 in **Figure 28**). By transferring 100 μL of this to subsequent wells, serial dilutions of the drug were made. 100 μL of bacterial suspension was added to all wells (except sterile control). The sterile control was 200 μL of caMHB. The growth control was 100 μL of bacterial suspension with 100 μL of caMHB. The outer wells were filled with 200 μL of sterile water and the plate wrapped with foil to reduce evaporation. The plates were incubated at 37°C for 24 h, shaken at 180 rpm, and MICs determined visually where possible. Three biological repeats with three technical replicates each were performed.

3.2.2.2 Minimum bactericidal concentration

In the same well-plate as used for the minimum inhibitory concentration assay, 5 mg/mL resazurin was added to each well (10% v/v) and left to incubate at 37°C for another 24 h before measuring fluorescence intensity (excitation at 530 nm and emission at 590 nm; Tecan Spark® Microplate Reader) to measure minimum bactericidal concentrations (MBCs). To correct for liposome contribution to fluorescence intensity measurements, loaded liposomes were incubated in caMHB without bacteria as another negative control. The number of viable cells was calculated as a percentage using the following formula:

$$\textbf{number of viable cells (\%)} = \frac{\textbf{fluorescence}_{treatment} - \textbf{fluorescence}_{sterile}}{\textbf{fluorescence}_{growth} - \textbf{fluorescence}_{sterile}} \times 100 \quad \textbf{(Eq. 3)}$$

where **fluorescence**$_{treatment}$ is the mean fluorescence signal of the corresponding treatment wells, **fluorescence**$_{sterile}$ is the mean fluorescence signal of the sterile (negative) control wells, and **fluorescence**$_{growth}$ is the mean fluorescence signal of the growth (positive) control wells. Three biological repeats with three technical replicates each were performed.

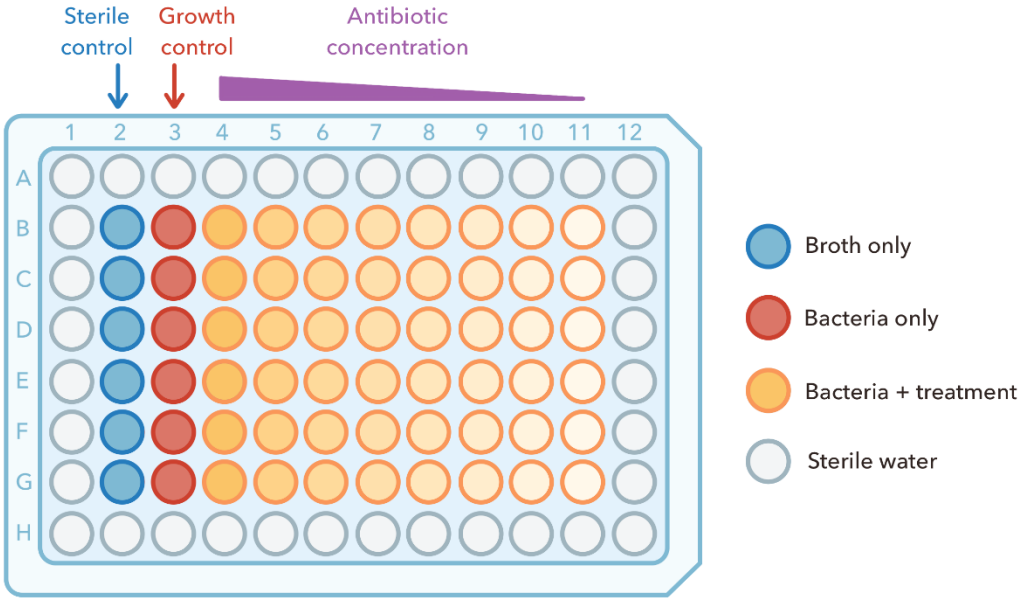


Figure 28 | Arrangement of samples in 96-well plate for MIC/MBC assays. Each row represents a repeat; there can be up to six repeats for each antibiotic treatment in the same well plate. The antibiotic treatment (free or liposomal) was serially diluted eight times to provide a sufficiently broad concentration range for determining an MIC value.

3.2.2.3 Minimum biofilm eradication concentration

A variation of the fluorometric-based biofilm assay described by Wannigama *et al.* (2019)[655] was used to measure minimum biofilm eradication concentrations (MBECs). Bacterial stocks were made in a similar fashion to that used for MIC and MBC assays described above, but the colonies were incubated in TSB instead of LB. The stock was diluted to 10^7 CFU/mL in TSB to make a working bacterial suspension. 500 µL of this suspension was added to each well (apart from the control wells) of a 24-well plate (**Figure 29**). 500 µL of sterile TSB was added to each control well and the plate incubated at 37°C for 24 h in static conditions. After 24 h, the liquid was removed and nonadherent cells were removed from the biofilms by a gentle wash with sterile PBS. Serial

dilutions of free drug or drug-loaded liposomes in TSB were made in separate conical tubes, based on maximum concentrations shown in **Table 5**. 500 μL of these drug preparations were added to the corresponding treatment wells. 500 μL of TSB was added to the negative control and growth control wells and the plate incubated at 37°C for another 24 h. The liquid bacterial suspension was aspirated and collected to determine the minimum biofilm-associated bactericidal concentration (MBaBC). Nonadherent cells were removed from the biofilms by one gentle wash with sterile PBS before 0.1% v/v CV in sterile water (500 μL) was added for 20 min at room temperature in the dark. The CV was disposed of and any excess removed by three gentle washes with sterile water. After the plate had dried, 30% acetic acid (500 μL) was added to each well for at least 20 min at room temperature before absorbance was measured at 594 nm (using a Tecan Spark® Microplate Reader). Biofilm biomass was calculated as a percentage using the following formula:

$$\textbf{biofilm biomass (\%)} = \frac{\textbf{absorbance}_{treatment} - \textbf{absorbance}_{sterile}}{\textbf{absorbance}_{growth} - \textbf{absorbance}_{sterile}} \times 100 \qquad \textbf{(Eq. 4)}$$

where $\textbf{absorbance}_{treatment}$ is the mean absorbance signal of the corresponding treatment wells, $\textbf{absorbance}_{sterile}$ is the mean absorbance signal of the sterile (negative) control wells, and $\textbf{absorbance}_{growth}$ is the mean absorbance signal of the growth (positive) control wells. Three biological repeats with three technical replicates each were performed.

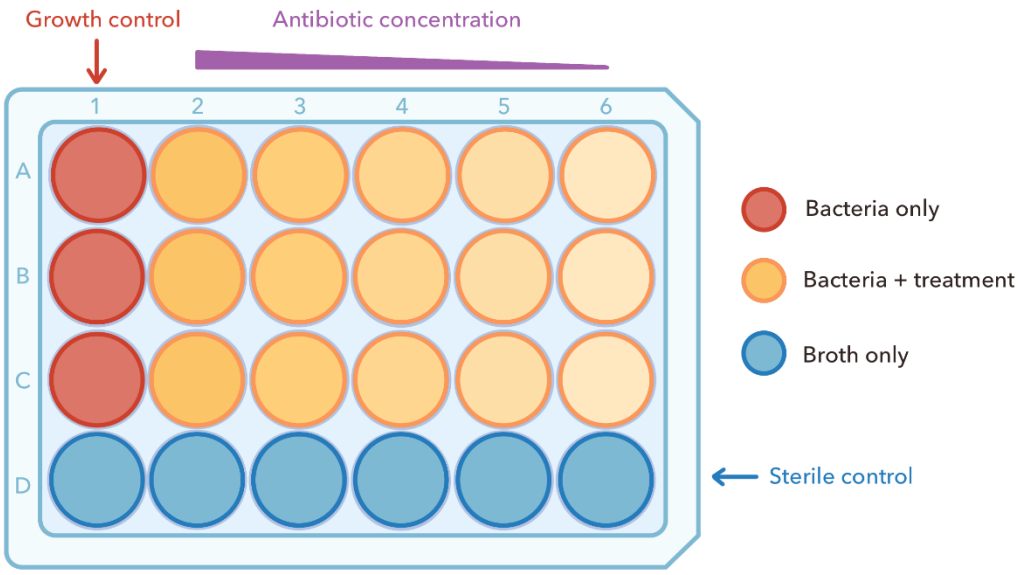


Figure 29 | Arrangement of samples in 24-well plate for MBEC assays. Each row represents a repeat; there can be up to three repeats for each antibiotic treatment in the same well plate. The last row contained sterile control repeats, with TSB medium only. The antibiotic treatment (free or liposomal) was serially diluted five times.

3.2.2.4 Minimum biofilm-associated bactericidal concentration

The liquid bacterial suspension associated with the biofilm collected during the MBEC assay was used in a follow-up experiment to assess the viability of biofilm-associated cells in a minimum biofilm-associated bactericidal concentration (MBaBC) assay. This assay is similar to the MBC assay but is performed on biofilm-associated bacteria instead of purely planktonic cells. 500 µL of the suspension from each well was added to a fresh plate. 5 mg/mL resazurin was then added to each well (10% v/v) and left to incubate at 37°C for another 24 h before measuring fluorescence intensity (excitation at 530 nm and emission at 590 nm; Tecan Spark® Microplate Reader). All assays were performed with three biological repeats, each with three technical repeats. The number of viable cells was calculated using **Eq. 3**.

Table 5 | Maximum drug concentrations used in each microbiological assay. Vancomycin and nitrofurantoin were used in minimum inhibitory/bactericidal concentration (MIC/MBC), minimum biofilm eradication concentration (MBEC), and minimum biofilm-associated bactericidal concentration (MBaBC) assays for *E. coli* and *E. faecalis* strains. These assays involved serial dilutions of the free drug or drug-loaded liposomes based on the maximum drug concentrations shown in this table. All concentrations are in mg/mL.

Assay	Drug	Bacterial species	
		E. coli	*E. faecalis*
MIC/MBC	Vancomycin	0.5	0.01
	Nitrofurantoin	0.5	0.5
MBEC	Vancomycin	5	2
	Nitrofurantoin	0.5	0.5

3.2.3 Confocal imaging with VAN-loaded liposomes

Bacterial suspensions of one *E. coli* strain (UTI89) and one *E. faecalis* strain (EF36) were prepared in the same way as for the MIC/MBC experiments described above (**3.2.2.1**). VAN-loaded DiD-labelled liposomes were added to each strain; total drug concentrations of 312.5 μg/mL and 4 μg/mL liposomal VAN were added to UTI89 and EF36 in caMHB, respectively. The samples were then incubated at 37°C, shaken at 180 rpm, for 24 h. Afterwards, 1 mL of treated culture was spun at 10,000 ×g for 10 min, the supernatant removed, and the pellet resuspended in sterile PBS. This washing process was repeated three times. 1.5 μL of SYTO 9 and 1.5 μL of PI dyes were incubated with the resuspension for 15 min at room temperature, protected from light. 10 μL of stained bacteria was pipetted onto a 35 mm ibidi μ-dish (ibidi GmbH, Germany). Images of the stained cells with labelled liposomes were then taken using a Nikon Eclipse Ti2 fluorescence microscope at 100× magnification using an oil-immersion objective, and 640 nm and 488 nm lasers. At least three images per sample were acquired from randomly selected points.

3.2.4 Super-resolution imaging

Liposome-treated bacterial samples were prepared in the same way as for the confocal imaging experiments described above (**3.2.3**). After incubation of the treated samples at 37°C for 24 h, 2 mL of treated culture was spun at 10,000 ×g for 10 min, the supernatant removed and the pellet resuspended in sterile PBS, repeated three times and finally resuspended in 1 mL of PBS to concentrate the sample for imaging. The on-chip staining protocol for super-resolution imaging of LNPs developed and optimised by ONI (Oxford Nanoimaging Ltd., Oxford, UK) was followed using a tailored version of the LNP Profiler Kit (**Figure 30**). Briefly, samples were immobilised on the poly-L-lysine (PLL)-coated lanes of an assay chip for 15 min. Unbound cells were washed off using 1X PBS and a fixative solution (4% paraformaldehyde) was added for 15 min to fix bacterial cells. A surface block solution (3% bovine serum albumin) and permeabilization buffer (0.1% Triton) were then added for 25 min to block excess PLL and permeabilise the cells before washing with 1X PBS. Proprietary pan-LNP detection (640 nm) and WGA (wheat germ agglutinin) conjugate (488 nm) were added for 15 min at room temperature, while protected from light, to label PEGylated liposomes and bacterial membranes, respectively. Excess label/dye was washed off with 1X PBS and the imaging buffer was then added to the assay chip lanes. The liposomes were imaged using an ONI Nanoimager S equipped with 640 nm and 488 nm lasers at 35% and 55% laser powers, respectively, and a 30 ms exposure time. Each acquisition was performed for at least 7000 frames. The super-resolution images were processed and analysed using ONI's Collaborative Discovery platform (CODI, www.alto.codi.bio) to obtain liposome and bacteria size and morphology data.

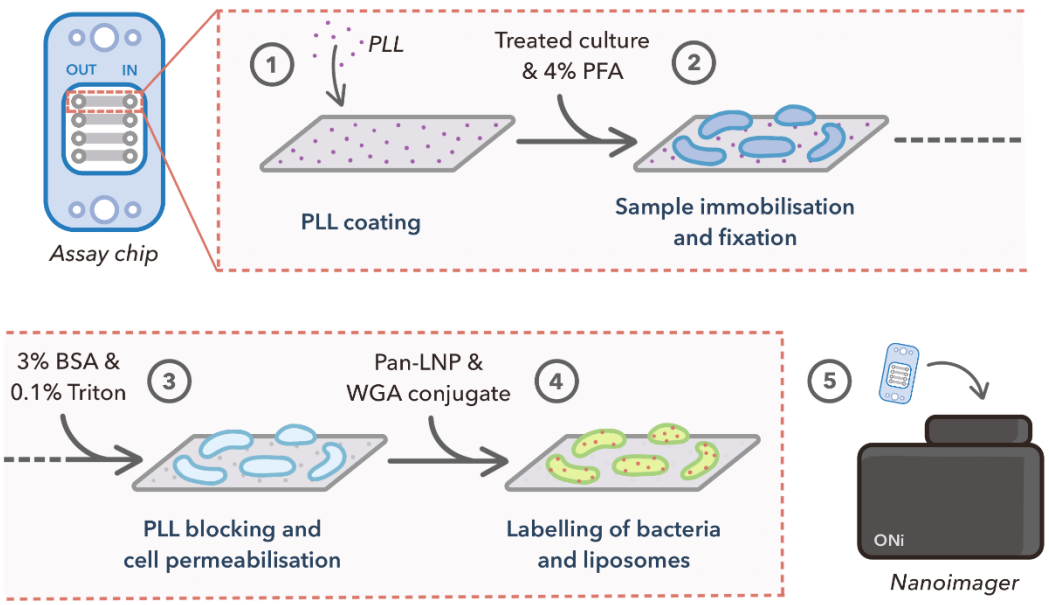


Figure 30 | Schematic of on-chip staining protocol for super-resolution imaging with ONI. ONI's assay chip has labelled inlets, outlets, and four flow lanes. Each lane was used to image a single sample and preparation followed the process of 'on-chip staining': (**1**) Poly-L-lysine (PLL) was flowed through the lane to coat the lane surface. (**2**) Bacterial cells were immobilised on the lane surface and fixed with 4% paraformaldehyde (PFA). (**3**) Excess PLL was blocked using 3% bovine serum albumin (BSA) and cells permeabilised using 0.1% Triton. (**4**) Pan-LNP detection and WGA conjugate were added to label bacteria and liposomes. (**5**) ONI's Nanoimager was used for super-resolution imaging.

3.2.5 Data processing

MIC, MBC, and MBEC data were visualised using GraphPad Prism 9 (version 9.4.1). Confocal images were processed using ImageJ (version 2.9.0/1.54k). The Live Dead Analysis macro written by Kerkhoff and Ludwig (2024)[656] was used to batch-process multi-channel images with a live and a dead fluorescence staining. Live-dead ratios (LDR) were calculated by dividing live cell count by dead cell count. The BIOP JACoP plugin was used to determine Pearson's correlation coefficients (PCC, r), which measures the strength and direction of linear correlation between two variables. It gives a value between -1 and +1, where $r = -1$ denotes a perfect negative correlation and $r = +1$ indicates a perfect positive correlation. It is used as a measure of colocalization to quantify how much one signal proportionally varies with another; here, it was used to measure the colocalization of signal associated with the liposome membrane with signal associated with the bacterial intracellular environment.

3.3 Results and Discussion

3.3.1 Investigating liposomal vancomycin activity against planktonic bacteria

To evaluate the antibacterial activity of the drug-loaded liposomes formulated in chapter **2**, MIC/MBC assays were performed against four *E. coli* strains (UTI89, CFT073, K12 and HM50) and three *E. faecalis* strains (EF12, EF36 and EF48) as described in **3.2.2**. Free VAN was tested against these selected bacterial strains as a baseline control. The efficacy of Cat-8-VAN and Fuso-1-PEG-VAN was then compared to the free VAN control to assess whether encapsulation within these liposome formulations affects the drug's efficacy and potency. Against planktonic bacteria, MIC values are the standard when reporting susceptibility of bacteria to an antibiotic. However, sometimes inhibition of growth does not translate to bacterial death, therefore, follow-on MBC assays were performed to gain a better understanding of what drug concentration effectively kills the bacteria. Additionally, in some cases, visual assessment of MIC values was difficult due to slow growth giving low turbidity—even in the growth control—or due to cloudiness introduced by adding of the liposomal treatment. This made an MBC assay valuable to supplement MIC findings. MBC values were determined using a microplate reader which is more reliable for quantification compared to visual assessment used for MIC values, and as such the MBC data are more informative. Both the MIC and MBC values of VAN treatment for each strain are summarised in **Table 6**.

Table 6 | Summary of MIC and MBC values of VAN treatments. Inhibitory or bactericidal drug concentrations that were above the corresponding free VAN baseline concentration are coloured in red; drug concentrations that were below the free VAN baseline are coloured in blue; and drug concentrations that were the same as the free VAN baseline are coloured in grey. All concentrations are in μg/mL.

	Strain	MIC (μg/mL)			MBC (μg/mL)		
		Free	Cat-8	Fuso-1-PEG	Free	Cat-8	Fuso-1-PEG
E. coli	UTI89	312.5	312.5	500	312.5	312.5	>500
	CFT073	312.5	156.25	500	312.5	312.5	>500
	K12	312.5	312.5	500	312.5	312.5	>500
	HM50	312.5	312.5	250	312.5–625	312.5	>500
E. faecalis	EF12	1.25	1.25	2.5	1.25	10	10
	EF36	1.25	2.5	5	10	5	5
	EF48	1.25	1.25	2.5	2.5–5	2.5–5	2.5–5

Liposomal VAN activity against planktonic *E. coli*

As *E. coli* is a Gram-negative bacterium that has natural resistance to VAN activity by virtue of its outer membrane, VAN is not a recommended antibiotic for *E. coli* infections and has no documented EUCAST breakpoint against *E. coli*. This fact is reflected in the very high drug concentrations needed to inhibit growth—312.5 μg/mL was the observed MIC of free VAN (**Table 6**), while EUCAST breakpoint values for other antibiotics against *E. coli* are typically 8 μg/mL or less[657]. A similar concentration was needed for bactericidal effects (MBC, **Table 6**); 312.5 μg/mL of free VAN was required to kill the *E. coli* cells. As VAN is a bactericidal antibiotic, an MBC:MIC ratio ≤ 4 is expected[658]. Here, the inhibitory and bactericidal concentrations are the

same (MBC:MIC = 1) likely because the inhibition of growth observed in an MIC assay is due to bacterial death, which is confirmed in an MBC assay.

Cat-8-VAN MIC and MBC values seemed to largely match that of free VAN (**Table 6**), suggesting that encapsulation did not increase antibiotic activity, but also did not impede it. This observation could be due to potential drug leakage occurring over the 24 to 48 hours of the assays, essentially releasing encapsulated VAN to mirror availability levels seen in free VAN samples. This could be elucidated by performing a drug release assay similar to that of chapter **2**, but using the MIC/MBC media over a 48-hour period instead, to assess whether VAN is completely released during that time. If drug release is actually incomplete, another reason for this observation could be that the cationic liposomes increase the local antibiotic concentration due to favourable interactions between the formulation and the cell membrane, as documented in the literature[366–368]. This would mean that despite incomplete release of VAN, the local availability and delivery is increased to levels that mirror free VAN treatment. One exception is CFT073 where Cat-8-VAN had an MIC half that of free VAN (156.25 μg/mL compared to 312.5 μg/mL), which may indicate that Cat-8-VAN improved delivery of VAN to this strain in particular. However, the MBC value matched that of free VAN at 312.5 μg/mL and of the other strains. This indicates that even though it appeared that CFT073 growth was inhibited at 156.25 μg/mL, the bacterial cells were still metabolically active at this antibiotic concentration, demonstrating why complementary MBC assays are beneficial. With an MBC:MIC ratio of 2, VAN is still having bactericidal effects on CFT073 and given the relative inaccuracy of visual assessment of MICs in this case, it is likely that the MBC value matching ones for free VAN and other *E. coli* strains more accurately reflects reality.

For Fuso-1-PEG-VAN, it appeared as though growth was inhibited at 500 μg/mL (the maximum concentration tested) for UTI89, CFT073 and K12, which is significantly above what was observed with free VAN and Cat-8-VAN. However, MBC assays revealed that none of the *E. coli* strains

were actually being fully killed; no MBC value was observed in the tested range (**Table 6** and **Figure 31**). In fact, encapsulation in fusogenic liposomes seemed to impair VAN activity, maybe through reduced interaction with bacteria and/or reduced release of VAN from this formulation. This contradicts the findings of Nicolosi *et al.* (2010) where a similar fusogenic formulation of VAN was used that inhibited bacterial growth of *E. coli* at much lower drug concentrations[449]. Apart from using different *E. coli* strains in this study, the PEGylation of the fusogenic formulation (to make Fuso-1-PEG-VAN) may have a part to play in the apparent impairment of VAN activity. Although PEGylation of liposomes is widely known for increasing liposome stability and circulation time, there are also reports of PEGylation negatively affecting binding ability depending on the molecular weight and abundance of PEG[659,660]. For example, PEGylated liposomes have actually shown reduced adsorption to bacteria within biofilm, as well as negatively interfered with the interaction between antimicrobial peptides and bacterial outer membrane components[661,662]. It is suggested that this effect is due to steric hindrance of the bulky PEG chains; in Fuso-1-PEG-VAN, the PEG chains have a molecular weight of 5000 Da which could serve as a significant obstruction, as seen in some examples in the literature[376,379,380]. To confirm if PEGylation is indeed contributing to the reduced VAN activity, this experiment should be repeated with a PEG-free version of this formulation.

Interestingly, for HM50, it appeared as though encapsulation did increase some form of antibacterial activity at the lowest concentrations (**Figure 31**); when treated with Cat-8-VAN, the number of viable cells was kept between 40% and 50%, before a brief spike in bacterial viability (~63%) followed by a sharp viability reduction to 0% to give an MBC similar to free VAN. HM50 specifically appeared to be more sensitive to Fuso-1-PEG-VAN with an MIC of 250 μg/mL, below that of free VAN and Cat-8-VAN. Even though no MBC value was recorded, **Figure 31** shows a 40% decrease in viable cells at 500 μg/mL, where the other strains showed no response. HM50 is a well-characterised asymptomatic bacteriuria bacterial strain that lacks the fimbriae found in invasive UPEC species associated with symptomatic UTIs, like UTI89 and CFT073[663].

This physiological difference may be responsible for the observed responses to both the liposome formulations, but the underlying mechanism is unclear. Perhaps the reduced capacity to form appendages allows for closer interactions with cationic liposomes and negates the steric hindrance caused by PEGylation of the fusogenic formulation, leading to an increased VAN uptake. Again, experiments with a non-PEGylated fusogenic formulation or neutral conventional liposomes could help clarify this result in HM50.

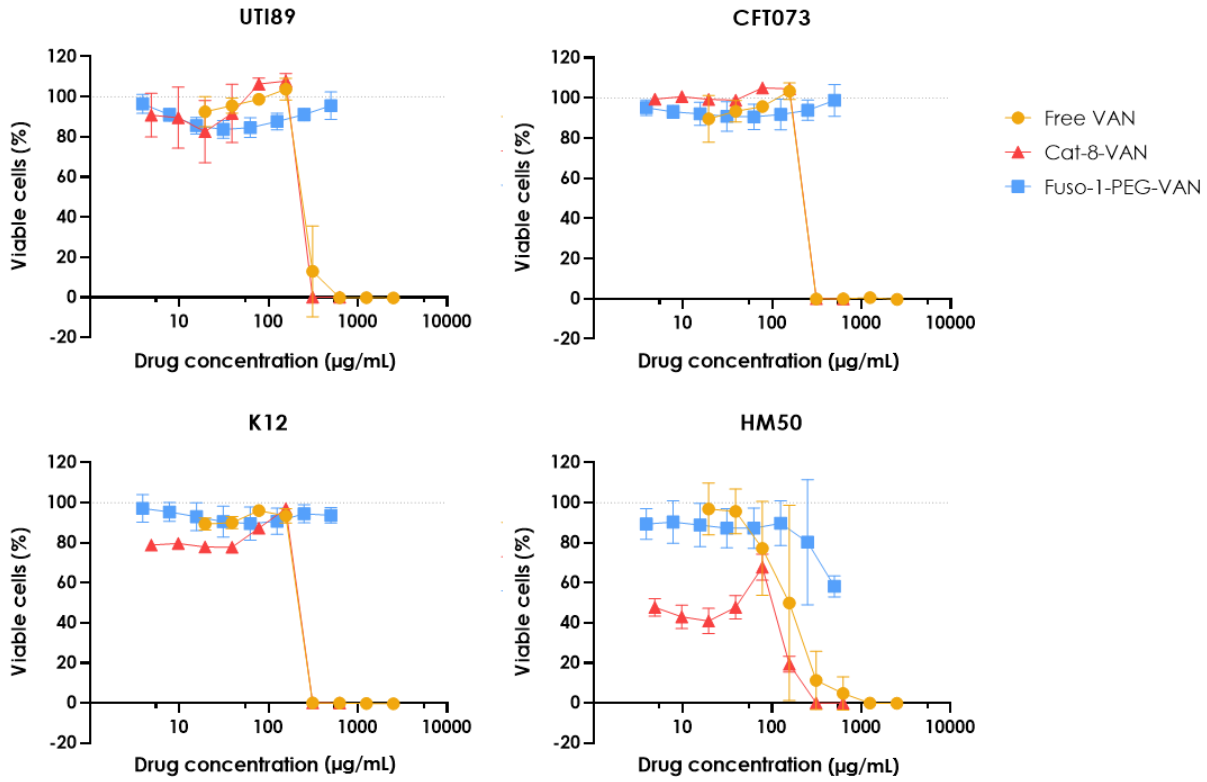


Figure 31 | Bacterial viability of four *E. coli* strains after treatment with VAN formulations in MBC assays. Four strains of *E. coli* (UTI89, CFT073, K12 and HM50) were treated with free VAN, cationic liposome-encapsulated VAN (Cat-8-VAN) or fusogenic liposome-encapsulated VAN (Fuso-1-PEG-VAN), matched for drug concentration, as part of an MBC assay. The average number of viable cells was calculated as a percentage compared to a growth control (no treatment) and plotted for each drug concentration tested.

Liposomal VAN activity against planktonic *E. faecalis*

To complement the studies on Gram-negative *E. coli* and see if the formulations interact differently based on bacterial class, three Gram-positive *E. faecalis* strains were also used in MIC and MBC assays. VAN is generally effective against Gram-positive species (due to the lack of an outer membrane) and can still be used for *E. faecalis* infections with a documented EUCAST breakpoint

of 4 μg/mL[657]. As such, the maximum concentrations used in the assays are much lower than that used for *E. coli* (10 μg/mL compared to 2500 μg/mL). The MIC value for all of these clinical isolates was 1.25 μg/mL for free VAN (**Table 6**), indicating the susceptibility of these strains to VAN. Again, Cat-8-VAN activity generally matched that of free VAN, apart from against EF36 where cationic encapsulation increased the MIC two-fold to 2.5 μg/mL. MICs also appeared to be increased further when encapsulated within fusogenic liposomes, doubling to 2.5 μg/mL for EF12 and EF48 and to 5 μg/mL for EF36. However, these MIC results deviate substantially from the observed MBC values. It is of importance to note that visual assessment of MICs was very difficult with the *E. faecalis* strains as their growth in caMHB was not as obvious as with *E. coli*, which could be down to their different size and shape influencing the visibility. Variation in growth in MHB between *E. faecalis* and *E. coli* has been observed in the literature, with *E. faecalis* showing up to a 1-log fold reduction in growth[664]. Therefore, MBCs for *E. faecalis* are a more reliable source of information on apparent VAN delivery to cells.

All of these clinical isolates showed different responses to the VAN treatments as exemplified by the mixed MBC values obtained (**Table 6**). Free VAN gave varying degrees of killing effect, requiring increasing concentrations to effect cell death in the order of EF12 (1.25 μg/mL), EF48 (2.5-5 μg/mL), then EF36 (10 μg/mL). For EF48, this MBC was matched by both the cationic and fusogenic formulations, indicating that VAN delivery was successful enough to mirror free VAN activity even though the MBC was not decreased (**Table 6** and **Figure 32**). Remarkably, Fuso-1-PEG-VAN worked to promote bacterial cell death within the tested concentration range for all *E. faecalis* species, where it failed to do at all so for *E. coli*. This implies that PEGylated liposomes may preferentially interact with Gram-positive species over Gram-negative species, a trend also shown with PEGylated peptides[665]. This could potentially be the result of favourable interactions between PEG and cell wall components of Gram-positive bacteria. It could also be that the lack of an outer membrane with constituent proteins doesn't provide the additional steric hindrance that obstructs interaction with PEGylated liposomes. Running an experiment where the

amount of PEGylated lipid is varied within the fusogenic formulation before testing on *E. faecalis* strains could be beneficial to confirm how PEGylation contributes to *E. faecalis* interaction and cell death.

Notably, both Cat-8-VAN and Fuso-1-PEG-VAN halved the MBC when used against EF36 but increased the MBC eight-fold when used against EF12 (**Table 6**). Therefore, liposome efficacy can differ within a species. As these are clinical isolates from different individuals, variation in antibiotic response is to be expected. This highlights the importance of using clinical samples in these tests to get an overall MBC profile that is representative of the clinical reality.

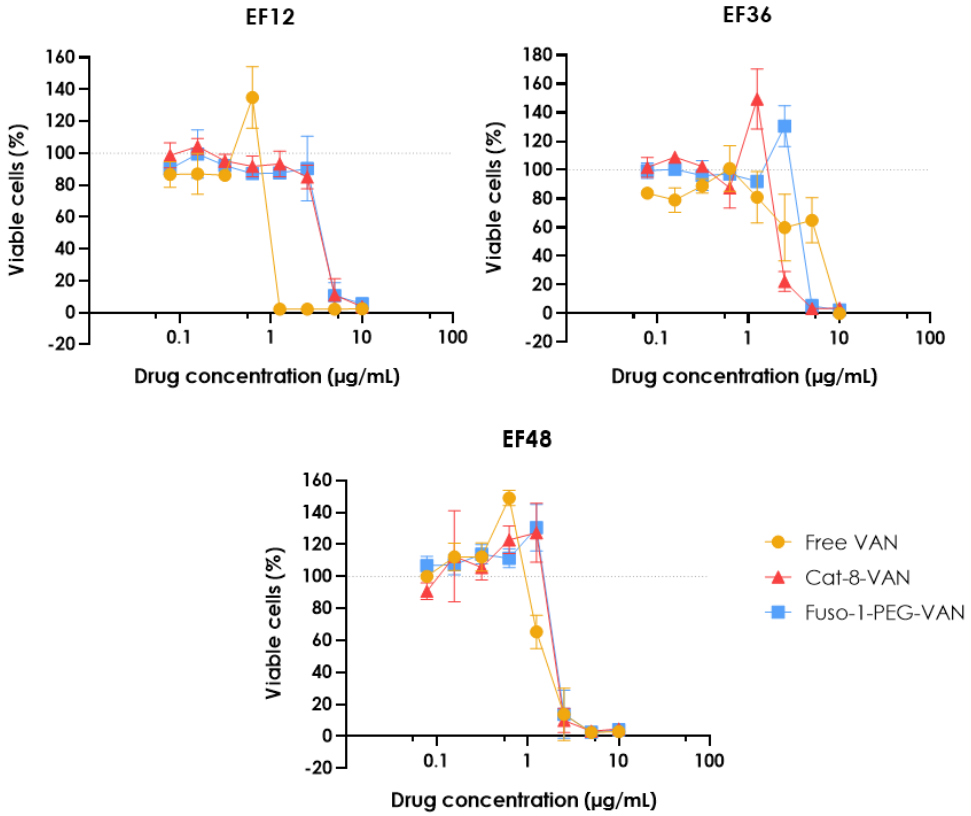


Figure 32 | Bacterial viability of three *E. faecalis* strains after treatment with VAN formulations in MBC assays. Three strains of *E. faecalis* (EF12, EF36, and EF48) were treated with free VAN, cationic liposome-encapsulated VAN (Cat-8-VAN) or fusogenic liposome-encapsulated VAN (Fuso-1-PEG-VAN), matched for drug concentration, as part of an MBC assay. The average number of viable cells was calculated as a percentage compared to a growth control (no treatment) and plotted for each drug concentration tested.

Another interesting trend was observed across both species where the number of viable cells slightly increases as drug concentration initially increases, just before bacterial viability plummets

(e.g. UTI89 in **Figure 31** and EF48 in **Figure 32**). This could be due to sufficient subinhibitory levels of antibiotic actually inducing bacterial virulence and stimulating bacterial growth[666,667]. At very low drug concentrations, there is no significant effect on bacterial viability but as the drug concentration increases, a sub-MIC is reached where bacterial virulence, growth and even biofilm formation is promoted. Once the MIC is reached, the number of viable cells would then drop, reflecting the complete bacterial cell death at this concentration. Moreover, these MBC assays are run for an additional 24 hours after MIC values have been collected. This may give more time for increased growth and biofilm formation effects to take place. Using a microplate reader to measure OD_{600} values in a time-kill assay to track growth changes over time, instead of visually assessing for a single MIC value, could reveal if the concentrations do have an effect on bacterial growth in this way. Running a 24-hour MBC assay in parallel with a 24-hour MIC assay could also potentially clarify if this effect is linked with longer incubation times.

The effect of unloaded liposomes on bacterial viability

Unloaded liposome formulations were also tested to confirm the contribution of the liposome formulation itself to antibacterial activity. In general, treatment with unloaded liposomes showed no reduction in planktonic growth for most strains, with the exceptions of HM50 and CFT073 (**Figure 33**). Given previous findings showing the increased sensitivity of HM50 to liposomal treatment compared to the other *E. coli* strains, it might be expected that even unloaded formulations decrease the number of viable cells. However, in the case of unloaded liposomes, both the fusogenic and cationic formulations affected bacterial viability following a similar pattern: viable cell count was kept between 40 and 80% with no significant trend as theoretical drug concentration increased (i.e. as liposome concentration increased). On the other hand, CFT073 did show a concentration-dependent response; as liposome concentration increased, viable cell count gradually decreased to 40-50% for both formulations. This is surprising, especially as the VAN-loaded fusogenic formulation did not increase CFT073 cell death. It is uncertain why

unloaded liposomes would affect CFT073 differently to UTI89, another UPEC strain associated with symptomatic UTIs. There has been a study on a cystitis model that demonstrated that CFT073 infections are cleared consistently quicker than UTI89, but the specifics of the underlying biochemistry are still not well understood[668]. This may, however, be relevant to explain the difference in response to unloaded liposomes. Empty liposomes have previously been shown to have therapeutic effects in sequestering bacterial toxins—perhaps unloaded liposomes may thus act to sequester toxins/nutrients needed for growth for particular strains[669,670]. Alternatively, the sheer number of liposomes could be interfering with intercellular communication by mimicking or obstructing bacteria-derived extracellular vesicles. However, it remains unclear why UTI89 and K12 wouldn't respond in the same way as CFT073 and HM50 if this was the case.

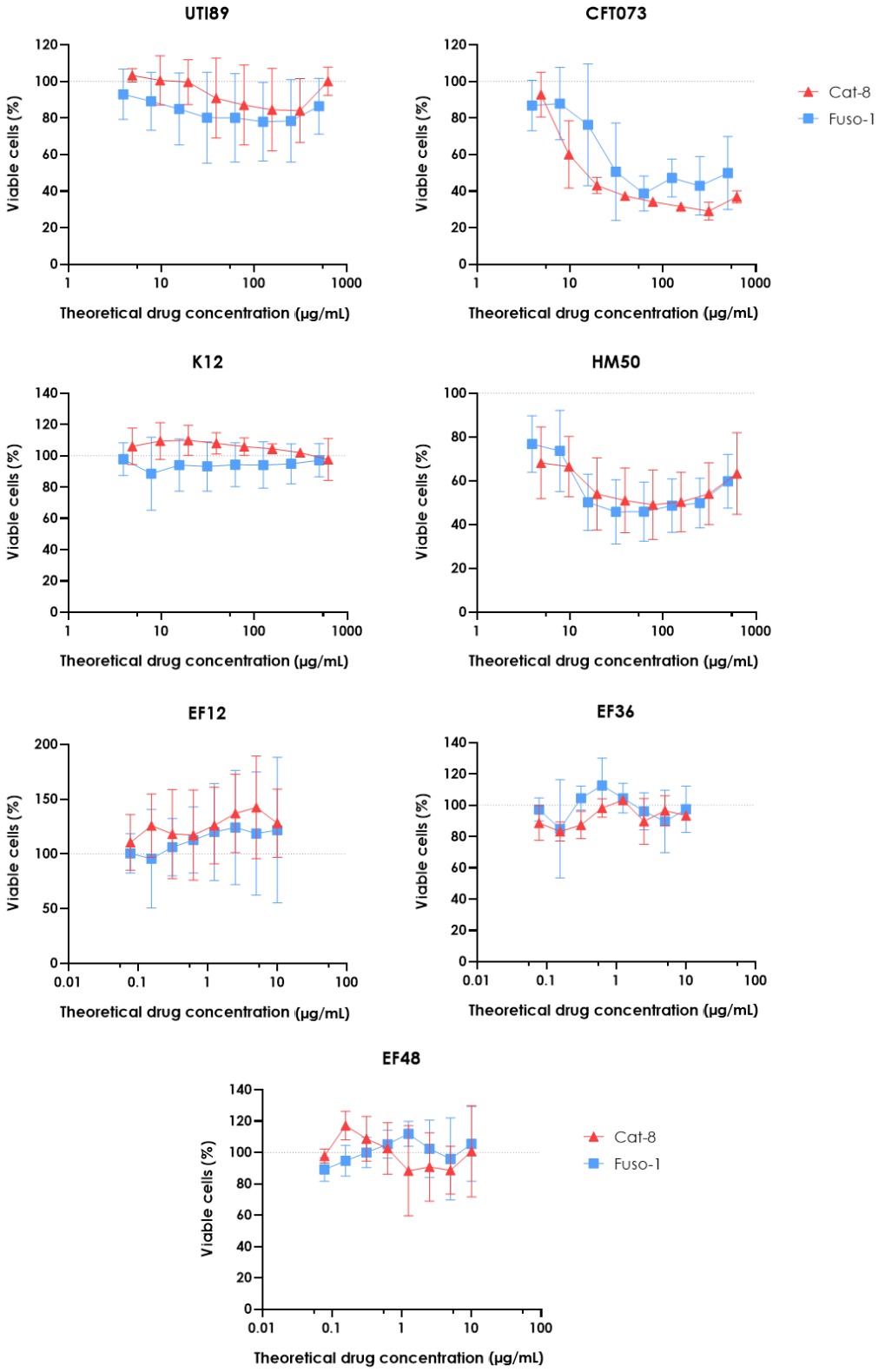


Figure 33 | Bacterial viability after treatment of planktonic monospecies models with unloaded liposomes. Four strains of *E. coli* (UTI89, CFT073, K12 and HM50) and three strains of *E. faecalis* (EF12, EF36, and EF48) were treated with unloaded cationic (Cat-8) or fusogenic (Fuso-1) liposome formulations, as part of an MBC assay. Liposomes concentrations of unloaded and VAN-loaded liposomes were matched to allow comparison with previous assays. The average number of viable cells was calculated as a percentage compared to a growth control (no treatment).

Although *E. faecalis* was found to be generally responsive to both VAN-loaded formulations, unloaded liposomes had no effect on bacterial growth, evidenced by the number of viable cells staying around 100% (**Figure 33**). It may even be the case that growth is promoted by the presence of the liposomes—EF12 show signs of such a trend, but there was no significant increase in bacterial viability to come to a solid conclusion. In combination with previous findings that liposomal encapsulation of VAN increased the MBC 4-fold against EF12, it is possible that this specific strain possesses features that make it more resilient in the presence of liposomes. Additionally, the lower liposome concentrations used against *E. faecalis* (to make these assays comparable with drug-loaded assays) may have been less obstructive to intercellular bacterial communication, which would explain why growth was not impaired for these strains. However, if this was the case, one might expect the increased liposome concentrations in *E. coli* samples to have diminished bacterial growth with both unloaded and drug-loaded liposomes of both types. Including more samples where equivalent liposome concentrations were used for both *E. coli* and *E. faecalis* may help to elucidate if the quantity of liposomes is indeed relevant for some of the observed bactericidal effects of unloaded liposomes. It would also be interesting to test various unloaded liposomes of different lipid compositions against these strains to assess whether any specific lipid components drive antibacterial effects independent of antibiotics used.

Overall, the current data suggest that Cat-8-VAN was generally equally as effective as free VAN against both planktonic *E. coli* and *E. faecalis*, except against EF12 where the MBC increased 4-fold upon liposomal encapsulation. Fuso-1-PEG-VAN seemed to show more of an affinity for Gram-positive bacteria, as it was able to facilitate complete bacterial death in all *E. faecalis* samples but not for any *E. coli* strains. Both formulations were particularly effective against planktonic EF36 where the MBC was halved. Unloaded liposomes generally did not impact bacterial viability on their own, except for in a couple of cases (HM50 and CFT073), where it is not quite understood why but further investigation into the underlying biochemistry would be beyond the scope of this project. From this data it appears as though Cat-8-VAN is the more suitable formulation given its

activity against both Gram-positive and Gram-negative species, but further probing into bacteria-liposome interactions for both formulations to understand whether and/or how the formulation affects these interactions may prove useful.

3.3.2 Preliminary findings from confocal imaging of *E. coli* and *E. faecalis* after liposome treatment

To get a clearer idea of whether observed bacterial cell death is likely due to interactions with the liposomes (i.e. via uptake or membrane fusion) instead of passive drug leakage/liposome bursting, one strain of *E. coli* (UTI89) and one strain of *E. faecalis* (EF36) were treated with DiD-labelled cationic or fusogenic VAN-loaded liposomes. UTI89 was chosen based on its status as a model UPEC organism and EF36 was chosen as the best-growing and most characterised of the clinical isolates used in this project[671]. After 24 hours of DiD-labelled VAN-loaded liposome exposure, the samples were live-dead stained and imaged with a confocal microscope (**Figure 34**). Overlap of fluorescence signal from labelled liposomes and stained cells was used as a proxy for interaction; if the liposomes were associated with or fused with the bacterial membrane, there should be increased colocalization of signal. Correlation of either dead cells or live cells with liposome signal was quantified via the Pearson's correlation coefficient (PCC, r). Live-dead ratios (LDR) were also calculated to compare the extent of visible cell death in the images, with both LDRs and PCCs summarised in **Figure 35**. Due to time and resources constraints, the following results are based on one biological repeat with at least three technical repeats. In addition to free VAN and no-treatment controls, more repeats are required to increase statistical power in comparisons.

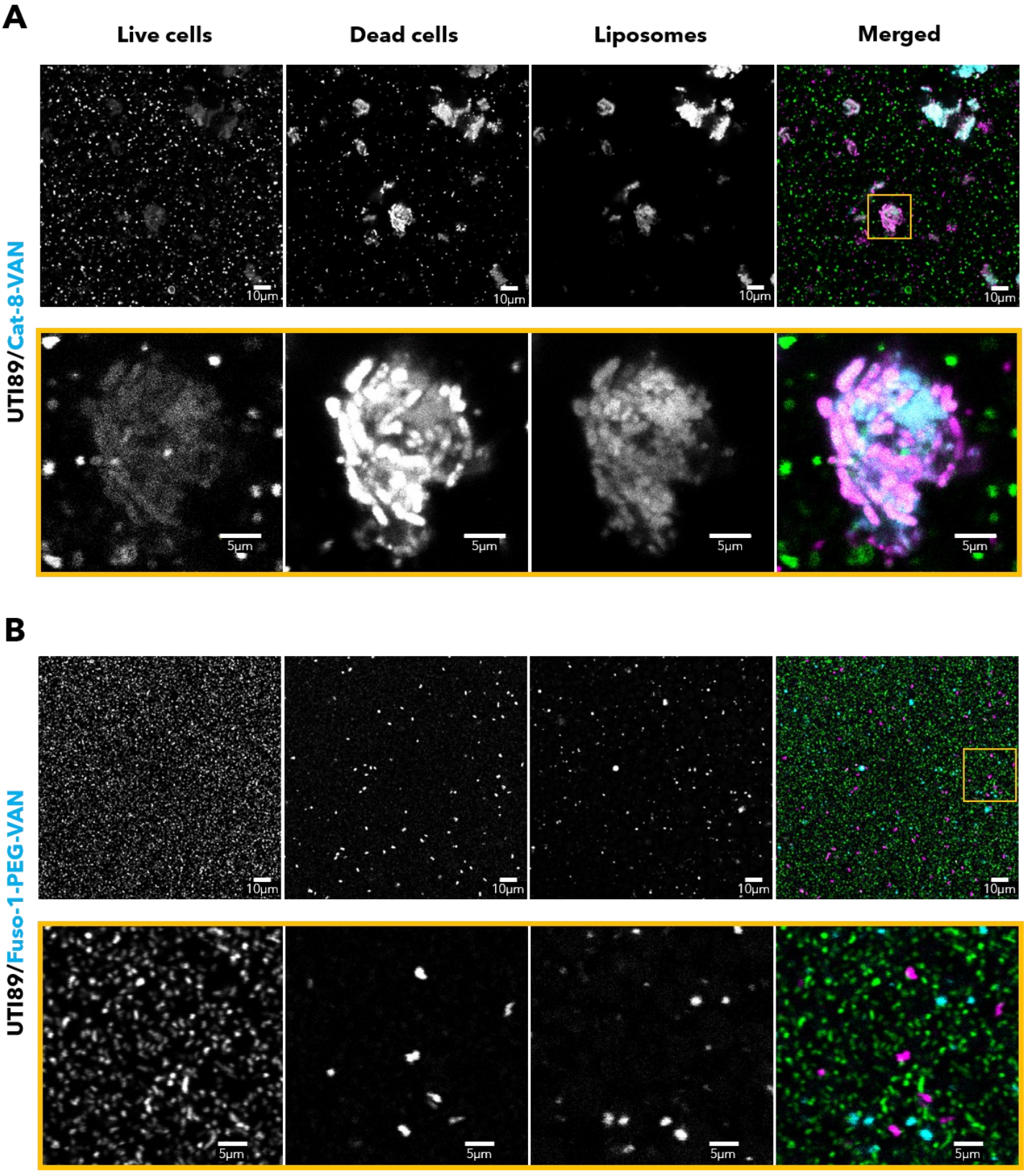
Confocal microscopy of treated UTI89 largely confirmed the trends observed in section **3.3.1**: comparing the treatment of UTI89 with Cat-8-VAN and Fuso-1-PEG-VAN, the cationic formulation was more effective at killing cells with a live-dead ratio of 1.92 ± 0.6 compared to 27.5 ± 12.7 (**Figure 35A**). Additionally, there was more colocalization of Cat-8-VAN with dead UTI89 cells signal (r =0.3) than with live cells signal (r =0.005), suggesting that liposome interaction is linked with bactericidal activity (**Figure 35B**). This colocalization is also visible in **Figure 34A**,

where dead cells and liposomes largely appear to be in the same location and forming structures of similar shapes. When treated with Fuso-1-PEG-VAN, cell death didn't appear to preferentially coincide with areas of liposome signal (**Figure 34B**)—there was essentially no difference in average PCC values between live cells (r=0.01) and dead cells (r=0.02).

One interesting observation to note is that the cationic liposomes appeared to be extensively aggregating; liposomes made to be around 100 nm in size were showing up in clumps that were tens of microns in size (**Figure 34A**). This is likely due to the high concentration of cationic liposomes interacting with negatively-charged components of the caMHB bacterial growth medium. This interaction was even more pronounced when Cat-8-VAN was added to standard MHB, which lacks the additional divalent cations found in caMHB; the liposomes appeared to precipitate out of the suspension with MHB, whereas with caMHB the suspension just became slightly cloudier (**Supplementary Figure 4**). This extent of clumping/aggregation was not seen with the neutral fusogenic liposomes (**Figure 34B**), neither was it seen when the liposomes were suspended in PBS (**Supplementary Figure 5**), which further suggests that electrostatic interactions may have a large part to play in the observed aggregation. PEGylation is also known to prevent aggregation which explains why this phenomenon was not observed with the PEGylated fusogenic formulation[378]. It is unclear whether this aggregation has any biological significance; as these aggregates were present even without the addition of bacteria, the increased colocalization of dead cells with these structures may have been because they were so large that there was a higher probability of colliding with bacteria. Once this interaction has occurred, the concentration of drug-loaded liposomes in the location would be relatively high to facilitate the increased killing observed. An alternative explanation could be that bacteria killed elsewhere (either naturally or through interactions with individual ~100 nm liposomes) are more likely to adhere to the large liposome aggregates that they collide with, essentially forming the basis of a biofilm[672]. Taking confocal images at different time-points over the 24 hours in a time-kill assay could help to elucidate how these structures influence overall liposome activity; this experiment might identify

whether live cells die before or after they come into contact with the liposome aggregates. Additionally, scanning electron microscopy (SEM) can be used to image the cells on these aggregates to understand if aggregates are coinciding with whole cells or dead cell fragments by looking at morphological differences[673,674]. Together, these follow-up experiments would give a better idea of the role that the liposome aggregates play. Furthermore, as these liposomes would not be administered into an environment that contains caMHB in a clinical context, it is important to test these particles in a physiological environment that the bacteria would normally be found in. A follow-up experiment that uses urine as growth medium instead would give more information about compatibility of the cationic formulation in a physiologically-relevant context, as it is clear that the medium has an effect on its physical properties and antimicrobial susceptibility[675].

Aside from the large liposome aggregates, it may be that many ~100 nm liposomes were actually present but not visible in these experiments due to resolution limits of the confocal equipment; confocal microscopy typically achieves a resolution limit around 250 nm[676]. As previously mentioned, Fuso-1-PEG-VAN did not appear to form such large aggregates but most of the visible particles were larger than 100 nm. This could mean that even though PCC comparison doesn't show an increased correlation between dead UTI89 cells and Fuso-1-PEG-VAN signal, individual ~100 nm liposomes may still be responsible for cell death but were just not detected. Super-resolution microscopy that allows for higher resolution probing of bacteria-liposome interactions would be beneficial to more confidently confirm that UTI89 cell death is likely linked to liposome uptake (or other forms of liposome-cell interaction).



(*Figure 34* continued on the next page)

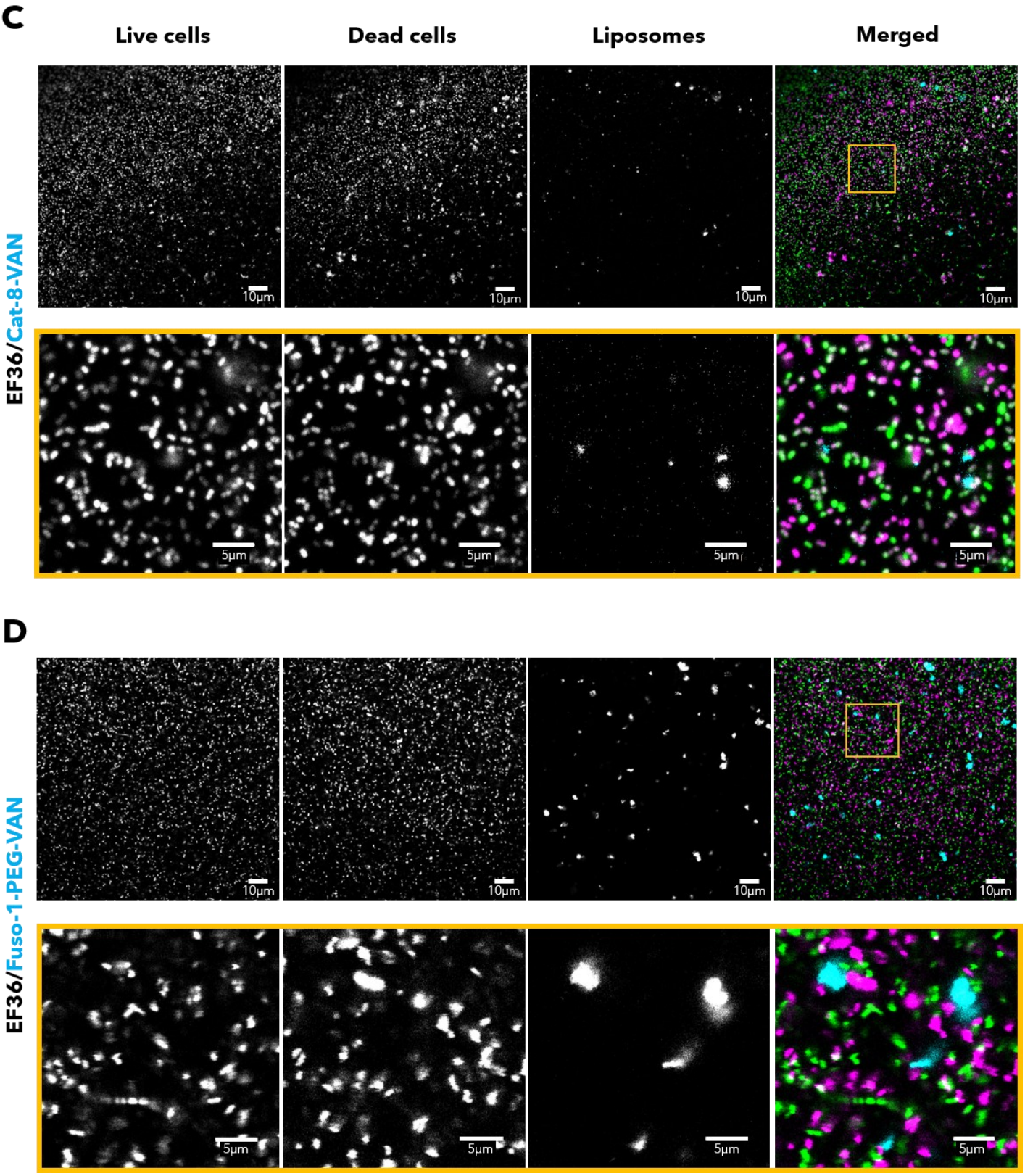


Figure 34 | Confocal images (100×) of UTI89 and EF36 after treatment with liposomal VAN. (A) UTI89 treated with Cat-8-VAN. (B) UTI89 treated with Fuso-1-PEG-VAN. (C) EF36 treated with Cat-8-VAN. (D) EF36 treated with Fuso-1-PEG-VAN. A selected area from each sample has been enlarged, highlighted in orange boxes. In the merged images, live cells are stained in green, dead cells in magenta and liposomes in cyan.

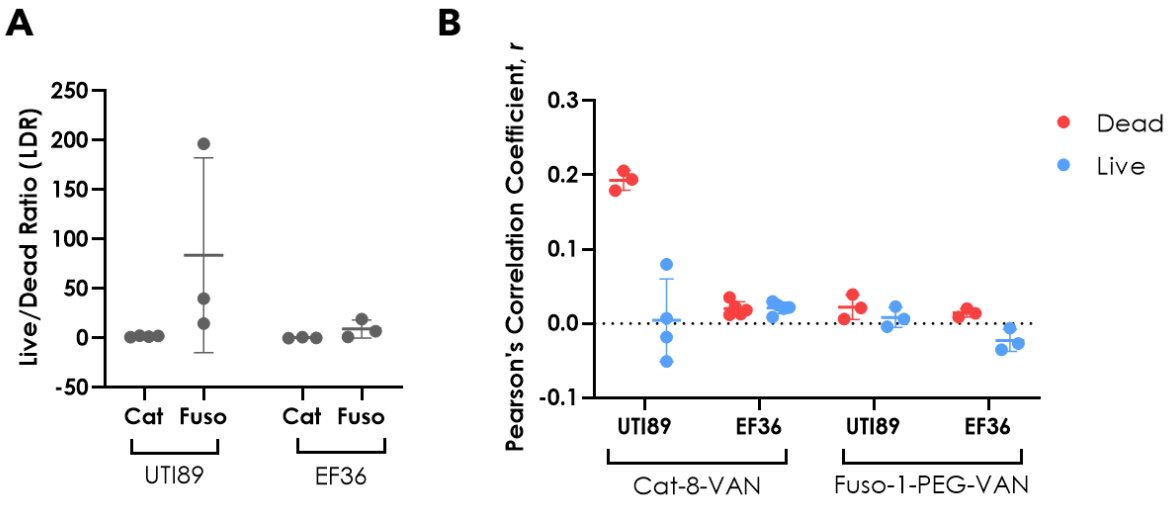


Figure 35 | Comparison of LDRs and PCCs from confocal images of UTI89 and EF36 after treatment with liposomes. (A) Live/dead ratios (LDRs) were calculated to quantify the extent of cell death relative to living cells after treatment with each formulation (Cat = Cat-8-VAN; Fuso = Fuso-1-PEG-VAN). (B) Pearson's correlation coefficient (PCC, *r*) values were determined to quantify the correlation between liposome signal and either dead cell signal (red) or live cell signal (blue). Data represents one biological experiment with at least three technical repeats.

For *E. faecalis*, the killing activity of both formulations was similar, as expected from previous findings; there wasn't a significant difference between the LDRs of Cat-8-VAN and Fuso-1-PEG-VAN with EF36 (**Figure 35A**). However, when analysing the confocal images, it appeared as though cell death did not coincide with the presence of liposomes (**Figure 34C/D**). This observation is supported by comparison of PCC values which revealed that there was no preferential correlation with dead cells seen for Cat-8-VAN, unlike what was observed with UTI89, suggesting that liposomal interaction was not linked to cell death here. Of note, at the lower VAN concentrations—and hence lower liposome concentrations—for *E. faecalis* treatment, the large Cat-8-VAN aggregates present in the UTI89 sample were not seen (**Figure 34C**). This indicates that aggregation of the cationic formulation may also be concentration dependent, which could restrict the formulation if an aggregate-free suspension is required further down the clinical pipeline to avoid immunogenic reactions and optimise interactions with bacterial cells[677–679]. This lower liposome concentration may also have been harder to visualise at the resolution of the confocal equipment used. Interestingly, signal correlation analysis seemed to indicate that there

was a slightly greater correlation between Fuso-1-PEG-VAN liposome signal and dead EF36 compared to live EF36 (**Figure 35B**). This result is not necessarily surprising given that it was previously shown that the PEGylated liposomes may preferentially interact with Gram-positive bacteria (see section **3.3.1**). However, the average PCC for this sample was close to zero (r=0.01) indicating no signal correlation, which seemed to better reflect what was seen in the acquired images (**Figure 34D**); detectable liposome signal thus did not really coincide with dead or live bacteria. Because previous findings suggested that liposome formulation increased VAN efficacy in EF36, it is unlikely that liposome interaction is not involved for both Cat-8-VAN and Fuso-1-PEG-VAN. It is possible that cell death is linked to liposome interaction but the resolution limit would prevent signal from ~100 nm liposomes being detected to confirm this hypothesis. Therefore, experiments using super-resolution microscopy would be the next step towards drawing a more confident conclusion on whether liposome interaction (i.e. uptake or membrane fusion) is largely responsible for bacterial cell death.

Overall, preliminary confocal microscopy studies to ascertain the involvement of liposome interaction in antibacterial activity have largely confirmed previous findings: Fuso-1-PEG-VAN activity was limited against UTI89 but showed promise against EF36, and Cat-8-VAN was effective at keeping the LDR relatively low for both species. A striking observation around the aggregation of Cat-8-VAN in caMHB was made, which may have implications on the antibacterial activity of the liposomes given that these aggregates greatly coincided with dead UTI89 cells. Microscopy at a higher resolution (i.e. super-resolution microscopy) would be beneficial to shed light on bacteria-liposome interactions that may be facilitating imaged cell death but were not detectable using the current setup due to its resolution limit.

3.3.3 Preliminary observations of liposome interactions using super-resolution microscopy

In an attempt to visualise bacteria-liposome interactions beyond the confocal microscopy resolution limit, pilot super-resolution microscopy studies were carried out using direct stochastic optical reconstruction microscopy (dSTORM). This technique utilises high-intensity lasers that activate single fluorophores to blink 'on' and 'off' in a stochastic manner, switching between a fluorescent state and dark state, to give an optical resolution of ~20 nm[680]. In this case, the photoswitchable fluorophores were conjugated either to antibodies specific to PEG or to WGA, which allowed marking of PEGylated liposomes and bacterial membranes, respectively. Due to this PEG requirement, Cat-8 liposomes which had no PEG content could not be imaged using this technique so Fuso-1-PEG-VAN was used to treat one strain of *E. coli* (UTI89) and one strain of *E. faecalis* (EF36) for imaging. The following data are from a single dSTORM run and have been interpreted qualitatively as a result. Further optimisation and more biological repeats are required which could not be achieved during the current study due to time and expertise constraints.

An on-chip staining protocol was followed as described in section **3.2.4**, which involved immobilising bacteria on the imaging chip before flowing through the fluorescent markers. This allowed for imaging of fixed bacteria and associated liposomes, as shown in **Figure 36**. Although the background signal was relatively high, particularly for EF36 (**Figure 36B**), structures that resemble bacterial cells could be made out for both samples. Using an in-solution staining protocol may help with reducing background signal as this method involves staining bacteria and liposomes before immobilisation on the imaging chip, reducing the chance of excess dye adhering to the chip.

When comparing the two samples, it looked as though more EF36 was captured on the imaging chip than UTI89, which may be down to variation in growth or sample preparation during staining—repeating this process with different replicates should help to clarify this. With UTI89, there didn't seem to be much colocalization of signal between the bacteria and Fuso-1-PEG-VAN (**Figure 36A**); most of the liposome signal found within proposed bacterial cells didn't look much

different from the surrounding background signal patterns, so was unlikely to be any real indication of liposomal uptake. From previous experiments, this is to be expected as Fuso-1-PEG-VAN showed virtually no correlation with UTI89, as well as had no effect on bacterial viability. On the other hand, with EF36, many of the assumed cell structures looked like they had a region of liposome signal within them that was not really visible outside these structures (**Figure 36B**). This might indicate that Fuso-1-PEG-VAN was taken up more readily by EF36 than UTI89, which would also align with previous findings detailed in sections **3.3.1** and **3.3.2**. Taking some confocal images to accompany these super-resolution images could help to confirm the presence and location of individual bacteria cells, so one can more confidently mark the observed structures as cells. dSTORM images of only Fuso-1-PEG-VAN were taken to improve confidence in identifying liposomes within a treated sample (**Supplementary Figure 6**) but the preparation process needs to be further optimised to help reduce the high background signal in these samples.

These preliminary dSTORM images appear to align with previous microscopy and MIC/MBC assay observations to suggest that EF36 does interact with Fuso-1-PEG-VAN more than UTI89 does. Taken together with prior findings, the evidence points to differential uptake of PEGylated liposomes between Gram-negative *E. coli* and Gram-positive *E. faecalis*.

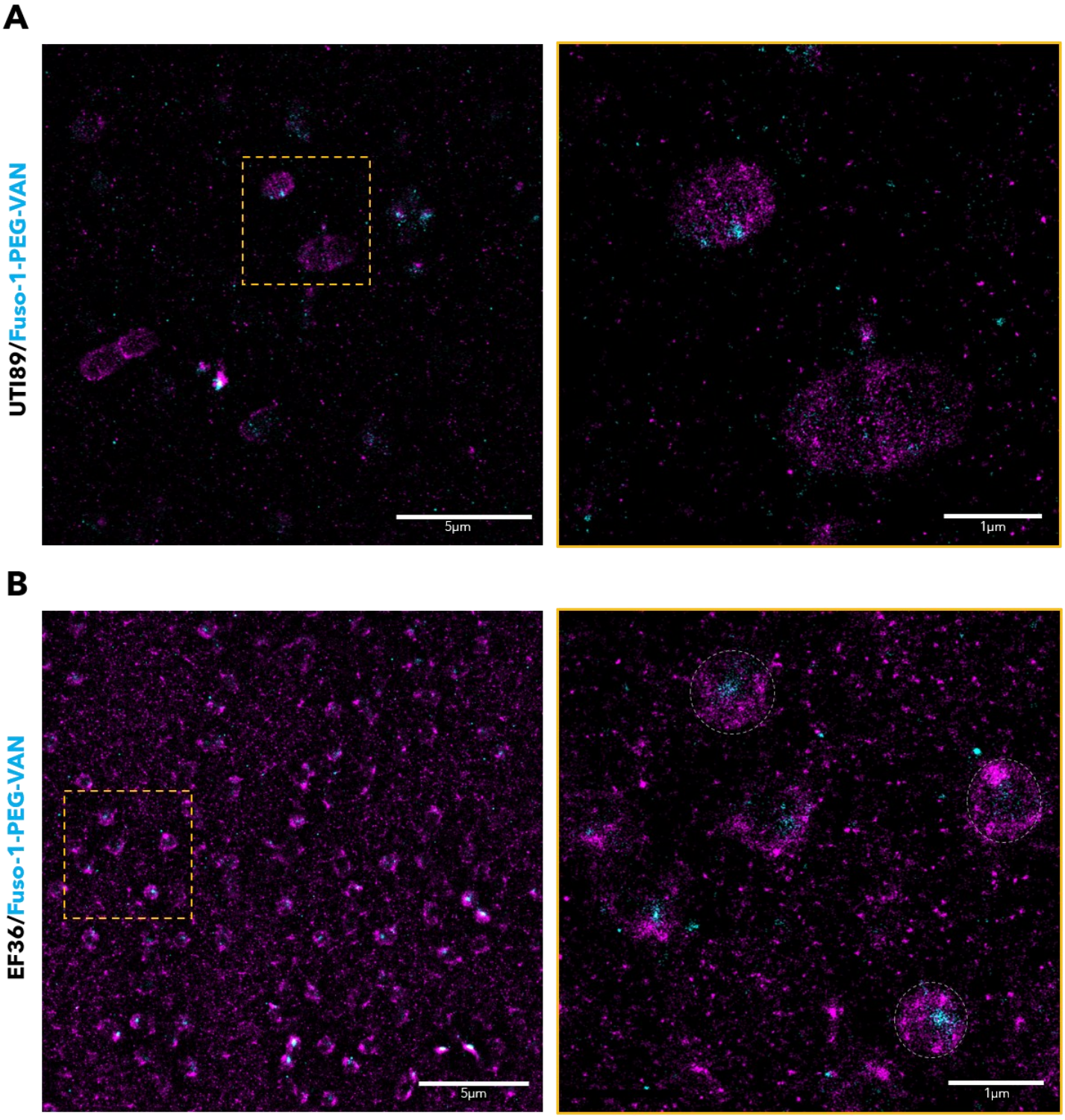


Figure 36 | Super-resolution images of UTI89 and EF36 after treatment with Fuso-1-PEG-VAN. Super-resolution dSTORM images of (A) UTI89 and (B) EF36 treated with Fuso-1-PEG-VAN. A selected area from each sample, highlighted in an orange box, has been enlarged as the right-hand-side image of each panel. Bacteria are shown in magenta and liposomes in cyan. Examples of assumed bacterial cell structures for EF36 are outlined in grey.

3.3.4 Investigating the effect of liposomal PEG content on bacterial interaction

To test the hypothesis that PEGylation hinders fusogenic liposome interaction with *E. coli* but not with *E. faecalis*, fusogenic liposomes with either 2.5% or 1% molar weight PEGylated lipid (instead of 5%) were produced. If PEGylation allows for preferential interaction with Gram-positive *E. faecalis* over Gram-negative *E. coli*, reducing the amount of PEG within the formulation, should theoretically allow the liposomes to facilitate killing of *E. coli* while reducing the effectiveness of the liposomes against *E. faecalis*.

During the manufacturing process, it was found that using lower PEG concentrations led to the formation of lipid films that did not successfully rehydrate; many large sediments of lipid film remained in the suspension before and after extrusion and were more prevalent with 1% PEG (**Supplementary Figure 7**). This was reminiscent of the difficulties encountered when producing the original non-PEGylated Fuso-1 formulation in chapter **2** (**Supplementary Figure 2**), highlighting the necessity of PEGylated lipids to stabilise this formulation right from manufacturing in the first place. Measuring particle size, concentration and encapsulation revealed that reduced PEG concentrations indeed influenced the properties of the liposomes, making them slightly different to the original Fuso-1-PEG (5%) formulation (**Table 7**). For example, as the PEG content decreased, the polydispersity index (PDI) increased, indicating that the suspensions were becoming less stable with a greater mix of smaller and larger particles. The encapsulation efficiency also increased to over 60% which could be a result of a higher particle concentration being able to encapsulate more drug molecules. Theoretically, these liposome suspensions were prepared with the same lipid concentrations, but 2.5% and 1% PEG preparations saw sedimentation and likely loss of lipid constituents, reducing the available lipid concentration. Despite this, larger particles, increased particle concentrations and encapsulation efficiencies were measured, which may lead to liposomes with reduced PEG content that are more prone to drug leakage; if fewer lipids go into making more and larger drug-loaded liposomes, the drug-to-lipid ratio would increase, producing particles that may not be as stable or impermeable[681]. This potential

impact on VAN release, in addition to the varying particle properties and observed sedimentation, points to 2.5% and 1% PEG liposomes being of a lower quality than the original 5% PEGylated formulation. Although only one batch of these reduced-PEG formulations was made, because the findings resemble that of previous experiments involving the non-PEGylated fusogenic formulation, it was assumed that these properties were representative. Therefore, reducing PEG amount in the fusogenic formulation likely negatively impacts the stability and structure of the particles, which may have downstream consequences on bacterial activity.

Table 7 | Summary of properties of fusogenic liposomes containing varying PEG content. Average size, polydispersity index (PDI), zeta potential, particle concentration and encapsulation efficiency for DiD-labelled Fuso-1-PEG-VAN liposomes containing either 5% (original), 2.5% or 1% PEG. Average values are from repeat measurements on a single batch.

PEG content (%)	Average size (nm)	Average PDI	Average zeta potential (mV)	Liposome concentration (particles/mL)	Encapsulation efficiency (%)
5	114 ± 0.9	0.086 ± 0.02	-3.52 ± 0.73	1.84×10^{11}	35.9
2.5	100 ± 11.6	0.181 ± 0.14	-4.53 ± 0.43	2.65×10^{11}	61.7
1	118 ± 23.1	0.353 ± 0.3	-4.26 ± 0.34	3.34×10^{11}	62.3

The reduced-PEG formulations were labelled with DiD and incubated with one strain of *E. coli* (UTI89) and one strain of *E. faecalis* (EF36). After 24 hours, the samples were live-dead stained and imaged using confocal microscopy, in the same fashion as in section **3.3.2** (**Figure 37**). Colocalization of fluorescence signal from labelled liposomes with stained cells was used as a proxy for interaction and quantified via the Pearson's correlation coefficient (PCC, r). Live-dead ratios (LDR) were calculated to quantify the extent of visible cell death in the images. PCCs and LDRs are summarised in **Figure 38**. Statistical analyses were not performed due to the limited sample size (one biological sample with at least three technical repeats).

At both 2.5% and 1% PEG content, a lower liposome concentration was reflected in the images (**Figure 37**), with fewer liposome signals being visible when compared to images in section **3.3.2**.

Although a higher liposome concentration was initially recorded for these reduced-PEG formulations, the increased PDI and sedimentation observed may have resulted in liposome deposition and accumulation at the bottom of the sample tube, effectively decreasing liposome concentration. Interestingly, despite this, reducing the PEG amount to 2.5% seemed to work towards increasing the antibacterial activity of the liposomes against UTI89 as the average LDR was decreased from 83.9 ± 80.4 with the original 5% PEG formulation to 3.6 ± 0.6, which would suggest 2.5% PEG resulted in fewer living cells and/or more dead cells, but this is not a certain conclusion given the large variation (**Figure 38A**). Liposome signal did not show increased colocalization with dead UTI89 signal over live cell signal, with ***r*** remaining around zero (**Figure 37A** and **Figure 38B**). This would suggest that changes in live/dead cell count are not due to direct liposome interactions, but perhaps due to VAN more readily released/leaked from the lower quality liposomes to give bactericidal concentrations. Alternatively, it could be that the active liposomes do show increased interaction as a result of lower PEG content but the liposomes are too small to be detected here. However, as this was the only biological replicate using a single liposome batch, it is also possible that there would be a natural variation in bacterial growth, so more repeats are needed to come to a confident conclusion.

For the 1% PEGylated formulation, this apparent effect on UTI89 growth is lost with the LDR increasing to 11.1 ± 2.5 (from 3.6 ± 0.6 with 2.5% PEG), and the correlation between liposome signal and dead or live cell signal being ~0 (**Figure 38**). This suggests that steric hindrance via PEGylation may not be the main factor impairing Fuso-1-PEG-VAN activity against UTI89, as decreasing PEG to 1% did not significantly increase bacterial cell death. However, if the fact that reducing PEGylation led to poorer liposome quality is taken into consideration, it is more likely this has a meaningful impact on drug delivery, resulting in less cell death and signal colocalization. One observed difference between 2.5% and 1% PEGylated liposomes was the amount of sedimentation present; liposomes suspensions with a greater size dispersity and larger sediments were observed at 1% PEG (**Table 7** and **Supplementary Figure 7**). This may have meant that

more of the 1% PEGylated liposomes sedimented at the bottom of the tube, effectively reducing chances for liposome interactions with bacteria and VAN release, giving an increased LDR compared to 2.5% PEG. However, again, it is also possible that this is the result of natural variation in bacterial growth, so more repeats are needed.

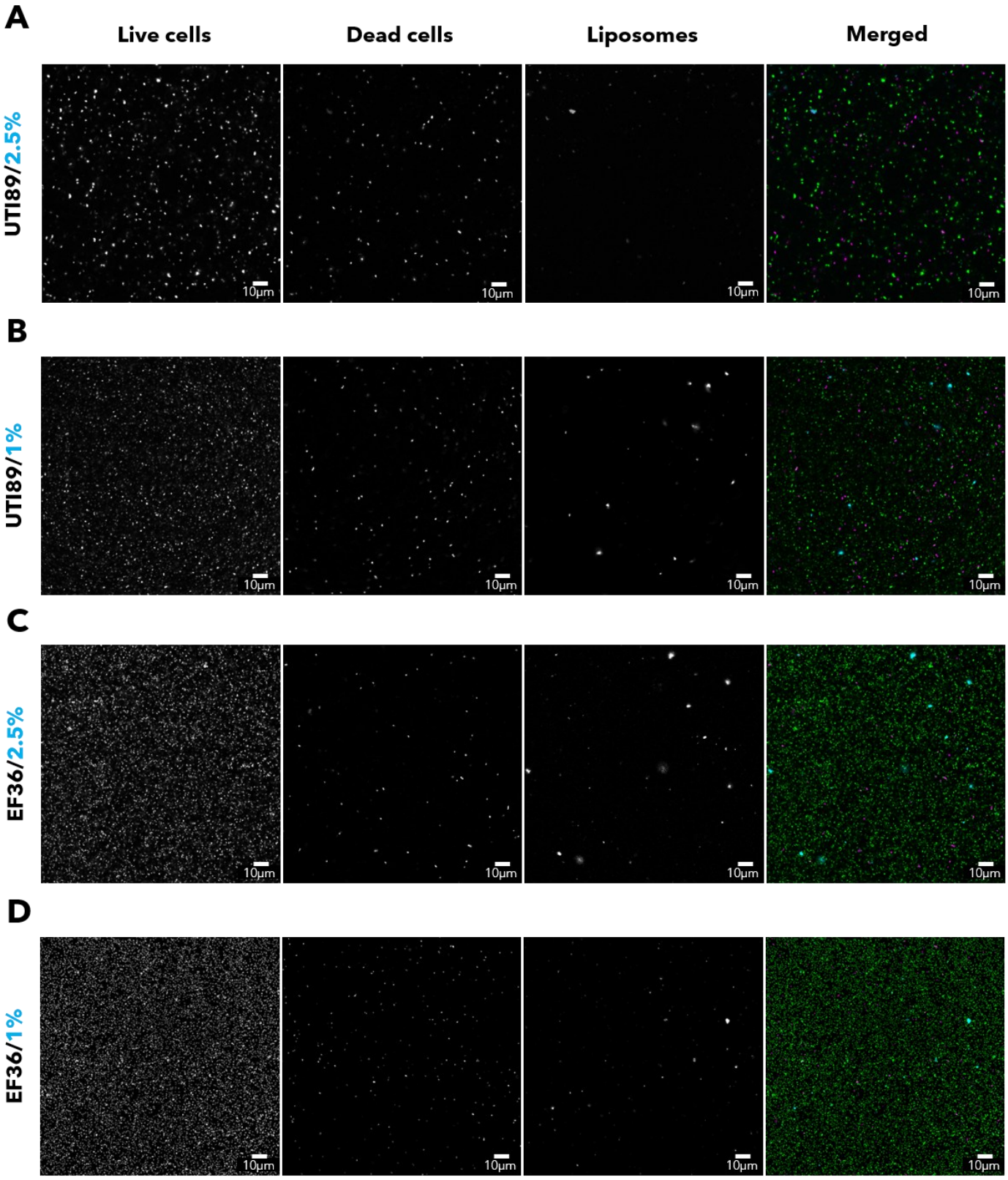


Figure 37 | Representative confocal images of UTI89 and EF36 after treatment with fusogenic formulations containing either 2.5% or 1% PEG. UTI89 treated with Fuso-1-PEG-VAN containing (**A**) 2.5% PEG or (**B**) 1% PEG. Below this, images of EF36 treated with Fuso-1-PEG-VAN containing (**C**) 2.5% PEG or (**D**) 1% PEG are shown. In the merged images, live cells are stained in green, dead cells in magenta and liposomes in cyan.

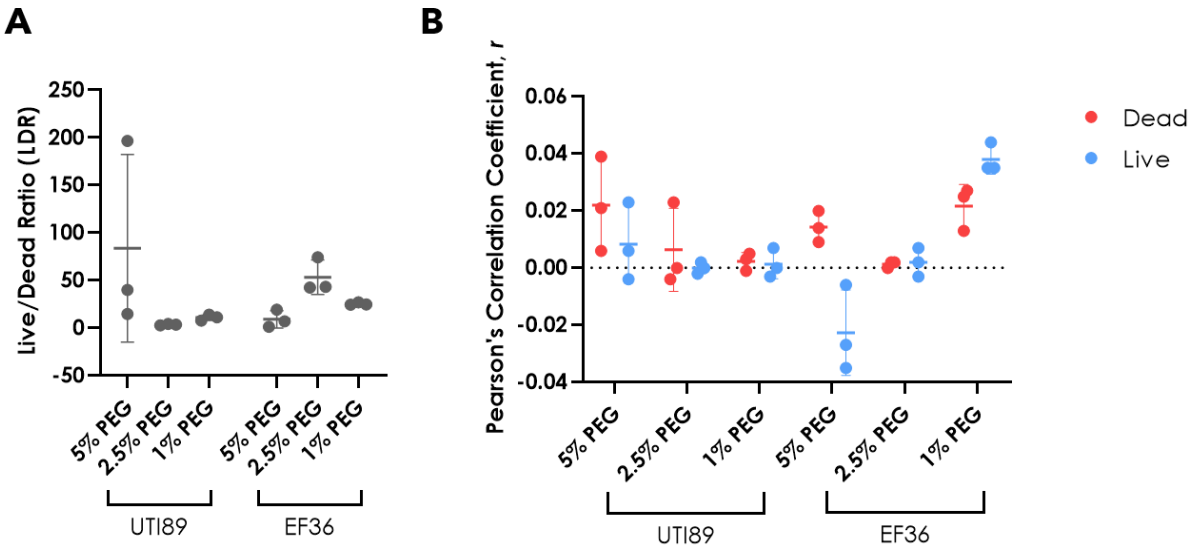


Figure 38 | Comparison of LDRs and PCCs from confocal images of UTI89 and EF36 after treatment with fusogenic liposomes containing either 5% (original), 2.5% or 1% PEG content. (**A**) Live/dead ratios (LDRs) were calculated to quantify the extent of cell death relative to living cells after treatment with each formulation. (**B**) Pearson's correlation coefficient (PCC, *r*) values were determined to quantify the correlation between liposome signal and either dead cell signal (red) or live cell signal (blue). Data represents one biological experiment with three technical repeats.

With EF36, reduced PEGylation appeared to have the opposite effect, with the number of live cells visibly outnumbering dead cells (**Figure 37C/D**). A relatively large reduction in antibacterial activity was observed as PEG content was halved from 5% to 2.5%; the average LDR increased from 9.3 ± 7.4 at 5% PEG to 53.5 ± 14.8 at 2.5% PEG (**Figure 38A**). Analysis of signal colocalization found that there was largely no correlation between liposomal signal and dead or live cells, which indicated that reduced PEGylation might result in reduced cell death-related interactions. Further reduction of PEG to 1% did not further decrease antibacterial activity; LDR was increased to 25.6 ± 1.1, not as high as seen with 2.5% PEG (**Figure 38A**). Additionally, liposome signal appeared to colocalise more with live EF36 cells than dead EF36 cells, although this correlation was still around 0 (**Figure 38B**). It is unclear why reduction to 1% PEG would increase antibacterial activity (giving a lower LDR) relative to 2.5% PEG—perhaps, the reduced liposome quality of 1% PEGylated liposomes led to more drug leakage and thus increased overall antibacterial activity compared to 2.5% PEG. When compared with 5% PEG, it still follows the trend that reduced PEG, on the whole, reduces antibacterial activity. The fact that these 1%

PEGylated liposomes also seemed to colocalise slightly more with live EF36 cells than dead cells suggests that the liposomes still interact with bacteria but are unable to facilitate a killing effect. This could be down to the poorer liposome quality, potentially with reduced intravesicular VAN concentrations due to leakage, overall showing reduced potency and efficacy on the cells that the liposomes interact with. It was previously suggested that the lower quality liposomes may more readily release/leak VAN into the surrounding media as a way to explain reduced LDRs (i.e. more killing) with UTI89 despite no signal colocalization. This could also be the case here as previous findings demonstrated that liposomal VAN was more effective than free VAN against EF36 (**Figure 32**), so leakage/release would not result in as much cell death. In fact, the presence of subinhibitory concentrations of VAN could promote bacterial growth and virulence, which could manifest in increased LDRs[666]. Including a control sample as an example of an expected LDR would give insights into whether the increased LDRs have a greater biological significance.

In a separate experiment, the antimicrobial activity of the reduced-PEG formulations was tested against UTI89 and EF36 in an MIC/MBC assay. There was found to be no effect on bacterial viability for either of the strains (**Figure 39**). This aligns with findings for EF36 where any reduction in PEG appeared to reduce bacterial killing effects, particularly when compared to the original 5% PEG formulation. At the drug concentration used for imaging studies on EF36 (4 μg/mL), it follows that bacterial viability (hence LDR) would be slightly elevated for 2.5% and 1% PEGylated liposomes. This MIC/MBC assay also largely aligns with UTI89 observations as the LDR was not definitively reduced after reducing PEG content from 5%, and at the drug concentration used for imaging studies on UTI89 (312.5 μg/mL), the viable cell count is not likely to vary much between the formulations. However, more repeats are necessary to make further comments on these differences.

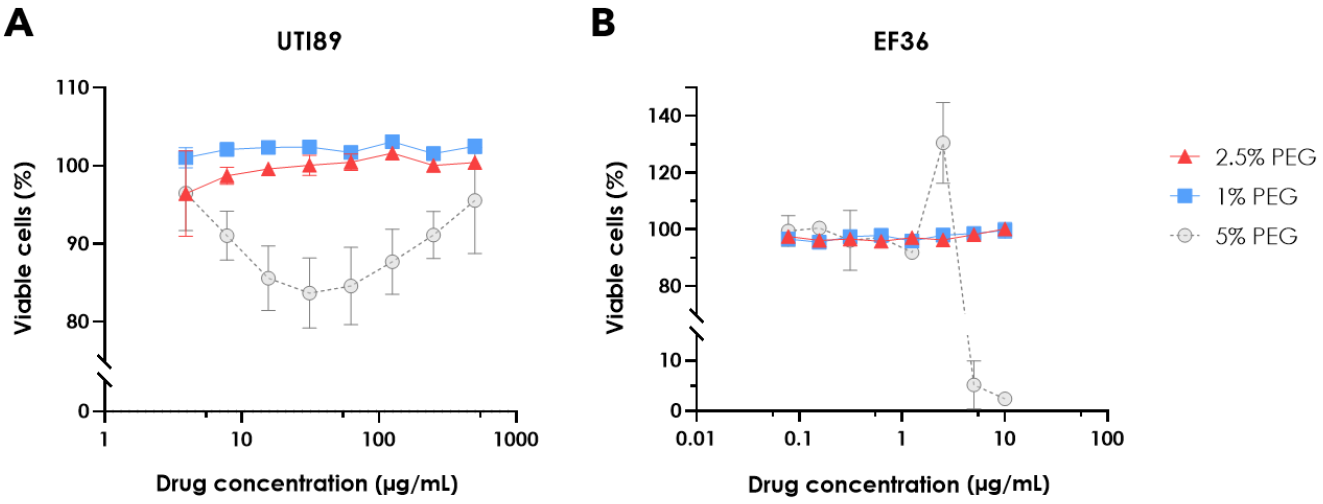


Figure 39 | Bacterial viability of UTI89 and EF36 after treatment with fusogenic liposomes containing either 5% (original), 2.5% or 1% PEG content in MBC assay. Bacterial viability of (A) UTI89 and (B) EF36. Fusogenic liposomes with varying PEG content were matched for drug concentration. The average number of viable cells was calculated as a percentage compared to a growth control (no treatment) and plotted for each drug concentration tested. Data for 2.5% and 1% PEG represents one biological experiment with three technical repeats.

With preliminary data that do not establish a clear concentration-dependent trend, it is hard to conclude how varying levels of PEG content within the fusogenic formulation affects its interactions with UTI89 and EF36. Although it appeared as though reducing PEG content below 5% increased antibacterial activity somewhat against UTI89 and decreased it against EF36, the liposome quality was relatively poor and the results were likely not an accurate reflection of downstream effects of solely varying PEGylation on bacterial interaction. Additionally, more practical repeats are required to confirm these preliminary findings, as these results may be due to natural biological variation. Furthermore, experiments using different Gram-positive and Gram-negative species, such as *K. pneumoniae* and *S. aureus*, might actually better clarify the extent that liposome PEGylation contributes to differential interaction with both classes of bacteria.

Overall, 5% PEG content gave the best results in terms of liposome quality and bacterial interaction, particularly against EF36, and confirmed by previous data (sections **3.3.1**, **3.3.2**, and **3.3.3**), so experiments were continued with this formulation.

3.3.5 Investigating liposomal nitrofurantoin activity against planktonic bacteria

To date, no published research involves liposomes loaded with nitrofurantoin (NIF) despite the widespread use of this antibiotic in UTI treatment. These novel cationic and fusogenic formulations were used to treat planktonic *E. coli* (UTI89, CFT073, K12, HM50) and *E. faecalis* (EF12, EF36, EF48) in a similar series of MIC/MBC assays to that of section **3.3.1**. Serial dilutions of free NIF were tested against the bacteria as a control to obtain the MIC and MBC values for these specific strains. The efficacy of Cat-8-NIF and Fuso-1-PEG-NIF was then compared to the free NIF control to assess whether encapsulation within these liposome formulations affects the drug's antibacterial efficacy. The MIC and MBC values of NIF treatment for each strain are summarised in **Table 8**.

NIF has a documented breakpoint of 64 μg/mL for both *E. coli* and *E. faecalis*[657]. Looking at the MICs of free NIF against all tested strains, they were all considered susceptible to NIF, with MICs below 64 μg/mL (**Table 8**). Further MBC assays revealed that 2-4 times higher concentrations of NIF where needed to facilitate bactericidal effects for every strain. The mechanism of action of NIF involves disruption of bacterial ribosomes and enzymes to interfere with DNA and cell wall synthesis, as well as other metabolic pathways, that results in bacterial cell death rather than an inhibition of growth, which is supported by the MBC:MIC ratios ≤ 4 observed here[258,262,658]. However, even though free NIF appeared to inhibit growth at 15.625 μg/mL for EF12 and EF48, MBC assays revealed that complete cell death was never really achieved (but viable cell count was significantly reduced); at and above 62.5 μg/mL, EF12 viability was reduced to ~6.3% and EF48 to ~15.8%, so it is debatable whether a true MBC value was actually reached in these samples. Perhaps increasing the maximum NIF concentration tested in this assay may yield results that bring viable cell count to 0. However, given that the significant reduction in bacterial viability was initially seen at 62.5 μg/mL and two-fold increments to 500 μg/mL did not cause any further drop in viability, it is possible that a 99.9% drop in cell viability would not be reached even within an extended concentration range. It is not clear why this is observed for these strains, especially given

that free NIF killed at least 99.9% of EF36 cells, albeit at a relatively high concentration (125 μg/mL). This may be a result of biofilm formation naturally occurring during the 48-hour time period of the MBC assay, with many prior studies having documented *E. faecalis* biofilms established within 24 hours[682,683]. A small subpopulation protected from NIF treatment could persist and show up as viable, but it is still expected that increasing drug concentrations would correspondingly decrease cell viability rather than keep it static, even in this scenario. Repeating these MBC assays in a 24-hour window (or less) instead of 48-hour can be used to probe the likelihood of early biofilm formation contributing to this apparent low-level tolerance to free NIF.

Table 8 | Summary of MIC and MBC values of NIF treatments. Inhibitory and bactericidal drug concentrations that were above the free NIF baseline concentration are coloured in red. All concentrations are in μg/mL. In some cases, the number of viable cells was significantly reduced but not completely to 0—such results are marked with an asterisk (*).

	Strain	MIC (μg/mL)			MBC (μg/mL)		
		Free	Cat-8	Fuso-1-PEG	Free	Cat-8	Fuso-1-PEG
E. coli	UTI89	15.625	62.5	250	31.25	125	500
	CFT073	15.625	62.5	250	62.5	250	500
	K12	15.625	62.5	125	31.25	250	500
	HM50	15.625	125	250	31.25–62.5	250	500
E. faecalis	EF12	15.625	62.5	125	62.5*	500*	500*
	EF36	31.25	125	500	125	>500	>500
	EF48	15.625	62.5	125	62.5*	250*	250*

Liposomal NIF activity against planktonic *E. coli*

Treating *E. coli* with liposomal NIF showed an overall decrease in antibiotic efficacy as evidenced by the increased concentrations needed for inhibitory/bactericidal effects, where the fusogenic formulation was less effective than the cationic formulation (**Table 8** and **Figure 40**). For example, Cat-8-NIF required a 4-fold increase in NIF concentration for the killing of UTI89 compared to the free drug, whereas Fuso-1-PEG-NIF increased the MIC/MBC 16-fold. This observation of increased MIC/MBC after liposomal encapsulation could be due to the chemical nature of NIF being more lipophilic than VAN, making it able to enter the lipid membrane and affect the packing of the phospholipids[619,631]. This could lead to an altered drug release profile compared to liposomes loaded with the more hydrophilic VAN, as a proportion of NIF may have been trapped within the lipid membrane, which would explain why a higher concentration of liposomal NIF is needed to facilitate equivalent killing effects. NIF could also differentially interact with the various lipids found in both formulations, and even PEG chains—PEG has been used as an additive to influence NIF solubility—which could contribute to the observation of the PEGylated fusogenic liposomes being less effective than cationic ones[684,685]. Performing drug release experiments with NIF-loaded liposomes would be necessary to explore how this drug is released over time in an aqueous environment. Additionally, cryo-TEM could be used to obtain detailed information on liposome structure and morphology, comparing liposomes before and after drug loading[421,686]. These added experiments would allow conclusions to be made on how NIF affects the liposome physicochemical properties and downstream drug delivery.

Another notable trend was that fusogenic liposomes loaded with NIF were able to significantly reduce the viable cell count of all *E. coli* strains (**Figure 40**), albeit at the highest concentration tested (500 μg/mL), whereas its VAN-loaded counterpart didn't work against any strains at any concentration. This data would potentially fit with the hypothesis that PEGylation hinders interactions with *E. coli* and if NIF has increased association and interference with the lipids that make up the liposome membrane, alteration of the phospholipid arrangement could relieve some

of that steric hindrance to allow for meaningful NIF delivery, but not so much as to match with Cat-8-NIF.

Again, HM50 shows increased sensitivity to liposomal NIF when compared with the other *E. coli* strains (**Figure 40**); encapsulation of NIF within the cationic formulation decreased viable cell count to about 50%, even at the lowest concentration tested (3.9 µg/mL). This is similar to its response to Cat-8-VAN and is consistent with the hypothesis that HM50 lacking the fimbriae found in invasive UPEC species associated with symptomatic UTIs allows for closer interactions with cationic liposomes and leads to better NIF delivery even at low concentrations[663].

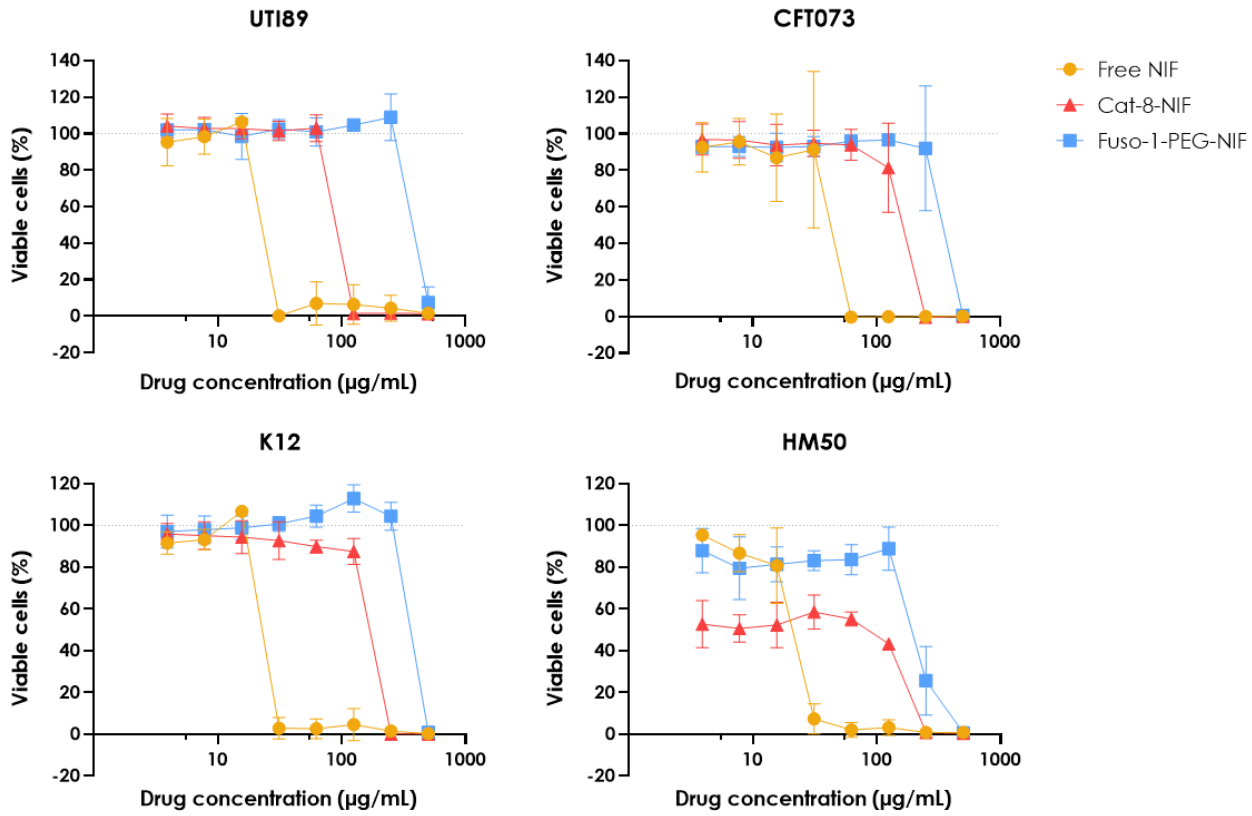


Figure 40 | Bacterial viability of four *E. coli* strains after treatment with NIF formulations in MBC assays. Four strains of *E. coli* (UTI89, CFT073, K12 and HM50) were treated with free NIF, cationic liposome-encapsulated NIF (Cat-8-NIF) or fusogenic liposome-encapsulated NIF (Fuso-1-PEG-NIF), matched for drug concentration, as part of an MBC assay. The average number of viable cells was calculated as a percentage compared to a growth control (no treatment) and plotted for each drug concentration tested.

Liposomal NIF activity against planktonic *E. faecalis*

Treatment of *E. faecalis* strains with liposomal NIF gave varied outcomes. As previously mentioned, for EF12 and EF48, complete killing (i.e. ≤0.1% viable cells) was not observed when treated with free NIF. Of note, sub-lethal concentrations of NIF may more effectively trigger upregulation of virulence and growth genes in *E. faecalis*; viable cells increased to ~250% relative to a growth control when EF12 and EF48 were treated with up to 15.625 μg/mL of free NIF, and when EF36 was treated with up to 31.25 μg/mL of free NIF (**Figure 41**). This mirrors data from previous assays involving VAN treatment, where increasing but sub-lethal concentrations of drug often resulted in an increasing viable cell count before a plummet at the lethal dose. Using NIF against *E. faecalis* gave a more pronounced response. This could be due to the mechanism of action of NIF requiring intracellular access to act on metabolic processes, which more effectively triggers upregulation of growth and virulence (compared to VAN that acts directly on the bacterial cell wall). This might also be responsible for the observation of viable cells not going below ~6.3% and ~15.8% for EF12 and EF48, respectively; perhaps specific genes were upregulated that allow for a small tolerant subpopulation to persist. It would be useful to have performed these experiments on a model *E. faecalis* strain, such as OG1RF, in addition to clinical isolates as its genetics and virulence are well-characterised[687].

In general, liposomal encapsulation of NIF increased the MIC/MBC values (i.e. reduced antibacterial activity) against *E. faecalis*. Against EF12, Cat-8-NIF appeared to be better than Fuso-1-PEG-NIF: at 62.5 μg/mL, viable cells were reduced to an average of 28.0% for the cationic formulation, but viability was around 134.9% for the fusogenic formulation at the same concentration. However, neither of these formulations managed to completely kill EF12 at the concentrations tested—viable cell count at the highest concentration tested (500 μg/mL) was eventually reduced to similar levels as with free NIF. Against EF48, Cat-8-NIF and Fuso-1-PEG-NIF showed essentially the same activity where substantial killing (8.6% and 11.6% viable cells, respectively) was observed at 250 μg/mL. Surprisingly, for EF36, liposomal NIF did not achieve

an MBC within the tested concentration range. In fact, it appeared as though increasing drug (and liposome) concentration resulted in a steady increase in viable cell count, particularly for Fuso-1-PEG-NIF (**Figure 41**). It is unclear why this would be the case, unless this increase in viable cells mirrors what has been observed to happen at increasing yet sub-lethal drug concentrations. Perhaps if drug concentrations higher than 500 μg/mL were tested, a drop in viability would follow the spike in viability, as seen with free NIF for these strains. However, when NIF was added to bacterial growth media at concentrations above 1 mg/mL, precipitate formed that settled as sediment at the bottom as well as a film at the liquid surface (**Supplementary Figure 8**), which made it difficult to be precise about the available NIF concentration in those samples. This could be due to interactions with broth constituents as this was not seen when powdered NIF was added to PBS or water to a concentration of up to 4000 μg/mL. Therefore, the NIF concentration for these assays was restricted to a maximum of 500 μg/mL.

In general, these studies have shown that liposomal encapsulation of NIF does not improve drug delivery to planktonic *E. coli* and *E. faecalis* compared to free NIF, with MIC and MBC values being higher in all cases of liposome treatment. Most interestingly, Fuso-1-PEG-NIF did show antibacterial effects on both *E. coli* and *E. faecalis* where the VAN-loaded counterpart did not facilitate killing of *E. coli*, which suggests that NIF loading could have affected liposome structure in a way that doesn't impair interactions of PEGylated liposomes with *E. coli* as much. This may be down to the way that NIF is compartmentalised in liposomal formulations; being lipid-soluble, it may be able to partition into the lipid membranes of liposomes, which would likely have downstream effects on drug delivery kinetics. However, further studies on drug release and liposome morphology would be necessary to confirm this hypothesis.

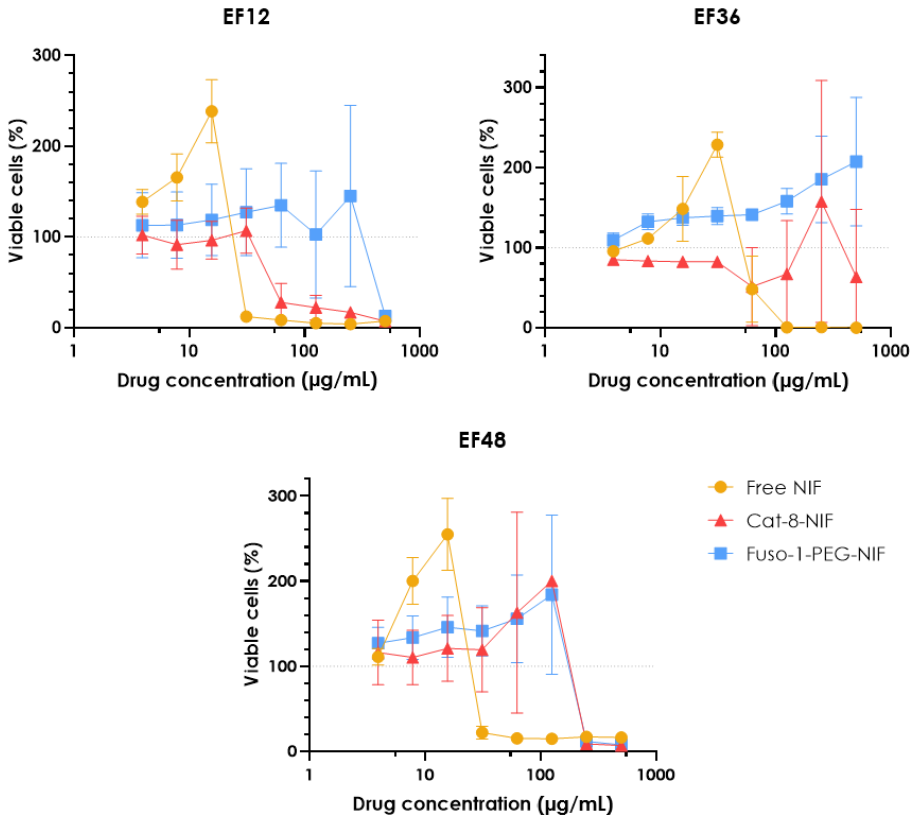


Figure 41 | Bacterial viability of three *E. faecalis* strains after treatment with NIF formulations in MBC assays. Three strains of *E. faecalis* (EF12, EF36 and EF48) were treated with free NIF, cationic liposome-encapsulated NIF (Cat-8-NIF) or fusogenic liposome-encapsulated NIF (Fuso-1-PEG-NIF), matched for drug concentration, as part of an MBC assay. The average number of viable cells was calculated as a percentage compared to a growth control (no treatment) and plotted for each drug concentration tested.

3.3.6 Testing liposomal antibiotics against monospecies biofilms

With the aim of developing an anti-biofilm strategy, it is useful to assess liposome activity on bacterial biofilms prior to conjugation with microbubbles. This was done by growing *E. coli* or *E. faecalis* monospecies biofilms in static conditions for 24 hours, treating them with free drug or liposomal drug for a further 24 hours and measuring the resulting change in biofilm biomass in an MBEC assay. Biofilms were treated after they were given 24 hours to grow in order to mirror what would be expected in a clinical context: a treatment to aid in clearance of an already established biofilm. As NIF is the first-line treatment for UTIs internationally, being one of the few antibiotics that are still effective against most Gram-positive and Gram-negative uropathogens[258,259], and since no NIF-loaded liposomes have been documented to date, NIF was chosen as the antibiotic to take

forward in subsequent experiments. Given previous observations of Cat-8 aggregation in bacterial growth media that has an unknown biological significance, the fusogenic formulation (Fuso-1-PEG) was also taken forward for subsequent experiments. Additionally, PEGylation of the liposomes would be necessary for future conjugation with microbubbles, which Fuso-1-PEG already has been characterised for, making it convenient to continue with this formulation. Therefore, the data in this section will primarily focus on the testing of Fuso-1-PEG-NIF against monospecies biofilm.

In the process of optimising the conditions of the assay, preliminary MBEC assays were performed on biofilms of *E. coli* (UTI89, CFT073, K12) and *E. faecalis* (EF12, EF36, EF48) that were grown in caMHB and treated with VAN formulations (see **Supplementary 6.6.1**). However, biofilm growth after 24 hours of both species was relatively low in caMHB (absorbance values <0.5 in the growth control) which likely made it hard to observe meaningful biofilm eradication. Changing the growth media to TSB improved biofilm growth greatly for *E. faecalis*, but remained largely the same for *E. coli* (**Supplementary Figure 11**). Due to time and resource constraints, two strains of *E. coli* (UTI89 and CFT073) and two strains of *E. faecalis* (EF36 and EF48) were used for reattempted MBEC assays in optimised conditions. The strains were chosen as they were the top two biofilm-forming strains in TSB for each species.

Biofilm biomass changes of *E. coli* biofilms after treatment with free NIF or Fuso-1-PEG-NIF at different concentrations are shown in **Figure 42**. Complete biofilm eradication (i.e. 0% biofilm biomass) was not observed for any of the tested strains or NIF formulations, which suggests that antibiotic/liposome treatment alone may not be very effective at clearing biofilm and/or much higher drug doses are required to do so. This is not surprising given that biofilms can be 10-1000 times more resistant to antibiotics than their planktonic counterparts[158], but for reasons previously described, it was not feasible to increase NIF concentration above 500 μg/mL in these assays. For *E. coli*, although complete eradication was not observed, treatment with free NIF saw a significant

reduction in biofilm biomass to around 40% at 125 μg/mL for UTI89 and at 62.5 μg/mL for CFT073 (**Figure 42A**). At the lowest concentration (31.25 μg/mL), however, there was an increase in biofilm biomass for both strains—to 130.1% for UTI89 and 119.2% for CFT073. This is consistent with findings in the literature that low/sub-inhibitory concentrations of antibiotics can lead to increased biofilm production and aggravate infection[667,688–690]. When UTI89 is treated with liposomal NIF, this trend is not seen, with biofilm biomass remaining between 50 and 100% at all concentrations tested. This suggests that delivery of lower drug concentrations into the biofilm may be increased using liposomes; perhaps liposomes improve the rate of delivery so that the bacteria have less time to upregulate biofilm production in response, resulting in the observed reduction in biofilm biomass while free NIF increased biomass. However, increasing the liposome (and drug) concentration didn't seem to improve biofilm eradication when treated with Fuso-1-PEG-NIF, but it did to a certain extent when treated with free NIF at and above 125 μg/mL. It is unclear why this would be the case but together with data from CFT073, it is apparent that Fuso-1-PEG-NIF is generally less effective at reducing *E. coli* biofilm biomass than free NIF, particularly at higher concentrations. Perhaps the liposomes do show increased penetration and retention within the biofilm, stopping further growth, but are not as efficient at physically clearing the dead material to manifest as a change in the measured biomass. This is one limitation of measuring biomass as an indication of biofilm eradication—biomass includes both living and dead material, and would not take into account the extent of death within the biofilm, unless this death is associated with detachment. Follow-up MBaBC assays were performed to get an insight into how the viability of the cells surrounding and/or released from the treated biofilm was affected (**Figure 42B**). Here, the trend is similar with free NIF performing better than Fuso-1-PEG-NIF; 125 μg/mL was the minimum concentration of free NIF needed to kill both UTI89 and CFT073, whereas there was no bactericidal concentration of Fuso-1-PEG-NIF observed (but there was a steady decrease in viable cells as concentration increased). The data suggest that the biofilm-associated cells show increased resistance to NIF treatment, with MBaBC of free NIF being up to

four times as high as it was for purely planktonic cells. This could also explain why there was no bactericidal concentration of Fuso-1-PEG-NIF here, as the MBC against planktonic cells was at the highest concentration (500 μg/mL) and likely increased beyond the tested range against biofilm-associated cells. This is in line with findings that biofilm production confers antibiotic resistance to bacteria. It would have been beneficial to carry out additional live-dead imaging using confocal microscopy or cell viability studies directly on the established biofilm (rather than on the suspension associated with biofilm) to get more accurate information about the effect that the treatments have on cells within the biofilm. Nevertheless, the response of biofilm-associated cells is very relevant to understand given the proposed flow of treatment, where biofilm is disrupted first to release associated cells that liposomes can act on.

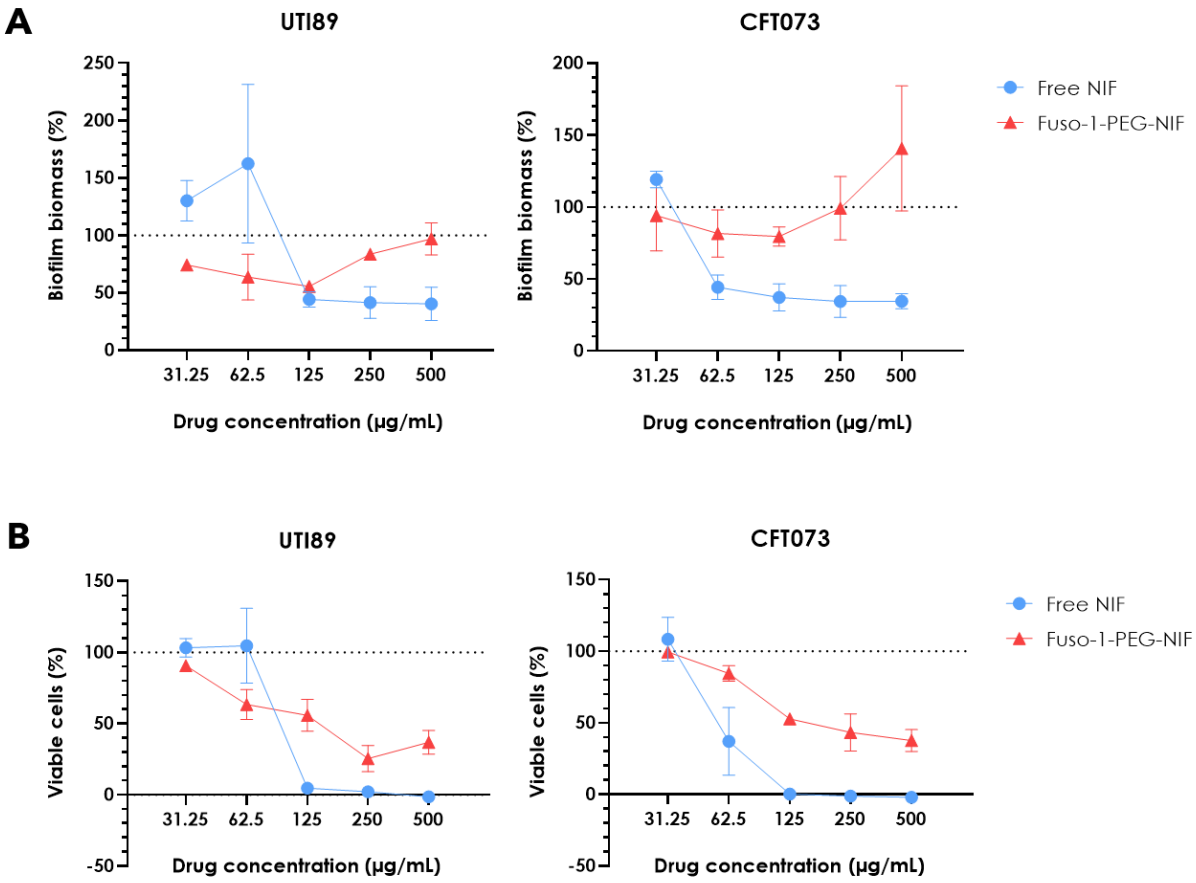


Figure 42 | Biofilm biomass and bacterial viability of *E. coli* in MBEC and MBaBC assays. Two strains of *E. coli* (UTI89 and CFT073) were treated with free NIF or fusogenic liposome-encapsulated NIF (Fuso-1-PEG-NIF), matched for drug concentration, as part of an MBEC assay. The bacterial cells in the suspension associated with the formed biofilm were removed and subject to an MBaBC assay. (**A**) The average biofilm biomass was calculated as a percentage compared to a growth control (no treatment) and plotted for each drug concentration tested. (**B**) The average number of viable cells from the MBaBC assay was calculated as a percentage compared to a growth control (no treatment) and plotted for each drug concentration tested.

For *E. faecalis* strains, both free NIF and Fuso-1-PEG-NIF were generally matched in terms of their effect on biofilm biomass; EF48 saw virtually no change in biomass for either treatment and EF36 saw a decrease by about 50% at 500 µg/mL for both treatments (**Figure 43A**). At the lowest concentration (31.25 µg/mL), it appeared as though Fuso-1-PEG-NIF more effectively cleared EF36 biofilm than free drug, clearing 58.5% biofilm compared to 18.6%, respectively. This mirrors what was observed with UTI89 where liposomes at the lowest concentration seemed to outperform free drug at the same concentration. Again, it is unclear why this would be the case, especially as biofilm eradication did not change in a concentration-dependent manner as concentration increases. In fact, it seemed as though a constant subset of liposomes had anti-

biofilm effects even as overall liposome (and drug) concentration changed. Perhaps there is a balance to be struck between liposome concentration and drug concentration for biofilm eradication effects. Repeating these assays with unloaded fusogenic liposomes at different concentrations might shed some light on the role that liposome concentration plays, particularly for a formulation that is proposed to facilitate anti-biofilm function through membrane destabilisation and fusion.

Once again, a lack of change in biofilm biomass is not necessarily indicative of a lack of antibacterial function which is evident when the viability of the biofilm-associated cells is considered. Although EF48 saw no change in biofilm biomass, bacterial viability dropped to 8.3% when treated with 250 μg/mL of free NIF, and then to 0 at 500 μg/mL (**Figure 43B**). The MBaBC value was four times higher, in line with the increased resistance associated with biofilm growth. Treatment with Fuso-1-PEG-NIF kept EF48 viability between 45 and 60% at all concentrations, with no MBaBC reached, similar to previous findings. For EF36, no MBaBC was achieved for either of the treatments likely due to the biofilm-induced resistance, but interestingly, Fuso-1-PEG-NIF kept biofilm-associated bacterial viability below 100% where it previously didn't with purely planktonic EF36. At 31.25 μg/mL bacterial viability was around 67%, which gradually reduced to 28% at 500 μg/mL in what seemed like a concentration-dependent manner. These data support the idea that biofilm-associated cells respond differently to purely planktonic cells, but also suggest that in the case of EF36 with Fuso-1-PEG-NIF, this may be in favour of showing meaningful antibacterial activity.

One outcome to note from this series of experiments on biofilms is that *E. coli* biofilm production was relatively poor, even when incubated in TSB (**Supplementary Figure 11**), which likely made it more difficult to be confident in any biomass changes observed. Additionally, large variations observed in biofilm growth could be a result of the manual setting up and washing of the biofilms; although extreme care was taken, pipetting actions may also have had an impact on biofilm growth

and/or biomass measurements. Perhaps using more mature and robust biofilms (>48 hours) would help limit the variation observed as well as more accurately reflect a clinically relevant long-established biofilm.

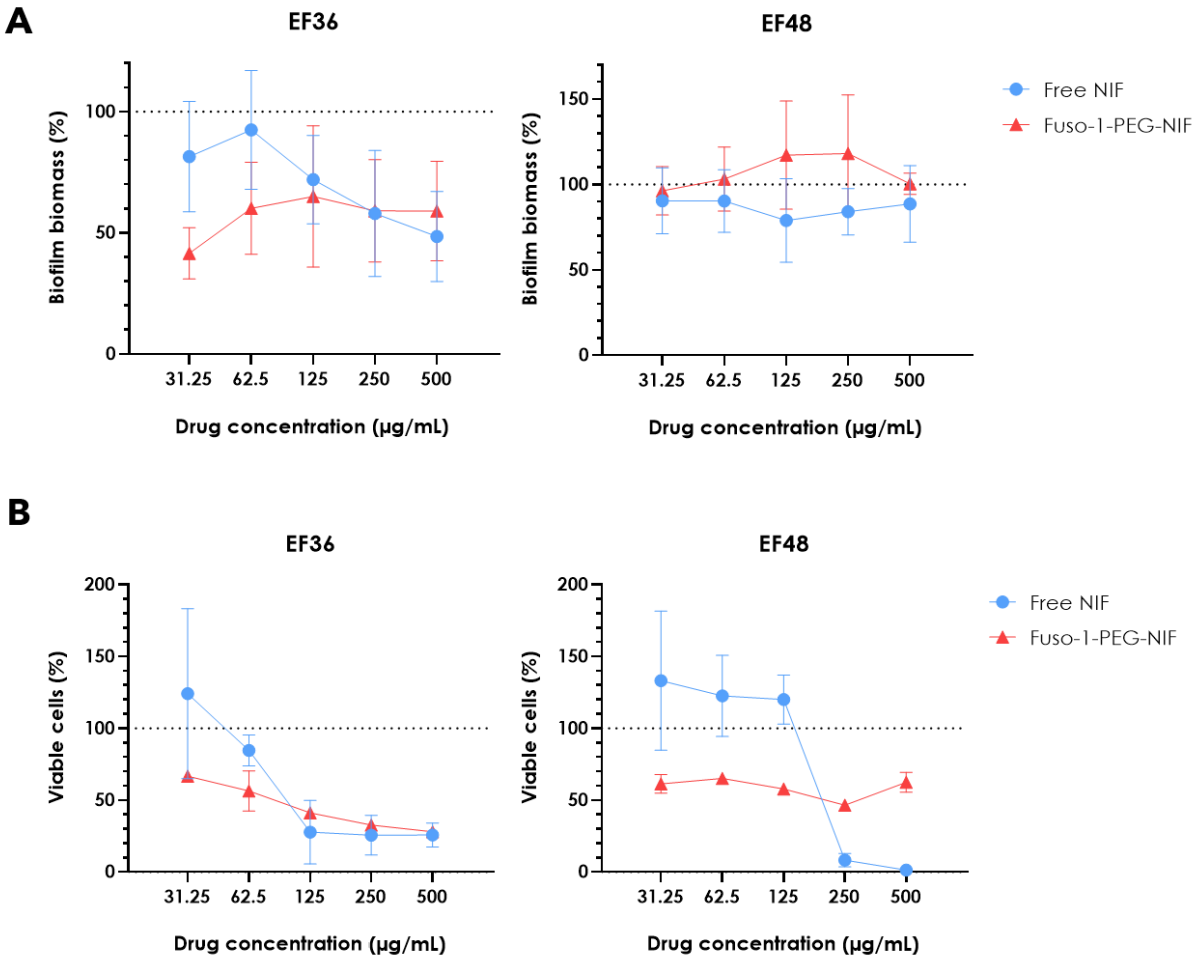


Figure 43 | Biofilm biomass and bacterial viability of *E. faecalis* in MBEC and MBaBC assays. Two strains of *E. faecalis* (EF36 and EF48) were treated with free NIF or fusogenic liposome-encapsulated NIF (Fuso-1-PEG-NIF), matched for drug concentration, as part of an MBEC assay. The bacterial cells in the suspension associated with the formed biofilm were removed and subject to an MBaBC assay. (A) The average biofilm biomass was calculated as a percentage compared to a growth control (no treatment) and plotted for each drug concentration tested. (B) The average number of viable cells was calculated as a percentage compared to a growth control (no treatment) and plotted for each drug concentration tested.

Together, these results indicate that NIF treatment can elicit strain-specific responses that differ noticeably from each other. It is important to consider differences between isolates within an infection, as exemplified by the variation in liposome anti-biofilm and bactericidal activity between all the tested strains. As bacterial communities that make up UTIs differ between patients, isolate-

specific testing may prove to be necessary for effective treatment and management[691]. It would be beneficial to repeat these experiments on a larger pool of strains from each species, and even repeating these assays on multi-species biofilm that are representative of actual bacterial communities present in UTIs[692,693].

3.4 Conclusions

Before drug-loaded liposomes were to be conjugated with microbubbles, it was important to understand and confirm the antibacterial properties of these nanoparticles. Microbiological assays were performed on bacteria in planktonic or biofilm form, with these experiments complemented by imaging studies. The current data suggests that Cat-8-VAN was essentially equally as effective as free VAN against both planktonic *E. coli* and *E. faecalis*. Even though Cat-8-VAN appears to possess the same activity as free VAN, encapsulation may provide added benefits in terms of reducing toxicity and improving retention in a physiological context. Fuso-1-PEG-VAN seemed to show more of an affinity for Gram-positive bacteria, as it was able to facilitate complete bacterial death in all *E. faecalis* samples but not for any *E. coli* strains. Both formulations were particularly effective against planktonic EF36 where the MBC was halved.

These findings were confirmed in preliminary confocal microscopy studies where Cat-8-VAN was effective at keeping the LDR relatively low for both species, and Fuso-1-PEG-VAN activity was limited against UTI89 but showed promise against EF36. Giant aggregates of Cat-8-VAN in caMHB were observed, which may have implications on the antibacterial activity of the liposomes given that these aggregates greatly coincided with dead bacterial cells. These confocal microscopy studies were done to visualise liposome interaction with bacterial cells and confirm its role in antibacterial activity. However, the resolution limit made it hard to confidently link cell death to liposomal uptake/interaction. Therefore, preliminary studies using super-resolution microscopy were done in an attempt to visualise this interaction at a higher resolution. The data indicated that

Fuso-1-PEG-VAN uptake was likely occurring with EF36 but there was not much interaction with UTI89, in line with previous findings. However, further protocol optimisation and data acquisition is needed for a quantitative conclusion.

It was thought that the presence of PEG may be interfering with bacteria-liposome interactions, particularly with *E. coli*, so a PEG-titration experiment was run to see how changing PEG content in the fusogenic formulation affected antibacterial activity. A decrease in PEG content resulted in a reduced quality of liposome which made it difficult to confirm the effect of solely varying liposomal PEG content. 5% PEG content gave the best results in terms of liposome quality and bacterial interaction, particularly against EF36, and confirmed by previous data, so the formulation remained unchanged.

Despite widespread NIF use in UTIs, no liposomal NIF has been reported in the literature. Assays on a novel liposomal formulation of NIF revealed that liposomal encapsulation of NIF did not improve drug delivery to planktonic *E. coli* and *E. faecalis* compared to free NIF. However, Fuso-1-PEG-NIF did show bactericidal effects on both *E. coli* and *E. faecalis* where the VAN-loaded counterpart did not facilitate killing of *E. coli*. This could be a result of differential drug loading chemistry between NIF and VAN that have different solubilities and lipophilicities. When used to treat monospecies biofilm, NIF treatment gave mixed results but, on the whole, none of the NIF treatments (free NIF or Fuso-1-PEG-NIF) were able to completely clear the biofilm, and in some cases had virtually no effect. Further studies were performed to probe the viability of the biofilm-associated cells and it was found that despite a high biofilm biomass, viability of cells associated with the biofilm was reduced as drug concentration increased. Against *E. coli*, free NIF was generally better at reducing biofilm biomass and bacterial viability than Fuso-1-PEG-NIF. Against *E. faecalis*, anti-biofilm activity of the two treatments largely matched each other, but strain-specific differences were observed when looking at the number of viable cells. Of note, a viable cell count of 0 was never reached for EF36 but both free NIF and Fuso-1-PEG-NIF seemed to gradually

reduce bacterial viability. This is noteworthy as Fuso-1-PEG-NIF was unable to reduce viability of purely planktonic EF36 but was able to for biofilm-associated EF36. These results highlight how strain-specific antibacterial responses can be and further studies with more strains and multi-species biofilms are recommended for a more accurate reflection of these treatments against UTIs in a clinical context.

Although the liposomal antibiotics did not show enhanced efficacy and potency compared to the free drug in most cases, especially when used against *E. coli* and *E. faecalis* biofilms, it is possible that biofilm dispersal—as a result of ultrasound treatment, for example—can work synergistically with liposome treatment. The fact that biofilm-associated EF36 was affected more than biofilm or purely planktonic EF36 by Fuso-1-PEG-NIF may indicate that biofilm dispersal can contribute to overall liposome activity.

The research presented in this chapter was necessary to confirm antibacterial and anti-biofilm properties of the formulated liposomes which aided in the selection of a candidate liposome, bacterial strain and experimental conditions under which to produce and test a final conjugate with. Due to the novelty and clinical relevance of liposomal NIF, Fuso-1-PEG-NIF was chosen as the candidate formulation to use in future work. Out of all the strains tested in this chapter, EF36 formed one of the best biofilms and gave noteworthy results when treated with Fuso-1-PEG-NIF, and therefore, was the selected monospecies biofilm strain. In order to assess a lipid-based anti-biofilm system consisting of drug-loaded liposomes and ultrasound-sensitive microbubbles, NIF-loaded fusogenic liposomes will be conjugated to microbubbles and tested on a monospecies EF36 biofilm model, which is explored in the next chapter.

4 Formulation of microbubbles, conjugation to drug-loaded liposomes, and assessment of the activity of the liposome-microbubble system

4.1 Introduction

Lipid-coated microbubbles (MBs) are the most common type of MB both pre-clinically and commercially, made of a lipid monolayer encapsulating an inert gas and between 0.1 and 10 μm in diameter[494,491,510]. As ultrasound (US) contrast agents, they have historically been used for diagnostic purposes to enhance the contrast in medical images by boosting the echo signal that can be detected[492]. The gas compressibility is fundamental to the mechanism of MB activity under US exposure, i.e. the volumetric oscillatory motion known as cavitation (see section **1.5.1** and **Figure 17** for more information)[482,497]. Non-inertial cavitation is when these oscillations are steady and repetitive, leading to a movement of local media surrounding the bubble, known as microstreaming. Inertial cavitation instead involves violent oscillations that result in bubble collapse, causing microjets or shockwaves. These physical actions can have permeabilization effects on nearby membranes through pore formation, 'massaging', or forming pits and invaginations[500–504]. Exposure of tissue to these extreme pressure changes can also cause thermal effects as a result of energy absorption, and can even induce chemical effects in the form of ROS production[505,506]. In most cases, exposure of MBs to US yields a combination of inertial and non-inertial behaviour and due to both the mechanical and biochemical outcomes of cavitation, the therapeutic applications of MBs are being increasingly researched in addition to their diagnostic use[483,500,509].

In the context of biofilm infections, US and MBs are effective at mechanically removing and sensitising bacteria within a biofilm (see section **1.5.3**), but often needs to be followed up with antibiotic treatment to achieve synergistic anti-biofilm effects that result in substantial bacterial death[322,509,551,552,557]. As such, the drug delivery capacity of MBs can be enhanced via a plethora of

different modifications (**Figure 18B**), such as loading an antibiotic agent into the gaseous core[694]. Unfortunately, these methods are generally limited by the low drug loading capacity intrinsic to MBs, so the more straightforward co-administration route is commonly utilised, where MBs are administered alongside free antibiotic to increase drug efficacy and biofilm penetration[322,551,552,557,564]. However, ensuring the drug is local to both the MBs and the target site is beneficial to take advantage of cavitation-induced effects (e.g., microstreaming and microjetting) to enhance drug penetration[562]. Additionally, spatial localisation of drug release to the US-treated area can potentially reduce side effects and unwanted interactions[567]. Therefore, the conjugation of MBs to drug carriers, such as liposomes, has been presented as a desirable and viable option to not only increase drug loading capacity but also localise drug release[562].

Attachment of drug-loaded liposomes to acoustically active MBs makes for an US-responsive drug delivery vehicle, combining the benefits offered by the two lipid-based systems. Conjugation is commonly achieved through non-covalent avidin-biotin linkage via functionalised liposome and MB lipids[570,572,573]. Although this option yields a very strong and stable bond, avidin displays high non-specificity and immunogenicity, so alternative conjugation methods, such as click chemistry, are gaining popularity[574,575]. Of these, the maleimide-thiol click chemistry reaction (**Figure 20**) has proven to be successful in the liposome-MB conjugation landscape as a process that can be carried out at room temperature and in aqueous buffer without any additional reagents or catalysts[575–577]. Many protocols for this conjugation involved adding pre-formed liposomes to a suspension of MB constituent lipids followed by high-speed mixing to form liposome-loaded MBs (LMBs)[576,577]. This is likely because MBs have a very short half-life (minutes to hours) that would limit how much time can be given to the conjugation process while maintaining the MB population[517,569,695,696]. However, the processes required to make MBs may be incompatible with the loaded drugs and liposomes, so combining pre-formed liposomes and MBs is also an option[570,572,573,581]. Although LMB conjugation has been widely studied for applications like oncology, there are currently very few studies around its bacterial applications; one study by Horsley *et al.* in 2019 has shown that

gentamicin-loaded LMBs can be used to kill intracellular UPEC in an organoid UTI model[323]. This single study utilising LMBs in UTI research highlights a current gap in the field despite the potential this approach has.

To address this gap and satisfy the objectives of this thesis, in this chapter I produced a MB formulation in line with what is already in commercial use, and characterised its physical and acoustic properties using microscopy and passive cavitation detection. A novel LMB formulation was also produced after optimisation of a conjugation protocol, consisting of the aforementioned MBs conjugated to NIF-loaded liposomes (produced and characterised in chapters **2** and **3**) via maleimide-thiol click chemistry. I investigated the anti-biofilm properties of these particles against a UTI-relevant monospecies biofilm model of *E. faecalis* through microscopy-based quantification of biofilm coverage and viability, as well as measuring the cavitation activity of these particles. The reporting of cavitation data here, which was not included in Horsley *et al.*'s study, is advantageous for a potentially better mechanistic and predictive understanding of the biological outcomes. This research aims to contribute to the emerging field of LMBs for antibacterial and anti-biofilm applications, particularly in the context of UTIs, using a novel NIF-containing and US-responsive lipid particle formulation.

4.2 Materials and Methods

4.2.1 Materials

1,2-distearoyl-sn-glycero-3-phosphocholine (DSPC, 25 mg/mL in chloroform) was purchased from Avanti Polar Lipids, USA. 1,2-distearoyl-sn-glycero-3-phosphoethanolamine-N-[methoxy(polyethylene glycol)-2000] (DSPE-PEG2000, 10 mg/mL in chloroform) and 10X phosphate-buffered saline (PBS) stock solution were purchased from Merck Life Sciences, UK. 1,2-distearoyl-sn-glycero-3-phosphoethanolamine-N-[thiol(polyethylene glycol)-5000] (DSPE-PEG5000-SH) was purchased from BroadPharm USA. Dioctadecyloxacarbocyanine (DiO) and

nitrofurantoin sodium (NIF) were purchased from Cambridge Bioscience, UK. Chloroform, methanol, UltraPure™ DNase/RNase-free distilled water and other solvents were of analytical grade (Thermo Fisher Scientific, UK).

Tryptic soy broth (TSB) and lysogeny broth (LB) were made by dissolving broth powder (Merck Life Sciences, UK) in distilled water according to the manufacturer's instructions and autoclaving at 121°C for 15 min to sterilise. Agar was also purchased from Merck Life Sciences, UK. The LIVE/DEAD™ *Bac*Light™ Bacterial Viability Kit, containing SYTO 9 and propidium iodide (PI) dyes, was purchased from Thermo Fisher Scientific, UK. Corning® human fibronectin was purchased from Scientific Laboratory Supplies Ltd, UK.

A frozen stock of clinical isolate of *Enterococcus faecalis* (EF36) was obtained from University College London (see **Table 4** for more information on this strain). The bacteria strain was stored at −80°C in cryovials containing 20% glycerol (v/v) in LB.

4.2.2 Ultrasound instrumentation and parameters

Ultrasound (US) was generated using a 1.1 MHz spherically focussed transducer (Sonic Concepts H102; outer diameter: 64 mm, inner diameter: 22.6 mm, focal distance: 63.2 mm). A 7.5 MHz unfocussed transducer (Olympus U8421035; diameter: 13 mm) was used for passive cavitation detection. A waveform generator (33600A Series Trueform Waveform Generator, Keysight Technologies, USA), 1020L RF amplifier (Electronics & Innovation, USA), and impedance matching network (Sonic Concepts Inc., USA) were used to send high amplitude voltage signals to the focussed transducer, generating cavitation within the sample. MB cavitation emissions were then received with the unfocussed transducer, sent through a high-pass filter (Allen Avionics Inc., USA) to filter out low frequency noise below 2 MHz, and finally digitized and stored using a TiePie HS6 handyscope (TiePie Engineering, The Netherlands) that was connected to a computer running the TiePie Multi Channel software (version 1.48.0.1). An oscilloscope (RS Pro

RSDS1052DL+, RS Components, UK) was additionally used to visualise the transmitted US signal and confirm consistent voltage amplification.

The two transducers were confocally aligned to channel slides (μ-Slide I Luer, ibidi GmbH, Germany) that were loaded with the sample to be insonated, and placed in a tank filled with degassed water at 25 °C. The sample was then exposed to 1.1 MHz US, bursts of 400 cycles at 50 Hz pulse repetition frequency (PRF) generating 1 MPa peak negative pressure (PNP; at the surface of the channel slide substrate where the biofilm was located) over a 40 s exposure time.

This setup is summarised in **Figure 44**.

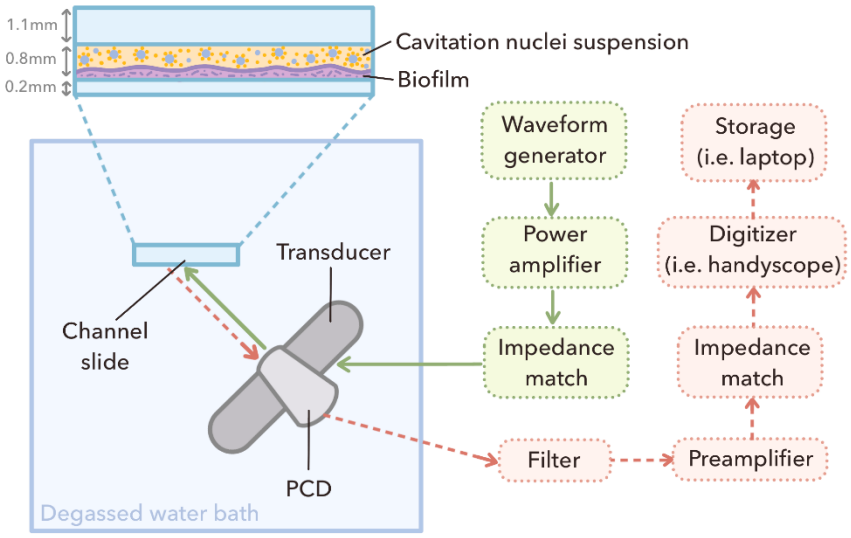


Figure 44 | Diagram of ultrasound setup. A 1.1 MHz focussed transducer was used to generate US and a passive cavitation detector (PCD, 7.5 MHz unfocussed transducer) was used to detect signal from the resultant cavitation. A channel slide (ibidi μ-Slide) containing 24-hour *E. faecalis* biofilm was placed onto the sample stage in the degassed water tank for US exposure. Steps and instrumentation involved in US propagation are highlighted in green with solid arrows; steps and instrumentation involved in passive detection of microbubble cavitation are highlighted in red with dashed arrows. Adapted from Keller *et al.* (2024)[697].

Signals detected by the PCD were analysed using a custom-made MATLAB script (The MathWorks Inc., USA; R2025b; see **Supplementary 6.9**), which computes the power spectral densities (PSD) to show how the emitted acoustic energy is distributed across a range of frequencies over time. The script also splits cavitation energy into harmonic, ultraharmonic, and

broadband signal, plotted on a power-time spectrum. Example spectra are explained in **Figure 45**. Acoustic energy data were visualised using GraphPad Prism 9 (version 9.4.1).

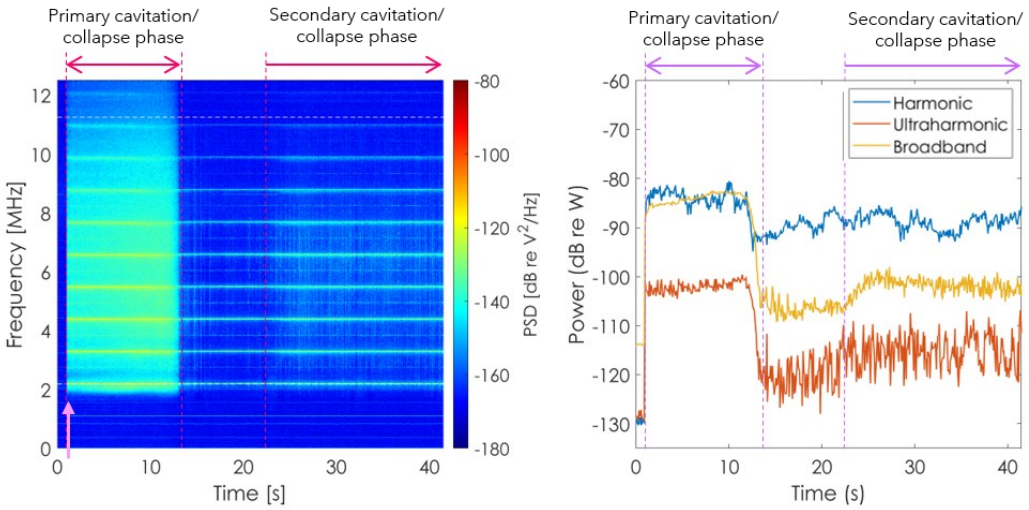


Figure 45 | Example spectra of analysed cavitation data. Passive cavitation data were recorded during the exposure of MB samples to US and these data were analysed using a custom MATLAB script to generate two different graphs, an example of which is shown here. (Left) Power spectral density (PSD) map showing the variation in power generated during the process of cavitation across different frequencies over time. Pink arrow indicates the start of US exposure. (Right) Power-time graph showing harmonic, ultraharmonic and broadband components of the signal over the exposure time period. The harmonic (blue line on the power-time graph) and ultraharmonic (red line on the power-time graph) components are thought to correspond to non-inertial cavitation and appear on the PSD map as bright horizontal bands (yellow/cyan) at discrete frequencies. The broadband noise (yellow line on the power-time graph) typically corresponds to inertial cavitation and collapse, appearing as regions of colour between the bright horizontal bands on the PSD map, with the power generated widely spread across more frequencies. This inertial cavitation typically occurs at the start of US exposure before the majority of the MBs collapse; here, this period of time is referred to as the primary cavitation/collapse phase. Secondary 'daughter' bubbles may be generated after the collapse of the primary bubbles and are able to cavitate again, starting the secondary collapse/cavitation phase[698–700]. The primary and secondary cavitation/collapse phases are indicated on each spectrum (in red on the PSD map; in purple on the power-time graph), corresponding to where increasing power generated from inertial cavitation events (i.e. greater broadband noise) was recorded.

4.2.3 Microbubble production

Microbubbles (MBs) were produced using an in-house tissue homogenisation protocol developed by O'Reilly *et al.* (unpublished). DSPC, DSPE-PEG2000, and DSPE-PEG5000-SH (90:5:5 molar ratio) dissolved in chloroform were added to a 7 mL glass vial (Supelco clear glass vial, Merck Life Sciences, UK). The organic solvent was removed using a concentrator (Eppendorf Concentrator Plus, Eppendorf, Germany) at 45°C for 45 min on vacuum setting 'V-AL', which resulted in the formation of a dry lipid cake. 0.1X PBS was added to hydrate the dry lipid cake (to achieve a total lipid concentration of 3 mg/mL) using a temperature-controlled mixer (HCM100-Pro Thermo

Mix, DLAB, China) at 90°C and 500 rpm for 60 min, above the phase transition temperature of the constituent lipids (DPSC at 55°C and DSPE at 74°C)[701]. 1 mL of the resulting suspension was pipetted into a 2 mL clear glass injection vial (VCDIN2R, Scientific Laboratory Supplies, UK) and the headspace of the vial was filled with perfluorobutane (PFB) gas before being crimped closed. The vial was placed in a custom-made vial holder and clamped down into the carousel of the tissue homogeniser (Precellys Evolution Touch Homogenizer, Bertin Technologies, France). Homogenisation was performed under the following settings: speed: 10,000 rpm; cycle: 1 × 45 s; pause: 1 s; temperature: 10°C. The vial was then placed on ice to bring the MB suspension below the phase transition temperature of the constituent lipids and reduce the gas diffusion rate. The MBs were then gently transferred to a 3 mL syringe and the syringe sealed with a luer lock cap (B. Braun™ Combi-Stopper, B Braun Medical Ltd, UK) before being placed in a centrifuge operated at 300 ×g for 10 min at 4°C to wash the MBs. Upon centrifugation, the MBs floated to the top of the suspension while the small-particle content (i.e. very small bubbles and lipid particles/aggregates) remained in the subnatant and were discarded. The remaining MBs were gently diluted in TSB back up to 1 mL in an Eppendorf tube and kept at 4°C.

4.2.4 Microbubble characterisation

MB size and concentration were characterised by bright-field microscopy. Immediately after production, the MB suspension was diluted up to 20 times in 0.1X PBS to obtain an MB concentration suitable for image analysis. 10 μL of MB suspension was pipetted onto a haemocytometer (Neubauer Improved Bright-Line Haemocytometer, Paul Marienfeld GmbH & Co. KG, Germany) and covered with a 0.2 mm thick glass cover slip. The haemocytometer was placed on the stage of an upright microscope (DM500 Binocular Educational Microscope, Leica Microsystems, UK) and 20 bright-field images were taken per sample from randomly selected locations at 40× magnification. A custom MATLAB script (The MathWorks Inc., USA; R2025b) was used to batch process the images to provide average MB size (i.e. diameter) and concentration. Briefly, the script converted the image to greyscale, segmented the image to trace the boundaries

of detected bubbles using automatic thresholding, fitted a circle equation to the detected bubbles to determine the pixel area for each bubble, and summarised this to give information about bubble diameter and concentration.

To characterise the acoustic response of the MBs, 200 μL of MBs (10^8 bubbles/mL) was injected into a channel slide (μ-Slide I Luer, ibidi GmbH, Germany) that was submerged in the water tank of the US setup and then exposed to the US field described in section **4.2.2**.

4.2.5 Liposome-microbubble conjugation optimisation and particle characterisation

Pre-formed liposomes functionalised with maleimide and pre-formed MBs functionalised with thiol were used to produce liposome-MB particles via maleimide-thiol click chemistry. Fuso-1-PEG-NIF liposomes labelled with DiO (produced in chapter **2**) corresponding to 0.5 mg/mL NIF (~10^8 liposomes/mL) were added to MBs (10^8 bubbles/mL) to a total volume of 2 mL in 0.1X PBS, in an Eppendorf tube on ice. To optimise the [Fuso-1-PEG-NIF]-loaded MB (FMB) conjugation protocol, several conditions for conjugation were compared: gentle mixing for 2 h at 4°C or for 24 h at room temperature (25°C); filling the Eppendorf tube headspace with room air or PFB gas; gentle mixing or stationary standing for 2 h at 4°C. For gentle mixing, a roller mixer (Stuart™ SRT9, Keison Products, UK) was used at a speed of 33 rpm. The suspension was protected from light during conjugation in all conditions.

Bright-field images were taken of the resulting particles using an upright microscope (DM500 Binocular Educational Microscope, Leica Microsystems, UK) at 40× magnification and 20 images were taken per sample from randomly selected points. The cavitation activity of the MB samples was assessed using the setup described in section **4.2.2** to confirm MB presence and acoustic response. Confocal microscopy images were taken of the FMBs produced using the final optimised conjugation protocol (see below) to further confirm conjugation: 10 μL of FMBs was pipetted onto a microscope slide (Superfrost™ Plus Adhesion Microscope Slides, Epredia, USA) and

covered with a 0.22 mm thick glass cover slip. Confocal microscopy images of the FMBs were then taken using a Nikon Eclipse Ti2 fluorescence microscope at 40× magnification. At least five images per sample were acquired from randomly selected locations. These images were processed using ImageJ (version 2.9.0/1.54k).

Optimised conjugation protocol

Following protocol optimisation experiments discussed in **Supplementary 6.7**, the following conjugation protocol was followed to produce FMBs: Fuso-1-PEG-NIF liposomes corresponding to 0.5 mg/mL NIF (~10^8 particles/mL) were added to MBs (10^8 particles/mL) to a total volume of 2 mL in TSB in an Eppendorf tube and left standing for 2 h at 4°C (no mechanical mixing), protected from light.

4.2.6 Assessment of anti-biofilm activity of liposome-microbubble particles

E. faecalis (EF36) was inoculated on LB agar plates (Thermo Fisher Scientific UK) from the frozen stock. After incubation at 37°C for 24 h, three separate colonies were transferred to TSB and incubated at 37°C (shaken at 180 rpm) until the optical density at 600 nm (OD_{600}) value was adjusted to approximately the equivalent of 10^8 CFU/ml as a bacterial stock. This stock was diluted to 10^7 CFU/ml in TSB to produce a working bacterial suspension. 200 μL of fibronectin (0.05 mg/mL) was injected into channel slides (μ-Slide I Luer, ibidi GmbH, Germany) and left at room temperature (25°C) for 60 min. The channel was washed with 1 mL of sterile 1X PBS and left to dry for 5 min. 300 μL of working bacterial suspension was injected into the channel and incubated at 37°C for 24 h in static conditions. The formed biofilm was then washed with 1 mL of sterile 1X PBS. 200 μL of one of the treatment samples listed in **Table 9** was slowly added to the channel slide and the slide was sealed with sterile combi-stoppers (B. Braun™ Combi-Stopper, B. Braun Medical Ltd, UK). The loaded channel slide was exposed to US depending on the loaded sample (**Table 9**; see section **4.2.2** for US parameters used). After exposure, the biofilm was incubated at 37°C for another 24 h. The biofilm was then washed with 1 mL of sterile 1X PBS. 3 μL of SYTO

9 and 3 μL of PI dyes were mixed into 1 mL of sterile water and 200 μL of the mixed stain solution was added to the channel slide for 30 min at room temperature, protected from light. The stained biofilm was then washed with 1 mL of sterile water. 200 μL of 1X PBS was then injected into the channel and images of the stained cells were then taken using a Nikon Eclipse Ti2 Inverted Microscope (Nikon Corporation, Japan). 3×3 tile scans were acquired at 10× magnification (corresponding to a 4.37 mm × 4.37 mm area) to cover the focal area of US exposure. At least two images per sample were also acquired at 40× magnification from an area of interest. These images were processed using ImageJ (version 2.9.0/1.54k) and mean pixel intensity of SYTO 9 and PI fluorescence were calculated. Biofilm coverage area was also measured using ImageJ (version 2.9.0/1.54k) by manual thresholding and calculation of the % area of the image covered by biofilm. Mean pixel intensity and biofilm coverage area data were plotted using GraphPad Prism 9 (version 9.4.1). Four biological replicates and three technical repeats per replicate were carried out for this experiment.

Table 9 | List of treatments used to evaluate anti-biofilm activity of liposome-loaded microbubbles. The contents of each sample are stated and the rationale behind their inclusion in these experiments are provided. All samples were suspended in TSB. Treatments marked with an asterisk (*) were not exposed to US after addition to the biofilm.

Treatment	Contents	Rationale
Control*	TSB broth only	No-treatment control
MB	10^8 bubbles/mL MBs	Control to confirm cavitation and biofilm disruption activity
NIF*	0.5 mg/mL free NIF	Control representing the current first-line treatment for UTIs
MB-NIF	10^8 bubbles/mL MBs + 0.5 mg/mL free NIF	Control representing treatment without liposome encapsulation
FMB	10^8 bubbles/mL MBs + 0.5 mg/mL NIF encapsulated in Fuso-1-PEG (~10^8 liposomes/mL)	Full treatment with conjugated liposome encapsulation

4.2.7 Statistical analysis

GraphPad Prism 9 (version 9.4.1) was used to perform ordinary one-way ANOVA with Dunnet's (to compare treatments to a control) or Tukey's (to compare between treatments) multiple comparisons tests, F-tests (to determine the significance of a linear regression model), and one-sample and unpaired t-tests. The standard p-value cut-off (≤ 0.05) was used to determine statistical significance.

4.3 Results and Discussion

4.3.1 Microbubble formulation and characterisation

Microbubbles made of DSPC, DSPE-PEG2000 and DSPE-PEG5000-SH were produced as described in section **4.2.3**. DSPC and DSPE-PEG are common lipid constituents of MBs used in the literature and in commercially available formulations, such as LUMASON® and Definity®[517,702,703]. DSPC typically makes up the bulk lipid that self-assembles around the gas pocket, while PEGylated DSPE acts as an emulsifier that stabilises the bubble monolayer shell during production and *in vivo* by providing a steric barrier that prevents coalescence and clearance[704]. The chosen lipid ratio for the current formulation was based off the most widely utilised molar ratio[704]—DSPC:DSPE-PEG = 9:1. DSPE-PEG5000-SH was additionally used as it contains a thiol functional group that is necessary for conjugation to maleimide-functionalised liposomes.

As part of the production process, the MB suspension was washed using centrifugation to remove any unincorporated lipid components and aggregates (**Figure 46A/B**). The average size (diameter) of the washed MBs was 1.00 ± 0.85 μm, comparable to commercially available MB formulations, LUMASON® and Definity®, with mean diameter ranges of 1.5-2.5 μm and 1.1-3.3 μm, respectively[702,703]. The slightly smaller average size of the MBs produced for this study was likely due to the homogenisation method of MB production used which has been found to generate smaller but more stable MBs compared to conventional sonication (O'Reilly *et al.*, unpublished). The MBs had an average concentration of 1.76×10^{8} bubbles/mL, which falls in the range of commercial MB concentrations (10^{8}-10^{10} bubbles/mL)[705]. Given the current lack of a gold-standard sizing method[532], it would be beneficial to use an additional particle and concentration counting technique, such as the Coulter Counter, in order to confirm the observed numbers.

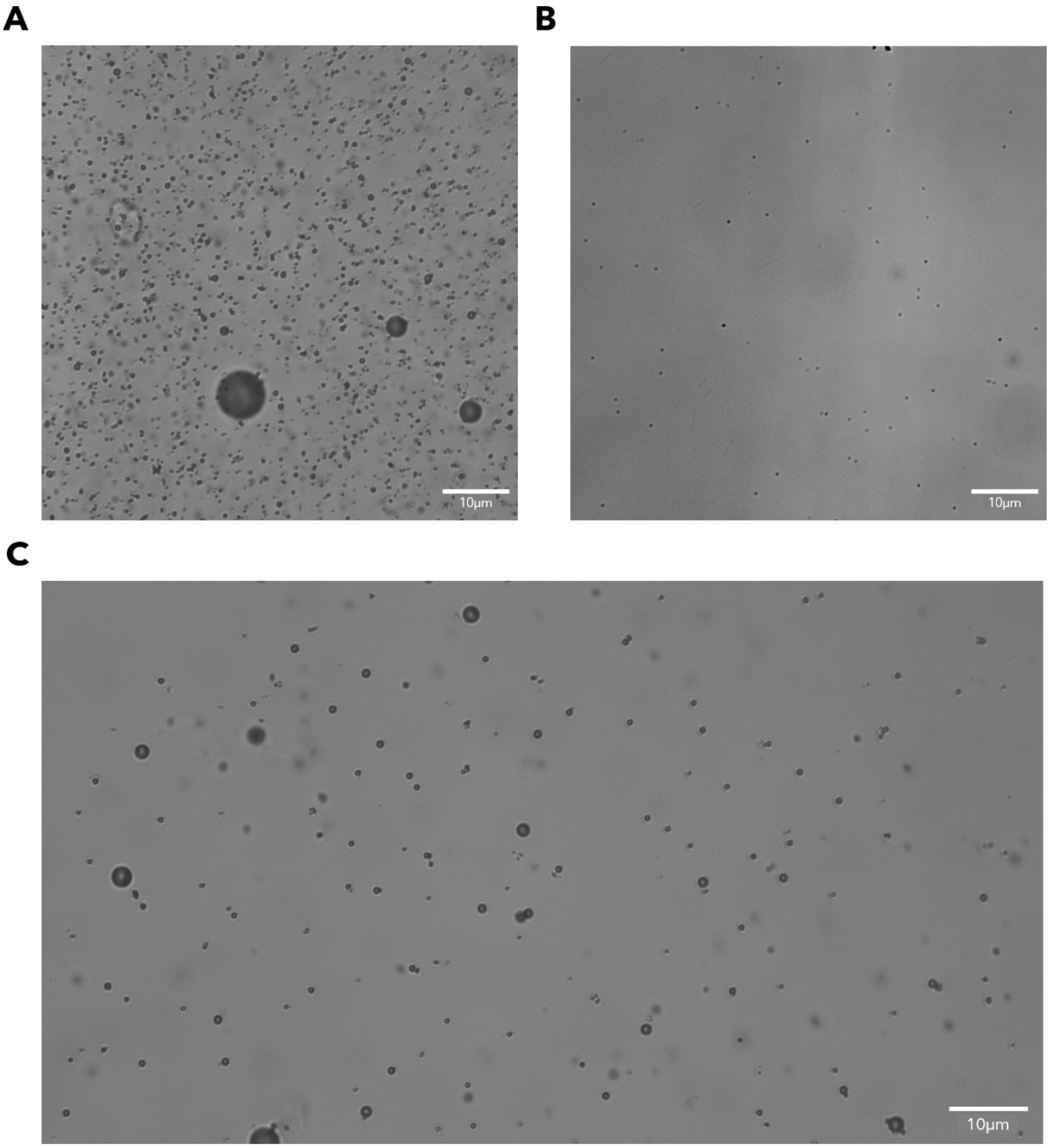


Figure 46 | Representative bright-field images of prepared microbubbles before and after washing. (A) Microbubble suspension before washing via centrifugation. (B) Post-wash subnatant with small-particle content, such as very small bubbles and lipid particles/aggregates. (C) Post-wash microbubble suspension. The images were taken with a 40× objective and scale bar is shown.

In order for the MB formulation to be deemed as suitable, the produced MBs needed to be responsive to the US parameters listed in section **4.2.2**. These parameters were chosen based on previous work by Keller *et al.* and Crowther *et al.* who used MBs to disrupt *S. aureus* and *P. aeruginosa* biofilms[697,706]. The cavitation profile of the MBs is shown in **Figure 47A** which confirmed the inertial cavitation period lasting around 10 seconds before the majority of the bubbles collapsed. Although the duration of cavitation depends on multiple variables, including MB size, concentration, shell properties, and US exposure parameters[707], the persistence of MB inertial collapse was observed to be longer than those in comparable studies (5 seconds or less)[697,706]. After the first 12 seconds, the detected signal was predominantly from non-inertial cavitation, as shown by the increased harmonic and ultraharmonic components (i.e. with power of detected signal being mostly at discrete frequencies) when compared to a negative control of buffer only (TSB; **Figure 47B**). In line with published findings on MBs suspended in PBS[708], TSB without MBs showed minimal cavitation activity; the total acoustic energy emitted by the MB sample was 0.370 ± 0.199 nJ, significantly higher than the 0.017 ± 0.003 nJ detected from the TSB sample ($p=0.0144$). Because this formulation and the US parameters used vary from what is already in the literature, it may be useful to include commercial MB formulations as a positive control in future experiments to assess how the acoustic activity compares to what is in clinical use. Interestingly, secondary cavitation events (i.e. a period of increased inertial collapse following the primary collapse phase; see the example spectra in **Figure 45** for clarification) appear to occur during the 40 seconds of US exposure, particularly from about 20 seconds after the start of exposure (**Figure 47A**). This is likely due to secondary 'daughter' bubbles generated after the collapse phase of the primary bubbles, which are then able to cavitate again[698–700]. A smaller gradual increase in broadband energy (likely corresponding to inertial collapse) is observed after the primary collapse and leading up to the secondary collapse phase (between 23 and 26 seconds in **Figure 47A**), which would align with the idea that inertially cavitating bubbles grow in size before collapsing violently[709]. It is thought that violent collapse events are major drivers of anti-biofilm effects and so having a secondary

collapse phase could potentially have significant anti-biofilm advantages, but this remains to be seen[710].

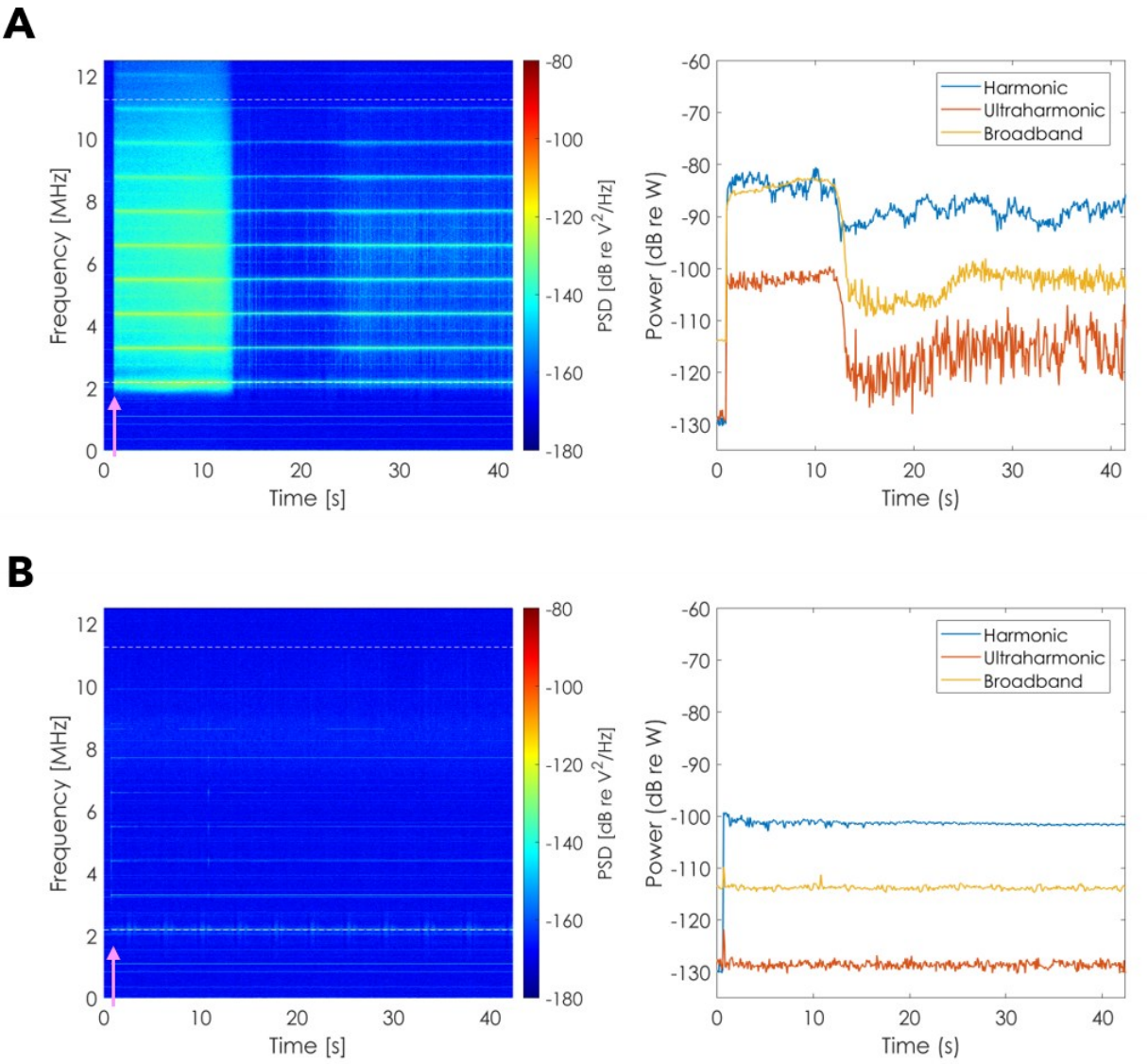


Figure 47 | Representative cavitation profile of microbubbles immediately after production. Representative cavitation profiles of (**A**) MBs in TSB (10^8 bubbles/mL) and (**B**) TSB only are shown. In each panel: (left) power spectral density (PSD) showing the variation in power generated by cavitation activity across different frequencies over time; (right) power-time graph showing harmonic, ultraharmonic and broadband components of the signal over the exposure time period. Pink arrows indicate the start of US exposure. Summary of US parameters used: 1.1 MHz with bursts of 400 cycles at 50 Hz PRF for 40 seconds, generating an acoustic pressure of 1 MPa peak negative pressure.

Thus far, the size and concentration of a novel MB formulation were characterised that appeared to be largely in line with published formulations, despite their suspension in bacterial growth medium, TSB, which has not been previously studied as a MB diluent. These MBs demonstrated

satisfactory acoustic activity in response to US exposure. This formulation was, therefore, taken forward as the candidate MBs for subsequent conjugation to drug-loaded liposomes.

4.3.2 Characterisation of optimised liposome-loaded microbubbles

To conjugate the chosen drug-loaded liposomes (Fuso-1-PEG-NIF) with the produced MBs, maleimide-thiol click chemistry was used to produce [Fuso-1-PEG-NIF]-loaded MBs (FMBs). The conjugation protocol for this study was optimised as discussed in **Supplementary 6.7**. Candidate FMBs were made by adding liposomes corresponding to 0.5 mg/mL NIF (i.e. ~10^8 liposomes/mL) to 10^8 bubbles/mL and leaving them to conjugate (without mixing) for 2 hours at 4°C. This gave FMBs that were on average 0.80 ± 0.31 μm in diameter and 2.85×10^8 particles/mL in concentration. The variation in overall size and concentration from the initial MBs (1.10 ± 1.10 μm and 1.64×10^8 bubbles/mL) could be reflective of the fact that liposomes and liposomal aggregates were also present in the suspension. An increased number of smaller particles (i.e. aggregates of liposomes) could have skewed the size distribution towards a smaller average diameter, as well as increase the overall particle concentration. Conjugation was confirmed via microscopy (**Figure 48**; **Supplementary Figure 14C**); non-labelled MBs became visible under both brightfield and widefield (fluorescence) microscopy after conjugation to DiO-labelled Fuso-1-PEG-NIF liposomes (normally non-labelled MBs are not visible under widefield microscopy). Liposome aggregates and lipid fragments were also visible in the microscopy images (e.g. non-bubble blotches in **Figure 48B**) which supports the hypothesis that liposome matter may have contributed to variation in measured particle size and concentration.

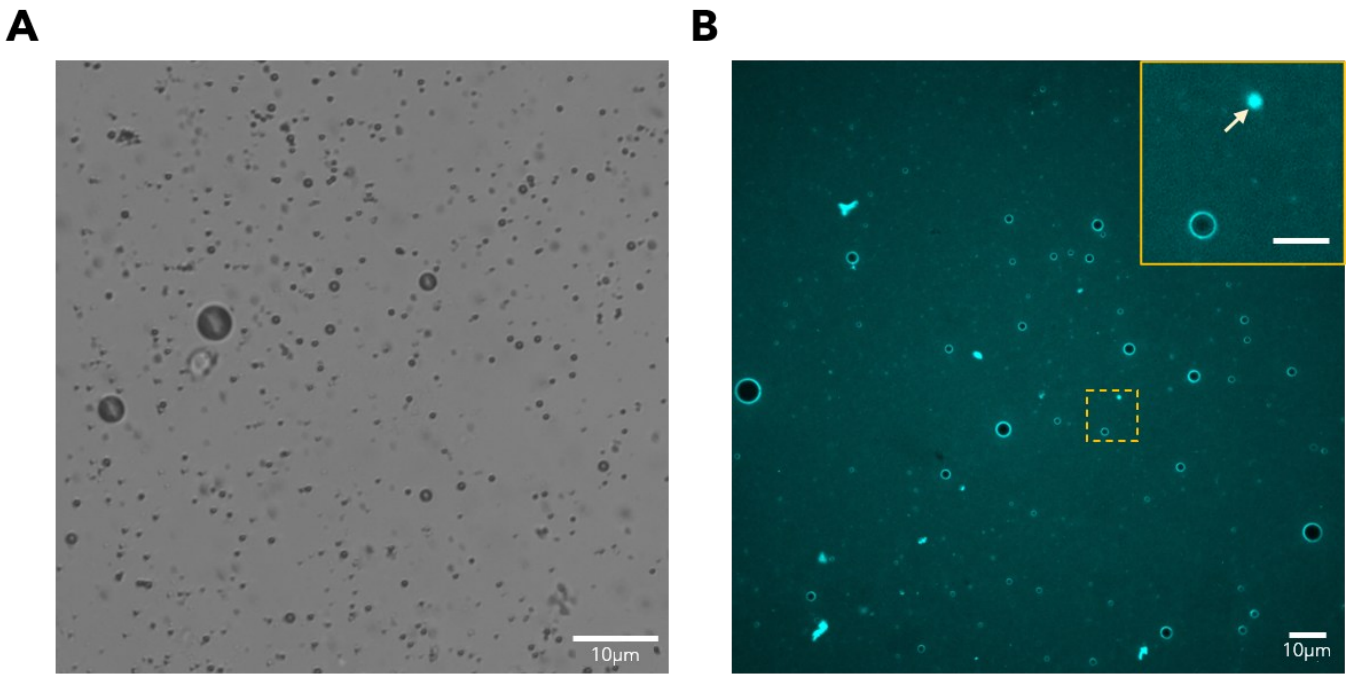


Figure 48 | Representative brightfield and widefield images of FMBs. (A) Brightfield and (B) widefield images of successfully conjugated FMBs. A selected area in panel (B) has been highlighted in an orange box and enlarged in the inset to show an example of a non-bubble particle (likely a lipid/liposomal aggregate) present in the FMB suspension, indicated by an arrow; the scale bar represents 5 μm. The images were taken with 40× objectives.

In preparation for subsequent experiments involving the produced FMBs, the cavitation activity and emitted acoustic energy was compared to that of unconjugated MBs (i.e. MBs only) and a TSB control. As previously observed in section **4.3.1**, unconjugated MBs emitted significantly more total acoustic energy compared to the TSB control, but FMBs did not emit significantly different total acoustic energy to either the control or unconjugated MBs (MBs: 0.370 ± 0.199 nJ; FMBs: 0.135 ± 0.049 nJ; control: 0.017 ± 0.003 nJ; **Figure 49**). From the cavitation profiles in **Figure 50**, it is clear that FMBs had a shortened period of inertial collapse events after US exposure (t=1 to t=4) compared to MBs (t=1 to t=11; p=0.0006) to give reduced overall acoustic energy; whilst the total power generated during collapse was similar (~ -85 dB re W), the duration of this inertial cavitation activity for FMBs was less than half that of MBs (**Figure 50B/C**). This suggests that there are less cavitating bubbles present in the FMB sample compared to the unconjugated MB sample; if there was an equivalent number of bubbles collapsing in a shorter period of time, there would have been greater power recorded during the collapse phase for the FMB sample. Together,

this suggests that conjugation to liposomes reduces the number of bubbles able to cavitate in the applied US field. This could be a result of the FMB suspension potentially containing less bubbles overall as a result of possible bubble dissolution induced by the introduction and conjugation of liposomes (even though the measured particle count was higher, likely as a result of added liposomes). However, further studies specifically counting the bubble and liposome components separately would be needed to confirm this. Alternatively, a reduced number of cavitating bubbles could be due to conjugated liposomes changing the MB shell properties, including stiffness and viscosity, and in turn altering its acoustic response—a hypothesis supported by previous work by McLaughlan *et al.*[571]. Perhaps, liposome conjugation increases the stiffness and viscosity of the bubble shell, making the bubbles generally less amenable to cavitation and collapse at the tested US parameters. Adjusting the US frequency and/or amplitude to account for the different resonance properties of FMBs could yield a cavitation response that is similar to that of MBs. The optimised conjugation process did not involve mechanical mixing (see **Supplementary 6.7**) that would normally increase the likelihood of the two types of particles being well-mixed. This could mean that there was a population of bubbles that were not (sufficiently) conjugated to liposomes in the suspension, and so would not have their cavitation ability dampened by conjugated liposomes. As such, this bubble sub-population would likely be the one contributing to the shorter collapse period observed. High-speed imaging[711] of the FMBs during US exposure would also be useful to assess whether a population of conjugated bubbles do not cavitate/collapse and stay intact, in line with this hypothesis. Probing of the conjugated bubble shell properties would also contribute towards understanding how conjugation affects this FMB formulation. Additionally, an assay measuring the cavitation of varying bubble concentrations (with and without liposomes) could quantify how cavitation activity varies with bubble concentration for this specific formulation. This would help clarify whether decreasing bubble concentration indeed decreases the duration of the collapse phase.

Again, secondary cavitation events were observed for both MBs and FMBs and it seemed as though the bulk of secondary collapse in the FMB sample occurred sooner after the primary collapse phase compared to the MB sample (~1 second compared to 3-5 seconds after, respectively; **Figure 50B/C**). Moreover, the power generated at the start of the secondary cavitation phase (about a second after the end of the primary collapse phase) was greater for FMBs (~ -95 dB re W) than for MBs (~ -105 dB re W). Together, this shows that a larger number of secondary bubbles collapsed sooner in the FMB sample, which might indicate that liposomes being present in the FMB suspension made the generated secondary bubbles unstable and more prone to immediate collapse, rather than gradually growing as a result of inertial cavitation before collapse. Interestingly, MB secondary collapse was more prolonged than FMB secondary collapse as evidenced by the secondary broadband peak not decaying as quickly in the MB sample (**Figure 50B**). This observation could be related to the hypothesis that conjugated liposomes make bubbles generally less amenable to cavitation and collapse; fewer cavitating bubbles would mean fewer secondary bubbles are generated and so the secondary cavitation events last for a shorter period of time. Over the secondary cavitation period, the power generated by non-inertial and inertial cavitation events were higher and lasted for longer with MBs compared to FMBs, as shown by the broadband and ultraharmonic components remaining ~10 dB re W higher for MBs from t=20 until the end of the US exposure period. This observation corresponds with the idea that a greater number of cavitating bubbles present in the MB sample would contribute to longer lasting cavitation activity and greater generated power over the duration of US exposure (and vice versa for the FMB sample). To evaluate how liposome presence/conjugation impacts bubble cavitation, it would be beneficial to test the cavitation activity of a fixed concentration of bubbles in suspension with varying concentrations of functionalised liposomes capable of conjugation or non-functionalised liposomes that cannot be conjugated. This will help elucidate the extent of the impact conjugation has on MB acoustic response or whether the mere presence of liposomes (without surface attachment) impacts cavitation in a concentration-dependent manner.

To summarise, microscopy was used to measure FMB particle size and concentration which didn't significantly differ from unconjugated MBs. FMB conjugation status was also confirmed by microscopy to show that the maleimide-thiol click chemistry reaction was successful following an optimised protocol. The produced FMBs displayed cavitation activity, although not as much as unconjugated MBs; FMBs showed a shorter period of inertial collapse and reduced total acoustic energy compared to MBs, possibly due to the presence of fewer cavitating bubbles. However, the FMBs were still acoustically responsive even after conjugation to liposomes, so they were suitable for subsequent testing on a monospecies biofilm model.

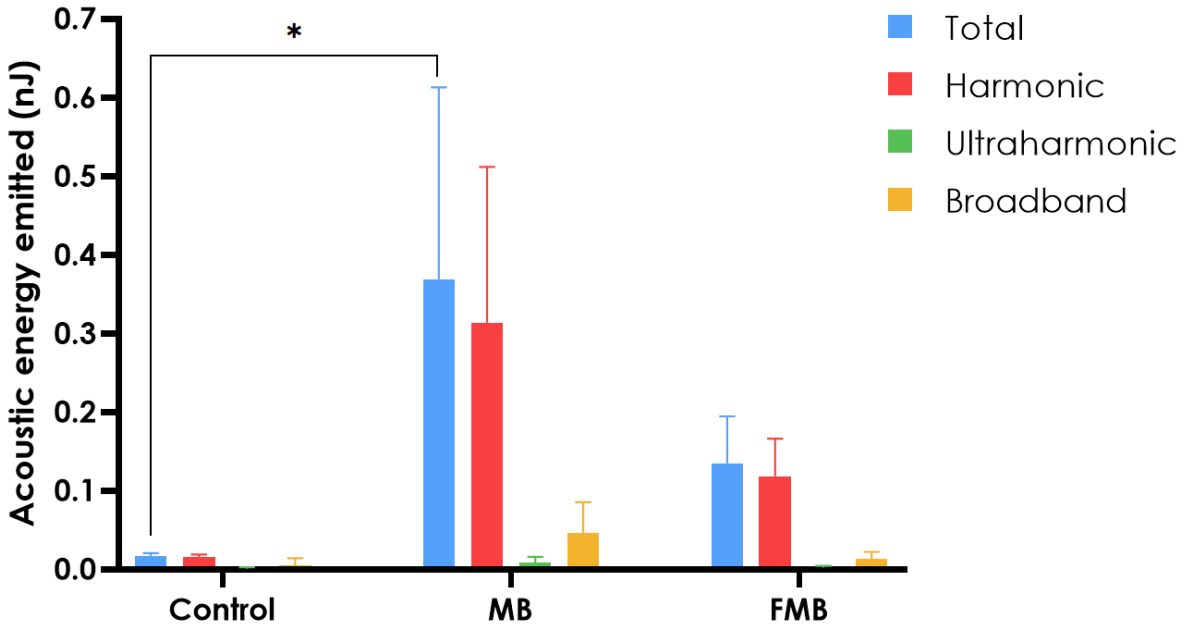


Figure 49 | Acoustic energy emitted by conjugated and non-conjugated microbubbles after exposure to US. Microbubbles only (MB) and Fuso-1-PEG-NIF liposomes conjugated to microbubbles (FMB) were exposed to US, and their cavitation activity was measured to calculate the total acoustic energy emitted. TSB broth (Control) was also exposed to US as a negative control. A one-way ANOVA with Dunnett's multiple comparison test, followed by an unpaired t-test, was performed on the total acoustic energies, where $p \leq 0.05$ indicated statistical significance. (*) = $p < 0.05$.

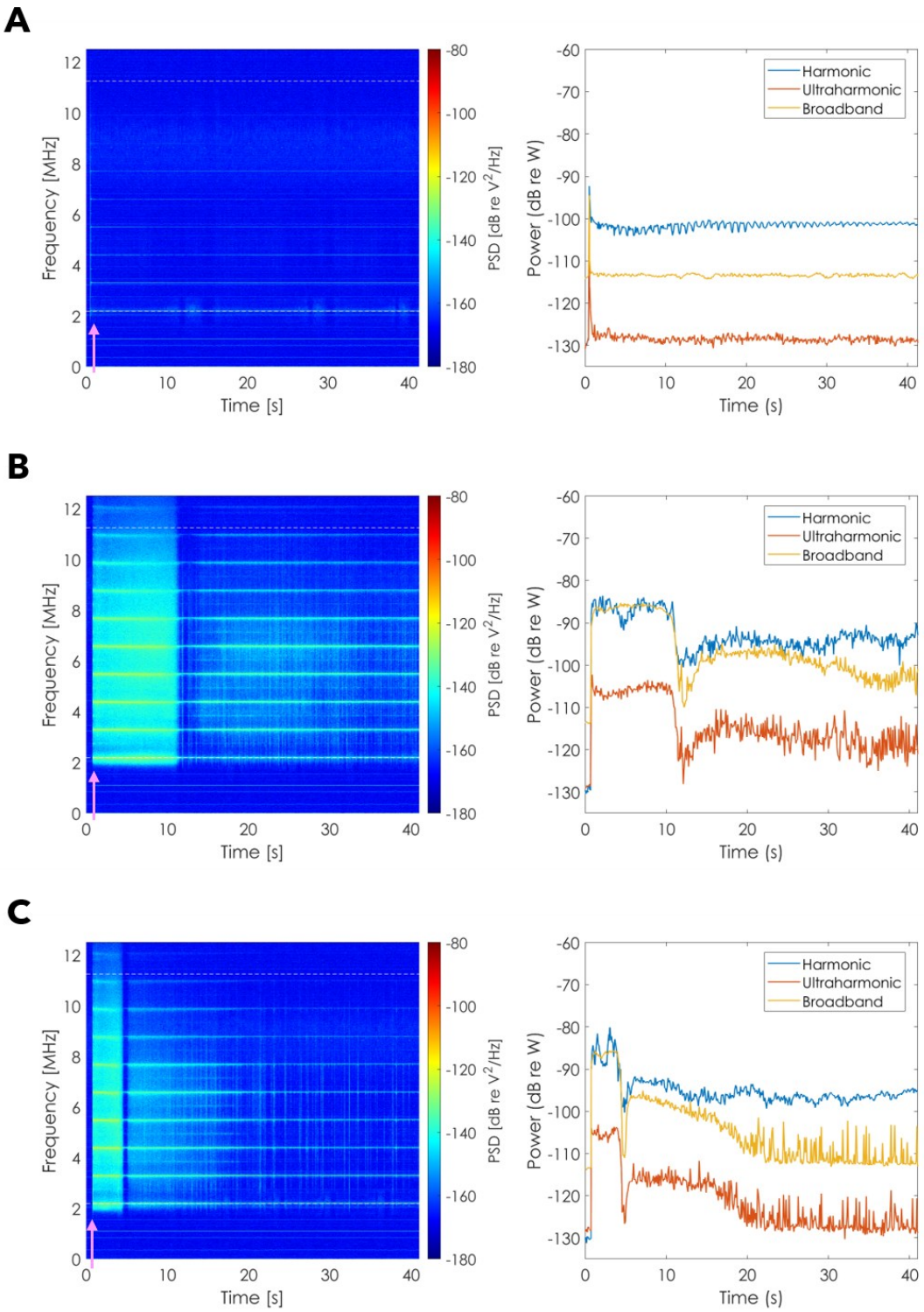


Figure 50 | Representative cavitation profile of conjugated and non-conjugated microbubbles. Representative cavitation profiles of (**A**) TSB control, (**B**) MBs and (**C**) FMBs are shown. In each panel: (left) power spectral density (PSD) showing the variation in power generated by cavitation activity across different frequencies over time; (right) power-time graph showing harmonic, ultraharmonic and broadband components of the signal over the exposure time period. Pink arrows indicate the start of US exposure. Summary of US parameters used: 1.1 MHz with bursts of 400 cycles at 50 Hz PRF for 40 seconds, generating an acoustic pressure of 1 MPa peak negative pressure. A one sample t-test found that the average FMB:MB collapse duration ratio (0.44 ± 0.06) significantly deviated from an expected average collapse duration ratio of 1.00 ($p=0.0006$).

4.3.3 Evaluation of anti-biofilm and cavitation activity of liposome-microbubble construct

4.3.3.1 Pre-application acoustic response of treatments

Before testing on an *E. faecalis* biofilm model, the cavitation activity of four treatments, along with a TSB control, were recorded in the absence of biofilm (treatments summarised in **Table 9**). In addition to the candidate FMB treatment, MB treatment was included as a positive cavitation control. MBs co-administered with free NIF (MB-NIF) served as a comparison to FMB treatment, where NIF was not liposome-encapsulated. A free NIF sample was included as another negative control to confirm there was no acoustic response as a result of adding NIF to the media. The data in this chapter were obtained from four practical repeats and three technical repeats.

As expected, due to the lack of MBs, energy emitted by the free NIF sample was comparable to the TSB control (**Figure 51**). Out of the three bubble-containing treatments—MB, MB-NIF, and FMB—the only one that emitted significantly more acoustic energy relative to the TSB control (0.017 ± 0.003 nJ) and NIF control (0.020 ± 0.008 nJ) was MB-NIF (0.644 ± 0.253 nJ; $p=0.0053$ and $p=0.0210$, respectively). Although there was no statistically significant difference between the energy emitted by the three bubble-containing treatments, the corresponding cavitation profiles show that MB-NIF had a prolonged inertial collapse phase of around 15 seconds compared to the 10 seconds of unconjugated MBs and the 3 seconds of FMBs (**Figure 52A-C**). The maximum power generated during this primary collapse phase was largely similar between the three groups (~ -85 dB re W) despite the difference in duration, suggesting that the MB-NIF sample contained more cavitating bubbles (rather than a comparable number of bubbles collapsing over a longer period of time). In line with what was previously observed, there was a secondary cavitation phase for all three treatments, with MB-NIF showing a gradual increase in power (broadband and ultraharmonic) leading up to secondary collapse, similar to unconjugated MBs. However, secondary cavitation events of MB-NIF generated greater total power than unconjugated MBs: e.g. at 35 seconds, the broadband and ultraharmonic components were about ~5 dB re W higher

for MB-NIF than MBs (**Figure 52A/B**). Interestingly, the time between the start of primary bubble collapse (i.e. when US exposure is started) and the start of secondary collapse was about 20 seconds for MBs and 25 seconds for MB-NIF, which might suggest that the secondary bubbles either take longer to form in the MB-NIF sample and/or are able to non-inertially cavitate for longer. Comparison of the power-time graphs (right panels of **Figure 52A/B**) suggests that there was increased non-inertial cavitation occurring as shown by the increased power of the ultraharmonic component between the two collapse phases of MB-NIF (~ -113 dB re W) compared to MB (~ -120 dB re W), while the broadband was similar for both samples (~ -105 dB re W). Together, the data indicates that NIF by itself did not contribute to cavitation activity but when added to bubbles, it worked to decrease bubble stability so that more of them were prone to collapse, resulting in the emission of more acoustic energy overall. It is possible that added free NIF in the MB-NIF sample was able to insert into and affect the packing of the lipid shell due to its lipophilicity, which in turn would impact the physicochemical properties of the bubble, such as elasticity and compressibility[619,631]. Although the effects of NIF on the constituent lipids used here (DSPE and DSPC) have not been tested in the literature, it is clear that free NIF influenced the properties of the bubble lipid shell and further studies probing this specific drug-lipid interaction would be beneficial.

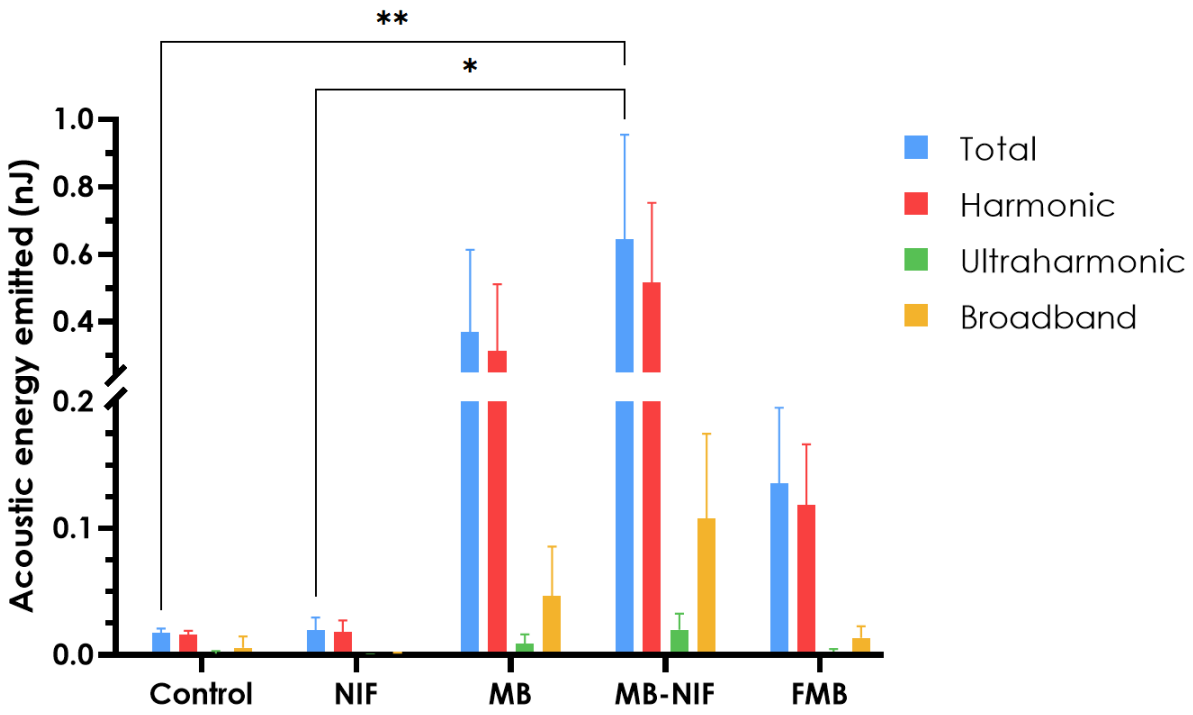
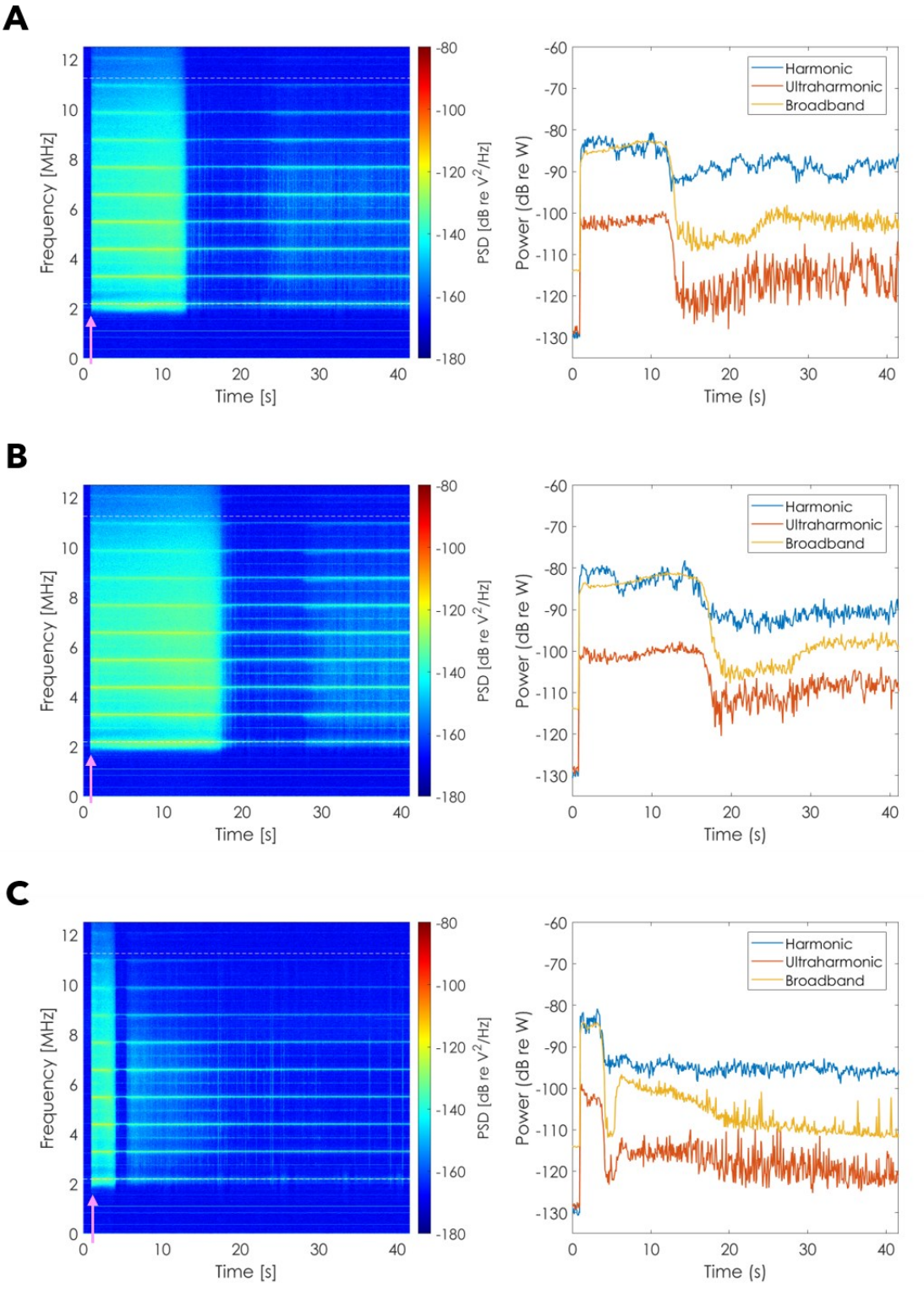


Figure 51 | Acoustic energy emitted by treatment samples after exposure to US in the absence of biofilm. Microbubbles only (MB), microbubbles co-administered with free nitrofurantoin (MB-NIF), and Fuso-1-PEG-NIF liposomes conjugated to microbubbles (FMB) were exposed to US and the cavitation activity was measured to calculate the total acoustic energy emitted. Free nitrofurantoin (NIF) and TSB broth (Control) were also exposed to US as negative controls. A one-way ANOVA with Dunnet's multiple comparison test, followed by Tukey's multiple comparison test, was performed on the total acoustic energies, where $p \leq 0.05$ indicated statistical significance. (*) = $p<0.05$; (**) = $p<0.01$.



(*Figure 52* continued on the next page)

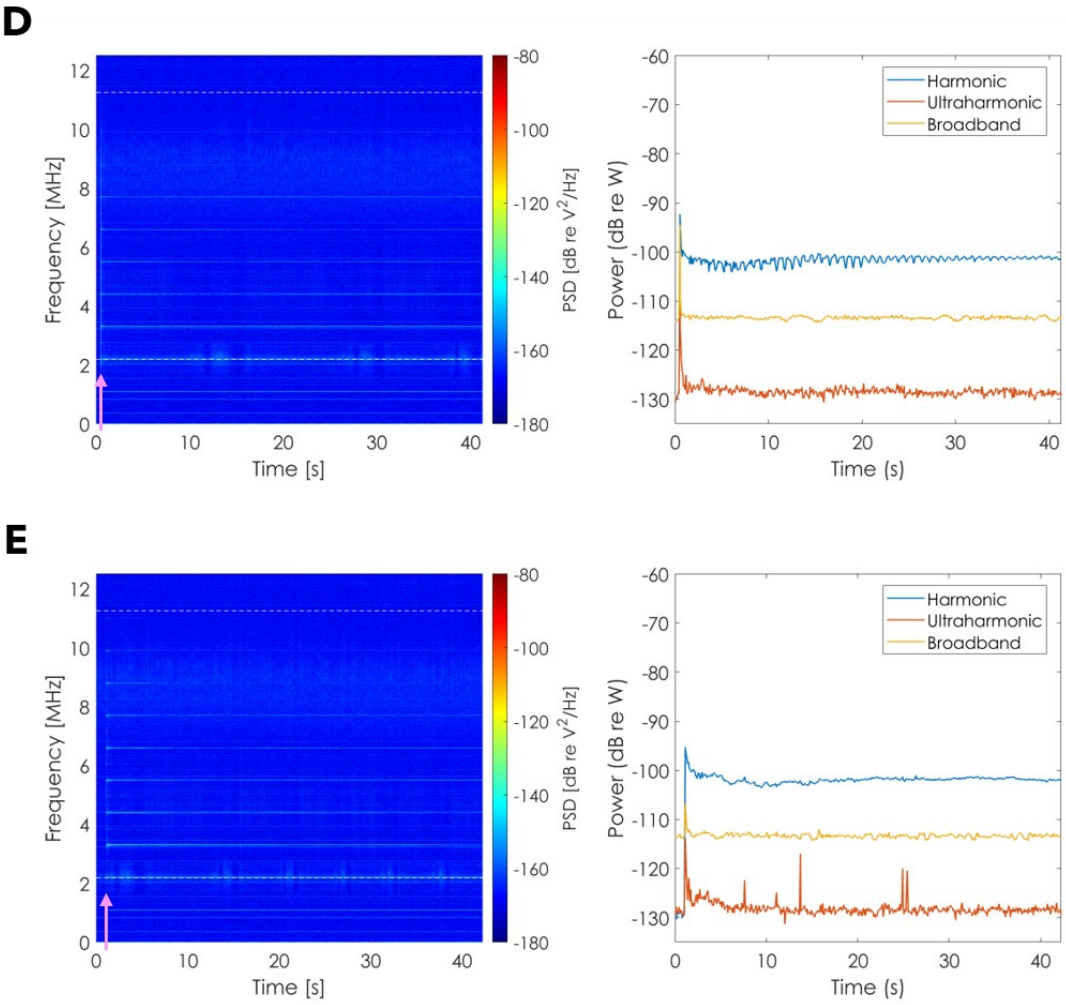


Figure 52 | Representative cavitation profiles of treatment samples in the absence of biofilm. Representative cavitation profiles of (**A**) MBs, (**B**) MBs + free NIF, (**C**) FMBs, (**D**) TSB and (**E**) free NIF in TSB are shown. In each panel: (left) power spectral density (PSD) showing the variation in power generated by cavitation activity across different frequencies over time; (right) power-time graph showing harmonic, ultraharmonic and broadband components of the signal over the exposure time period. Pink arrows indicate the start of US exposure. Summary of US parameters used: 1.1 MHz with bursts of 400 cycles at 50 Hz PRF for 40 seconds, generating an acoustic pressure of 1 MPa peak negative pressure.

4.3.3.2 Post-application acoustic response and anti-biofilm activity of treatments

To assess anti-biofilm activity of the produced FMBs, a 24-hour *E. faecalis* (EF36) biofilm was grown in a channel slide and incubated with different treatments (listed in **Table 9**) after US exposure, as described in section **4.2.6**. In addition to the candidate FMB treatment, MB treatment was included as a positive cavitation control, as well as to provide a baseline for anti-biofilm activity of bubbles in the absence of antibiotics. MBs co-administered with free NIF (MB-NIF) served as a comparison to FMB treatment but without liposome-encapsulation of NIF; this was to assess

whether liposome encapsulation specifically affects the efficacy of the antibiotic when used together with MBs. A solution of NIF dissolved in TSB (i.e. free NIF) sample was included as a control representing the current first-line treatment for UTIs and so was not exposed to US. TSB was included as a no-treatment control and so it was also not exposed to US. Acoustic response was recorded in the form of acoustic energy and cavitation profiles, and anti-biofilm efficacy was measured by calculating biofilm clearance around the US-exposed area and comparing live-dead staining intensities and ratios. The data in this chapter were obtained from four practical repeats and three technical repeats.

In the presence of biofilm, the acoustic energies emitted by the bubble-containing treatments—MB, MB-NIF and FMB—were generally much lower than in the absence of biofilm (**Figure 53**); in the presence of biofilm, total energies were at most half what they were in the absence of biofilm. This could be due to increased attenuation of transducer-generated US waves and/or MB-emitted acoustic energy by the biofilm matrix within the channel slide[712,713]. Additionally, cavitation activity can be significantly impacted by the proximity of MBs to a surface, such as biofilm, the channel wall, or even each other; short distances to a solid wall or nearby bubbles can limit bubble growth and oscillation amplitudes[714,715]. The presence of biofilm could effectively reduce the channel thickness and, hence, reduce surface proximities to suppress cavitation. Furthermore, the presence of PEG chains in the lipid particles could also possibly be facilitating interactions with Gram-positive EF36 (as proposed in section **3.3.1**), working to increase MB-biofilm proximity. However, the general trend observed in the previous section (**4.3.3.1**) was the same; MB-NIF emitted the most acoustic energy followed by MBs and then FMBs. This was also reflected in the corresponding cavitation profiles (**Figure 54**) where the duration of primary inertial collapse was reduced for all the treatments but still followed the order of MB-NIF > MB > FMB.

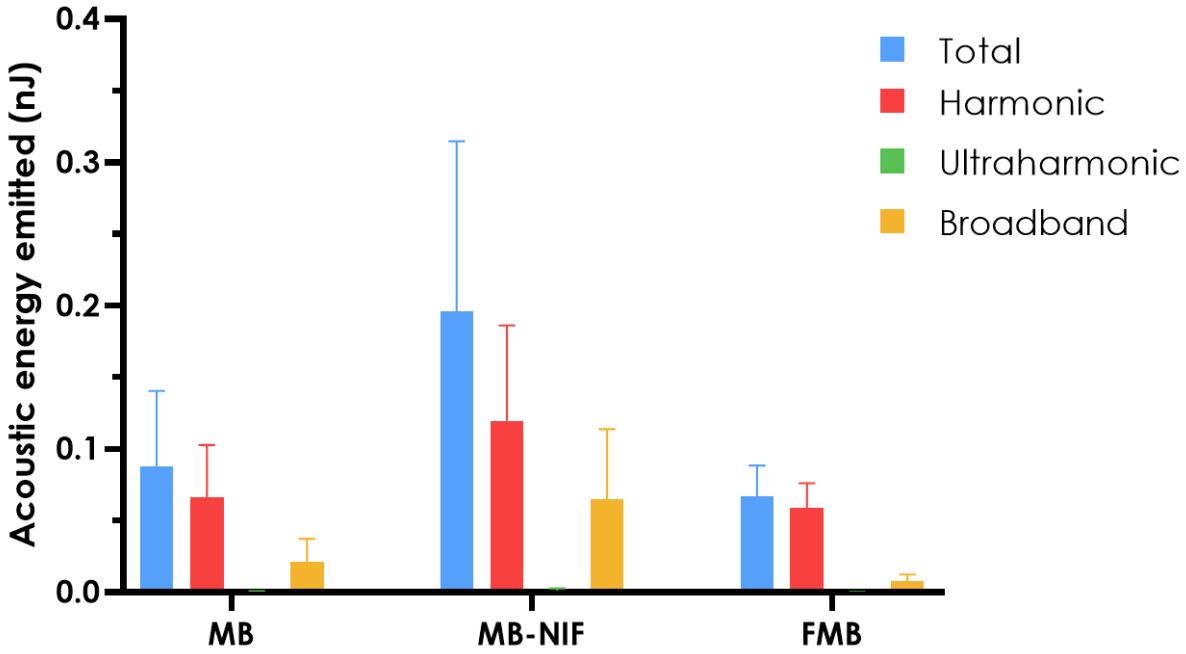


Figure 53 | Acoustic energy emitted by microbubble preparations after exposure to US in the presence of biofilm. Microbubbles only (MB), microbubbles co-administered with free nitrofurantoin (MB-NIF), and Fuso-1-PEG-NIF liposomes conjugated to microbubbles (FMB) were exposed to US and the cavitation activity was measured to calculate the total acoustic energy emitted. A one-way ANOVA with Tukey's multiple comparison test was performed on the total acoustic energies—no statistically significant difference between the total acoustic energies emitted by the three treatments was found ($p=0.0842$).

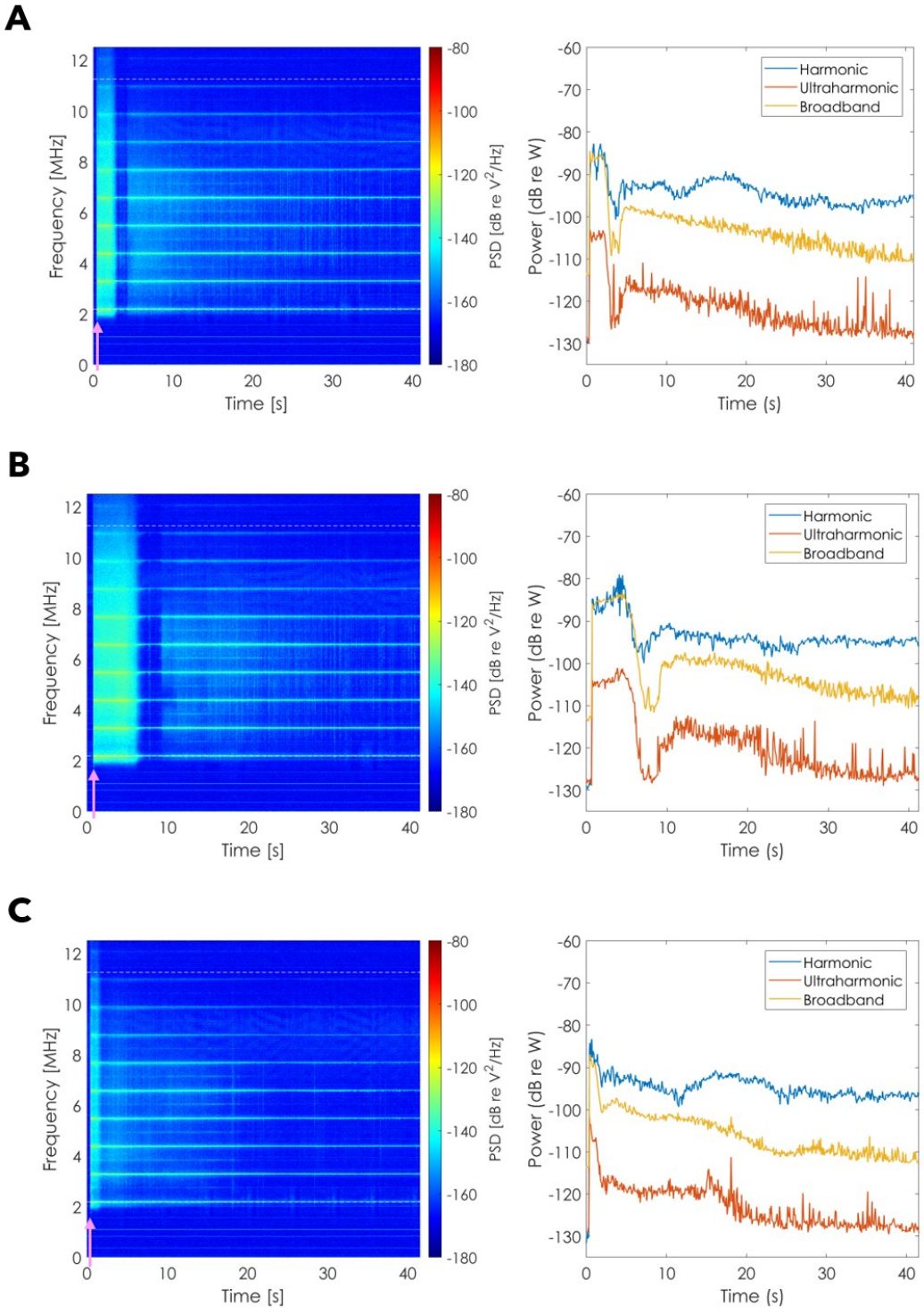


Figure 54 | Representative cavitation profiles of microbubble preparations exposed to US in the presence of biofilm. Representative cavitation profiles of (**A**) MBs, (**B**) MBs + free NIF (i.e. MB-NIF) and (**C**) FMBs are shown. In each panel: (left) power spectral density (PSD) showing the variation in power generated by cavitation activity across different frequencies over time; (right) power-time graph showing harmonic, ultraharmonic and broadband components of the signal over the exposure time period. Pink arrows indicate the start of US exposure. Summary of US parameters used: 1.1 MHz with bursts of 400 cycles at 50 Hz PRF for 40 seconds, generating an acoustic pressure of 1 MPa peak negative pressure.

In line with findings from section **3.3.6**, confocal microscopy revealed that free NIF and FMB treatment (0.5 mg/mL NIF) did not significantly reduce biofilm coverage area compared to the control (**Figure 55B/E/F**); NIF reduced biofilm coverage by 24 percentage points to 63%, while FMBs reduced it by 12 percentage points to 75%. MBs, on the other hand, significantly reduced the amount of biofilm to 52% (**Figure 55C/F**; p=0.0118), which is in agreement with findings of MB-facilitated biofilm clearance in the literature[322,509,548,557]. The formation of large pores and streaks in the biofilm (**Figure 55C**), but also smaller ones (**Figure 55E**, **Supplementary Figure 18**), in the MB and FMB treated samples (but not the control or NIF treated samples) suggests that bubble-associated cavitation activity is driving biofilm clearance in this way. Again, these findings are supported by previous studies that show similar patterns of clearance upon exposure of MB-treated biofilm to US[716]. Most interestingly, MB-NIF was the best treatment in reducing biofilm coverage very significantly to 25% (**Figure 55D/F**; p<0.0001 compared to the control). Additionally, when compared to free NIF and FMB treatments, biofilm clearance by MB-NIF was significantly greater (p=0.0269 and p=0.0040, respectively) which implies that MBs co-administered with 'free' NIF (which may become incorporated into the MB shell) was more effective than conjugation to liposome-encapsulated NIF, a finding that has not previously been tested or reported in the literature. Many large streaks of removed bacteria can be seen in the resultant biofilm (**Figure 55D**). This finding may be specific to MB co-administration with NIF, but could also be a trend that holds true for other lipophilic drugs—MB co-administration studies with other lipophilic antibiotics, such as ciprofloxacin, could be carried out to assess whether cavitation and anti-biofilm activity are also greatly increased. Together with the cavitation data, these results indicate that increased emitted acoustic energy associated with longer inertial collapse phases is likely the primary driver of biofilm clearance (**Figure 56A**); notably, the extent of biofilm clearance of the different bubble-containing treatments follows the same trend as the emitted acoustic energy and inertial collapse duration—MB-NIF > MB > FMB (**Figure 55F**; **Figure 56B**).

In addition to calculating the resultant biofilm coverage area, the mean pixel intensities of the SYTO 9 and PI staining (for live and dead cells, respectively) were measured and the PI/SYTO 9 intensity ratio calculated as a measure of cell death within the biofilm[706]. Within the control biofilm, much of the cells were dead (**Figure 57**), which could be a reflection of the growth conditions used (e.g. TSB not being a rich enough broth) or the biofilm formation of this particular strain (EF36). However, a high number of dead cells (up to 65%) within *K. pneumoniae* biofilms have been reported in the literature, which aligns with this observation[717]. Although FMBs did not clear biofilm as effectively as MBs and MB-NIF, when considering the viability of the remaining biofilm, FMBs were the only treatment that resulted in cell death significantly greater than the control (**Figure 57**); both the mean pixel intensity of PI ($p=0.0382$) and the PI/SYTO 9 ratio ($p=0.0285$) were greater than the control. This indicates that even though the reduced acoustic response of FMBs may reduce the amount of mechanical biofilm clearance, this doesn't appear to hamper antibiotic activity and may, in fact, enhance it; previously, it was observed that Fuso-1-PEG-NIF anti-biofilm activity largely matched that of free NIF at 0.5 mg/mL (**Figure 43**) but after conjugation to MBs and exposure to US, liposomal NIF facilitated more bacterial death than free NIF representative of the current first-line treatment. Perhaps the biophysical effects of cavitation, such as microstreaming, help to drive liposomal interaction and uptake in the biofilm, an effect that is not present with the NIF treatment. In future experiments, it would be useful to include Fuso-1-PEG-NIF with and without US exposure as a treatment. This would give insights into how US exposure with liposomes alone contributes to biofilm clearance and viability reduction, i.e. confirming if MBs meaningfully contribute to the antibiotic activity observed with FMBs or if liposomes alone would give the same outcome.

NIF treatments did not significantly increase cell death, which complements previous findings from section **3.3.6** where biofilm-associated cells were not completely killed at 0.5 mg/mL free NIF (note that the viability of the biofilm itself was not directly probed in section **3.3.6**). MBs similarly did not significantly decrease biofilm viability compared to the control even though it was

observed that biofilm coverage was reduced. This result could be due to the fact that the reduced biofilm biomass impacted the quantification of the stain ratios, or could be because MB-associated biofilm clearance does not necessarily mean cell death. As mentioned in section **1.5.3**, US and MBs are known to be effective at biofilm clearance but should be followed up with antibiotic treatment to facilitate bacterial killing, hence why this result may be expected[557]. However, MB-NIF also did not decrease biofilm viability despite significant biofilm clearance and the presence of antibiotic (**Figure 57**). Again, this could be due to the relatively small number of bacterial cells present in the resultant biofilm, so quantification of staining was not reflective of what the broader biofilm population would have been. Alternatively, it could be indicative of free NIF not being as effective against cells in the biofilm even with added MB activity, contrary to what is in the literature; perhaps the value of NIF in this formulation comes from increasing cavitation activity and mechanical biofilm clearance rather than being available to kill bacteria through chemical means, especially given that NIF potentially intercalates with the MB shell. It might be beneficial to measure the amount of truly free NIF (i.e. not interacting with the MB shell) that is available in the suspension by separating it into a bubble and aqueous fraction, which could help explain why MB-NIF does not seem to decrease biofilm viability.

Together, these results indicate that NIF on its own is insufficient treatment for EF36 biofilm infections as it neither clears biofilm nor reduces biofilm viability, especially in comparison to the bubble-containing treatments tested. As expected, MBs alone are efficient at biofilm clearance but the remaining biofilm does not have any increased cell death, and likely needs added antibiotics to facilitate bacterial killing. Upon adding NIF to MBs, however, even though the biofilm viability was not significantly reduced according to the quantification of PI and SYTO 9, the biofilm clearance ability was greatly enhanced. This is likely linked to the increase in cavitation activity and emitted energy of MB-NIF, with the inertial collapse events contributing to mechanical removal of the biofilm. FMBs did not show efficient biofilm clearance, which might be expected due to the reduced acoustic energy emitted and fewer inertial collapse events compared to MBs and MB-

NIF. Despite this, the biofilm viability was significantly reduced by FMBs which suggests there may be a balance to be struck between energy emission by cavitation for biofilm clearance and liposomal encapsulation that facilitates increased cell death. For example, changing the US parameters or the MB:liposome ratio in the conjugate could result in increased cavitation energy while maintaining antibiotic efficacy. All things considered, it is clear that further optimisation is necessary to get the best outcome in both biofilm clearance and bacterial killing. Currently, these data indicate that MB-NIF may be the most promising anti-biofilm treatment modality, using the existing US parameters and particle formulations.

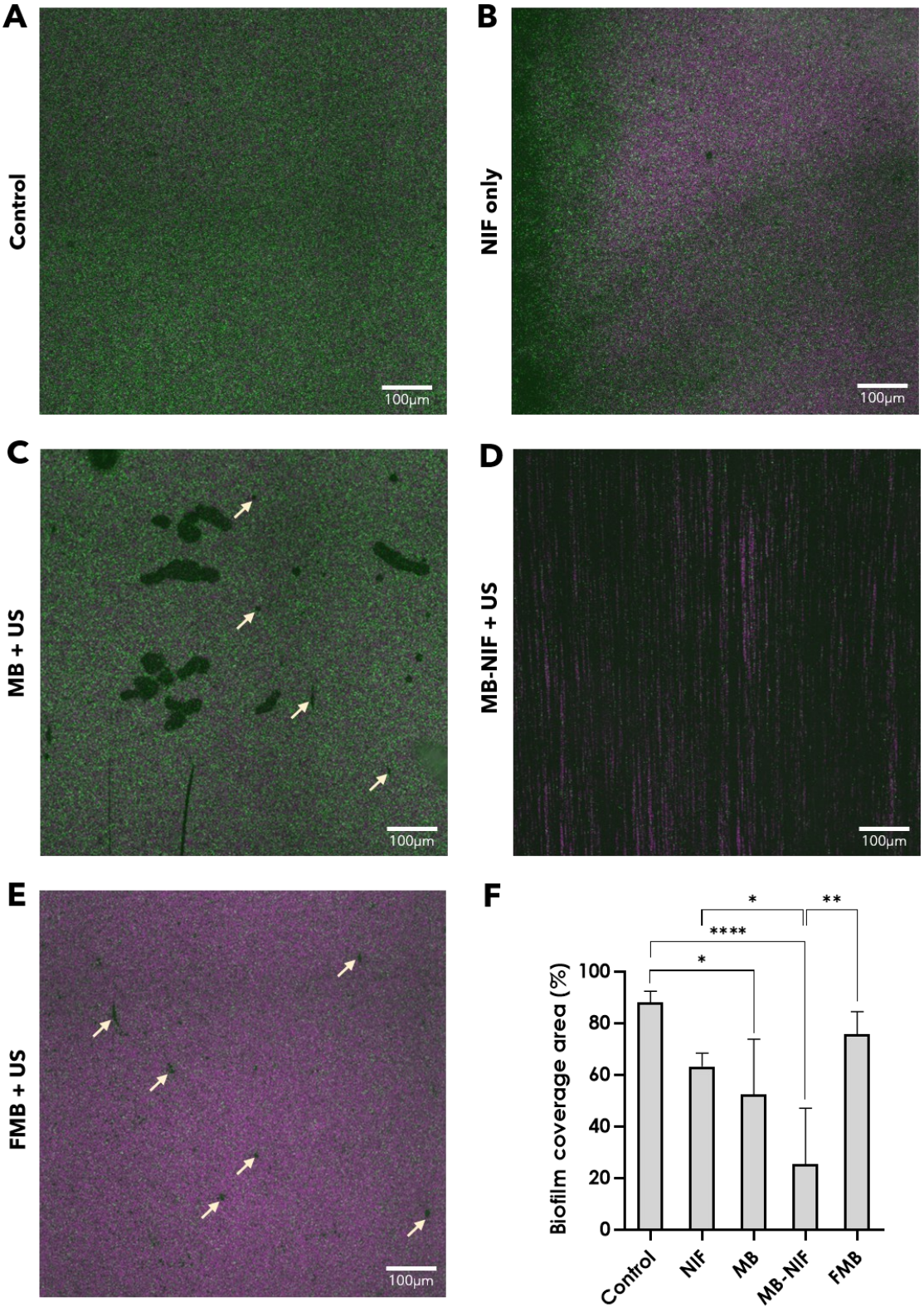


Figure 55 | Confocal images (10×) of *E. faecalis* biofilm after incubation with different US-exposed treatments. Biofilm after treatment with (A) TSB (no US), (B) free NIF (no US), (C) MBs (+ US), (D) MB-NIF (+ US) and (E) FMBs (+ US). In the images, live cells are stained in green and dead cells in magenta. Examples of small pores and streaks are indicated by arrows. (F) Average biofilm coverage area (%) quantified for each treatment. A one-way ANOVA with Dunnet's and Tukey's multiple comparison test was performed on the biofilm coverage area, where $p \leq 0.05$ indicated statistical significance. (*) = $p<0.05$; (**) = $p<0.01$; (****) = $p<0.0001$.

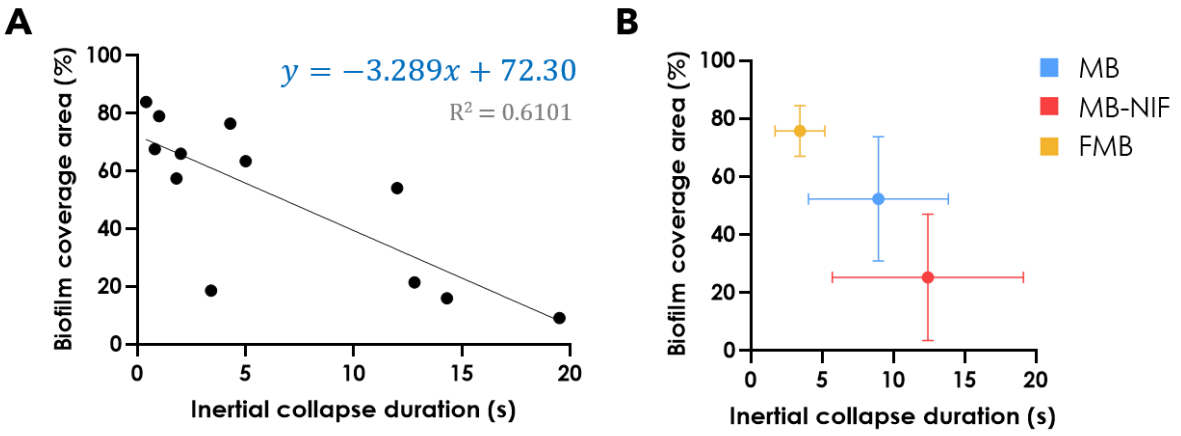


Figure 56 | Biofilm coverage area vs. inertial collapse duration comparisons. (A) Scatterplot showing how biofilm coverage area varies with the duration of (primary) inertial collapse. The 12 experimental points, (corresponding to four practical repeats each for MB, MB-NIF, and FMB) were fit with a linear regression model and the calculated equation and R^2 value is shown. A F-test found that the slope was significantly non-zero (p=0.0027); a significant linear relationship exists between biofilm coverage area and the inertial collapse duration. (B) The average biofilm coverage area and inertial collapse duration summarised for each treatment (MB, MB-NIF, FMB). The vertical error bars represent standard deviation in biofilm coverage area; the horizontal error bars represent standard deviation in inertial collapse duration.

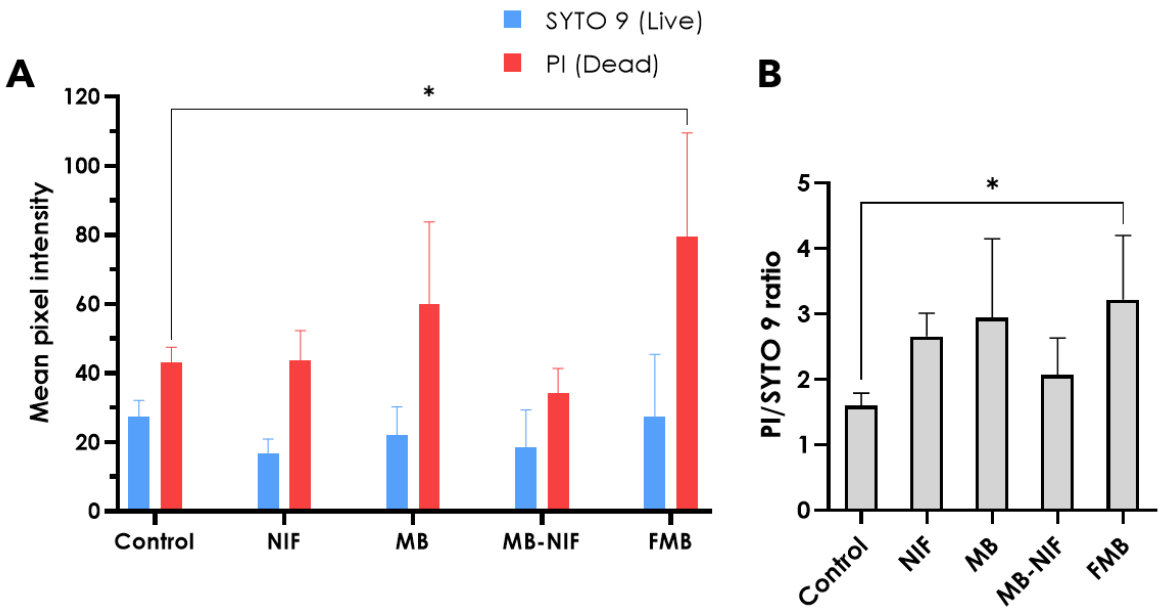


Figure 57 | Mean pixel intensities and ratios of treated biofilm staining with SYTO 9 and PI. *E. faecalis* (EF36) biofilms were incubated with microbubbles only (MB), microbubbles co-administered with free nitrofurantoin (MB-NIF), and Fuso-1-PEG-NIF liposomes conjugated to microbubbles (FMB) after US exposure with the treatments. Free nitrofurantoin (NIF) and TSB broth (Control) were controls not exposed to US. Confocal microscopy images were taken and mean pixel intensities of the SYTO 9/PI (live/dead) staining measured. (A) Mean pixel intensities of SYTO 9 (live; blue bars) and PI (dead; red bars) from the images of treated biofilm and (B) their respective PI/SYTO 9 ratios as an indicator of biofilm viability are plotted. A one-way ANOVA with Dunnet's and Tukey's multiple comparison test was performed on the mean pixel intensity of PI as well as the PI/SYTO 9 ratios of the different treated biofilm, where p≤0.05 indicated statistical significance. (*) = p<0.05.

4.4 Conclusions

This chapter focussed on producing a MB formulation that was suitable for conjugation to Fuso-1-PEG-NIF liposomes, physically characterising these MBs and optimised liposome-MB particles, and testing the liposome-MB particles against a monospecies biofilm to assess anti-biofilm activity.

A MB formulation consisting of the two most commonly used lipids for lipid-coated MBs, DSPC and DSPE-PEG[517], was successfully produced using a homogenisation protocol (O'Reilly *et al.*, unpublished). The MBs were physically characterised via optical microscopy—the average size and concentration of the bubbles was 1.00 ± 0.85 μm and 1.76×10^8 bubbles/mL, respectively. The acoustic response was measured via PCD that confirmed cavitation activity with the chosen US parameters (1.1 MHz, 400 cycles at 50 Hz PRF, 1 MPa PNP, 40-second exposure). These MBs were then conjugated to Fuso-1-PEG-NIF via maleimide-thiol click chemistry following an optimised protocol. The success of conjugation was assessed via fluorescence microscopy where DiO-labelled Fuso-1-PEG-NIF made unlabelled MBs visible if conjugated. The conjugated particles (FMBs) had an average size of 0.80 ± 0.31 μm and concentration of 2.85×10^8 particles/mL. Conjugation was shown to reduce the acoustic response of the MBs, likely through changing the properties of the MB shell and reducing the number of bubbles capable of cavitating and collapsing in the chosen US field. When compared to other bubble-containing treatments, MBs and MB-NIF, FMBs emitted the least amount of acoustic energy, while MB-NIF emitted the greatest. It is possible that the addition of NIF to MBs also changed the properties of the MB shell in a way that made the bubbles more prone to cavitation and collapse; NIF could intercalate into the lipid shell due to its lipophilicity, as has been reported elsewhere[619,631].

When exposed to US in the presence of biofilm, the trend in emitted acoustic energy remained the same (i.e. MB-NIF > MB > FMB), but the overall acoustic energy decreased across all treatments, likely due to increased signal attenuation caused by the presence of the biofilm. These energies also corresponded with the amount of biofilm clearance achieved, where MB-NIF decreased

biofilm coverage area the most (to 25%), followed by MBs (to 52%) and then FMBs (to 75%). However, when looking at biofilm viability, FMBs were the only treatment that significantly increased cell death more than the no-treatment control, which could indicate that even though this formulation was not effective at clearing biofilm, it had enhanced antibacterial activity against cells remaining in the biofilm. Free NIF representative of the current first-line treatment against UTIs did not manage to significantly clear biofilm or reduce biofilm viability within the same setup.

The research presented in this chapter was the final step towards the objective of this project to create a novel ultrasound-mediated lipid-based drug delivery system that is efficient at both disrupting biofilms of UTI-related species and delivering NIF to bacteria. On the whole, the bubble-containing treatments performed better than NIF alone, highlighting the potential for US and MBs to enhance antibacterial and anti-biofilm activity. In particular, MB co-administration with NIF showed the most promise of significant biofilm clearance, associated with increased cavitation activity, compared to both MBs alone and FMBs. The results indicate that prolonged cavitation, particularly inertial collapse, is important for biofilm clearance and this needs to be paired with increased bacterial killing within the remaining biofilm. A NIF-loaded LMB formulation (i.e. FMB) was produced that was acoustically responsive, which has not been done previously. Further optimisation of either this FMB formulation or the US parameters used (or both) is required in order to get the best of both worlds—increased energy output from bubble cavitation and increased cell death from US-enhanced liposomal uptake. The analysis of cavitation data in this study was essential to draw conclusions on how the acoustic response informs biological outcomes; this provides valuable insight into the mechanism of action of bubble-containing treatments, as well as highlights areas where adjustments and modifications can be made to potentially improve anti-biofilm effects.

5 Conclusions

5.1 Summary of research

The overall aim of this research was to develop a novel LMB formulation that combines US-mediated disruption of bacterial biofilms with bacterial killing by antibiotic-loaded liposomes.

The first objective was to formulate and characterise antibiotic-loaded liposomes suitable, in terms of stability and encapsulation efficiency, for subsequent antibacterial treatment. Several cationic and fusogenic formulations were produced and their average size, size distribution, and zeta potential measured to assess their short-term stability (7 days). From this, one cationic formulation (Cat-8; 126 nm, +25 mV) and one fusogenic formulation (Fuso-1-PEG; 111 nm, -3 mV) were selected as the most stable liposomes. They were successfully loaded with VAN or NIF and labelled with DiD or DiO in preparation for bacterial susceptibility tests. Experiments probing passive drug release of the VAN-loaded cationic formulation (Cat-8-VAN) at temperatures representing storage conditions (4°C) or a physiological environment (37°C) revealed that temperature had no significant effect on the drug release profile of this formulation. Additionally, Cat-8-VAN was found to maintain its physical size and zeta potential for up to 120 days in long-term stability studies. The primary outcome of this chapter was that NIF-loaded liposomes were successfully formulated and characterised to address the gap in liposomal formulations of NIF for UTI treatment.

The second objective was to assess the antibacterial properties of the selected liposomes against UTI-relevant monospecies planktonic and biofilm models, which would allow for the selection of the most suitable formulation for later use with MBs and US. MIC and MBC assays found that Cat-8-VAN was essentially equally as effective as free VAN against both planktonic *E. coli* and *E. faecalis*, whereas Fuso-1-PEG-VAN was only able to facilitate bacterial death in planktonic *E. faecalis* but not *E. coli*. Preliminary confocal microscopy studies found that Cat-8-VAN could

exhibit extreme aggregation in growth media (caMHB) and indicated that uptake/interaction was likely responsible for the cell death observed in both species. Preliminary super-resolution studies suggested that Fuso-1-PEG-VAN uptake was likely occurring with *E. faecalis* (EF36) but there was not much interaction with *E. coli* (UTI89). To explore the hypothesis that liposome PEGylation may be interfering with bacteria-liposomes, particularly with *E. coli*, a PEG-titration experiment was attempted but a reduction in Fuso-1-PEG-VAN liposome quality, corresponding to a reduction in PEG content, made it difficult to confirm the effect of solely varying liposomal PEG content.

MIC and MBC assays using liposomal formulations of NIF showed they did not improve drug delivery to planktonic *E. coli* and *E. faecalis* compared to free NIF, although Fuso-1-PEG-NIF did show bactericidal effects on *E. coli* where the VAN-loaded counterpart did not. Due to the novelty and clinical relevance of NIF-loaded liposomes, the large particle aggregation associated with the Cat-8 formulation, as well as time-constraints, Fuso-1-PEG-NIF was selected for MBEC and MBaBC assays on monospecies biofilm. On the whole, anti-biofilm activities of NIF and Fuso-1-PEG-NIF gave mixed results: against *E. coli*, free NIF was generally better at reducing biofilm biomass and viability than Fuso-1-PEG-NIF; against *E. faecalis*, anti-biofilm activity of the two treatments was largely comparable but strain-specific differences were observed where EF36 biomass was reduced slightly more than EF48. Additionally, Fuso-1-PEG-NIF seemed to outperform free NIF at lower concentrations when evaluating the viability of biofilm-associated cells, but at higher concentrations either showed comparable performance or underperformed relative to free NIF, depending on the strain (EF36 in the former case, EF48 in the latter). Interestingly, Fuso-1-PEG-NIF showed increased activity against biofilm-associated 'planktonic' EF36 compared to its biofilm form or purely planktonic EF36, which may indicate that biofilm dispersal—that can be facilitated by US and MBs—could contribute to overall liposome activity. Therefore, Fuso-1-PEG-NIF and EF36 were chosen as the formulation and biofilm strain, respectively, for subsequent US experiments.

The third objective was to formulate and characterise acoustically-responsive MBs before and after conjugation to liposomes. MBs (1 μm, ~2×10^8 bubbles/mL) were successfully produced following a homogenisation protocol and physically characterised using microscopy. The cavitation activity of these MBs at 1.1 MHz US and 1 MPa PNP was recorded using PCD, and confirmed an acoustic response of the bubbles in this US field. Maleimide-thiol click chemistry was used to conjugate maleimide-functionalised Fuso-1-PEG-NIF liposomes to thiol-functionalised MBs following an optimised protocol, which was confirmed via fluorescence microscopy. The produced FMBs (0.8 μm, ~3×10^8 particles/mL) showed a reduced acoustic response: a shorter period of inertial collapse and less acoustic energy emitted overall. These findings added a new characterised formulation to the emerging field of LMB technology and the results could provide useful insight into downstream anti-biofilm observations.

The final objective was to evaluate the anti-biofilm activity of the LMBs against a UTI-relevant monospecies biofilm model. In the absence of biofilm, it was found that MBs co-administered with free NIF (MB-NIF) emitted more acoustic energy and showed a longer inertial collapse period than both MBs and FMBs. In the presence of biofilm, this trend remained (MB-NIF > MB > FMB) but the overall acoustic energy emitted was reduced across all treatments. These energies also corresponded with the amount of biofilm clearance achieved, where MB-NIF decreased biofilm coverage area the most, followed by MBs and then FMBs. However, when evaluating biofilm viability, FMBs were the only treatment that significantly increased cell death more than the no-treatment control. These results highlight the antibacterial potential of LMBs in a UTI context, paving the way for the exploration of LMB formulation and US field modifications that can increase the acoustic response and corresponding anti-biofilm properties. More notably, the significant role free NIF had in enhancing MB acoustic activity and downstream anti-biofilm effects may also prompt further investigation into combining lipophilic drugs with MB technology against UTIs, as a potentially more promising anti-biofilm strategy.

5.2 Perspectives and future work

5.2.1 Limitations of the study

At different stages of this project, a number of limitations were identified that highlight areas for future investigation which are listed below.

I. There were changes that had to be made to the fusogenic formulation, Fuso-1, to overcome production and stability difficulties that unexpectedly arose, reasons for which are unclear (see sections **2.3.1** and **6.1.2**). Because of this, a non-PEGylated version of this fusogenic formulation was unavailable for comparative studies on how PEGylation potentially impacts bacteria-liposome interactions, as attempted in section **3.3.4**. Additionally, comparative studies probing how MB co-administration with fusogenic liposomes (rather than conjugation) affected bubble cavitation activity and downstream anti-biofilm effects could not be performed. Given the impact that co-administration with free NIF had on MB activity (see section **4.3.3**), there is reason to believe that co-administration with drug-loaded liposomes could also influence the acoustic response of surrounding MBs.

II. Microbiological assays performed in chapter **3** that evaluated MBC values involved incubating the bacterial suspension with resazurin for a further 24 hours (after the 24 hours needed for MIC recordings). This meant that the bacterial suspension was incubated in unchanged media for up to 48 hours, with two different measurements occurring at different points within that timeframe. Bacterial activity may have been significantly different as nutrients were depleted over time[718]. Furthermore, this additional 24 hours may have been sufficiently long to allow bacterial regrowth and/or biofilm growth and so the more immediate antibiotic effect could have been masked at the point of MBC measurement[719]. Therefore, running concurrent MIC and MBC assays to take measurements in matching bacterial environments may have given different values.

Additionally, time-kill assays would have been useful to measure the rate of killing as well as track potential population (re)growth kinetics.

III. The visualisation of liposomes using dSTORM super-resolution microscopy could only be accomplished using antibody detection (proprietary to Oxford Nanoimaging, UK) that were specific to PEG chains. As such, only the PEGylated formulation (Fuso-1-PEG) could be imaged using this technique and Cat-8 treatments could not be included in this experiment. Producing and characterising a PEGylated version of the cationic formulation would prove useful in visualising bacteria-liposomal interactions and aid in comparisons to Fuso-1-PEG behaviour documented in section **3.3.3**.

IV. There were some limitations of the design of the US setup used in chapter **4**. In order to minimise US wave attenuation by the channel slide itself during exposure of the sample, the orientation of the channel slide in the water tank was restricted to what was illustrated in **Figure 44**: the thinner lower wall of the channel slide (0.2 mm) facing downwards and the thicker upper wall (1.1 mm) facing upwards. However, this channel slide orientation might not have been the most ideal for biofilm treatment; biofilm grew primarily along the lower wall of the channel slide and when the treatment was added, it occupied the space above the biofilm. Since suspended bubbles naturally rise, it would have been preferable to place the treatment media at the bottom of the channel slide and have the biofilm develop along the upper wall. This way, as the bubbles ascend, they distance between them and the biofilm above would be reduced for potentially greater localised effects[720,721]. Unfortunately, bacterial incubation was not possible with a flipped channel slide (due to its geometry) to allow for biofilm growth along the upper wall, and restrictions within the US setup mentioned earlier meant that the channel slide could not be in a flipped orientation in the tank. Overall, this meant that the bubbles may not have been as close in proximity to the biofilm as desired. In a clinical scenario, the location of the surface-attached biofilm on the urothelium, the position of the transducer relative to the biofilm

and bubble-containing treatment suspension (especially when using an US probe from outside the body), as well as the physical positioning of the patient are all likely to contribute to variation in bubble-biofilm proximity and the downstream anti-biofilm effects. Additionally, greater US attenuation would be expected as the US wave would have to travel through the body, across the bladder lining and, ultimately, through the surface-attached biofilm on the urothelium before it reaches the bubble-containing treatment suspension held in the bladder. Exploration of different US setups that allow for the systematic investigation of the effect of bubble-biofilm proximity and US attenuation on anti-biofilm activity would possibly allow for better assessment and adjustment of LMB and MB properties, where the location of biofilm growth, direction and attenuation of US exposure, as well as the tendency of bubbles to rise are taken into account.

5.2.2 Suggestions for future work

This research has identified several promising directions for future investigation, which are outlined in this section.

I. For super-resolution imaging of bacteria and liposomes utilised in section **3.3.3**, an on-chip staining method was used (see methods **3.2.4**). Because staining was done after the bacteria had been immobilised on the assay chip, it is likely that the large amount of background signal came from dye that had non-specifically bound to the lysine-coated chip. Therefore, in order to reduce this background signal, it is proposed that an in-solution staining protocol should be used instead (see **Supplementary 6.3.2**). Briefly, this would involve staining the bacteria in suspension before immobilisation on the assay chip to reduce the risk of non-specific binding of dye. In this way, more confident conclusions on visualised cell and liposome structures can be made.

II. All experiments involving bacteria in chapters **3** and **4** used either caMHB or TSB as growth media. While these are standard microbiological media, it is widely acknowledged

that these growth media are not representative of a clinical bacterial/biofilm environment, e.g. not containing physiological proteins or missing host-bacteria interaction cues[722,723]. This can lead to experimental outcomes that do not translate clinically and, as such, it is important to replicate physiological conditions for more accurate and translatable results. In the context of UTIs, growing of bacteria in urine or under flow, for example, have proven to be better models that take the complexities of infection into consideration[724,725]. Additionally, the use of human cell-attached biofilm models, such as organoids that attempt to reproduce the host microenvironment, provide even more information *in vitro* on host interactions with both the colonising bacteria and tested treatments[726–728].

III. From the results generated in chapter **3**, it seemed as though the cationic liposomes had great antibacterial potential, particularly against Gram-negative *E. coli*. However, the formation of large aggregates potentially poses a clinical risk down the line[677–679]. PEGylation is known to help prevent liposome aggregation and so including PEG chains in the cationic formulation could prove effective at resolving this problem (although PEGylation could also somewhat reduce the antibacterial effects observed)[376,378–380]. This PEGylation would also allow for super-resolution experiments to be performed on the cationic formulation, to visualise any differences compared with the behaviour of the fusogenic formulation, complementing the experiments in section **3.3.3**. Including maleimide-functionalised PEG chains to the formulation would additionally allow for the conjugation of these liposomes to thiol-functionalised MBs. This, again, would allow for comparative US experiments to those involving FMBs in chapter **4** for the evaluation of the efficacy of treatments containing two different types of liposomes.

IV. To successfully make acoustically-responsive FMBs in chapter **4**, an optimised protocol was used that involved adding the liposomes and MBs into a sample tube and leaving them to stand for two hours at 4°C (see **Supplementary 6.7**). The lack of mechanical mixing of the two components may have resulted in a non-uniform FMB suspension containing a

mix of conjugated and non-conjugated particles. In the literature, a 'pre-formation' method where liposomes are mixed with MB lipids before vigorous shaking to produce MBs with liposome attached is often used[576,577]. The period of mixing likely allows for more uniform conjugation without risking MB dissolution during conjugation, and perhaps increases reproducibility. Therefore, FMBs could be produced using the 'pre-formation' method in line with the literature. However, this would require additional recharacterization of the attached liposomes to ensure the shaking used to form the MBs does not significantly affect their structure and properties. Using this protocol and characterising the resulting particles could potentially contribute to the standardisation of a production protocol for LMBs, giving future researchers the confidence to develop new formulations based on established methods.

V. To address the limitations of the US setup used in chapter **4**, future work could explore differently designed US setups for biofilm assays: if better biofilm models are to be included in these experiments, such as urinary organoids, investigating instrumentation similar to that of Horsley *et al.*[323] could address some of these challenges, e.g. removing the need for channel slides, and allowing for more comparative studies. Additionally, the experimental design of the US experiments could be improved on to include different bubble and treatment concentrations, as well as the testing of different US parameters. This would give further insights into how liposome and MB concentrations (both separately and within a conjugated sample) affect cavitation and anti-biofilm activity, and if there's a balance that gives optimal results. Adjusting the US parameters (while keeping to clinical standards) to maximise the cavitation of the produced FMBs to match that of corresponding MBs (see section **4.3.2**) could also be the next step in enhancing the anti-biofilm potential of the FMB formulation from this research.

5.3 Closing remarks

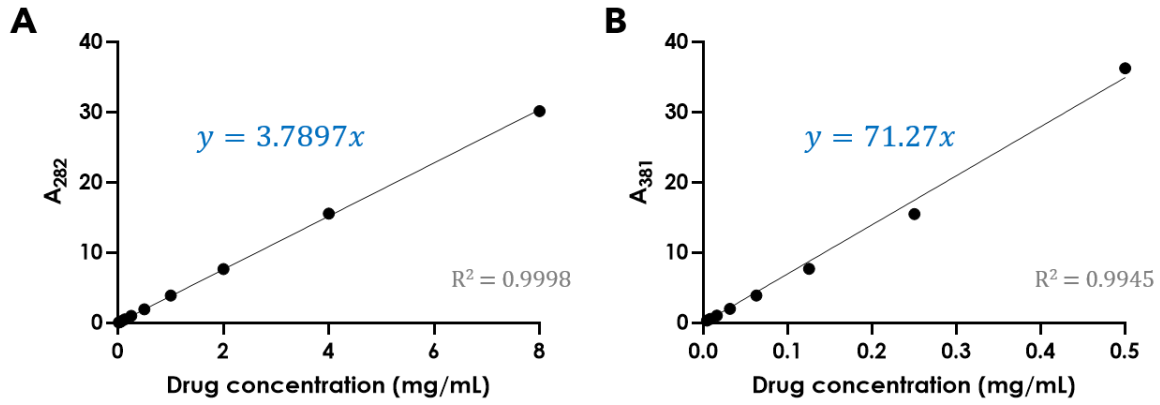
The research presented in this thesis has demonstrated the potential for the US-mediated disruption of bacterial biofilms alongside liposomal drug delivery as a therapeutic approach to UTIs. This study highlights the bactericidal potential of LMBs in a UTI context and lays the foundation for the versatility of LMBs in anti-biofilm applications to be explored. The significant role free NIF had in enhancing bubble acoustics and anti-biofilm activity also presents the combination of lipophilic drugs with MB technology as a promising strategy against UTIs. The limitations identified during this research brought attention to the importance of incorporating bacterial models that accurately reflect clinical conditions, as well as designing experiments and protocols with future industrial and clinical applications in mind.

Overall, this work significantly contributes to pre-clinical research in the fields of LMB technologies and anti-biofilm strategies, underpinned by a focus on the clinical context of UTIs. Interdisciplinary efforts are necessary for continued innovation and development of effective therapeutic approaches for the disruption of bacterial biofilm paired with the delivery of antibacterial agents against UTIs, and beyond.

6 Supplementary

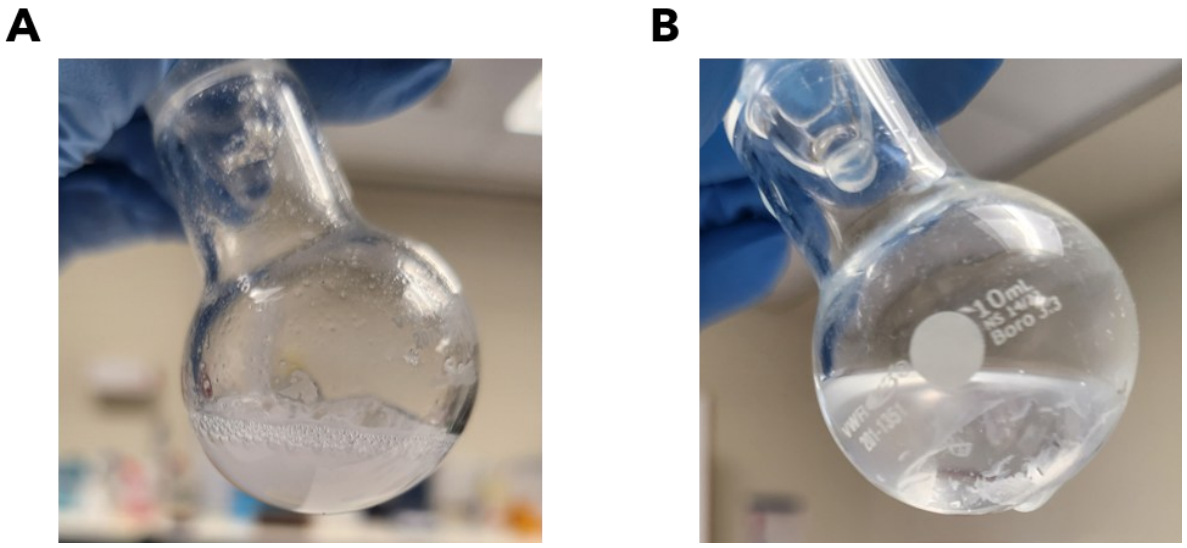
6.1 Liposome manufacturing

6.1.1 Calibration curves



Supplementary Figure 1 | Calibration curves used for encapsulation efficiency calculations. These curves were used to calculate the sample concentration from measured UV absorbance of (**A**) VAN and (**B**) NIF. Serial dilutions of each drug were made and detected by UV-Visible spectroscopy (Implen NanoPhotometer® NP80), so known concentrations could be correlated to UV absorbances. Absorbance at 282 nm was used for VAN and absorbance at 381 nm was used for NIF measurements. The specific equations of these curves are shown.

6.1.2 Rehydration difficulties



Supplementary Figure 2 | Photographs of thin film during hydration step. (**A**) Expected uniform cloudy appearance of a good quality liposome suspension after hydration of thin film. (**B**) Appearance of non-PEGylated Fuso-1 after hydration. There were many flakes of non-hydrated film that did not break down even after prolonged hydration at the phase transition temperature or after several rounds of probe sonication.

6.1.3 Freeze-thaw method attempts

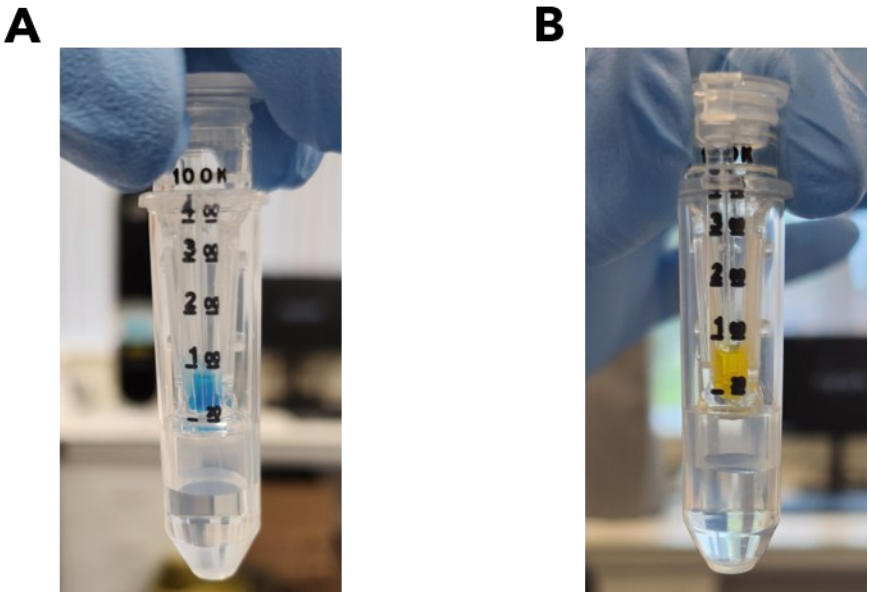
The freeze-thaw method is one that has been long used to improve encapsulation of drugs within liposomes[407,408,729]. Multiple cycles of freezing and thawing are thought to increase drug encapsulation through cryo-concentration, where drug molecules are concentrated into zones upon freezing which increases diffusion into liposomes as thawing occurs[399].

Therefore, I utilised this method to aid with drug encapsulation before extruding the liposomes. I initially used three cycles of the following: 5 min in a dry ice bath (-79°C), 10 min in an ice bath (0°C) and 10 min at the highest phase transition temperature of the lipids (45°C). Unfortunately, this yielded a very low encapsulation efficiency of ~3%. Since holding liposomes at a sub-zero temperature during the thawing process is thought to be the point at which drug diffusion into liposomes take place, it was recommended that anneal phases be included in the cycles, to make freeze-anneal-thaw cycles[399]. Therefore, I tried a variation of the freeze-anneal-thaw method recommended in a study by Costa *et al.* (2014)[399]: three cycles of 5 min in a dry ice bath (-79°C) to freeze, 30 min in an ice bath (0°C) to anneal, and 10 min at the highest phase transition temperature of the lipids (45°C) to thaw. Unfortunately, this did not improve the encapsulation efficiency which remained around 3%. Surprisingly, encapsulation efficiencies were able to get as high as 64% without this process, so freeze-thaw cycles were no longer performed; liposomes were immediately extruded after hydration.

6.1.4 Liposome contribution to absorbance

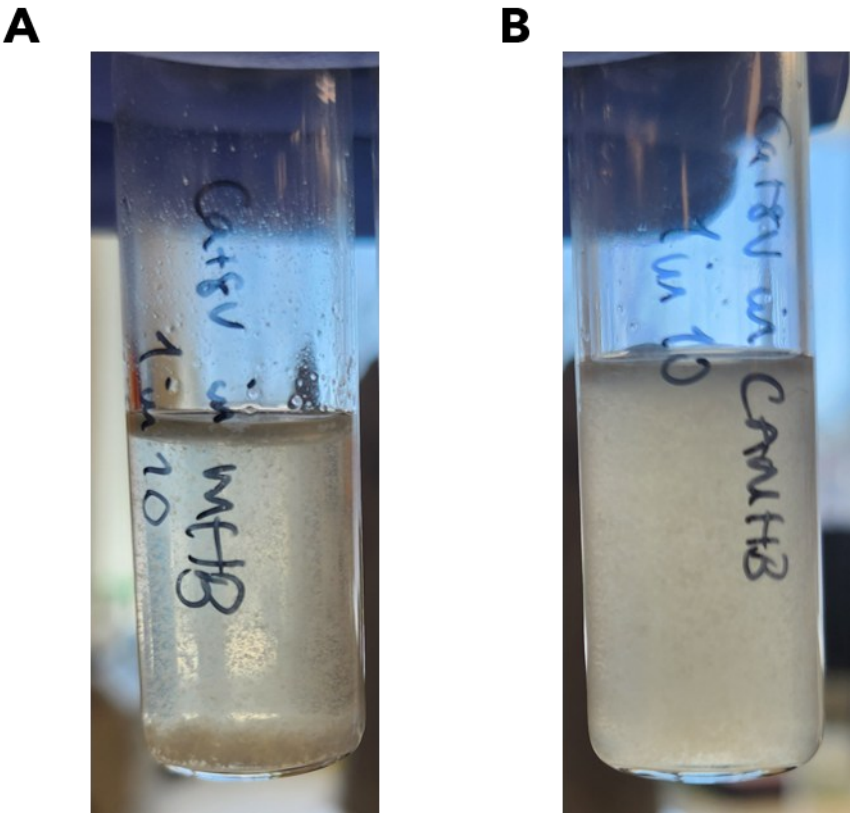
Measuring the drug amount present in the ultrafiltration flowthrough (free drug) fractions and the original total drug solution was the method used to measure EE, rather than direct lysis of manufactured liposomes as is frequently done in the literature[428]. This method was chosen because it avoided having to destroy the liposomes required for downstream experiments and, in this way, EE could be efficiently measured for every batch. It was also found that, even after liposome lysis with methanol, the presence of lipid still interfered with drug absorbance values to give inaccurate results. Therefore, only the flowthrough fractions and free drug fractions were measured for EE quantification.

Flowthrough fractions were tested for the presence of liposomes that may have squeezed through the centrifugal filter: a flowthrough fraction was spun at 21,000 ×g for 30 min to pellet any liposomes present. An equivalent flowthrough fraction was not spun as a control. There was no difference in the drug concentration found in the spun and not-spun samples, indicating that a negligible number of liposomes was present in the flowthrough sample. Therefore, I could be confident that absorbance by stray liposomes was minimised in any EE measurements. The clean separation of liposomes from the aqueous buffer after ultrafiltration was also visible, particularly when the liposomes were dyed with either DiD or DiO (**Supplementary Figure 3**).

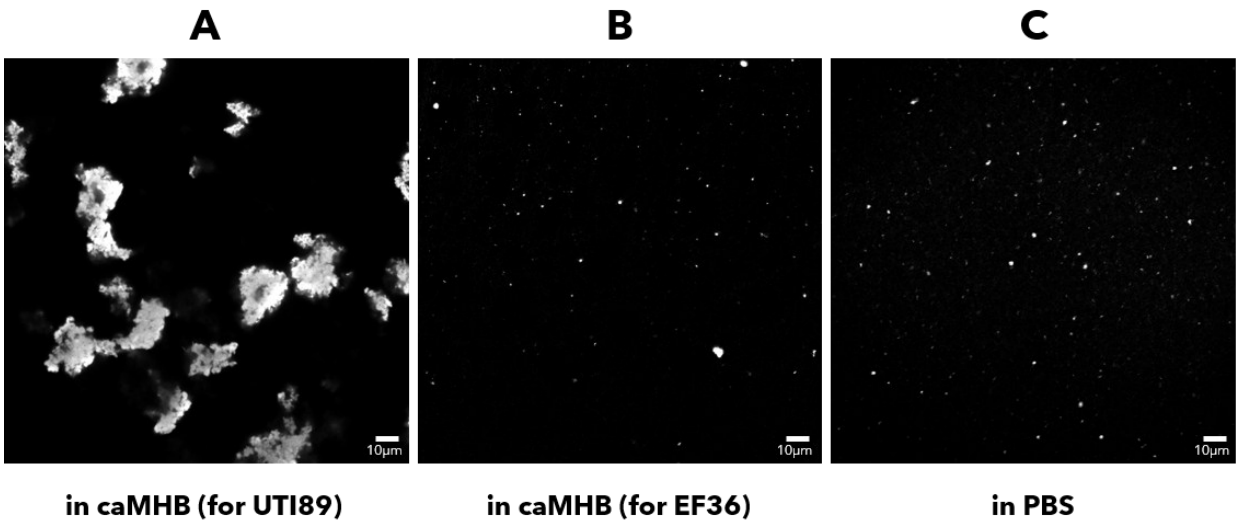


Supplementary Figure 3 | Photographs of Amicon® filter after ultrafiltration of liposome suspension. (A) Liposome suspensions separated into a liposome fraction and free drug fraction via ultrafiltration. The liposomes were retained in the filter, while the free drug dissolved in the aqueous buffer moved past the filter to end up at the bottom of the tube. Liposomes dyed with (**A**) DiD or (**B**) DiO made this separation clearly visible.

6.2 Cationic liposome aggregation observations



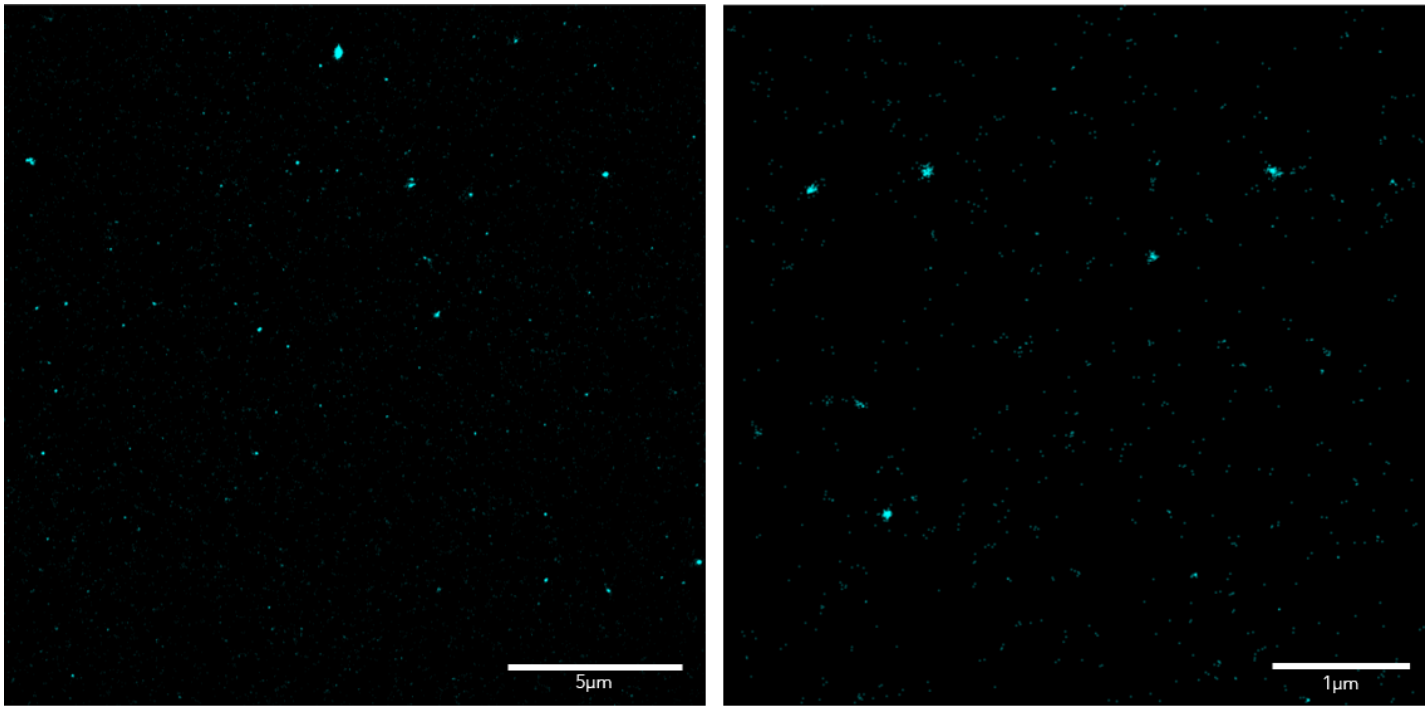
Supplementary Figure 4 | Photographs comparing Cat-8-VAN aggregation in MHB and caMHB. (A) Cat-8-VAN in MHB and (B) in caMHB.



Supplementary Figure 5 | Confocal images comparing Cat-8-VAN aggregation in caMHB or PBS. (A) Cat-8-VAN in caMHB at concentrations used for *E. coli*; (B) in caMHB at concentrations used for *E. faecalis*; and (C) in PBS.

6.3 Super-resolution microscopy

6.3.1 Liposome-only sample images



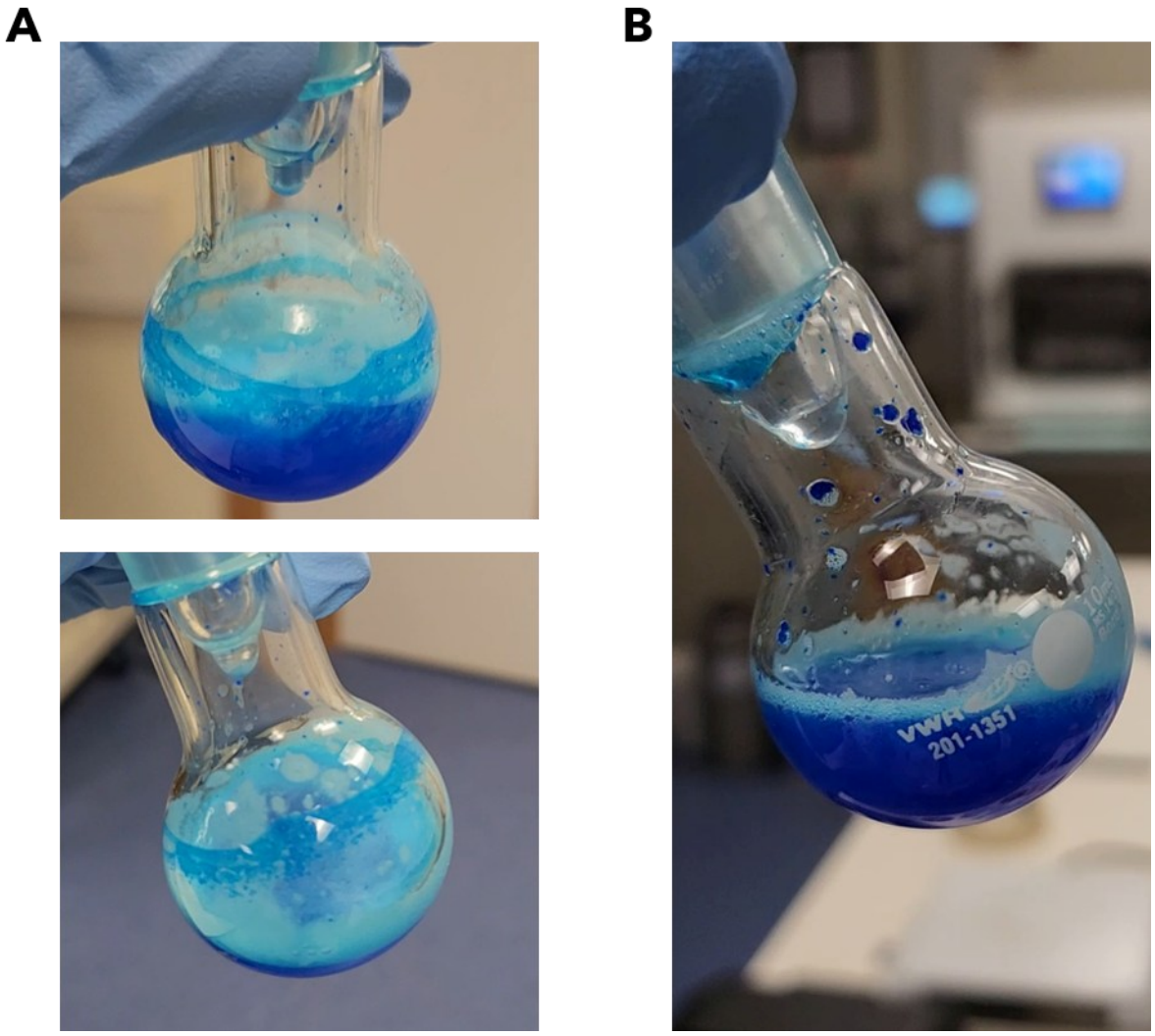
Supplementary Figure 6 | Super-resolution dSTORM image of sample containing only Fuso-1-PEG-VAN labelled with proprietary pan-LNP detection (640 nm, Oxford Nanoimaging, UK).

6.3.2 Proposed in-solution staining protocol

The proposed in-chip staining protocol would use a tailored version of the LNP Profiler Kit (Oxford Nanoimaging Ltd., Oxford, UK). Drug- or liposome-treated bacterial samples would be prepared in the same way as for the confocal imaging experiments described in section **3.2.3**. After incubation of the treated samples at 37°C for 24 h, 2 mL of treated culture would be spun at 10,000 ×g for 10 min, the supernatant removed and the pellet resuspended in sterile 1X PBS to wash the cells. This washing process would be repeated three times, resuspending the pellet in 1X PBS the first two times, before resuspending the pellet in 4% paraformaldehyde (PFA) for 15 min after the third wash to fix the bacteria cells. The PFA is then removed by washing the cells twice as previously, resuspending the pellet in 1X PBS each time. A permeabilization buffer (0.1% Triton) would then be added for 10 min to permeabilise the cells before washing the cells twice as previously, resuspending the pellet in 1X PBS each time. Proprietary pan-LNP detection (640 nm)

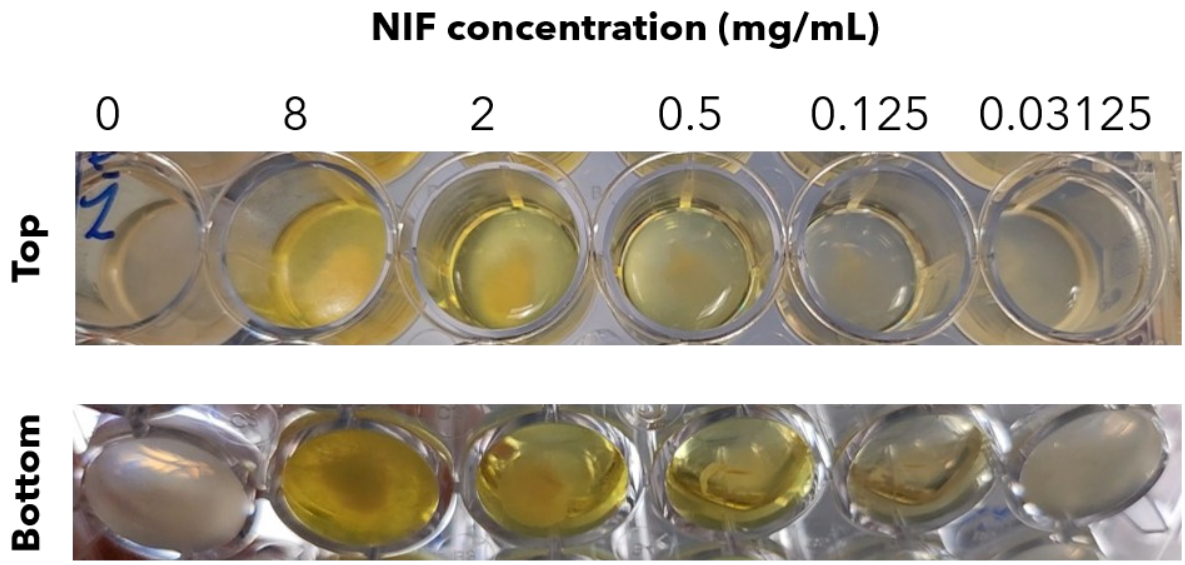
and WGA (wheat germ agglutinin) conjugate (488 nm) would be added (to a final concentration of 5 μg/mL of each stain) for 30 min at room temperature, while protected from light, to label PEGylated liposomes and bacterial membranes, respectively. Excess stain would then be removed by washing the cells twice as previously, resuspending the pellet in 1X PBS each time. Stained samples would then be immobilised on the poly-L-lysine (PLL)-coated lanes of an assay chip for 15 min before imaging using an ONI Nanoimager S (Oxford Nanoimaging Ltd., Oxford, UK).

6.4 Fusogenic liposome PEG titration



Supplementary Figure 7 | Photographs comparing Fuso1-PEG-VAN containing varying amounts of PEG during the rehydration step. (**A**) Fuso-1-PEG-VAN with 2.5% PEG and (**B**) 1% PEG. These formulations were stained with DiD so appear blue. As PEG content decreased, there was an increasing presence of large masses of lipid film that did not resuspend after prolonged hydration at the phase transition temperature or after several rounds of probe sonication.

6.5 NIF precipitation in microbiological assays



Supplementary Figure 8 | Photograph of NIF precipitation at high concentrations in caMHB. A row from a microbiological assay plate is shown with bacteria incubated with serial dilutions of free NIF. The top and bottom views of the plate are shown. At 8 and 2 mg/mL, a significant amount of NIF precipitate was observed that settled at the bottom of the wells, and a hydrophobic film (presumably of NIF) formed at the liquid-air interface. At concentrations below 2 mg/mL this precipitate was not observed—the cloudiness here was from the bacterial growth in the wells.

6.6 MBEC assays

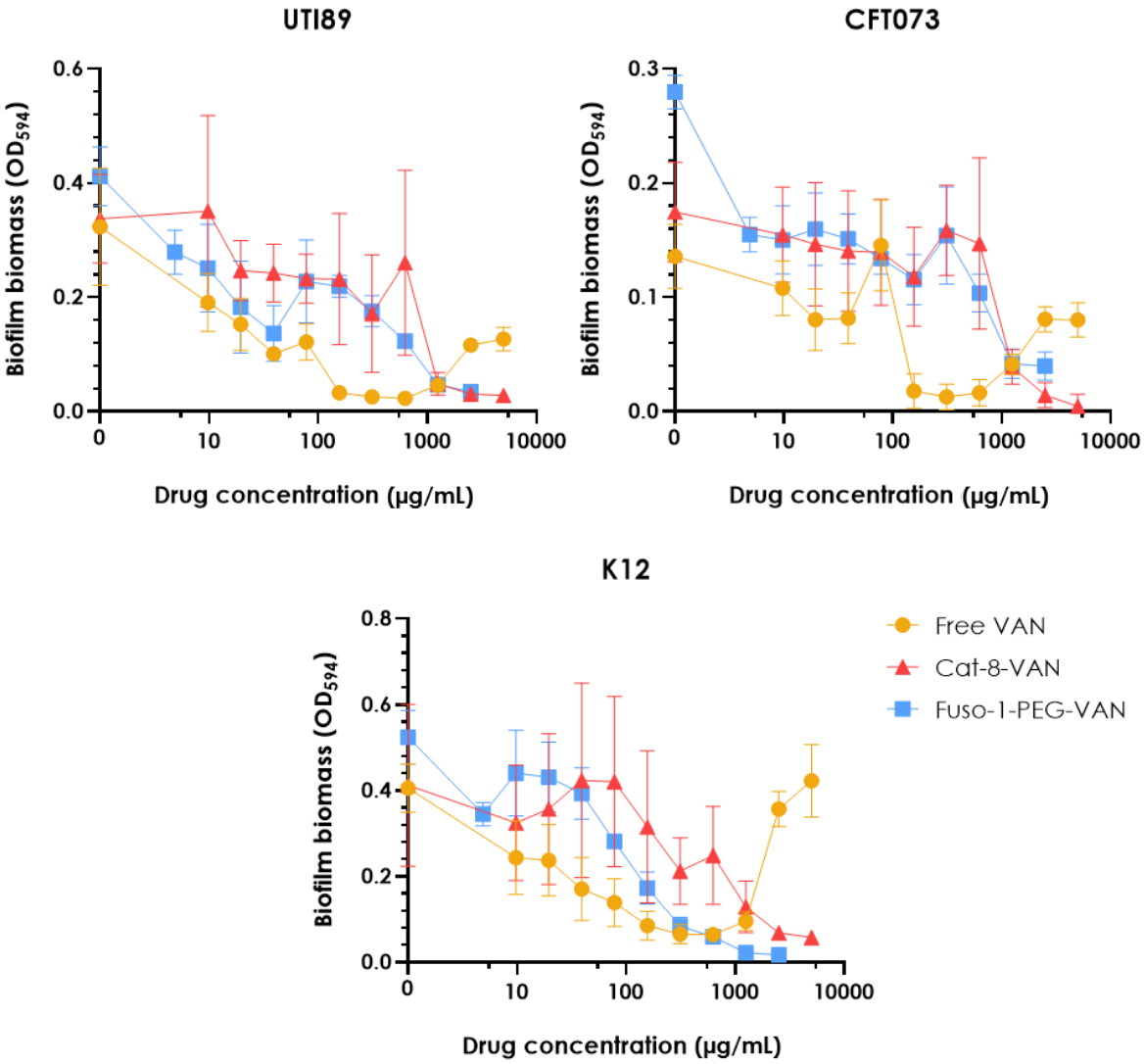
6.6.1 MBEC assay optimisation

As part of the optimisation of the MBEC assays, *E. coli* and *E. faecalis* monospecies biofilm were grown as described in section **3.2.2.3**, but instead of incubating in TSB, caMHB was used as bacterial growth media. Additionally, instead of using a 24-well plate, these initial MBEC assays used a 96-well Calgary device (Thermo Fisher Scientific, UK) for growing of *E. coli* strains (UTI89, CFT073, and K12). The Calgary device is a popular option for assessing biofilm susceptibility to antibiotics[652]. Unfortunately, the 96-well Calgary device became unavailable for purchase during the course of these experiments, so *E. faecalis* (EF12, EF36, and EF48) biofilms were grown in a 24-well plate, as described in section **3.2.2.3**. The biofilms were grown in static conditions for 24 hours, treated with free VAN or liposomal VAN for a further 24 hours and the resulting change in biofilm biomass measured in an MBEC assay

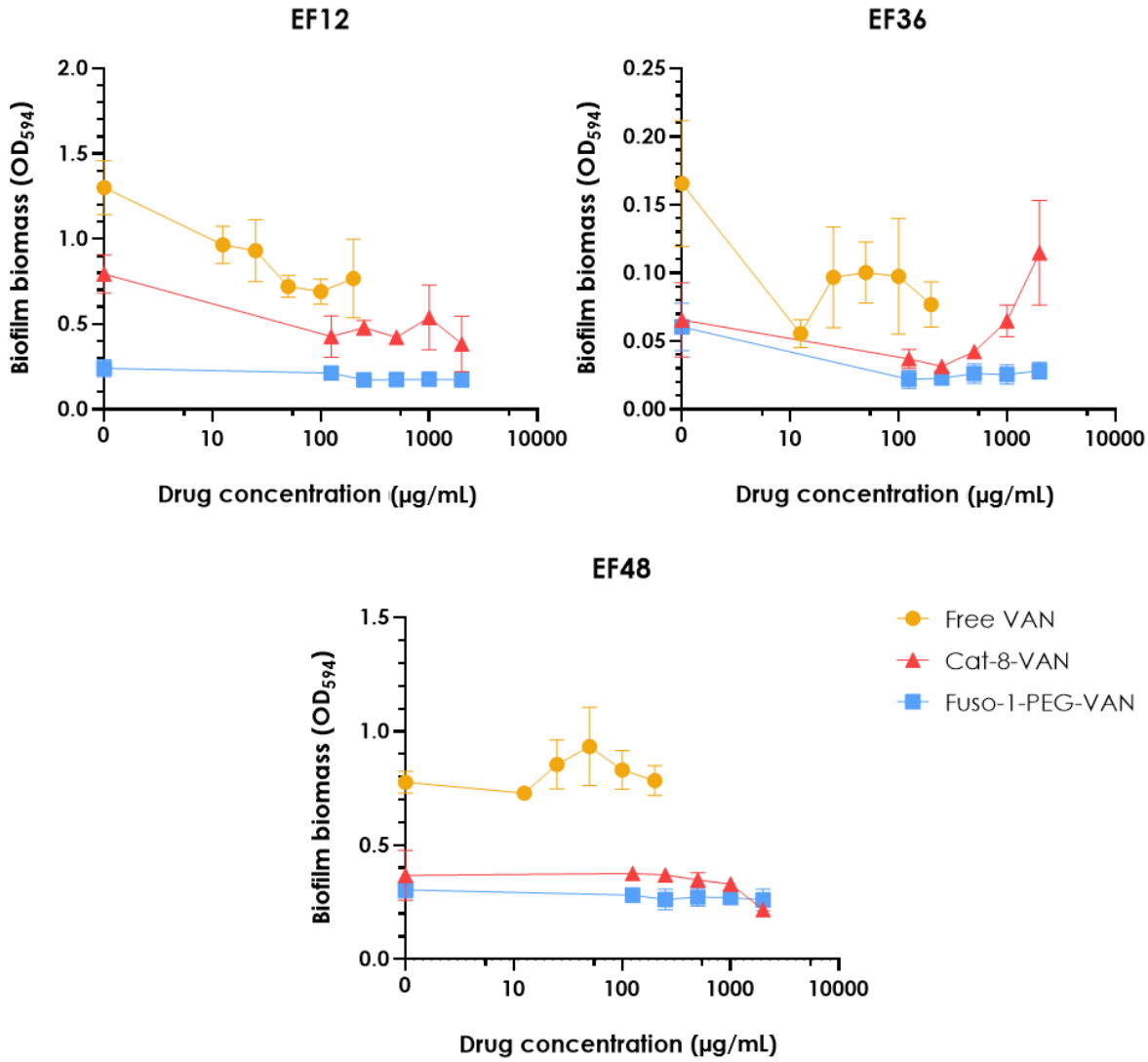
Biofilm biomass of *E. coli* was generally reduced in a concentration-dependent manner (**Supplementary Figure 9**), but it seemed as though neither of the liposomal VAN formulations were more effective at reducing biofilm biomass as free VAN. However, the large variation in recorded biomass between repeats and the relatively low biofilm growth even in the growth control likely made it more difficult to perceive any meaningful trends. Therefore, it would be worth optimising the growth conditions for *E. coli* biofilm (e.g. different media or longer incubation times) to produce denser biofilms. One noteworthy observation is that at free VAN concentrations greater than 1000 μg/mL, the biofilm biomass started to increase as drug concentration increased for every strain. It is unclear why this is the case, especially as VAN is very water-soluble and should remain dissolved even at these concentrations—perhaps dilution in caMHB shows significantly lower solubility and so results in the reduction of available VAN in the suspension. Visibly, this did not seem to be the case; there was no precipitate observed in the VAN solution at any concentration but solubility tests, like filtration and evaporation, could be performed to confirm this. Interestingly, encapsulation of VAN in liposomes appeared to reverse this

phenomenon; there was no increase in biofilm biomass at liposomal VAN concentrations above 1000 μg/mL. This could be due to liposomal encapsulation potentially improving the apparent solubility by providing another compartment that drug can partition into.

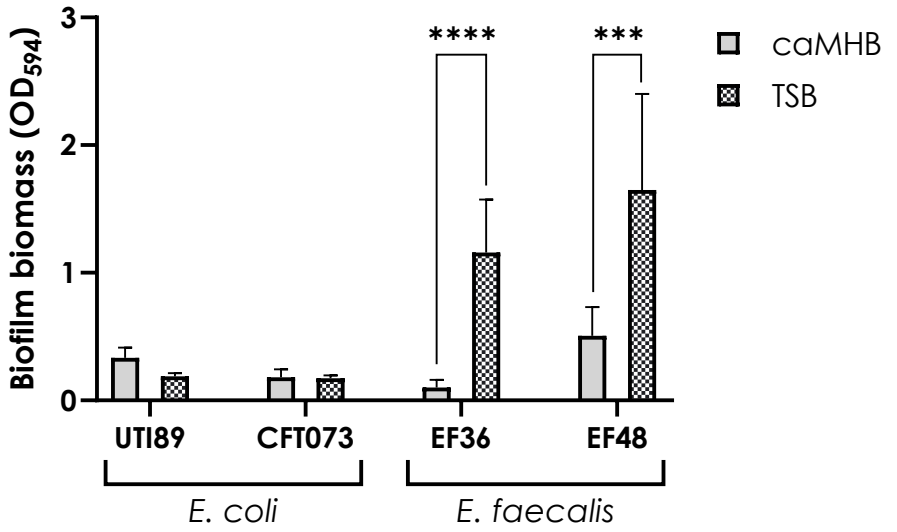
For *E. faecalis*, biofilm growth was also low when grown in caMHB, particularly EF36, and so this experiment was terminated early in order to find a better growth medium for these strains (**Supplementary Figure 10**). When biofilms were grown in TSB instead of caMHB, the average biofilm biomass was much greater for the *E. faecalis* strains tested (EF36 and EF48; **Supplementary Figure 11**). However, the *E. coli* strains saw virtually no change in biofilm biomass when grown in the two different media (**Supplementary Figure 11**). Due to time constraints, other growth media could not be tested in an attempt to improve *E. coli* biofilm growth and TSB was used as the growth media for subsequent assays on *E. coli* and *E. faecalis* biofilms.



Supplementary Figure 9 | Biofilm biomass of *E. coli* after treatment with VAN formulations in MBEC assays. Three strains of *E. coli* (UTI89, CFT073 and K12) were treated with free VAN or liposomal VAN, matched for drug concentration, as part of an MBEC assay. The average absorbance of crystal violet at 594 nm was used as a measure of biofilm biomass and plotted against drug concentration. The data represents three biological experiments with three technical repeats.

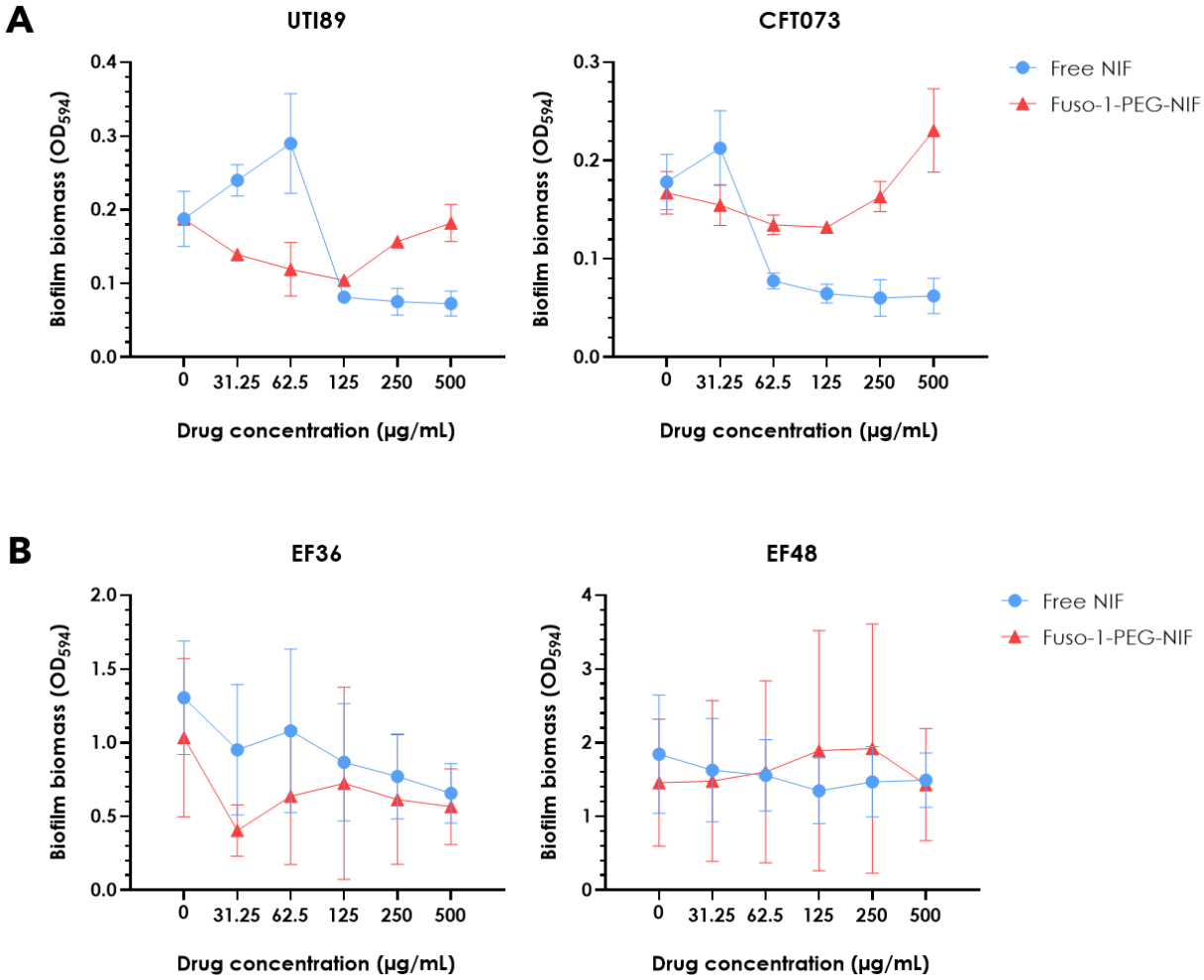


Supplementary Figure 10 | Biofilm biomass of *E. faecalis* after treatment with VAN formulations in MBEC assays. Three strains of *E. faecalis* (EF12, EF36 and EF48) were treated with free VAN or liposomal VAN, matched for drug concentration, as part of an MBEC assay. The average absorbance of crystal violet at 594 nm was used as a measure of biofilm biomass and plotted against drug concentration. The data for Fuso-1-PEG-VAN represents one biological experiment with three technical repeats.



Supplementary Figure 11 | Comparison of bacterial biofilm biomass when grown in caMHB or TSB for 24 hours. Two strains of *E. coli* (UTI89 and CFT073) and two strains of *E. faecalis* (EF12 and EF36) were incubated in either caMHB or TSB and given 24 hours to form biofilm in a microplate. The average absorbance of crystal violet at 594 nm was used as a measure of biofilm biomass for each sample. *E. coli* biofilm growth was relatively poor in both media; however, *E. faecalis* strains saw a significant increase in biofilm formation when grown in TSB compared to caMHB ($p<0.000001$ for EF36 and $p=0.00014$ for EF48). T-tests were performed on the biofilm biomass, where $p \leq 0.05$ indicated statistical significance. (***) = $p<0.001$; (****) = $p<0.0001$.

6.6.2 Biofilm biomass as absorbance values (complementary to Figure 42A and Figure 43A)



Supplementary Figure 12 | Biofilm biomass (as absorbance values) in MBEC assays. Two strains of *E. coli* (UTI89 and CFT073) and two strains of *E. faecalis* (EF36 and EF48) were treated with free NIF or fusogenic liposome-encapsulated NIF (Fuso-1-PEG-NIF), matched for drug concentration, as part of an MBEC assay. The average absorbance of crystal violet at 594 nm was used as a measure of biofilm biomass and plotted against drug concentration.

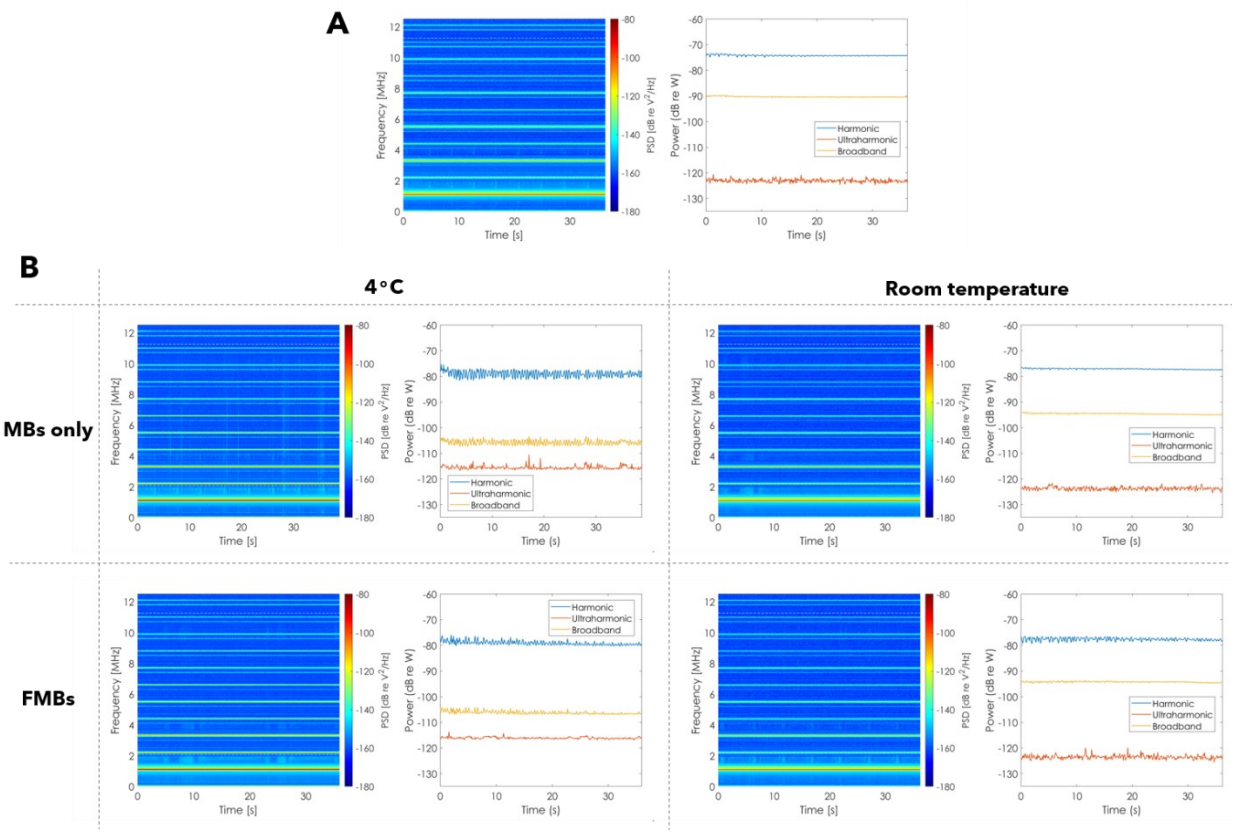
6.7 Optimisation of liposome-microbubble conjugation

Maleimide-functionalised Fuso-1-PEG-NIF liposomes can form covalent bonds with thiol-functionalised MBs via the maleimide-thiol click chemistry reaction (**Figure 20**) to produce [Fuso-1-PEG-NIF]-loaded MBs (FMBs). The prepared FMBs were then exposed to US and cavitation activity measured. Unfortunately, a faulty high-pass filter was mistakenly used as part of the US setup which impacted the recorded cavitation profiles and accuracy of the calculated acoustic energies: there was a lower signal-to-noise ratio and strong harmonics recorded, even in the absence of MBs. Due to time constraints, this set of optimisation experiments could not be repeated and the optimisation choices were based off of qualitative observations from one practical replicate and one technical replicate. More repeats are required for quantitative comparisons between the samples subjected to the different conjugation protocols (listed in section **4.2.5**), that include acoustic energies. Fuso-1-PEG-NIF was also labelled with DiO that allowed for visualisation of conjugation to non-labelled MBs: non-labelled MBs are visible under brightfield but not fluorescence microscopy; if conjugation was successful, MBs should become visible under both brightfield and widefield (fluorescence) microscopy.

It is known that this conjugation process is very simple and straightforward—it can be performed at room temperature and in aqueous buffer, without any additional reagents or catalysts[575]. Many protocols for this reaction in the context of liposome-MB conjugation involved adding pre-formed liposomes to a suspension of MB constituent lipids, followed by high-speed mixing to form LMBs[576,577]. Although the practical details have not been specified in the literature, it is likely that the liposome-lipid mixture would initially be kept above the phase transition temperature to aid MB production, which in this case is 74°C—much higher than the 41°C of Fuso-1-PEG-NIF. This may promote premature drug leakage from the liposomes during conjugation and MB production[730], such as the passive drug release observed at 4°C and 37°C (**Figure 27**). Therefore, I opted to conjugate pre-formed liposomes to pre-formed MBs. To optimise the conjugation

protocol for the lipid particles used in this study, multiple conditions were compared: variation of temperature, of gas in the vial headspace, and of mixing motion.

To assess the optimal temperature, the particles were gently mixed either at 4°C or room temperature. In line with protocols for the conjugation of pre-formed particles, they were gently mixed[572,731] and even though the maleimide-thiol reaction can occur at room temperature, MBs are more stable at lower temperatures so it was beneficial to evaluate conjugation at 4°C[732,733]. There was minimal cavitation activity from FMBs when mixed at 4°C or at room temperature, with cavitation profiles that matched the control sample (TSB only; **Supplementary Figure 13**). Brightfield and widefield microscopy revealed that there were indeed successfully conjugated FMBs present in both samples but at slightly lower MB quantities than the initial 2.35×10^8 bubbles/mL they started with (**Supplementary Table 1**; **Supplementary Figure 14**), which may explain why minimal US response was recorded. It may be expected that liposome conjugation would affect the MB cavitation profile as it likely changes the shell properties, but when compared with a MB-only control that was treated in the same way, there was no observed difference in acoustic response. Conjugating at 4°C did appear to keep the particle size similar to that of the initial MB suspension (0.93 ± 0.59 μm; **Supplementary Table 1**), and perhaps even narrow the size distribution, so this temperature was the one used in further optimisation tests. It should be noted that as this data is from one repeat, the variation in size and concentration may not be substantial; more repeats are required to make confident conclusions correlating size and concentration with cavitation activity for this study.

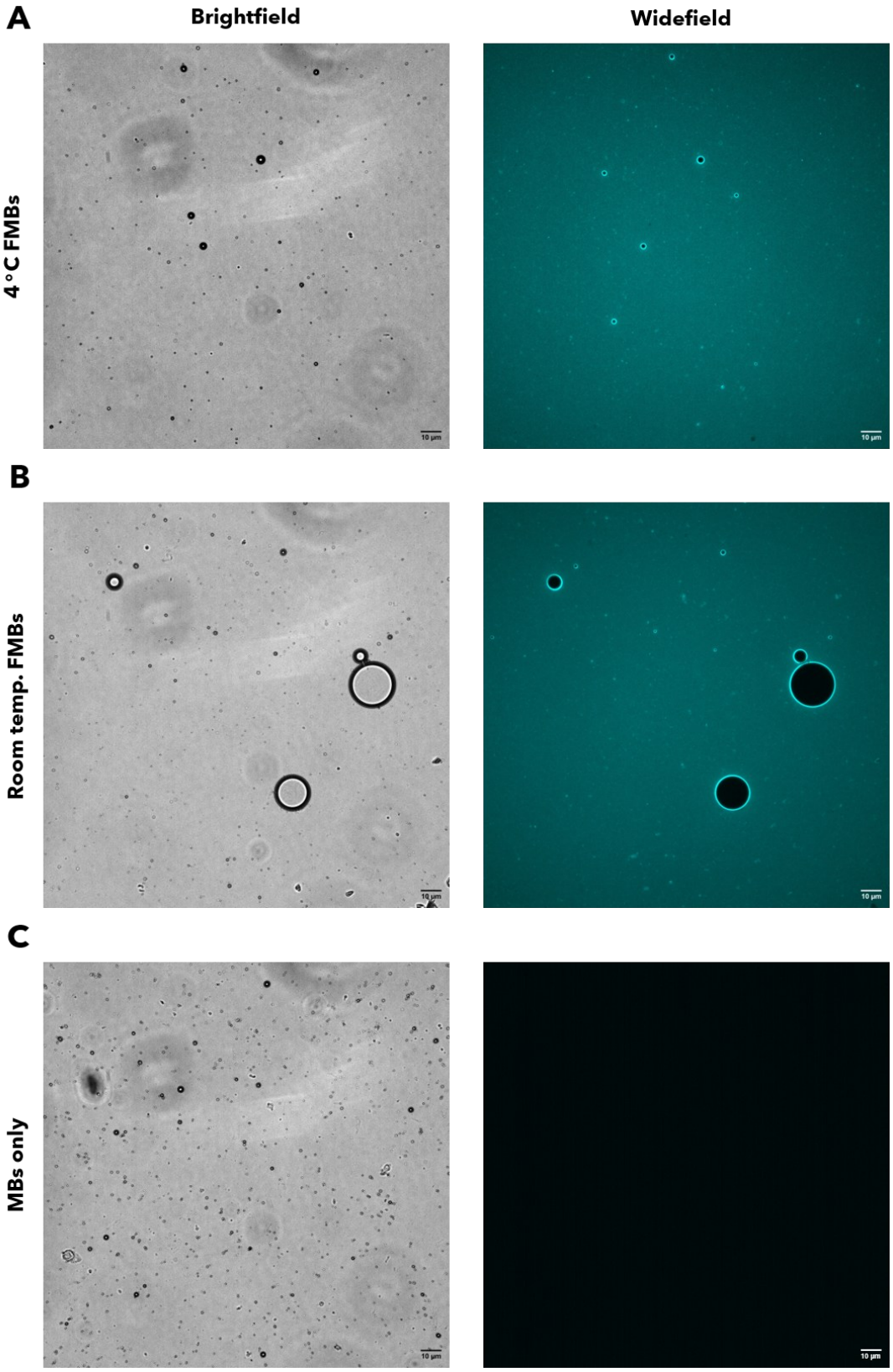


Supplementary Figure 13 | Cavitation profiles of MBs and FMBs conjugated at 4 °C or at room temperature. Cavitation profiles of (**A**) TSB only and (**B**) MB-only sample after gently mixing at 4°C (top left) and at room temperature (top right); FMB sample after gentle mixing at 4°C (bottom left) and at room temperature (bottom right). In each panel: (left) power spectral density (PSD) showing the variation in power generated by cavitation activity across different frequencies over time; (right) power-time graph showing harmonic, ultraharmonic and broadband components of the signal over the exposure time period. Summary of US parameters used: 1.1 MHz with bursts of 400 cycles at 50 Hz PRF for 40 seconds, generating an acoustic pressure of 1 MPa peak negative pressure.

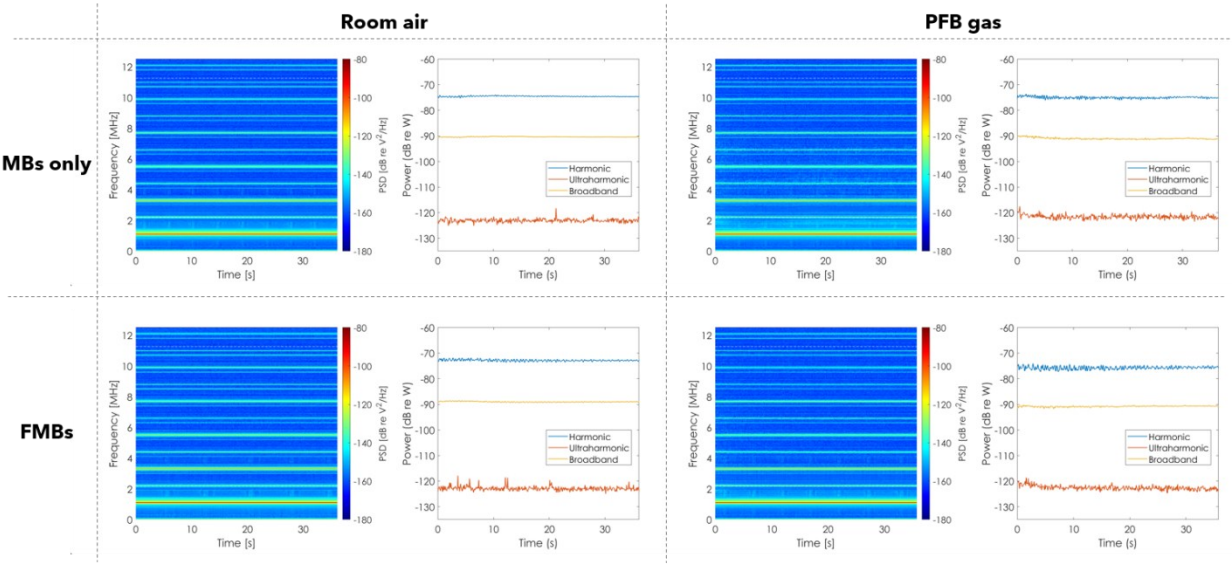
Supplementary Table 1 | Average size and concentration of MBs and FMBs after being subject to various conjugation conditions. This data is from one practical repeat and one technical repeat; more repeats are necessary to come to concrete solutions based on measured bubble size and concentration.

Condition	Particle	Size (μm)	Concentration (particles/mL)
4°C, mixing	MB	0.82 ± 0.21	8.87×10^{6}
	FMB	0.91 ± 0.40	1.57×10^{6}
Room temp., mixing	MB	1.05 ± 0.49	1.82×10^{7}
	FMB	1.23 ± 0.60	4.69×10^{7}
Mixing, room air	MB	0.97 ± 0.45	8.06×10^{7}
	FMB	0.84 ± 0.24	4.22×10^{7}
Mixing, PFB	MB	0.96 ± 0.58	1.53×10^{8}
	FMB	0.91 ± 0.69	4.83×10^{7}
Standing, room air	MB	0.84 ± 0.44	1.49×10^{8}
	FMB	0.79 ± 0.22	3.03×10^{8}
Standing, PFB	MB	2.56 ± 1.51	1.73×10^{7}
	FMB	0.89 ± 0.72	3.14×10^{7}

As the particles were mixed for at least two hours, it is possible that gas leakage and MB dissolution occurred during the process due to gas exchange and exposure to dissolved air[634,734,735] that potentially contributed to the observed lower MB count and reduced cavitation activity. Therefore, the particles were gently mixed at 4°C either with room air or insoluble PFB gas occupying the Eppendorf headspace. Again, there was no apparent increase in cavitation activity compared to the control (**Supplementary Figure 13A**) or MB-only samples (**Supplementary Figure 15**), which suggests that gas exchange was not the primary factor reducing MB and FMB cavitation activity.



Supplementary Figure 14 | Brightfield and widefield images of FMBs and MBs conjugated by mixing at 4°C or at room temperature. (**A**) FMBs conjugated at 4°C and (**B**) FMBs conjugated at room temperature and (**C**) MBs only before conjugation. In each panel, (**Left**) brightfield and corresponding (**Right**) widefield images of the same sample. The images were taken with a 40× objective.

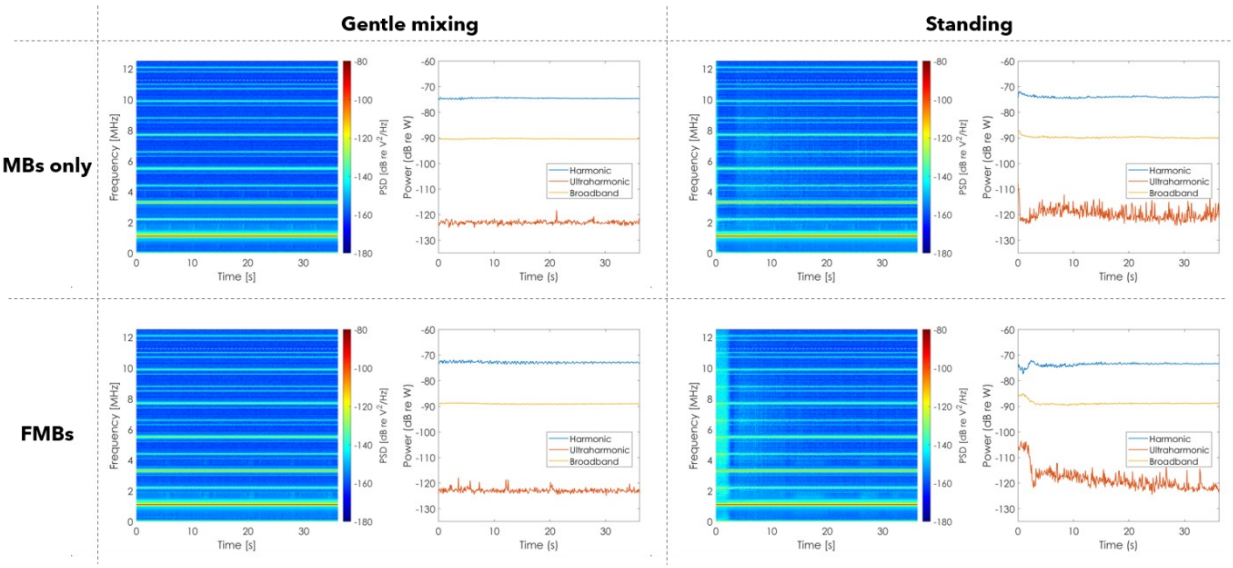


Supplementary Figure 15 | Cavitation profiles of MBs and FMBs conjugated in the presence of room air or PFB gas. Cavitation profiles of MB-only sample gently mixed in the presence of room air (top left) and in PFB (top right); FMB sample conjugated in the presence of room air (bottom left) and in PFB (bottom right). In each panel: (left) power spectral density (PSD) showing the variation in power generated by cavitation activity across different frequencies over time; (right) power-time graph showing harmonic, ultraharmonic and broadband components of the signal over the exposure time period. Summary of US parameters used: 1.1 MHz with bursts of 400 cycles at 50 Hz PRF for 40 seconds, generating an acoustic pressure of 1 MPa peak negative pressure.

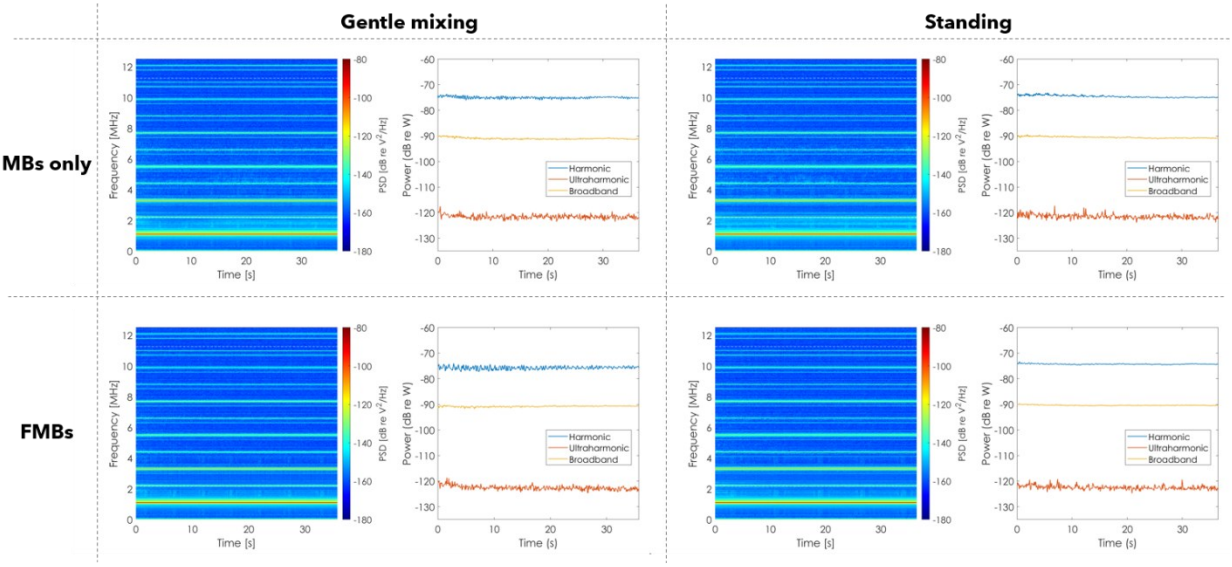
Although mixing is a step in published methods[572,731], MBs are relatively 'fragile' with a short circulation half-life[736]. Therefore, it was hypothesised that the mixing motion may be contributing to bubble instability and collapse during the conjugation process. To test this, the particles were either gently mixed or left standing at 4°C. When in the presence of room air, only the particles that were left standing showed any increased cavitation activity compared to the control (**Supplementary Figure 16**); MB-only and FMB samples left standing both showed a brief period of increased cavitation with an increased ultraharmonic component, but no activity was recorded from the samples that were mixed. This suggests that the motion of mixing of the particles disrupts the MBs to such an extent that cavitation activity is greatly reduced. Interestingly, when this comparison was repeated in the presence of PFB gas, neither mixing nor standing FMB samples yielded any significant acoustic response (**Supplementary Figure 17**). This may be due to the fact that to replace room air with PFB in the sample Eppendorf, PFB was flowed from a cannister through a needle that exerted a visible burst of pressure on the sample surface for several seconds.

This pressure burst could have introduced motion akin to mixing that disrupted suspended MBs in the standing sample to give cavitation profiles similar to those of the mixed sample. Furthermore, the PFB flow was manually controlled which meant different samples may have been exposed to different pressure bursts. This might explain the discrepancies in MB size and concentration measured for the samples involving PFB. Perhaps repeating this comparison but using equipment capable of finely controlling gas pressure to introduce PFB would help minimise any inadvertent mixing.

Out of all the variables tested, only one gave a sample capable of cavitating more than control samples upon US exposure; particles left standing at 4°C for 2 hours was chosen as the optimised protocol for liposome-MB conjugation in subsequent experiments.

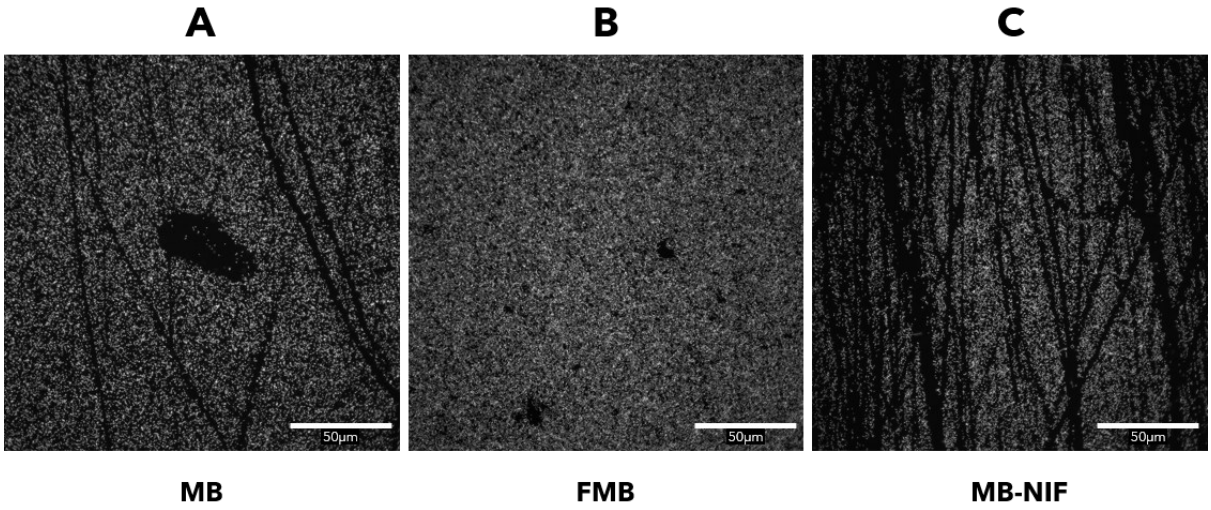


Supplementary Figure 16 | Cavitation profiles of MBs and FMBs after gentle mixing or standing at 4°C in the presence of room air. Cavitation profiles of MB-only sample gently mixed (top left) and left standing (top right); FMB sample gently mixed (bottom left) and left standing (bottom right). In each panel: (left) power spectral density (PSD) showing the variation in power generated by cavitation activity across different frequencies over time; (right) power-time graph showing harmonic, ultraharmonic and broadband components of the signal over the exposure time period. Summary of US parameters used: 1.1 MHz with bursts of 400 cycles at 50 Hz PRF for 40 seconds, generating an acoustic pressure of 1 MPa peak negative pressure.



Supplementary Figure 17 | Cavitation profiles of MBs and FMBs after gentle mixing or standing at 4°C in the presence of PFB. Cavitation profiles of MB-only sample gently mixed (top left) and left standing (top right); FMB sample gently mixed (bottom left) and left standing (bottom right). In each panel: (left) power spectral density (PSD) showing the variation in power generated by cavitation activity across different frequencies over time; (right) power-time graph showing harmonic, ultraharmonic and broadband components of the signal over the exposure time period. Summary of US parameters used: 1.1 MHz with bursts of 400 cycles at 50 Hz PRF for 40 seconds, generating an acoustic pressure of 1 MPa peak negative pressure.

6.8 Confocal images of biofilm clearance



Supplementary Figure 18 | Confocal images (40×) of pores and streaks in *E. faecalis* (EF36) biofilm after US exposure with bubble-containing treatments. Biofilm incubated with (**A**) microbubbles only (MB); (**B**) fuso-1-PEG-NIF conjugated to microbubbles (FMB); and (**C**) microbubbles co-administered with free NIF (MB-NIF) after exposure to US. Cleared areas of biofilm appear as black regions in the images.

6.9 Passive cavitation detection analysis MATLAB script

```
clear all;%close all; clc
clc

%% 1. SETUP

W = 1800:12000;
f0 = 1.1e6;
gaindB=40;
gain = 10^(gaindB/20);

myDir = uigetdir; % choose directory
myFiles = dir(fullfile(myDir,'*.mat')); %gets all .mat files in file
n_files = length(myFiles);

 %% 2. PREALLOCATE ARRAYS BASED ON FIRST DATA

% Load first file to get parameters
data = load(strcat(myDir, "/",myFiles(1).name));
fs = double(data.tpd.SampleFrequency);

window = W;

% Identify harmonics and ultraharmonics

% Second harmonic is lower bound
fmin = 2*f0;
% Use Nyquist to set upper bound
fmax = min([12e6 0.9*(fs / 2)]);
f_harm =  fmin:f0:fmax;
f_ultra = (fmin+0.5*f0):f0:fmax;
% Make length the smaller to have same size
len_fh = min([length(f_harm) length(f_ultra)]);

% Spectrum parameters

bin = 5e3;                % spectrum resolution (Hz)
Nfft = round(fs/bin);     % samples needed for desired binsize
Novr = 0.5*Nfft;          % sample overlap Welch method

% Run first spectrum to confirm data size
remove_trend = detrend(double(data.tpd.Data(1,window)));
[~,F] = pwelch(remove_trend/gain,Nfft,Novr,Nfft,fs);

% Define indices for harmonics and ultraharmonics.

% Calculate number of bins around each tone [harm, ult. harm]
nbin = [5 5];
% Define relative indices
bw{1} = -(nbin(1)-1)/2:(nbin(1)-1)/2;
bw{2} = -(nbin(2)-1)/2:(nbin(2)-1)/2;

% Preallocate for indices
index_f_harm = zeros(nbin(1)*len_fh,1);
index_f_ultra = zeros(nbin(2)*len_fh,1);
```

```
for i = 1:len_fh
    % Get index of harmonic tone
    [~, ind] = min(abs(F - f_harm(i)));
    % Store indices of the binned area around the harmonic
    index_f_harm((1:nbin(1))+(i-1)*nbin(1)) = ind + bw{1};

    % Get index of ultraharmonic tone
    [~, ind] = min(abs(F - f_ultra(i)));
    % Store indices of the binned area around the ultraharmonic
    index_f_ultra((1:nbin(2))+(i-1)*nbin(2)) = ind + bw{2};
end

f_MHz = F*1e-6;
f_MHz_harm = f_MHz(index_f_harm);
f_MHz_ultra = f_MHz(index_f_ultra);

% Pre-size data storage
P.total = zeros(length(F),n_files);
P.harm = zeros(length(index_f_harm), n_files);
P.ultra = zeros(length(index_f_ultra), n_files);

%% 3. LOOP OVER FILES

time = zeros(n_files,1);

wb = waitbar(0,'file loop');
for ii = 1:n_files

        % Load file
        data = load(strcat(myDir, "/",myFiles(ii).name));

        % Get date/time
        tmp = datevec(data.tpd.DateTime);
        time(ii) = tmp(4)*60^2 + tmp(5)*60 + tmp(6); %hour, min, sec

        % Power spectral density
        [P.total(:,ii),~] =
pwelch(double(data.tpd.Data(1,window))/gain,Nfft,Novr,Nfft,fs);

        % Collect harmonics and ultraharmonics
        P.harm(:,ii) = P.total(index_f_harm,ii);
        P.ultra(:,ii) = P.total(index_f_ultra,ii);

        waitbar(ii/n_files,wb)

end
close(wb)


%% 4. FINISH PROCESSING

    % Sort by file acquisition time in case file names are ambiguous
    [file_times,ind] = sort(time);
    % Give time relative to the first aquisition
    file_times = file_times - file_times(1);

    % Also sort the PSDs
    P.total = P.total(:,ind);
    P.harm = P.harm(:,ind);
```

```
    P.ultra = P.ultra(:,ind);



%     If you don't want to show the entire recording, you can choose where
%     to start
    file_times_window = (file_times>4 & file_times<580);
%
%     Find the indices of these times
    start_ind = find(file_times_window,1,'first');
    last_ind = find(file_times_window,1,'last');
    win_ind = start_ind:last_ind;
    file_times = file_times(win_ind); %Only contains elements between 10s and 120s
    file_times = file_times - file_times(1);

%    Also sort the PSDs
    P.total = P.total(:,win_ind);
    P.harm = P.harm(:,win_ind);
    P.ultra = P.ultra(:,win_ind);

    % Signal power by type, units are Watts (divide PSD by 50 Ohms for true
electrical power from receiver)
    ze = 50;
    ub = min([index_f_harm(1) index_f_ultra(1)]):max([index_f_harm(end)
index_f_ultra(end)]); % freq range for power calcs, spanning Ph, Pu
    Pwr(:,1) = sum(P.total(ub,:),1)*bin/ze;                    % total
    Pwr(:,2) = sum(P.harm,1)*bin/ze;                          % harmonic
    Pwr(:,3) = sum(P.ultra,1)*bin/ze;                          % ultraharmonic
    Pwr(:,4) = Pwr(:,1) - sum(Pwr(:,2:3),2);             % broadband

    % Energy (J) sum the powers and multiply by the time duration of the
    % window
    t_window = diff(window([1, end]))/fs;
    E = sum(Pwr,1)*t_window*1e9 % convert to nJ by 1e9 multiplication
    E=E'

    TotalEnergy = E(1);


%% 5. DISPLAY

% previous colourbar limits: caxis([-80 0]+mx)
    mx = 0.5*db(max(P.total(:)));

    % the folder where I will save my figures
    %fig_folder = strcat(fig_folder, "\");

    figure,set(gcf,'Position',[10 160 2000 500])
    %f.Position = [10 100 540 400];
    tiledlayout (1,2)

    %figure, set(gcf,'name','Spectrogram','Position',[10 160 920 710])
    nexttile
    pcolor(file_times,f_MHz,0.5*db(P.total)), shading flat, colormap jet
    xlabel('Time [s]'), ylabel('Frequency [MHz]')
    %title("Spectrogram")
    xlim([0 diff(file_times([1 end]))])
    hb=colorbar('vert'); hb.Label.String='PSD [dB re V^2/Hz]'; set(hb,
'FontSize',14);
```

```
    caxis([-180 -80]), ylim([ 0 12.5 ])
    hold on; fmin = min([f_MHz_harm; f_MHz_ultra])*1e6; % indicate min-max
frequencies used
    plot(file_times([1 end]),fmin*[1 1]*1e-6,'--w', file_times([1 end]),fmax*[1
1]*1e-6,'--w')
    ax = gca;
    fontname(ax, "Century Gothic");
    ax.FontSize = 15;

    nexttile
    plot(file_times, 0.5*db(Pwr(:,2:4)),'LineWidth',1)
    xlabel('Time (s)'), ylabel('Power (dB re W)')
    legend({'Harmonic','Ultraharmonic','Broadband'},'location','best')
    %title(['Spectral Content, ',num2str(F(ub(1))*1e-6,'%1.2f'),' - ', ...
        %num2str(F(ub(end))*1e-6,'%1.2f'),' MHz'])
    xlim([0 diff(file_times([1 end]))])
    ylim([-135 -60])
    ax = gca;
    fontname(ax, "Century Gothic");
    ax.FontSize = 15;
```

References

(1) Tan, S. Y.; Tatsumura, Y. Alexander Fleming (1881–1955): Discoverer of Penicillin. *Singapore Med. J.* **2015**, *56* (7), 366–367. https://doi.org/10.11622/smedj.2015105.

(2) Bud, R. Antibiotics: The Epitome of a Wonder Drug. *BMJ* **2007**, *334* (suppl 1), s6–s6. https://doi.org/10.1136/bmj.39021.640255.94.

(3) Ratner, A. J.; Weiser, J. N. Pneumonia before Antibiotics Therapeutic Evolution and Evaluation in Twentieth-Century America. *J. Clin. Invest.* **2006**, *116* (9), 2311. https://doi.org/10.1172/JCI29920.

(4) Austrian, R.; Gold, J. Pneumococcal Bacteremia with Especial Reference to Bacteremic Pneumococcal Pneumonia. *Ann. Intern. Med.* **2008**. https://doi.org/10.7326/0003-4819-60-5-759.

(5) Shlaes, D. M.; Bradford, P. A. Antibiotics—From There to Where?: How the Antibiotic Miracle Is Threatened by Resistance and a Broken Market and What We Can Do about It. *Pathog. Immun.* **2018**, *3* (1), 19–43. https://doi.org/10.20411/pai.v3i1.231.

(6) Armstrong, G. L.; Conn, L. A.; Pinner, R. W. Trends in Infectious Disease Mortality in the United States During the 20th Century. *JAMA* **1999**, *281* (1), 61–66. https://doi.org/10.1001/jama.281.1.61.

(7) Hutchings, M. I.; Truman, A. W.; Wilkinson, B. Antibiotics: Past, Present and Future. *Curr. Opin. Microbiol.* **2019**, *51*, 72–80. https://doi.org/10.1016/j.mib.2019.10.008.

(8) Stennett, H. L.; Back, C. R.; Race, P. R. Derivation of a Precise and Consistent Timeline for Antibiotic Development. *Antibiotics* **2022**, *11* (9), 1237. https://doi.org/10.3390/antibiotics11091237.

(9) Matei, A. T.; Visan, A. I. Mechanism, Efficacy, and Safety of Natural Antibiotics. *Antibiotics* **2025**, *14* (10), 981. https://doi.org/10.3390/antibiotics14100981.

(10) Ferraz, M. P. Antimicrobial Resistance: The Impact from and on Society According to One Health Approach. *Societies* **2024**, *14* (9), 187. https://doi.org/10.3390/soc14090187.

(11) Murugaiyan, J.; Kumar, P. A.; Rao, G. S.; Iskandar, K.; Hawser, S.; Hays, J. P.; Mohsen, Y.; Adukkadukkam, S.; Awuah, W. A.; Jose, R. A. M.; Sylvia, N.; Nansubuga, E. P.; Tilocca, B.; Roncada, P.; Roson-Calero, N.; Moreno-Morales, J.; Amin, R.; Kumar, B. K.; Kumar, A.; Toufik, A.-R.; Zaw, T. N.; Akinwotu, O. O.; Satyaseela, M. P.; van Dongen, M. B. M. Progress in Alternative Strategies to Combat Antimicrobial Resistance: Focus on Antibiotics. *Antibiotics* **2022**, *11* (2), 200. https://doi.org/10.3390/antibiotics11020200.

(12) Murray, C. J. L.; Ikuta, K. S.; Sharara, F.; Swetschinski, L.; Aguilar, G. R.; Gray, A.; Han, C.; Bisignano, C.; Rao, P.; Wool, E.; Johnson, S. C.; Browne, A. J.; Chipeta, M. G.; Fell, F.; Hackett, S.; Haines-Woodhouse, G.; Hamadani, B. H. K.; Kumaran, E. A. P.; McManigal, B.; Achalapong, S.; Agarwal, R.; Akech, S.; Albertson, S.; Amuasi, J.; Andrews, J.; Aravkin, A.; Ashley, E.; Babin, F.-X.; Bailey, F.; Baker, S.; Basnyat, B.; Bekker, A.; Bender, R.; Berkley, J. A.; Bethou, A.; Bielicki, J.; Boonkasidecha, S.; Bukosia, J.; Carvalheiro, C.; Castañeda-Orjuela, C.; Chansamouth, V.; Chaurasia, S.; Chiurchiù, S.; Chowdhury, F.; Donatien, R. C.; Cook, A. J.; Cooper, B.; Cressey, T. R.; Criollo-Mora, E.; Cunningham, M.; Darboe, S.; Day, N. P. J.; Luca, M. D.; Dokova, K.; Dramowski, A.; Dunachie, S. J.; Bich, T. D.; Eckmanns, T.; Eibach, D.; Emami, A.; Feasey, N.; Fisher-Pearson, N.; Forrest, K.; Garcia, C.; Garrett, D.; Gastmeier, P.; Giref, A. Z.; Greer, R. C.; Gupta, V.; Haller, S.; Haselbeck, A.; Hay, S. I.; Holm, M.; Hopkins, S.; Hsia, Y.; Iregbu, K. C.; Jacobs, J.; Jarovsky, D.; Javanmardi, F.; Jenney, A. W. J.; Khorana, M.; Khusuwan, S.; Kissoon, N.; Kobeissi, E.; Kostyanev, T.; Krapp, F.; Krumkamp, R.; Kumar, A.; Kyu, H. H.; Lim, C.; Lim, K.; Limmathurotsakul, D.; Loftus, M. J.; Lunn, M.; Ma, J.; Manoharan, A.; Marks, F.; May, J.; Mayxay, M.; Mturi, N.; Munera-Huertas, T.; Musicha, P.; Musila, L. A.; Mussi-Pinhata, M. M.; Naidu, R. N.;

Nakamura, T.; Nanavati, R.; Nangia, S.; Newton, P.; Ngoun, C.; Novotney, A.; Nwakanma, D.; Obiero, C. W.; Ochoa, T. J.; Olivas-Martinez, A.; Olliaro, P.; Ooko, E.; Ortiz-Brizuela, E.; Ounchanum, P.; Pak, G. D.; Paredes, J. L.; Peleg, A. Y.; Perrone, C.; Phe, T.; Phommasone, K.; Plakkal, N.; Ponce-de-Leon, A.; Raad, M.; Ramdin, T.; Rattanavong, S.; Riddell, A.; Roberts, T.; Robotham, J. V.; Roca, A.; Rosenthal, V. D.; Rudd, K. E.; Russell, N.; Sader, H. S.; Saengchan, W.; Schnall, J.; Scott, J. A. G.; Seekaew, S.; Sharland, M.; Shivamallappa, M.; Sifuentes-Osornio, J.; Simpson, A. J.; Steenkeste, N.; Stewardson, A. J.; Stoeva, T.; Tasak, N.; Thaiprakong, A.; Thwaites, G.; Tigoi, C.; Turner, C.; Turner, P.; Doorn, H. R. van; Velaphi, S.; Vongpradith, A.; Vongsouvath, M.; Vu, H.; Walsh, T.; Walson, J. L.; Waner, S.; Wangrangsimakul, T.; Wannapinij, P.; Wozniak, T.; Sharma, T. E. M. W. Y.; Yu, K. C.; Zheng, P.; Sartorius, B.; Lopez, A. D.; Stergachis, A.; Moore, C.; Dolecek, C.; Naghavi, M. Global Burden of Bacterial Antimicrobial Resistance in 2019: A Systematic Analysis. *The Lancet* **2022**, *399* (10325), 629–655. https://doi.org/10.1016/S0140-6736(21)02724-0.

(13) O'Neill, J. *Tackling Drug-Resistant Infections Globally: Final Report and Recommendations*. https://amr-review.org/sites/default/files/160518_Final%20paper_with%20cover.pdf (accessed 2025-12-17).

(14) IACG on AMR. *no-time-to-wait-securing-the-future-from-drug-resistant-infections-en*. https://www.who.int/docs/default-source/documents/no-time-to-wait-securing-the-future-from-drug-resistant-infections-en.pdf (accessed 2025-12-17).

(15) WHO GLASS. *Global antibiotic resistance surveillance report 2025*. https://www.who.int/publications/i/item/9789240116337 (accessed 2025-12-17).

(16) NAO. Investigation into How Government Is Addressing Antimicrobial Resistance. **2025**.

(17) Laurence, T.; Lamberti, O.; Smith, R.; Drake, T.; McDonnell, A. The Global Direct Inpatient Cost of Antimicrobial Resistance: A Modelling Study. **2025**.

(18) World Bank. *Drug-Resistant Infections: A Threat to Our Economic Future*. https://documents1.worldbank.org/curated/en/323311493396993758/pdf/final-report.pdf (accessed 2025-12-17).

(19) Rupasinghe, N.; Machalaba, C.; Muthee, T.; Mazimba, A. *Stopping the Grand Pandemic: A Framework for Action - Addressing Antimicrobial Resistance through World Bank Operations*; World Bank, 2024. https://doi.org/10.1596/41533.

(20) Global Leaders Group on AMR. *Amid the escalating impact of antimicrobial resistance, the Global Leaders Group calls on UN Member States to take bold and specific action*. https://www.amrleaders.org/news-and-events/news/item/03-04-2024-amid-the-escalating-impact-of-antimicrobial-resistance-the-global-leaders-group-calls-on-un-member-states-to-take-bold-and-specific-action (accessed 2025-12-17).

(21) WOAH; World Bank. *Forecasting the Fallout from AMR: Economic Impacts of Antimicrobial Resistance in Humans. A Report from the EcoAMR Series*; WOAH & WorldBank, 2024. https://doi.org/10.20506/ecoAMR.3539.

(22) United Nations Environment Programme. *Bracing for Superbugs: Strengthening Environmental Action in the One Health Response to Antimicrobial Resistance*; United Nations, 2023. https://doi.org/10.18356/9789210025799.

(23) McCarthy, M.; BMA. *Tackling antimicrobial resistance*. The British Medical Association is the trade union and professional body for doctors in the UK. https://www.bma.org.uk/news-and-opinion/tackling-antimicrobial-resistance (accessed 2025-12-17).

(24) Food and Agriculture Organization of the United Nations. Why Should Policymakers Act on Antimicrobial Resistance in Agrifood Systems? **2023**.

(25) Harvey, E. J.; De Brún, C.; Casale, E.; Finistrella, V.; Ashiru-Oredope, D. Influence of Factors Commonly Known to Be Associated with Health Inequalities on Antibiotic Use in High-Income Countries: A Systematic Scoping Review. *J. Antimicrob. Chemother.* **2023**, *78* (4), 861–870. https://doi.org/10.1093/jac/dkad034.

(26) Gilham, E.; Ashiru-Oredope, D. *Antimicrobial resistance: improving understanding and addressing inequalities*. https://www.rcpath.org/resource-report/antimicrobial-resistance-improving-understanding-and-addressing-inequalities-.html (accessed 2025-12-17).
(27) WHO. *Overcoming stigma and discrimination in pursuit of reducing antimicrobial resistance: a Swedish approach*. https://www.who.int/europe/news-room/feature-stories/item/overcoming-stigma-and-discrimination-in-pursuit-of-reducing-antimicrobial-resistance--a-swedish-approach (accessed 2025-12-17).
(28) WHO. *Antimicrobial resistance*. https://www.who.int/news-room/fact-sheets/detail/antimicrobial-resistance (accessed 2025-12-17).
(29) WHO. *WHO Global research agenda for AMR in human health - Policy brief*. https://cdn.who.int/media/docs/default-source/antimicrobial-resistance/amr-spc-npm/who-global-research-agenda-for-amr-in-human-health---policy-brief.pdf?sfvrsn=f86aa073_4&download=true (accessed 2025-07-01).
(30) WHO. *Global leaders set first targets to control antimicrobial resistance crisis*. https://www.who.int/europe/news/item/27-09-2024-global-leaders-set-first-targets-to-control-antimicrobial-resistance-crisis (accessed 2025-07-01).
(31) Endale, H.; Mathewos, M.; Abdeta, D. Potential Causes of Spread of Antimicrobial Resistance and Preventive Measures in One Health Perspective-A Review. *Infect. Drug Resist.* **2023**, *16*, 7515–7545. https://doi.org/10.2147/IDR.S428837.
(32) Karakonstantis, S.; Kalemaki, D. Antimicrobial Overuse and Misuse in the Community in Greece and Link to Antimicrobial Resistance Using Methicillin-Resistant *S. Aureus* as an Example. *J. Infect. Public Health* **2019**, *12* (4), 460–464. https://doi.org/10.1016/j.jiph.2019.03.017.
(33) Dolk, F. C. K.; Pouwels, K. B.; Smith, D. R. M.; Robotham, J. V.; Smieszek, T. Antibiotics in Primary Care in England: Which Antibiotics Are Prescribed and for Which Conditions? *J. Antimicrob. Chemother.* **2018**, *73* (suppl_2), ii2–ii10. https://doi.org/10.1093/jac/dkx504.
(34) Smieszek, T.; Pouwels, K. B.; Dolk, F. C. K.; Smith, D. R. M.; Hopkins, S.; Sharland, M.; Hay, A. D.; Moore, M. V.; Robotham, J. V. Potential for Reducing Inappropriate Antibiotic Prescribing in English Primary Care. *J. Antimicrob. Chemother.* **2018**, *73* (suppl_2), ii36–ii43. https://doi.org/10.1093/jac/dkx500.
(35) Lathakumari, R. H.; Vajravelu, L. K.; Satheesan, A.; Ravi, S.; Thulukanam, J. Antibiotics and the Gut Microbiome: Understanding the Impact on Human Health. *Med. Microecol.* **2024**, *20*, 100106. https://doi.org/10.1016/j.medmic.2024.100106.
(36) Fahmi, A.; Yang, Y.-T.; Zhong, X.; Pate, A.; Sharma, A.; Watts, S.; Ashcroft, D. M.; Goldacre, B.; MacKenna, B.; Massey, J.; Mehrkar, A.; Bacon, S.; McMillan, B.; Dark, P.; Hand, K.; Palin, V.; van Staa, T. P. Antibiotics for Common Infections in Primary Care before, during and after the COVID-19 Pandemic: Cohort Study of Extent of Prescribing Based on Risks of Infection-Related Hospital Admissions. *J. R. Soc. Med.* **2025**, *118* (4), 126–137. https://doi.org/10.1177/01410768251328997.
(37) Tiseo, K.; Huber, L.; Gilbert, M.; Robinson, T. P.; Van Boeckel, T. P. Global Trends in Antimicrobial Use in Food Animals from 2017 to 2030. *Antibiotics* **2020**, *9* (12), 918. https://doi.org/10.3390/antibiotics9120918.
(38) Coe, S.; Balogun, B.; Sutherland, N. The Use of Antibiotics on Healthy Farm Animals and Antimicrobial Resistance. **2023**.
(39) Hayek, M. N. The Infectious Disease Trap of Animal Agriculture. *Sci. Adv.* **2022**, *8* (44), eadd6681. https://doi.org/10.1126/sciadv.add6681.
(40) Zhang, T.; Nickerson, R.; Zhang, W.; Peng, X.; Shang, Y.; Zhou, Y.; Luo, Q.; Wen, G.; Cheng, Z. The Impacts of Animal Agriculture on One Health—Bacterial Zoonosis, Antimicrobial Resistance, and Beyond. *One Health* **2024**, *18*, 100748. https://doi.org/10.1016/j.onehlt.2024.100748.

(41) Blokhuis, H. J.; Hopster, H.; Geverink, N. A.; Korte, S. M.; van Reenen, C. G. Studies of Stress in Farm Animals. *Comp. Haematol. Int.* **1998**, *8* (2), 94–101. https://doi.org/10.1007/BF02642498.

(42) Van Boeckel, T. P.; Brower, C.; Gilbert, M.; Grenfell, B. T.; Levin, S. A.; Robinson, T. P.; Teillant, A.; Laxminarayan, R. Global Trends in Antimicrobial Use in Food Animals. *Proc. Natl. Acad. Sci.* **2015**, *112* (18), 5649–5654. https://doi.org/10.1073/pnas.1503141112.

(43) Snyder, H. L.; Niebuhr, S. E.; Dickson, J. S. Transfer of Methicillin-Resistant *Staphylococcus Aureus* from Retail Pork Products onto Food Contact Surfaces and the Potential for Consumer Exposure. *J. Food Prot.* **2013**, *76* (12), 2087–2092. https://doi.org/10.4315/0362-028X.JFP-13-143.

(44) Larsson, D. G. J.; Flach, C.-F. Antibiotic Resistance in the Environment. *Nat. Rev. Microbiol.* **2022**, *20* (5), 257–269. https://doi.org/10.1038/s41579-021-00649-x.

(45) Polianciuc, S. I.; Gurzău, A. E.; Kiss, B.; Ştefan, M. G.; Loghin, F. Antibiotics in the Environment: Causes and Consequences. *Med. Pharm. Rep.* **2020**, *93* (3), 231–240. https://doi.org/10.15386/mpr-1742.

(46) Wang, Y.; Li, G.; Zhu, Q.; Liao, C. Occurrence of Parabens, Triclosan and Triclocarban in Paired Human Urine and Indoor Dust from Two Typical Cities in China and Its Implications for Human Exposure. *Sci. Total Environ.* **2021**, *786*, 147485. https://doi.org/10.1016/j.scitotenv.2021.147485.

(47) Mahnert, A.; Moissl-Eichinger, C.; Zojer, M.; Bogumil, D.; Mizrahi, I.; Rattei, T.; Martinez, J. L.; Berg, G. Man-Made Microbial Resistances in Built Environments. *Nat. Commun.* **2019**, *10* (1), 968. https://doi.org/10.1038/s41467-019-08864-0.

(48) Cave, R.; Cole, J.; Mkrtchyan, H. V. Surveillance and Prevalence of Antimicrobial Resistant Bacteria from Public Settings within Urban Built Environments: Challenges and Opportunities for Hygiene and Infection Control. *Environ. Int.* **2021**, *157*, 106836. https://doi.org/10.1016/j.envint.2021.106836.

(49) Hooban, B.; Fitzhenry, K.; Cahill, N.; Joyce, A.; O' Connor, L.; Bray, J. E.; Brisse, S.; Passet, V.; Abbas Syed, R.; Cormican, M.; Morris, D. A Point Prevalence Survey of Antibiotic Resistance in the Irish Environment, 2018–2019. *Environ. Int.* **2021**, *152*, 106466. https://doi.org/10.1016/j.envint.2021.106466.

(50) Qamar, A. K. A.; Habboub, T. M.; Elmanama, A. A. Antimicrobial Resistance of Bacteria Isolated at the European Gaza Hospital before and after the Great March of Return Protests: A Retrospective Study. *The Lancet* **2022**, *399*, S14. https://doi.org/10.1016/S0140-6736(22)01149-7.

(51) Ebied, M. *How Human Conflict Accelerates Antimicrobial Resistance*. ASM.org. https://asm.org:443/articles/2025/september/how-human-conflict-accelerates-antimicrobial-resis (accessed 2025-12-18).

(52) Pallett, S. J. C.; Boyd, S. E.; O'Shea, M. K.; Martin, J.; Jenkins, D. R.; Hutley, E. J. The Contribution of Human Conflict to the Development of Antimicrobial Resistance. *Commun. Med.* **2023**, *3* (1), 153. https://doi.org/10.1038/s43856-023-00386-7.

(53) Hutin, Y. J.-F. *Invisible frontlines: tackling antimicrobial resistance amid conflict and fragility*. https://www.who.int/news-room/commentaries/detail/invisible-frontlines--tackling-antimicrobial-resistance-amid-conflict-and-fragility (accessed 2025-12-18).

(54) Okeke, I. N.; Edelman, R. Dissemination of Antibiotic-Resistant Bacteria across Geographic Borders. *Clin. Infect. Dis.* **2001**, *33* (3), 364–369. https://doi.org/10.1086/321877.

(55) Kenyon, T. A.; Valway, S. E.; Ihle, W. W.; Onorato, I. M.; Castro, K. G. Transmission of Multidrug-Resistant Mycobacterium Tuberculosis during a Long Airplane Flight. *N. Engl. J. Med.* **1996**, *334* (15), 933–938. https://doi.org/10.1056/NEJM199604113341501.

(56) Belay, W. Y.; Getachew, M.; Tegegne, B. A.; Teffera, Z. H.; Dagne, A.; Zeleke, T. K.; Abebe, R. B.; Gedif, A. A.; Fenta, A.; Yirdaw, G.; Tilahun, A.; Aschale, Y. Mechanism of Antibacterial Resistance, Strategies and next-Generation Antimicrobials to Contain Antimicrobial Resistance: A Review. *Front. Pharmacol.* **2024**, *15*. https://doi.org/10.3389/fphar.2024.1444781.

(57) Fernández, L.; Hancock, R. E. W. Adaptive and Mutational Resistance: Role of Porins and Efflux Pumps in Drug Resistance. *Clin. Microbiol. Rev.* **2012**, *25* (4), 661–681. https://doi.org/10.1128/cmr.00043-12.

(58) Rappuoli, R.; Young, P.; Ron, E.; Pecetta, S.; Pizza, M. Save the Microbes to Save the Planet. A Call to Action of the International Union of the Microbiological Societies (IUMS). *One Health Outlook* **2023**, *5*, 5. https://doi.org/10.1186/s42522-023-00077-2.

(59) Garde, S.; Chodisetti, P. K.; Reddy, M. Peptidoglycan: Structure, Synthesis, and Regulation. *EcoSal Plus* **2021**, *9* (2), eESP-0010-2020. https://doi.org/10.1128/ecosalplus.ESP-0010-2020.

(60) Salton, M. R. J.; Kim, K.-S. Structure. In *Medical Microbiology*; Baron, S., Ed.; University of Texas Medical Branch at Galveston: Galveston (TX), 1996.

(61) Silhavy, T. J.; Kahne, D.; Walker, S. The Bacterial Cell Envelope. *Cold Spring Harb. Perspect. Biol.* **2010**, *2* (5), a000414. https://doi.org/10.1101/cshperspect.a000414.

(62) Seltmann, G.; Holst, O. Periplasmic Space and Rigid Layer. In *The Bacterial Cell Wall*; Seltmann, G., Holst, O., Eds.; Springer: Berlin, Heidelberg, 2002; pp 103–132. https://doi.org/10.1007/978-3-662-04878-8_3.

(63) Erickson, H. P. How Teichoic Acids Could Support a Periplasm in Gram-Positive Bacteria, and Let Cell Division Cheat Turgor Pressure. *Front. Microbiol.* **2021**, *12*. https://doi.org/10.3389/fmicb.2021.664704.

(64) Atanasova, K. Interactions between Porcine Respiratory Coronavirus and Bacterial Cell-Wall Toxins in Th Elungs of Pigs, 2010.

(65) Bertani, B.; Ruiz, N. Function and Biogenesis of Lipopolysaccharides. *EcoSal Plus* **2018**, *8* (1), 10.1128/ecosalplus.ESP-0001–2018. https://doi.org/10.1128/ecosalplus.esp-0001-2018.

(66) Delcour, A. H. Outer Membrane Permeability and Antibiotic Resistance. *Biochim. Biophys. Acta* **2009**, *1794* (5), 808–816. https://doi.org/10.1016/j.bbapap.2008.11.005.

(67) Saxena, D.; Maitra, R.; Bormon, R.; Czekanska, M.; Meiers, J.; Titz, A.; Verma, S.; Chopra, S. Tackling the Outer Membrane: Facilitating Compound Entry into Gram-Negative Bacterial Pathogens. *Npj Antimicrob. Resist.* **2023**, *1* (1), 17. https://doi.org/10.1038/s44259-023-00016-1.

(68) Fernández, L.; Hancock, R. E. W. Adaptive and Mutational Resistance: Role of Porins and Efflux Pumps in Drug Resistance. *Clin. Microbiol. Rev.* **2012**, *25* (4), 661–681. https://doi.org/10.1128/CMR.00043-12.

(69) Schindler, H.; Rosenbusch, J. P. Matrix Protein from Escherichia Coli Outer Membranes Forms Voltage-Controlled Channels in Lipid Bilayers. *Proc. Natl. Acad. Sci.* **1978**, *75* (8), 3751–3755. https://doi.org/10.1073/pnas.75.8.3751.

(70) Duret, G.; Simonet, V.; Delcour, A. H. Modulation of Vibrio Cholerae Porin Function by Acidic pH. *Channels* **2007**, *1* (2), 70–79. https://doi.org/10.4161/chan.3983.

(71) Iyer, R.; Delcour, A. H. Complex Inhibition of OmpF and OmpC Bacterial Porins by Polyamines. *J. Biol. Chem.* **1997**, *272* (30), 18595–18601. https://doi.org/10.1074/jbc.272.30.18595.

(72) Ebbensgaard, A. E.; Løbner-Olesen, A.; Frimodt-Møller, J. The Role of Efflux Pumps in the Transition from Low-Level to Clinical Antibiotic Resistance. *Antibiotics* **2020**, *9* (12), 855. https://doi.org/10.3390/antibiotics9120855.

(73) Blair, J. M.; Piddock, L. J. Structure, Function and Inhibition of RND Efflux Pumps in Gram-Negative Bacteria: An Update. *Curr. Opin. Microbiol.* **2009**, *12* (5), 512–519. https://doi.org/10.1016/j.mib.2009.07.003.

(74) Zack, K. M.; Sorenson, T.; Joshi, S. G. Types and Mechanisms of Efflux Pump Systems and the Potential of Efflux Pump Inhibitors in the Restoration of Antimicrobial Susceptibility, with a Special Reference to Acinetobacter Baumannii. *Pathogens* **2024**, *13* (3), 197. https://doi.org/10.3390/pathogens13030197.

(75) WHO. *WHO Bacterial Priority Pathogens List 2024: Bacterial Pathogens of Public Health Importance, to Guide Research, Development, and Strategies to Prevent and Control Antimicrobial Resistance*, 1st ed.; World Health Organization: Geneva, 2024.
(76) Coculescu, B. Antimicrobial Resistance Induced by Genetic Changes. *J. Med. Life* **2009**, *2* (2), 114–123.
(77) Martinez, J. L.; Baquero, F. Mutation Frequencies and Antibiotic Resistance. *Antimicrob. Agents Chemother.* **2000**, *44* (7), 1771–1777. https://doi.org/10.1128/aac.44.7.1771-1777.2000.
(78) Poulton, N. C.; Rock, J. M. Unraveling the Mechanisms of Intrinsic Drug Resistance in Mycobacterium Tuberculosis. *Front. Cell. Infect. Microbiol.* **2022**, *12*. https://doi.org/10.3389/fcimb.2022.997283.
(79) Darby, E. M.; Trampari, E.; Siasat, P.; Gaya, M. S.; Alav, I.; Webber, M. A.; Blair, J. M. A. Molecular Mechanisms of Antibiotic Resistance Revisited. *Nat. Rev. Microbiol.* **2023**, *21* (5), 280–295. https://doi.org/10.1038/s41579-022-00820-y.
(80) Jacoby, G. A.; Munoz-Price, L. S. The New β-Lactamases. *N. Engl. J. Med.* **2005**, *352* (4), 380–391. https://doi.org/10.1056/NEJMra041359.
(81) Bush, K.; Bradford, P. A. β-Lactams and β-Lactamase Inhibitors: An Overview. *Cold Spring Harb. Perspect. Med.* **2016**, *6* (8), a025247. https://doi.org/10.1101/cshperspect.a025247.
(82) Papp-Wallace, K. M.; Endimiani, A.; Taracila, M. A.; Bonomo, R. A. Carbapenems: Past, Present, and Future ▿. *Antimicrob. Agents Chemother.* **2011**, *55* (11), 4943–4960. https://doi.org/10.1128/AAC.00296-11.
(83) Blair, J. M. A.; Webber, M. A.; Baylay, A. J.; Ogbolu, D. O.; Piddock, L. J. V. Molecular Mechanisms of Antibiotic Resistance. *Nat. Rev. Microbiol.* **2015**, *13* (1), 42–51. https://doi.org/10.1038/nrmicro3380.
(84) Ramirez, M. S.; Tolmasky, M. E. Aminoglycoside Modifying Enzymes. *Drug Resist. Updat.* **2010**, *13* (6), 151–171. https://doi.org/10.1016/j.drup.2010.08.003.
(85) Krause, K. M.; Serio, A. W.; Kane, T. R.; Connolly, L. E. Aminoglycosides: An Overview. *Cold Spring Harb. Perspect. Med.* **2016**, *6* (6), a027029. https://doi.org/10.1101/cshperspect.a027029.
(86) Courvalin, P.; Fiandt, M. Aminoglycoside-Modifying Enzymes of *Staphylococcus Aureus*; Experssion in *Escherichia Coli*. *Gene* **1980**, *9* (3), 247–269. https://doi.org/10.1016/0378-1119(90)90326-M.
(87) Ahmadian, L.; Norouzi Bazgir, Z.; Ahanjan, M.; Valadan, R.; Goli, H. R. Role of Aminoglycoside-Modifying Enzymes (AMEs) in Resistance to Aminoglycosides among Clinical Isolates of Pseudomonas Aeruginosa in the North of Iran. *BioMed Res. Int.* **2021**, *2021* (1), 7077344. https://doi.org/10.1155/2021/7077344.
(88) Rizo, J.; Encarnación-Guevara, S. Bacterial Protein Acetylation: Mechanisms, Functions, and Methods for Study. *Front. Cell. Infect. Microbiol.* **2024**, *14*. https://doi.org/10.3389/fcimb.2024.1408947.
(89) Fang, Z.; Lai, F.; Cao, K.; Zhang, Z.; Cao, L.; Liu, S.; Duan, Y.; Yin, X.; Ge, R.; He, Q.-Y.; Sun, X. Potential Role of Lysine Acetylation in Antibiotic Resistance of Escherichia Coli. *mSystems* **2022**, *7* (6), e00649-22. https://doi.org/10.1128/msystems.00649-22.
(90) Reygaert, W. C. An Overview of the Antimicrobial Resistance Mechanisms of Bacteria. *AIMS Microbiol.* **2018**, *4* (3), 482–501. https://doi.org/10.3934/microbiol.2018.3.482.
(91) Periasamy, H.; Joshi, P.; Palwe, S.; Shrivastava, R.; Bhagwat, S.; Patel, M. High Prevalence of Escherichia Coli Clinical Isolates in India Harbouring Four Amino Acid Inserts in PBP3 Adversely Impacting Activity of Aztreonam/Avibactam. *J. Antimicrob. Chemother.* **2020**, *75* (6), 1650–1651. https://doi.org/10.1093/jac/dkaa021.
(92) Long, K. S.; Poehlsgaard, J.; Kehrenberg, C.; Schwarz, S.; Vester, B. The Cfr rRNA Methyltransferase Confers Resistance to Phenicols, Lincosamides, Oxazolidinones, Pleuromutilins, and Streptogramin A Antibiotics. *Antimicrob. Agents Chemother.* **2006**, *50* (7), 2500–2505. https://doi.org/10.1128/aac.00131-06.

(93) Hegde, S. S.; Vetting, M. W.; Roderick, S. L.; Mitchenall, L. A.; Maxwell, A.; Takiff, H. E.; Blanchard, J. S. A Fluoroquinolone Resistance Protein from Mycobacterium Tuberculosis That Mimics DNA. *Science* **2005**, *308* (5727), 1480–1483. https://doi.org/10.1126/science.1110699.

(94) Li, W.; Atkinson, G. C.; Thakor, N. S.; Allas, Ü.; Lu, C.; Chan, K.-Y.; Tenson, T.; Schulten, K.; Wilson, K. S.; Hauryliuk, V.; Frank, J. Mechanism of Tetracycline Resistance by Ribosomal Protection Protein Tet(O). *Nat. Commun.* **2013**, *4* (1), 1477. https://doi.org/10.1038/ncomms2470.

(95) Foster, T. J. Antibiotic Resistance in Staphylococcus Aureus. Current Status and Future Prospects. *FEMS Microbiol. Rev.* **2017**, *41* (3), 430–449. https://doi.org/10.1093/femsre/fux007.

(96) Stogios, P. J.; Savchenko, A. Molecular Mechanisms of Vancomycin Resistance. *Protein Sci. Publ. Protein Soc.* **2020**, *29* (3), 654–669. https://doi.org/10.1002/pro.3819.

(97) Jian, Z.; Zeng, L.; Xu, T.; Sun, S.; Yan, S.; Yang, L.; Huang, Y.; Jia, J.; Dou, T. Antibiotic Resistance Genes in Bacteria: Occurrence, Spread, and Control. *J. Basic Microbiol.* **2021**, *61* (12), 1049–1070. https://doi.org/10.1002/jobm.202100201.

(98) Olivares Pacheco, J. A.; Bernardini, A.; Garcia-Leon, G.; Corona, F.; Sanchez, M. B.; Martinez, J. L. The Intrinsic Resistome of Bacterial Pathogens. *Front. Microbiol.* **2013**, *4*. https://doi.org/10.3389/fmicb.2013.00103.

(99) Lloyd, G. S.; Thomas, C. M. Microbial Primer: The Logic of Bacterial Plasmids. *Microbiology* **2023**, *169* (7), 001336. https://doi.org/10.1099/mic.0.001336.

(100) Ochman, H. Bacterial Evolution: Chromosome Arithmetic and Geometry. *Curr. Biol.* **2002**, *12* (12), R427–R428. https://doi.org/10.1016/S0960-9822(02)00916-8.

(101) Svara, F.; Rankin, D. J. The Evolution of Plasmid-Carried Antibiotic Resistance. *BMC Evol. Biol.* **2011**, *11*, 130. https://doi.org/10.1186/1471-2148-11-130.

(102) Shintani, M.; Vestergaard, G.; Milaković, M.; Kublik, S.; Smalla, K.; Schloter, M.; Udiković-Kolić, N. Integrons, Transposons and IS Elements Promote Diversification of Multidrug Resistance Plasmids and Adaptation of Their Hosts to Antibiotic Pollutants from Pharmaceutical Companies. *Environ. Microbiol.* **2023**, *25* (12), 3035–3051. https://doi.org/10.1111/1462-2920.16481.

(103) Bennett, P. M. Genome Plasticity. In *Genomics, Proteomics, and Clinical Bacteriology: Methods and Reviews*; Woodford, N., Johnson, A. P., Eds.; Humana Press: Totowa, NJ, 2004; pp 71–113. https://doi.org/10.1385/1-59259-763-7:071.

(104) Patel, S. Drivers of Bacterial Genomes Plasticity and Roles They Play in Pathogen Virulence, Persistence and Drug Resistance. *Infect. Genet. Evol.* **2016**, *45*, 151–164. https://doi.org/10.1016/j.meegid.2016.08.030.

(105) Coluzzi, C.; Rocha, E. P. C. The Spread of Antibiotic Resistance Is Driven by Plasmids Among the Fastest Evolving and of Broadest Host Range. *Mol. Biol. Evol.* **2025**, *42* (3), msaf060. https://doi.org/10.1093/molbev/msaf060.

(106) Partridge, S. R.; Kwong, S. M.; Firth, N.; Jensen, S. O. Mobile Genetic Elements Associated with Antimicrobial Resistance. *Clin. Microbiol. Rev.* **2018**, *31* (4), e00088-17. https://doi.org/10.1128/CMR.00088-17.

(107) Munita, J. M.; Arias, C. A. Mechanisms of Antibiotic Resistance. *Microbiol. Spectr.* **2016**, *4* (2), 10.1128/microbiolspec.vmbf-0016–2015. https://doi.org/10.1128/microbiolspec.vmbf-0016-2015.

(108) Sun, D. Pull in and Push Out: Mechanisms of Horizontal Gene Transfer in Bacteria. *Front. Microbiol.* **2018**, *9*. https://doi.org/10.3389/fmicb.2018.02154.

(109) von Wintersdorff, C. J. H.; Penders, J.; van Niekerk, J. M.; Mills, N. D.; Majumder, S.; van Alphen, L. B.; Savelkoul, P. H. M.; Wolffs, P. F. G. Dissemination of Antimicrobial Resistance in Microbial Ecosystems through Horizontal Gene Transfer. *Front. Microbiol.* **2016**, *7*, 173. https://doi.org/10.3389/fmicb.2016.00173.

(110) Cantón, R.; González-Alba, J. M.; Galán, J. C. CTX-M Enzymes: Origin and Diffusion. *Front. Microbiol.* **2012**, *3*, 110. https://doi.org/10.3389/fmicb.2012.00110.
(111) Hakenbeck, R. Transformation in Streptococcus Pneumoniae: Mosaic Genes and the Regulation of Competence. *Res. Microbiol.* **2000**, *151* (6), 453–456. https://doi.org/10.1016/S0923-2508(00)00170-4.
(112) Johnston, C.; Martin, B.; Fichant, G.; Polard, P.; Claverys, J.-P. Bacterial Transformation: Distribution, Shared Mechanisms and Divergent Control. *Nat. Rev. Microbiol.* **2014**, *12* (3), 181–196. https://doi.org/10.1038/nrmicro3199.
(113) Billard-Pomares, T.; Fouteau, S.; Jacquet, M. E.; Roche, D.; Barbe, V.; Castellanos, M.; Bouet, J. Y.; Cruveiller, S.; Médigue, C.; Blanco, J.; Clermont, O.; Denamur, E.; Branger, C. Characterization of a P1-Like Bacteriophage Carrying an SHV-2 Extended-Spectrum β-Lactamase from an Escherichia Coli Strain. *Antimicrob. Agents Chemother.* **2014**, *58* (11), 6550–6557. https://doi.org/10.1128/aac.03183-14.
(114) Mazaheri Nezhad Fard, R.; Barton, M. D.; Heuzenroeder, M. W. Bacteriophage-mediated Transduction of Antibiotic Resistance in Enterococci. *Lett. Appl. Microbiol.* **2011**, *52* (6), 559–564. https://doi.org/10.1111/j.1472-765X.2011.03043.x.
(115) Domingues, S.; Nielsen, K. M. Membrane Vesicles and Horizontal Gene Transfer in Prokaryotes. *Curr. Opin. Microbiol.* **2017**, *38*, 16–21. https://doi.org/10.1016/j.mib.2017.03.012.
(116) Dubey, G. P.; Ben-Yehuda, S. Intercellular Nanotubes Mediate Bacterial Communication. *Cell* **2011**, *144* (4), 590–600. https://doi.org/10.1016/j.cell.2011.01.015.
(117) Bárdy, P.; Füzik, T.; Hrebík, D.; Pantůček, R.; Thomas Beatty, J.; Plevka, P. Structure and Mechanism of DNA Delivery of a Gene Transfer Agent. *Nat. Commun.* **2020**, *11*, 3034. https://doi.org/10.1038/s41467-020-16669-9.
(118) Muteeb, G.; Kazi, R. N. A.; Aatif, M.; Azhar, A.; Oirdi, M. E.; Farhan, M. Antimicrobial Resistance: Linking Molecular Mechanisms to Public Health Impact. *SLAS Discov.* **2025**, *33*, 100232. https://doi.org/10.1016/j.slasd.2025.100232.
(119) Magiorakos, A.-P.; Srinivasan, A.; Carey, R. B.; Carmeli, Y.; Falagas, M. E.; Giske, C. G.; Harbarth, S.; Hindler, J. F.; Kahlmeter, G.; Olsson-Liljequist, B.; Paterson, D. L.; Rice, L. B.; Stelling, J.; Struelens, M. J.; Vatopoulos, A.; Weber, J. T.; Monnet, D. L. Multidrug-Resistant, Extensively Drug-Resistant and Pandrug-Resistant Bacteria: An International Expert Proposal for Interim Standard Definitions for Acquired Resistance. *Clin. Microbiol. Infect.* **2012**, *18* (3), 268–281. https://doi.org/10.1111/j.1469-0691.2011.03570.x.
(120) Preda, V. G.; Săndulescu, O. Communication Is the Key: Biofilms, Quorum Sensing, Formation and Prevention. *Discoveries* **2019**, *7* (3), e100. https://doi.org/10.15190/d.2019.13.
(121) Muhammad, M. H.; Idris, A. L.; Fan, X.; Guo, Y.; Yu, Y.; Jin, X.; Qiu, J.; Guan, X.; Huang, T. Beyond Risk: Bacterial Biofilms and Their Regulating Approaches. *Front. Microbiol.* **2020**, *11*. https://doi.org/10.3389/fmicb.2020.00928.
(122) Kragh, K. N.; Tolker-Nielsen, T.; Lichtenberg, M. The Non-Attached Biofilm Aggregate. *Commun. Biol.* **2023**, *6* (1), 898. https://doi.org/10.1038/s42003-023-05281-4.
(123) Nealson, K. H.; Platt, T.; Hastings, J. W. Cellular Control of the Synthesis and Activity of the Bacterial Luminescent System. *J. Bacteriol.* **1970**, *104* (1), 313–322. https://doi.org/10.1128/jb.104.1.313-322.1970.
(124) Verma, S. C.; Miyashiro, T. Quorum Sensing in the Squid-Vibrio Symbiosis. *Int. J. Mol. Sci.* **2013**, *14* (8), 16386–16401. https://doi.org/10.3390/ijms140816386.
(125) Markowska, K.; Szymanek-Majchrzak, K.; Pituch, H.; Majewska, A. Understanding Quorum-Sensing and Biofilm Forming in Anaerobic Bacterial Communities. *Int. J. Mol. Sci.* **2024**, *25* (23), 12808. https://doi.org/10.3390/ijms252312808.

(126) Kuo, A.; Blough, N. V.; Dunlap, P. V. Multiple N-Acyl-L-Homoserine Lactone Autoinducers of Luminescence in the Marine Symbiotic Bacterium Vibrio Fischeri. *J. Bacteriol.* **1994**, *176* (24), 7558–7565. https://doi.org/10.1128/jb.176.24.7558-7565.1994.

(127) Kumar, L.; Patel, S. K. S.; Kharga, K.; Kumar, R.; Kumar, P.; Pandohee, J.; Kulshresha, S.; Harjai, K.; Chhibber, S. Molecular Mechanisms and Applications of N-Acyl Homoserine Lactone-Mediated Quorum Sensing in Bacteria. *Molecules* **2022**, *27* (21), 7584. https://doi.org/10.3390/molecules27217584.

(128) Dragoš, A.; Kiesewalter, H.; Martin, M.; Hsu, C.-Y.; Hartmann, R.; Wechsler, T.; Eriksen, C.; Brix, S.; Drescher, K.; Stanley-Wall, N.; Kümmerli, R.; Kovács, Á. T. Division of Labor during Biofilm Matrix Production. *Curr. Biol.* **2018**, *28* (12), 1903-1913.e5. https://doi.org/10.1016/j.cub.2018.04.046.

(129) Sharma, S.; Mohler, J.; Mahajan, S. D.; Schwartz, S. A.; Bruggemann, L.; Aalinkeel, R. Microbial Biofilm: A Review on Formation, Infection, Antibiotic Resistance, Control Measures, and Innovative Treatment. *Microorganisms* **2023**, *11* (6), 1614. https://doi.org/10.3390/microorganisms11061614.

(130) Afrasiabi, S.; Partoazar, A. Targeting Bacterial Biofilm-Related Genes with Nanoparticle-Based Strategies. *Front. Microbiol.* **2024**, *15*. https://doi.org/10.3389/fmicb.2024.1387114.

(131) Sutherland, I. W. Biofilm Exopolysaccharides: A Strong and Sticky Framework. *Microbiology* **2001**, *147* (1), 3–9. https://doi.org/10.1099/00221287-147-1-3.

(132) Fong, J. N. C.; Yildiz, F. H. Biofilm Matrix Proteins. *Microbiol. Spectr.* **2015**, *3* (2), 10.1128/microbiolspec.mb-0004–2014. https://doi.org/10.1128/microbiolspec.mb-0004-2014.

(133) Okshevsky, M.; Meyer, R. L. The Role of Extracellular DNA in the Establishment, Maintenance and Perpetuation of Bacterial Biofilms. *Crit. Rev. Microbiol.* **2015**, *41* (3), 341–352. https://doi.org/10.3109/1040841X.2013.841639.

(134) Véscovi, E. G.; Ayala, Y. M.; Cera, E. D.; Groisman, E. A. Characterization of the Bacterial Sensor Protein PhoQ: Evidence for Distinct Binding Sites for Mg2+ And Ca2+. *J. Biol. Chem.* **1997**, *272* (3), 1440–1443. https://doi.org/10.1074/jbc.272.3.1440.

(135) Wimpenny, J.; Manz, W.; Szewzyk, U. Heterogeneity in Biofilms. *FEMS Microbiol. Rev.* **2000**, *24* (5), 661–671. https://doi.org/10.1016/S0168-6445(00)00052-8.

(136) Bridier, A.; Dubois-Brissonnet, F.; Boubetra, A.; Thomas, V.; Briandet, R. The Biofilm Architecture of Sixty Opportunistic Pathogens Deciphered Using a High Throughput CLSM Method. *J. Microbiol. Methods* **2010**, *82* (1), 64–70. https://doi.org/10.1016/j.mimet.2010.04.006.

(137) Guzmán-Soto, I.; McTiernan, C.; Gonzalez-Gomez, M.; Ross, A.; Gupta, K.; Suuronen, E. J.; Mah, T.-F.; Griffith, M.; Alarcon, E. I. Mimicking Biofilm Formation and Development: Recent Progress in in Vitro and in Vivo Biofilm Models. *iScience* **2021**, *24* (5). https://doi.org/10.1016/j.isci.2021.102443.

(138) Rather, M. A.; Gupta, K.; Mandal, M. Microbial Biofilm: Formation, Architecture, Antibiotic Resistance, and Control Strategies. *Braz. J. Microbiol.* **2021**, *52* (4), 1701–1718. https://doi.org/10.1007/s42770-021-00624-x.

(139) Jo, J.; Price-Whelan, A.; Dietrich, L. E. P. Gradients and Consequences of Heterogeneity in Biofilms. *Nat. Rev. Microbiol.* **2022**, *20* (10), 593–607. https://doi.org/10.1038/s41579-022-00692-2.

(140) Zhao, X.; Zhao, F.; Wang, J.; Zhong, N. Biofilm Formation and Control Strategies of Foodborne Pathogens: Food Safety Perspectives. *RSC Adv.* **2017**, *7* (58), 36670–36683. https://doi.org/10.1039/C7RA02497E.

(141) Dufour, D.; Leung, V.; Lévesque, C. M. Bacterial Biofilm: Structure, Function, and Antimicrobial Resistance. *Endod. Top.* **2010**, *22* (1), 2–16. https://doi.org/10.1111/j.1601-1546.2012.00277.x.

(142) Rabin, N.; Zheng, Y.; Opoku-Temeng, C.; Du, Y.; Bonsu, E.; Sintim, H. O. Biofilm Formation Mechanisms and Targets for Developing Antibiofilm Agents. *Future Med. Chem.* **2015**, *7* (4), 493–512. https://doi.org/10.4155/fmc.15.6.

(143) Jefferson, K. K. What Drives Bacteria to Produce a Biofilm? *FEMS Microbiol. Lett.* **2004**, *236* (2), 163–173. https://doi.org/10.1111/j.1574-6968.2004.tb09643.x.

(144) Zhao, A.; Sun, J.; Liu, Y. Understanding Bacterial Biofilms: From Definition to Treatment Strategies. *Front. Cell. Infect. Microbiol.* **2023**, *13*, 1137947. https://doi.org/10.3389/fcimb.2023.1137947.

(145) Sadiq, F. A.; Burmølle, M.; Heyndrickx, M.; Flint, S.; Lu, W.; Chen, W.; Zhao, J.; Zhang, H. Community-Wide Changes Reflecting Bacterial Interspecific Interactions in Multispecies Biofilms. *Crit. Rev. Microbiol.* **2021**, *47* (3), 338–358. https://doi.org/10.1080/1040841X.2021.1887079.

(146) Singh, S.; Singh, S. K.; Chowdhury, I.; Singh, R. Understanding the Mechanism of Bacterial Biofilms Resistance to Antimicrobial Agents. *Open Microbiol. J.* **2017**, *11*, 53–62. https://doi.org/10.2174/1874285801711010053.

(147) Sørensen, S. J.; Bailey, M.; Hansen, L. H.; Kroer, N.; Wuertz, S. Studying Plasmid Horizontal Transfer in Situ: A Critical Review. *Nat. Rev. Microbiol.* **2005**, *3* (9), 700–710. https://doi.org/10.1038/nrmicro1232.

(148) Madsen, J. S.; Burmølle, M.; Hansen, L. H.; Sørensen, S. J. The Interconnection between Biofilm Formation and Horizontal Gene Transfer. *FEMS Immunol. Med. Microbiol.* **2012**, *65* (2), 183–195. https://doi.org/10.1111/j.1574-695X.2012.00960.x.

(149) Fan, Y.; Xiao, Y.; Momeni, B.; Liu, Y.-Y. Horizontal Gene Transfer Can Help Maintain the Equilibrium of Microbial Communities. *J. Theor. Biol.* **2018**, *454*, 53–59. https://doi.org/10.1016/j.jtbi.2018.05.036.

(150) Sharma, D. K.; Rajpurohit, Y. S. Multitasking Functions of Bacterial Extracellular DNA in Biofilms. *J. Bacteriol.* **2024**, *206* (4), e00006-24. https://doi.org/10.1128/jb.00006-24.

(151) Chiang, W.-C.; Nilsson, M.; Jensen, P. Ø.; Høiby, N.; Nielsen, T. E.; Givskov, M.; Tolker-Nielsen, T. Extracellular DNA Shields against Aminoglycosides in Pseudomonas Aeruginosa Biofilms. *Antimicrob. Agents Chemother.* **2013**, *57* (5), 2352–2361. https://doi.org/10.1128/aac.00001-13.

(152) Lewis, K. Riddle of Biofilm Resistance. *Antimicrob. Agents Chemother.* **2001**, *45* (4), 999–1007. https://doi.org/10.1128/aac.45.4.999-1007.2001.

(153) Giwercman, B.; Jensen, E. T.; Høiby, N.; Kharazmi, A.; Costerton, J. W. Induction of Beta-Lactamase Production in Pseudomonas Aeruginosa Biofilm. *Antimicrob. Agents Chemother.* **1991**, *35* (5), 1008–1010. https://doi.org/10.1128/aac.35.5.1008.

(154) Walters, M. C.; Roe, F.; Bugnicourt, A.; Franklin, M. J.; Stewart, P. S. Contributions of Antibiotic Penetration, Oxygen Limitation, and Low Metabolic Activity to Tolerance of Pseudomonas Aeruginosa Biofilms to Ciprofloxacin and Tobramycin. *Antimicrob. Agents Chemother.* **2003**, *47* (1), 317–323. https://doi.org/10.1128/aac.47.1.317-323.2003.

(155) Harms, A.; Maisonneuve, E.; Gerdes, K. Mechanisms of Bacterial Persistence during Stress and Antibiotic Exposure. *Science* **2016**, *354* (6318), aaf4268. https://doi.org/10.1126/science.aaf4268.

(156) Fauvart, M.; De Groote, V. N.; Michiels, J. Role of Persister Cells in Chronic Infections: Clinical Relevance and Perspectives on Anti-Persister Therapies. *J. Med. Microbiol.* **2011**, *60* (6), 699–709. https://doi.org/10.1099/jmm.0.030932-0.

(157) Fleming, D.; Rumbaugh, K. P. Approaches to Dispersing Medical Biofilms. *Microorganisms* **2017**, *5* (2), 15. https://doi.org/10.3390/microorganisms5020015.

(158) Mah, T.-F. C.; O'Toole, G. A. Mechanisms of Biofilm Resistance to Antimicrobial Agents. *Trends Microbiol.* **2001**, *9* (1), 34–39. https://doi.org/10.1016/S0966-842X(00)01913-2.

(159) Ali, A.; Zahra, A.; Kamthan, M.; Husain, F. M.; Albalawi, T.; Zubair, M.; Alatawy, R.; Abid, M.; Noorani, M. S. Microbial Biofilms: Applications, Clinical Consequences, and Alternative Therapies. *Microorganisms* **2023**, *11* (8), 1934. https://doi.org/10.3390/microorganisms11081934.

(160) Bhagirath, A. Y.; Li, Y.; Somayajula, D.; Dadashi, M.; Badr, S.; Duan, K. Cystic Fibrosis Lung Environment and Pseudomonas Aeruginosa Infection. *BMC Pulm. Med.* **2016**, *16* (1), 174. https://doi.org/10.1186/s12890-016-0339-5.

(161) Linares, J. F.; Gustafsson, I.; Baquero, F.; Martinez, J. L. Antibiotics as Intermicrobial Signaling Agents Instead of Weapons. *Proc. Natl. Acad. Sci.* **2006**, *103* (51), 19484–19489. https://doi.org/10.1073/pnas.0608949103.

(162) Wu, Y.-K.; Cheng, N.-C.; Cheng, C.-M. Biofilms in Chronic Wounds: Pathogenesis and Diagnosis. *Trends Biotechnol.* **2019**, *37* (5), 505–517. https://doi.org/10.1016/j.tibtech.2018.10.011.

(163) Mustoe, T. Understanding Chronic Wounds: A Unifying Hypothesis on Their Pathogenesis and Implications for Therapy. *Am. J. Surg.* **2004**, *187* (5), S65–S70. https://doi.org/10.1016/S0002-9610(03)00306-4.

(164) Cavallo, I.; Sivori, F.; Mastrofrancesco, A.; Abril, E.; Pontone, M.; Di Domenico, E. G.; Pimpinelli, F. Bacterial Biofilm in Chronic Wounds and Possible Therapeutic Approaches. *Biology* **2024**, *13* (2), 109. https://doi.org/10.3390/biology13020109.

(165) Verbanic, S.; Shen, Y.; Lee, J.; Deacon, J. M.; Chen, I. A. Microbial Predictors of Healing and Short-Term Effect of Debridement on the Microbiome of Chronic Wounds. *Npj Biofilms Microbiomes* **2020**, *6* (1), 21. https://doi.org/10.1038/s41522-020-0130-5.

(166) Yallowitz, A. W.; Decker, L. C. Infectious Endocarditis. In *StatPearls*; StatPearls Publishing: Treasure Island (FL), 2025.

(167) Elgharably, H.; Hussain, S. T.; Shrestha, N. K.; Blackstone, E. H.; Pettersson, G. B. Current Hypotheses in Cardiac Surgery: Biofilm in Infective Endocarditis. *Semin. Thorac. Cardiovasc. Surg.* **2016**, *28* (1), 56–59. https://doi.org/10.1053/j.semtcvs.2015.12.005.

(168) Cremieux, A.-C.; Maziere, B.; Vallois, J.-M.; Ottaviani, M.; Azancot, A.; Raffoul, H.; Bouvet, A.; Pocidalo, J.-J.; Carbon, C. Evaluation of Antibiotic Diffusion into Cardiac Vegetations by Quantitative Autoradiography. *J. Infect. Dis.* **1989**, *159* (5), 938–944. https://doi.org/10.1093/infdis/159.5.938.

(169) Parsek, M. R.; Singh, P. K. Bacterial Biofilms: An Emerging Link to Disease Pathogenesis. *Annu. Rev. Microbiol.* **2003**, *57* (Volume 57, 2003), 677–701. https://doi.org/10.1146/annurev.micro.57.030502.090720.

(170) Arciola, C. R.; Campoccia, D.; Montanaro, L. Implant Infections: Adhesion, Biofilm Formation and Immune Evasion. *Nat. Rev. Microbiol.* **2018**, *16* (7), 397–409. https://doi.org/10.1038/s41579-018-0019-y.

(171) Lila, A. S. A.; Rajab, A. A. H.; Abdallah, M. H.; Rizvi, S. M. D.; Moin, A.; Khafagy, E.-S.; Tabrez, S.; Hegazy, W. A. H. Biofilm Lifestyle in Recurrent Urinary Tract Infections. *Life* **2023**, *13* (1), 148. https://doi.org/10.3390/life13010148.

(172) Delcaru, C.; Alexandru, I.; Podgoreanu, P.; Grosu, M.; Stavropoulos, E.; Chifiriuc, M. C.; Lazar, V. Microbial Biofilms in Urinary Tract Infections and Prostatitis: Etiology, Pathogenicity, and Combating Strategies. *Pathogens* **2016**, *5* (4), 65. https://doi.org/10.3390/pathogens5040065.

(173) Flores-Mireles, A. L.; Walker, J. N.; Bauman, T. M.; Potretzke, A. M.; Schreiber, H. L.; Park, A. M.; Pinkner, J. S.; Caparon, M. G.; Hultgren, S. J.; Desai, A. Fibrinogen Release and Deposition on Urinary Catheters Placed during Urological Procedures. *J. Urol.* **2016**, *196* (2), 416–421. https://doi.org/10.1016/j.juro.2016.01.100.

(174) Khatoon, Z.; McTiernan, C. D.; Suuronen, E. J.; Mah, T.-F.; Alarcon, E. I. Bacterial Biofilm Formation on Implantable Devices and Approaches to Its Treatment and Prevention. *Heliyon* **2018**, *4* (12). https://doi.org/10.1016/j.heliyon.2018.e01067.

(175) Kafazi, A.; Apostolopoulou, E.; Andreou, E.; Gavala, A.; Stefanidis, E.; Antwniadou, F.; Stylianou, C.; Katsoulas, T.; Myrianthefs, P. Device-Associated Infections in Adult Intensive Care Units: A Prospective Surveillance Study. *Acta Microbiol. Hell.* **2025**, *70* (2), 15. https://doi.org/10.3390/amh70020015.

(176) Rosenthal, V. D.; Yin, R.; Nercelles, P.; Rivera-Molina, S. E.; Jyoti, S.; Dongol, R.; Aguilar-De-Moros, D.; Tumu, N.; Alarcon-Rua, J.; Stagnaro, J. P.; Alkhawaja, S.; Jimenez-Alvarez, L. F.; Cano-Medina, Y. A.; Valderrama-Beltran, S. L.; Henao-Rodas, C. M.; Zuniga-Chavarria, M. A.; El-Kholy, A.; Agha, H. M.; Sahu, S.; Anusandhan, S. O.; Bhattacharyya, M.; Kharbanda, M.; Poojary, A.; Nair, P. K.; Myatra, S. N.; Chawla, R.; Sandhu, K.; Mehta, Y.; Rajhans, P.; Zand, F.; Abdellatif-Daboor, M.; Tai, C.-W.; Gan, C. S.; Nor, M.-B. M.; Aguirre-Avalos, G.; Hernandez-Chena, B. E.; Sassoe-Gonzalez, A.; Villegas-Mota, I.; Bocanegra, M. C. A.-; Bat-Erdene, I.; Carreazo, N. Y.; Castaneda-Sabogal, A.; Janc, J.; Belskiy, V.; Hlinkova, S.; Yildizdas, D.; Havan, M.; Koker, A.; Sungurtekin, H.; Dinleyici, E. C.; Guclu, E.; Tao, L.; Memish, Z. A.; Jin, Z. International Nosocomial Infection Control Consortium (INICC) Report of Health Care Associated Infections, Data Summary of 45 Countries for 2015 to 2020, Adult and Pediatric Units, Device-Associated Module. *Am. J. Infect. Control* **2024**, *52* (9), 1002–1011. https://doi.org/10.1016/j.ajic.2023.12.019.

(177) Reportlinker. *Global Implantable Biomaterials Market Outlook (2014-2022) - Reportlinker Review*. https://www.prnewswire.com/news-releases/global-implantable-biomaterials-market-outlook-2014-2022---reportlinker-review-300148728.html (accessed 2025-12-31).

(178) McConoughey, S. J.; Howlin, R.; Granger, J. F.; Manring, M. M.; Calhoun, J. H.; Shirtlif, M.; Kathju, S.; Stoodley, P. Biofilms in Periprosthetic Orthopedic Infections. *Future Microbiol.* **2014**, *9* (8), 987–1007. https://doi.org/10.2217/fmb.14.64.

(179) Knott, S.; Curry, D.; Zhao, N.; Metgud, P.; Dastgheyb, S. S.; Purtill, C.; Harwood, M.; Chen, A. F.; Schaer, T. P.; Otto, M.; Hickok, N. J. Staphylococcus Aureus Floating Biofilm Formation and Phenotype in Synovial Fluid Depends on Albumin, Fibrinogen, and Hyaluronic Acid. *Front. Microbiol.* **2021**, *12*. https://doi.org/10.3389/fmicb.2021.655873.

(180) De Bleeckere, A.; van Charante, F.; Debord, T.; Vandendriessche, S.; De Cock, M.; Verstraete, M.; Lamret, F.; Lories, B.; Boelens, J.; Reffuveille, F.; Steenackers, H. P.; Coenye, T. A Novel Synthetic Synovial Fluid Model for Investigating Biofilm Formation and Antibiotic Susceptibility in Prosthetic Joint Infections. *Microbiol. Spectr.* **2024**, *13* (1), e01980-24. https://doi.org/10.1128/spectrum.01980-24.

(181) Lee, S. W.; Gu, H.; Kilberg, J. B.; Ren, D. Sensitizing Bacterial Cells to Antibiotics by Shape Recovery Triggered Biofilm Dispersion. *Acta Biomater.* **2018**, *81*, 93–102. https://doi.org/10.1016/j.actbio.2018.09.042.

(182) Zhang, K.; Li, X.; Yu, C.; Wang, Y. Promising Therapeutic Strategies Against Microbial Biofilm Challenges. *Front. Cell. Infect. Microbiol.* **2020**, *10*. https://doi.org/10.3389/fcimb.2020.00359.

(183) Bari, A. K.; Belalekar, T. S.; Poojary, A.; Rohra, S. Combination Drug Strategies for Biofilm Eradication Using Synthetic and Natural Agents in KAPE Pathogens. *Front. Cell. Infect. Microbiol.* **2023**, *13*, 1155699. https://doi.org/10.3389/fcimb.2023.1155699.

(184) Kemnic, T. R.; Coleman, M. Trimethoprim Sulfamethoxazole. In *StatPearls*; StatPearls Publishing: Treasure Island (FL), 2025.

(185) Andrade, F. F.; Silva, D.; Rodrigues, A.; Pina-Vaz, C. Colistin Update on Its Mechanism of Action and Resistance, Present and Future Challenges. *Microorganisms* **2020**, *8* (11), 1716. https://doi.org/10.3390/microorganisms8111716.

(186) Petrosillo, N.; Taglietti, F.; Granata, G. Treatment Options for Colistin Resistant Klebsiella Pneumoniae: Present and Future. *J. Clin. Med.* **2019**, *8* (7), 934. https://doi.org/10.3390/jcm8070934.

(187) Capone, A.; Giannella, M.; Fortini, D.; Giordano, A.; Meledandri, M.; Ballardini, M.; Venditti, M.; Bordi, E.; Capozzi, D.; Balice, M. P.; Tarasi, A.; Parisi, G.; Lappa, A.; Carattoli, A.; Petrosillo, N. High Rate of Colistin Resistance among Patients with Carbapenem-Resistant Klebsiella Pneumoniae Infection Accounts for an Excess of Mortality. *Clin. Microbiol. Infect.* **2013**, *19* (1), E23–E30. https://doi.org/10.1111/1469-0691.12070.

(188) Finnegan, S.; Percival, S. L. EDTA: An Antimicrobial and Antibiofilm Agent for Use in Wound Care. *Adv. Wound Care* **2015**, *4* (7), 415–421. https://doi.org/10.1089/wound.2014.0577.
(189) Shein, A. M. S.; Wannigama, D. L.; Higgins, P. G.; Hurst, C.; Abe, S.; Hongsing, P.; Chantaravisoot, N.; Saethang, T.; Luk-in, S.; Liao, T.; Nilgate, S.; Rirerm, U.; Kueakulpattana, N.; Laowansiri, M.; Srisakul, S.; Muhummudaree, N.; Techawiwattanaboon, T.; Gan, L.; Xu, C.; Kupwiwat, R.; Phattharapornjaroen, P.; Rojanathanes, R.; Leelahavanichkul, A.; Chatsuwan, T. Novel Colistin-EDTA Combination for Successful Eradication of Colistin-Resistant Klebsiella Pneumoniae Catheter-Related Biofilm Infections. *Sci. Rep.* **2021**, *11* (1), 21676. https://doi.org/10.1038/s41598-021-01052-5.
(190) Nyhoegen, C.; Bonhoeffer, S.; Uecker, H. The Many Dimensions of Combination Therapy: How to Combine Antibiotics to Limit Resistance Evolution. *Evol. Appl.* **2024**, *17* (8), e13764. https://doi.org/10.1111/eva.13764.
(191) Miller, A.; Nasir, M.; Bou-Akl, T.; Pawlitz, P.; Markel, D. C. Efficacy of Commercially Available Irrigation Solutions on Removal of Biofilms Grown on Porous Titanium Implants: An *In Vitro* Study. *J. Arthroplasty* **2025**, 1–6. https://doi.org/10.1016/j.arth.2025.10.041.
(192) Ousey, K.; Ovens, L. Comparing Methods of Debridement for Removing Biofilm in Hard-to-Heal Wounds. *J. Wound Care* **2023**, *32* (Sup3b), S4–S10. https://doi.org/10.12968/jowc.2023.32.Sup3b.S4.
(193) Rodríguez-Merchán, E. C.; Davidson, D. J.; Liddle, A. D. Recent Strategies to Combat Infections from Biofilm-Forming Bacteria on Orthopaedic Implants. *Int. J. Mol. Sci.* **2021**, *22* (19), 10243. https://doi.org/10.3390/ijms221910243.
(194) Chen, X.; Zhou, J.; Qian, Y.; Zhao, L. Antibacterial Coatings on Orthopedic Implants. *Mater. Today Bio* **2023**, *19*, 100586. https://doi.org/10.1016/j.mtbio.2023.100586.
(195) Lorenzo-Gómez, M.-F.; Foley, S.; Nickel, J. C.; García-Cenador, M.-B.; Padilla-Fernández, B.-Y.; González-Casado, I.; Martínez-Huélamo, M.; Yang, B.; Blick, C.; Ferreira, F.; Caballero, R.; Saz-Leal, P.; Casanovas, M. Sublingual MV140 for Prevention of Recurrent Urinary Tract Infections. *NEJM Evid.* **2022**, *1* (4), EVIDoa2100018. https://doi.org/10.1056/EVIDoa2100018.
(196) Sevilla, C. R.; Lanza, E. G.; Manzanera, J. L.; Herrando, A. C.; Pallàs, J. M. P. A Focus on Long-Term Follow-Up of Immunoprophylaxis to Recurrent Urinary Tract Infections: 10 Years of Experience with MV140 Vaccine in a Cohort of 1003 Patients Support High Efficacy and Safety. *Arch. Esp. Urol.* **2022**, *75* (9), 753–757. https://doi.org/10.56434/j.arch.esp.urol.20227509.110.
(197) Kanabar, S.; Foley, S. J.; Yang, B. Pd63-01 Evaluating the Safety and Effectiveness of Uromune® Bacterial Vaccine over a 9-Year Period in the Uk: A Study on Managing Recurrent Urinary Tract Infections in Men and Women in the Initial Cohort. *J. Urol.* **2024**, *211* (5S), e1292. https://doi.org/10.1097/01.JU.0001009384.23104.ca.01.
(198) Eker, F.; Duman, H.; Akdaşçi, E.; Bolat, E.; Sarıtaş, S.; Karav, S.; Witkowska, A. M. A Comprehensive Review of Nanoparticles: From Classification to Application and Toxicity. *Molecules* **2024**, *29* (15), 3482. https://doi.org/10.3390/molecules29153482.
(199) Zhang, Y.; Lin, S.; Fu, J.; Zhang, W.; Shu, G.; Lin, J.; Li, H.; Xu, F.; Tang, H.; Peng, G.; Zhao, L.; Chen, S.; Fu, H. Nanocarriers for Combating Biofilms: Advantages and Challenges. *J. Appl. Microbiol.* **2022**, *133* (3), 1273–1287. https://doi.org/10.1111/jam.15640.
(200) Shkodenko, L.; Kassirov, I.; Koshel, E. Metal Oxide Nanoparticles Against Bacterial Biofilms: Perspectives and Limitations. *Microorganisms* **2020**, *8* (10), 1545. https://doi.org/10.3390/microorganisms8101545.
(201) Joshi, A. A.; Patil, R. H. Nanoparticles Targeting Biofilms: A New Era in Combating Antimicrobial Resistance. *Med. Microecol.* **2025**, *26*, 100156. https://doi.org/10.1016/j.medmic.2025.100156.
(202) Aflakian, F.; Hashemitabar, G. Biosynthesized Silver Nanoparticles at Subinhibitory Concentrations as Inhibitors of Quorum Sensing, Pathogenicity, and Biofilm Formation in

Pseudomonas Aeruginosa PAO1. *Heliyon* **2025**, *11* (4), e42899. https://doi.org/10.1016/j.heliyon.2025.e42899.

(203) Rai, M. k.; Deshmukh, S. d.; Ingle, A. p.; Gade, A. k. Silver Nanoparticles: The Powerful Nanoweapon against Multidrug-Resistant Bacteria. *J. Appl. Microbiol.* **2012**, *112* (5), 841–852. https://doi.org/10.1111/j.1365-2672.2012.05253.x.

(204) Pontes, J. T. C. de; Toledo Borges, A. B.; Roque-Borda, C. A.; Pavan, F. R. Antimicrobial Peptides as an Alternative for the Eradication of Bacterial Biofilms of Multi-Drug Resistant Bacteria. *Pharmaceutics* **2022**, *14* (3), 642. https://doi.org/10.3390/pharmaceutics14030642.

(205) Yasir, M.; Willcox, M. D. P.; Dutta, D. Action of Antimicrobial Peptides against Bacterial Biofilms. *Materials* **2018**, *11* (12), 2468. https://doi.org/10.3390/ma11122468.

(206) Pulido, D.; Nogués, M. V.; Boix, E.; Torrent, M. Lipopolysaccharide Neutralization by Antimicrobial Peptides: A Gambit in the Innate Host Defense Strategy. *J. Innate Immun.* **2012**, *4* (4), 327–336. https://doi.org/10.1159/000336713.

(207) Peng, J.; Long, H.; Liu, W.; Wu, Z.; Wang, T.; Zeng, Z.; Guo, G.; Wu, J. Antibacterial Mechanism of Peptide Cec4 against *Acinetobacter Baumannii*. *Infect. Drug Resist.* **2019**, *12*, 2417–2428. https://doi.org/10.2147/IDR.S214057.

(208) Overhage, J.; Campisano, A.; Bains, M.; Torfs, E. C. W.; Rehm, B. H. A.; Hancock, R. E. W. Human Host Defense Peptide LL-37 Prevents Bacterial Biofilm Formation. *Infect. Immun.* **2008**, *76* (9), 4176–4182. https://doi.org/10.1128/iai.00318-08.

(209) de la Fuente-Núñez, C.; Reffuveille, F.; Mansour, S. C.; Reckseidler-Zenteno, S. L.; Hernández, D.; Brackman, G.; Coenye, T.; Hancock, R. E. W. D-Enantiomeric Peptides That Eradicate Wild-Type and Multidrug-Resistant Biofilms and Protect against Lethal *Pseudomonas Aeruginosa* Infections. *Chem. Biol.* **2015**, *22* (2), 196–205. https://doi.org/10.1016/j.chembiol.2015.01.002.

(210) Gordya, N.; Yakovlev, A.; Kruglikova, A.; Tulin, D.; Potolitsina, E.; Suborova, T.; Bordo, D.; Rosano, C.; Chernysh, S. Natural Antimicrobial Peptide Complexes in the Fighting of Antibiotic Resistant Biofilms: Calliphora Vicina Medicinal Maggots. *PLoS ONE* **2017**, *12* (3), e0173559. https://doi.org/10.1371/journal.pone.0173559.

(211) Peláez Coyotl, E. A.; Barrios Palacios, J.; Muciño, G.; Moreno-Blas, D.; Costas, M.; Montiel Montes, T.; Diener, C.; Uribe-Carvajal, S.; Massieu, L.; Castro-Obregón, S.; Espinosa, O. R.; Mata Espinosa, D.; Barrios-Payan, J.; León Contreras, J. C.; Corzo, G.; Hernández-Pando, R.; Del Rio, G. Antimicrobial Peptide against Mycobacterium Tuberculosis That Activates Autophagy Is an Effective Treatment for Tuberculosis. *Pharmaceutics* **2020**, *12* (11), 1071. https://doi.org/10.3390/pharmaceutics12111071.

(212) Campos, J. V.; Pontes, J. T. C.; Canales, C. S. C.; Roque-Borda, C. A.; Pavan, F. R. Advancing Nanotechnology: Targeting Biofilm-Forming Bacteria with Antimicrobial Peptides. *BME Front.* **2025**, *6*, 0104. https://doi.org/10.34133/bmef.0104.

(213) Carrera, E. T.; Dias, H. B.; Corbi, S. C. T.; Marcantonio, R. A. C.; Bernardi, A. C. A.; Bagnato, V. S.; Hamblin, M. R.; Rastelli, A. N. S. The Application of Antimicrobial Photodynamic Therapy (aPDT) in Dentistry: A Critical Review. *Laser Phys.* **2016**, *26* (12), 123001. https://doi.org/10.1088/1054-660X/26/12/123001.

(214) Qi, M.; Chi, M.; Sun, X.; Xie, X.; Weir, M. D.; Oates, T. W.; Zhou, Y.; Wang, L.; Bai, Y.; Xu, H. H. Novel Nanomaterial-Based Antibacterial Photodynamic Therapies to Combat Oral Bacterial Biofilms and Infectious Diseases. *Int. J. Nanomedicine* **2019**, *14*, 6937–6956. https://doi.org/10.2147/IJN.S212807.

(215) Osman, A.-H.; Darkwah, S.; Kotey, F. C. N.; Asante-Poku, A.; Donkor, E. S. Lytic Bacteriophages as Alternative to Overcoming Antibiotic-Resistant Biofilms Formed by Clinically Significant Bacteria. *Ther. Adv. Infect. Dis.* **2025**, *12*, 20499361251356057. https://doi.org/10.1177/20499361251356057.

(216) Chan, B. K.; Abedon, S. T.; Loc-Carrillo, C. Phage Cocktails and the Future of Phage Therapy. *Future Microbiol.* **2013**, *8* (6), 769–783. https://doi.org/10.2217/fmb.13.47.
(217) Henriksen, K.; Rørbo, N.; Rybtke, M. L.; Martinet, M. G.; Tolker-Nielsen, T.; Høiby, N.; Middelboe, M.; Ciofu, O. P. Aeruginosa Flow-Cell Biofilms Are Enhanced by Repeated Phage Treatments but Can Be Eradicated by Phage–Ciprofloxacin Combination: —Monitoring the Phage–P. Aeruginosa Biofilms Interactions. *Pathog. Dis.* **2019**, *77* (2), ftz011. https://doi.org/10.1093/femspd/ftz011.
(218) Akturk, E.; Melo, L. D. R.; Oliveira, H.; Crabbé, A.; Coenye, T.; Azeredo, J. Combining Phages and Antibiotic to Enhance Antibiofilm Efficacy against an *in Vitro* Dual Species Wound Biofilm. *Biofilm* **2023**, *6*, 100147. https://doi.org/10.1016/j.bioflm.2023.100147.
(219) Łusiak-Szelachowska, M.; Weber-Dąbrowska, B.; Górski, A. Bacteriophages and Lysins in Biofilm Control. *Virol. Sin.* **2020**, *35* (2), 125–133. https://doi.org/10.1007/s12250-019-00192-3.
(220) Al-Madboly, L. A.; Aboulmagd, A.; El-Salam, M. A.; Kushkevych, I.; El-Morsi, R. M. Microbial Enzymes as Powerful Natural Anti-Biofilm Candidates. *Microb. Cell Factories* **2024**, *23* (1), 343. https://doi.org/10.1186/s12934-024-02610-y.
(221) Wang, S.; Zhao, Y.; Breslawec, A. P.; Liang, T.; Deng, Z.; Kuperman, L. L.; Yu, Q. Strategy to Combat Biofilms: A Focus on Biofilm Dispersal Enzymes. *Npj Biofilms Microbiomes* **2023**, *9* (1), 63. https://doi.org/10.1038/s41522-023-00427-y.
(222) Redman, W. K.; Welch, G. S.; Williams, A. C.; Damron, A. J.; Northcut, W. O.; Rumbaugh, K. P. Efficacy and Safety of Biofilm Dispersal by Glycoside Hydrolases in Wounds. *Biofilm* **2021**, *3*, 100061. https://doi.org/10.1016/j.bioflm.2021.100061.
(223) Vaikundamoorthy, R.; Rajendran, R.; Selvaraju, A.; Moorthy, K.; Perumal, S. Development of Thermostable Amylase Enzyme from *Bacillus Cereus* for Potential Antibiofilm Activity. *Bioorganic Chem.* **2018**, *77*, 494–506. https://doi.org/10.1016/j.bioorg.2018.02.014.
(224) Sujith, S.; Solomon, A. P.; Rayappan, J. B. B. Comprehensive Insights into UTIs: From Pathophysiology to Precision Diagnosis and Management. *Front. Cell. Infect. Microbiol.* **2024**, *14*, 1402941. https://doi.org/10.3389/fcimb.2024.1402941.
(225) Zeng, Z.; Zhan, J.; Zhang, K.; Chen, H.; Cheng, S. Global, Regional, and National Burden of Urinary Tract Infections from 1990 to 2019: An Analysis of the Global Burden of Disease Study 2019. *World J. Urol.* **2022**, *40* (3), 755–763. https://doi.org/10.1007/s00345-021-03913-0.
(226) He, Y.; Zhao, J.; Wang, L.; Han, C.; Yan, R.; Zhu, P.; Qian, T.; Yu, S.; Zhu, X.; He, W. Epidemiological Trends and Predictions of Urinary Tract Infections in the Global Burden of Disease Study 2021. *Sci. Rep.* **2025**, *15* (1), 4702. https://doi.org/10.1038/s41598-025-89240-5.
(227) NHS England. *New awareness campaign to help reduce hospital admissions for urinary tract infections*. https://www.england.nhs.uk/2023/10/new-awareness-campaign-to-help-reduce-hospital-admissions-for-urinary-tract-infections/ (accessed 2026-04-14).
(228) UKHSA. *Understanding the burden of UTI hospitalisations in England*. GOV.UK. https://www.gov.uk/government/publications/understanding-the-burden-of-uti-hospitalisations-in-england/understanding-the-burden-of-uti-hospitalisations-in-england (accessed 2025-11-26).
(229) Ernstmeyer, K. Chapter 8 Renal and Urinary System Alterations. In *Health Alterations [Internet]*; Chippewa Valley Technical College, 2024.
(230) Lacerda Mariano, L.; Ingersoll, M. A. The Immune Response to Infection in the Bladder. *Nat. Rev. Urol.* **2020**, *17* (8), 439–458. https://doi.org/10.1038/s41585-020-0350-8.
(231) Hou, Y.; Lv, Z.; Hu, Q.; Zhu, A.; Niu, H. The Immune Mechanisms of the Urinary Tract against Infections. *Front. Cell. Infect. Microbiol.* **2025**, *15*. https://doi.org/10.3389/fcimb.2025.1540149.
(232) Mancuso, G.; Midiri, A.; Gerace, E.; Marra, M.; Zummo, S.; Biondo, C. Urinary Tract Infections: The Current Scenario and Future Prospects. *Pathogens* **2023**, *12* (4), 623. https://doi.org/10.3390/pathogens12040623.

(233) Bonkat, G.; Wagenlehner, F.; Cai, T.; Geerlings, S.; Medina-Polo, J.; Köves, B.; Pilatz, A.; Schneidewind, L.; Schubert, S.; Veeratterapillay, R.; Bausch, K.; Devlies, W.; Leitner, L.; Mantica, G.; Stangl, F. P.; Kranz, J. Classification of Urinary Tract Infections in 2025: Moving Beyond Uncomplicated and Complicated. *Eur. Urol. Open Sci.* **2025**, *75*, 44–47. https://doi.org/10.1016/j.euros.2025.03.010.

(234) Flores-Mireles, A. L.; Walker, J. N.; Caparon, M.; Hultgren, S. J. Urinary Tract Infections: Epidemiology, Mechanisms of Infection and Treatment Options. *Nat. Rev. Microbiol.* **2015**, *13* (5), 269–284. https://doi.org/10.1038/nrmicro3432.

(235) Medina, M.; Castillo-Pino, E. An Introduction to the Epidemiology and Burden of Urinary Tract Infections. *Ther. Adv. Urol.* **2019**, *11*, 1756287219832172. https://doi.org/10.1177/1756287219832172.

(236) Griebling, T. L. Urologic Diseases in America Project: Trends in Resource Use for Urinary Tract Infections in Men. *J. Urol.* **2005**, *173* (4), 1288–1294. https://doi.org/10.1097/01.ju.0000155595.98120.8e.

(237) Aggarwal, N.; Leslie, S. W. Recurrent Urinary Tract Infections. In *StatPearls*; StatPearls Publishing: Treasure Island (FL), 2025.

(238) Aydin, A.; Ahmed, K.; Zaman, I.; Khan, M. S.; Dasgupta, P. Recurrent Urinary Tract Infections in Women. *Int. Urogynecology J.* **2015**, *26* (6), 795–804. https://doi.org/10.1007/s00192-014-2569-5.

(239) Sgarabotto, D.; Andretta, E.; Sgarabotto, C. Recurrent Urinary Tract Infections (UTIs): A Review and Proposal for Clinicians. *Antibiotics* **2025**, *14* (1), 22. https://doi.org/10.3390/antibiotics14010022.

(240) Swatesutipun, V. Can Recurrent UTIs in Women Be Cured? Review Article. *Cont. Rep.* **2023**, *5*, 100021. https://doi.org/10.1016/j.contre.2023.100021.

(241) Dudzik, Ł.; Krzyżek, P.; Dworniczek, E. A Review on the Current and Future State of Urinary Tract Infection Diagnostics. *Int. J. Mol. Sci.* **2025**, *26* (22), 10847. https://doi.org/10.3390/ijms262210847.

(242) Cortes-Penfield, N. W.; Trautner, B. W.; Jump, R. L. P. Urinary Tract Infection and Asymptomatic Bacteriuria in Older Adults. *Infect. Dis. Clin. North Am.* **2017**, *31* (4), 673–688. https://doi.org/10.1016/j.idc.2017.07.002.

(243) Kaur, R.; Kaur, R. Symptoms, Risk Factors, Diagnosis and Treatment of Urinary Tract Infections. *Postgrad. Med. J.* **2021**, *97* (1154), 803–812. https://doi.org/10.1136/postgradmedj-2020-139090.

(244) Shah, C.; Baral, R.; Bartaula, B.; Shrestha, L. B. Virulence Factors of Uropathogenic Escherichia Coli (UPEC) and Correlation with Antimicrobial Resistance. *BMC Microbiol.* **2019**, *19* (1), 204. https://doi.org/10.1186/s12866-019-1587-3.

(245) Bien, J.; Sokolova, O.; Bozko, P. Role of Uropathogenic Escherichia Coli Virulence Factors in Development of Urinary Tract Infection and Kidney Damage. *Int. J. Nephrol.* **2012**, *2012*, 681473. https://doi.org/10.1155/2012/681473.

(246) Zhao, F.; Yang, H.; Bi, D.; Khaledi, A.; Qiao, M. A Systematic Review and Meta-Analysis of Antibiotic Resistance Patterns, and the Correlation between Biofilm Formation with Virulence Factors in Uropathogenic *E. Coli* Isolated from Urinary Tract Infections. *Microb. Pathog.* **2020**, *144*, 104196. https://doi.org/10.1016/j.micpath.2020.104196.

(247) Naziri, Z.; Kilegolan, J. A.; Moezzi, M. S.; Derakhshandeh, A. Biofilm Formation by Uropathogenic Escherichia Coli: A Complicating Factor for Treatment and Recurrence of Urinary Tract Infections. *J. Hosp. Infect.* **2021**, *117*, 9–16. https://doi.org/10.1016/j.jhin.2021.08.017.

(248) Ramírez Castillo, F. Y.; Guerrero Barrera, A. L.; Harel, J.; Avelar González, F. J.; Vogeleer, P.; Arreola Guerra, J. M.; González Gámez, M. Biofilm Formation by Escherichia Coli Isolated from Urinary Tract Infections from Aguascalientes, Mexico. *Microorganisms* **2023**, *11* (12), 2858. https://doi.org/10.3390/microorganisms11122858.

(249) Lila, A. S. A.; Rajab, A. A. H.; Abdallah, M. H.; Rizvi, S. M. D.; Moin, A.; Khafagy, E.-S.; Tabrez, S.; Hegazy, W. A. H. Biofilm Lifestyle in Recurrent Urinary Tract Infections. *Life* **2023**, *13* (1), 148. https://doi.org/10.3390/life13010148.

(250) Uruén, C.; Chopo-Escuin, G.; Tommassen, J.; Mainar-Jaime, R. C.; Arenas, J. Biofilms as Promoters of Bacterial Antibiotic Resistance and Tolerance. *Antibiotics* **2021**, *10* (1), 3. https://doi.org/10.3390/antibiotics10010003.

(251) Delcaru, C.; Alexandru, I.; Podgoreanu, P.; Grosu, M.; Stavropoulos, E.; Chifiriuc, M. C.; Lazar, V. Microbial Biofilms in Urinary Tract Infections and Prostatitis: Etiology, Pathogenicity, and Combating Strategies. *Pathogens* **2016**, *5* (4), 65. https://doi.org/10.3390/pathogens5040065.

(252) Molin, S.; Tolker-Nielsen, T. Gene Transfer Occurs with Enhanced Efficiency in Biofilms and Induces Enhanced Stabilisation of the Biofilm Structure. *Curr. Opin. Biotechnol.* **2003**, *14* (3), 255–261. https://doi.org/10.1016/S0958-1669(03)00036-3.

(253) Werneburg, G. T. Catheter-Associated Urinary Tract Infections: Current Challenges and Future Prospects. *Res. Rep. Urol.* **2022**, *14*, 109–133. https://doi.org/10.2147/RRU.S273663.

(254) Schaffer, J. N.; Pearson, M. M. Proteus Mirabilis and Urinary Tract Infections. *Microbiol. Spectr.* **2015**, *3* (5), 10.1128/microbiolspec.uti-0017–2013. https://doi.org/10.1128/microbiolspec.uti-0017-2013.

(255) Flores-Mireles, A. L.; Pinkner, J. S.; Caparon, M. G.; Hultgren, S. J. EbpA Vaccine Antibodies Block Binding of Enterococcus Faecalis to Fibrinogen to Prevent Catheter-Associated Bladder Infection in Mice. *Sci. Transl. Med.* **2014**, *6* (254), 254ra127. https://doi.org/10.1126/scitranslmed.3009384.

(256) Govindarajan, D. K.; Kandaswamy, K. Virulence Factors of Uropathogens and Their Role in Host Pathogen Interactions. *Cell Surf.* **2022**, *8*, 100075. https://doi.org/10.1016/j.tcsw.2022.100075.

(257) Nickel, J. C. Management of Urinary Tract Infections: Historical Perspective and Current Strategies: Part 2— Modern Management. *J. Urol.* **2005**, *173* (1), 27–32. https://doi.org/10.1097/01.ju.0000141497.46841.7a.

(258) Squadrito, F. J.; del Portal, D. Nitrofurantoin. In *StatPearls*; StatPearls Publishing: Treasure Island (FL), 2025.

(259) Kashouris, E.; Joseph, A.; Lewis, T. Nitrofurantoin: What Is the Evidence for Current UK Guidance? *J. Antimicrob. Chemother.* **2023**, *78* (11), 2605–2611. https://doi.org/10.1093/jac/dkad287.

(260) Teoh, X.-Y.; bt Mahyuddin, F. N.; Ahmad, W.; Chan, S.-Y. Formulation Strategy of Nitrofurantoin: Co-Crystal or Solid Dispersion? *Pharm. Dev. Technol.* **2020**, *25* (2), 245–251. https://doi.org/10.1080/10837450.2019.1689401.

(261) Fransen, F.; Melchers, M. J. B.; Lagarde, C. M. C.; Meletiadis, J.; Mouton, J. W. Pharmacodynamics of Nitrofurantoin at Different pH Levels against Pathogens Involved in Urinary Tract Infections. *J. Antimicrob. Chemother.* **2017**, *72* (12), 3366–3373. https://doi.org/10.1093/jac/dkx313.

(262) Mahdizade Ari, M.; Dashtbin, S.; Ghasemi, F.; Shahroodian, S.; kiani, P.; Bafandeh, E.; Darbandi, T.; Ghanavati, R.; Darbandi, A. Nitrofurantoin: Properties and Potential in Treatment of Urinary Tract Infection: A Narrative Review. *Front. Cell. Infect. Microbiol.* **2023**, *13*, 1148603. https://doi.org/10.3389/fcimb.2023.1148603.

(263) Hrbacek, J.; Cermak, P.; Zachoval, R. Current Antibiotic Resistance Trends of Uropathogens in Central Europe: Survey from a Tertiary Hospital Urology Department 2011–2019. *Antibiotics* **2020**, *9* (9), 630. https://doi.org/10.3390/antibiotics9090630.

(264) ten Doesschate, T.; Hendriks, K.; van Werkhoven, C. H.; van der Hout, E. C.; Platteel, T. N.; Groenewegen, I. A. M.; Muller, A. E.; Hoepelman, A. I. M.; Bonten, M. J. M.; Geerlings, S. E.

Nitrofurantoin 100 Mg versus 50 Mg Prophylaxis for Urinary Tract Infections, a Cohort Study. *Clin. Microbiol. Infect.* **2022**, *28* (2), 248–254. https://doi.org/10.1016/j.cmi.2021.05.048.

(265) Jick, S. S.; Jick, H.; Walker, A. M.; Hunter, J. R. Hospitalizations for Pulmonary Reactions Following Nitrofurantoin Use. *CHEST* **1989**, *96* (3), 512–515. https://doi.org/10.1378/chest.96.3.512.

(266) Claussen, K.; Stocks, E.; Bhat, D.; Fish, J.; Rubin, C. D. How Common Are Pulmonary and Hepatic Adverse Effects in Older Adults Prescribed Nitrofurantoin? *J. Am. Geriatr. Soc.* **2017**, *65* (6), 1316–1320. https://doi.org/10.1111/jgs.14796.

(267) Whelan, S.; O'Grady, M. C.; Corcoran, G. D.; Finn, K.; Lucey, B. Effect of Sub-Inhibitory Concentrations of Nitrofurantoin, Ciprofloxacin, and Trimethoprim on In Vitro Biofilm Formation in Uropathogenic Escherichia Coli (UPEC). *Med. Sci.* **2022**, *11* (1), 1. https://doi.org/10.3390/medsci11010001.

(268) Gümüş, D.; Kalaycı-Yüksek, F.; Yörük, E.; Uz, G.; Çelik, E.; Arslan, C.; Aydın, E. M.; Canlı, C.; Anğ-Küçüker, M. Alterations of Growth Rate and Gene Expression Levels of UPEC by Antibiotics at Sub-MIC. *Folia Microbiol. (Praha)* **2018**, *63* (4), 451–457. https://doi.org/10.1007/s12223-017-0582-z.

(269) Zaitseva, J.; Granik, V.; Belik, A.; Koksharova, O.; Khmel, I. Effect of Nitrofurans and NO Generators on Biofilm Formation by *Pseudomonas Aeruginosa* PAO1 and *Burkholderia Cenocepacia* 370. *Res. Microbiol.* **2009**, *160* (5), 353–357. https://doi.org/10.1016/j.resmic.2009.04.007.

(270) Rundle, J. S.; Scott, R. Co-Trimoxazole and Trimethoprim in Complicated Urinary Tract Infection. *Urology* **1983**, *21* (6), 645–647. https://doi.org/10.1016/0090-4295(83)90216-9.

(271) Leblebicioglu, H.; Ozaras, R.; Sunbul, M. Role of Co-Trimoxazole for Urinary Tract Infections in Developing Countries. *Lancet Infect. Dis.* **2015**, *15* (7), 764–765. https://doi.org/10.1016/S1473-3099(15)00076-6.

(272) Poey, M. E.; de los Santos, E.; Aznarez, D.; García-Laviña, C. X.; Laviña, M. Genetics of Resistance to Trimethoprim in Cotrimoxazole Resistant Uropathogenic Escherichia Coli: Integrons, Transposons, and Single Gene Cassettes. *Front. Microbiol.* **2024**, *15*. https://doi.org/10.3389/fmicb.2024.1395953.

(273) British Medical Journal Publishing. Bacterial Resistance to Trimethoprim. *Br Med J* **1980**, *281* (6240), 571–572. https://doi.org/10.1136/bmj.281.6240.571.

(274) Pouwels, K. B.; Batra, R.; Patel, A.; Edgeworth, J. D.; Robotham, J. V.; Smieszek, T. Will Co-Trimoxazole Resistance Rates Ever Go down? Resistance Rates Remain High despite Decades of Reduced Co-Trimoxazole Consumption. *J. Glob. Antimicrob. Resist.* **2017**, *11*, 71–74. https://doi.org/10.1016/j.jgar.2017.07.013.

(275) Sihra, N.; Goodman, A.; Zakri, R.; Sahai, A.; Malde, S. Nonantibiotic Prevention and Management of Recurrent Urinary Tract Infection. *Nat. Rev. Urol.* **2018**, *15* (12), 750–776. https://doi.org/10.1038/s41585-018-0106-x.

(276) Bono, M. J.; Leslie, S. W. Uncomplicated Urinary Tract Infections. In *StatPearls*; StatPearls Publishing: Treasure Island (FL), 2025.

(277) Pulipati, S.; Babu, P. S.; Narasu, M. L.; Anusha, N. An Overview on Urinary Tract Infections and Effective Natural Remedies. **2017**.

(278) Luís, Â.; Domingues, F.; Pereira, L. Can Cranberries Contribute to Reduce the Incidence of Urinary Tract Infections? A Systematic Review with Meta-Analysis and Trial Sequential Analysis of Clinical Trials. *J. Urol.* **2017**, *198* (3), 614–621. https://doi.org/10.1016/j.juro.2017.03.078.

(279) Fu, Z.; Liska, D.; Talan, D.; Chung, M. Cranberry Reduces the Risk of Urinary Tract Infection Recurrence in Otherwise Healthy Women: A Systematic Review and Meta-Analysis. *J. Nutr.* **2017**, *147* (12), 2282–2288. https://doi.org/10.3945/jn.117.254961.

(280) Aroutcheva, A.; Gariti, D.; Simon, M.; Shott, S.; Faro, J.; Simoes, J. A.; Gurguis, A.; Faro, S. Defense Factors of Vaginal Lactobacilli. *Am. J. Obstet. Gynecol.* **2001**, *185* (2), 375–379. https://doi.org/10.1067/mob.2001.115867.

(281) Falagas, M. E.; Betsi, G. I.; Tokas, T.; Athanasiou, S. Probiotics for Prevention of Recurrent Urinary Tract Infections in Women. *Drugs* **2006**, *66* (9), 1253–1261. https://doi.org/10.2165/00003495-200666090-00007.

(282) Grin, P. M.; Kowalewska, P. M.; Alhazzan, W.; Fox-Robichaud, A. E. Lactobacillus for Preventing Recurrent Urinary Tract Infections in Women: Meta-Analysis. *Can. J. Urol.* **2013**, *20* (1), 6607–6614.

(283) Nickel, J. C.; Doiron, R. C. An Effective Sublingual Vaccine, MV140, Safely Reduces Risk of Recurrent Urinary Tract Infection in Women. *Pathogens* **2023**, *12* (3), 359. https://doi.org/10.3390/pathogens12030359.

(284) Lorenzo-Gómez, M. F.; Padilla-Fernández, B.; García-Cenador, M. B.; Virseda-Rodríguez, Á. J.; Martín-García, I.; Sánchez-Escudero, A.; Vicente-Arroyo, M. J.; Mirón-Canelo, J. A. Comparison of Sublingual Therapeutic Vaccine with Antibiotics for the Prophylaxis of Recurrent Urinary Tract Infections. *Front. Cell. Infect. Microbiol.* **2015**, *5*, 50. https://doi.org/10.3389/fcimb.2015.00050.

(285) Parker, V.; Giles, M.; Graham, L.; Suthers, B.; Watts, W.; O'Brien, T.; Searles, A. Avoiding Inappropriate Urinary Catheter Use and Catheter-Associated Urinary Tract Infection (CAUTI): A Pre-Post Control Intervention Study. *BMC Health Serv. Res.* **2017**, *17*, 314. https://doi.org/10.1186/s12913-017-2268-2.

(286) Wickins, J.; Rickard, C. M.; Kasper, K.; Morton, L.; Doellinger, J.; Thomas-Gabbett, P.; Marsh, N. Indwelling Urinary Catheter Use and Adherence to Clinical Practice Guidelines: A Point Prevalence Study in Adult Hospital Inpatients. *J. Infect. Prev.* **2025**, *26* (1), 11–18. https://doi.org/10.1177/17571774241270995.

(287) Zhou, T. Z., Guiqin Du,Xuan. *Inappropriate urinary catheterisation: a review of the prevalence, risk factors and measures to reduce incidence*. British Journal of Nursing. https://www.britishjournalofnursing.com/content/inappropriate-catheterisation/inappropriate-urinary-catheterisation-a-review-of-the-prevalence-risk-factors-and-measures-to-reduce-incidence (accessed 2026-01-09).

(288) Umscheid, C. A.; Mitchell, M. D.; Doshi, J. A.; Agarwal, R.; Williams, K.; Brennan, P. J. Estimating the Proportion of Healthcare-Associated Infections That Are Reasonably Preventable and the Related Mortality and Costs. *Infect. Control Hosp. Epidemiol.* **2011**, *32* (2), 101–114. https://doi.org/10.1086/657912.

(289) Letica-Kriegel, A. S.; Salmasian, H.; Vawdrey, D. K.; Youngerman, B. E.; Green, R. A.; Furuya, E. Y.; Calfee, D. P.; Perotte, R. Identifying the Risk Factors for Catheter-Associated Urinary Tract Infections: A Large Cross-Sectional Study of Six Hospitals. *BMJ Open* **2019**, *9* (2), e022137. https://doi.org/10.1136/bmjopen-2018-022137.

(290) Nicolle, L. E. Catheter Associated Urinary Tract Infections. *Antimicrob. Resist. Infect. Control* **2014**, *3*, 23. https://doi.org/10.1186/2047-2994-3-23.

(291) Al-Hazmi, H. Role of Duration of Catheterization and Length of Hospital Stay on the Rate of Catheter-Related Hospital-Acquired Urinary Tract Infections. *Res. Rep. Urol.* **2015**, *7*, 41–47. https://doi.org/10.2147/RRU.S75419.

(292) Hooton, T. M.; Bradley, S. F.; Cardenas, D. D.; Colgan, R.; Geerlings, S. E.; Rice, J. C.; Saint, S.; Schaeffer, A. J.; Tambayh, P. A.; Tenke, P.; Nicolle, L. E. Diagnosis, Prevention, and Treatment of Catheter-Associated Urinary Tract Infection in Adults: 2009 International Clinical Practice Guidelines from the Infectious Diseases Society of America. *Clin. Infect. Dis.* **2010**, *50* (5), 625–663. https://doi.org/10.1086/650482.

(293) Patel, P. K.; Advani, S. D.; Kofman, A. D.; Lo, E.; Maragakis, L. L.; Pegues, D. A.; Pettis, A. M.; Saint, S.; Trautner, B.; Yokoe, D. S.; Meddings, J. Strategies to Prevent Catheter-Associated

Urinary Tract Infections in Acute-Care Hospitals: 2022 Update. *Infect. Control Hosp. Epidemiol.* **2023**, *44* (8), 1209–1231. https://doi.org/10.1017/ice.2023.137.

(294) Zhang, Q.; Zong, Q.; Feng, X.; Luo, M.; Sun, W.; Zhai, Y. Antibacterial and Antifouling Materials for Urinary Catheter Coatings. *Acta Biomater.* **2025**, *192*, 28–47. https://doi.org/10.1016/j.actbio.2024.12.040.

(295) Al-Qahtani, M.; Safan, A.; Jassim, G.; Abadla, S. Efficacy of Anti-Microbial Catheters in Preventing Catheter Associated Urinary Tract Infections in Hospitalized Patients: A Review on Recent Updates. *J. Infect. Public Health* **2019**, *12* (6), 760–766. https://doi.org/10.1016/j.jiph.2019.09.009.

(296) Johnson, J. R.; Berggren, T.; Conway, A. J. Activity of a Nitrofurazone Matrix Urinary Catheter against Catheter-Associated Uropathogens. *Antimicrob. Agents Chemother.* **1993**, *37* (9), 2033–2036. https://doi.org/10.1128/aac.37.9.2033.

(297) Lam, T. B.; Omar, M. I.; Fisher, E.; Gillies, K.; MacLennan, S. Types of Indwelling Urethral Catheters for Short-term Catheterisation in Hospitalised Adults. *Cochrane Database Syst. Rev.* **2014**, *2014* (9), CD004013. https://doi.org/10.1002/14651858.CD004013.pub4.

(298) Saini, H.; Chhibber, S.; Harjai, K. Antimicrobial and Antifouling Efficacy of Urinary Catheters Impregnated with a Combination of Macrolide and Fluoroquinolone Antibiotics against Pseudomonas Aeruginosa. *Biofouling* **2016**, *32* (5), 511–522. https://doi.org/10.1080/08927014.2016.1155564.

(299) Rupp, M. E.; Fitzgerald, T.; Marion, N.; Helget, V.; Puumala, S.; Anderson, J. R.; Fey, P. D. Effect of Silver-Coated Urinary Catheters: Efficacy, Cost-Effectiveness, and Antimicrobial Resistance. *Am. J. Infect. Control* **2004**, *32* (8), 445–450. https://doi.org/10.1016/j.ajic.2004.05.002.

(300) Saint, S.; Elmore, J. G.; Sullivan, S. D.; Emerson, S. S.; Koepsell, T. D. The Efficacy of Silver Alloy-Coated Urinary Catheters in Preventing Urinary Tract Infection: A Meta-Analysis. *Am. J. Med.* **1998**, *105* (3), 236–241. https://doi.org/10.1016/S0002-9343(98)00240-X.

(301) Seymour, C. Audit of Catheter-Associated UTI Using Silver Alloy-Coated Foley Catheters. *Br. J. Nurs.* **2006**, *15* (11), 598–603. https://doi.org/10.12968/bjon.2006.15.11.21227.

(302) Srinivasan, A.; Karchmer, T.; Richards, A.; Song, X.; Perl, T. M. A Prospective Trial of a Novel, Silicone-Based, Silver-Coated Foley Catheter for the Prevention of Nosocomial Urinary Tract Infections. *Infect. Control Hosp. Epidemiol.* **2006**, *27* (1), 38–43. https://doi.org/10.1086/499998.

(303) Desai, D. G.; Liao, K. S.; Cevallos, M. E.; Trautner, B. W. Silver or Nitrofurazone Impregnation of Urinary Catheters Has a Minimal Effect on Uropathogen Adherence. *J. Urol.* **2010**, *184* (6), 2565–2571. https://doi.org/10.1016/j.juro.2010.07.036.

(304) Alam, M. S.; Anwar, M. J.; Akhtar, M. S.; Alam, P.; Mohammad, A. A. S.; Almutairy, A. F.; Nazmi, A. S.; Mukherjee, T. K. A Systematic Review of Recent Advances in Urinary Tract Infection Interventions and Treatment Technology. **2024**.

(305) Crintea, A.; Carpa, R.; Mitre, A.-O.; Petho, R. I.; Chelaru, V.-F.; Nădăşan, S.-M.; Neamti, L.; Dutu, A. G. Nanotechnology Involved in Treating Urinary Tract Infections: An Overview. *Nanomaterials* **2023**, *13* (3), 555. https://doi.org/10.3390/nano13030555.

(306) El-Batal, A. I.; El-Sayyad, G. S.; Al-Hazmi, N. E.; Gobara, M. Antibiofilm and Antimicrobial Activities of Silver Boron Nanoparticles Synthesized by PVP Polymer and Gamma Rays Against Urinary Tract Pathogens. *J. Clust. Sci.* **2019**, *30* (4), 947–964. https://doi.org/10.1007/s10876-019-01553-4.

(307) Bhande, R. M.; Khobragade, C. N.; Mane, R. S.; Bhande, S. Enhanced Synergism of Antibiotics with Zinc Oxide Nanoparticles against Extended Spectrum β-Lactamase Producers Implicated in Urinary Tract Infections. *J. Nanoparticle Res.* **2013**, *15* (1), 1413. https://doi.org/10.1007/s11051-012-1413-4.

(308) Esim, O.; Kiymaci, M. E.; Hascicek, C. Ciprofloxacin HCl-Loaded Albumin Nanoparticles for the Treatment of Recurrent Urinary Tract Infections: Preparation, Optimization, and Evaluation of

Antibacterial Activity. *J. Pharm. Innov.* **2023**, *18* (3), 1100–1110. https://doi.org/10.1007/s12247-023-09709-6.

(309) Becknell, B.; Schwaderer, A.; Hains, D. S.; Spencer, J. D. Amplifying Renal Immunity: The Role of Antimicrobial Peptides in Pyelonephritis. *Nat. Rev. Nephrol.* **2015**, *11* (11), 642–655. https://doi.org/10.1038/nrneph.2015.105.

(310) Kai-Larsen, Y.; Lüthje, P.; Chromek, M.; Peters, V.; Wang, X.; Holm, Å.; Kádas, L.; Hedlund, K.-O.; Johansson, J.; Chapman, M. R.; Jacobson, S. H.; Römling, U.; Agerberth, B.; Brauner, A. Uropathogenic Escherichia Coli Modulates Immune Responses and Its Curli Fimbriae Interact with the Antimicrobial Peptide LL-37. *PLoS Pathog.* **2010**, *6* (7), e1001010. https://doi.org/10.1371/journal.ppat.1001010.

(311) Neumann, A.; Berends, E. T. M.; Nerlich, A.; Molhoek, E. M.; Gallo, R. L.; Meerloo, T.; Nizet, V.; Naim, H. Y.; von Köckritz-Blickwede, M. The Antimicrobial Peptide LL-37 Facilitates the Formation of Neutrophil Extracellular Traps. *Biochem. J.* **2014**, *464* (1), 3–11. https://doi.org/10.1042/BJ20140778.

(312) Al-Anany, A. M.; Hooey, P. B.; Cook, J. D.; Burrows, L. L.; Martyniuk, J.; Hynes, A. P.; German, G. J. Phage Therapy in the Management of Urinary Tract Infections: A Comprehensive Systematic Review. *PHAGE* **2023**, *4* (3), 112–127. https://doi.org/10.1089/phage.2023.0024.

(313) Lehman, S. M.; Donlan, R. M. Bacteriophage-Mediated Control of a Two-Species Biofilm Formed by Microorganisms Causing Catheter-Associated Urinary Tract Infections in an In Vitro Urinary Catheter Model. *Antimicrob. Agents Chemother.* **2015**, *59* (2), 1127–1137. https://doi.org/10.1128/AAC.03786-14.

(314) Bedi, M. S.; Verma, V.; Chhibber, S. Amoxicillin and Specific Bacteriophage Can Be Used Together for Eradication of Biofilm of Klebsiella Pneumoniae B5055. *World J. Microbiol. Biotechnol.* **2009**, *25* (7), 1145–1151. https://doi.org/10.1007/s11274-009-9991-8.

(315) Huttner, A.; Hatz, C.; Dobbelsteen, G. van den; Abbanat, D.; Hornacek, A.; Frölich, R.; Dreyer, A. M.; Martin, P.; Davies, T.; Fae, K.; Nieuwenhof, I. van den; Thoelen, S.; Vallière, S. de; Kuhn, A.; Bernasconi, E.; Viereck, V.; Kavvadias, T.; Kling, K.; Ryu, G.; Hülder, T.; Gröger, S.; Scheiner, D.; Alaimo, C.; Harbarth, S.; Poolman, J.; Fonck, V. G. Safety, Immunogenicity, and Preliminary Clinical Efficacy of a Vaccine against Extraintestinal Pathogenic Escherichia Coli in Women with a History of Recurrent Urinary Tract Infection: A Randomised, Single-Blind, Placebo-Controlled Phase 1b Trial. *Lancet Infect. Dis.* **2017**, *17* (5), 528–537. https://doi.org/10.1016/S1473-3099(17)30108-1.

(316) Inoue, M.; Ogawa, T.; Tamura, H.; Hagiwara, Y.; Saito, Y.; Abbanat, D.; van den Dobbelsteen, G.; Hermans, P.; Thoelen, S.; Poolman, J.; Ibarra de Palacios, P. Safety, Tolerability and Immunogenicity of the ExPEC4V (JNJ-63871860) Vaccine for Prevention of Invasive Extraintestinal Pathogenic Escherichia Coli Disease: A Phase 1, Randomized, Double-Blind, Placebo-Controlled Study in Healthy Japanese Participants. *Hum. Vaccines Immunother.* **2018**, *14* (9), 2150–2157. https://doi.org/10.1080/21645515.2018.1474316.

(317) Starks, C. M.; Miller, M. M.; Broglie, P. M.; Cubbison, J.; Martin, S. M.; Eldridge, G. R. Optimization and Qualification of an Assay That Demonstrates That a FimH Vaccine Induces Functional Antibody Responses in Women with Histories of Urinary Tract Infections. *Hum. Vaccines Immunother.* **2021**, *17* (1), 283–292. https://doi.org/10.1080/21645515.2020.1770034.

(318) Lopatto, E. D. B.; Santiago-Borges, J. M.; Sanick, D. A.; Malladi, S. K.; Azimzadeh, P. N.; Timm, M. W.; Fox, I. F.; Schmitz, A. J.; Turner, J. S.; Sayed Ahmed, S. M.; Ortinau, L.; Gualberto, N. C.; Pinkner, J. S.; Dodson, K. W.; Ellebedy, A. H.; Kau, A. L.; Hultgren, S. J. Monoclonal Antibodies Targeting the FimH Adhesin Protect against Uropathogenic E. Coli UTI. *Sci. Adv.* **2025**, *11* (25), eadw0698. https://doi.org/10.1126/sciadv.adw0698.

(319) Butler, D.; Ambite, I.; Wan, M. L. Y.; Tran, T. H.; Wullt, B.; Svanborg, C. Immunomodulation Therapy Offers New Molecular Strategies to Treat UTI. *Nat. Rev. Urol.* **2022**, *19* (7), 419–437. https://doi.org/10.1038/s41585-022-00602-4.

(320) Ambite, I.; Puthia, M.; Nagy, K.; Cafaro, C.; Nadeem, A.; Butler, D. S. C.; Rydström, G.; Filenko, N. A.; Wullt, B.; Miethke, T.; Svanborg, C. Molecular Basis of Acute Cystitis Reveals Susceptibility Genes and Immunotherapeutic Targets. *PLoS Pathog.* **2016**, *12* (10), e1005848. https://doi.org/10.1371/journal.ppat.1005848.

(321) Pinto, R. M.; Soares, F. A.; Reis, S.; Nunes, C.; Van Dijck, P. Innovative Strategies Toward the Disassembly of the EPS Matrix in Bacterial Biofilms. *Front. Microbiol.* **2020**, *11*. https://doi.org/10.3389/fmicb.2020.00952.

(322) Dong, Y.; Xu, Y.; Li, P.; Wang, C.; Cao, Y.; Yu, J. Antibiofilm Effect of Ultrasound Combined with Microbubbles against *Staphylococcus Epidermidis* Biofilm. *Int. J. Med. Microbiol.* **2017**, *307* (6), 321–328. https://doi.org/10.1016/j.ijmm.2017.06.001.

(323) Horsley, H.; Owen, J.; Browning, R.; Carugo, D.; Malone-Lee, J.; Stride, E.; Rohn, J. L. Ultrasound-Activated Microbubbles as a Novel Intracellular Drug Delivery System for Urinary Tract Infection. *J. Controlled Release* **2019**, *301*, 166–175. https://doi.org/10.1016/j.jconrel.2019.03.017.

(324) Alidriss, O. M.; AlSudais, H.; Alhumaidan, O. S.; Altwaijry, H. D.; Bakhsh, A.; Almuhanna, Y.; Alkudmani, Z. S.; Alqarni, I. A.; Alenazi, D.; Aljasham, A. T.; Jamous, Y. F. Targeted Drug Delivery Strategies in Overcoming Antimicrobial Resistance: Advances and Future Directions. *Pharmaceutics* **2025**, *17* (11), 1426. https://doi.org/10.3390/pharmaceutics17111426.

(325) Hua, S.; de Matos, M. B. C.; Metselaar, J. M.; Storm, G. Current Trends and Challenges in the Clinical Translation of Nanoparticulate Nanomedicines: Pathways for Translational Development and Commercialization. *Front. Pharmacol.* **2018**, *9*, 790. https://doi.org/10.3389/fphar.2018.00790.

(326) Mitchell, M. J.; Billingsley, M. M.; Haley, R. M.; Wechsler, M. E.; Peppas, N. A.; Langer, R. Engineering Precision Nanoparticles for Drug Delivery. *Nat. Rev. Drug Discov.* **2021**, *20* (2), 101–124. https://doi.org/10.1038/s41573-020-0090-8.

(327) Mukherjee, D.; Sil, M.; Goswami, A.; Lahiri, D.; Nag, M. Antibiofilm Activities of Carbon-Based Nanoparticles and Nanocomposites: A Comparative Review. *J. Inorg. Organomet. Polym. Mater.* **2023**, *33* (12), 3961–3983. https://doi.org/10.1007/s10904-023-02732-7.

(328) Shi, J.; Wang, B.; Wang, L.; Lu, T.; Fu, Y.; Zhang, H.; Zhang, Z. Fullerene (C60)-Based Tumor-Targeting Nanoparticles with "off-on" State for Enhanced Treatment of Cancer. *J. Controlled Release* **2016**, *235*, 245–258. https://doi.org/10.1016/j.jconrel.2016.06.010.

(329) Kim, T.; Hyeon, T. Applications of Inorganic Nanoparticles as Therapeutic Agents. *Nanotechnology* **2013**, *25* (1), 012001. https://doi.org/10.1088/0957-4484/25/1/012001.

(330) Gurunathan, S.; Lee, K.-J.; Kalishwaralal, K.; Sheikpranbabu, S.; Vaidyanathan, R.; Eom, S. H. Antiangiogenic Properties of Silver Nanoparticles. *Biomaterials* **2009**, *30* (31), 6341–6350. https://doi.org/10.1016/j.biomaterials.2009.08.008.

(331) Yin, I. X.; Zhang, J.; Zhao, I. S.; Mei, M. L.; Li, Q.; Chu, C. H. The Antibacterial Mechanism of Silver Nanoparticles and Its Application in Dentistry. *Int. J. Nanomedicine* **2020**, *15*, 2555–2562. https://doi.org/10.2147/IJN.S246764.

(332) S, S.; Sangeetha, M. S.; Martin, T. M.; Kumar, M. S. K. Phytogenic Silver Nanoparticles from Betanin: A Novel Approach to Suppress Angiogenesis and Tumor Progression. *Lex Localis - J. Local Self-Gov.* **2025**, *23* (S6), 3818–3835. https://doi.org/10.52152/rn6x0t68.

(333) Liao, S.; Zhang, Y.; Pan, X.; Zhu, F.; Jiang, C.; Liu, Q.; Cheng, Z.; Dai, G.; Wu, G.; Wang, L.; Chen, L. Antibacterial Activity and Mechanism of Silver Nanoparticles against Multidrug-Resistant Pseudomonas Aeruginosa. *Int. J. Nanomedicine* **2019**, *14*, 1469–1487. https://doi.org/10.2147/IJN.S191340.

(334) Premanathan, M.; Karthikeyan, K.; Jeyasubramanian, K.; Manivannan, G. Selective Toxicity of ZnO Nanoparticles toward Gram-Positive Bacteria and Cancer Cells by Apoptosis through Lipid Peroxidation. *Nanomedicine Nanotechnol. Biol. Med.* **2011**, *7* (2), 184–192. https://doi.org/10.1016/j.nano.2010.10.001.

(335) Huang, Z.; Zheng, X.; Yan, D.; Yin, G.; Liao, X.; Kang, Y.; Yao, Y.; Huang, D.; Hao, B. Toxicological Effect of ZnO Nanoparticles Based on Bacteria. *Langmuir* **2008**, *24* (8), 4140–4144. https://doi.org/10.1021/la7035949.

(336) Mitragotri, S.; Patrick, S. Organic Nanoparticles for Drug Delivery and Imaging. *MRS Bull.* **2014**, *39* (3), 219–223. https://doi.org/10.1557/mrs.2014.11.

(337) MaHam, A.; Tang, Z.; Wu, H.; Wang, J.; Lin, Y. Protein-Based Nanomedicine Platforms for Drug Delivery. *Small* **2009**, *5* (15), 1706–1721. https://doi.org/10.1002/smll.200801602.

(338) Kratz, F. Albumin as a Drug Carrier: Design of Prodrugs, Drug Conjugates and Nanoparticles. *J. Controlled Release* **2008**, *132* (3), 171–183. https://doi.org/10.1016/j.jconrel.2008.05.010.

(339) Gradishar, W. J. Albumin-Bound Paclitaxel: A next-Generation Taxane. *Expert Opin. Pharmacother.* **2006**, *7* (8), 1041–1053. https://doi.org/10.1517/14656566.7.8.1041.

(340) De, R.; Mahata, M. K.; Kim, K.-T. Structure-Based Varieties of Polymeric Nanocarriers and Influences of Their Physicochemical Properties on Drug Delivery Profiles. *Adv. Sci.* **2022**, *9* (10), 2105373. https://doi.org/10.1002/advs.202105373.

(341) Cerqueira, B. B. S.; Lasham, A.; Shelling, A. N.; Al-Kassas, R. Development of Biodegradable PLGA Nanoparticles Surface Engineered with Hyaluronic Acid for Targeted Delivery of Paclitaxel to Triple Negative Breast Cancer Cells. *Mater. Sci. Eng. C* **2017**, *76*, 593–600. https://doi.org/10.1016/j.msec.2017.03.121.

(342) Wu, T.; Wu, C.; Fu, S.; Wang, L.; Yuan, C.; Chen, S.; Hu, Y. Integration of Lysozyme into Chitosan Nanoparticles for Improving Antibacterial Activity. *Carbohydr. Polym.* **2017**, *155*, 192–200. https://doi.org/10.1016/j.carbpol.2016.08.076.

(343) Taghiloo, S.; Ghajari, G.; Zand, Z.; Kabiri-Samani, S.; Kabiri, H.; Rajaei, N.; Piri-Gharaghie, T. Designing Alginate/Chitosan Nanoparticles Containing Echinacea Angustifolia: A Novel Candidate for Combating Multidrug-Resistant Staphylococcus Aureus. *Chem. Biodivers.* **2023**, *20* (7), e202201008. https://doi.org/10.1002/cbdv.202201008.

(344) Mehta, M.; Bui, T. A.; Yang, X.; Aksoy, Y.; Goldys, E. M.; Deng, W. Lipid-Based Nanoparticles for Drug/Gene Delivery: An Overview of the Production Techniques and Difficulties Encountered in Their Industrial Development. *ACS Mater. Au* **2023**, *3* (6), 600–619. https://doi.org/10.1021/acsmaterialsau.3c00032.

(345) Wilson, B.; Geetha, K. M. Lipid Nanoparticles in the Development of mRNA Vaccines for COVID-19. *J. Drug Deliv. Sci. Technol.* **2022**, *74*, 103553. https://doi.org/10.1016/j.jddst.2022.103553.

(346) Lamb, Y. N. BNT162b2 mRNA COVID-19 Vaccine: First Approval. *Drugs* **2021**, *81* (4), 495–501. https://doi.org/10.1007/s40265-021-01480-7.

(347) Mishra, V.; Bansal, K. K.; Verma, A.; Yadav, N.; Thakur, S.; Sudhakar, K.; Rosenholm, J. M. Solid Lipid Nanoparticles: Emerging Colloidal Nano Drug Delivery Systems. *Pharmaceutics* **2018**, *10* (4), 191. https://doi.org/10.3390/pharmaceutics10040191.

(348) Viegas, C.; Patrício, A. B.; Prata, J. M.; Nadhman, A.; Chintamaneni, P. K.; Fonte, P. Solid Lipid Nanoparticles vs. Nanostructured Lipid Carriers: A Comparative Review. *Pharmaceutics* **2023**, *15* (6), 1593. https://doi.org/10.3390/pharmaceutics15061593.

(349) Tenchov, R.; Bird, R.; Curtze, A. E.; Zhou, Q. Lipid Nanoparticles─From Liposomes to mRNA Vaccine Delivery, a Landscape of Research Diversity and Advancement. *ACS Nano* **2021**, *15* (11), 16982–17015. https://doi.org/10.1021/acsnano.1c04996.

(350) Makino, K.; Shibata, A. Chapter 2: Surface Properties of Liposomes Depending on Their Composition. In *Advances in Planar Lipid Bilayers and Liposomes*; Academic Press, 2006; Vol. 4, pp 49–77. https://doi.org/10.1016/S1554-4516(06)04002-6.
(351) Liu, P.; Chen, G.; Zhang, J. A Review of Liposomes as a Drug Delivery System: Current Status of Approved Products, Regulatory Environments, and Future Perspectives. *Molecules* **2022**, *27* (4), 1372. https://doi.org/10.3390/molecules27041372.
(352) Rudzińska, M.; Grygier, A.; Knight, G.; Kmiecik, D. Liposomes as Carriers of Bioactive Compounds in Human Nutrition. *Foods* **2024**, *13* (12), 1814. https://doi.org/10.3390/foods13121814.
(353) Soni, V.; Chandel, S.; Jain, P.; Asati, S. Role of Liposomal Drug-Delivery System in Cosmetics. In *Nanobiomaterials in Galenic Formulations and Cosmetics*; William Andrew Publishing, 2016; pp 93–120. https://doi.org/10.1016/B978-0-323-42868-2.00005-X.
(354) Bulbake, U.; Doppalapudi, S.; Kommineni, N.; Khan, W. Liposomal Formulations in Clinical Use: An Updated Review. *Pharmaceutics* **2017**, *9* (2), 12. https://doi.org/10.3390/pharmaceutics9020012.
(355) Luiz, H.; Oliveira Pinho, J.; Gaspar, M. M. Advancing Medicine with Lipid-Based Nanosystems—The Successful Case of Liposomes. *Biomedicines* **2023**, *11* (2), 435. https://doi.org/10.3390/biomedicines11020435.
(356) Shao, X.-R.; Wei, X.-Q.; Zhang, S.; Fu, N.; Lin, Y.-F.; Cai, X.-X.; Peng, Q. Effects of Micro-Environmental pH of Liposome on Chemical Stability of Loaded Drug. *Nanoscale Res. Lett.* **2017**, *12*, 504. https://doi.org/10.1186/s11671-017-2256-9.
(357) Luo, M.; Oomah, B. D.; Akoetey, W.; Zhang, Y.; Daneshfozoun, H.; Hosseinian, F. Liposomes as Sustainable Delivery Systems in Food, Cosmetic, and Pharmaceutical Applications. *J. Am. Oil Chem. Soc.* **2025**, *102* (3), 547–568. https://doi.org/10.1002/aocs.12907.
(358) Gatto, M. S.; Johnson, M. P.; Najahi-Missaoui, W. Targeted Liposomal Drug Delivery: Overview of the Current Applications and Challenges. *Life* **2024**, *14* (6), 672. https://doi.org/10.3390/life14060672.
(359) Okafor, N. I.; Omoteso, O. A.; Choonara, Y. E. The Modification of Conventional Liposomes for Targeted Antimicrobial Delivery to Treat Infectious Diseases. *Discov. Nano* **2025**, *20* (1), 19. https://doi.org/10.1186/s11671-024-04170-x.
(360) Cˇeh, B.; Winterhalter, M.; Frederik, P. M.; Vallner, J. J.; Lasic, D. D. Stealth® Liposomes: From Theory to Product. *Adv. Drug Deliv. Rev.* **1997**, *24* (2), 165–177. https://doi.org/10.1016/S0169-409X(96)00456-5.
(361) Van Etten, E. W. M.; Ten Kate, M. T.; Snijders, S. V.; Bakker-Woudenberg, I. A. J. M. Administration of Liposomal Agents and Blood Clearance Capacity of the Mononuclear Phagocyte System. *Antimicrob. Agents Chemother.* **1998**, *42* (7), 1677–1681. https://doi.org/10.1128/AAC.42.7.1677.
(362) Nongkhlaw, R.; Nongrum, R.; Arunachalam, J.; Kalia, N. P.; Agnivesh, P. K.; Nongkhlaw, R. Drug-Loaded Liposomes for Macrophage Targeting in Mycobacterium Tuberculosis: Development, Characterization and Macrophage Infection Study. *3 Biotech* **2025**, *15* (2), 52. https://doi.org/10.1007/s13205-025-04208-6.
(363) Narenji, M.; Talaee, M. R.; Moghimi, H. R. Effect of Charge on Separation of Liposomes upon Stagnation. *Iran. J. Pharm. Res. IJPR* **2017**, *16* (2), 423–431.
(364) Murugova, T. N.; Balgavý, P. Molecular Volumes of DOPC and DOPS in Mixed Bilayers of Multilamellar Vesicles. *Phys. Chem. Chem. Phys.* **2014**, *16* (34), 18211–18216. https://doi.org/10.1039/C4CP01980F.
(365) Shim, G.; Kim, M.-G.; Park, J. Y.; Oh, Y.-K. Application of Cationic Liposomes for Delivery of Nucleic Acids. *Asian J. Pharm. Sci.* **2013**, *8* (2), 72–80. https://doi.org/10.1016/j.ajps.2013.07.009.

(366) Zhao, F.; Nayyar, D.; Hwang, Y. S.; Bartucci, R.; Salvati, A. Effect of Positive Charges on Liposome Stability, Uptake Efficacy and Impact on Cells. *Int. J. Pharm.* **2025**, *681*, 125881. https://doi.org/10.1016/j.ijpharm.2025.125881.

(367) Forest, V.; Pourchez, J. Preferential Binding of Positive Nanoparticles on Cell Membranes Is Due to Electrostatic Interactions: A Too Simplistic Explanation That Does Not Take into Account the Nanoparticle Protein Corona. *Mater. Sci. Eng. C* **2017**, *70*, 889–896. https://doi.org/10.1016/j.msec.2016.09.016.

(368) Gandek, T. B.; van der Koog, L.; Nagelkerke, A. A Comparison of Cellular Uptake Mechanisms, Delivery Efficacy, and Intracellular Fate between Liposomes and Extracellular Vesicles. *Adv. Healthc. Mater.* **2023**, *12* (25), 2300319. https://doi.org/10.1002/adhm.202300319.

(369) Reginald-Opara, J. N.; Svirskis, D.; Paek, S. Y.; Tang, M.; O'Carroll, S. J.; Dean, J. M.; Chamley, L. W.; Wu, Z. The Involvement of Extracellular Vesicles in the Transcytosis of Nanoliposomes through Brain Endothelial Cells, and the Impact of Liposomal pH-Sensitivity. *Mater. Today Bio* **2022**, *13*, 100212. https://doi.org/10.1016/j.mtbio.2022.100212.

(370) Pei, D.; Buyanova, M. Overcoming Endosomal Entrapment in Drug Delivery. *Bioconjug. Chem.* **2019**, *30* (2), 273–283. https://doi.org/10.1021/acs.bioconjchem.8b00778.

(371) Sachetelli, S.; Khalil, H.; Chen, T.; Beaulac, C.; Sénéchal, S.; Lagacé, J. Demonstration of a Fusion Mechanism between a Fluid Bactericidal Liposomal Formulation and Bacterial Cells. *Biochim. Biophys. Acta BBA - Biomembr.* **2000**, *1463* (2), 254–266. https://doi.org/10.1016/S0005-2736(99)00217-5.

(372) Farid, M.; Faber, T.; Dietrich, D.; Lamprecht, A. Cell Membrane Fusing Liposomes for Cytoplasmic Delivery in Brain Endothelial Cells. *Colloids Surf. B Biointerfaces* **2020**, *194*, 111193. https://doi.org/10.1016/j.colsurfb.2020.111193.

(373) Scheeder, A.; Brockhoff, M.; Ward, E. N.; Kaminski Schierle, G. S.; Mela, I.; Kaminski, C. F. Molecular Mechanisms of Cationic Fusogenic Liposome Interactions with Bacterial Envelopes. *J. Am. Chem. Soc.* **2023**, *145* (51), 28240–28250. https://doi.org/10.1021/jacs.3c11463.

(374) Kowalska, M.; Broniatowski, M.; Mach, M.; Płachta, Ł.; Wydro, P. The Effect of the Polyethylene Glycol Chain Length of a Lipopolymer (DSPE-PEGn) on the Properties of DPPC Monolayers and Bilayers. *J. Mol. Liq.* **2021**, *335*, 116529. https://doi.org/10.1016/j.molliq.2021.116529.

(375) Li, M.; Jiang, S.; Simon, J.; Paßlick, D.; Frey, M.-L.; Wagner, M.; Mailänder, V.; Crespy, D.; Landfester, K. Brush Conformation of Polyethylene Glycol Determines the Stealth Effect of Nanocarriers in the Low Protein Adsorption Regime. *Nano Lett.* **2021**, *21* (4), 1591–1598. https://doi.org/10.1021/acs.nanolett.0c03756.

(376) Nosova, A. S.; Koloskova, O. O.; Nikonova, A. A.; Simonova, V. A.; Smirnov, V. V.; Kudlay, D.; Khaitov, M. R. Diversity of PEGylation Methods of Liposomes and Their Influence on RNA Delivery. *MedChemComm* **2019**, *10* (3), 369–377. https://doi.org/10.1039/c8md00515j.

(377) Suk, J. S.; Xu, Q.; Kim, N.; Hanes, J.; Ensign, L. M. PEGylation as a Strategy for Improving Nanoparticle-Based Drug and Gene Delivery. *Adv. Drug Deliv. Rev.* **2016**, *99*, 28–51. https://doi.org/10.1016/j.addr.2015.09.012.

(378) Feng, S.-J.; Liu, C.-H.; Xia, X.-M.; Yu, B.-Y.; Chu, G.-W.; Li, H.; Chen, J.-F. Unraveling the Role of PEGylation in the Anti-Aggregation Stability of Lipid Nanoparticles. *Nanoscale* **2025**, *17* (47), 27530–27537. https://doi.org/10.1039/D5NR03266K.

(379) Gaston, J. P.; Meepat, S.; Islam, M. S.; Li, J.; Daljit Singh, J. K.; Booth, M. J.; Wickham, S. FJ.; Baker, M. AB. The Effect of PEGylation on Surface Tethering of Liposomes via DNA Nanotechnology. *J. Lipid Res.* **2026**, *67* (1), 100940. https://doi.org/10.1016/j.jlr.2025.100940.

(380) Fang, Y.; Xue, J.; Gao, S.; Lu, A.; Yang, D.; Jiang, H.; He, Y.; Shi, K. Cleavable PEGylation: A Strategy for Overcoming the "PEG Dilemma" in Efficient Drug Delivery. *Drug Deliv.* **2017**, *24* (2), 22–32. https://doi.org/10.1080/10717544.2017.1388451.

(381) Allen, T. M.; Cullis, P. R. Liposomal Drug Delivery Systems: From Concept to Clinical Applications. *Adv. Drug Deliv. Rev.* **2013**, *65* (1), 36–48. https://doi.org/10.1016/j.addr.2012.09.037.
(382) Alshaer, W.; Hillaireau, H.; Vergnaud, J.; Ismail, S.; Fattal, E. Functionalizing Liposomes with Anti-CD44 Aptamer for Selective Targeting of Cancer Cells. *Bioconjug. Chem.* **2015**, *26* (7), 1307–1313. https://doi.org/10.1021/bc5004313.
(383) Paolino, D.; Cosco, D.; Gaspari, M.; Celano, M.; Wolfram, J.; Voce, P.; Puxeddu, E.; Filetti, S.; Celia, C.; Ferrari, M.; Russo, D.; Fresta, M. Targeting the Thyroid Gland with Thyroid-Stimulating Hormone (TSH)-Nanoliposomes. *Biomaterials* **2014**, *35* (25), 7101–7109. https://doi.org/10.1016/j.biomaterials.2014.04.088.
(384) Zhou, X.; Zhang, M.; Yung, B.; Li, H.; Zhou, C.; Lee, L. J.; Lee, R. J. Lactosylated Liposomes for Targeted Delivery of Doxorubicin to Hepatocellular Carcinoma. *Int. J. Nanomedicine* **2012**, *7*, 5465–5474. https://doi.org/10.2147/IJN.S33965.
(385) Kirpotin, D. B.; Drummond, D. C.; Shao, Y.; Shalaby, M. R.; Hong, K.; Nielsen, U. B.; Marks, J. D.; Benz, C. C.; Park, J. W. Antibody Targeting of Long-Circulating Lipidic Nanoparticles Does Not Increase Tumor Localization but Does Increase Internalization in Animal Models. *Cancer Res.* **2006**, *66* (13), 6732–6740. https://doi.org/10.1158/0008-5472.CAN-05-4199.
(386) Lee, Y.; Thompson, D. H. Stimuli-Responsive Liposomes for Drug Delivery. *Wiley Interdiscip. Rev. Nanomed. Nanobiotechnol.* **2017**, *9* (5), 10.1002/wnan.1450. https://doi.org/10.1002/wnan.1450.
(387) Fan, Y.; Chen, C.; Huang, Y.; Zhang, F.; Lin, G. Study of the pH-Sensitive Mechanism of Tumor-Targeting Liposomes. *Colloids Surf. B Biointerfaces* **2017**, *151*, 19–25. https://doi.org/10.1016/j.colsurfb.2016.11.042.
(388) Alrbyawi, H.; Poudel, I.; Annaji, M.; Boddu, S. H. S.; Arnold, R. D.; Tiwari, A. K.; Babu, R. J. pH-Sensitive Liposomes for Enhanced Cellular Uptake and Cytotoxicity of Daunorubicin in Melanoma (B16-BL6) Cell Lines. *Pharmaceutics* **2022**, *14* (6), 1128. https://doi.org/10.3390/pharmaceutics14061128.
(389) Wang, D.-Y.; van der Mei, H. C.; Ren, Y.; Busscher, H. J.; Shi, L. Lipid-Based Antimicrobial Delivery-Systems for the Treatment of Bacterial Infections. *Front. Chem.* **2020**, *7*, 872. https://doi.org/10.3389/fchem.2019.00872.
(390) Li, Y.; Liu, R.; Yang, J.; Shi, Y.; Ma, G.; Zhang, Z.; Zhang, X. Enhanced Retention and Anti-Tumor Efficacy of Liposomes by Changing Their Cellular Uptake and Pharmacokinetics Behavior. *Biomaterials* **2015**, *41*, 1–14. https://doi.org/10.1016/j.biomaterials.2014.11.010.
(391) Yatvin, M. B.; Weinstein, J. N.; Dennis, W. H.; Blumenthal, R. Design of Liposomes for Enhanced Local Release of Drugs by Hyperthermia. *Science* **1978**, *202* (4374), 1290–1293. https://doi.org/10.1126/science.364652.
(392) Yavlovich, A.; Singh, A.; Blumenthal, R.; Puri, A. A Novel Class of Photo-Triggerable Liposomes Containing DPPC:DC8,9PC as Vehicles for Delivery of Doxorubcin to Cells. *Biochim. Biophys. Acta BBA - Biomembr.* **2011**, *1808* (1), 117–126. https://doi.org/10.1016/j.bbamem.2010.07.030.
(393) Andra, V. V. S. N. L.; Pammi, S. V. N.; Bhatraju, L. V. K. P.; Ruddaraju, L. K. A Comprehensive Review on Novel Liposomal Methodologies, Commercial Formulations, Clinical Trials and Patents. *BioNanoscience* **2022**, *12* (1), 274–291. https://doi.org/10.1007/s12668-022-00941-x.
(394) Eugster, R.; Luciani, P. Liposomes: Bridging the Gap from Lab to Pharmaceuticals. *Curr. Opin. Colloid Interface Sci.* **2025**, *75*, 101875. https://doi.org/10.1016/j.cocis.2024.101875.
(395) Peruš, M.; Knez Marevci, M.; Kotnik, P. Liposomes: Recent Progress on Nanoparticles Production and Their Usage in Medicine. *Biomater. Adv.* **2026**, *180*, 214585. https://doi.org/10.1016/j.bioadv.2025.214585.
(396) Lombardo, D.; Kiselev, M. A. Methods of Liposomes Preparation: Formation and Control Factors of Versatile Nanocarriers for Biomedical and Nanomedicine Application. *Pharmaceutics* **2022**, *14* (3), 543. https://doi.org/10.3390/pharmaceutics14030543.

(397) Bangham, A. D.; Standish, M. M.; Watkins, J. C. Diffusion of Univalent Ions across the Lamellae of Swollen Phospholipids. *J. Mol. Biol.* **1965**, *13* (1), 238-IN27. https://doi.org/10.1016/S0022-2836(65)80093-6.

(398) Zhang, H. Thin-Film Hydration Followed by Extrusion Method for Liposome Preparation. *Methods Mol. Biol. Clifton NJ* **2017**, *1522*, 17–22. https://doi.org/10.1007/978-1-4939-6591-5_2.

(399) Costa, A. P.; Xu, X.; Burgess, D. J. Freeze-Anneal-Thaw Cycling of Unilamellar Liposomes: Effect on Encapsulation Efficiency. *Pharm. Res.* **2014**, *31* (1), 97–103. https://doi.org/10.1007/s11095-013-1135-z.

(400) Gould-Fogerite, S.; Mannino, R. J. Rotary Dialysis: Its Application to the Preparation of Large Liposomes and Large Proteoliposomes (Protein-Lipid Vesicles) with High Encapsulation Efficiency and Efficient Reconstitution of Membrane Proteins. *Anal. Biochem.* **1985**, *148* (1), 15–25. https://doi.org/10.1016/0003-2697(85)90622-0.

(401) Basak, S.; Das, T. K. Liposome-Based Drug Delivery Systems: From Laboratory Research to Industrial Production—Instruments and Challenges. *ChemEngineering* **2025**, *9* (3). https://doi.org/10.3390/chemengineering9030056.

(402) Batzri, S.; Korn, E. D. Single Bilayer Liposomes Prepared without Sonication. *Biochim. Biophys. Acta BBA - Biomembr.* **1973**, *298* (4), 1015–1019. https://doi.org/10.1016/0005-2736(73)90408-2.

(403) Gouda, A.; Sakr, O. S.; Nasr, M.; Sammour, O. Ethanol Injection Technique for Liposomes Formulation: An Insight into Development, Influencing Factors, Challenges and Applications. *J. Drug Deliv. Sci. Technol.* **2021**, *61*, 102174. https://doi.org/10.1016/j.jddst.2020.102174.

(404) Wagner, A.; Vorauer-Uhl, K. Liposome Technology for Industrial Purposes. *J. Drug Deliv.* **2011**, *2011* (1), 591325. https://doi.org/10.1155/2011/591325.

(405) Szoka, F.; Papahadjopoulos, D. Procedure for Preparation of Liposomes with Large Internal Aqueous Space and High Capture by Reverse-Phase Evaporation. *Proc. Natl. Acad. Sci. U. S. A.* **1978**, *75* (9), 4194–4198. https://doi.org/10.1073/pnas.75.9.4194.

(406) Akbarzadeh, A.; Rezaei-Sadabady, R.; Davaran, S.; Joo, S. W.; Zarghami, N.; Hanifehpour, Y.; Samiei, M.; Kouhi, M.; Nejati-Koshki, K. Liposome: Classification, Preparation, and Applications. *Nanoscale Res. Lett.* **2013**, *8* (1), 102. https://doi.org/10.1186/1556-276X-8-102.

(407) Mayer, L. D.; Hope, M. J.; Cullis, P. R.; Janoff, A. S. Solute Distributions and Trapping Efficiencies Observed in Freeze-Thawed Multilamellar Vesicles. *Biochim. Biophys. Acta* **1985**, *817* (1), 193–196. https://doi.org/10.1016/0005-2736(85)90084-7.

(408) Aliño, S. F.; García, M.; Lejarreta, M.; Bobadilla, M.; Pérez-Yarza, G.; Unda, F. J. Trapping Drug Efficiency in Liposomes Produced by Extrusion of Freeze-Thaw Multilamellar Vesicles. *Biochem. Soc. Trans.* **1989**, *17* (6), 1000–1001. https://doi.org/10.1042/bst0171000.

(409) Haran, G.; Cohen, R.; Bar, L. K.; Barenholz, Y. Transmembrane Ammonium Sulfate Gradients in Liposomes Produce Efficient and Stable Entrapment of Amphipathic Weak Bases. *Biochim. Biophys. Acta BBA - Biomembr.* **1993**, *1151* (2), 201–215. https://doi.org/10.1016/0005-2736(93)90105-9.

(410) Fritze, A.; Hens, F.; Kimpfler, A.; Schubert, R.; Peschka-Süss, R. Remote Loading of Doxorubicin into Liposomes Driven by a Transmembrane Phosphate Gradient. *Biochim. Biophys. Acta BBA - Biomembr.* **2006**, *1758* (10), 1633–1640. https://doi.org/10.1016/j.bbamem.2006.05.028.

(411) Alyane, M.; Barratt, G.; Lahouel, M. Remote Loading of Doxorubicin into Liposomes by Transmembrane pH Gradient to Reduce Toxicity toward H9c2 Cells. *Saudi Pharm. J. SPJ* **2016**, *24* (2), 165–175. https://doi.org/10.1016/j.jsps.2015.02.014.

(412) Barenholz, Y. (Chezy). Doxil® — The First FDA-Approved Nano-Drug: Lessons Learned. *J. Controlled Release* **2012**, *160* (2), 117–134. https://doi.org/10.1016/j.jconrel.2012.03.020.

(413) U.S. Food and Drug Administration. Liposome Drug Products: Chemistry, Manufacturing, and Controls; Human Pharmacokinetics and Bioavailability; and Labeling Documentation. **2018**.

(414) Sheikholeslami, B.; Lam, N. W.; Dua, K.; Haghi, M. Exploring the Impact of Physicochemical Properties of Liposomal Formulations on Their *in Vivo* Fate. *Life Sci.* **2022**, *300*, 120574. https://doi.org/10.1016/j.lfs.2022.120574.

(415) Zhang, M.; Xiang, C.; Niu, R.; He, X.; Luo, W.; Liu, W.; Gu, R. Liposomes as Versatile Agents for the Management of Traumatic and Nontraumatic Central Nervous System Disorders: Drug Stability, Targeting Efficiency, and Safety. *Neural Regen. Res.* **2025**, *20* (7), 1883. https://doi.org/10.4103/NRR.NRR-D-24-00048.

(416) Hallett, F. R. Scattering and Particle Sizing, Applications. **1999**, 2067–2074. https://doi.org/10.1006/rwsp.2000.0273.

(417) Danaei, M.; Dehghankhold, M.; Ataei, S.; Hasanzadeh Davarani, F.; Javanmard, R.; Dokhani, A.; Khorasani, S.; Mozafari, M. R. Impact of Particle Size and Polydispersity Index on the Clinical Applications of Lipidic Nanocarrier Systems. *Pharmaceutics* **2018**, *10* (2), 57. https://doi.org/10.3390/pharmaceutics10020057.

(418) Beit-Yannai, E.; Tabak, S.; Stamer, W. D. Physical Exosome:Exosome Interactions. *J. Cell. Mol. Med.* **2018**, *22* (3), 2001–2006. https://doi.org/10.1111/jcmm.13479.

(419) Malvern Panalytical. How to Choose a Light Scattering Instrument for Nanoparticle Size and Zeta Potential Measurements, 2025.

(420) Filipe, V.; Hawe, A.; Jiskoot, W. Critical Evaluation of Nanoparticle Tracking Analysis (NTA) by NanoSight for the Measurement of Nanoparticles and Protein Aggregates. *Pharm. Res.* **2010**, *27* (5), 796–810. https://doi.org/10.1007/s11095-010-0073-2.

(421) Baxa, U. Imaging of Liposomes by Transmission Electron Microscopy. In *Characterization of Nanoparticles Intended for Drug Delivery*; McNeil, S. E., Ed.; Springer: New York, NY, 2018; pp 73–88. https://doi.org/10.1007/978-1-4939-7352-1_8.

(422) Trucillo, P.; Campardelli, R.; Reverchon, E. Liposomes: From Bangham to Supercritical Fluids. *Processes* **2020**, *8* (9), 1022. https://doi.org/10.3390/pr8091022.

(423) Kiselev, M. A.; Zemlyanaya, E. V.; Ryabova, N. Y.; Hauss, T.; Almasy, L.; Funari, S. S.; Zbytovska, J.; Lombardo, D. Influence of Ceramide on the Internal Structure and Hydration of the Phospholipid Bilayer Studied by Neutron and X-Ray Scattering. *Appl. Phys. A* **2014**, *116* (1), 319–325. https://doi.org/10.1007/s00339-013-8123-3.

(424) Rabanel, J.-M.; Hildgen, P.; Banquy, X. Assessment of PEG on Polymeric Particles Surface, a Key Step in Drug Carrier Translation. *J. Controlled Release* **2014**, *185*, 71–87. https://doi.org/10.1016/j.jconrel.2014.04.017.

(425) Weber, F.; Rahnfeld, L.; Luciani, P. Analytical Profiling and Stability Evaluation of Liposomal Drug Delivery Systems: A Rapid UHPLC-CAD-Based Approach for Phospholipids in Research and Quality Control. *Talanta* **2020**, *220*, 121320. https://doi.org/10.1016/j.talanta.2020.121320.

(426) Wallace, S. J.; Li, J.; Nation, R. L.; Boyd, B. J. Drug Release from Nanomedicines: Selection of Appropriate Encapsulation and Release Methodology. *Drug Deliv. Transl. Res.* **2012**, *2* (4), 284–292. https://doi.org/10.1007/s13346-012-0064-4.

(427) Ran, C.; Chen, D.; Xu, M.; Du, C.; Li, Q.; Jiang, Y. A Study on Characteristic of Different Sample Pretreatment Methods to Evaluate the Entrapment Efficiency of Liposomes. *J. Chromatogr. B* **2016**, *1028*, 56–62. https://doi.org/10.1016/j.jchromb.2016.06.008.

(428) Gonzalez Gomez, A.; Syed, S.; Marshall, K.; Hosseinidoust, Z. Liposomal Nanovesicles for Efficient Encapsulation of Staphylococcal Antibiotics. *ACS Omega* **2019**, *4* (6), 10866–10876. https://doi.org/10.1021/acsomega.9b00825.

(429) Ball, R. L.; Bajaj, P.; Whitehead, K. A. Achieving Long-Term Stability of Lipid Nanoparticles: Examining the Effect of pH, Temperature, and Lyophilization. *Int. J. Nanomedicine* **2016**, *12*, 305–315. https://doi.org/10.2147/IJN.S123062.

(430) Crommelin, D. J. A.; Fransen, G. J.; Salemink, P. J. M. Stability of Liposomes on Storage. In *Targeting of Drugs With Synthetic Systems*; Gregoriadis, G., Senior, J., Poste, G., Eds.; Springer US: Boston, MA, 1986; pp 277–287. https://doi.org/10.1007/978-1-4684-5185-6_20.

(431) Adler-Moore, J.; Proffitt, R. T. AmBisome: Liposomal Formulation, Structure, Mechanism of Action and Pre-Clinical Experience. *J. Antimicrob. Chemother.* **2002**, *49* (suppl_1), 21–30. https://doi.org/10.1093/jac/49.suppl_1.21.

(432) Schmidt-Erfurth, U.; Hasan, T. Mechanisms of Action of Photodynamic Therapy with Verteporfin for the Treatment of Age-Related Macular Degeneration. *Surv. Ophthalmol.* **2000**, *45* (3), 195–214. https://doi.org/10.1016/S0039-6257(00)00158-2.

(433) He, Y.; Zhang, W.; Xiao, Q.; Fan, L.; Huang, D.; Chen, W.; He, W. Liposomes and Liposome-like Nanoparticles: From Anti-Fungal Infection to the COVID-19 Pandemic Treatment. *Asian J. Pharm. Sci.* **2022**, *17* (6), 817–837. https://doi.org/10.1016/j.ajps.2022.11.002.

(434) Shirley, M. Amikacin Liposome Inhalation Suspension: A Review in Mycobacterium Avium Complex Lung Disease. *Drugs* **2019**, *79* (5), 555–562. https://doi.org/10.1007/s40265-019-01095-z.

(435) Kenaan, H. T.; Duncan, R. M.; Al-Jamal, W. T.; Jones, D. S.; Andrews, G. P.; Gilmore, B.; Yardley, V.; Farrington, N.; Stott, K. E.; Lawrence, D.; Jarvis, J. N.; Harrison, T. S.; Robinson, S.; Ribeiro, I.; Hope, W.; Tian, Y. Liposomal Antimicrobials in the Fight against Bacterial and Fungal Pathogens: Clinical Successes and Development Challenges. *Int. J. Pharm. X* **2026**, *11*, 100478. https://doi.org/10.1016/j.ijpx.2025.100478.

(436) Sizar, O.; Rahman, S.; Sundareshan, V. Amikacin. In *StatPearls*; StatPearls Publishing: Treasure Island (FL), 2025.

(437) Thy, M.; Timsit, J.-F.; de Montmollin, E. Aminoglycosides for the Treatment of Severe Infection Due to Resistant Gram-Negative Pathogens. *Antibiotics* **2023**, *12* (5), 860. https://doi.org/10.3390/antibiotics12050860.

(438) Ramirez, M. S.; Tolmasky, M. E. Amikacin: Uses, Resistance, and Prospects for Inhibition. *Mol. J. Synth. Chem. Nat. Prod. Chem.* **2017**, *22* (12), 2267. https://doi.org/10.3390/molecules22122267.

(439) Meers, P.; Neville, M.; Malinin, V.; Scotto, A. W.; Sardaryan, G.; Kurumunda, R.; Mackinson, C.; James, G.; Fisher, S.; Perkins, W. R. Biofilm Penetration, Triggered Release and in Vivo Activity of Inhaled Liposomal Amikacin in Chronic Pseudomonas Aeruginosa Lung Infections. *J. Antimicrob. Chemother.* **2008**, *61* (4), 859–868. https://doi.org/10.1093/jac/dkn059.

(440) Zhang, J.; Leifer, F.; Rose, S.; Chun, D. Y.; Thaisz, J.; Herr, T.; Nashed, M.; Joseph, J.; Perkins, W. R.; DiPetrillo, K. Amikacin Liposome Inhalation Suspension (ALIS) Penetrates Non-Tuberculous Mycobacterial Biofilms and Enhances Amikacin Uptake Into Macrophages. *Front. Microbiol.* **2018**, *9*. https://doi.org/10.3389/fmicb.2018.00915.

(441) FDA. *ARIKAYCE (amikacin liposome inhalation suspension), for oral inhalation use - label.* https://www.accessdata.fda.gov/drugsatfda_docs/label/2018/207356s000lbl.pdf (accessed 2026-02-06).

(442) Malinin, V.; Neville, M.; Eagle, G.; Gupta, R.; Perkins, W. R. Pulmonary Deposition and Elimination of Liposomal Amikacin for Inhalation and Effect on Macrophage Function after Administration in Rats. *Antimicrob. Agents Chemother.* **2016**, *60* (11), 6540–6549. https://doi.org/10.1128/aac.00700-16.

(443) Ferreira, M.; Ogren, M.; Dias, J. N. R.; Silva, M.; Gil, S.; Tavares, L.; Aires-da-Silva, F.; Gaspar, M. M.; Aguiar, S. I. Liposomes as Antibiotic Delivery Systems: A Promising Nanotechnological Strategy against Antimicrobial Resistance. *Molecules* **2021**, *26* (7), 2047. https://doi.org/10.3390/molecules26072047.

(444) Ghosh, R.; De, M. Liposome-Based Antibacterial Delivery: An Emergent Approach to Combat Bacterial Infections. *ACS Omega* **2023**, *8* (39), 35442–35451. https://doi.org/10.1021/acsomega.3c04893.

(445) Sande, L.; Sanchez, M.; Montes, J.; Wolf, A. J.; Morgan, M. A.; Omri, A.; Liu, G. Y. Liposomal Encapsulation of Vancomycin Improves Killing of Methicillin-Resistant Staphylococcus Aureus in a Murine Infection Model. *J. Antimicrob. Chemother.* **2012**, *67* (9), 2191–2194. https://doi.org/10.1093/jac/dks212.
(446) Muppidi, K.; Wang, J.; Betageri, G.; Pumerantz, A. S. PEGylated Liposome Encapsulation Increases the Lung Tissue Concentration of Vancomycin. *Antimicrob. Agents Chemother.* **2011**, *55* (10), 4537–4542. https://doi.org/10.1128/aac.00713-11.
(447) Zhu, R.; Yin, Z.; Liu, N.; Wang, Z.; Zhang, H.; Li, J.; Shen, L.; Zheng, A. Polymyxin B-Modified Fosfomycin Liposomes Target Gram-Negative Bacteria and Exert Synergistic Antibacterial Effect. *ACS Omega* **2023**, *8* (48), 45914–45923. https://doi.org/10.1021/acsomega.3c06719.
(448) Alipour, M.; Halwani, M.; Omri, A.; Suntres, Z. E. Antimicrobial Effectiveness of Liposomal Polymyxin B against Resistant Gram-Negative Bacterial Strains. *Int. J. Pharm.* **2008**, *355* (1), 293–298. https://doi.org/10.1016/j.ijpharm.2007.11.035.
(449) Nicolosi, D.; Scalia, M.; Nicolosi, V. M.; Pignatello, R. Encapsulation in Fusogenic Liposomes Broadens the Spectrum of Action of Vancomycin against Gram-Negative Bacteria. *Int. J. Antimicrob. Agents* **2010**, *35* (6), 553–558. https://doi.org/10.1016/j.ijantimicag.2010.01.015.
(450) Fernandes, P. Fusidic Acid: A Bacterial Elongation Factor Inhibitor for the Oral Treatment of Acute and Chronic Staphylococcal Infections. *Cold Spring Harb. Perspect. Med.* **2016**, *6* (1), a025437. https://doi.org/10.1101/cshperspect.a025437.
(451) Biedenbach, D. J.; Rhomberg, P. R.; Mendes, R. E.; Jones, R. N. Spectrum of Activity, Mutation Rates, Synergistic Interactions, and the Effects of pH and Serum Proteins for Fusidic Acid (CEM-102). *Diagn. Microbiol. Infect. Dis.* **2010**, *66* (3), 301–307. https://doi.org/10.1016/j.diagmicrobio.2009.10.014.
(452) Nicolosi, D.; Cupri, S.; Genovese, C.; Tempera, G.; Mattina, R.; Pignatello, R. Nanotechnology Approaches for Antibacterial Drug Delivery: Preparation and Microbiological Evaluation of Fusogenic Liposomes Carrying Fusidic Acid. *Int. J. Antimicrob. Agents* **2015**, *45* (6), 622–626. https://doi.org/10.1016/j.ijantimicag.2015.01.016.
(453) Nacucchio, M. C.; Bellora, M. J.; Sordelli, D. O.; D'Aquino, M. Enhanced Liposome-Mediated Activity of Piperacillin against Staphylococci. *Antimicrob. Agents Chemother.* **1985**, *27* (1), 137–139. https://doi.org/10.1128/aac.27.1.137.
(454) Makhlouf, Z.; Ali, A. A.; Al-Sayah, M. H. Liposomes-Based Drug Delivery Systems of Anti-Biofilm Agents to Combat Bacterial Biofilm Formation. *Antibiotics* **2023**, *12* (5), 875. https://doi.org/10.3390/antibiotics12050875.
(455) Ahsan, A.; Thomas, N.; Barnes, T. J.; Subramaniam, S.; Loh, T. C.; Joyce, P.; Prestidge, C. A. Lipid Nanocarriers-Enabled Delivery of Antibiotics and Antimicrobial Adjuvants to Overcome Bacterial Biofilms. *Pharmaceutics* **2024**, *16* (3), 396. https://doi.org/10.3390/pharmaceutics16030396.
(456) Forier, K.; Raemdonck, K.; De Smedt, S. C.; Demeester, J.; Coenye, T.; Braeckmans, K. Lipid and Polymer Nanoparticles for Drug Delivery to Bacterial Biofilms. *J. Controlled Release* **2014**, *190*, 607–623. https://doi.org/10.1016/j.jconrel.2014.03.055.
(457) Sugano, M.; Morisaki, H.; Negishi, Y.; Endo-Takahashi, Y.; Kuwata, H.; Miyazaki, T.; Yamamoto, M. Potential Effect of Cationic Liposomes on Interactions with Oral Bacterial Cells and Biofilms. *J. Liposome Res.* **2016**, *26* (2), 156–162. https://doi.org/10.3109/08982104.2015.1063648.
(458) Dong, D.; Thomas, N.; Thierry, B.; Vreugde, S.; Prestidge, C. A.; Wormald, P.-J. Distribution and Inhibition of Liposomes on Staphylococcus Aureus and Pseudomonas Aeruginosa Biofilm. *PLOS ONE* **2015**, *10* (6), e0131806. https://doi.org/10.1371/journal.pone.0131806.
(459) Amer, A. M.; Charnock, C.; Nguyen, S. The Impact of Surface Charge on the Interaction of Cholesterol-Free Fusogenic Liposomes with Planktonic Microbial Cells and Biofilms. *Int. J. Pharm.* **2025**, *669*, 125088. https://doi.org/10.1016/j.ijpharm.2024.125088.

(460) Scriboni, A. B.; Couto, V. M.; Ribeiro, L. N. de M.; Freires, I. A.; Groppo, F. C.; de Paula, E.; Franz-Montan, M.; Cogo-Müller, K. Fusogenic Liposomes Increase the Antimicrobial Activity of Vancomycin Against Staphylococcus Aureus Biofilm. *Front. Pharmacol.* **2019**, *10*. https://doi.org/10.3389/fphar.2019.01401.

(461) Hou, Y.; Wang, Z.; Zhang, P.; Bai, H.; Sun, Y.; Duan, J.; Mu, H. Lysozyme Associated Liposomal Gentamicin Inhibits Bacterial Biofilm. *Int. J. Mol. Sci.* **2017**, *18* (4), 784. https://doi.org/10.3390/ijms18040784.

(462) Fang, J.-Y.; Chou, W.-L.; Lin, C.-F.; Sung, C. T.; Alalaiwe, A.; Yang, S.-C. Facile Biofilm Penetration of Cationic Liposomes Loaded with DNase I/Proteinase K to Eradicate Cutibacterium Acnes for Treating Cutaneous and Catheter Infections. *Int. J. Nanomedicine* **2021**, *16*, 8121–8138. https://doi.org/10.2147/IJN.S335804.

(463) Lamichhane, N.; Udayakumar, T. S.; D'Souza, W. D.; Simone, C. B.; Raghavan, S. R.; Polf, J.; Mahmood, J. Liposomes: Clinical Applications and Potential for Image-Guided Drug Delivery. *Mol. J. Synth. Chem. Nat. Prod. Chem.* **2018**, *23* (2), 288. https://doi.org/10.3390/molecules23020288.

(464) Nsairat, H.; Khater, D.; Sayed, U.; Odeh, F.; Al Bawab, A.; Alshaer, W. Liposomes: Structure, Composition, Types, and Clinical Applications. *Heliyon* **2022**, *8* (5), e09394. https://doi.org/10.1016/j.heliyon.2022.e09394.

(465) Sercombe, L.; Veerati, T.; Moheimani, F.; Wu, S. Y.; Sood, A. K.; Hua, S. Advances and Challenges of Liposome Assisted Drug Delivery. *Front. Pharmacol.* **2015**, *6*, 286. https://doi.org/10.3389/fphar.2015.00286.

(466) Narang, A.; Chang, R.-K.; Hussain, M. A. Pharmaceutical Development and Regulatory Considerations for Nanoparticles and Nanoparticulate Drug Delivery Systems. *J. Pharm. Sci.* **2013**, *102* (11), 3867–3882. https://doi.org/10.1002/jps.23691.

(467) Tinkle, S.; McNeil, S. E.; Mühlebach, S.; Bawa, R.; Borchard, G.; Barenholz, Y. (Chezy); Tamarkin, L.; Desai, N. Nanomedicines: Addressing the Scientific and Regulatory Gap. *Ann. N. Y. Acad. Sci.* **2014**, *1313* (1), 35–56. https://doi.org/10.1111/nyas.12403.

(468) Ulrich, A. S. Biophysical Aspects of Using Liposomes as Delivery Vehicles. *Biosci. Rep.* **2002**, *22* (2), 129–150. https://doi.org/10.1023/A:1020178304031.

(469) Stark, B.; Pabst, G.; Prassl, R. Long-Term Stability of Sterically Stabilized Liposomes by Freezing and Freeze-Drying: Effects of Cryoprotectants on Structure. *Eur. J. Pharm. Sci.* **2010**, *41* (3), 546–555. https://doi.org/10.1016/j.ejps.2010.08.010.

(470) Gonzalez Gomez, A.; Xu, C.; Hosseinidoust, Z. Preserving the Efficacy of Glycopeptide Antibiotics during Nanoencapsulation in Liposomes. *ACS Infect. Dis.* **2019**, *5* (10), 1794–1801. https://doi.org/10.1021/acsinfecdis.9b00232.

(471) Campbell, R. E.; Chen, C. H.; Edelstein, C. L. Overview of Antibiotic-Induced Nephrotoxicity. *Kidney Int. Rep.* **2023**, *8* (11), 2211–2225. https://doi.org/10.1016/j.ekir.2023.08.031.

(472) Rukavina, Z.; Vanić, Ž. Current Trends in Development of Liposomes for Targeting Bacterial Biofilms. *Pharmaceutics* **2016**, *8* (2), 18. https://doi.org/10.3390/pharmaceutics8020018.

(473) Szoka, F.; Papahadjopoulos, D. Procedure for Preparation of Liposomes with Large Internal Aqueous Space and High Capture by Reverse-Phase Evaporation. *Proc. Natl. Acad. Sci. U. S. A.* **1978**, *75* (9), 4194–4198. https://doi.org/10.1073/pnas.75.9.4194.

(474) Yu, J.; Zhang, H.; Li, Y.; Sun, S.; Gao, J.; Zhong, Y.; Sun, D.; Zhang, G. Metabolomics Revealed the Toxicity of Cationic Liposomes in HepG2 Cells Using UHPLC-Q-TOF/MS and Multivariate Data Analysis. *Biomed. Chromatogr. BMC* **2017**, *31* (12). https://doi.org/10.1002/bmc.4036.

(475) Omri, A.; Ravaoarinoro, M. Comparison of the Bactericidal Action of Amikacin, Netilmicin and Tobramycin in Free and Liposomal Formulation against Pseudomonas Aeruginosa. *Chemotherapy* **2009**, *42* (3), 170–176. https://doi.org/10.1159/000239438.

(476) Meng, Y.; Hou, X.; Lei, J.; Chen, M.; Cong, S.; Zhang, Y.; Ding, W.; Li, G.; Li, X. Multi-Functional Liposomes Enhancing Target and Antibacterial Immunity for Antimicrobial and Anti-Biofilm Against Methicillin-Resistant Staphylococcus Aureus. *Pharm. Res.* **2016**, *33* (3), 763–775. https://doi.org/10.1007/s11095-015-1825-9.

(477) Messiaen, A.-S.; Forier, K.; Nelis, H.; Braeckmans, K.; Coenye, T. Transport of Nanoparticles and Tobramycin-Loaded Liposomes in Burkholderia Cepacia Complex Biofilms. *PLOS ONE* **2013**, *8* (11), e79220. https://doi.org/10.1371/journal.pone.0079220.

(478) Grogan, S. P.; Mount, C. A. Ultrasound Physics and Instrumentation. In *StatPearls*; StatPearls Publishing: Treasure Island (FL), 2023.

(479) Poggi, C.; Palavecino, M. Ultrasound Principles and Instrumentation. *Surg. Open Sci.* **2024**, *18*, 123–128. https://doi.org/10.1016/j.sopen.2024.02.005.

(480) Zuckerwar, A. J. Acoustical Measurement. **2003**, 91–115. https://doi.org/10.1016/B0-12-227410-5/00008-9.

(481) Pitt, W. G.; Husseini, G. A.; Staples, B. J. Ultrasonic Drug Delivery – A General Review. *Expert Opin. Drug Deliv.* **2004**, *1* (1), 37–56. https://doi.org/10.1517/17425247.1.1.37.

(482) Deprez, J.; Lajoinie, G.; Engelen, Y.; De Smedt, S. C.; Lentacker, I. Opening Doors with Ultrasound and Microbubbles: Beating Biological Barriers to Promote Drug Delivery. *Adv. Drug Deliv. Rev.* **2021**, *172*, 9–36. https://doi.org/10.1016/j.addr.2021.02.015.

(483) Miller, D.; Smith, N.; Bailey, M.; Czarnota, G.; Hynynen, K.; Makin, I. Overview of Therapeutic Ultrasound Applications and Safety Considerations. *J. Ultrasound Med. Off. J. Am. Inst. Ultrasound Med.* **2012**, *31* (4), 623–634. https://doi.org/10.7863/jum.2012.31.4.623.

(484) Wang, T.-Y.; Wilson, K. E.; Machtaler, S.; Willmann, J. K. Ultrasound and Microbubble Guided Drug Delivery: Mechanistic Understanding and Clinical Implications. *Curr. Pharm. Biotechnol.* **2014**, *14* (8), 743–752. https://doi.org/10.2174/1389201014666131226114611.

(485) ter Haar, G. Therapeutic Applications of Ultrasound. *Prog. Biophys. Mol. Biol.* **2007**, *93* (1), 111–129. https://doi.org/10.1016/j.pbiomolbio.2006.07.005.

(486) Mason, T. J. Therapeutic Ultrasound an Overview. *Ultrason. Sonochem.* **2011**, *18* (4), 847–852. https://doi.org/10.1016/j.ultsonch.2011.01.004.

(487) Ihnatsenka, B.; Boezaart, A. P. Ultrasound: Basic Understanding and Learning the Language. *Int. J. Shoulder Surg.* **2010**, *4* (3), 55–62. https://doi.org/10.4103/0973-6042.76960.

(488) Carovac, A.; Smajlovic, F.; Junuzovic, D. Application of Ultrasound in Medicine. *Acta Inform. Medica* **2011**, *19* (3), 168–171. https://doi.org/10.5455/aim.2011.19.168-171.

(489) Recker, F.; Gembruch, U.; Strizek, B. Clinical Ultrasound Applications in Obstetrics and Gynecology in the Year 2024. *J. Clin. Med.* **2024**, *13* (5), 1244. https://doi.org/10.3390/jcm13051244.

(490) Paefgen, V.; Doleschel, D.; Kiessling, F. Evolution of Contrast Agents for Ultrasound Imaging and Ultrasound-Mediated Drug Delivery. *Front. Pharmacol.* **2015**, *6*, 197. https://doi.org/10.3389/fphar.2015.00197.

(491) Frinking, P.; Segers, T.; Luan, Y.; Tranquart, F. Three Decades of Ultrasound Contrast Agents: A Review of the Past, Present and Future Improvements. *Ultrasound Med. Biol.* **2020**, *46* (4), 892–908. https://doi.org/10.1016/j.ultrasmedbio.2019.12.008.

(492) Calliada, F.; Campani, R.; Bottinelli, O.; Bozzini, A.; Sommaruga, M. G. Ultrasound Contrast Agents: Basic Principles. *Eur. J. Radiol.* **1998**, *27*, S157–S160. https://doi.org/10.1016/S0720-048X(98)00057-6.

(493) Stride, E. P.; Coussios, C. C. Cavitation and Contrast: The Use of Bubbles in Ultrasound Imaging and Therapy. *Proc. Inst. Mech. Eng. [H]* **2010**, *224* (2), 171–191. https://doi.org/10.1243/09544119JEIM622.

(494) Jangjou, A.; Meisami, A. H.; Jamali, K.; Niakan, M. H.; Abbasi, M.; Shafiee, M.; Salehi, M.; Hosseinzadeh, A.; Amani, A. M.; Vaez, A. The Promising Shadow of Microbubble over Medical

Sciences: From Fighting Wide Scope of Prevalence Disease to Cancer Eradication. *J. Biomed. Sci.* **2021**, *28*, 49. https://doi.org/10.1186/s12929-021-00744-4.

(495) Sirsi, S.; Borden, M. Microbubble Compositions, Properties and Biomedical Applications. *Bubble Sci. Eng. Technol.* **2009**, *1* (1–2), 3–17. https://doi.org/10.1179/175889709X446507.

(496) Ignee, A.; Atkinson, N. S. S.; Schuessler, G.; Dietrich, C. F. Ultrasound Contrast Agents. *Endosc. Ultrasound* **2016**, *5* (6), 355–362. https://doi.org/10.4103/2303-9027.193594.

(497) Roovers, S.; Segers, T.; Lajoinie, G.; Deprez, J.; Versluis, M.; De Smedt, S. C.; Lentacker, I. The Role of Ultrasound-Driven Microbubble Dynamics in Drug Delivery: From Microbubble Fundamentals to Clinical Translation. *Langmuir* **2019**, *35* (31), 10173–10191. https://doi.org/10.1021/acs.langmuir.8b03779.

(498) Xin, Z.; Lin, G.; Lei, H.; Lue, T. F.; Guo, Y. Clinical Applications of Low-Intensity Pulsed Ultrasound and Its Potential Role in Urology. *Transl. Androl. Urol.* **2016**, *5* (2), 255–266. https://doi.org/10.21037/tau.2016.02.04.

(499) Neppiras, E. A. Acoustic Cavitation. *Phys. Rep.* **1980**, *61* (3), 159–251. https://doi.org/10.1016/0370-1573(80)90115-5.

(500) Kooiman, K.; Roovers, S.; Langeveld, S. A. G.; Kleven, R. T.; Dewitte, H.; O'Reilly, M. A.; Escoffre, J.-M.; Bouakaz, A.; Verweij, M. D.; Hynynen, K.; Lentacker, I.; Stride, E.; Holland, C. K. Ultrasound-Responsive Cavitation Nuclei for Therapy and Drug Delivery. *Ultrasound Med. Biol.* **2020**, *46* (6), 1296–1325. https://doi.org/10.1016/j.ultrasmedbio.2020.01.002.

(501) Lentacker, I.; De Cock, I.; Deckers, R.; De Smedt, S. C.; Moonen, C. T. W. Understanding Ultrasound Induced Sonoporation: Definitions and Underlying Mechanisms. *Adv. Drug Deliv. Rev.* **2014**, *72*, 49–64. https://doi.org/10.1016/j.addr.2013.11.008.

(502) Delalande, A.; Leduc, C.; Midoux, P.; Postema, M.; Pichon, C. Efficient Gene Delivery by Sonoporation Is Associated with Microbubble Entry into Cells and the Clathrin-Dependent Endocytosis Pathway. *Ultrasound Med. Biol.* **2015**, *41* (7), 1913–1926. https://doi.org/10.1016/j.ultrasmedbio.2015.03.010.

(503) Tan, J.-K. Y.; Pham, B.; Zong, Y.; Perez, C.; Maris, D. O.; Hemphill, A.; Miao, C. H.; Matula, T. J.; Mourad, P. D.; Wei, H.; Sellers, D. L.; Horner, P. J.; Pun, S. H. Microbubbles and Ultrasound Increase Intraventricular Polyplex Gene Transfer to the Brain. *J. Controlled Release* **2016**, *231*, 86–93. https://doi.org/10.1016/j.jconrel.2016.02.003.

(504) Prentice, P.; Cuschieri, A.; Dholakia, K.; Prausnitz, M.; Campbell, P. Membrane Disruption by Optically Controlled Microbubble Cavitation. *Nat. Phys.* **2005**, *1* (2), 107–110. https://doi.org/10.1038/nphys148.

(505) Holt, R. G.; Roy, R. A. Measurements of Bubble-Enhanced Heating from Focused, Mhz-Frequency Ultrasound in a Tissue-Mimicking Material. *Ultrasound Med. Biol.* **2001**, *27* (10), 1399–1412. https://doi.org/10.1016/S0301-5629(01)00438-0.

(506) Juffermans, L. J. M.; Dijkmans, P. A.; Musters, R. J. P.; Visser, C. A.; Kamp, O. Transient Permeabilization of Cell Membranes by Ultrasound-Exposed Microbubbles Is Related to Formation of Hydrogen Peroxide. *Am. J. Physiol.-Heart Circ. Physiol.* **2006**, *291* (4), H1595–H1601. https://doi.org/10.1152/ajpheart.01120.2005.

(507) Tacker, J. R.; Anderson, R. U. Delivery of Antitumor Drug to Bladder Cancer by Use of Phase Transition Liposomes and Hyperthermia. *J. Urol.* **1982**, *127* (6), 1211–1214. https://doi.org/10.1016/s0022-5347(17)54299-8.

(508) Dong, H.-Q.; Fu, X.-F.; Wang, M.-Y.; Zhu, J. Research Progress on Reactive Oxygen Species Production Mechanisms in Tumor Sonodynamic Therapy. *World J. Clin. Cases* **2023**, *11* (22), 5193–5203. https://doi.org/10.12998/wjcc.v11.i22.5193.

(509) Nakonechny, F.; Nisnevitch, M. Different Aspects of Using Ultrasound to Combat Microorganisms. *Adv. Funct. Mater.* **2021**, *31* (44), 2011042. https://doi.org/10.1002/adfm.202011042.

(510) Lyons, B.; Balkaran, J. P. R.; Dunn-Lawless, D.; Lucian, V.; Keller, S. B.; O'Reilly, C. S.; Hu, L.; Rubasingham, J.; Nair, M.; Carlisle, R.; Stride, E.; Gray, M.; Coussios, C. Sonosensitive Cavitation Nuclei—A Customisable Platform Technology for Enhanced Therapeutic Delivery. *Molecules* **2023**, *28* (23), 7733. https://doi.org/10.3390/molecules28237733.

(511) Kwan, J. J.; Myers, R.; Coviello, C. M.; Graham, S. M.; Shah, A. R.; Stride, E.; Carlisle, R. C.; Coussios, C. C. Ultrasound-Propelled Nanocups for Drug Delivery. *Small* **2015**, *11* (39), 5305–5314. https://doi.org/10.1002/smll.201501322.

(512) Zhang, W.; Shi, Y.; Shukor, S. A.; Vijayakumaran, A.; Vlatakis, S.; Wright, M.; Thanou, M. Phase-Shift Nanodroplets as an Emerging Sonoresponsive Nanomaterial for Imaging and Drug Delivery Applications. *Nanoscale* **2022**, *14* (8), 2943–2965. https://doi.org/10.1039/D1NR07882H.

(513) Paul, S.; Nahire, R.; Mallik, S.; Sarkar, K. Encapsulated Microbubbles and Echogenic Liposomes for Contrast Ultrasound Imaging and Targeted Drug Delivery. *Comput. Mech.* **2014**, *53* (3), 413–435. https://doi.org/10.1007/s00466-013-0962-4.

(514) Dayton, P. A.; Morgan, K. E.; Klibanov, A. L.; Brandenburger, G. H.; Ferrara, K. W. Optical and Acoustical Observations of the Effects of Ultrasound on Contrast Agents. *IEEE Trans. Ultrason. Ferroelectr. Freq. Control* **1999**, *46* (1), 220–232. https://doi.org/10.1109/58.741536.

(515) Yang, H.; Sun, Y.; Wei, J.; Xu, L.; Tang, Y.; Yang, L.; Zhang, X.; Lu, Y. The Effects of Ultrasound-Targeted Microbubble Destruction (UTMD) Carrying IL-8 Monoclonal Antibody on the Inflammatory Responses and Stability of Atherosclerotic Plaques. *Biomed. Pharmacother.* **2019**, *118*, 109161. https://doi.org/10.1016/j.biopha.2019.109161.

(516) Cochran, M. C.; Eisenbrey, J.; Ouma, R. O.; Soulen, M.; Wheatley, M. A. Doxorubicin and Paclitaxel Loaded Microbubbles for Ultrasound Triggered Drug Delivery. *Int. J. Pharm.* **2011**, *414* (1), 161–170. https://doi.org/10.1016/j.ijpharm.2011.05.030.

(517) Upadhyay, A.; Dalvi, S. V. Microbubble Formulations: Synthesis, Stability, Modeling and Biomedical Applications. *Ultrasound Med. Biol.* **2019**, *45* (2), 301–343. https://doi.org/10.1016/j.ultrasmedbio.2018.09.022.

(518) Tartis, M. S.; McCallan, J.; Lum, A. F. H.; LaBell, R.; Stieger, S. M.; Matsunaga, T. O.; Ferrara, K. W. Therapeutic Effects of Paclitaxel-Containing Ultrasound Contrast Agents. *Ultrasound Med. Biol.* **2006**, *32* (11), 1771–1780. https://doi.org/10.1016/j.ultrasmedbio.2006.03.017.

(519) Liang, Z.; Chen, H.; Gong, X.; Shi, B.; Lin, L.; Tao, F.; Wu, Q.; Fang, M.; Li, H.; Lu, C.; Xu, H.; Zhao, Y.; Chen, B. Ultrasound-Induced Destruction of Nitric Oxide–Loaded Microbubbles in the Treatment of Thrombus and Ischemia–Reperfusion Injury. *Front. Pharmacol.* **2022**, *12*. https://doi.org/10.3389/fphar.2021.745693.

(520) Lafond, M.; Shekhar, H.; Panmanee, W.; Collins, S. D.; Palaniappan, A.; McDaniel, C. T.; Hassett, D. J.; Holland, C. K. Bactericidal Activity of Lipid-Shelled Nitric Oxide-Loaded Microbubbles. *Front. Pharmacol.* **2020**, *10*, 1540. https://doi.org/10.3389/fphar.2019.01540.

(521) Grishenkov, D.; Gonon, A.; Weitzberg, E.; Lundberg, J. O.; Harmark, J.; Cerroni, B.; Paradossi, G.; Janerot-Sjoberg, B. Ultrasound Contrast Agent Loaded with Nitric Oxide as a Theranostic Microdevice. *Drug Des. Devel. Ther.* **2015**, *9*, 2409–2419. https://doi.org/10.2147/DDDT.S77790.

(522) Kooiman, K.; Vos, H. J.; Versluis, M.; de Jong, N. Acoustic Behavior of Microbubbles and Implications for Drug Delivery. *Adv. Drug Deliv. Rev.* **2014**, *72*, 28–48. https://doi.org/10.1016/j.addr.2014.03.003.

(523) Navarro-Becerra, J. A.; Borden, M. A. Targeted Microbubbles for Drug, Gene, and Cell Delivery in Therapy and Immunotherapy. *Pharmaceutics* **2023**, *15* (6), 1625. https://doi.org/10.3390/pharmaceutics15061625.

(524) Fernandes, D. A. Comprehensive Review on Bubbles: Synthesis, Modification, Characterization and Biomedical Applications. *Bioconjug. Chem.* **2024**, *35* (11), 1639–1686. https://doi.org/10.1021/acs.bioconjchem.4c00137.

(525) Stride, E.; Edirisinghe, M. Novel Microbubble Preparation Technologies. *Soft Matter* **2008**, *4* (12), 2350–2359. https://doi.org/10.1039/B809517P.
(526) Hettiarachchi, K.; Talu, E.; Longo, M. L.; Dayton, P. A.; Lee, A. P. On-Chip Generation of Microbubbles as a Practical Technology for Manufacturing Contrast Agents for Ultrasonic Imaging. *Lab. Chip* **2007**, *7* (4), 463–468. https://doi.org/10.1039/b701481n.
(527) Dalla Palma, L.; Bertolotto, M. Introduction to Ultrasound Contrast Agents: Physics Overview. *Eur. Radiol.* **1999**, *9* (3), S338–S342. https://doi.org/10.1007/PL00014069.
(528) Barak, M.; Katz, Y. Microbubbles. *Chest* **2005**, *128* (4), 2918–2932. https://doi.org/10.1378/chest.128.4.2918.
(529) Daeichin, V.; Van Rooij, T.; Skachkov, I.; Ergin, B.; Specht, P. A. C.; Lima, A.; Ince, C.; Bosch, J. G.; Van Der Steen, A. F. W.; De Jong, N.; Kooiman, K. Microbubble Composition and Preparation for High-Frequency Contrast-Enhanced Ultrasound Imaging: *In Vitro* and *In Vivo* Evaluation. *IEEE Trans. Ultrason. Ferroelectr. Freq. Control* **2017**, *64* (3), 555–567. https://doi.org/10.1109/TUFFC.2016.2640342.
(530) Davoodi, P.; Feng, F.; Xu, Q.; Yan, W.-C.; Tong, Y. W.; Srinivasan, M. P.; Sharma, V. K.; Wang, C.-H. Coaxial Electrohydrodynamic Atomization: Microparticles for Drug Delivery Applications. *J. Controlled Release* **2015**, *205*, 70–82. https://doi.org/10.1016/j.jconrel.2014.12.004.
(531) Chen, C.; Liu, W.; Jiang, P.; Hong, T. Coaxial Electrohydrodynamic Atomization for the Production of Drug-Loaded Micro/Nanoparticles. *Micromachines* **2019**, *10* (2), 125. https://doi.org/10.3390/mi10020125.
(532) van den Broek, M. R. P.; Sikkema, H. G.; Satpathi, N. S.; Kleinsmit, L.; van den Berg, A.; Versluis, M.; Segers, T. Accurate Sizing of Monodisperse Microbubble Suspensions by Optical Attenuation Spectroscopy. *Ultrasound Med. Biol.* **2026**, *52* (2), 305–314. https://doi.org/10.1016/j.ultrasmedbio.2025.08.022.
(533) Rhyner, M. N. The Coulter Principle for Analysis of Subvisible Particles in Protein Formulations. *AAPS J.* **2011**, *13* (1), 54–58. https://doi.org/10.1208/s12248-010-9245-6.
(534) Izadifar, Z.; Babyn, P.; Chapman, D. Ultrasound Cavitation/Microbubble Detection and Medical Applications. *J. Med. Biol. Eng.* **2019**, *39* (3), 259–276. https://doi.org/10.1007/s40846-018-0391-0.
(535) Madanshetty, S. I.; Roy, R. A.; Apfel, R. E. Acoustic Microcavitation: Its Active and Passive Acoustic Detection. *J. Acoust. Soc. Am.* **1991**, *90* (3), 1515–1526. https://doi.org/10.1121/1.401891.
(536) Garay, G.; Abraham, Y.; Cortela, G.; Benech, N.; Negreira, C. Passive and Active Cavitation Detection Methods: Inception and Persistence during HIFU Sonication. In *2023 IEEE International Ultrasonics Symposium (IUS)*; 2023; pp 1–4. https://doi.org/10.1109/IUS51837.2023.10307234.
(537) Wu, P.; Wang, X.; Lin, W.; Bai, L. Acoustic Characterization of Cavitation Intensity: A Review. *Ultrason. Sonochem.* **2022**, *82*, 105878. https://doi.org/10.1016/j.ultsonch.2021.105878.
(538) Shinar, H.; Ilovitsh, T. Volumetric Passive Acoustic Mapping and Cavitation Detection of Nanobubbles under Low-Frequency Insonation. *ACS Mater. Au* **2025**, *5* (1), 159–169. https://doi.org/10.1021/acsmaterialsau.4c00064.
(539) Salgaonkar, V. A.; Datta, S.; Holland, C. K.; Mast, T. D. Passive Cavitation Imaging with Ultrasound Arrays. *J. Acoust. Soc. Am.* **2009**, *126* (6), 3071–3083. https://doi.org/10.1121/1.3238260.
(540) Starkoff, B. Ultrasound Physical Principles in Today's Technology. *Australas. J. Ultrasound Med.* **2014**, *17* (1), 4–10. https://doi.org/10.1002/j.2205-0140.2014.tb00086.x.
(541) Gu, Y.; Chen, C.; Tu, J.; Guo, X.; Wu, H.; Zhang, D. Harmonic Responses and Cavitation Activity of Encapsulated Microbubbles Coupled with Magnetic Nanoparticles. *Ultrason. Sonochem.* **2016**, *29*, 309–316. https://doi.org/10.1016/j.ultsonch.2015.10.006.

(542) Li, J.; Ahn, J.; Liu, D.; Chen, S.; Ye, X.; Ding, T. Evaluation of Ultrasound-Induced Damage to Escherichia Coli and Staphylococcus Aureus by Flow Cytometry and Transmission Electron Microscopy. *Appl. Environ. Microbiol.* **2016**, *82* (6), 1828–1837. https://doi.org/10.1128/AEM.03080-15.

(543) Pitt, W. G.; McBride, M. O.; Lunceford, J. K.; Roper, R. J.; Sagers, R. D. Ultrasonic Enhancement of Antibiotic Action on Gram-Negative Bacteria. *Antimicrob. Agents Chemother.* **1994**, *38* (11), 2577–2582. https://doi.org/10.1128/aac.38.11.2577.

(544) Klibanov, A. L.; Shevchenko, T. I.; Raju, B. I.; Seip, R.; Chin, C. T. Ultrasound-Triggered Release of Materials Entrapped in Microbubble–Liposome Constructs: A Tool for Targeted Drug Delivery. *J. Controlled Release* **2010**, *148* (1), 13–17. https://doi.org/10.1016/j.jconrel.2010.07.115.

(545) Zevnik, J.; Dular, M. Liposome Destruction by a Collapsing Cavitation Microbubble: A Numerical Study. *Ultrason. Sonochem.* **2021**, *78*, 105706. https://doi.org/10.1016/j.ultsonch.2021.105706.

(546) Zhu, H.-X.; Cai, X.-Z.; Shi, Z.-L.; Hu, B.; Yan, S.-G. Microbubble-Mediated Ultrasound Enhances the Lethal Effect of Gentamicin on Planktonic Escherichia Coli. *BioMed Res. Int.* **2014**, *2014* (1), 142168. https://doi.org/10.1155/2014/142168.

(547) Lattwein, K. R.; Shekhar, H.; Kouijzer, J. J. P.; van Wamel, W. J. B.; Holland, C. K.; Kooiman, K. Sonobactericide: An Emerging Treatment Strategy for Bacterial Infections. *Ultrasound Med. Biol.* **2020**, *46* (2), 193–215. https://doi.org/10.1016/j.ultrasmedbio.2019.09.011.

(548) He, N.; Hu, J.; Liu, H.; Zhu, T.; Huang, B.; Wang, X.; Wu, Y.; Wang, W.; Qu, D. Enhancement of Vancomycin Activity against Biofilms by Using Ultrasound-Targeted Microbubble Destruction. *Antimicrob. Agents Chemother.* **2011**, *55* (11), 5331–5337. https://doi.org/10.1128/aac.00542-11.

(549) Ronan, E.; Edjiu, N.; Kroukamp, O.; Wolfaardt, G.; Karshafian, R. USMB-Induced Synergistic Enhancement of Aminoglycoside Antibiotics in Biofilms. *Ultrasonics* **2016**, *69*, 182–190. https://doi.org/10.1016/j.ultras.2016.03.017.

(550) Carmen, J. C.; Nelson, J. L.; Beckstead, B. L.; Runyan, C. M.; Robison, R. A.; Schaalje, G. B.; Pitt, W. G. Ultrasonic-Enhanced Gentamicin Transport through Colony Biofilms of Pseudomonas Aeruginosa and Escherichia Coli. *J. Infect. Chemother. Off. J. Jpn. Soc. Chemother.* **2004**, *10* (4), 193–199. https://doi.org/10.1007/s10156-004-0319-1.

(551) Vyas, N.; Wang, Q. X.; Manmi, K. A.; Sammons, R. L.; Kuehne, S. A.; Walmsley, A. D. How Does Ultrasonic Cavitation Remove Dental Bacterial Biofilm? *Ultrason. Sonochem.* **2020**, *67*, 105112. https://doi.org/10.1016/j.ultsonch.2020.105112.

(552) Dong, Y.; Chen, S.; Wang, Z.; Peng, N.; Yu, J. Synergy of Ultrasound Microbubbles and Vancomycin against Staphylococcus Epidermidis Biofilm. *J. Antimicrob. Chemother.* **2013**, *68* (4), 816–826. https://doi.org/10.1093/jac/dks490.

(553) Wang, G.; Wu, W.; Zhu, J.-J.; Peng, D. The Promise of Low-Intensity Ultrasound: A Review on Sonosensitizers and Sonocatalysts by Ultrasonic Activation for Bacterial Killing. *Ultrason. Sonochem.* **2021**, *79*, 105781. https://doi.org/10.1016/j.ultsonch.2021.105781.

(554) Rediske, A. M.; Roeder, B. L.; Brown, M. K.; Nelson, J. L.; Robison, R. L.; Draper, D. O.; Schaalje, G. B.; Robison, R. A.; Pitt, W. G. Ultrasonic Enhancement of Antibiotic Action on Escherichia Coli Biofilms: An In Vivo Model. *Antimicrob. Agents Chemother.* **1999**, *43* (5), 1211–1214. https://doi.org/10.1128/aac.43.5.1211.

(555) Liu, X.; Yin, H.; Weng, C.-X.; Cai, Y. Low-Frequency Ultrasound Enhances Antimicrobial Activity of Colistin–Vancomycin Combination against Pan-Resistant Biofilm of Acinetobacter Baumannii. *Ultrasound Med. Biol.* **2016**, *42* (8), 1968–1975. https://doi.org/10.1016/j.ultrasmedbio.2016.03.016.

(556) Cai, Y.; Wang, J.; Liu, X.; Wang, R.; Xia, L. A Review of the Combination Therapy of Low Frequency Ultrasound with Antibiotics. *BioMed Res. Int.* **2017**, *2017* (1), 2317846. https://doi.org/10.1155/2017/2317846.

(557) Hu, J.; Zhang, N.; Li, L.; Zhang, N.; Ma, Y.; Zhao, C.; Wu, Q.; Li, Y.; He, N.; Wang, X. The Synergistic Bactericidal Effect of Vancomycin on UTMD Treated Biofilm Involves Damage to Bacterial Cells and Enhancement of Metabolic Activities. *Sci. Rep.* **2018**, *8* (1), 192. https://doi.org/10.1038/s41598-017-18496-3.

(558) Grari, O.; Ezrari, S.; El Yandouzi, I.; Benaissa, E.; Ben Lahlou, Y.; Lahmer, M.; Saddari, A.; Elouennass, M.; Maleb, A. A Comprehensive Review on Biofilm-Associated Infections: Mechanisms, Diagnostic Challenges, and Innovative Therapeutic Strategies. *The Microbe* **2025**, *8*, 100436. https://doi.org/10.1016/j.microb.2025.100436.

(559) Pitt, W. G.; Ross, S. A. Ultrasound Increases the Rate of Bacterial Cell Growth. *Biotechnol. Prog.* **2003**, *19* (3), 1038–1044. https://doi.org/10.1021/bp0340685.

(560) Erriu, M.; Blus, C.; Szmukler-Moncler, S.; Buogo, S.; Levi, R.; Barbato, G.; Madonnaripa, D.; Denotti, G.; Piras, V.; Orrù, G. Microbial Biofilm Modulation by Ultrasound: Current Concepts and Controversies. *Ultrason. Sonochem.* **2014**, *21* (1), 15–22. https://doi.org/10.1016/j.ultsonch.2013.05.011.

(561) Yu, H.; Liu, Y.; Li, L.; Guo, Y.; Xie, Y.; Cheng, Y.; Yao, W. Ultrasound-Involved Emerging Strategies for Controlling Foodborne Microbial Biofilms. *Trends Food Sci. Technol.* **2020**, *96*, 91–101. https://doi.org/10.1016/j.tifs.2019.12.010.

(562) Suzuki, R.; Klibanov, A. L. Co-Administration of Microbubbles and Drugs in Ultrasound-Assisted Drug Delivery: Comparison with Drug-Carrying Particles. In *Therapeutic Ultrasound*; Escoffre, J.-M., Bouakaz, A., Eds.; Springer International Publishing: Cham, 2016; pp 205–220. https://doi.org/10.1007/978-3-319-22536-4_12.

(563) Endoh, M.; Koibuchi, N.; Sato, M.; Morishita, R.; Kanzaki, T.; Murata, Y.; Kaneda, Y. Fetal Gene Transfer by Intrauterine Injection with Microbubble-Enhanced Ultrasound. *Mol. Ther.* **2002**, *5* (5), 501–508. https://doi.org/10.1006/mthe.2002.0577.

(564) Plazonic, F.; LuTheryn, G.; Hind, C.; Clifford, M.; Gray, M.; Stride, E.; Glynne-Jones, P.; Hill, M.; Sutton, J. M.; Carugo, D. Bactericidal Effect of Ultrasound-Responsive Microbubbles and Sub-Inhibitory Gentamicin against *Pseudomonas Aeruginosa* Biofilms on Substrates With Differing Acoustic Impedance. *Ultrasound Med. Biol.* **2022**, *48* (9), 1888–1898. https://doi.org/10.1016/j.ultrasmedbio.2022.05.019.

(565) Fu, Y.-Y.; Zhang, L.; Yang, Y.; Liu, C.-W.; He, Y.-N.; Li, P.; Yu, X. Synergistic Antibacterial Effect of Ultrasound Microbubbles Combined with Chitosan-Modified Polymyxin B-Loaded Liposomes on Biofilm-Producing Acinetobacter Baumannii. *Int. J. Nanomedicine* **2019**, *14*, 1805–1815. https://doi.org/10.2147/IJN.S186571.

(566) Rastegar, G.; Salman, M. M.; Sirsi, S. R. Remote Loading: The Missing Piece for Achieving High Drug Payload and Rapid Release in Polymeric Microbubbles. *Pharmaceutics* **2023**, *15* (11), 2550. https://doi.org/10.3390/pharmaceutics15112550.

(567) Lentacker, I.; Smedt, S. C. D.; Sanders, N. N. Drug Loaded Microbubble Design for Ultrasound Triggered Delivery. *Soft Matter* **2009**, *5* (11), 2161–2170. https://doi.org/10.1039/B823051J.

(568) Ferrara, K. W. Driving Delivery Vehicles with Ultrasound. *Adv. Drug Deliv. Rev.* **2008**, *60* (10), 1097–1102. https://doi.org/10.1016/j.addr.2008.03.002.

(569) Ferrara, K.; Pollard, R.; Borden, M. Ultrasound Microbubble Contrast Agents: Fundamentals and Application to Gene and Drug Delivery. *Annu. Rev. Biomed. Eng.* **2007**, *9* (Volume 9, 2007), 415–447. https://doi.org/10.1146/annurev.bioeng.8.061505.095852.

(570) Kheirolomoom, A.; Dayton, P. A.; Lum, A. F. H.; Little, E.; Paoli, E. E.; Zheng, H.; Ferrara, K. W. Acoustically-Active Microbubbles Conjugated to Liposomes: Characterization of a Proposed Drug Delivery Vehicle. *J. Controlled Release* **2007**, *118* (3), 275–284. https://doi.org/10.1016/j.jconrel.2006.12.015.

(571) McLaughlan, J. R.; Harput, S.; Abou-Saleh, R. H.; Peyman, S. A.; Evans, S.; Freear, S. Characterisation of Liposome-Loaded Microbubble Populations for Subharmonic Imaging. *Ultrasound Med. Biol.* **2017**, *43* (1), 346–356. https://doi.org/10.1016/j.ultrasmedbio.2016.09.011.

(572) Malik, R.; Pancholi, K.; Melzer, A. Microbubble–Liposome Conjugate: Payload Evaluation of Potential Theranostic Vehicle. *Nanobiomedicine* **2016**, *3*, 1849543516670806. https://doi.org/10.1177/1849543516670806.

(573) Lentacker, I.; De Smedt, S. C.; Demeester, J.; Van Marck, V.; Bracke, M.; Sanders, N. N. Lipoplex-Loaded Microbubbles for Gene Delivery: A Trojan Horse Controlled by Ultrasound. *Adv. Funct. Mater.* **2007**, *17* (12), 1910–1916. https://doi.org/10.1002/adfm.200700106.

(574) Jain, A.; Cheng, K. The Principles and Applications of Avidin-Based Nanoparticles in Drug Delivery and Diagnosis. *J. Control. Release Off. J. Control. Release Soc.* **2017**, *245*, 27–40. https://doi.org/10.1016/j.jconrel.2016.11.016.

(575) Nwe, K.; Brechbiel, M. W. Growing Applications of "Click Chemistry" for Bioconjugation in Contemporary Biomedical Research. *Cancer Biother. Radiopharm.* **2009**, *24* (3), 289–302. https://doi.org/10.1089/cbr.2008.0626.

(576) Geers, B.; Lentacker, I.; Sanders, N. N.; Demeester, J.; Meairs, S.; De Smedt, S. C. Self-Assembled Liposome-Loaded Microbubbles: The Missing Link for Safe and Efficient Ultrasound Triggered Drug-Delivery. *J. Controlled Release* **2011**, *152* (2), 249–256. https://doi.org/10.1016/j.jconrel.2011.02.024.

(577) Dwivedi, P.; Kiran, S.; Han, S.; Dwivedi, M.; Khatik, R.; Fan, R.; Mangrio, F. A.; Du, K.; Zhu, Z.; Yang, C.; Huang, F.; Ejaz, A.; Han, R.; Si, T.; Xu, R. X. Magnetic Targeting and Ultrasound Activation of Liposome–Microbubble Conjugate for Enhanced Delivery of Anticancer Therapies. *ACS Appl. Mater. Interfaces* **2020**, *12* (21), 23737–23751. https://doi.org/10.1021/acsami.0c05308.

(578) Baldwin, A. D.; Kiick, K. L. Tunable Degradation of Maleimide-Thiol Adducts in Reducing Environments. *Bioconjug. Chem.* **2011**, *22* (10), 1946–1953. https://doi.org/10.1021/bc200148v.

(579) Browning, R.; Thomas, N.; Marsh, L. K.; Tear, L. R.; Owen, J.; Stride, E.; Farrer, N. J. Ultrasound-Triggered Delivery of Iproplatin from Microbubble-Conjugated Liposomes. *ChemistryOpen* **2021**, *10* (12), 1170–1176. https://doi.org/10.1002/open.202100222.

(580) Armistead, F. J.; Batchelor, D. V. B.; Johnson, B. R. G.; Evans, S. D. QCM-D Investigations on Cholesterol–DNA Tethering of Liposomes to Microbubbles for Therapy. *J. Phys. Chem. B* **2023**, *127* (11), 2466–2474. https://doi.org/10.1021/acs.jpcb.2c07256.

(581) Chapla, R.; Huynh, K. T.; Schutt, C. E. Microbubble–Nanoparticle Complexes for Ultrasound-Enhanced Cargo Delivery. *Pharmaceutics* **2022**, *14* (11), 2396. https://doi.org/10.3390/pharmaceutics14112396.

(582) Gao, J.; Nesbitt, H.; Logan, K.; Burnett, K.; White, B.; Jack, I. G.; Taylor, M. A.; Love, M.; Callan, B.; McHale, A. P.; Callan, J. F. An Ultrasound Responsive Microbubble-Liposome Conjugate for Targeted Irinotecan-Oxaliplatin Treatment of Pancreatic Cancer. *Eur. J. Pharm. Biopharm.* **2020**, *157*, 233–240. https://doi.org/10.1016/j.ejpb.2020.10.012.

(583) Yoon, Y. I.; Kwon, Y.-S.; Cho, H.-S.; Heo, S.-H.; Park, K. S.; Park, S. G.; Lee, S.-H.; Hwang, S. I.; Kim, Y. I.; Jae, H. J.; Ahn, G.-J.; Cho, Y.-S.; Lee, H.; Lee, H. J.; Yoon, T.-J. Ultrasound-Mediated Gene and Drug Delivery Using a Microbubble-Liposome Particle System. *Theranostics* **2014**, *4* (11), 1133–1144. https://doi.org/10.7150/thno.9945.

(584) Yan, F.; Li, L.; Deng, Z.; Jin, Q.; Chen, J.; Yang, W.; Yeh, C.-K.; Wu, J.; Shandas, R.; Liu, X.; Zheng, H. Paclitaxel-Liposome–Microbubble Complexes as Ultrasound-Triggered Therapeutic Drug Delivery Carriers. *J. Controlled Release* **2013**, *166* (3), 246–255. https://doi.org/10.1016/j.jconrel.2012.12.025.

(585) Zhao, G.; Huang, Q.; Wang, F.; Zhang, X.; Hu, J.; Tan, Y.; Huang, N.; Wang, Z.; Wang, Z.; Cheng, Y. Targeted shRNA-Loaded Liposome Complex Combined with Focused Ultrasound for

Blood Brain Barrier Disruption and Suppressing Glioma Growth. *Cancer Lett.* **2018**, *418*, 147–158. https://doi.org/10.1016/j.canlet.2018.01.035.

(586) Franco-Urquijo, C. A.; Navarro-Becerra, J. Á.; Ríos, A.; Escalante, B. Release of Vascular Agonists from Liposome-Microbubble Conjugate by Ultrasound-Mediated Microbubble Destruction: Effect on Vascular Function. *Drug Deliv. Transl. Res.* **2022**, *12* (5), 1175–1186. https://doi.org/10.1007/s13346-021-00994-7.

(587) Zhang, S.; Wen, K.; Wu, W.; Li, W.; Zhao, J. Efficacy of HGF Carried by Ultrasound Microbubble-Cationic Nano-Liposomes Complex for Treating Hepatic Fibrosis in a Bile Duct Ligation Rat Model, and Its Relationship with the Diffusion-Weighted MRI Parameters. *Clin. Res. Hepatol. Gastroenterol.* **2013**, *37* (6), 602–607. https://doi.org/10.1016/j.clinre.2013.05.011.

(588) Yang, D.; Gao, Y.-H.; Tan, K.-B.; Zuo, Z.-X.; Yang, W.-X.; Hua, X.; Li, P.-J.; Zhang, Y.; Wang, G. Inhibition of Hepatic Fibrosis with Artificial microRNA Using Ultrasound and Cationic Liposome-Bearing Microbubbles. *Gene Ther.* **2013**, *20* (12), 1140–1148. https://doi.org/10.1038/gt.2013.41.

(589) LuTheryn, G.; Glynne-Jones, P.; Webb, J. S.; Carugo, D. Ultrasound-Mediated Therapies for the Treatment of Biofilms in Chronic Wounds: A Review of Present Knowledge. *Microb. Biotechnol.* **2020**, *13* (3), 613–628. https://doi.org/10.1111/1751-7915.13471.

(590) Ellbogen, M. H.; Olsen, K. M.; Gentry-Nielsen, M. J.; Preheim, L. C. Efficacy of Liposome-Encapsulated Ciprofloxacin Compared with Ciprofloxacin and Ceftriaxone in a Rat Model of Pneumococcal Pneumonia. *J. Antimicrob. Chemother.* **2003**, *51* (1), 83–91. https://doi.org/10.1093/jac/dkg024.

(591) Nicolosi, D.; Scalia, M.; Nicolosi, V. M.; Pignatello, R. Encapsulation in Fusogenic Liposomes Broadens the Spectrum of Action of Vancomycin against Gram-Negative Bacteria. *Int. J. Antimicrob. Agents* **2010**, *35* (6), 553–558. https://doi.org/10.1016/j.ijantimicag.2010.01.015.

(592) Bakker-Woudenberg, I. A. J. M.; Schiffelers, R. M.; Storm, G.; Becker, M. J.; Guo, L. Long-Circulating Sterically Stabilized Liposomes in the Treatment of Infections. In *Methods in Enzymology*; Elsevier, 2005; Vol. 391, pp 228–260. https://doi.org/10.1016/S0076-6879(05)91014-8.

(593) Ghosh, R.; De, M. Liposome-Based Antibacterial Delivery: An Emergent Approach to Combat Bacterial Infections. *ACS Omega* **2023**, *8* (39), 35442–35451. https://doi.org/10.1021/acsomega.3c04893.

(594) Hajiahmadi, F.; Alikhani, M. Y.; Shariatifar, H.; Arabestani, M. R.; Ahmadvand, D. The Bactericidal Effect of Lysostaphin Coupled with Liposomal Vancomycin as a Dual Combating System Applied Directly on Methicillin-Resistant *Staphylococcus Aureus* Infected Skin Wounds in Mice. *Int. J. Nanomedicine* **2019**, *14*, 5943–5955. https://doi.org/10.2147/IJN.S214521.

(595) Bastari, K.; Arshath, M.; NG, Z. H. M.; Chia, J. H.; Yow, Z. X. D.; Sana, B.; Tan, M. F. C.; Lim, S.; Loo, S. C. J. A Controlled Release of Antibiotics from Calcium Phosphate-Coated Poly(Lactic-Co-Glycolic Acid) Particles and Their in Vitro Efficacy against Staphylococcus Aureus Biofilm. *J. Mater. Sci. Mater. Med.* **2014**, *25* (3), 747–757. https://doi.org/10.1007/s10856-013-5125-9.

(596) Loureiro, J. A.; Gomes, B.; Fricker, G.; Cardoso, I.; Ribeiro, C. A.; Gaiteiro, C.; Coelho, M. A. N.; Pereira, M. do C.; Rocha, S. Dual Ligand Immunoliposomes for Drug Delivery to the Brain. *Colloids Surf. B Biointerfaces* **2015**, *134*, 213–219. https://doi.org/10.1016/j.colsurfb.2015.06.067.

(597) Drulis-Kawa, Z.; Dorotkiewicz-Jach, A.; Gubernator, J.; Gula, G.; Bocer, T.; Doroszkiewicz, W. The Interaction between *Pseudomonas Aeruginosa* Cells and Cationic PC:Chol:DOTAP Liposomal Vesicles versus Outer-Membrane Structure and Envelope Properties of Bacterial Cell. *Int. J. Pharm.* **2009**, *367* (1), 211–219. https://doi.org/10.1016/j.ijpharm.2008.09.043.

(598) Zhou, Z.; Hu, F.; Hu, S.; Kong, M.; Feng, C.; Liu, Y.; Cheng, X.; Ji, Q.; Chen, X. pH-Activated Nanoparticles with Targeting for the Treatment of Oral Plaque Biofilm. *J. Mater. Chem. B* **2018**, *6* (4), 586–592. https://doi.org/10.1039/C7TB02682J.

(599) Wardlow, R.; Bing, C.; VanOsdol, J.; Maples, D.; Ladouceur-Wodzak, M.; Harbeson, M.; Nofiele, J.; Staruch, R.; Ramachandran, A.; Malayer, J.; Chopra, R.; Ranjan, A. Targeted Antibiotic Delivery Using Low Temperature-Sensitive Liposomes and Magnetic Resonance-Guided High-Intensity Focused Ultrasound Hyperthermia. *Int. J. Hyperthermia* **2016**, *32* (3), 254–264. https://doi.org/10.3109/02656736.2015.1134818.

(600) Wang, D.-Y.; van der Mei, H. C.; Ren, Y.; Busscher, H. J.; Shi, L. Lipid-Based Antimicrobial Delivery-Systems for the Treatment of Bacterial Infections. *Front. Chem.* **2020**, *7*. https://doi.org/10.3389/fchem.2019.00872.

(601) Liu, C.; Zhang, L.; Zhu, W.; Guo, R.; Sun, H.; Chen, X.; Deng, N. Barriers and Strategies of Cationic Liposomes for Cancer Gene Therapy. *Mol. Ther. Methods Clin. Dev.* **2020**, *18*, 751–764. https://doi.org/10.1016/j.omtm.2020.07.015.

(602) Safinya, C. R.; Ewert, K. K.; Majzoub, R. N.; Leal, C. Cationic Liposome–Nucleic Acid Complexes for Gene Delivery and Gene Silencing. *New J. Chem.* **2014**, *38* (11), 5164–5172. https://doi.org/10.1039/C4NJ01314J.

(603) Guo, R.; Liu, Y.; Li, K.; Tian, B.; Li, W.; Niu, S.; Hong, W. Direct Interactions between Cationic Liposomes and Bacterial Cells Ameliorate the Systemic Treatment of Invasive Multidrug-Resistant *Staphylococcus Aureus* Infections. *Nanomedicine Nanotechnol. Biol. Med.* **2021**, *34*, 102382. https://doi.org/10.1016/j.nano.2021.102382.

(604) Ibaraki, H.; Kanazawa, T.; Chien, W.-Y.; Nakaminami, H.; Aoki, M.; Ozawa, K.; Kaneko, H.; Takashima, Y.; Noguchi, N.; Seta, Y. The Effects of Surface Properties of Liposomes on Their Activity against *Pseudomonas Aeruginosa* PAO-1 Biofilm. *J. Drug Deliv. Sci. Technol.* **2020**, *57*, 101754. https://doi.org/10.1016/j.jddst.2020.101754.

(605) Miatmoko, A.; Asmoro, F. H.; Azhari, A. A.; Rosita, N.; Huang, C.-S. The Effect of 1,2-Dioleoyl-3-Trimethylammonium Propane (DOTAP) Addition on the Physical Characteristics of β-Ionone Liposomes. *Sci. Rep.* **2023**, *13* (1), 4324. https://doi.org/10.1038/s41598-023-31560-5.

(606) Mihailescu, M.; Worcester, D. L.; Carroll, C. L.; Chamberlin, A. R.; White, S. H. DOTAP: Structure, Hydration, and the Counterion Effect. *Biophys. J.* **2023**, *122* (6), 1086–1093. https://doi.org/10.1016/j.bpj.2023.01.031.

(607) Sharma, A.; Khushika; Chaudhary, M.; Jana, P. K.; Parveen, N. Helper Lipids Accelerate the Mass Transfer of Cationic Lipid Nanoparticles Resulting in an Efficient Gene Delivery. *Nanoscale* **2026**, *18* (3), 1420–1432. https://doi.org/10.1039/D5NR03142G.

(608) Siegel, D. P.; Epand, R. M. The Mechanism of Lamellar-to-Inverted Hexagonal Phase Transitions in Phosphatidylethanolamine: Implications for Membrane Fusion Mechanisms. *Biophys. J.* **1997**, *73* (6), 3089–3111. https://doi.org/10.1016/S0006-3495(97)78336-X.

(609) BenchChem Technical Support Team. The Fusogenic Properties of DOPE: A Technical Guide for Drug Development Professionals. **2025**.

(610) Kolašinac, R.; Kleusch, C.; Braun, T.; Merkel, R.; Csiszár, A. Deciphering the Functional Composition of Fusogenic Liposomes. *Int. J. Mol. Sci.* **2018**, *19* (2). https://doi.org/10.3390/ijms19020346.

(611) Cheng, X.; Lee, R. J. The Role of Helper Lipids in Lipid Nanoparticles (LNPs) Designed for Oligonucleotide Delivery. *Adv. Drug Deliv. Rev.* **2016**, *99*, 129–137. https://doi.org/10.1016/j.addr.2016.01.022.

(612) Kamo, T.; Handa, T.; Nakano, M. Lateral Pressure Change on Phase Transitions of Phosphatidylcholine/Diolein Mixed Membranes. *Colloids Surf. B Biointerfaces* **2013**, *104*, 128–132. https://doi.org/10.1016/j.colsurfb.2012.11.024.

(613) Rappolt, M.; Hickel, A.; Bringezu, F.; Lohner, K. Mechanism of the Lamellar/Inverse Hexagonal Phase Transition Examined by High Resolution X-Ray Diffraction. *Biophys. J.* **2003**, *84*, 3111–3122. https://doi.org/10.1016/S0006-3495(03)70036-8.

(614) Parra Ortiz, E. Effects of Pulmonary Surfactant Proteins SP-B and SP-C on the Physical Properties of Biological Membranes, 2013. https://doi.org/10.13140/RG.2.1.3930.3522.
(615) Eugster, R.; Luciani, P. Liposomes: Bridging the Gap from Lab to Pharmaceuticals. *Curr. Opin. Colloid Interface Sci.* **2025**, *75*, 101875. https://doi.org/10.1016/j.cocis.2024.101875.
(616) Hung, S.-Y.; Chancellor, D. D.; Chancellor, M. B.; Chuang, Y.-C. Role of Liposome in Treatment of Overactive Bladder and Interstitial Cystitis. *Urol. Sci.* **2015**, *26* (1), 3–6. https://doi.org/10.1016/j.urols.2014.12.008.
(617) Tyagi, P.; Kashyap, M.; Majima, T.; Kawamorita, N.; Yoshizawa, T.; Yoshimura, N. Intravesical Liposome Therapy for Interstitial Cystitis. *Int. J. Urol.* **2017**, *24* (4), 262–271. https://doi.org/10.1111/iju.13317.
(618) Mustafa, N. R.; Spelbos, V. S.; Witkamp, G.-J.; Verpoorte, R.; Choi, Y. H. Solubility and Stability of Some Pharmaceuticals in Natural Deep Eutectic Solvents-Based Formulations. *Molecules* **2021**, *26* (9), 2645. https://doi.org/10.3390/molecules26092645.
(619) Machado, A. C.; Caseli, L. Ultrathin Films to Investigate the Interaction of Nitrofurantoin with Phospholipids. *Thin Solid Films* **2021**, *725*, 138638. https://doi.org/10.1016/j.tsf.2021.138638.
(620) Michaud, J. E.; Morrill, C. C.; Haffar, A.; Di Carlo, H. N.; Gearhart, J. P. Intravesical Vancomycin for the Treatment of Corynebacterium Cystitis and Struvite Bladder Stones: A Case Report. *Urol. Case Rep.* **2024**, *57*, 102857. https://doi.org/10.1016/j.eucr.2024.102857.
(621) Ellens, H.; Bentz, J.; Szoka, F. C. pH-Induced Destabilization of Phosphatidylethanolamine-Containing Liposomes: Role of Bilayer Contact. *Biochemistry* **1984**, *23* (7), 1532–1538. https://doi.org/10.1021/bi00302a029.
(622) Kolašinac, R.; Kleusch, C.; Braun, T.; Merkel, R.; Csiszár, A. Deciphering the Functional Composition of Fusogenic Liposomes. *Int. J. Mol. Sci.* **2018**, *19* (2), 346. https://doi.org/10.3390/ijms19020346.
(623) Cavalcanti, R. R. M.; Lira, R. B.; Riske, K. A. Membrane Fusion Biophysical Analysis of Fusogenic Liposomes. *Langmuir* **2022**, *38* (34), 10430–10441. https://doi.org/10.1021/acs.langmuir.2c01169.
(624) Liu, H.; Zhang, Q.; Wang, S.; Weng, W.; Jing, Y.; Su, J. Bacterial Extracellular Vesicles as Bioactive Nanocarriers for Drug Delivery: Advances and Perspectives. *Bioact. Mater.* **2022**, *14*, 169–181. https://doi.org/10.1016/j.bioactmat.2021.12.006.
(625) Hu, F.; Zhou, Z.; Xu, Q.; Fan, C.; Wang, L.; Ren, H.; Xu, S.; Ji, Q.; Chen, X. A Novel pH-Responsive Quaternary Ammonium Chitosan-Liposome Nanoparticles for Periodontal Treatment. *Int. J. Biol. Macromol.* **2019**, *129*, 1113–1119. https://doi.org/10.1016/j.ijbiomac.2018.09.057.
(626) Furneri, P. M.; Fresta, M.; Puglisi, G.; Tempera, G. Ofloxacin-Loaded Liposomes: In Vitro Activity and Drug Accumulation in Bacteria. *Antimicrob. Agents Chemother.* **2000**, *44* (9), 2458–2464.
(627) Moyá, M. L.; López-López, M.; Lebrón, J. A.; Ostos, F. J.; Pérez, D.; Camacho, V.; Beck, I.; Merino-Bohórquez, V.; Camean, M.; Madinabeitia, N.; López-Cornejo, P. Preparation and Characterization of New Liposomes. Bactericidal Activity of Cefepime Encapsulated into Cationic Liposomes. *Pharmaceutics* **2019**, *11* (2), 69. https://doi.org/10.3390/pharmaceutics11020069.
(628) Hafez, I. M.; Cullis, P. R. Cholesteryl Hemisuccinate Exhibits pH Sensitive Polymorphic Phase Behavior. *Biochim. Biophys. Acta BBA - Biomembr.* **2000**, *1463* (1), 107–114. https://doi.org/10.1016/S0005-2736(99)00186-8.
(629) Padín-González, E.; Lancaster, P.; Bottini, M.; Gasco, P.; Tran, L.; Fadeel, B.; Wilkins, T.; Monopoli, M. P. Understanding the Role and Impact of Poly (Ethylene Glycol) (PEG) on Nanoparticle Formulation: Implications for COVID-19 Vaccines. *Front. Bioeng. Biotechnol.* **2022**, *10*. https://doi.org/10.3389/fbioe.2022.882363.
(630) Gao, P. PEGylated Lipids in Lipid Nanoparticle Delivery Dynamics and Therapeutic Innovation. *Beilstein J. Nanotechnol.* **2025**, *16*, 1914–1930. https://doi.org/10.3762/bjnano.16.133.

(631) Machado, A. C.; Caseli, L. Interaction of Nitrofurantoin with Lipid Langmuir Monolayers as Cellular Membrane Models Distinguished with Tensiometry and Infrared Spectroscopy. *Colloids Surf. B Biointerfaces* **2020**, *188*, 110794. https://doi.org/10.1016/j.colsurfb.2020.110794.

(632) Rahim, M. A.; Zahran, H. A.; Jaffar, H. M.; Ambreen, S.; Ramadan, M. F.; Al-Asmari, F.; Castro-Muñoz, R.; Zongo, E. Liposomal Encapsulation in Food Systems: A Review of Formulation, Processing, and Applications. *Food Sci. Nutr.* **2025**, *13* (8), e70587. https://doi.org/10.1002/fsn3.70587.

(633) Takács-Novák, K.; Noszál, B.; Tókés-Kövesdi, M.; Szász, G. Acid-Base Properties and Proton-Speciation of Vancomycin. *Int. J. Pharm.* **1993**, *89* (3), 261–263. https://doi.org/10.1016/0378-5173(93)90252-B.

(634) Stride, E.; Segers, T.; Lajoinie, G.; Cherkaoui, S.; Bettinger, T.; Versluis, M.; Borden, M. Microbubble Agents: New Directions. *Ultrasound Med. Biol.* **2020**, *46* (6), 1326–1343. https://doi.org/10.1016/j.ultrasmedbio.2020.01.027.

(635) Navarro-Becerra, J. A.; Song, K.-H.; Martinez, P.; Borden, M. A. Microbubble Size and Dose Effects on Pharmacokinetics. *ACS Biomater. Sci. Eng.* **2022**, *8* (4), 1686–1695. https://doi.org/10.1021/acsbiomaterials.2c00043.

(636) NHS. *Intravesical gentamicin treatment*. https://www.royalberkshire.nhs.uk/media/pyqdxt0z/intravesical-gentamicin-treatment_jun24.pdf (accessed 2026-01-29).

(637) NHS. *Bladder Instillation of Gentamicin*. Alder Hey Children's Hospital Trust. https://www.alderhey.nhs.uk/conditions/patient-information-leaflets/bladder-instillation-of-gentamicin/ (accessed 2026-01-29).

(638) Klibanov, A. L.; Shevchenko, T. I.; Raju, B. I.; Seip, R.; Chin, C. T. Ultrasound-Triggered Release of Materials Entrapped in Microbubble-Liposome Constructs: A Tool for Targeted Drug Delivery. *J. Control. Release Off. J. Control. Release Soc.* **2010**, *148* (1), 13–17. https://doi.org/10.1016/j.jconrel.2010.07.115.

(639) Janicki, J. J.; Chancellor, M. B.; Kaufman, J.; Gruber, M. A.; Chancellor, D. D. Potential Effect of Liposomes and Liposome-Encapsulated Botulinum Toxin and Tacrolimus in the Treatment of Bladder Dysfunction. *Toxins* **2016**, *8* (3), 81. https://doi.org/10.3390/toxins8030081.

(640) Ribeiro, L. N. de M.; de Paula, E.; Rossi, D. A.; Monteiro, G. P.; Júnior, E. C. V.; Silva, R. R.; Franco, R. R.; Espíndola, F. S.; Goulart, L. R.; Fonseca, B. B. Hybrid Pectin-Liposome Formulation against Multi-Resistant Bacterial Strains. *Pharmaceutics* **2020**, *12* (8), 769. https://doi.org/10.3390/pharmaceutics12080769.

(641) Moyá, M. L.; López-López, M.; Lebrón, J. A.; Ostos, F. J.; Pérez, D.; Camacho, V.; Beck, I.; Merino-Bohórquez, V.; Camean, M.; Madinabeitia, N.; López-Cornejo, P. Preparation and Characterization of New Liposomes. Bactericidal Activity of Cefepime Encapsulated into Cationic Liposomes. *Pharmaceutics* **2019**, *11* (2), 69. https://doi.org/10.3390/pharmaceutics11020069.

(642) Alarfaj, R. E.; Alkhulaifi, M. M.; Al-Fahad, A. J.; Aljihani, S.; Yassin, A. E. B.; Alghoribi, M. F.; Halwani, M. A. Antibacterial Efficacy of Liposomal Formulations Containing Tobramycin and N-Acetylcysteine against Tobramycin-Resistant Escherichia Coli, Klebsiella Pneumoniae, and Acinetobacter Baumannii. *Pharmaceutics* **2022**, *14* (1), 130. https://doi.org/10.3390/pharmaceutics14010130.

(643) Hossain, T. J. Methods for Screening and Evaluation of Antimicrobial Activity: A Review of Protocols, Advantages, and Limitations. *Eur. J. Microbiol. Immunol.* **2024**, *14* (2), 97–115. https://doi.org/10.1556/1886.2024.00035.

(644) Thieme, L.; Hartung, A.; Tramm, K.; Klinger-Strobel, M.; Jandt, K. D.; Makarewicz, O.; Pletz, M. W. MBEC Versus MBIC: The Lack of Differentiation between Biofilm Reducing and Inhibitory Effects as a Current Problem in Biofilm Methodology. *Biol. Proced. Online* **2019**, *21*, 18. https://doi.org/10.1186/s12575-019-0106-0.

(645) Kadeřábková, N.; Mahmood, A. J. S.; Mavridou, D. A. I. Antibiotic Susceptibility Testing Using Minimum Inhibitory Concentration (MIC) Assays. *Npj Antimicrob. Resist.* **2024**, *2* (1), 37. https://doi.org/10.1038/s44259-024-00051-6.
(646) EUCAST. *MIC Determination*. https://www.eucast.org/bacteria/methodology-and-instructions/mic-determination/ (accessed 2026-03-04).
(647) CLSI. *M100: Performance Standards for Antimicrobial Susceptibility Testing, 30th Edition*. https://www.nih.org.pk/wp-content/uploads/2021/02/CLSI-2020.pdf (accessed 2026-01-26).
(648) Sanchez Armengol, E.; Laffleur, F. The Progress on Sulfhydryl Modified Polymers with Regard to Synthesis, Characterization and Mucoadhesion. *Int. J. Pharm.* **2021**, *592*, 120016. https://doi.org/10.1016/j.ijpharm.2020.120016.
(649) Coenye, T. Biofilm Antimicrobial Susceptibility Testing: Where Are We and Where Could We Be Going? *Clin. Microbiol. Rev.* **2023**, *36* (4), e00024-23. https://doi.org/10.1128/cmr.00024-23.
(650) Fernández-Olmos, A.; García-Castillo, M.; Maiz, L.; Lamas, A.; Baquero, F.; Cantón, R. In Vitro Prevention of *Pseudomonas Aeruginosa* Early Biofilm Formation with Antibiotics Used in Cystic Fibrosis Patients. *Int. J. Antimicrob. Agents* **2012**, *40* (2), 173–176. https://doi.org/10.1016/j.ijantimicag.2012.04.006.
(651) Thöming, J. G.; Häussler, S. Pseudomonas Aeruginosa Is More Tolerant Under Biofilm Than Under Planktonic Growth Conditions: A Multi-Isolate Survey. *Front. Cell. Infect. Microbiol.* **2022**, *12*. https://doi.org/10.3389/fcimb.2022.851784.
(652) Ceri, H.; Olson, M. E.; Stremick, C.; Read, R. R.; Morck, D.; Buret, A. The Calgary Biofilm Device: New Technology for Rapid Determination of Antibiotic Susceptibilities of Bacterial Biofilms. *J. Clin. Microbiol.* **1999**, *37* (6), 1771–1776. https://doi.org/10.1128/jcm.37.6.1771-1776.1999.
(653) Kragh, K. N.; Alhede, M.; Kvich, L.; Bjarnsholt, T. Into the Well—A Close Look at the Complex Structures of a Microtiter Biofilm and the Crystal Violet Assay. *Biofilm* **2019**, *1*, 100006. https://doi.org/10.1016/j.bioflm.2019.100006.
(654) Magana, M.; Sereti, C.; Ioannidis, A.; Mitchell, C. A.; Ball, A. R.; Magiorkinis, E.; Chatzipanagiotou, S.; Hamblin, M. R.; Hadjifrangiskou, M.; Tegos, G. P. Options and Limitations in Clinical Investigation of Bacterial Biofilms. *Clin. Microbiol. Rev.* **2018**, *31* (3), e00084-16. https://doi.org/10.1128/CMR.00084-16.
(655) Wannigama, D. L.; Hurst, C.; Pearson, L.; Saethang, T.; Singkham-in, U.; Luk-in, S.; Storer, R. J.; Chatsuwan, T. Simple Fluorometric-Based Assay of Antibiotic Effectiveness for Acinetobacter Baumannii Biofilms. *Sci. Rep.* **2019**, *9* (1), 6300. https://doi.org/10.1038/s41598-019-42353-0.
(656) Kerkhoff, Y.; Ludwig, K. Automatic Quantification of Fluorescence-Imaged Live Dead Assays Using Fiji (ImageJ), 2024. https://doi.org/10.5281/zenodo.10395753.
(657) The European Committee on Antimicrobial Susceptibility Testing. *Breakpoint tables for interpretation of MICs and zone diameters. Version 16.0, 2026*. https://www.eucast.org/fileadmin/eucast/pdf/breakpoints/v_16.0_Breakpoint_Tables.pdf (accessed 2026-02-12).
(658) Patel, P.; Wermuth, H. R.; Calhoun, C.; Hall, G. A. Antibiotics. In *StatPearls*; StatPearls Publishing: Treasure Island (FL), 2025.
(659) Klibanov, A. L.; Maruyama, K.; Beckerleg, A. M.; Torchilin, V. P.; Huang, L. Activity of Amphipathic Poly(Ethylene Glycol) 5000 to Prolong the Circulation Time of Liposomes Depends on the Liposome Size and Is Unfavorable for Immunoliposome Binding to Target. *Biochim. Biophys. Acta BBA - Biomembr.* **1991**, *1062* (2), 142–148. https://doi.org/10.1016/0005-2736(91)90385-L.
(660) Botosoa, Eliot. P.; Maillasson, M.; Mougin-Degraef, M.; Remaud-Le Saëc, P.; Gestin, J.-F.; Jacques, Y.; Barbet, J.; Faivre-Chauvet, A. Antibody-Hapten Recognition at the Surface of Functionalized Liposomes Studied by SPR: Steric Hindrance of Pegylated Phospholipids in Stealth

Liposomes Prepared for Targeted Radionuclide Delivery. *J. Drug Deliv.* **2011**, *2011*, 368535. https://doi.org/10.1155/2011/368535.

(661) Ahmed, K.; Muiruri, P. W.; Jones, G. H.; Scott, M. J.; Jones, M. N. The Effect of Grafted Poly(Ethylene Glycol) on the Electrophoretic Properties of Phospholipid Liposomes and Their Adsorption to Bacterial Biofilms. *Colloids Surf. Physicochem. Eng. Asp.* **2001**, *194* (1), 287–296. https://doi.org/10.1016/S0927-7757(01)00817-2.

(662) Singh, S.; Papareddy, P.; Mörgelin, M.; Schmidtchen, A.; Malmsten, M. Effects of PEGylation on Membrane and Lipopolysaccharide Interactions of Host Defense Peptides. *Biomacromolecules* **2014**, *15* (4), 1337–1345. https://doi.org/10.1021/bm401884e.

(663) Hull, R. Escherichia Coli, Strain 83972 Catalog No. HM-50 For Research Use Only. Not for Use in Humans. **2023**.

(664) Wulkersdorfer, B.; Jaros, D.; Eberl, S.; Poschner, S.; Jäger, W.; Cosentini, E.; Zeitlinger, M.; Schwameis, R. Human Bile Reduces Antimicrobial Activity of Selected Antibiotics against Enterococcus Faecalis and Escherichia coliIn Vitro. *Antimicrob. Agents Chemother.* **2017**, *61* (8), 10.1128/aac.00527-17. https://doi.org/10.1128/aac.00527-17.

(665) Dennison, S. R.; Reddy, S. M.; Morton, L. H. G.; Harris, F.; Badiani, K.; Phoenix, D. A. PEGylation Enhances the Antibacterial and Therapeutic Potential of Amphibian Host Defence Peptides. *Biochim. Biophys. Acta BBA - Biomembr.* **2022**, *1864* (1), 183806. https://doi.org/10.1016/j.bbamem.2021.183806.

(666) Gao, P.; Wei, Y.; Wan, R. E.; Wong, K. W.; Iu, H. T. V.; Tai, S. S. C.; Li, Y.; Yam, H. C. B.; Halebeedu Prakash, P.; Chen, J. H. K.; Ho, P. L.; Yuen, K. Y.; Davies, J.; Kao, R. Y. T. Subinhibitory Concentrations of Antibiotics Exacerbate Staphylococcal Infection by Inducing Bacterial Virulence. *Microbiol. Spectr.* **2022**, *10* (4), e00640-22. https://doi.org/10.1128/spectrum.00640-22.

(667) Liu, J.; Huang, T.; Xu, Z.; Mao, Y.; Soteyome, T.; Liu, G.; Qu, C.; Yuan, L.; Ma, Q.; Zhou, F.; Seneviratne, G. Sub-MIC Streptomycin and Tetracycline Enhanced *Staphylococcus Aureus* Guangzhou-SAU749 Biofilm Formation, an in-Depth Study on Transcriptomics. *Biofilm* **2023**, *6*, 100156. https://doi.org/10.1016/j.bioflm.2023.100156.

(668) O'Brien, V. P.; Dorsey, D. A.; Hannan, T. J.; Hultgren, S. J. Host Restriction of Escherichia Coli Recurrent Urinary Tract Infection Occurs in a Bacterial Strain-Specific Manner. *PLoS Pathog.* **2018**, *14* (12), e1007457. https://doi.org/10.1371/journal.ppat.1007457.

(669) Henry, B. D.; Neill, D. R.; Becker, K. A.; Gore, S.; Bricio-Moreno, L.; Ziobro, R.; Edwards, M. J.; Mühlemann, K.; Steinmann, J.; Kleuser, B.; Japtok, L.; Luginbühl, M.; Wolfmeier, H.; Scherag, A.; Gulbins, E.; Kadioglu, A.; Draeger, A.; Babiychuk, E. B. Engineered Liposomes Sequester Bacterial Exotoxins and Protect from Severe Invasive Infections in Mice. *Nat. Biotechnol.* **2015**, *33* (1), 81–88. https://doi.org/10.1038/nbt.3037.

(670) Azeredo Da Silveira, S.; Perez, A. Liposomes as Novel Anti-Infectives Targeting Bacterial Virulence Factors? *Expert Rev. Anti Infect. Ther.* **2015**, *13* (5), 531–533. https://doi.org/10.1586/14787210.2015.1028367.

(671) Lau, W. K.; Dharmasena, D.; Horsley, H.; Jafari, N. V.; Malone-Lee, J.; Stride, E.; Edirisinghe, M.; Rohn, J. L. Novel Antibiotic-Loaded Particles Conferring Eradication of Deep Tissue Bacterial Reservoirs for the Treatment of Chronic Urinary Tract Infection. *J. Controlled Release* **2020**, *328*, 490–502. https://doi.org/10.1016/j.jconrel.2020.08.048.

(672) Bayles, K. W. The Biological Role of Death and Lysis in Biofilm Development. *Nat. Rev. Microbiol.* **2007**, *5* (9), 721–726. https://doi.org/10.1038/nrmicro1743.

(673) Rozali, S. N. M.; Milani, E. A.; Deed, R. C.; Silva, F. V. M. Bacteria, Mould and Yeast Spore Inactivation Studies by Scanning Electron Microscope Observations. *Int. J. Food Microbiol.* **2017**, *263*, 17–25. https://doi.org/10.1016/j.ijfoodmicro.2017.10.008.

(674) Zmerli, O.; Boukili, M.; Bellali, S.; Bou Khalil, J. The Return of a Forgotten Ally: Tabletop Scanning Electron Microscopy in the Realm of Bacteriology. *Front. Cell. Infect. Microbiol.* **2026**, *15*, 1697696. https://doi.org/10.3389/fcimb.2025.1697696.

(675) Garcia-Maset, R.; Chu, V.; Yuen, N.; Blumgart, D.; Yoon, J.; Murray, B. O.; Joseph, A. A.; Rohn, J. L. Effect of Host Microenvironment and Bacterial Lifestyles on Antimicrobial Sensitivity and Implications for Susceptibility Testing. *Npj Antimicrob. Resist.* **2025**, *3* (1), 42. https://doi.org/10.1038/s44259-025-00113-3.

(676) MacDonald, L.; Baldini, G.; Storrie, B. Does Super Resolution Fluorescence Microscopy Obsolete Previous Microscopic Approaches to Protein Co-Localization? *Methods Mol. Biol. Clifton NJ* **2015**, *1270*, 255–275. https://doi.org/10.1007/978-1-4939-2309-0_19.

(677) Szebeni, J.; Barenholz, Y. (Chezy). Complement Activation, Immunogenicity, and Immune Suppression as Potential Side Effects of Liposomes. In *Advances in Clinical Immunology, Medical Microbiology, COVID-19, and Big Data*; Jenny Stanford Publishing, **2021**.

(678) Szebeni, J.; Moghimi, S. M. Liposome Triggering of Innate Immune Responses: A Perspective on Benefits and Adverse Reactions: Biological Recognition and Interactions of Liposomes. *J. Liposome Res.* **2009**, *19* (2), 85–90. https://doi.org/10.1080/08982100902792855.

(679) Sercombe, L.; Veerati, T.; Moheimani, F.; Wu, S. Y.; Sood, A. K.; Hua, S. Advances and Challenges of Liposome Assisted Drug Delivery. *Front. Pharmacol.* **2015**, *6*, 286. https://doi.org/10.3389/fphar.2015.00286.

(680) Endesfelder, U.; Heilemann, M. Direct Stochastic Optical Reconstruction Microscopy (dSTORM). In *Advanced Fluorescence Microscopy: Methods and Protocols*; Verveer, P. J., Ed.; Springer: New York, NY, 2015; pp 263–276. https://doi.org/10.1007/978-1-4939-2080-8_14.

(681) Xu, X.; Khan, M. A.; Burgess, D. J. A Quality by Design (QbD) Case Study on Liposomes Containing Hydrophilic API: II. Screening of Critical Variables, and Establishment of Design Space at Laboratory Scale. *Int. J. Pharm.* **2012**, *423* (2), 543–553. https://doi.org/10.1016/j.ijpharm.2011.11.036.

(682) Zheng, J.; Bai, B.; Lin, Z.; Pu, Z.; Yao, W.; Chen, Z.; Li, D.; Deng, X.; Deng, Q.; Yu, Z. Characterization of Biofilm Formation by Enterococcus Faecalis Isolates Derived from Urinary Tract Infections in China. *J. Med. Microbiol.* **2018**, *67* (1), 60–67. https://doi.org/10.1099/jmm.0.000647.

(683) Seneviratne, C. J.; Yip, J. W. Y.; Chang, J. W. W.; Zhang, C. F.; Samaranayake, L. P. Effect of Culture Media and Nutrients on Biofilm Growth Kinetics of Laboratory and Clinical Strains of *Enterococcus Faecalis*. *Arch. Oral Biol.* **2013**, *58* (10), 1327–1334. https://doi.org/10.1016/j.archoralbio.2013.06.017.

(684) Wang, X.; Ji, X.; Cai, T.; Guo, M. Mechanistic Insight of Polymer Effects on the Kinetic of Solution-Mediated Phase Transformation of Nitrofurantoin Anhydrate to Monohydrate. *Pharm. Res.* **2023**, *40* (6), 1587–1598. https://doi.org/10.1007/s11095-023-03513-0.

(685) Bhosale, D. S.; Kalshetti, M. S. Enhanced Drug Dissolution of Nitrofurantoin Using a Solid Dispersion Technique. *BIO Integr.* **2024**, *5*, 977. https://doi.org/10.15212/bioi-2024-0025.

(686) Robson, A.-L.; Dastoor, P. C.; Flynn, J.; Palmer, W.; Martin, A.; Smith, D. W.; Woldu, A.; Hua, S. Advantages and Limitations of Current Imaging Techniques for Characterizing Liposome Morphology. *Front. Pharmacol.* **2018**, *9*. https://doi.org/10.3389/fphar.2018.00080.

(687) Bourgogne, A.; Garsin, D. A.; Qin, X.; Singh, K. V.; Sillanpaa, J.; Yerrapragada, S.; Ding, Y.; Dugan-Rocha, S.; Buhay, C.; Shen, H.; Chen, G.; Williams, G.; Muzny, D.; Maadani, A.; Fox, K. A.; Gioia, J.; Chen, L.; Shang, Y.; Arias, C. A.; Nallapareddy, S. R.; Zhao, M.; Prakash, V. P.; Chowdhury, S.; Jiang, H.; Gibbs, R. A.; Murray, B. E.; Highlander, S. K.; Weinstock, G. M. Large Scale Variation in Enterococcus Faecalis Illustrated by the Genome Analysis of Strain OG1RF. *Genome Biol.* **2008**, *9* (7), R110. https://doi.org/10.1186/gb-2008-9-7-r110.

(688) Ranieri, M. R.; Whitchurch, C. B.; Burrows, L. L. Mechanisms of Biofilm Stimulation by Subinhibitory Concentrations of Antimicrobials. *Curr. Opin. Microbiol.* **2018**, *45*, 164–169. https://doi.org/10.1016/j.mib.2018.07.006.
(689) Berlutti, F.; Frioni, A.; Natalizi, T.; Pantanella, F.; Valenti, P. Influence of Sub-Inhibitory Antibiotics and Flow Condition on Staphylococcus Aureus ATCC 6538 Biofilm Development and Biofilm Growth Rate: BioTimer Assay as a Study Model. *J. Antibiot. (Tokyo)* **2014**, *67* (11), 763–769. https://doi.org/10.1038/ja.2014.66.
(690) Elawady, R.; Aboulela, A. G.; Gaballah, A.; Ghazal, A. A.; Amer, A. N. Antimicrobial Sub-MIC Induces Staphylococcus Aureus Biofilm Formation without Affecting the Bacterial Count. *BMC Infect. Dis.* **2024**, *24*, 1065. https://doi.org/10.1186/s12879-024-09790-3.
(691) Tang, P.-C.; Sánchez-Hevia, D. L.; Westhoff, S.; Fatsis-Kavalopoulos, N.; Andersson, D. I. Within-Species Variability of Antibiotic Interactions in Gram-Negative Bacteria. *mBio* **2024**, *15* (3), e00196-24. https://doi.org/10.1128/mbio.00196-24.
(692) Gaston, J. R.; Johnson, A. O.; Bair, K. L.; White, A. N.; Armbruster, C. E. Polymicrobial Interactions in the Urinary Tract: Is the Enemy of My Enemy My Friend? *Infect. Immun.* **2021**, IAI.00652-20. https://doi.org/10.1128/IAI.00652-20.
(693) Azevedo, A. S.; Almeida, C.; Melo, L. F.; Azevedo, N. F. Impact of Polymicrobial Biofilms in Catheter-Associated Urinary Tract Infections. *Crit. Rev. Microbiol.* **2017**, *43* (4), 423–439. https://doi.org/10.1080/1040841X.2016.1240656.
(694) LuTheryn, G.; Hind, C.; Campbell, C.; Crowther, A.; Wu, Q.; Keller, S. B.; Glynne-Jones, P.; Sutton, J. M.; Webb, J. S.; Gray, M.; Wilks, S. A.; Stride, E.; Carugo, D. Bactericidal and Anti-Biofilm Effects of Uncharged and Cationic Ultrasound-Responsive Nitric Oxide Microbubbles on Pseudomonas Aeruginosa Biofilms. *Front. Cell. Infect. Microbiol.* **2022**, *12*, 956808. https://doi.org/10.3389/fcimb.2022.956808.
(695) Wu, S.-K.; Chu, P.-C.; Chai, W.-Y.; Kang, S.-T.; Tsai, C.-H.; Fan, C.-H.; Yeh, C.-K.; Liu, H.-L. Characterization of Different Microbubbles in Assisting Focused Ultrasound-Induced Blood-Brain Barrier Opening. *Sci. Rep.* **2017**, *7*, 46689. https://doi.org/10.1038/srep46689.
(696) Lentacker, I.; De Geest, B. G.; Vandenbroucke, R. E.; Peeters, L.; Demeester, J.; De Smedt, S. C.; Sanders, N. N. Ultrasound-Responsive Polymer-Coated Microbubbles That Bind and Protect DNA. *Langmuir* **2006**, *22* (17), 7273–7278. https://doi.org/10.1021/la0603828.
(697) Keller, S. B.; LuTheryn, G.; Gray, M. D.; Lyons, B.; Cleveland, R. O.; Stride, E.; Coussios, C. C. Quantitative Evaluation of Anti-Biofilm Cavitation Activity Seeded from Microbubbles or Protein Cavitation Nuclei by Passive Acoustic Mapping. *Phys. Med. Biol.* **2024**, *69* (21), 215008. https://doi.org/10.1088/1361-6560/ad7f1a.
(698) Chen, T.; Zhang, C.; Zhao, Y.; Wang, Y.; Li, M.; Liu, Y.; Wang, X.; Liu, S.; Mu, D.; Yang, F. Multi-Interfacial Microbubbles Controlled Sequential Cavitation for Synergistic Vascular Destruction/Chemotherapeutic Therapy. *J. Controlled Release* **2025**, *388*, 114287. https://doi.org/10.1016/j.jconrel.2025.114287.
(699) Fu, L.; Wang, J.; Wang, S.; Zhang, Z.; Vogel, A.; Liang, X.; Yao, C. Secondary Cavitation Bubble Dynamics during Laser-Induced Bubble Formation in a Small Container. *Opt. Express* **2024**, *32* (6), 9747–9766. https://doi.org/10.1364/OE.516264.
(700) Arita, Y.; Antkowiak, M.; Venugopalan, V.; Gunn-Moore, F. J.; Dholakia, K. Dynamics of Primary and Secondary Microbubbles Created by Laser-Induced Breakdown of an Optically Trapped Nanoparticle. *Phys. Rev. E Stat. Nonlin. Soft Matter Phys.* **2012**, *85* (1 Pt 2), 016319. https://doi.org/10.1103/PhysRevE.85.016319.
(701) Avanti Research. *Phase Transition Temperatures for Glycerophospholipids | Avanti Research*. https://www.avantiresearch.com/en-gb/support-hub/physical-properties/phase-transition-temps (accessed 2026-03-30).

(702) FDA. *LUMASON (sulfur hexafluoride lipid-type A microspheres) for injectable suspension, for intravenous use or intravesical use*. https://www.accessdata.fda.gov/drugsatfda_docs/label/2016/203684s002lbl.pdf (accessed 2026-03-31).
(703) FDA. *DEFINITY® (Perflutren Lipid Microsphere) Injectable Suspension*. https://www.accessdata.fda.gov/drugsatfda_docs/label/2011/021064s011lbl.pdf (accessed 2026-03-31).
(704) Kilic, S.; Ozdemir, E. Lipid Monolayer Composition and Production Efficiency in DSPC/PEG40St Microbubbles for Ultrasound Applications. *Int. J. Pharm.* **2025**, *685*, 126254. https://doi.org/10.1016/j.ijpharm.2025.126254.
(705) Sonne, C.; Xie, F.; Lof, J.; Oberdorfer, J.; Phillips, P.; Carr Everbach, E.; Porter, T. R. Differences in Definity and Optison Microbubble Destruction Rates at a Similar Mechanical Index with Different Real-Time Perfusion Systems. *J. Am. Soc. Echocardiogr.* **2003**, *16* (11), 1178–1185. https://doi.org/10.1067/j.echo.2003.07.001.
(706) Crowther, A.; Carugo, D. D.; LuTheryn, D. G.; Parhizkar, M. The Combined Effects of Biofilm Dispersal Agents and Ultrasound: A Novel Therapeutic Strategy for Biofilm-Associated Infections, 2025.
(707) Qin, D.; Zou, Q.; Lei, S.; Wang, W.; Li, Z. Cavitation Dynamics and Inertial Cavitation Threshold of Lipid Coated Microbubbles in Viscoelastic Media with Bubble–Bubble Interactions. *Micromachines* **2021**, *12* (9), 1125. https://doi.org/10.3390/mi12091125.
(708) Song, R.; Zhang, C.; Teng, F.; Tu, J.; Guo, X.; Fan, Z.; Zheng, Y.; Zhang, D. Cavitation-Facilitated Transmembrane Permeability Enhancement Induced by Acoustically Vaporized Nanodroplets. *Ultrason. Sonochem.* **2021**, *79*, 105790. https://doi.org/10.1016/j.ultsonch.2021.105790.
(709) Shanei, A.; Sazgarnia, A. An Overview of Therapeutic Applications of Ultrasound Based on Synergetic Effects with Gold Nanoparticles and Laser Excitation. *Iran. J. Basic Med. Sci.* **2019**, *22* (8), 848–855. https://doi.org/10.22038/ijbms.2019.29584.7142.
(710) Vyas, N.; Manmi, K.; Wang, Q.; Jadhav, A. J.; Barigou, M.; Sammons, R. L.; Kuehne, S. A.; Walmsley, A. D. Which Parameters Affect Biofilm Removal with Acoustic Cavitation? A Review. *Ultrasound Med. Biol.* **2019**, *45* (5), 1044–1055. https://doi.org/10.1016/j.ultrasmedbio.2019.01.002.
(711) Bellotti, A. A Review of High-Speed Optical Imaging Technology for the Analysis of Ultrasound Contrast Agents in an Acoustic Field. *iRADIOLOGY* **2023**, *1* (1), 78–90. https://doi.org/10.1002/ird3.8.
(712) Nahum, Y.; Gross, N.; Cerrone, A.; Matouš, K.; Nerenberg, R. Effect of Biofilm Physical Characteristics on Their Susceptibility to Antibiotics: Impacts of Low-Frequency Ultrasound. *Npj Biofilms Microbiomes* **2024**, *10* (1), 70. https://doi.org/10.1038/s41522-024-00544-2.
(713) Anastasiadis, P.; Mojica, K. D. A.; Allen, J. S.; Matter, M. L. Detection and Quantification of Bacterial Biofilms Combining High-Frequency Acoustic Microscopy and Targeted Lipid Microparticles. *J. Nanobiotechnology* **2014**, *12*, 24. https://doi.org/10.1186/1477-3155-12-24.
(714) Zhang, Y.; Xie, X.; Zhang, Y.; Zhang, Y.; Du, X. Experimental Study of Influences of a Particle on the Collapsing Dynamics of a Laser-Induced Cavitation Bubble near a Solid Wall. *Exp. Therm. Fluid Sci.* **2019**, *105*, 289–306. https://doi.org/10.1016/j.expthermflusci.2019.04.005.
(715) Qin, D.; Zou, Q.; Lei, S.; Wang, W.; Li, Z. Cavitation Dynamics and Inertial Cavitation Threshold of Lipid Coated Microbubbles in Viscoelastic Media with Bubble–Bubble Interactions. *Micromachines* **2021**, *12* (9), 1125. https://doi.org/10.3390/mi12091125.
(716) Batchelor, D. V. B.; Lad, A.; Burr, K. L.; Hollie, K.; McLaughlan, J. R.; Turnbull, W. B.; Sandoe, J. A. T.; Evans, S. D. *S. Aureus* Biofilm Disruption Using Ultrasound and Microbubbles: Influence of Radiation Force, Bubble Dynamics and Biofilm Growth Conditions. *Biofilm* **2025**, *10*, 100327. https://doi.org/10.1016/j.bioflm.2025.100327.

(717) Desai, S.; Sanghrajka, K.; Gajjar, D. High Adhesion and Increased Cell Death Contribute to Strong Biofilm Formation in Klebsiella Pneumoniae. *Pathogens* **2019**, *8* (4), 277. https://doi.org/10.3390/pathogens8040277.
(718) Nguyen, J.; Fernandez, V.; Pontrelli, S.; Sauer, U.; Ackermann, M.; Stocker, R. A Distinct Growth Physiology Enhances Bacterial Growth under Rapid Nutrient Fluctuations. *Nat. Commun.* **2021**, *12*, 3662. https://doi.org/10.1038/s41467-021-23439-8.
(719) Laekas-Hameder, M.; Daigle, F. Only Time Will Tell: Lipopolysaccharide Glycoform and Biofilm-Formation Kinetics in Salmonella Species and Escherichia Coli. *J. Bacteriol.* **2024**, *206* (10), e00318-24. https://doi.org/10.1128/jb.00318-24.
(720) Jung, J. W.; Jeon, H. M.; Pyo, J.; Lim, J.-H.; Weon, B. M.; Kohmura, Y.; Ishikawa, T.; Je, J. H. Four-Dimensional Visualization of Rising Microbubbles. *Sci. Rep.* **2014**, *4* (1), 5083. https://doi.org/10.1038/srep05083.
(721) Sassaroli, E.; Hynynen, K. Cavitation Threshold of Microbubbles in Gel Tunnels by Focused Ultrasound. *Ultrasound Med. Biol.* **2007**, *33* (10), 1651–1660. https://doi.org/10.1016/j.ultrasmedbio.2007.04.018.
(722) Vyas, H. K. N.; Xia, B.; Mai-Prochnow, A. Clinically Relevant in Vitro Biofilm Models: A Need to Mimic and Recapitulate the Host Environment. *Biofilm* **2022**, *4*, 100069. https://doi.org/10.1016/j.bioflm.2022.100069.
(723) Shi, D.; Mi, G.; Wang, M.; Webster, T. J. In Vitro and Ex Vivo Systems at the Forefront of Infection Modeling and Drug Discovery. *Biomaterials* **2019**, *198*, 228–249. https://doi.org/10.1016/j.biomaterials.2018.10.030.
(724) Abbott, I. J.; van Gorp, E.; Wijma, R. A.; Meletiadis, J.; Mouton, J. W.; Peleg, A. Y. Evaluation of Pooled Human Urine and Synthetic Alternatives in a Dynamic Bladder Infection *in Vitro* Model Simulating Oral Fosfomycin Therapy. *J. Microbiol. Methods* **2020**, *171*, 105861. https://doi.org/10.1016/j.mimet.2020.105861.
(725) Andersen, T. E.; Kingshott, P.; Palarasah, Y.; Benter, M.; Alei, M.; Kolmos, H. J. A Flow Chamber Assay for Quantitative Evaluation of Bacterial Surface Colonization Used to Investigate the Influence of Temperature and Surface Hydrophilicity on the Biofilm Forming Capacity of Uropathogenic *Escherichia Coli*. *J. Microbiol. Methods* **2010**, *81* (2), 135–140. https://doi.org/10.1016/j.mimet.2010.02.009.
(726) Jafari, N. V.; Rohn, J. L. An Immunoresponsive Three-Dimensional Urine-Tolerant Human Urothelial Model to Study Urinary Tract Infection. *Front. Cell. Infect. Microbiol.* **2023**, *13*, 1128132. https://doi.org/10.3389/fcimb.2023.1128132.
(727) Flores, C.; Ling, J.; Loh, A.; Maset, R. G.; Aw, A.; White, I. J.; Fernando, R.; Rohn, J. L. A Human Urothelial Microtissue Model Reveals Shared Colonization and Survival Strategies between Uropathogens and Commensals. *Sci. Adv.* **2023**, *9* (45), eadi9834. https://doi.org/10.1126/sciadv.adi9834.
(728) Andersen, T. E.; Khandige, S.; Madelung, M.; Brewer, J.; Kolmos, H. J.; Møller-Jensen, J. Escherichia Coli Uropathogenesis In Vitro: Invasion, Cellular Escape, and Secondary Infection Analyzed in a Human Bladder Cell Infection Model. *Infect. Immun.* **2012**, *80* (5), 1858–1867. https://doi.org/10.1128/iai.06075-11.
(729) Pick, U. Liposomes with a Large Trapping Capacity Prepared by Freezing and Thawing of Sonicated Phospholipid Mixtures. *Arch. Biochem. Biophys.* **1981**, *212* (1), 186–194. https://doi.org/10.1016/0003-9861(81)90358-1.
(730) Hays, L. M.; Crowe, J. H.; Wolkers, W.; Rudenko, S. Factors Affecting Leakage of Trapped Solutes from Phospholipid Vesicles during Thermotropic Phase Transitions. *Cryobiology* **2001**, *42* (2), 88–102. https://doi.org/10.1006/cryo.2001.2307.

(731) Chandan, R.; Banerjee, R. Pro-Apoptotic Liposomes-Nanobubble Conjugate Synergistic with Paclitaxel: A Platform for Ultrasound Responsive Image-Guided Drug Delivery. *Sci. Rep.* **2018**, *8* (1), 2624. https://doi.org/10.1038/s41598-018-21084-8.

(732) Park, B.; Yoon, S.; Choi, Y.; Jang, J.; Park, S.; Choi, J. Stability of Engineered Micro or Nanobubbles for Biomedical Applications. *Pharmaceutics* **2020**, *12* (11), 1089. https://doi.org/10.3390/pharmaceutics12111089.

(733) Rovers, T. A. M.; Sala, G.; van der Linden, E.; Meinders, M. B. J. Temperature Is Key to Yield and Stability of BSA Stabilized Microbubbles. *Food Hydrocoll.* **2016**, *52*, 106–115. https://doi.org/10.1016/j.foodhyd.2015.05.038.

(734) Sarkar, K.; Katiyar, A.; Jain, P. Growth and Dissolution of an Encapsulated Contrast Microbubble: Effects of Encapsulation Permeability. *Ultrasound Med. Biol.* **2009**, *35* (8), 1385–1396. https://doi.org/10.1016/j.ultrasmedbio.2009.04.010.

(735) Kwan, J. J.; Borden, M. A. Microbubble Dissolution in a Multigas Environment. *Langmuir* **2010**, *26* (9), 6542–6548. https://doi.org/10.1021/la904088p.

(736) Wu, S.-K.; Chu, P.-C.; Chai, W.-Y.; Kang, S.-T.; Tsai, C.-H.; Fan, C.-H.; Yeh, C.-K.; Liu, H.-L. Characterization of Different Microbubbles in Assisting Focused Ultrasound-Induced Blood-Brain Barrier Opening. *Sci. Rep.* **2017**, *7*, 46689. https://doi.org/10.1038/srep46689.